NOTE TO USERS

THE CHEMICAL AND PHYSICAL PROPERTIES OF POLYCHALCOGENS

Eli Zysman-Colman

A thesis submitted to the Faculty of Graduate Studies and Research of McGill University
in partial fulfillment of the requirements of the degree of
Doctor of Philosophy

Department of Chemistry
McGill University
Montréal, Québec, Canada
October, 2003

Your file Votre référence
ISBN: 0-612-98398-6
Our file Notre référence
ISBN: 0-612-98398-6

To my parents without whom
I would be a fraction of the person I am today.

For my sister, Zofia

The life so short; the craft so long to learn

Hippocrates

There is a single light of science, and to brighten it anywhere is to brighten it everywhere.

Isaac Asimov

Chance favours the prepared mind

Louis Pasteur

ABSTRACT

The optimized synthesis of acyclic dialkoxy disulfides and aromatic polysulfides is described and their physical properties probed. A theoretical survey of dialkoxy disulfides and thionosulfites was undertaken in order to determine the most efficacious method for accurately modeling these compounds. In particular, the origin of the high barrier to rotation in the dialkoxy disulfides was determined to be due to a generalized anomeric effect resulting from two lone pair donations of each sulfur atom into each of their respective sulfur-oxygen antibonding orbitals. The origin of the high rotational barrier was also verified experimentally, in particular with respect to solvent and substituent effects. Complimentary to this thermal process, the decomposition of dialkoxy disulfides was also investigated. It was determined that these compounds decompose under first order kinetics *via* an initial asymmetric S-O homolytic cleavage. Activation parameters for both of these processes were determined.

Theoretical modeling on the relative ground state energies of dialkoxy disulfides is also described. It has been ascertained that the equilibrium position between the two isomers can be influenced by the ring size of the molecule; larger rings promote the dialkoxy disulfide isomer. These modeling studies were successfully corroborated experimentally. Of note is the synthesis of a new 8-membered ring dialkoxy disulfides as well as novel 7-membered ring thionosulfites. These compounds were also confirmed by single X-ray crystallography.

The kinetics of desulfurization of acyclic aromatic tri- and tetrasulfides is described. Tetrasulfides were found to transfer a sulfur atom to triphenylphosphine over ten times faster than their trisulfide analogues.

RÉSUMÉ

La synthèse optimisée et les propriétés physiques de dialkoxy disulphides acycliques et de polysulphides aromatiques est décrite. Une étude théorique des dialkoxy disulphides et thionosulphites a permis de déterminer la méthode la plus efficace pour la modélisation exacte de ces composés. En particulier, l'origine l'élévation de la barrière de rotation des liens présents dans les dialkoxy disulphides a été déterminée. Elle est attribuée à un effet anomérique général résultant d'un partage de deux paires d'électrons de valences provenant de chaque atome de souffre vers les orbitales anti-liantes souffre-oxygène. L'origine de cette barrière de rotation a été aussi vérifiée par expérimentation, plus précisément en étudiant l'effet du solvant et des substituants. Parce qu'elle représente une réaction similaire, la décomposition des dialkoxy disulphides a aussi été investiguée. Il a été déterminé que ces molécules décomposent suivant une cinétique de premier ordre entamée par une scission homolytique et asymétrique du lien souffre-oxygène. Les paramètres d'activation pour ces deux processus ont été déterminés.

La modélisation théorique des énergies relatives de différents dialkoxy disulfides à l'état fondamental a aussi été étudiée. Il a été constaté que la position d'équilibre entre les deux isomères est influencée par l'encombrement stérique. Ainsi les grosses molécules ont tendance à former l'isomère dialkoxy disulphide. Ces conclusions ont été corroborées par des expériences en laboratoire. Des résultats particulièrement intéressants ont été obtenus avec un dialkoxy disulphide contenant un cycle de huit atomes, et un thionosulphite contenant un cycle de sept atomes. Ces composés ont été préparés par synthèse et leur structure a été confirmée par cristallographie à rayons X.

Finalement, la cinétique des réactions de désulfurisation des tri- et tétra-sulphides a aussi été étudiée. Les résultats obtenus suggèrent que les tétrasulphides transfèrent un atome de souffre au triphenylphosphine au moins dix fois plus vite que leurs trisulphides analogues.

ACKOWLEDGEMENTS

I would be remiss if I did not acknowledge that it would have been impossible to complete my doctoral work without the help and support of a great many people. Without forethought, I am most indebted to my supervisor, Dr. David Harpp. He enthusiastically provided me with all the tools necessary to become a researcher. He is a gifted teacher but more importantly, he is a true mentor. Dr. Harpp possesses intangible qualities not only as a professor but also as a human being. I am consistently awed and inspired by his generous caring and compassionate personality. His support has been near incalculable and invaluable for me, a guy with Crohn's who came from Physics to do Organic Chemistry. Thank you for believing in me.

I would never have joined the Department of Chemistry to do post-graduate work if it weren't for the enthusiastic and graceful teaching that I received from Dr. Bruce Lennox. He inspired me first during my undergraduate scholarship then nudged me into applying to do graduate work and finally facilitated the transition from physicist to chemist. I am eternally grateful for the career change that you help to catalyze.

Dr. Patrick Farrell has been, in many important ways, a second mentor to me. He has been wonderfully supportive not only in terms of direct collaborative efforts but also as one who was only too happy to listen to both chemistry-related and unrelated stories. His introspection has proven to be quite important over the years. I also wish to acknowledge his collaboration in my polysulfide kinetics work.

I wish to thank Dr. James Snyder of Emory University who has taught me all I know about computational chemistry. I am indebted to him for providing me the opportunity to go to Emory University for the summer of 1999. I wish to further acknowledge his contributions over the years, most specifically in terms of our many collaborative efforts. He is a wealth of knowledge and someone who looks at chemistry problems critically and logically. From his analytical techniques, I have learned much and I gratefully acknowledge many helpful discussions.

Other collaborators need also be acknowledged. I am grateful to Dr. Neysa Nevins (Glaxo Smith Kline), Pahk Chepatkri (Emory University) and Dr. Mark S. Workentin (University of Western Ontario).

I am endebted to the following people who helped to edit the thesis: Dr. David Harpp, Dr. Patrick Farrell, Dr. James Snyder and Alain Ajamian. I would also like to thank Zofia Zysman-Colman for aiding in and Dr. Karine Auclair for proof-reading the French translation of the abstract.

There are so many who have provided important and helpful discussions and/or advice during the course of my doctoral work. I wish to acknowledge the following for their contributions: Dr. Lodovico Lunazzi (Università di Bologna), Dr. Keith Ingold (Steacie Institute for Molecular Sciences), Dr. Alexander Greer (CUNY-Brooklyn), Dr. Kent Gates (University of Missouri-Columbia), Dr. Hans Reich (University of Wisconsin at Madison), Dr. Adrian Schwan (University of Guelph), Dr. John Tebby (University of

Staffordshire), Dr. Harry S. Hudson (University of North London), Dr. Scott Bohle (McGill University), Dr. Karine Auclair (McGill University), Dr. George Just (McGill University), Dr. Paul Wiseman (McGill University), Dr. Nicolas Moitessier (McGill University) and Dr. John Harrod (McGill University).

I was extremely fortunate to have fantastic teachers who were always willing to respond to each and every one of my myriad questions. Grateful acknowledgements go to Drs. Hanadi Sleiman, Bruce Arndtsen, D.F.R. Gilson, Romas Kazlauskas and James Gleason. I would also like to single out Drs. Hanadi Sleiman and Masad Damha for encouraging me to continue teaching and providing me unique opportunities to do so.

The assistance and technical expertise of Dr. Zhicheng Xia has been invaluable throughout the course of my doctoral work. The success of much of the thesis relies on the use of NMR spectroscopy. I thank Dr. Xia for his patience in aiding me throughout critical stages of this work.

I wish to thank Drs. Anne-Marie Lebuis and Francine Bélanger-Gariépy for their solution of the six crystal structures contained within this work. Thank you also to Vasa Sindolic and Rick Rossi for their help with the acquisition of the Raman spectra.

The administrative staff provides a helpful atmosphere that allows me to go about my work that much more smoothly. I am most appreciative for their kindness and

generosity. I wish to thank Renée Charron, Chantal Marotte, Fay Nurse, Sandra Aerssen, Paulette Henault and Carol Brown for their tireless assistance.

Thank you to all those colleagues who help make it a pleasure to come into work every day. I am truly beholden to Alain Ajamian who has been such a superb friend over the past four years. I have learned much from Drs. Yihua Hou and Erwin Schultz. They helped me acclimatize to life in the lab and taught me the little things that only lab-mates could teach. Thank you Aaron Kosar for your help in using the FT-IR, DSC and UV-Vis machines.

Financial assistance from McGill University (Alma Matter Travel Grant) and the Fonds pour la Formation de Chercheurs et l'Aide à la Recherche (B1 and B2 Graduate Fellowships) is gratefully acknowledged.

Life during the past four years has been made so much more pleasurable thanks to the continued presence of life-long friends. Thanks so much to Matthew, Sarah, Denton, Kristi, Chantal, Andrea, Dan, Danistan and Andy.

Johanne, I cannot begin to acknowledge how much your emotional support and inner strength have so favourably impacted the last two years of my life. I will always be thankful for your constant encouragement and friendship.

To my extended family that has constantly shown their support, enthusiasm and love before and during my chemistry adventure, I am eternally grateful. I would like to especially acknowledge my Zajda. From his example amongst many of his fine attributes, I have learned perseverance. To my sister, Zofia, who is the smartest and hardest worker I know, you are simply the best. Finally, to my parents, Margo and Neil, what can I say but simply thank you. Words need not be written to express how deeply important you are and have always been to me.

TABLE OF CONTENTS

LIST OF ABBREVIATIONS

Å	Angstrom, 1x 10^{-10} m
A	Arrhenius pre-exponential factor
$A^{1,3}$	1,3-allylic
Ac	acetyl
AC	alternating current
Addn	addition
Adm	adamantyl
AIDS	acquired immunodeficiency syndrome
All	allyl
AM1	Austin Model 1 - a semi-empirical method
AMBER	assisted model building with energy refinement - a force field
Anal.	analysis
AO	atomic orbital
aq	aqueous
Ar	Aryl
av, avg	average
β	isokinetic temperature
b	y-intercept
B	Becke's correlation functional - a DFT method
BLYP	a gradient corrected DFT method
B3	Becke's 3 parameter correlational functional - a DFT method
B3LYP	a hybrid DFT method
BDE	homolytic bond dissociation energy
Bn	benzyl
bp	boiling point
br	broad (spectral)
Bu	butyl
°C	degrees Celcius
c	centi; at the coalescence temperature
ca	circa
cal	calorie
calcd	calculated
cc-pVQZ	a correlation-consisten basis set that includes polarization functions
CC	coupled cluster calculation - a correlated *ab initio* method
CCSD(T)	coupled cluster calculation perturbatively possessing triple excitations - an *ab initio* method
CHARMM	chemistry at Harvard macromolecular mechanics - a force field
CI	chemical ionization (in mass spectrometry); configuration interaction - a correlated *ab initio* method
CIP	Cahn-Ingold-Prelog (in nomenclature)
cmpd	compound
CMV	cytomegalovirus, a member of a group of herpes-type viruses
CNDO	complete neglect of differential overlap
concd	concentrated
Cp	cyclopentadienyl
Cp*	η^5-$CH_3C_5H_4$
Cys, cyst	cystine
Δ	reflux/heat or change

δ	chemical shift in parts per million downfield from tetramethylsilane
d	decomposition
d_n	*n* deuterated protons
d	day(s); doublet (spectral)
D	debye
dd	doublet of doublets (spectral)
DABCO	4-diazabicyclo[2.2.2]octane
DAD	di-*tert*-adamantyl disulfide
del	delocalization
DFT	density functional theory
DMA	*N,N*-dimethylacetamide
DMAAN	*N,N*-dimethylacrylonitrile
DMF	*N,N*-dimethylformamide
DMPO	*4-N,N*-dimethylpyridine-*N*-oxide
DMSO	dimethyl sulfoxide
DNA	deoxyribonucleic acid
DNMR	dynamic NMR
DSC	differential scanning calorimetry
DZP	Dunning-Hay double ζ basis set plus polarization functions
E	energy
E_A	activation energy
EC_{50}	effective concentration
ED	electron diffraction
EDITH	3-ethoxy-1,2,4-dithiazoline-5-one
EH	extended Hückel theory
EI	electronic implact (in mass spectrometry)
EN	electronegativity
eq	equation
ESR	electron spin resonance
Expt	experimental
Et	ethyl
E_T	Dimroth-Reichardt solvent polarity parameter
ESR	electron-spin-resonance spectroscopy
eu	entropy unit
f	formation
FAB	fast atom bombardment (in mass spectrometry)
FWHH	full width at half height (in NMR spectroscopy)
g	gram(s); gas phase
G	free energy
GC	gas chromatography
GE	General Electric Company
GLC	gas-liquid chromatography
G*n*	Gaussian theory methods such as G2 and G3 - a semi-empirical method
GTO	Gaussian-type orbital(s)
h	Planck's constant
h	hour(s)
H	enthalpy
HF	Hartree-Fock - an *ab initio* method
HFIP	hexafluoroisopropyl alcohol
HMO	Hückel molecular orbital

HMQC	heteronuclear multiple-quantum correlation
HOMO	highest occupied molecular orbital
HPLC	high performance liquid chromatography
HRMS	high-resolution mass spectroscopy
Hz	hertz
i	iso
I	integration
IBX	*o*-iodoxybenzoic acid
IL-1	interleukin-1
INDO	intermediate neglect of differential overlap
IR	infrared
J	coupling constant (in NMR spectrometry)
J	joule
k	rate constant
k	kilo
K	Kelvin(s) (degrees of absolute temperature)
k_B	Boltzmann's constant
L	liter(s)
LAH	lithium aluminum hydride
LCAO	linear combination of atomic orbitals
LDA	lithium diisopropylamide
Lew	Lewis
LFER	linear free energy relationship
lit.	literature
LSA	line shape analysis (in NMR spectroscopy)
LUMO	lowest unoccupied molecular orbital
LYP	Lee, Yang and Parr's non-local exchange functional - a DFT method
μ	micro
m	slope
m	multiplet (spectral); meter(s); milli; medium (in IR spectroscopy)
M	molar (moles pre liter); mega; a conformation with a positive helicity
max	maximum
m-CPBA, MCPBA	*m*-cholroperoxybenzoic acid
Me	methyl
min	minute(s); minimum
MINDO	modified intermediate neglect of differential overlap - a semi-empirical method
MINI-*i* (*i* = 1-4)	a minimum *ab initio* basis set with one contraction per orbital
MM1	Allinger's first generation molecular mechanics force field
MM2	Allinger's second generation molecular mechanics force field
MM3	Allinger's third generation molecular mechanics force field
MM3*	a modification of MM3 implemented in Macromodel®
MMFF	Merck molecular force field - a molecular mechanics force field
MNDO	modified neglect of diatomic overlap - a semi-empirical method
MO	molecular orbitals
mol	mole(s); molecular (as in mol wt)
Mp	melting point
MPn	n^{th} order Møller-Plesset pertubation function - a correlated *ab initio* method
mRNA	messenger RNA
Ms	methanesulfonyl (mesyl)
MS	mass spectrometry

MW or mol wt	microwave; molecular weight
m/z	mass to charge ratio (in mass spectrometry)
n	number; normal
n	nano
NBO	natural bond order
NMR	nuclear magnetic resonance
NO	nitric oxide
NOE	nuclear Overhauser effect
NOESY	nuclear Overhauser effect spectroscopy
NRMS	neutralization-reionization mass spectrometry
Nu	nucleophile
obs	observed
P	a conformation with a negative helicity
P86	Perdew's gradient-corrected functional - a DFT method
PADS	phenylacyl disulfide
PCILO	pertubative configuration interaction using localized orbitals - a semi-empirical method
PES	photoelectron spectroscopy
PG	prostaglandin
Ph	phenyl
PM3	parameterization method 3 - a semi-empirical method
ppm	parts per million
Pr	propyl
PTC	phase transfer catalyst
PW91	Perdew and Wang's gradient corrected functional - a DFT method
QCI	quadratic configuration interaction - a correlated *ab initio* method
q	quartet (spectral)
R	universal gas constant
R^2	Pearson regression factor
rac	racemic
Ref	reference
rel	relative
R_f	retention factor (in chromatography)
RHF	restricted HF - an *ab intio* method
RSV	respiratory syncytial virus
RT	room temperature
s	secondary
s	singlet (spectral); second(s); strong (in IR spectroscopy)
σ	standard deviation
S	entropy
SCF	self-consistent field - a procedure for solving the HF equation
SD	single and double excitation calculations included - used to describe *ab initio* methods such as CI-SD
STO	Slater-type orbital(s)
SVWN	Slater's exchange with Vosko Wilk and Nusar's correlational functional - a DFT method
t, tert	tertiary
t	triplet (spectral)
temp	temperature
TETD	tetraethylthiuram disulfide
TFAA	trifluoroacetic anhydride
THF	tetrahydrofuran

TLC	thin-layer chromatography
TMEDA	tetramethylethenediamine
TMS	trimethylsilyl; tetramethylsilane
TNF	tumour necrosis factor
tol	4-methylphenyl (tolyl)
Tos	4-toluenesulfonyl (tosyl)
tot	total
Tr	triphenylmethyl (trityl)
tRNA	transfer RNA
TS	transition state
UV	ultraviolet
V	volt
V_n	n-fold torsional parameter
vic	vicinal
vis	visible
vol	volume
w	weak (in IR spectroscopy)
W	watt
WBI	Wiberg bond index
Xα	a simple DFT method
ZDO	zero differential overlap
ZDMC	zinc dimethyldithiocarbamate
ZPE, ZPVE	zero point vibrational energy

INDEX OF FIGURES

INDEX OF TABLES

Chapter 1

Introduction

1.1 History of Sulfur

It is tasteless and odourless. It is one of the elements found most often in a pure crystalline form. It is sulfur and knowledge of this element goes back to antiquity. The etymology of sulfur may come from the German or Scandinavian (schwelfel/svovel/svavl) which are themselves derived from the Indo-European *suelphlos* which comes from the word *swel* which means to burn slowly. Sulfur taxonomically is derived from the Latin *sulpur* meaning "burning stone" and was itself synonymously used with the term fire, though its origins may come from the Sanskrit word *sulveri* meaning the enemy of copper.[1]

The Bible contains more than 15 references for the term brimstone – sulfur as it was known in antiquity. Most references thematically deal with death and destruction. For example:

Revelation 19:20 And the beast was taken, and with him the false prophet that wrought miracles before him, with which he deceived them that had received the mark of the beast, and them that worshipped his image. These both were cast alive into a lake of fire burning with brimstone.

The term brimstone though is most closely identified with the Biblical destruction of Soddom and Gomorrah. Pre-Roman civilizations used burned brimstone as a medicine and used burning sulfur as fumigants and as bleaching and purification agents. The

Egyptians employed sulfur to concoct dyes more than 2600 years ago (most probably in the form of metal sulfides).

The ancient literature is replete with references to this element. Homer, in the Odyssey (850 BCE) wrote:

Bring me sulfur, old nurse, that cleanses all pollution and bring me fire, that I may purify the house with sulfur. As well as *Bring me fire that I may burn sulfur, the divine curer of ills.*

Pliny the Elder (23-27 CE) reported in his book "Historia Naturalis" that sulfur was a

most singular kind of earth and an agent of great power on other substances, and had *medicinal [sic] virtues* and *burning sulfur will keep out enchantments – yea, and drive away foul fiends.*

Both the Greeks and the Romans discovered sulfur's combustibility property and exploited it first for pyrotechnic displays then in wartime as a catalyst in incendiary weaponry. Indeed, sulfur is one of the main components in gunpowder (along with saltpeter, KNO_3 and charcoal), a mixture discovered in Europe in the 14^{th} century though known to the Chinese since the time of Confucius (557-479 BCE). It was only in 1777 that sulfur was finally confirmed to be an element by French chemist Antoine Lavoisier.

Interest in elemental sulfur and its organic derivatives has been and continues to be extensive. Currently, there are at least four journals substantially devoted to its organic chemistry.

1.2 Layout of Thesis

The title of this thesis generally relates to the physical organic chemistry of polychalcogens specifically containing sulfur. The thesis is subdivided into two main sections: the first dealing with alkoxy disulfide (ROSSOR) chemistry and the second dealing with polysulfide (RS_nR) chemistry. Each section contains its own introduction. Relevant synthetic experimental work is detailed at the end of each chapter. Figures, tables, schemes, equations and compounds are numbered sequentially throughout the thesis. References are numbered sequentially for each chapter and may be found as endnotes at the completion of the chapter.

1.3 A Note on Nomenclature

Systematic as well as common nomenclature[2] used in this thesis is outlined in Tables 1 and 2 and are used interchangeably throughout the thesis. Common nomenclature is used more often as it allows for the efficient description of key compounds given that the official IUPAC terminology for highly functionalized polychalcogens is often long, unwieldy and non-intuitive. Throughout the thesis, there are references to "S". This does

not imply that atomic sulfur is a reactive intermediate or product but simply refers to an as yet unidentified sulfur species. From a mass balance point of view the term "*n*S" is equivalent to $^{n}/_{8}$ S_8; S_8 is the most stable sulfur allotrope at the reaction temperatures described in this work.

Table 1 Nomenclature for some acyclic sulfur compounds

IUPAC	Common	Structure
monosulfane	sulfide	
monosulfane oxide	sulfoxide	
sulfenic acid ester	sulfenate	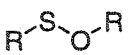
sulfinic acid ester	sulfinate	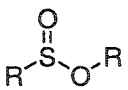
sulfonic acid ester	sulfonate	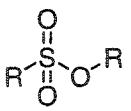
disulfane	disulfide	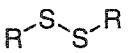
disulfane monoxide	thiosulfinate	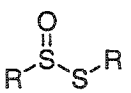
disulfane 1,1-dioxide	thiosulfonate	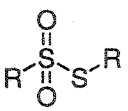
disulfane 1,2-dioxide	α-disulfoxide	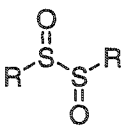
trisulfane	trisulfide	
tetrasulfane	tetrasulfide	
polysulfane	polysulfide	
[sulfanediylbis(oxy)]-dialkane	sulfoxylate	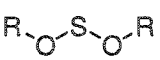
sulfite	sulfite	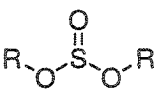
O,O-dimethyl thiosulfite	thionosulfite	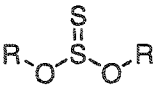
sulfate	sulfate	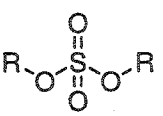
[disulfanediylbis(oxy)]-dialkane	alkoxy disulfide	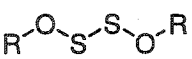

Table 2 Nomenclature for some sulfur-containing heterocycles

Ring Size	IUPAC		Common	Structure
	saturated	unsaturated		
3	-irane	-iren		
4	-etane	-ete		
5	-olane	-ole		
6	-ane	-in	in thesis these are referred to as:	
7	-epane	-epin	*n*-membered - functional group	
8	-ocane	-ocin		
9	-onane	-onin		
10	-ecane	-ecin		
	Examples:			
	1,3,2-dioxathiolane		5-membered saturated sulfoxylate	
	1,3,2-dioxathiole		5-membered unsaturated sulfoxylate	
	1,3,2-dioxathiolane 2-oxide		5-membered sulfite	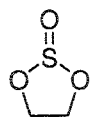
	1,3,2-dioxathiolane 2-sulfide		5-membered thionosulfite	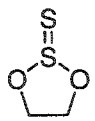
	1,4,2,3-dioxadithiane		6-membered alkoxy disulfide	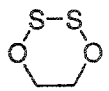
	1,3,2-dioxathiepin 2-sulfide		7-membered unsaturated thionosulfite	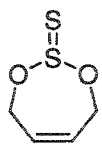

1.4 A Note on Computations

Throughout this thesis much computational work is reported. It should be noted that this is not a thesis centered on theoretical work; rather computational chemistry is used as

a tool to help understand the organic chemistry. We believe that calculations can prove to be invaluable as a predictive tool. The following is a brief, and by no means comprehensive, summary of computational methods. It is placed here in order to acquaint and aid the reader in understanding the computational nomenclature and methodology used throughout this thesis.[3] For a complete listing of computational methods, see the Index of abbreviations.

There are two main computational methods used to elucidate structural and electronic properties of modeled compounds. They are molecular mechanics and electronic structure methods. The latter term globally represents all methods which aim to approximate the Schrödinger equation, an equation that when solved for a specific system, encapsulates the quantum mechanical energy and other related properties of that system. These methods include semi-empirical methods, *ab initio* methods and density functional theory (DFT) methods.

Molecular mechanics simulations use the laws of classical mechanics to predict the structures and properties of molecules. The main computer program used within this thesis is Macromodel®. Though there are many different methods, each characterized with its own force field such as AMBER, MMFF or CHARMM, the predominant ones seen here include MM2, MM3 and MM3*. The last method specifically refers to our own modified MM3* force field (which is itself implemented within the Macromodel program) in which we have added new atom types and parameter sets to better model our compounds of interest.

Semi-empirical methods such as EH, AM1, PM3 and MINDO/n (n = 1-3) are implemented in programs such as MOPAC or Gaussian. These methods distinguish themselves as their parameters are in part derived from experimental data and account only for valence electrons. Different semi-empirical methods, each characterized by their own distinct parameter sets, each solve an approximation to the Schrödinger equation that depends on these input parameters.

Ab initio methods solve the Schrödinger equation using a series of mathematical approximations. Two of the most important are the Born-Oppenheimer and the central-field approximations. The Born-Oppenheimer approximation deconvolutes nuclear and electronic motions such that they can be treated separately. This is reasonable given the large mass difference that exists between the two. A result of this is that the nuclei are assumed to be fixed relative to the motion of the surrounding electrons of the atoms in the molecule. Hartree-Fock (HF) calculations average the electrons' motions and thus do not take into account electron correlation. In other words when using HF theory, each electron reacts to the average electron density of the molecule while methods which include electron correlation such as MPn (n = 2-4 and represents the order of correlation) or CC or CI account for explicit instantaneous repulsion interactions. Because of the central-field approximation, all HF energies are greater than the exact energy of the system (variational principle). In contrast to semi-empirical methods, which are computationally cheap, *ab initio* methods provide highly accurate quantitative results and greater computational cost.

The wave function as described by the Schrödinger equation must be described by some mathematical function which is solvable. The functions used most often are linear combinations of Gaussian-type orbitals of the form $\exp(-ar^2)$. These linear combinations of atomic orbitals or basis functions describe the molecular wave function. Basis functions are specified by abbreviations such as 6-31G*.

Basis set notation can be tricky. A major class of basis sets used in this thesis is the Pople basis sets and are indicated by the notation 6-31G. This notation indicates that each core orbital is described by a single contraction of six GTO primitives and each valence shell orbital is described by two contractions, one with three primitives and the other with one primitive. The basis set can be modified by the inclusion of polarization functions such as 6-31G*. The "*" indicates that a set of *d* primitives has been added to heavy atoms. Larger polarization functions also exist such as 6-31G(2df); here a set of 2 *d* and 1 *f* primitives has been added to the heavy atoms in the molecule. Polarization functions are added in order to modify the shape of the wave function. The inclusion of such functions usually leads to more accurate predictions. The addition of diffuse functions is denoted by a "+" such as in 6-31+G*. Diffuse functions describe the shape of the wave function far from the nucleus and are usually used to describe compounds with large electron density distributions such as anions.

DFT methods are similar to *ab initio* methods but are computationally less demanding and inherently include electron correlation. DFT methods calculate the energy of the

molecule not from the wave function but from its electron density. Many methods have been developed including the popular B3LYP, B3PW91, B3PW86, SVWN and Xα. As with *ab initio* methods, DFT calculations require the use of basis sets.

1.5 References

(1) For a review on the history of sulfur see: Woolins, J. D. *Encyclopedia of Inorganic Chemistry*; King, R. B., Ed.; John Wiley & Sons: Toronto, **1994**, *7*, 3954

(2) For a review on nomenclature see: Steudel, R. *Chem. Rev.* **2002**, *102*, 3905

(3) For a review on basic concepts relating to computational chemistry see: Young, D. C.; John Wiley & Sons, Inc.: Toronto, **2001**, 381

Chapter 2

A Context for the Study of Alkoxy Disulfides

2.1 Introduction to Compounds containing the OSSO moiety

Molecules of the form ROSSOR **1**, ester derivatives of hydrothiosulfurous acid HOSSOH, have been known for over a century.[1] It was not until 1964 that Thompson and co-workers[2-4] were able to confirm that this functionality could potentially exist in two separate constitutional forms, namely dialkoxy disulfides **1** (in this thesis, alkoxy disulfide is used as an interchangeable term) and a branch-bonded arrangement, the thionosulfites **2**. Other isomers such as the thiosulfite **3** or the thiosulfonate ester (RSO_2SR) **4** earlier proposed by Zinner[5] were readily ruled out by ^1H NMR spectroscopy, while other early work[6-9] (Raman,[10,11] dipole moment measurements[10]) failed to fully distinguish **1** from **2** though they did suggest the connectivity in **1**.

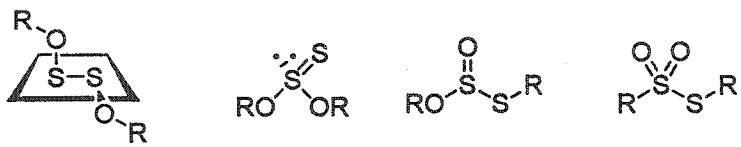

1 **2** **3** **4**

For R = Et, Thompson observed a characteristic magnetic non-equivalence of the methylene protons in the ^1H NMR at room temperature. The origin of this diastereotopicity of the methylene protons was not determined. One of two possible conclusions could be drawn. The compound could have connectivity of form **2**, in which case there would be an associated high thermal barrier to pyramidal inversion[12-14] about the branched sulfur as does exist with analogous sulfite[15-17] and sulfoxide[18-27] systems. As examples, Thompson has reported that the nonequivalence of the methylene protons in diethyl sulfite was maintained at 145 °C[28] and the barrier to inversion for DMSO is

reported[27] to be 39.7 kcal/mol. Conversely, an inherently high barrier about the sulfur-sulfur bond could be responsible. Here, the compound would adopt a *gauche* conformation in the ground state and would have form **1** (a detailed investigation of barriers about S-S bonds is covered in Chapter 2.4).[29] A coalescence of the ABX_3 pattern to that of a simple A_2X_3 pattern for **1** was observed at 100 °C suggesting the connectivity of **1** over that of the branched **2** (barriers[22] for sulfoxide inversion can be as high as 85 kcal/mol).

Since Thompson's seminal work, few investigations into the physical properties of alkoxy disulfides have been published.[30-34] Other work on this system is worthy of mention.[35,36] The results contained within these recent references are profiled in detail throughout this thesis. Besides their unusual physical properties, substituted benzyloxy disulfides have been shown to inhibit the growth of certain microorganisms (*E. coli* and *S. aureus*).[37]

Although compounds with a branched sulfur are known,[38] there are relatively few examples. Foss[39] had originally elucidated the notion that valence expansion of the branched sulfur could be stabilized by adjoining electronegative atoms (F, O). Those of form **2** are rare, having been characterized[2,40-42] only four times with each of the thionosulfites containing a 5-membered ring core (**5a-5n**). The only systems where the thionosulfite connectivity has been structurally verified (**5g**, **5i**, **5m** and **5n** by X-ray) are in cyclic compounds.[40-42]

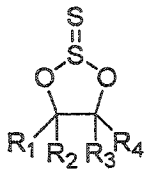

5

5a $R_1 = R_4 = Me$ (*cis*); $R_2 = R_3 = H$
5b $R_1 = R_3 = Me$ (*trans*); $R_2 = R_4 = H$
5c $R_1 = R_2 = R_3 = R_4 = H$
5d $R_1 = R_2 = R_3 = H$; $R_4 = Me$
5e $R_1 = R_4 = Ph$ (*cis*); $R_2 = R_3 = H$
5f $R_1 = R_3 = Ph$ (*trans*); $R_2 = R_4 = H$
5g $R_1,R_2 = R_3,R_4 = -(CH_2)_5-$
5h $R_1,R_2 = R_3,R_4 = -(CH_2)_4-$
5i $R_1,R_2 = R_3,R_4 = -(CH_2)_6-$
5j $R_1,R_2 = R_3,R_4 = -(CH_2)_7-$
5k $R_1,R_2 = -(CH_2)_5-$; $R_3 = R_4 = Me$
5l $R_1,R_2 = -(CH_2)_6-$; $R_3 = R_4 = Me$

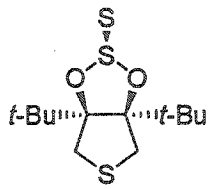

5m

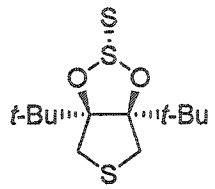

5n

2.2 Synthesis of Alkoxy Disulfides

Alkoxy disulfides 1 (where R = Me **6**, Et 7) were originally synthesized from reaction of S_2Cl_2 with a suspension of the sodium alkoxide in ligroin[43] (Scheme 1).[1]

$$2\ RONa \xrightarrow[\text{Ligroin}]{S_2Cl_2} ROSSOR$$

1

Scheme 1.

Larger homologues (where R = *n*-Pr **8**, *n*-Bu **9**) were subsequently synthesized by Stamm[44] using the same procedure. Hacklin[45] reported the synthesis of fluorinated derivatives (R = $(CF_3)_2CH$- **10**, CF_3CH_2- **11**) using lithium alkoxides at 50 °C. As will become evident, the use of S_2Cl_2 at elevated temperatures is quite uncommon. Although not strictly alkoxy disulfides as they are derived from silver acid salts not alcohols, **12a-12c** synthesized by Wang[46] in excellent yield (> 90%), are included for completeness. These compounds are thermally unstable and decompose readily to form the anhydride, SO_2 and sulfur.[47]

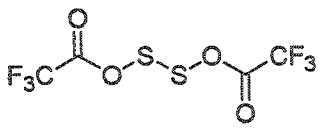

12a

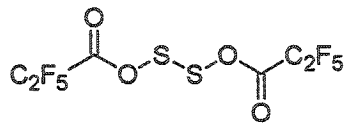

12b

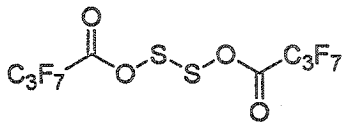

12c

In 1965, Thompson modified the procedure as it became increasingly difficult to prepare dry alcohol-free sodium alcoholates of higher molecular weight homologues. He synthesized a number of alkoxy disulfides in good yield by coupling S_2Cl_2 to the alcohol **13** in the presence of an amine base (in his case NEt_3) which would serve as an HCl scavenger (Scheme **2**). His work is highlighted within Tables **3**, **5-7**.

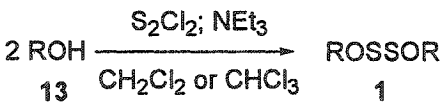

Scheme **2**.

Thompson used long addition times under relatively dilute conditions ($[S_2Cl_2] = 3.3$ M) employing a slight excess of alcohol at temperatures in the 10-15 °C range though the reaction could be performed at room temperature. This work has been patented.[48] This general procedure has been used as is by others.[33,35,49-51] Other groups claimed better yields with ethereal solvents[52,53] and low temperature work-up. Still others have synthesized **1** in THF[54] (no yield was reported) or have used pyridine[55] as the HCl acceptor. Our current work on the optimization of the synthesis of form **1** is summarized in Chapter **4**.

It appears that formation of alkoxy disulfides occurs *via* two simple nucleophilic displacements of chloride by the alcohol but Steudel[56] as well as Möckel[57,58] reported the presence of many other homologs ROS_nOR (with R = Me, n = 1, 2, 4-15; with R = Bu, n

= 1-15) by reverse-phase HPLC; peaks were identified based on the relationship that the natural logarithm of the retention time is linearly related to the number of sulfur atoms. The addition of Na_2S_x (from Na_2S and S_8) in the reaction promoted the formation of sulfur allotropes S_7 and S_8.

The formation of **1** is not limited to the use of S_2Cl_2 as the sulfur transfer reagent, though it is the one most frequently used and the one whereby the highest yields have been reported. Blanschette[59] recently reported the synthesis of dibutoxy disulfide **9** in moderate yield (46 %) using **14** in CH_2Cl_2 at RT whereas the use of other sulfur transfer reagents such as **15a** and **15b**,[51] developed in our lab,[60] has had limited success.

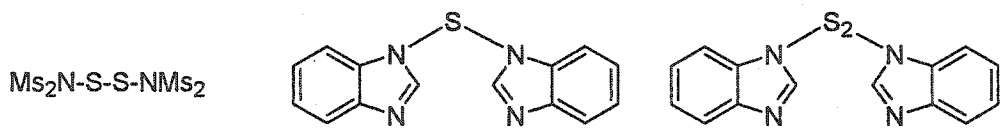

14 **15a** **15b**

Wenschuh and Rotzel[61] reported the formation of di-*n*-propoxy disulfide **8** and di-*iso*propoxy disulfide **16** through the metathesis of *n*-Bu_3SnOR (where R = *n*-Pr, *i*-Pr) with S_2Cl_2 in excellent yields. This method has not been exploited, most likely due to the need to use toxic stannyl alkoxides as the alcohol derivatives.

Tables 3-7 represent the exhaustive list of alkoxy disulfides synthesized to date in the literature (our current work excluded).

Table 3. Conditions and yields for the synthesis of some simple alkoxy disulfides

Entry	R	Cmpd	Method[a]	Solvent	Temp (°C)[b]	Yield (%)[e]	bp °C (mm Hg)	Mp (°C)	Ref[c]
1	Me	6	A	ligroin		37[1]			1,11
2	Et	7	A	ligroin		41[1]			1,10
3	*n*-Pr	8	A	ligroin					44
4	*n*-Pr	8	C	CH_2Cl_2	10-15	74[3]			3
5	*n*-Pr	8	G			94	36-38 (3.9)		61
6	*i*-Pr	16	C	CH_2Cl_2	10-15	71[3]	48 (100.0)		3,49
7	*i*-Pr	16	G			87	55-56 (2.0)		61
8	*n*-Bu	9	A	ligroin					44
9	*n*-Bu	9	C	CH_2Cl_2	10-15	70[3]	71 (0.7)		3
10	*n*-Bu	9	E		RT	46	71 (0.7)		59
11	*s*-Bu	17	C	CH_2Cl_2	10-15		58 (1.0)		49
12	*t*-Bu	18	C	CH_2Cl_2	10-15		49 (1.0)		49
13	*t*-Bu, Me[d]	19	C	CH_2Cl_2	10-15				33
14	*t*-Bu-CH_2-	20	C	CH_2Cl_2	10-15		72 (0.8)		49

a) Method **A** - 2 RONa + S_2Cl_2; Method **C** - 2 ROH + S_2Cl_2 + 2 NEt_3, 1 h addition time, 1.25 h total reaction time; Method **E** - 2 ROH + $(Ms_2N)_2S_2$, 4 h; Method **G** - 2 Bu_3SnOR + S_2Cl_2. b) Refers to temperature during the addition of S_2Cl_2 or if none, the reaction temperature. c) References reported for all those who synthesized the compound. d) Only known asymmetric alkoxy disulfide. e) Yields reported after distillation and correcting for impurities by GLC.

Table 4. Conditions and yields for the synthesis of some fluorinated alkoxy disulfides and related compounds

Entry	R	Cmpd	Method[a]	Solvent	Temp (°C)[b]	Yield (%)	bp °C (mm Hg)	Mp (°C)	Ref[c]
1	$(CF_3)_2CH$-	10	B		50	80	61 (30.0)		45
2	CF_3CH_2-	11	B		50	80	78 (76.0)		45
3	CF_3CO_2	12a	F			>90		TU[h]	46
4	$C_2F_5CO_2$	12b	F			>90		TU[h]	46
5	$C_3F_7CO_2$	12c	F			>90		TU[h]	46

a) Method **B** - 2 ROLi + S_2Cl_2; Method **F** - ROAg + S_2Cl_2, under vacuum. b) Refers to temperature during the addition of S_2Cl_2 or if none, the reaction temperature. c) References reported for all those who synthesized the compound. d) TU - thermally unstable.

Table 5. Conditions and yields for the synthesis of aliphatic alkoxy disulfides

Entry	R	Cmpd	Method[a]	Solvent	Temp (°C)[b]	Yield (%)	bp °C (mm Hg)	Mp (°C)	Ref[c]
1	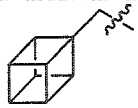	21	C	CH_2Cl_2	0	85			50
2	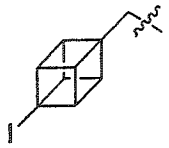	22	C	CH_2Cl_2	0	89			50
3[e]	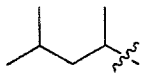	23	C	CH_2Cl_2	10-15	83	67 (0.8)		3
4		24	C	CH_2Cl_2	10-15	80			3
5	n-C_8H_{17}	25	C	CH_2Cl_2	10-15	90		-22	3
6[e]	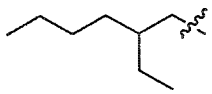	26	C	CH_2Cl_2	10-15	85	147 (0.8)[d]		3
7	n-$C_{12}H_{25}$	27	C	CH_2Cl_2	10-15	85		15-16	3
8	n-$C_{18}H_{37}$	28	C	CH_2Cl_2	10-15	85		50-51	3
9[e]	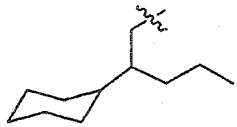	29	C	CH_2Cl_2	10-15	90			3
10	cholesteryl	30	C	CH_2Cl_2	10-15	48		179-180[d]	3
11	$EtSCH_2CH_2$-	31	C	CH_2Cl_2	10-15	70	135 (0.5)[d]		3
12	$EtOCH_2CH_2$-	32	C	CH_2Cl_2	10-15	85	117 (1.1)[d]		3
13	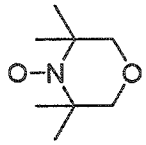	33	C		-30	68		100-104	55

a) Method C - 2 ROH + S_2Cl_2 + 2 NEt_3, 1 h addition time, 1.25 h total reaction time. b) Refers to temperature during the addition of S_2Cl_2 or if none, the reaction temperature. c) References reported for all those who synthesized the compound. d) Decomposed upon heating. e) No stereochemistry reported.

Table 6. Conditions and yields for the synthesis of allylic and propargylic alkoxy disulfides

Entry	R	Cmpd	Method[a]	Solvent	Temp (°C)[b]	Yield (%)	bp °C (mm Hg)	Mp (°C)	Ref[c]
1	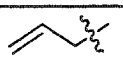	34	C	Et_2O[d]	0	87[52]			3,52
2[e]	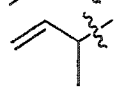	35	C	Et_2O[d]	0	62			52
3	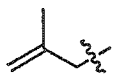	36	C	Et_2O[d]	0	95			52
4	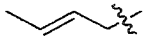	37	C	Et_2O[d]	0	98			52
5	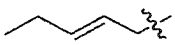	38	C	Et_2O[d]	0	87			52
6	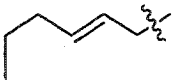	39	C	Et_2O[d]	0	90			52
7	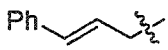	40	C	Et_2O[d]	0	95			52
8	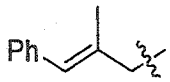	41	C	Et_2O[d]	0	93			52
9	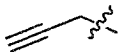	42	C	Et_2O[d]	0	98			53
10[e]	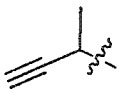	43	C	Et_2O[d]	0	>91, <98			53
11[e]	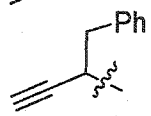	44	C	Et_2O[d]	0	>91, <98			53
12		45	C	Et_2O[d]	0	>91, <98			53
13	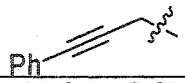	46	C	Et_2O[d]	0	>91, <98			53

a) Method C - 2 ROH + S_2Cl_2 + 2 NEt_3, 1 h addition time, 1.25 h total reaction time. b) Refers to temperature during the addition of S_2Cl_2 or if none, the reaction temperature. c) References reported for all those who synthesized the compound. d) Low temperature work-up. e) No stereochemistry reported.

Table 7. Conditions and yields for the synthesis of some aryl and benzyl alkoxy disulfides

Entry	R	Cmpd	Method[a]	Solvent	Temp (°C)[b]	Yield (%)	bp °C (mm Hg)	Mp (°C)	Ref[c]
1	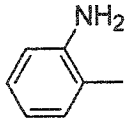	47	C	THF	0-4			84.2	54
2	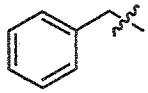	48	C	CH_2Cl_2	0	88[35]		50-51;[35] 58-59[49]	3,35,49
3	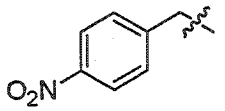	49	C	CH_2Cl_2	0	90[35]		92-93;[35] 100-101[33]	33,35
4	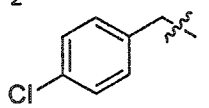	50	C	CH_2Cl_2	0	86		45-47	35
5	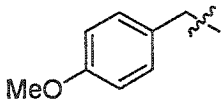	51	C	CH_2Cl_2	0	62		34-36	35
6	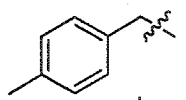	52	C	CH_2Cl_2	0	82		liquid	35
7	*rac-* 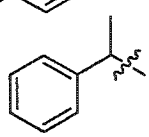	53	C	CH_2Cl_2	0	80			51
8	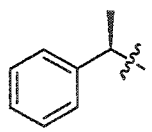	54	C	CH_2Cl_2	0				51
9	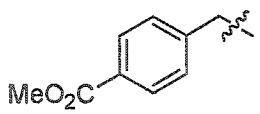	55	C	CH_2Cl_2	0	63	44-46		51
10	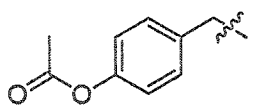	56	C	CH_2Cl_2	0	25			51
11	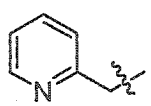	57	C	CH_2Cl_2	0	75[d]			51
12	*rac-* 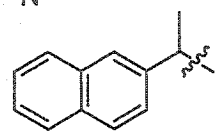	58	C	CH_2Cl_2	0	12			51

13	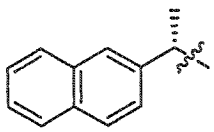	59	C	CH_2Cl_2	0	69	51

a) Method C - 2 ROH + S_2Cl_2 + 2 NEt_3, 1 h addition time, 1.25 h total reaction time. b) Refers to temperature during the addition of S_2Cl_2 or if none, the reaction temperature. c) Reference reported for all those who synthesized the compound. d) Decomposed entirely upon chromatography.

As can be seen, the synthesis of alkoxy disulfides using the method developed by Thompson[3] or derivatives thereof is extremely tolerant to substitution. In general, as the amount of substitution and steric bulk increases on the α-carbon, the yield decreases.

2.3 Synthesis and Characterization of Thionosulfites

In 1964, Thompson treated *dl*-2,3-butanediol with S_2Cl_2 and NEt_3 at 10 °C under high dilution conditions in CH_2Cl_2; the unstable product (43% for the **5a**; 21% for pure **5b** from *meso*-butanediol) did not exhibit coalescence of the AB pattern and was proposed to exist as a thionosulfite (form **2**).[2] Evidence for this conclusion derived from the close similarities between the ^1H NMR of this class of compounds compared to the sulfite analog as well as similar UV and IR data; in general, **2** are not shelf-stable.[36] Thompson prepared and isolated pure thionosulfites **5e** and **5f** from *meso*-hydrobenzoin **61a** in low yield (5-44%) through fractional recrystallization.[2,62] In this particular case, he synthesized the products from the magnesium alcoholates as shown in Scheme **3**. Interestingly, the corresponding sulfites[63] for the two isomeric forms of **5e** and of **5f** were thermally more stable (130-131 °C, 129-131 °C, 85-86 °C respectively – Scheme **3**) than the thionosulfites. This is most probably due to the greater S=O bond strength. Also of note is the increased thermal stability of the *cis*-configuration of the phenyl groups.

A diagnostic feature of thionosulfites is the presence of non-equivalent protons on the α-carbons in the proton NMR spectrum. It is similar to the spectrum of the corresponding sulfites suggesting a similar orientation of the S=S bond with respect to that of the S=O moiety. For instance **5c**, a lachrymatory liquid, displays an A_2B_2 pattern. A detailed analysis as to the factors that influence the formation of the thionosulfite isomer **2** over its valence bond isomeric alkoxy disulfide **1** is covered in Chapter **5**.

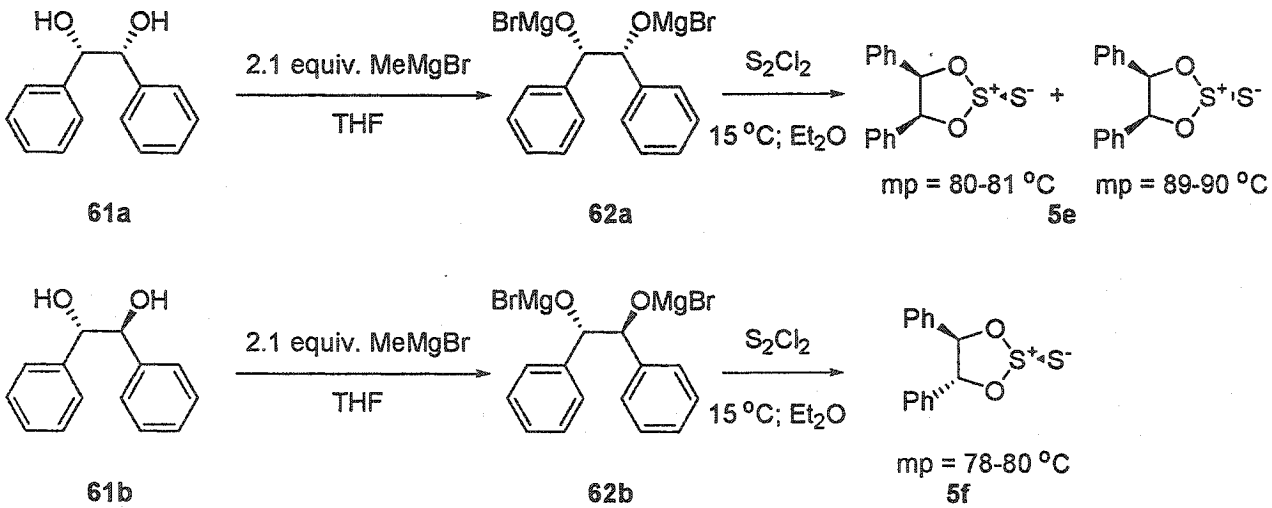

Scheme **3**.

Thompson[62] proposed that the reaction pathway involved the formation of a polymer under high dilution conditions of sulfur monochloride. He suggested (Scheme **4**) that an alkoxide-catalyzed unzipping of the proposed polymeric intermediate would yield a thionosulfite as a cyclic monomeric product (this reaction was performed under reduced pressure at 80-120 °C).

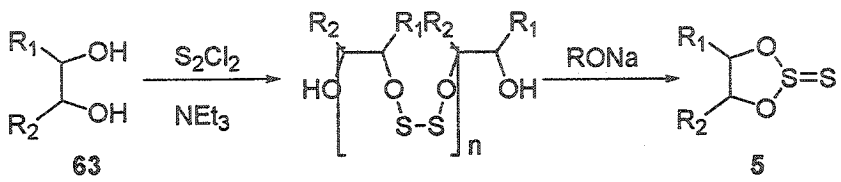

Scheme 4. Proposed mechanism for the formation of thionosulfites

Our method[41] of preparation,[§] using sulfur transfer reagents **15a** and **15b**, resulted in similar yields but with no polymeric side products (Scheme 5). It is important to note that while both **15a** and **15b** were effective sulfur transfer reagents in the synthesis of thionosulfites, they proved quite ineffective during the synthesis of isomeric alkoxy disulfides (*vide supra*). In this manner, thionosulfites **5g-5l** were synthesized (Table 8). The *mono*sulfur transfer reagent **15a**, produced thionosulfites in moderate yield (21-50%) while the *di*sulfur transfer reagent **15b** was generally more effective (14-80%) and was used for all the precursor 1,2-diols **63** examined. For all thionosulfites, column chromatography was sufficient to obtain analytically pure samples. While isolable, some of the thionosulfites were nevertheless unstable at room temperature or upon extended exposure to light.

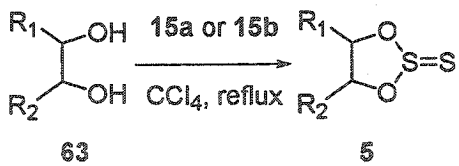

Scheme 5 Synthesis of thionosulfites using either Method A or B (*cf.* Table 8).

[§] This work has been published: Harpp, D. N.; Zysman-Colman, E.; Abrams, C. B. *J. Org. Chem.* **2003**, *68*, 7059.

Table 8. Yields of some thionosulfites

Entry	R_1	R_2	R_3	R_4	Diol	Product	Yield (%)
1	$-(CH_2)_5-$		$-(CH_2)_5-$		**63a**	**5g**	50[a]; 41[b]
2	$-(CH_2)_4-$		$-(CH_2)_4-$		**63b**	**5h**[c]	21[a]; 80[b]
3	$-(CH_2)_6-$		$-(CH_2)_6-$		**63c**	**5i**	47[b]
4	$-(CH_2)_7-$		$-(CH_2)_7-$		**63d**	**5j**	14[b]
5	$-(CH_2)_5-$		Me	Me	**63e**	**5k**[c]	72[b]
6	$-(CH_2)_6-$		Me	Me	**63f**	**5l**	77[b]

a) **Method A**: 1:1 diol:**15a** in refluxing CCl_4. b) **Method B**: 1:1 diol:**15b** in refluxing CCl_4. c) ^1H NMR data is missing for these 2 entries; the characterization is therefore incomplete although existing data is consistent with the assigned structures.

The mechanism of the formation of thionosulfites remains unclear particularly with respect to the involvement of *mono*sulfur reagent **15a**. The lack of polymeric side products leads to the conclusion that the mechanism for the process in Scheme 5 is different than that originally advanced by Thompson (Scheme 4). No evidence for the formation of a sulfoxylate ester (ROSOR) intermediate has been found though Nakayama[42] postulated its existence in the formation of his thionosulfites **5m** and **5n**. Moreover, the only by-product observed was that of benzimidazole; Nakayama[42] postulated the formation of bibenzimidazole which was never directly detected.

The proton decoupled ^{13}C NMR spectra of thionosulfites **5g-5l** reveal the expected magnetic anisotropy. There is a lack of degeneracy as each carbon is now anisochronous. This is due to the tetrahedral nature of the branched sulfur in the thionosulfite which effectively acts as a stereogenic center. The extent of the influence of the branch-bonded sulfur atom is hypothesized to be due to its pseudo-axial position with respect to the 5-

membered ring core as well as its diffuse electron cloud. Indeed, Steudel and co-workers showed *via* calculations that the branched sulfur-sulfur bond is in fact polarized, with the terminal sulfur being negatively charged.[30] This is evidenced by the observed downfield shift of the signal of carbon atoms four-carbons away from the sulfur-sulfur moiety as compared with the parent diol **63**. Thus the deshielding and shielding zones of the thionosulfite functionality are analogous to that of the sulfite (this is extensively reviewed in Chapter **5**).

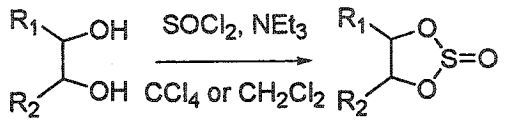

63 **64**

Scheme **6**. Formation of sulfites

Although very similar, the NMR spectra of the thionosulfites are distinct from the analogous sulfites, prepared according to Scheme **6**, Table **9**. In addition, the absence of a strong band between 1180-1240 cm^{-1} indicates the absence of the sulfite (S=O) moiety. A consistent feature in the infrared of the thionosulfites synthesized is the presence of a strong band at 655 cm^{-1} indicating an S-S (S=S) stretch; this is in clear agreement with the literature.[36] Nakayama reported similar IR and Raman S=S stretching absorptions.[42]

Table 9. Yields of 5-membered ring cyclic sulfites

Entry	R_1	R_2	R_3	R_4	Sulfite	Yield (%)
1	$-(CH_2)_5-$		$-(CH_2)_5-$		**64g**	60
2	$-(CH_2)_6-$		$-(CH_2)_6-$		**64i**	64

Mass spectrometric data provides further evidence to support the existence of new thionosulfites **5g-5l**. One characteristic feature of the MS common to all the thionosulfites is the base peak representing the loss of the HS_2O_2 (*m/z* 97) moiety from the parent ion. The feature common to the MS of alkoxy disulfides is the initial loss of SO (*m/z* 48) from the parent ion (*vide infra* – Chapter **3**).

Most recently, using our procedure (solvent: MeCN at RT), Nakayama[42] reported the synthesis of a fused 5,5-bicycle containing thionosulfite moiety in two diastereomeric forms. These were isolated by column chromatography then by HPLC to afford **5m** 45% and **5n** 10%. No thermal isomerization between **5m** and **5n** was possible even at temperatures of 120 °C.

To the extent that it has been explored, formation of larger ring homologues has to date proven unsuccessful. The reaction with 1,3-butanediols **65** with S_2Cl_2 primarily gave a low molecular weight polymeric product which when subjected to an alkoxide catalyzed degradation, afforded sulfite **66**, sulfoxylate **67** as well as transient formation of what was believed to be thionosulfite **68**. This latter compound decomposed to the sulfoxylate **67** due to facile loss of ⅛ S_8 (Scheme 7). Attempts to form thionosulfites from 1,4-

butanediols proved completely unsuccessful, affording only polymeric mixtures of products. No other attempts with larger diols have been reported.

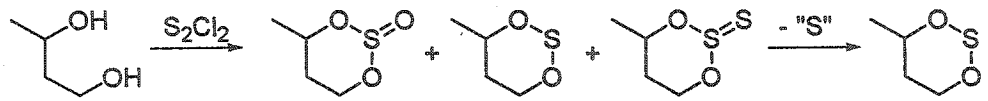

65 66 67 68 67

Scheme 7.

2.4 Conformational Analysis of and The Origins of Barriers to Rotation in X-S-S-X Systems & Systems Containing an S=S Bond

The S-S single bond is ubiquitous in structural biology as a vital secondary structural unit essential for the activity in a diversity of proteins of which insulin, oxytocin and vasopressin,[64,65] ribonuclease A, phospholipase A_2 and immunoglobins are illustrative.[66] One of the reasons for Nature's use of the S-S bond in conferring structural rigidity is the high bond energy of this functionality, which at *ca.* 63 kcal/mol, is the third strongest homonuclear single bond.[67] Nevertheless, it is considered a weak bond as compared to other bonds that normally break in chemical reactions. Apart from serving to tailor the three-dimensional structure of proteins, disulfide bonds make their appearance in rubber vulcanization,[68] drugs[69] such as Antabuse (TETD),[70] molecules used in marine organisms,[71,72] and as aqueous gelators.[73]

In order to best understand and provide a context for the conformational analysis and theoretical calculations highlighted in this thesis, a detailed investigation of the

geometries of related disulfides, HSSH, ClSSCl, BrSSBr and FSSF is presented. Geometries for all these compounds are defined according to Figure 1.

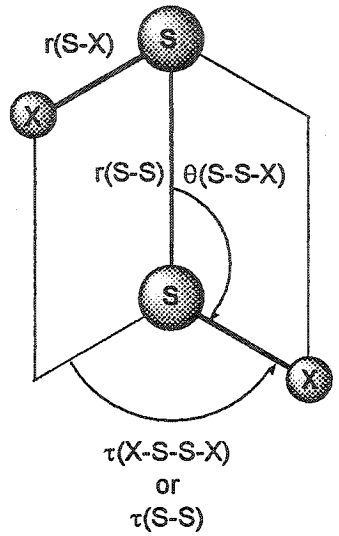

Figure 1. Structural parameters for the XSSX systems. Bond lengths are defined as r(S-S) and r(S-X), bond and dihedral angles are defined as θ(S-S-X) and τ(S-S) respectively.

The origin of the S-S barrier to rotation is explored. A comparison of experimental and theoretical work is also undertaken to determine the minimum level of theory needed in order to accurately describe these systems.

2.4.1 The HSSH System

The geometry of dihydrogen disulfide HSSH **69a** as well as its isotopic derivatives has been determined by electron diffraction[74] and microwave spectroscopy.[75-83] Often with those that determine the geometry by microwave spectroscopy (MW), the parameters have been recalculated from the same data set and then re-reported. Disulfane **69a** has an

analogous structure to that of HOOH **70a**. The experimental structural parameters of some investigators are highlighted in Table **10**.

Table **10**. Experimentally derived parameters for **69a**.

r(S-S) Å			r(S-H) Å			θ(H-S-S) °			τ(H-S-S-H) °			method	Ref
2.055	±	0.001	1.327	±	0.003	92.00	±	0.50	90.60	±	0.10	MW	[75]
2.055	±	0.001	1.327	±	0.003	91.30	±	0.05	90.60	±	0.05	MW	[76]
2.058	±	0.003	1.345	±	0.003	98.10	±	0.30	90.80	±	0.30	MW	[83]
2.0611	±	0.0001	1.3410	±	0.0003	97.42	±	0.04	90.75	±	0.05	MW	[82]
2.055	±			±		98.10	±		89.60	±		MW	[84]
2.056	±		1.342	±		97.90	±		90.30	±		MW	[81]
2.057	±	0.002	1.336	±	0.009	95.80	±	3.23	90.44	±	0.45	Average	

The initial work[75,76] underestimated both the r(S-H) bond length and θ(H-S-S) bond angle. This is most likely due to the fact that here the authors based their microwave geometries on flawed electron diffraction[74] data which served as a reference for the θ(H-S-S) bond angle. In general, the location of hydrogen atoms in the presence of heavier atoms is problematic by diffraction techniques. Given that bond lengths derived from rotational constants are correlated to the bond angle, an inappropriate determination of the latter parameter will thus affect the two former; torsional angles are weakly correlated with other structural parameters and remain consistent throughout. The average bond angle of 95.8° is slightly larger than that of H_2S (92.2°)[85] but is substantially smaller than that for alkyl or halogenated disulfides (*vide infra*). The small bulk of the hydrogen atoms and the subsequent decrease in the H-H and S-S repulsions may explain this smaller bond angle.

Theoretical modeling of this system proves quite accurate, even with smaller basis sets as summarized in Table **11**; though the inclusion of polarization functions on heavy

atoms is essential for determining accurate parameters.[86,87] It has also been suggested that addition of correlation corrections is required to obtain good structural parameters for the analogous H_2O_2 **70a** system[88,89] though this does not seem to be the case here. The bond order for the S-S bond was calculated[90] to be 0.95, an indication of the single bond character of this parent compound; thus the covalent radius of sulfur can now be derived as 2.055 Å / 2 =1.03 Å, where we have used the most recent MW[84] S-S bond length.

Table **11**. Calculated structural parameters for **69a**

r(S-S) Å	r(S-H) Å	θ(H-S-S) °	τ(H-S-S-H) °	method	Ref
2.081	1.356	98.3	91.7	SCF/DZ+P	91
2.063	1.336	98.9	90.3	SCF/3-21G*	92
1.958	1.327	99.1	88.1	*ab initio* STO-3G*	93
2.067	1.331	98.2	89.7	SCF-CI/DZ+P	94
2.066	1.327	98.6	89.9	MP2/4-31G*	95
2.066	1.328	99.0	90.0	HF-SCF/6-31G*	90
2.063	1.327	99.1	89.8	HF/6-31G*	96
2.070	1.333	98.7	90.5	MP2/6-31G**	97
2.082	1.336	98.1	90.4	MP2/6-311G**	98
2.092	1.333	97.5	90.8	MP2/6-311G(2d,2p)	97
2.092	1.333	97.5	91.2	MP2/6-311G++(2d,2p)	97
2.064	1.338	97.8	91.0	MP2/6-311G++(2df,2p)	97
2.067	1.343	98.0	90.7	CCSD(T)/cc-pVQZ	99
2.064	1.334	98.4	90.3	Average[100]	
0.034	0.008	0.6	0.9	Error	

A characteristic feature of the bonding in X-S-S-X systems is the presence of a *gauche* conformation about the S-S bond. The bonds formed are almost entirely p in character. Thus there exists a non-bonding electron pair that resides in a perpendicular 3p orbital on each sulfur atom (Figure 2). The size of these orbitals leads to a partial overlap of these MOs. The lone pair–lone pair repulsion inherently caused by the formed π- and π*-MOs results in a destabilization (and subsequent lengthening) of the S-S bond that is maximized when $\tau = 0$ and $\tau = 180°$; this destabilization is diminished when $\tau = 90°$ and τ

= -90° due to the orthogonality of the two 3 p orbitals. Recall that the splitting of AOs to form MOs is asymmetric.[101] This is illustrated in Figure **3a**. As a corollary to this MO argument is the fact that when H_2S_2 (or any other XSSX system) is in the *gauche* conformation, there is a maximum stabilizing overlap which occurs with each of the lone pair 3p orbitals to that of the adjacent S-H (or S-X as the case may be) σ* MO (Figure **3b**); the above MO description is indicative of a hyperconjugative mechanism. Mulliken[102] population analyses show that the largest S-S overlap population does indeed occur at this (*ca.* 90°) dihedral angle thus indicating that the total energy of the compound is lowest.[103] The origin of this stabilizing interaction will be explored in greater detail in Chapters **3** and **4**. It is for these reasons that the observed dihedral angle in **69a** is *ca.* 90° which represents an energy minimum for the compound. Thus there are two energetically degenerate conformations of **69a** which are antipodal in the S-S unit. Inherently chiral though XSSX systems are, they remain optically inactive and unresolvable if the substituent X is achiral and the magnitude of the S-S rotational barrier is sufficiently low.

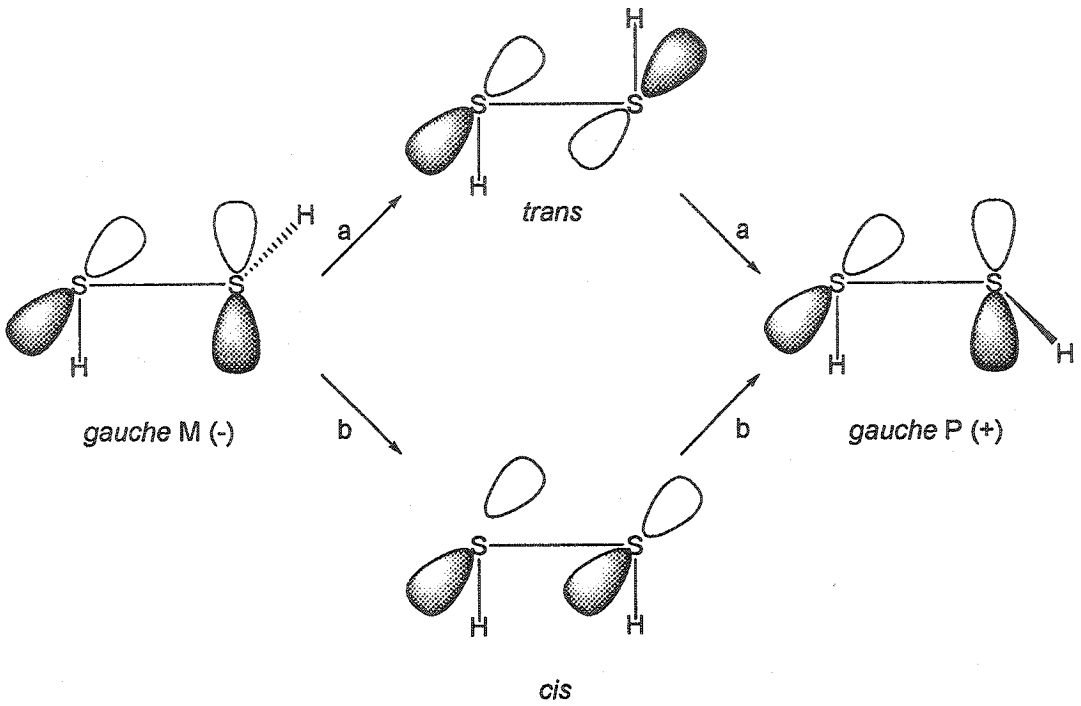

Figure 2. 3p orbital orientation in the ground and *cis* and *trans* transition states.

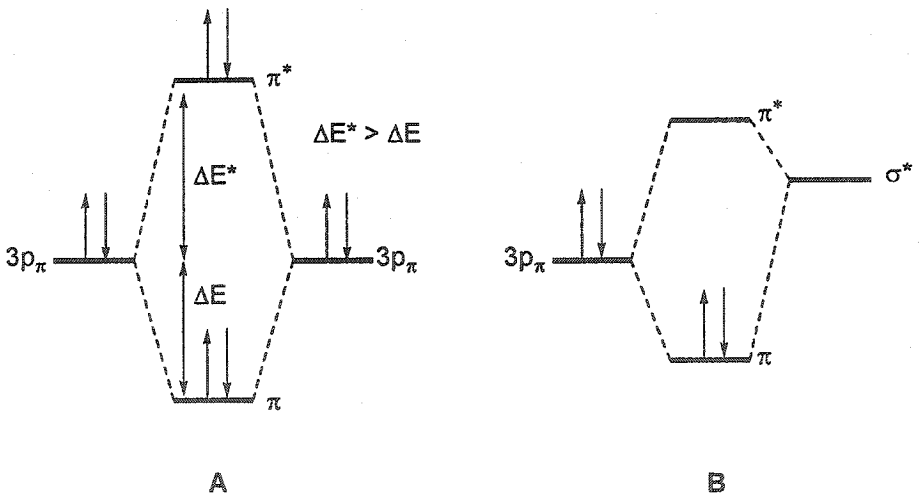

Figure 3. a) Splitting of adjacent S-3p_π-orbitals. b) Splitting of S-3p_π-orbital with that of an adjacent S-X antibonding orbital. The magnitude of the splitting in each case is dependent on the dihedral angle τ and on the origin of X.

The geometries of the *cis* and *trans* transition state structures in Figure 2 indicate distortions from the ground state geometry. The calculated r(S-S) is *ca.* 0.04-0.05 Å

longer and the θ(S-S-H) is 1° and 4° smaller respectively while the r(S-H) remains essentially unchanged.[94] These sorts of changes are not unusual and similar results have been observed in sulfur homocycles wherein τ = *ca.* 0°.[104]

The barrier to rotation about the S-S bond is of course also dependent on the dihedral angle due to the same molecular orbital considerations (*vide supra*). Although there is much variation in the measured and calculated barriers (Table **12**), the *cis* barrier (*via* path **b** in Figure **2**) is consistently higher than that of the *trans* barrier (*via path* **a** in Figure **2**). Some of this variation may be caused by the use of inaccurate structural parameters as well as the assumption that rotation is rigid (that is all other bond angles are constrained as the energies are calculated during the rotational profile about the S-S bond). Others did not optimize transition state geometries prior to obtaining single point energies. In general, it is well known that *ab initio* calculations can reproduce rotational barriers at the HF level given the use of a large enough basis set;[105] the lack thereof is evident in the barriers calculated by Laitinen (geometry optimization using the same method was also poor).[106] Inclusion of electron correlation did not change the barrier heights.[82,94] It should be noted that full optimization of the energy surface using appropriately large basis sets is standard in modern theoretical work for rotational barriers. Thus the HF predictions of Samdal[96] and co-workers (last Entry of Table **12**) should be viewed as the most accurate.

Table 12. Measured and calculated barriers to rotation about the S-S bond in **69a**

Measured[a]	Calculated[a]		$\Delta^{a,b}$	Method	Ref[c]
	cis	*trans*			
6.9			-	Far IR	77
d			-	Millimeter wave	75
	9.3	6.0	3.3	SCF[e]	107
	1.5	0.9	0.6	EH	103
	6.4	3.5	2.9	STO-3G	93
	12.5	10.8	1.7	STO-3G*	93
	9.0	5.2	3.8	HF-SCF[f]	108
	8.7	6.1	2.6	SCF/3-21G*	92
	7.6	5.1	2.5	SCF/ZPE	94
	7.5	5.0	2.5	CI-SD/ZPE	94
	22.5	4.1	18.4	MINI-1	106
	26.4	14.3	12.1	MINI-1*	106
	7.7	5.1	2.6	SCF[e]	82
	7.8	5.0	2.8	MP2//SCF	82
8.2			-	IR	84
	8.1	5.8	2.3	MW	81
	8.4		-	HF/STO-3G(M3*)	90
	8.5	6.1	2.5	HF/6-31G*	96

a) Barriers in kcal/mol. b) Difference between *cis* and *trans* barriers. c) References are in chronological order. d) No value determined but authors quote almost equal barriers. e) Included the use of a double ζ basis set augmented by polarization functions. f) Included the use of an extended polarized basis set

The increased height of the *cis* barrier is most probably due to a relatively decreased stabilizing hyperconjugative $\sigma_{S\text{-}H} \rightarrow \sigma^*_{S\text{-}H}$ interaction (similar to that found in ethane[109-112]) as compared with the *trans* transition state.[113] The slightly lower calculated *trans* barrier as compared with the measured barriers (which as a matter of course are in fact measurements of the *trans* barrier) is due to geometry relaxation.[108] The barrier height is also a function of the van der Waals radii and the electronegativities of the respective atoms about the X-X bond (in this case S-S). This is illustrated in Table **13** wherein moving from a first row element to a second row element may lead to a decreased barrier but this effect can be compensated by moving from left to right across the periodic table.

Table 13. Barriers to rotation about C-X bonds where X = C, Si, N, P, O, S

Cmpd	Barrier[a,b]	Cmpd	Barrier[a,b]	Cmpd	Barrier[a,b]
CH_3-CH_3	2.93	CH_3-NH_2	1.98	CH_3-OH	1.07
CH_3-SiH_3	1.66	CH_3-PH_2	1.96	CH_3-SH	1.27
Δ	-1.27	Δ	-0.02	Δ	0.20

a) Barriers and differences measured in kcal/mol. b) From Ref [114].

A more important comparison is that between HOOH **70a** and HSSH **69a**. The barriers for **70a** are shown in Table 14.

Table 14. Calculated barrier to rotation for HOOH **70a**

Calculated[a]		Δ[a,b]	Method	Ref[c]
cis	*trans*			
10.9	0.6	10.3	SCF	[115]
7.3	1.1	6.2	MW	[81]
9.1	0.9	8.2	HF/ 6-31G*	[96]

a) Barriers in kcal/mol. b) Difference between *cis* and *trans* barriers. c) References are in chronological order.

A comparison of barrier heights clearly shows that for all cases except those values reported by Boyd,[103] HSSH has the higher *trans* barrier (by *ca.* 6 kcal/mol); the *cis* barrier for both compounds is of a comparable energy. Given that **70a** has a similar geometry (τ = *ca.* 115°) to that of **69a**, the increased *trans* barrier must be due to increased lone pair–lone pair repulsion afforded by the larger, more diffuse 3p orbitals of adjoining sulfurs as compared to the 2p orbitals of adjoining oxygens. This results in a 2-fold torsional barrier[116] component for **69a** (the MP2[82] two-fold component is 3.21 kcal/mol) that is *ca.* double that of the experimentally[117] determined one in **70a** (1.81 kcal/mol). Counteracting this two-fold torsional component is the fact that in H_2S_2 **69a**, there are decreased dipole-dipole and atom-atom interactions and decreased polarity in the S-H bond as compared to the O-H bond.[82]

The calculated dipole moments of the transition state and ground state geometries of **69a** are shown in Table 15. The indicated difference in gas phase dipole moments between the *trans* transition state and the ground state suggest that the barrier to rotation may be solvent dependent.

Table 15. Calculated dipole moments for **69a**

Calculated Dipole Moment (D)[a]		
cis	*trans*	equilibrium[b]
1.82	0.00	1.36

a) From Ref [108]. b) Calculated for the ground state geometry - Expt[118] = 1.17 D.

Here, there has been an extensive overview of the geometry and torsional barrier for **69a**. It was necessary to introduce concepts in conformational analysis and molecular modeling. These themes will reoccur throughout the thesis. Analysis in the following systems is undertaken as a comparison to the HSSH **69a** system.

2.4.2 The MeSSMe System

The structure of dimethyl disulfide **71a** resembles that of **69a**. The structural parameters, both experimental and theoretical are outlined in Table 16.

Table 16. Experimental and theoretical structural parameters for **71a**

r(S-S) Å	r(S-C) Å	θ(C-S-S) °	τ(C-S-S-C) °	method	Ref[a]
2.038	1.810	102.8	84.7	MW[b]	119
2.022 ± 0.003	1.806 ± 0.002	104.1 ± 0.3	83.9 ± 0.9	ED	120
2.029 ± 0.003	1.816 ± 0.003	103.2 ± 0.2	85.0 ± 4.0	ED	121
2.030 ± 0.008	1.811 ± 0.005	103.4 ± 0.7	84.5 ± 0.6	Average[100]	
1.842	c	103.2	85.0	CNDO/2	122
2.030	1.818	103.7	83.2	MM1	123
2.064	1.809	100.0	90.6	*ab initio* STO-3G	93
1.950	1.803	102.9	87.4	*ab initio* STO-3G*	93
2.050	1.823	102.3	88.4	SCF/3-21G*	92
2.054	1.812	102.1	85.1	MP2/6-31G**	97
2.072	1.819	101.5	84.7	MP2/6-311G(2d,2p)	97
2.064	1.807	100.8	83.7	MP2/6-311G**	98
2.016 ± 0.080	1.813 ± 0.007	102.1 ± 1.2	86.0 ± 2.6	Average[100]	

a) References are ordered chronologically per section. b) No errors reported. c) Not determined.

All calculations accurately predict the r(S-C) bond length as well as the bond and τ(S-S) angles. Most calculations seem to overestimate the experimental r(S-S) by as much as 2% from the average experimental value. This is especially true when electron correlation is added (last three entries). The addition of polarization functions to the STO-3G basis set severely underestimated the r(S-S) bond length. Semi-empirical methods also underestimate the r(S-S) though molecular mechanics methods accurately predict the geometry of **71a**. As with **69a**, the r(S-S) is a true single bond and compares favourably with rhombohedral S_6 (r(S-S)[124] = 2.057 Å) and orthorhombic-S_8 (r(S-S)[125] = 2.037 Å).

The main structural difference between **71a** and **69a** is in the bond angle, which is *ca.* 7° wider in **71a**; whereas the r(S-S) is *ca.* 1% shorter. The widening of the bond angle is ostensibly due to increased Me-S_β repulsive interactions. The intramolecular r(C---S) is

ca. 3.0 Å is less that of the sum of the respective van der Waals radii of the constituent atoms (3.4 Å).

The experimental and calculated barriers to rotation for **71a** are reported in Table 17.

Table 17. Measured and calculated barriers to rotation about the S-S bond for **71a**

Measured[a]	Calculated[a]		$\Delta^{a,b}$	Method	Ref[c]
	cis	*trans*			
9.5[d]				Raman	126
6.8				Calorimetric data[e]	127
7.3				IR	128
10[f]				Raman	129
	2.9	1.3	1.6	PCILO	130
	45.9	14.5	31.4	ZDO-SCF	131
	7.0	2.2	4.8	EH	103
	17.7	10.8	6.9	CNDO/2	122
	10.6	7	3.6	MM1	123
	18.0	4.4	13.6	STO-3G (rigid rotor)	93
	21.1	12.7	8.4	STO-3G* (rigid rotor)	93
	7.5	2.9	4.6	SCF/3-21G	92
	12.0	5.7	6.3	SCF/3-21G*	92
	11.4	5.7	5.7	HF/6-31G*[g]	78
	11.3	5.5	5.8	HF/6-31G*[g,h]	132
	11.4	6.3	5.1	MP4/6-311G**[h]	132
	11.6	6.1	5.5	MP2/6-31G*[i]	133

a) Barriers in kcal/mol. b) Difference between *cis* and *trans* barriers. c) References are in chronological order. d) Caution: Assumed symmetrical barrier shape and neglected effects of coupling between S-S rotation and vibrational degrees of freedom in MeSSMe. e) Estimated from calculated and observed entropy and heat capacity. f) Approximate value reported. g) Based on HF/6-31G* optimized geometry. h) Calculations reported do not include ZPE correction. i) Based on MP2/6-31G* optimized geometry.

The best experimental estimates suggest a barrier of *ca.* 7 kcal/mol. It is expected that with **71a**, rotation proceeds through a *trans* transition state. *Ab initio* calculated results seem to converge with larger basis sets (last three Entries) however these seem to underestimate the *trans* barrier by *ca.* 1 kcal/mol. Deconvolution of the torsional potential function[134] indicates that the two-fold term (V_2) predominates.[132,135] Of those

reported in the literature, only barriers derived from Allinger's MM1 force field[123] suitably reproduce the experimental results. It is evident, as was the case for **69a**, that the addition of polarization functions is essential in barrier determination (contrast last six entries). It is also evident that electron correlation increases slightly the *trans* barrier (contrast last four entries). The calculated and experimental barriers for **71a** are comparable with those of **69a** (Table **12**).

The barrier for MeSSH **72** was calculated by Ha and co-workers at the SCF/3-21G*.[92] They reported a *cis* barrier of 8.9 kcal/mol and a *trans* barrier of 5.9 kcal/mol. Comparing this result to that obtained for **70a** and **69a** suggests that the inclusion of methyl groups increases only the *cis* barrier and that the *trans* barrier is defined solely through an electronic interaction (that is the methyl group is not substantially bulky to affect this barrier – see Chapter **2.4.3** for examples).

2.4.3 Other Disulfides with the C-S-S-C Moiety

In general, organic disulfides have a similar geometry to that of MeSSMe **71a**.[136-138] The geometries of a representative set of disulfides is shown in Table **18**. Unlike **71a**, the next smallest disulfide, EtSSEt (Entry 1), is predicted to show a 1% increase in its r(S-C); other parameters remaining essentially the same. In fact this small increase in this bond length is true with most dialkyl disulfides (where C_α is sp^3 hybridized) and is most likely due to the increased steric demands of larger R groups (*cf.* Table **18**).

One of the shortest registered r(S-S) for a disulfide is 1.999 Å for tetraethylthiuram disulfide (TETD), (Entry 6). Even for this molecule, there is but a 1.5% decrease in bond length from that of **71a**; recently an extremely short r(S-S) = 1.858 Å has been reported for the double helical cyclic peptide $(Adm\text{-}Cyst)_3$.[139,140] The corresponding longest reported r(S-S) is 2.110 Å in Entry 12. This longer bond (*ca.* 3.5% longer than in **71a**) is almost certainly due to the bulky tris(trimethylsilyl) methyl groups as is its highly unusual τ(S-S) of 180°. Interestingly, whereas Entry 12 compensates for the bulky R group through a long S-S bond, Tr-SS-Tr (Entry 13) does so with the longest reported r(S-C) of 1.931 Å.

Dicubyl disulfide (Entry 7) has an unusually small τ(S-S) for disulfides bearing a tertiary carbon (τ_{av}(S-S) = 112.4° from Entries 5, 8, 13, 26). This has been attributed to the strained nature of the cubyl geometry wherein the τ(C-S) are distorted which enables a minimimization of steric interactions between the β-carbon and the S-S moiety. The accompanying short r(S-C) is *ca.* 5% smaller than the average bond length for a disulfide with a tertiary-substituted carbon. This is a structural manifestation of the high s-character of the C_{cubyl} moiety. This can be seen by comparing the r(S-C) for this case with those of disulfides containing an sp^2 carbon attached to the S-S functionality (Entries 11, 14-22). In fact, except for the τ(S-S) dihedral angle, the other structural parameters for these cases are unresponsive to substitution changes about the benzene ring which alter the electronics of the respective systems though Entry 11 does have an unusually small bond angle. Entry 11 also has one of the smallest τ(S-S) and both angle deformations from the ideal are most probably caused by the lack of conformational

flexibility afforded by the biphenyl system. Entry 23 also has a massively distorted torsional angle and S-S bond length but as can be seen Entries 11 and 23 are exceptional cases. It is unclear why Entries 16-18 and 25 have unusually small τ(S-S) (*ca.* 12% smaller than in **71a**) but this may be in part related to the extensive intermolecular hydrogen bonding observed in the solid state (Entries 16 and 25).

Table 18. The structural parameters of some dialkyl and diaryl disulfides

Entry	Disulfide	r(S-S) Å	r(S-C) Å	θ(C-S-S) °	τ(C-S-S-C) °	method	Ref
1	Et-SS-Et	2.038	1.832	103.7	90.0	CNDO/2	141
2	*n*Pr-SS-*n*Pr	2.051	1.830	102.9	-89.3	HF/6-31G*	98
3	Allyl-SS-Allyl	2.052	1.834	103.3	-86.9	HF/6-31G*	98
4	Allyl-SS-*n*Pr	2.066	1.807		84.0	HF/6-31G*	98
5	di-*t*-butyl disulfide	2.029	1.847	106.2	113.8	MM1	142
6	TETD	1.999	1.820 ± 0.030	103.5 ± 0.3	90.0	X-Ray	143
7	Cubyl-SS-Cubyl	2.044 ± 0.001	1.771 ± 0.002	104.6 ± 0.1	-86.5 ± 0.1	X-Ray	144
8	DAD	2.048 ± 0.007	1.840 ± 0.020	107.3 ± 0.6	110.5 ± 0.9	X-Ray	145
9	DAD	2.029	1.845	106.2	113.8	MM1	146
10	Bn-SS-Bn	2.020		103.3	92.0	X-Ray	147
11	2,2'-biphenyl disulfide	2.050 ± 0.003	1.750 ± 0.010	98.3 ± 0.2	69.0	X-Ray	148
12	$(Me_3Si)_3C$-SS-$C(SiMe_3)_3$	2.110 ± 0.010	1.844 ± 0.002	105.7 ± 0.1	180.0	X-Ray	149
13	Tr-SS-Tr	2.012 ± 0.001	1.931 ± 0.030	110.9 ± 0.1	110.3	X-Ray	149
14	Ph-SS-Ph	2.023 ± 0.001	1.788 ± 0.003	105.9 ± 0.1	90	X-Ray	150
15	2,2'-dinitrophenyl disulfide	2.045 ± 0.004	1.797 ± 0.009	104.4 ± 0.3	85.1	X-Ray	151
16	3,3'-dicarboxy-4'4'dinitrophenyl disulfide	2.023 ± 0.002	1.779 ± 0.005	105.5 ± 0.2	76.0	X-Ray	152
17	4,4'dinitrophenyl disulfide	2.019 ± 0.005	1.767 ± 0.010	106.2 ± 0.3	72.0	X-Ray	153
18	dipentafluorophenyl disulfide	2.059 ± 0.004	1.770 ± 0.007	101.3 ± 0.3	76.5	X-Ray	154
19	2,2'-diaminophenyl disulfide	2.060 ± 0.003	1.760 ± 0.007	103.3 ± 0.3	90.5	X-Ray	155
20	di-2-pyrimidyl disulfide dihydrate	2.016 ± 0.001	1.781 ± 0.002	104.7 ± 0.1	82.5	X-Ray	156
21	di-2-pyridyl disulfide	2.016 ± 0.002	1.785 ± 0.002	105.7 ± 0.1	87.1	X-Ray	150
22	3,3'-dihydroxydi-2-pyridyl disulfide	2.018 ± 0.001	1.785 ± 0.002	104.8 ± 0.7	93.2	X-Ray	157
23	5-[1-(2'-deoxy-α-D-ribofuranosyl)uracilyl] disulfide	2.108 ± 0.003	1.756 ± 0.007	102.0 ± 0.2	50.0	X-Ray	158
24	4-[1-(α-D-ribofuranyl)uracilyl] disulfide	2.022 ± 0.004	1.790 ± 0.020	104.0 ± 0.4	87.0	X-Ray	159
25	5-(1-methyluracil) disulfide	2.074 ± 0.003	1.750 ± 0.010	100.7 ± 0.3	78.0	X-Ray	160
26	D-penicillamine disulfide	2.049	1.866	105.5	115.0	X-Ray	161
27	L-cystine hexagonal	2.032 ± 0.004	1.820 ± 0.012	114.5 ± 0.3	106.0 ± 1.0	X-Ray	162

In general, deviations to smaller angles from an idealized τ(S-S) of *ca.* 90° are accompanied by a corresponding increase in the r(S-S). For instance, introduction of the S-S moiety into a ring as in 1,2-dithiolane[163] **73** or in natural products bearing the piperazinedione core such as the Sporidesmins[164] **74** greatly enhances the lone pair–lone pair repulsion thereby leading to an increased r(S-S).

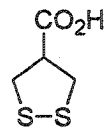

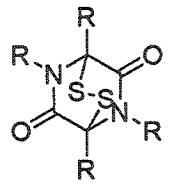

τ = 27° τ = 8.5°

r(S-S) = 2.096 Å r(S-S) = 2.096 Å

73 **74**

Few studies have been done on the barrier to rotation about disulfides bearing larger substituents. The results of some disulfides are shown in Table **19**.

Table **19**. Calculated and measured barriers to rotation for some disulfides

Entry	Disulfide	Measured[a]	Calculated[a]		Δ[a,b]	Method	Ref
			cis	*trans*			
1	diethyl disulfide		19.5	5.1	14.4	STO-3G	93
2	diethyl disulfide		12.2	7	5.2	MM1	165
3	*t*-butyl methyl disulfide		17.2	6.6	10.6	MM1	165
4	*t*-butyl ethyl disulfide		17.7	6.6	11.1	MM1	165
5	*t*-butyl *i*-propyl disulfide		19.6	6.7	12.9	MM1	165
6	di-*t*-butyl disulfide		28.8	5	23.8	MM1	165
7	di-*t*-butyl disulfide			6		B3LYP/6-31G*[d]	144
8	dicubyl disulfide			5.2		B3LYP/6-31G*[d]	144
9	DAD (di-*tert*-adamantyl disulfide)		29.7	5.3	24.4	MM1	146
10	benzyl trichloromethyl disulfide	9.4[c]				DNMR	166
11	benzyl trifluoromethyl disulfide	8.3[c]				DNMR	166
12	benzyl *t*-butyl disulfide	7.8[c]				DNMR	166
13	benzyl trityl disulfide	8.8[c]				DNMR	166
14	L-cystine		23.1	6	17.1	STO-3G	93
15	diphenyl disulfide		7.5	6.8	0.7	MP2/3-21G*[e]	167
16	bis(1,3,5-tri-*i*-Pr-phenyl) disulfide	16.2				DNMR	168

a) Barriers in kcal/mol. b) Difference between *cis* and *trans* barriers. c) $\Delta G^{\ddagger} = \pm 0.3$ kcal/mol. d) Geometry optimized at B3LYP/6-31G*. e) Geometry optimized at MP2/3-21G*.

The highest barrier reported and one of the more interesting results is that of bis(1,3,5-tri-*i*-Pr-phenyl) disulfide (Entry 16). Kessler and Rundel[168] determined by low temperature DNMR a barrier of 16.2 kcal/mol, *ca.* 9 kcal/mol greater than that of **71a**. This situation, compared to Entry 15, represents an extreme case of steric interactions influencing barrier height. According to the authors, the torsional barriers of less sterically demanding derivatives displayed only C-S bond hindrance.

Although Fraser[166] originally attributed the observed barriers for Entries 10-13 to rotation *via* a *cis* transition state, a conclusion diametrically opposed to the literature, his barrier measurements, coupled with others (*cf.* Table **19**), did clearly indicate that the barrier height does increase with increasing steric bulk.[167,169] Interestingly, barrier measurements for Entry 10 over three solvents (vinyl chloride, CS_2 and toluene) differed little. The authors also reported that barrier height was influenced by the inductive effects of the substituents attached to the S-S bond (*cf.* Entries 10-11, Table **19**).

Gas phase calculations for the barrier of dicubyl disulfide, Entry 8, indicate a $S_n \rightarrow \sigma^*_{C\text{-}C}$ interaction leading to a stabilization of the *trans* transition state and thus a counterintuitive small decrease in the S-S barrier. In general, gas phase calculations faithfully reproduced the expected lower *trans* barrier of *ca.* 6.5 kcal/mol.

It is therefore possible to influence torsional barriers both stereoelectronically as well as sterically. Influence based on the former will be self-evident in the next section.

2.4.4 Disulfides Bearing an Electronegative Atom Next to the S-S Bond

Electronegative atoms immediately attached to a S-S bond influence substantially the structural properties of the moiety. Geometries of FSSF **75a**, BrSSBr **76a** and ClSSCl **77a** are shown in Table **20**.

Table **20**. Experimental and theoretical structural parameters for dihalo disulfanes

Entry	X	r(S-S) Å	θ(X-S-S) °	τ(X-S-S-X) °	method	Ref[a]
1	Br	1.980 ± 0.040	105.0 ± 3.0	83.5 ± 11.0	ED	170
2	Br	1.948 ± 0.002	109.2 ± 0.1	83.9 ± 0.1	X-ray	171
3	Br	1.964 ± 0.020	107.1 ± 2.9	83.7 ± 0.3	Average[100]	
4	Cl	2.040 ± 0.050	105.0 ± 5.0	90.0	ED	172
5	Cl	2.050 ± 0.030	103.0 ± 2.0		ED	173
6	Cl	1.970 ± 0.030	107.0 ± 2.5	82.5 ± 12.0	ED	170
7	Cl	1.931 ± 0.005	108.2 ± 0.3	84.8 ± 1.3	ED	174
8	Cl		111.0	85.0	CNDO/2	175
9	Cl	1.950 ± 0.001	107.7 ± 0.1	85.2 ± 0.1	MW	176
10	Cl	1.943 ± 0.001	107.1 ± 0.0	84.8 ± 0.1	X-ray	171
11	Cl	2.005	105.9	94.8	HF-SCF/6-31G*	90
12	Cl	2.004	105.9	85.1	HF/6-31G*	96
13	Cl	1.979	107.5	85.8	MP2/6-311G**	97
14	Cl	1.976	107.5	85.7	MP2/6-311G(2d,2p)	97
15	Cl	1.985 ± 0.040	106.9 ± 2.0	86.4 ± 3.5	Average[100]	
16	F	1.888 ± 0.010	108.3 ± 0.5	87.9 ± 1.5	MW	177
17	F		110.0	89.0	CNDO/2	175
18	F	1.890 ± 0.002	108.3 ± 0.2	87.7 ± 0.4	ED	178
19	F	1.953	104.2	92.7	HF-SCF/6-31G*	90
20	F	1.953	104.3	88.7	HF/6-31G*	96
21	F	1.953	104.3	88.6	HF/6-31G*	179
22	F	1.923	106.6	88.9	MP2/6-311G**	97
23	F	1.921	108.3	88.6	MP2/6-311G(2d,2p)	97
24	F	1.894	110.4	88.1	X_α/DZP	97
25	F	1.952	106.6	88.9	MP2/6-31G*	180
26	F	1.944	105.6	88.9	QCISD/6-31G*	180
27	F	1.910	110.5	89.3	SVWN/6-31G*	180
28	F	1.937	110.6	89.4	BP86/6-31G*	180
29	F	1.942	108.4	89.1	B3LYP/6-31G*	180
30	F	1.928 ± 0.025	107.6 ± 2.4	89.0 ± 1.2	Average[100]	

a) References are ordered chronologically per section.

Comparing the electron diffraction structures of each of **75a**-**77a** (Entries 1, 7 and 18), we observe a characteristic decrease in r(S-S), and increases in both the bond and torsional angles for increasing electronegativity of the X substituent. However this is not the whole story as $(CF_3)_2S_2$ has a normal r(S-S)[181] of *ca.* 2.03 Å even though the inductive effect of the trifluoromethyl group amounts to an electronegativity of 3.7;[182] similarly R_2NSSNR_2 has an $r_{X\text{-}ray}$(S-S) = 2.021 Å for R = CH_3SO_2.[59] Cárdenas-Jirón[90] calculated the S-S bond orders for S_2Cl_2 **77a** and S_2F_2 **75a** and found them to be 1.09 and 1.36 respectively, indicating that in the latter case a substantial degree of double bond character exists. Given such a short reported S-S bond for **75a**, it is entirely reasonable that this bond would possess a large degree of double bond character. All three sulfur monohalides possess C_2 symmetry as with **69a**.

It should be noted that early electron diffraction work on S_2Cl_2 **77a** contained larger errors with poorly defined structures (these were included for completeness) and Entry 7 or Entry 9 should be used as the optimal geometry; the ED data has uncertainties related to electron correlation while the MW data has uncertainties related to zero-point vibrations. Kniep and co-workers[171] are the only ones to report crystal structures of S_2Cl_2 **77a** (1.943 Å) and S_2Br_2 **76a** (1.970 Å). Their reported structure for **77a** is intermediate between that of the ED and MW data (*cf.* Table **20**). Interestingly, their r(S-S) for **76a** is much closer to that of **77a** and is shorter by *ca.* 0.03 Å than that determined by Hirota.[170]

In general, electron correlation is required to accurately predict the geometric parameters of these halodisulfanes. For instance Entry 12 overestimates the r(S-S) while

Entry 14 approaches the experimental geometry with an r(S-S) < 2 Å. Das and Whittenburg[183] recently published a high level theoretical study on **77a**. They report that the inclusion of diffuse and d and f polarization functions was necessary to shorten the S-S bond (though they had little effect on increasing the accuracy of the predictions of bond and dihedral angles) and that their inclusion was additive; the MP2 method shows the best agreement among theoretical models (the best basis sets were that of the 6-311+G(2df) and 6-311+G(3df)).

For the FSSF **75a**, system, even with the addition of electron correlation and the inclusion of larger basis sets as in Entry 23, there still is no convergence in the geometry; the r(S-S) is overestimated by *ca.* 2%. In fact, using DFT methods[180,184] (Entries 24 and 27) provide much more accurate predictive methods. As can be seen, modeling these systems, electronically related to the alkoxy disulfides, is non trivial.

To date, the barriers to rotation of halosulfanes have not been experimentally determined. Some have calculated their barriers and the results are shown in Table **21**.

Table **21**. Calculated barriers to rotation for some halo disulfane and dihalo disulfanes

Cmpd		Calculated[a]		$\Delta^{a,b}$	Method	Ref
		cis	*trans*			
HSSCl	**78**	10.7			HF/6-31+G*	90
ClSSCl	**77a**	17.0			HF/6-31+G*	90
		17.1	11.9	5.2	HF/6-31G*	96
		20.2	15.4	4.8	MP2/6-311+G(3df)	183
HSSF	**79**	12.8			HF/6-31+G*	90
FSSF	**75a**	25.3			HF/6-31+G*	90
		24.2	18.9	5.2	HF/6-31G*	96

a) Barriers in kcal/mol. b) Difference between *cis* and *trans* barriers.

As can be seen, the addition of one halogen increases the *cis* barrier by *ca.* 3-5 kcal/mol over that of **69a**. The effect is multiplicative when two halogens are attached with an increase of *ca.* 10-17 kcal/mol depending on the nature of the halogen. Those barrier calculations done using the HF method should be taken with a degree of caution as it has previously been shown (*vide supra*) that this method is poor when it comes to predicting barrier height. Nevertheless, the calculations do indicate that the S-S barrier is sensitive to the nature of the attached substituents; the sensitivity and barrier magnitudes here are much greater than those of the XOOX analogs.[96]

The high barrier calculated for FSSF **75a** coupled with the short r(S-S) has been attributed to two hyperconjugative interactions between the 3p lone pairs of each sulfur which are partially delocalized into the adjacent $\sigma^*_{S\text{-}F}$ antibonding orbitals. This delocalization is maximized given a *gauche* conformation. The MO overlap is maximized as the energy of the σ^* orbital is lowered, so we would expect that the more electronegative the atom, the higher the barrier (Figure **3b**). This interaction exists in HSSH **69a**, ClSSCl **77a**, HOOH **70a** as well as FOOF **80** and has previously been discussed.[185,186]

A detailed overview of the experimental geometries of alkoxy disulfides and the ability of different methods to predict them is covered in Chapter **3**. The origin of the barriers to rotation about the S-S bond for these compounds is explored extensively in Chapters **3** and **4**, particularly as a comparison with other common rotational processes.

2.4.5 Compounds Containing Hypervalent Sulfur Atoms Directly Bonded to Sulfur

There exist but a few examples of stable molecules containing a hypervalent sulfur atom directly bonded to another sulfur atom.[38] The S-S bond in these compounds is classically written as if it were a true double bond. Their r(S-S) are shown in Table 22.

Table 22. The experimentally determined r(S-S) for hypervalent sulfur-sulfur bond-containing compounds.

Cmpd	r(S-S) Å			Method	Ref
F_2S=S **75b**	1.860	±	0.015	ED, MW	177,187
O=S=S	1.884	±	0.010	MW	188
S=S	1.892			MW	189
RN=S=S	1.898			X-ray	190
$(RO)_2S$=S **5g**	1.901			X-ray	40
$(RO)_2S$=S **5i**	1.910			X-ray	41
$(RO)_2S$=S **5m**	1.9154	±	0.0006	X-ray	42
$(RO)_2S$=S **5n**	1.8964	±	0.0013	X-ray	42
Ph_3P=NSN=S=S	1.908	±	0.002	X-ray	191
O=S=S=O	2.024			ED	192

The structure of **75b** was confirmed by a second ED study and contains the shortest known S-S bond.[178] The long S-S bond for planar S_2O_2 has been ascribed to a partial delocalization of the oxygen lone pairs into the $\sigma^*_{S\text{-}S}$ bond leading to a strengthening of the S-O bond at the expense of the S-S bond. Nevertheless, most compounds in Table 22 possess an extremely short S-S bond indicative of the double bond character present; of special note are the thionosulfites **5g**, **5i**, **5m** and **5n** (r_{av}(S-S) = 1.906 ± 0.009 Å). Thus, the short bond in FSSF **75a** (1.890, 1.888 Å; ED and MW, respectively, Table 20) demonstrates that in this case, there is also increased double bond character.

The geometry of branched structures $F_2S{=}S$ **75b**,[97,175,179,180,184] $Cl_2S{=}S$ **77b**,[97,175,183] $H_2S{=}S$ **69b**,[97,98] and $Me_2S{=}S$ **71b**[97,98] have all been modeled at high levels of theory. MP2 methods using a minimum of the 6-31G* basis set accurately predict the geometry of **75b**. In fact, only DFT calculations overestimated the r(S-S) bond length, and then only by *ca.* 2%. Assuming that these methods can handle electronically less demanding compounds **77b**, **69b** and **71b**, their r_{av}(S-S) bond lengths should respectively be *ca.* 1.879, 2.004, 2.019 Å. The latter two results suggest that in these thiosulfoxides the S-S bond has little double bond character. Steudel[98] also investigated larger alkyl homologues S_2Pr_2, S_2All_2 and they both possess similar structural parameters as that of **71b**.

To our knowledge, there are currently no comprehensive theoretical studies for thionosulfite structures. One of the major goals of the current work is to find a method, at minimum computational cost, which can equally model both isomeric forms of ROSSOR as well as predict their physical organic properties. In the next section, the relationship between these two forms is explored in the context of valence bond isomerization.

2.5 Valence-bond Isomerism

Eliel[193] classically defined valence-bond isomers as:

"Isomers that differ only by the position and order of the bonds between their atoms, which latter may, however, move slightly."

In particular, aromatic valence bond isomerization has received considerable attention.[194] A prime example of valence bond isomers is that between 1,3,5-cyclooctatriene **81** and bicyclo[4.2.0]octa-2,4-diene **82** (Scheme 8).

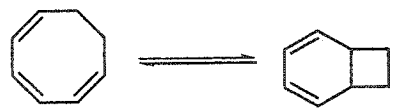

81 **82**

Scheme 8.

Alkyl-substituted benzenes,[195,196] perfluoroalkyl-substituted benzenes[197] and related aromatics have been shown to transform into their Dewar counterparts upon continuous UV irradiation as in the case of naphthalene/hemi-Dewar naphthalene (Scheme 9).[198,199] Theoretical studies[200] suggest that these isomerizations occur through a two-electron excitation from the HOMO to the LUMO which alters the geometry of the aromatic favouring new bonding between C1 and C4. These reactions are reversible.

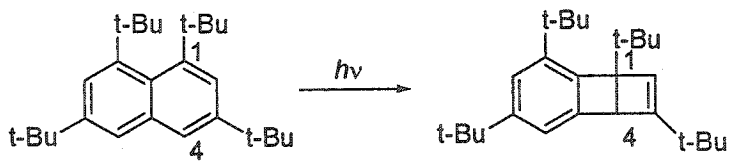

83 **84**

Scheme 9.

The concept of valence bond isomerization is not limited to simple substituted aromatics. In the following heteroatomic example,[201] irradiation of 5-methyl-thiazolo[3,2-*a*]pyridinium-8-olate **85** gave its valence bond isomer 6-methyl-2-thia-5-azatricyclo-[4.3.0.$0^{1,5}$]non-7-en-9-one **86**, which upon further irradiation isomerized to the corresponding 8-methyl-thiazolo[3,2-*a*]pyridine-5-one **87** (Scheme **10**). The extensive rearrangement of **85** to **86** corresponds to a photochemically allowed disrotatory ring closure.

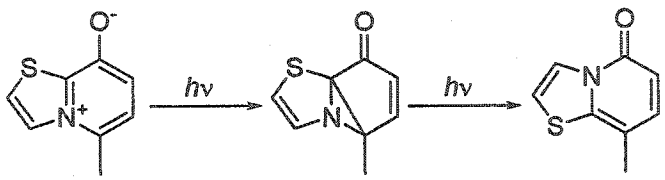

85 **86** **87**

Scheme **10**.

Although many of these examples are photolytically induced, this is not universally the case. Kurita[202] and co-workers thermalized related tricyclic heptane derivatives **88a-91a** to form interesting and synthetically useful 7-membered ring heterocycles **88b-91b** in excellent yield (70-90%). This isomerization may either proceed *via* a biradical intermediate or an ionic mechanism; the concerted mechanism was deemed less likely to occur without comment from the authors and they reported no photolytic reaction in the attempted conversion of **88a-91a** to **88b-91b** (Scheme **11**).

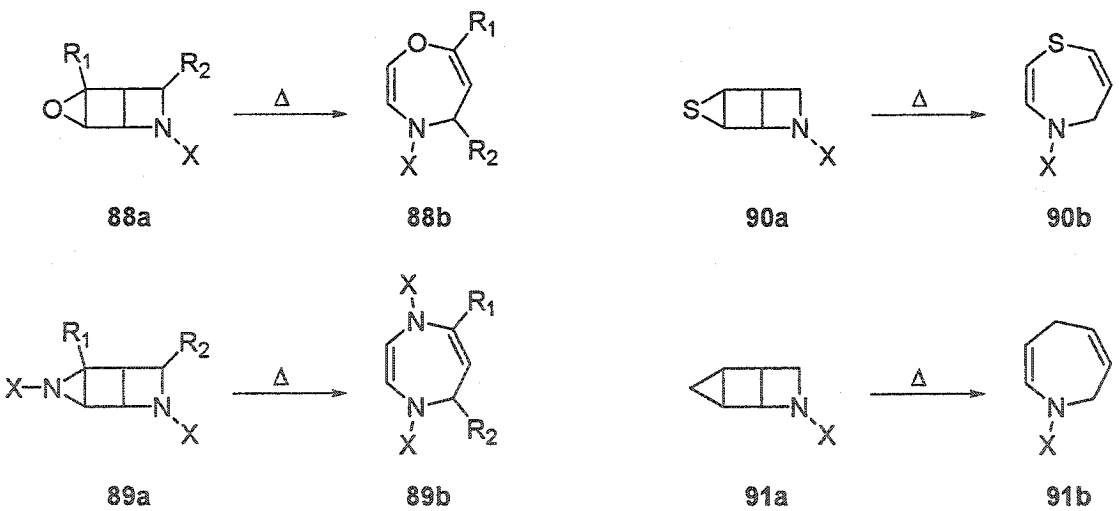

88a **88b** **90a** **90b**

89a **89b** **91a** **91b**

R_1, R_2 = H, Me, Ph
X = CO_2R
R = Me, Bn

Scheme **11**.

There also exist examples of valence-bond isomerization involving solely heteroatoms. In this interesting case, Scheme 12, Messmer[203] and co-workers observed the formation of triazine isomer **92** *via* nucleophilic attack of the pyridine nitrogen onto the diazonium functionality of **93**. Valence bond isomerization of related triazolium salts[204] and more highly nitrated heteroatomic ring systems[205] have also been investigated.

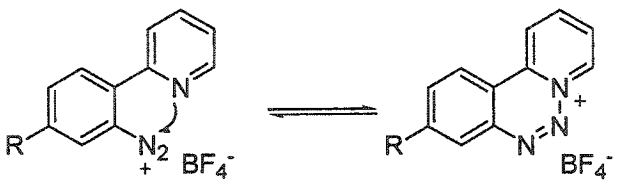

93 **92**

R = H, Cl, OMe, Me

Scheme 12.

An important feature of the work covered in this thesis revolves around the stability and mechanism of isomerization of divalent disulfide isomer **94a** to thiosulfoxide-like isomer **94b** (Scheme 13). The S-S bond in **94b** may either be considered as having double bond[206] character or containing a single semipolar[207] bond depending on the electronegativity of the substituent X. The double bond character in **94a** is also influenced by the inductive nature of X as was seen in Chapter 2.4.

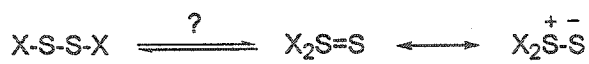

94a **94b**

X = F, Br, Cl, OR, alkyl

Scheme 13.

We are using the term valence-bond isomerism (or valence tautomerism) to describe this particular form of constitutional isomerization even though it does not strictly meet

the classical definition set by Eleil.[193] We feel that the term valence-bond isomerization is a most accurate description here due to the unusual valence-bond expansion that accompanies the transformation between **94a** to **94b**.

2.5.1 General Commentary on X-S-S-X / X_2S=S Systems

The concept of the existence of branch-bonded S-S species has generated considerable debate and investigation.[208] Foss first popularized the notion that branch-bonded sulfur molecules of the form **94b** bonded *via* S_{3d}-S_p orbital interactions and that these were only stabilized when the branched sulfur was attached to an electronegative group.[39,208] In the following sections, an overview of related isomerization reactions involving sulfur and the respective stabilities of each isomer are highlighted in order to provide a context for the work covered herein. Here we are interested in situations where X in Scheme **13** is an electronegative group; an overview wherein X = H or Me is covered in Chapter 7.

2.5.2 The F-S-S-F / F_2S=S System

As will be seen, isomer **94a** (with C_2 symmetry) is the most common isomer. In some special cases the thiosulfoxide isomer **94b** (with C_s symmetry) has also been detected. Historically, the first isolation and identification (*via* IR, MW and MS) of each of the valence-bond isomers in Scheme **13** was that of the sulfur monofluoride (S_2F_2) system. Kuczkowski's[177,187,209] seminal work has since been experimentally[178,210-218] and theoretically[91,97,175,178-180] confirmed by others. The unbranched isomer FSSF **75a** had

been initially regarded[213] as the less stable isomer as it was reported to isomerize to the branch-bonded F_2S_2 **75b** at temperatures above -100 °C.[210,212,213] To complicate the analysis, Seel and Budenz postulated that **75b** in the gas phase is transformed into the complex [FSSF, F_2S_2](g) upon cooling the sample to -80 °C.[210] This would seem to indicate that at lower temperatures **75a** is the most stable isomer. These two observations would seem to be initially at odds yet nevertheless demonstrate that the two isomers **75a** and **75b** are of comparable ground state energies. The physical properties of **75a** and **75b** are outlined in Table **23**.

Table **23**. Physical properties of sulfur monofluoride **75**

Cmpd.[a]	Connectivity	Mp (°C)	bp (°C)
75a	F-S-S-F	-133[b]	15[b]
75b	F_2S=S	-164.6[c]	-10.6[c]

a) Each isomer is a colourless gas at RT. b) From Ref [212]. c) From Ref [217].

Brown and Pez[212] were the first to investigate the isomerization of **75a** to **75b**. They noted that Lewis acids such as HF or BF_3 catalyzed the conversion of liquid **75a** to **75b** and postulated a possible mechanism, Scheme **14**.

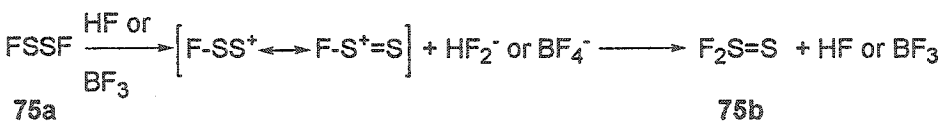

Scheme **14**.

When **75b** experiences the same conditions, it decomposes into S_8 and SF_4; thiothionyl fluoride **75b** is a stable gas up to at least 400 °C in the absence of a Lewis Acid. Their[212] preliminary kinetics measurements indicated that the Lewis Acid promoted isomerization was first order and that **75b** was the more stable isomer at RT (21.8 ± 0.3 °C); **75a** had a

$t_{½}$ = 4.7 h. They did however determine that it was **75a** that was the more stable isomer at -50 °C over CsF, in general agreement with that observed by Seel.[210] It seems that the CsF stabilizes **75a** relative to **75b**. Lösking[219] reported that the **75b** is more stable by 2.7 ± 0.4 kcal/mol.

Recently Cao[218,220] and co-workers reported the PES spectra of **75a** and **75b** as well as the isomerization between the two. They determined that **75a** is the more stable isomer *above* -80 °C and determined that the kinetics of isomerization of **75b** to **75a** were first order ($k_{296\ K}$ = 3.8 ± 0.4 x 10^{-5} s^{-1}) with an activation barrier E_A for the forward direction of 5.8 kcal/mol. This observed reversal of stability as compared to that of the literature should be viewed with great skepticism.

Several groups have probed the isomerization of sulfur monofluoride **75** computationally. Solouki and Bock[175] investigated the isomerization in Scheme **13** by semi-empirical methods (CNDO/2). They determined that as the electronegativity of X increases, the thiosulfoxide isomer **94b** becomes more stabilized. Solouki and Bock determined that there existed a substantial isomerization barrier between **75a** and **75b** of 23-46 kcal/mol.[221]

More recently Bickelhaupt[97] and co-workers explored the relative energies of **75a** and **75b** and related systems. They corroborated the earlier work[175] which stated that the ground state energy difference between **94a** and **94b** decreases as the electronegativity of X increases. They determined that the energy difference for **75a** and **75b** was small and

dependent on the level of *ab initio* theory used. For instance, at QCISD(T)/6-31G**//MP2/6-31G** **75b** is the more stable by 0.3 kcal/mol whereas at QCISD(T)/6-31+G**//MP2/6-31G** **75a** is the more stable by 3 kcal/mol. Such a range in energies is due to the polarized nature of **75b** wherein both the terminal sulfur and the fluorines acquire a substantial negative charge. Diffuse and polarization functions were thus required to accurately describe such compounds although these had a net neutralizing effect on the overall energy difference (total stabilization effect is 1.7 kcal/mol for **75a**). This confirmed the early *ab initio* work done by Marsden[178] and co-workers, though at the time Marsden believed that **75b** was the more stable isomer and had difficulty rectifying this with his theoretical results (this apparent conflict can be explained *vide infra*). Jursic[184] recently published a comprehensive DFT study wherein geometries converged (B3P86 was the best method) but energies predicted the wrong isomer **75a** as the more stable; he conjectured that using the MP2 method would yield better energies. A summary of relative ground state energies for S_2X_2 systems is shown in Table **24**.

In investigating the mechanism for the rearrangement between **75a** and **75b**, they[97] confirmed the earlier barrier calculations assuming that the isomerization proceeds *via* a 1,2-F shift in a unimolecular mechanism (40.7-51.5 kcal/mol depending on level of theory, ZPE correction included). The addition of electron correlation and diffuse functions reduced this barrier substantially yet the barrier still remains high. DFT (NL BP86) energies[180] of the same barrier are corroborative.

Such calculated barriers are disconnected from the experimental observations of an equilibrium between the two isomers at low temperatures (-100 °C).[210,213] This inconsistency implies that the pathway is not unimolecular (as had been originally proposed by Bock and Solouki involving a 1,2-F shift *via* a three-membered ring transition state – **TS 2**) and the authors[97] have suggested a bimolecular mechanism with possible transition states as outlined in Scheme **15** (**TS 1**).

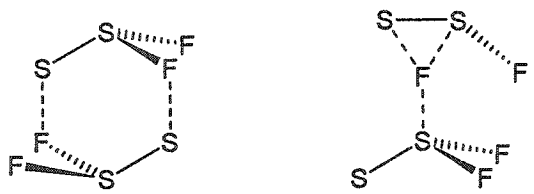

TS 1 **TS 2**

Scheme **15**. Possible bimolecular transition states in the isomerization of **75**.

Careful attention must be taken when interpreting theoretical energies as these are usually calculated without any consideration of temperature. Torrent[180] and co-workers recently calculated the respective energies of **75a** and **75b** with ZPE and thermal corrections and determined that at RT, **75b** is the more stable isomer whereas at low temperatures, **75a** is the more stable isomer. The low temperature activation parameters agree well with earlier work reported by Marsden[178] and Bickelhaupt[97] as well as that observed experimentally (though Marsden did not acknowledge the thermal dependence on the relative stability of isomers **75a** and **75b**).

To summarize, disulfide **75a** appears to be the more stable isomer at low temperatures (*ca.* -100 °C) whereas branch-bonded **75b** is the more stable isomer at higher temperatures (-80 – 400 °C). To date, no plausible mechanism for this isomerization has

been posited based on experimental findings though the calculated 1,2-F shift reported by some possesses a barrier that is too large to account for the observed low temperature isomerization.

Table 24. Relative energies of S_2X_2 **94b** with respect to XSSX **94a** isomers.[97]

		QCISD(T)/6-31G**//MP2/6-31G**			QCISD(T)/6-31+G**//MP2/6-31G**			
X	EN[a]	XSSX[b]	S_2X_2[b]	Δ[c,d]	XSSX[b]	S_2X_2[b]	Δ[c,d]	$\Delta\Delta$[e]
F	4.1	-994.46225	-994.46273	-0.3	-994.50082	-994.49610	3.0	3.3
Cl	2.8	-1714.51823	-1714.49275	16.0	-1714.52799	-1714.50400	15.1	-0.9
H	2.5	-796.47540	-796.42237	33.3	-796.47907	-796.42663	32.9	-0.4
Me	2.2	-874.82574	-874.79478	19.4	-874.83390	-874.80481	18.3	-1.2

a) Allred-Rochow electronegativities; Ref [222]. b) In Hartrees. c) In kcal/mol. d) Energy difference between two isomeric forms; a '-' sign signifies that S_2X_2 is more stable. e) Energy difference (kcal/mol) relative to the inclusion of diffuse functions.

2.5.3 The Cl-S-S-Cl / Cl_2S=S & Br-S-S-Br / Br_2S=S Systems

Relative to S_2F_2, much less work exists in the literature on the relative stabilities of isomeric forms of sulfur monochloride **77a** and sulfur monobromide **76a**. Though thiothionyl chloride **77b** has been suggested as a minor equilibrium contributor by some,[223-225] the ED,[170,172-174] Raman,[226-230] IR,[228] PES,[231] dipole moment,[10] quasielastic neutron scattering[232] and MW[176] studies all suggest that S_2Cl_2 exits in one isomeric form as **77a**. Chadwick and co-workers[233] and Feuerhahn and Vahl[234] both reported the presence of low concentrations of **77b** once **77a**, deposited in argon matrices at low temperature (8-20 K), had been UV photolyzed. These last two reports should be taken as artifacts of the observation technique.

Bock[175] and Solouki calculated that the most stable isomer was that of the unbranched **77a** and that the interconversion barrier was only *ca.* 3.5 kcal/mol based on the CNDO/2 hyperenergy surface. However, Das[235] at a high level of theory (QCISD/6-311+G(3df)// QCISD/6-311G(3d)) determined the barrier at 0 K to be *ca.* 51 kcal/mol; the latter case presumes a unimolecular mechanism involving a 1,2-Cl shift with a 3-membered ring transition state, similar to that reported for the S_2F_2 system (*vide supra*). Similar to the S_2F_2 system, Bickelhaupt[97] calculated the relative ground state energies of **77a** and **77b**. At the QCISD(T)/6-31G**//MP2/6-31G** **77a** is more stable by *ca.* 16.0 kcal/mol while adding diffuse functions in QCISD(T)/6-31+G**//MP2/6-31G** destabilized **77a** slightly relative to **77b** (15.1 kcal/mol). In general, the addition of diffuse functions destabilized the XSSX isomer but not significantly so. A higher barrier than that calculated by Bock would be expected given the lack of experimental evidence for the existence of the branched structure.

The little work on the isomerization of S_2Br_2 **76** suggests that it too exists in its unbranched form[170,228,230,232] though as with S_2Cl_2, Feuerhahn and Vahl[234] claim to have observed thiothionyl bromide.

2.5.4 Commentary on the RO-S-S-OR / $(RO)_2S{=}S$ System (R = H, R')

Outside this work, only Steudel has investigated the isomerization between alkoxydisulfides and thionosulfites. The transient preparation of dihydroxy disulfide HOSSOH **95a**, the unbranched form of thiosulfurous acid, has been reported[236,237] however no reports of its physical properties exist though **95a** has been observed in the

EI mass spectrometry of parent ROSSOR compounds (R = alkyl), which are themselves known to exist (see Chapter **2.1**).[238]

There are at least 11 isomeric structures of HOSSOH **95** and their geometries and energies have been calculated. The four lowest energy isomers are shown in Table **25**.[30]

Table **25**. Calculated[30] relative energies (kcal/mol) of the four most stable isomers of HOSSOH **95**

	HO–S–S–OH	HO–S(=O)–SH	HO–S(=S)–OH	H–S(=O)(=O)–SH
	95a	**95b**	**95c**	**95d**
HF/6-31G*//MP4/6-31G*	0	3.2	3.9	23.5

The relative energies of the first three structures (**95a-95c**) are small as compared with the fourth, **95d**. When the energies of these three structures are further refined using larger basis sets (MP2/6-311G**//HF/6-311G** + ZPE), their relative energy differences decrease (**95a** = 0, **95b** = -0.3, **95c** = 3.2 kcal/mol); **95b** has not been experimentally detected. Related tetrasulfide HSSSSH **96a** is 33.0 kcal/mol more stable than its branch-bonded analog $(HS)_2S{=}S$ **96b**[178] whereas the branch-bonded S_2F_2 **75b** is the more stable isomer in that system (*vide supra*).[239] So the inclusion of electronegative atoms such as oxygen stabilizes the branch bonded form **95b** over the unbranched **95a**.

As has been seen in Chapter **2.2**, esters of dihydroxy disulfide can be easily prepared. To date, *only* the unbranched geometry ROSSOR has ever been structurally resolved in acyclic form (R = Me **6**,[31,32,240] *p*-NO_2-Bn **49**,[35,36] *p*-Cl-Bn **50**[51]).

As highlighted in Chapters **2.1** and **2.3**, thionosulfites containing a 5-membered ring core can be synthesized. To our knowledge, no other ring-sized thionosulfite and no acyclic thionosulfite is known to exist. As well, to date no one has experimentally investigated the origin of the barrier to isomerization of this class of compound.

2.6 The Chemistry of Alkoxy Disulfides

2.6.1 A Brief Note on the Importance and Interest of S_2

Unlike O_2 which is readily stable at biological temperatures, S_2 is extremely reactive and labile, concatenating readily to S_8; for instance, S_2 UV photodissociates in 7.5 min at Earth's heliocentric distance.[241] In fact, S_2 is the prevailing sulfur allotrope at elevated temperatures (>500 °C) but likely in the triplet, spin unpaired form. Diatomic sulfur has been reported as a blue-violet gas[242] at these elevated temperatures and has been detected celestially. Its relevance in our own solar system manifests in its detection (MW and near IR) in the volcanic plumes of the Jovian moon Io;[243,244] the red colour of the moon surface being attributed to energy transitions resulting from ejected S_2 gas which instantly cools upon landing on the surface and quickly rearranges to more stable S_3 and S_4 allotropes.[245,246] Diatomic sulfur has also been detected in other astronomical contexts as

in the near-nucleus commae of comets[241] and at the impact sites of comet Shoemaker-Levy 9 on Jupiter.[247]

Diatomic sulfur can be trapped at low temperatures by rare gas matrices[248] or synthetically generated and subsequently trapped by, for instance, dienes as Diels-Alder-like adducts (Scheme 16).[249] The generation and trapping of diatomic sulfur has been well reviewed in the literature.[250-253] The Diels-Alder trapping of $^1S_2$ is symmetry allowed by Woodward-Hoffmann rules[101] and mirrors analogous reactions with singlet oxygen;[250,254,255] it is the singlet state of diatomic sulfur which is its excited state (*ca.* 13 kcal/mol above that of the ground state).[256]

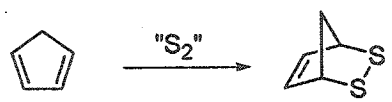

Scheme 16. Example of a synthetic trap using cyclopentadiene; acyclic dienes have also been used to trap 2-sulfur units.

Of particular interest in the current context of this thesis is the recent report that alkoxy disulfides at higher temperatures efficiently (> 75% trapped 97) deliver a 2-sulfur unit.[35] It has originally been suggested that such S_2 generation results from the concerted disproportionation of the parent alkoxy disulfide (Scheme 17)[3,35] though the actual source of sulfur in these thermolysis reactions has been questioned.[257] In particular, Thompson[3] observed that the origin of the R group of the alkoxy disulfide affected their thermal stability (secondary > primary > allyl > propargyl). This observation provided the sole evidence for the cyclic transition shown in Scheme 17. In Chapter 4 we will investigate the validity of this mechanism.

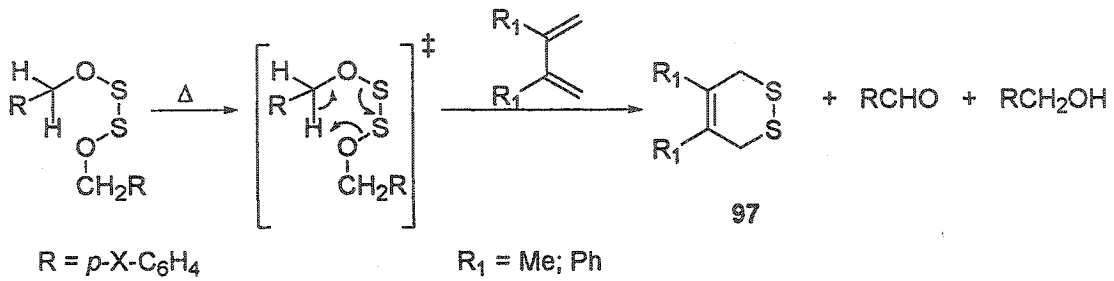

Scheme 17. Proposed mechanism in the thermolysis of alkoxy disulfides

Besides the trapping experiments profiled in Chapter **2.7.1**, the usefulness of alkoxy disulfides in organic synthesis has not been exploited. A summary of the use of **1** is provided in the following subsections.

2.6.2 Thermochemistry of Alkoxy Disulfides

Recently, Lunazzi[49,258] showed that photolysis of *t*-alkoxy disulfides and trapping with fullerene-C_{60} or fullerene-C_{70} provided an alternate source of alkoxyl radicals. This chemistry is reviewed in detail in Chapter **4**.

Braverman,[52,53] in two related papers, outlined the thermal rearrangements of diallyloxy disulfides **34-41** and dipropargyloxy disulfides **42-46**. Reaction times were influenced by substitution patterns of the starting alcohols. Diallyloxy disulfides[52] in refluxing acetonitrile were shown to undergo double [2,3]-sigmatropic rearrangements to the corresponding *vic*-disulfoxides **34a-39a**, which then rearranged further to the more stable thiosulfonate isomers **34b-39b** (Scheme **18a**). Cinnamyl alkoxydisulfides **40-41** (R_1 = H, R_3 = Ph, R_2 = H or Me) do not undergo this tandem rearrangement but instead disproportionate to the corresponding alcohol, aldehyde and elemental sulfur. This is not

surprising given that cinnamyl sulfenates[259] also do not thermally rearrange due to the loss of conjugation which would result during the allylic shift. It has been supposed that detected **34d** and **36d**, could be formed *via* the intermolecular self [4+2]-cycloadditions of the corresponding conjugated vinyl sulfines **34c** and **36c**. These intermediates in turn would have been generated by either H-abstraction from a sulfinyl radical by another *in situ* radical species or by a cycloelimination reaction of precursors **34a** or **36a** (Scheme **18b**).

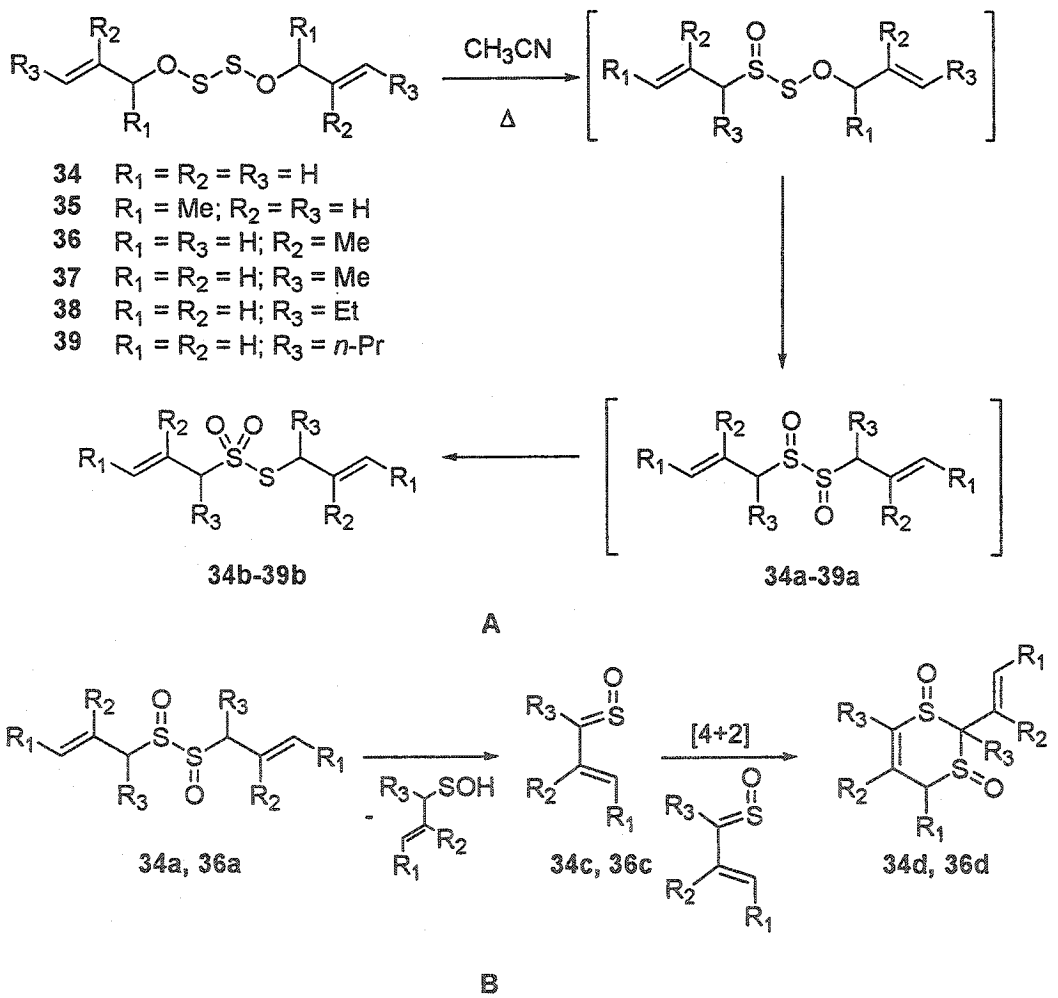

Scheme **18.**

Analogously, propargyloxy disulfides[53] **42-46** undergo a double [2,3]-sigmatropic shift to afford the corresponding diallenic *vic*-disulfoxide (Scheme 19). These intermediates now undergo tandem [2,3]-, [3,3]-sigmatropic rearrangements to form **42b-46b**. This is then followed by a head-to-tail intramolecular [2+2] cycloaddition to afford the dithiabicyclo product **42c-46c**. To date, this represents the only method to access these types of substituted dithiabicycles, which have similar functionality to the natural product class of bioactive zwiebelanes found in onions.[260]

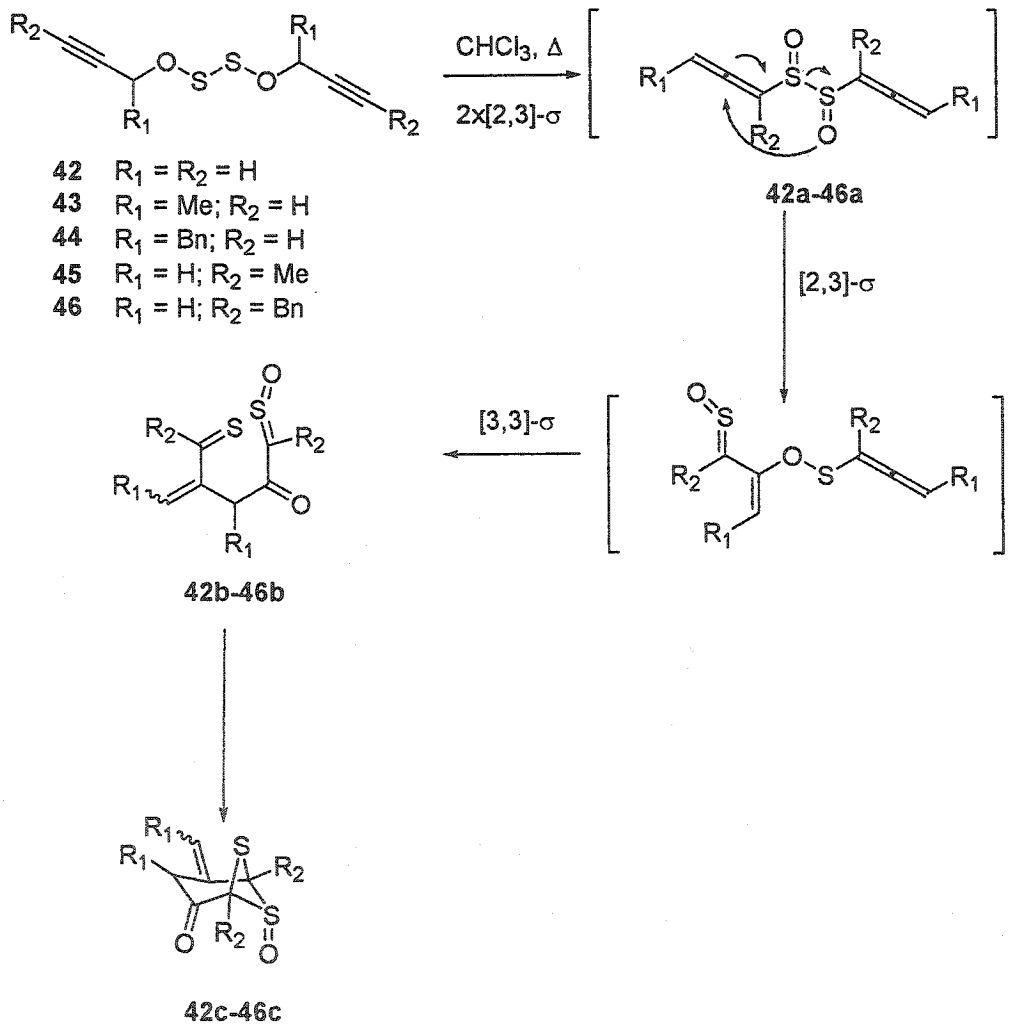

42 $R_1 = R_2 = H$
43 $R_1 = Me$; $R_2 = H$
44 $R_1 = Bn$; $R_2 = H$
45 $R_1 = H$; $R_2 = Me$
46 $R_1 = H$; $R_2 = Bn$

42a-46a

42b-46b

42c-46c

Scheme 19.

2.6.3 Chemistry Involving the Alkoxy Disulfides as the Nucleophile

Dialkoxy disulfides are acid labile. In the presence of a stoichiometric amount of Lewis Acid, MeOSSOMe **6** was found to readily decompose *via* alkylation to the corresponding sulfite **98** with trace amounts of the sulfinate **99**; sulfur was observed as a precipitate in the reaction (Scheme **20**).[261]

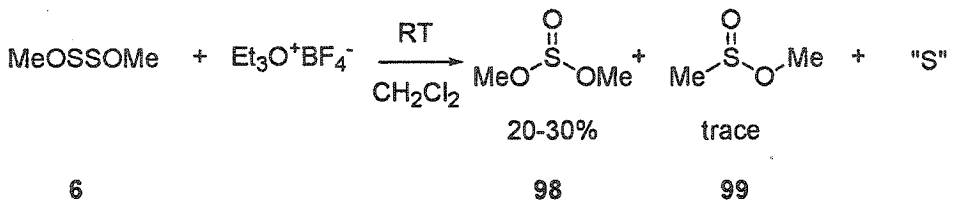

Scheme **20**.

The yield of sulfinate **99** increased when only a catalytic amount of triethyloxonium tetrafluoroborate was used. Other Lewis acids such as $SbCl_5$ and $BF_3{\cdot}OEt_2$ also effected the same decomposition. When the decomposition was followed by ^1H NMR, other low boiling products were observed including, dimethyl sulfate and dimethyl ether. The decomposition products most likely result from the concomitant desulfurization/disproportionation/isomerization of **6**.[261]

Decomposition of ROSSOR **1** has also been observed on acidic and basic alumina during chromatography. In the latter case, it has been proposed[3] that there is S-S bond cleavage resulting in hydrolysis to the parent alcohol **13** according to Scheme **21**, fragment a; the use of MeOH as an eluant was required to saponify the aluminum ester which then afforded another equivalent of alcohol and *ca.* ½ of the remaining sulfur, fragment b.

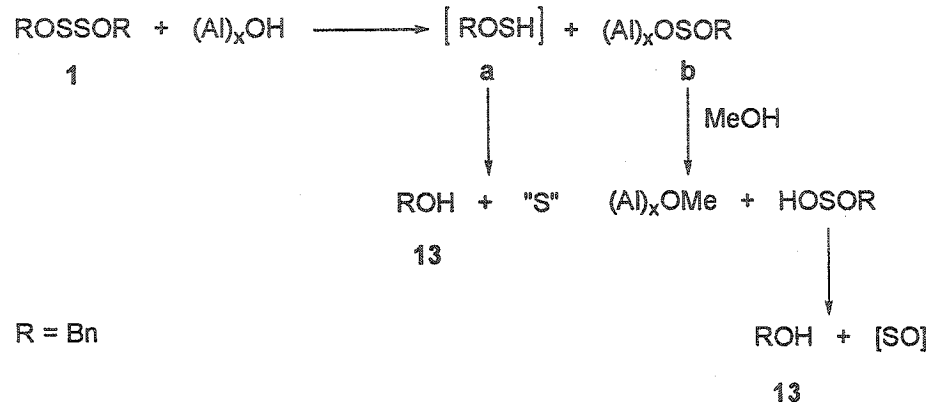

Scheme **21**. Decomposition on basic alumina

Disproportionation to the alcohol **13**, aldehyde **100** and sulfur was observed when using acidic alumina.

When alkoxydisulfides are allowed to stand in solution in the presence of pyridine hydrochloride, decomposition ensues with formation of the alcohol **13**, sulfite (*ca.* 30 %) **101**, sulfoxylate **102** (trace) and sulfur. A rationale was provided to account the product distribution as outlined in Scheme **22**. The observed percentage of sulfite is similar to that observed by Kobayashi.[261]

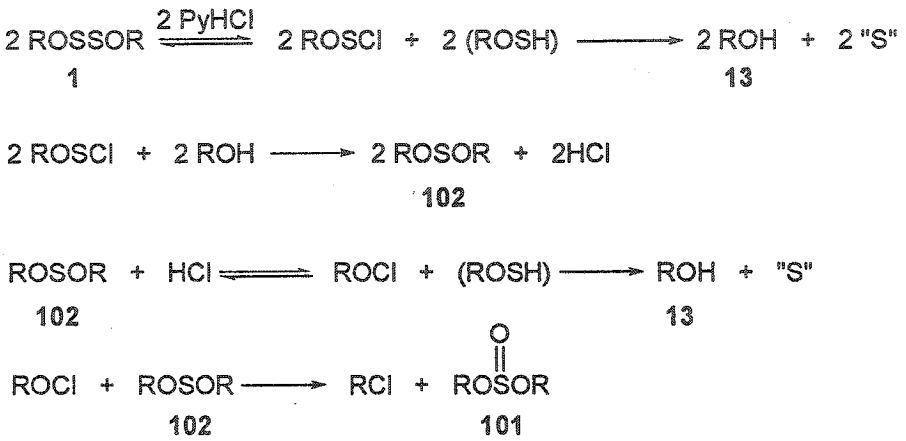

Scheme 22. Decomposition of ROSSOR with pyridine hydrochloride. In this scheme 75% of the sulfur is converted to elemental sulfur while the rest can be found as the sulfite **101**.[262]

2.6.4 Chemistry Involving Nucleophilic attack on Alkoxy Disulfides

Kagami[263] showed that alkoxy disulfides could serve as an SSOR source to form **103** when he reacted alkylthio acids with R'OSSOR' (R' = Me **6**, Et 7, *n*-Pr **8**, *i*-Pr **16**) in CCl_4 in moderate yield (29-58%). A plausible mechanism for this reaction is outlined in Scheme **23**.

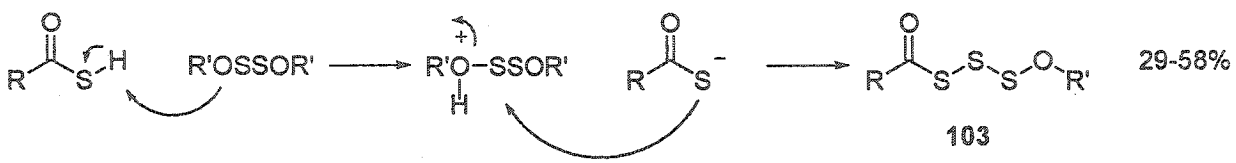

Scheme 23.

In related work, Kagami[264] demonstrated that the SSOR moiety could also be transferred when amines or thiols were used as nucleophiles. These substitution reactions

also proceed in moderate yield. Steudel[265] has also used thiols as nucleophiles in related substitution reactions. The work is generally outlined in Scheme **24**.

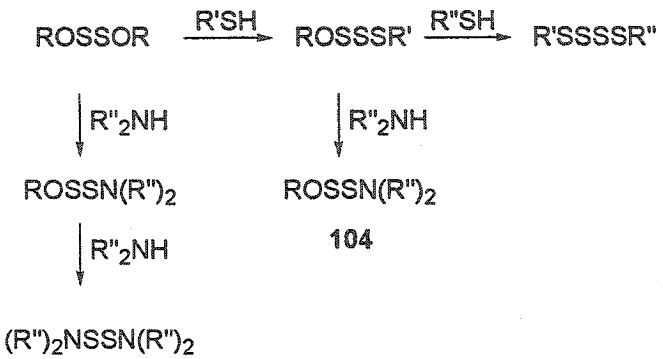

Scheme **24**.

Their sequential addition of nucleophiles illustrates well the increasing leaving group capacity of N < S < O. The reaction of EtOSSOEt **7** with primary amines was less straightforward than that of the thiols. For instance when **7** was reacted with **105** in refluxing benzene, it resulted in the initial formation of **106**, which then eliminated EtOH to form *N*-thiosulfinylaniline **107** (Scheme **25**). This reaction was characterized with a colour change in the solution to deep violet.

105 **106** **107**

Scheme **25**.

When the amine was changed to one which contained protons α but not β to the amine functionality as in benzylamine **108a** or furfurylamine **108b**, under similar reaction conditions, tetrasulfides **109a-109b** were formed *via* intermediate **110** (Scheme **26a**). When β protons are present (**111a-111b**), α-ketonthioamides **112a-112b** are isolated after column chromatography (Scheme **26b**); it should be noted that no ν_{NH} or $\nu_{C=O}$ stretches

were detected in the IR of the crude mixture suggesting that **112** is formed as a result of decomposition on the column from some unknown intermediate. No attempts were made to trap the extruded sulfur from **113**.

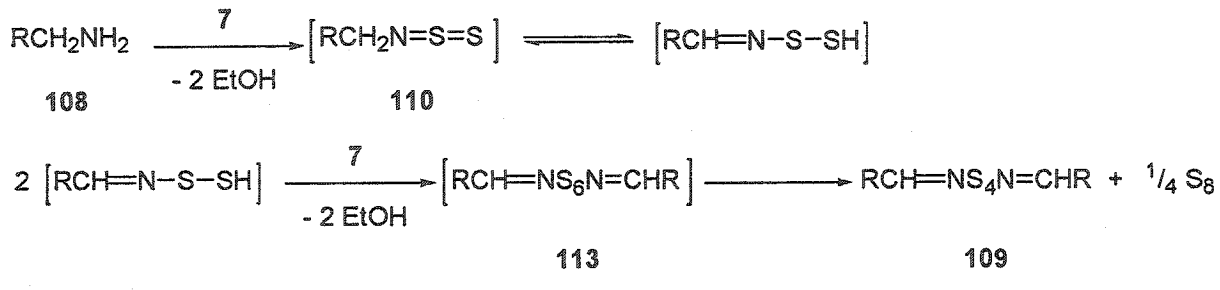

108 **110** **113** **109**

R' = RCH_2 = Bn,

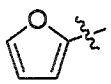

108a **108b**

A

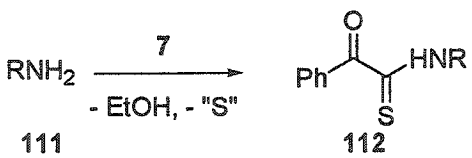

111 **112**

R = $PhCH_2CH_2$-, PhCH(Me)-

111a **111b**

B

Scheme 26.

Kagami[266] also investigated the corresponding reaction with hydrazines **114** ($RNHNH_2$) and found that not only is the alkoxy group displaced as with their other work highlighted in this section, but in addition there is the elimination of sulfur and nitrogen. Analogously to attack by amines (*vide supra*), it is reasonable to assume that in this case a thiosulfinyl intermediate is formed (**115**). It is then believed that after tautomerization of **115**, a second equivalent of EtOSSOEt **7** is attacked forming a highly unstable arylazo ethoxy tetrasulfide **116**. In a radical decomposition mechanism, nitrogen would then

evolve with the formation of aryl and highly chalcogenized radicals. Indeed, the formation of aryl radical from thermal decomposition of diazonium salts is well-known.[267] These radicals then concatenate together or react with the solvent to give biphenyl **117** (0-27%) or aryl ethoxy tetrasulfide **118** (0-29%). This latter compound can then self-react to form aryl tetrasulfides **119** (13-38%). Reported yields were low due to difficulty in separating the products by chromatography. The results are summarized in Scheme **27**.

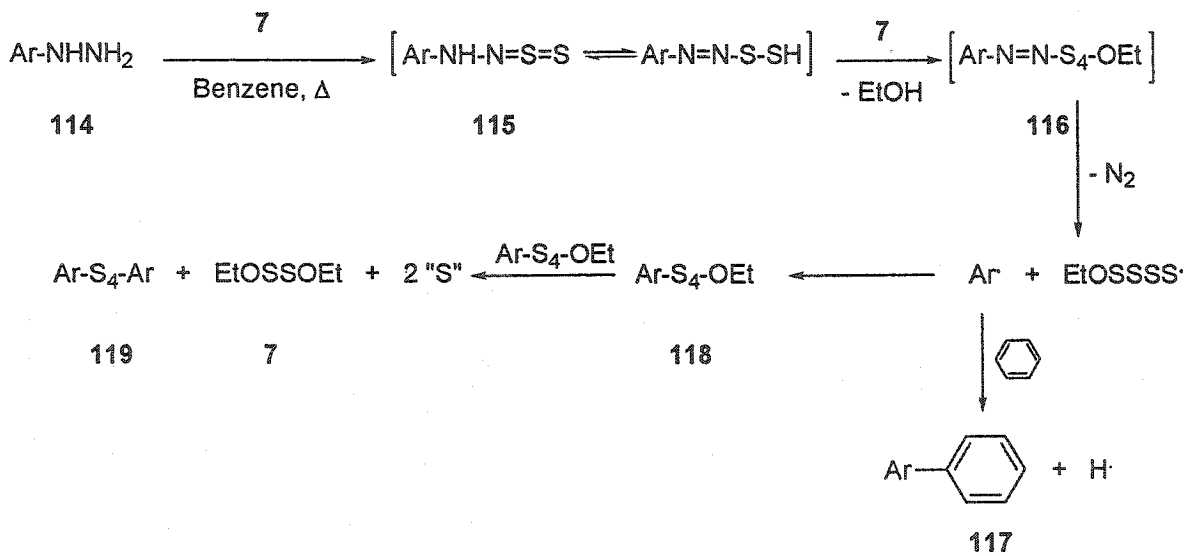

Scheme **27**.

Derivatives of hydrazobenzene **120** reacted much more simply with **7** to afford azobenzenes **121** in near quantitative yields. Their synthesis is rationalized in Scheme **28**. Here **7** acts as an oxidizing agent.

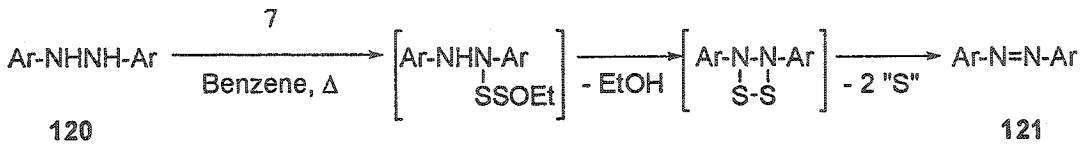

120 **121**

Ar = C_6H_5, 2-BrC_6H_4

Scheme **28**.

Reaction of 7 with $(PhNHNH)_2C(=S)$ **122** gave tetrazoliumthiolate **123** *via* **124** (Scheme **29**).

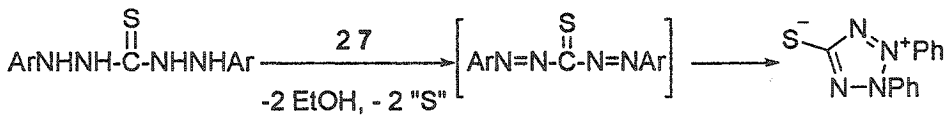

122 **124** **123**

Scheme **29**.

Not all nucleophilic attack is so straight forward. Kagami reported[268] the formation of carbodiimdides **125**, cyanamides **126**, tetrasulfides **127** or thiadiazoles **128** from the sequential attack of 1 or 2 equivalents of thiourea **129** on 7; unsubstituted thioureas were needed in order to obtain the thiadiazoles. The product formation is rationalized in Scheme **30**.

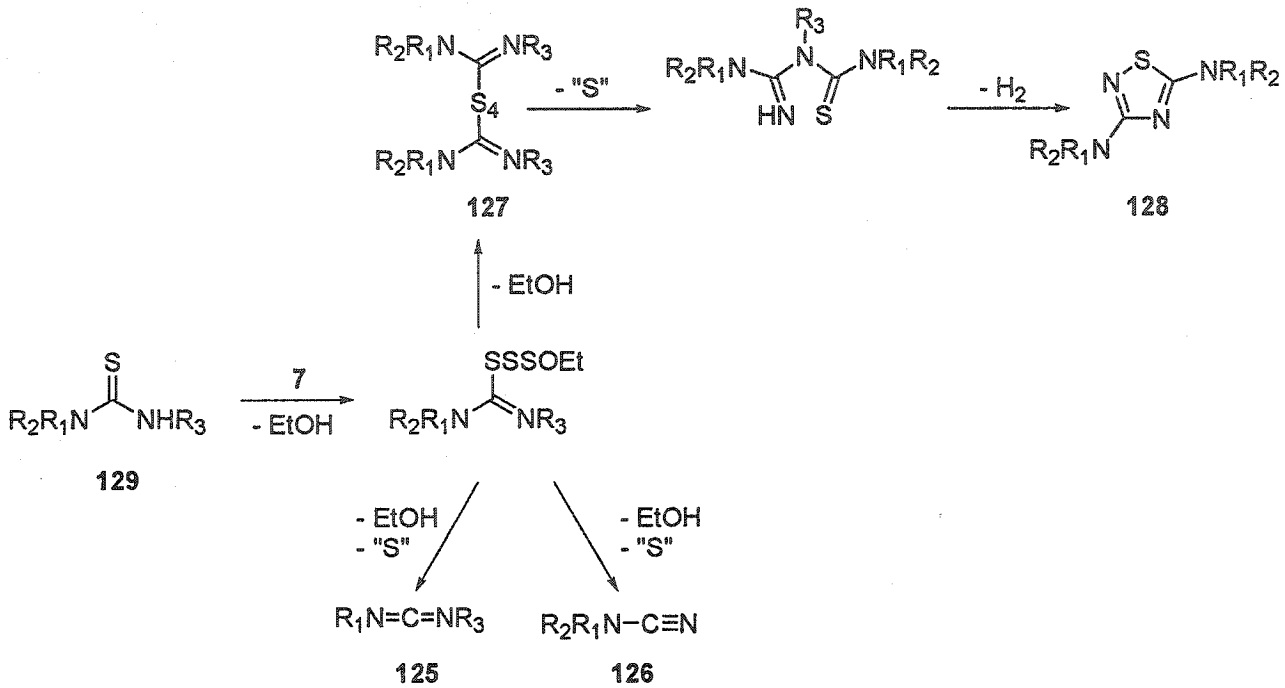

Scheme 30.

Cyanamides **126** are most probably formed by a similar mechanism to that proposed[264] for the formation of benzonitrile **130** from thiobenzamide **131** (Scheme **31**). It should be noted that a common intermediate in Schemes **25-27** is a substituted-*N*-thiosulfinylamine (**107**, **110**, **115**). Interestingly, no reaction was observed when benzamide was used as the nucleophile. The proposed mechanism includes the desulfurization of **133** which would involve the loss of an "S_3" unit. Transfer of S_3 is rare and it would have been interesting to see whether there was real S_3 extrusion as the authors allege. Another possibility (not shown) is sequential extrusion of "S_2" followed by "S", though this seems less likely as thioamides (the product of initial S_2 loss) are themselves stable species.

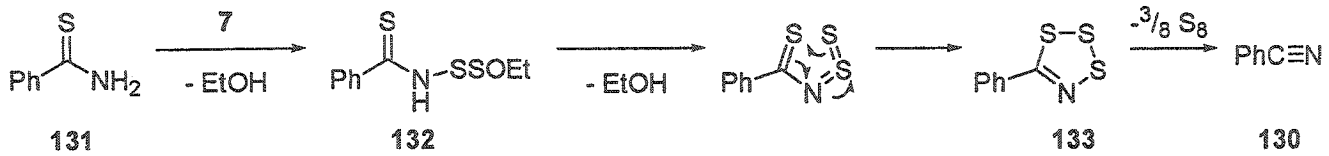

Scheme 31.

Reaction of *p*-toluenesulfinic acid **134** with alkoxy disulfides does not undergo the same chemistry as that of the thioamides. Instead, simple nucleophilic displacement of alkoxide followed by O-S migration occurs at room temperature to afford di-*p*-toluenesulfonyl disulfide **135** in good yield (68-75%), depending on the alkoxy disulfide used. At elevated temperatures, disproportionation occurs to afford a mixture of di-*p*-toluenesulfonyl sulfide **136** and di-*p*-toluenesulfonyl trisulfide **137** in yields of *ca.* 30% each (Scheme **32**). Indeed, when **135** was heated **136** and **137** were obtained in yields of 36 and 33% respectively.

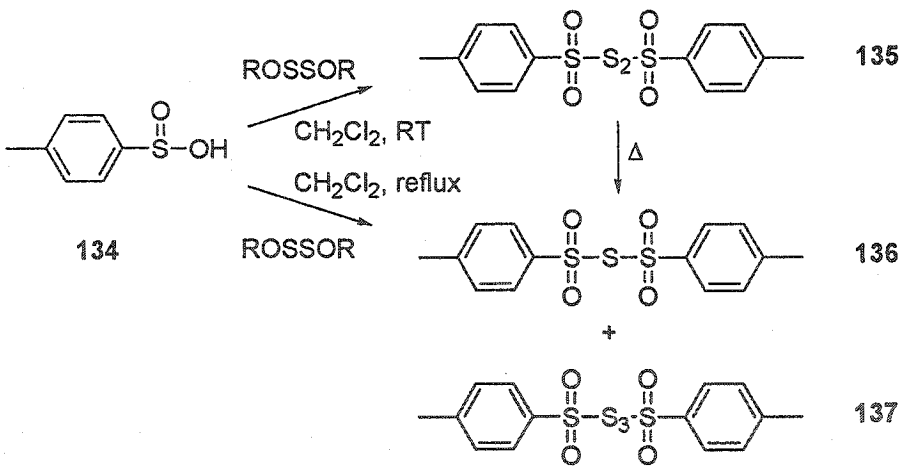

Scheme 32.

Hoepping[269] recently reported the synthesis of α-ketothio esters **138** in moderate-to-good yields from aryl or *t*-alkyl methyl ketones **139**. A mechanism is proposed, though not confirmed, involving a highly strained dithiirane intermediate **140**. It is outlined in Scheme **33**.

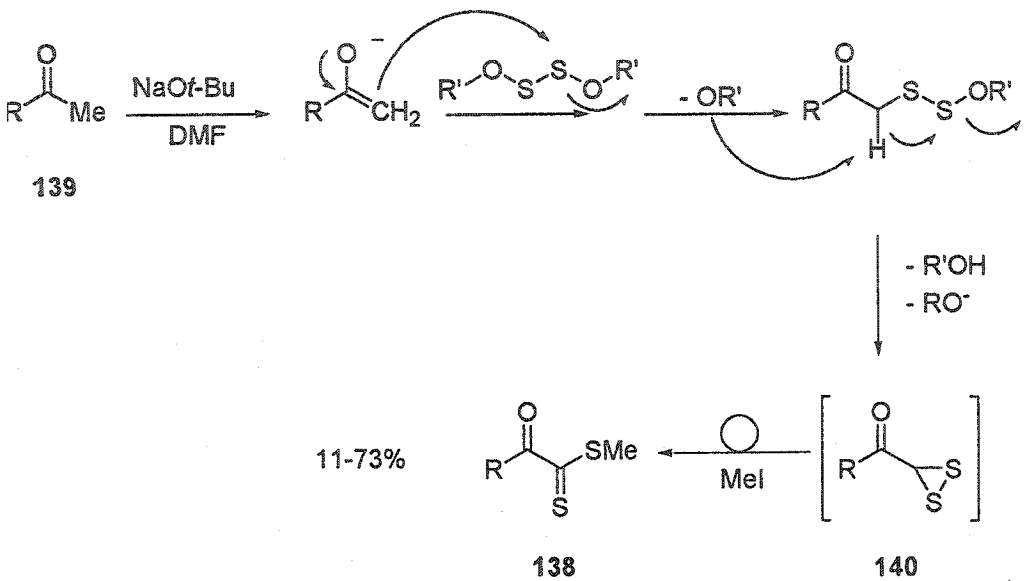

139 138 140

ne **33**.

:hemistry has been used[270] in the facile synthesis of the dye thioindigo **141** (56%)

as chlorinated derivatives thereof. Its synthesis is outlined in Scheme **34**.

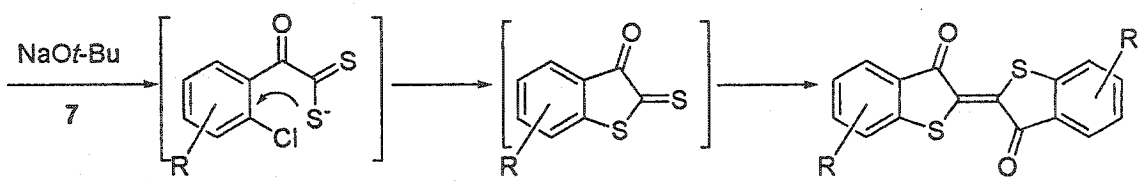

141

ne **34**.

stingly, when the enolate of β-diketone **142** is reacted with MeOSSOMe **6**, the

lated product was that of the sulfide **143** (Scheme **35**).

In a recent report,[271] gas phase nucleophilic substitution with hard nucleophiles on alkoxy disulfides (R = Me **6**, Et **7**) was detected on carbon, sulfur and oxygen (attack on oxygen occurs less frequently than on carbon or sulfur). Meuwsen hypothesized that nucleophilic attack in the solution phase by hard nucleophiles such as potassium hydroxide[8] (Scheme **36a**) or sodium alkoxides[272,273] (Scheme **36b**) or alkyl lithium reagents[3,272] (Scheme **36c**) occurs at sulfur which is consistent with that observed in the gas phase by Smith and O'Hair.[271] This is intriguing as sulfur would normally be considered the soft site.

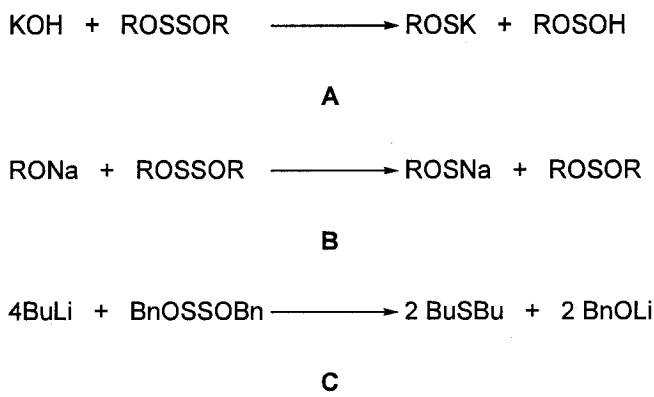

Scheme **36**.

Under careful conditions, ROSSCl can be formed from ROSSOR **1** and SCl_2. Steudel[238] used this key intermediate in his synthesis of a nonasulfide (see Chapter **7** for details). The formation of ROSSCl is quantitative due to the fact that by-product ROSCl decomposes to form a highly stable sulfite, Scheme **37**.

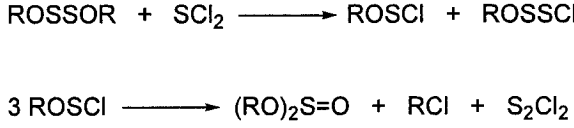

Scheme **37**.

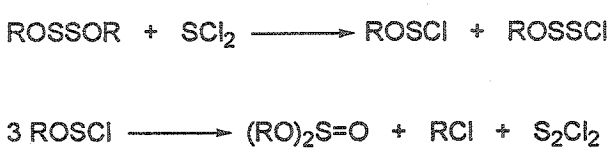

Scheme 37.

2.6.5 Alkoxy Disulfides as Catalysts

Catalytic use of MeOSSOMe **6** promotes the transylidation of sulfur ylids containing two electron-withdrawing groups ($R_1R_2S^+C^-(CO_2Me)_2$) on carbon (Scheme **38**).[274] Examples of transylidation are rare in the literature owing to the very strong stability of the sulfur ylid due to the two electon-withdrawing groups attached to carbon. Therefore, a synthetically useful procedure is desirable. The reaction proceeds quite easily and affords good to excellent yields of the transylidated product. Increased steric bulk of R_3 and R_4 (Scheme **38**) decrease the efficiency of the reaction. Other catalysts that were successfully employed for this reaction include thiocyanogen (NC-SS-CN) and benzoyl disulfide (Bz-SS-Bz). It would seem that electron-withdrawing groups adjacent to the disulfide moiety of the catalyst are key to proper reactivity; during the reaction the catalyst does not decompose but in the absence of the sulfide, the ylid does (leading to an olefinic by-product).[275] Although no mechanism was given, a zwitterionic sulfonium ylid complex most probably forms[276] in an analogous fashion to that when Cu(II) sulfate reacts with ylids to quantitatively decompose them.[277]

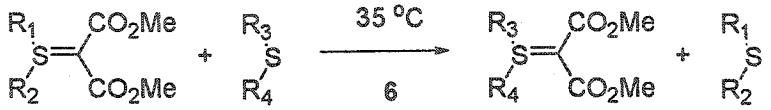

Scheme 38.

2.6.6 The Chemistry of Thionosulfites

The chemistry of thionosulfites remains a relatively unexplored topic. Recently, Nakayama synthesized two diastereomeric thionosulfites **5m** and **5n** and explored some of their chemistry.[42] When these thionosulfites were thermalized, they gave decomposition products thiophene **144** and sulfide **145** in different relative yields, Scheme 39. While **5m** decomposed in 96 h at 120 °C to afford ratio of 39:13:48 of **144:145:5m**, **5n** decomposed completely in 24 h to solely produce a 6:94 ratio of **144:145**. The increased yield of **145** in the thermolysis of **5n** was thought to be due to the retardation of the formation of **144** due to steric reasons. Though compound **5m** proved to be the thermodynamically most stable thionosulfite, the relative yield between the two isomers (in an 82:18 ratio – see Chapter 2.3) and the lack of isomerization between the two indicate that the synthesis is kinetically controlled. DFT calculations correctly predicted that **5m** would be the more stable isomer by 1.69 kcal/mol.

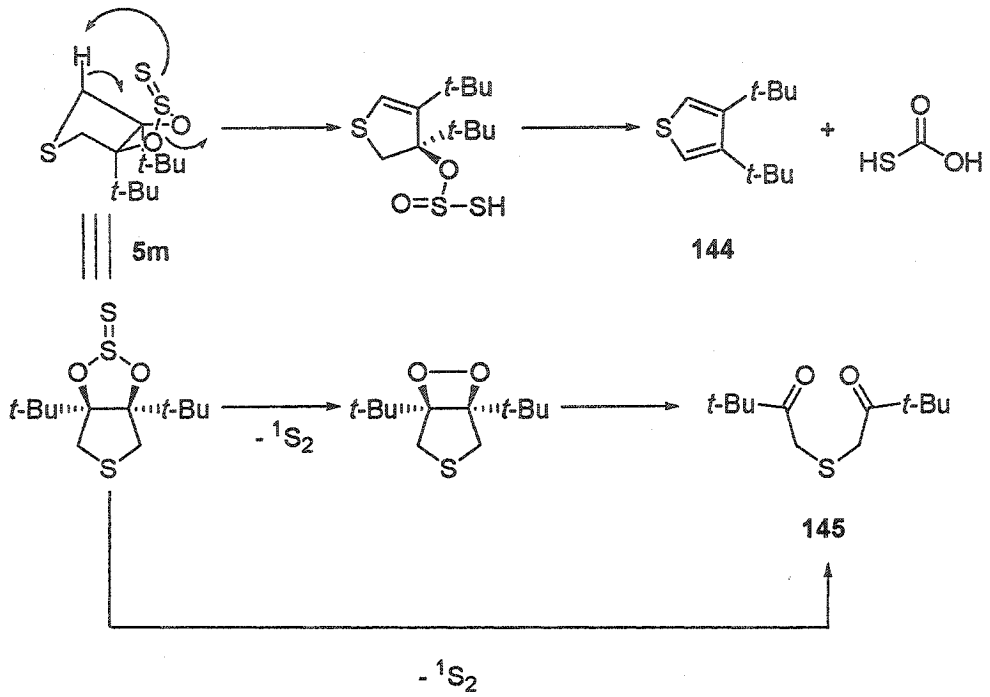

Scheme **39**

These two thionosulfites were also readily hydrolyzed under alkaline conditions. For instance, **5m** was hydrolyzed (1:1 H_2O/THF) in the presence of $NaHCO_3$ to give diol **63m** in 93%.

Oxidation of **5m** with 1.1 equivalents of MCPBA afforded a 94:6 ratio of **146:147** (**146** was isolated in 77% yield). Oxidation of **5m** in excess (3.3 equivalent) MCPBA gave a 90:10 ratio of **147:148**. These results indicate that the S=S bond is more resistant to oxidation than a simple sulfide sulfur atom. More interestingly is the inversion of stereochemistry in **147**. A mechanism for this inversion is posited in the supporting information of the paper. The product ratios are summarized in Scheme **40**.

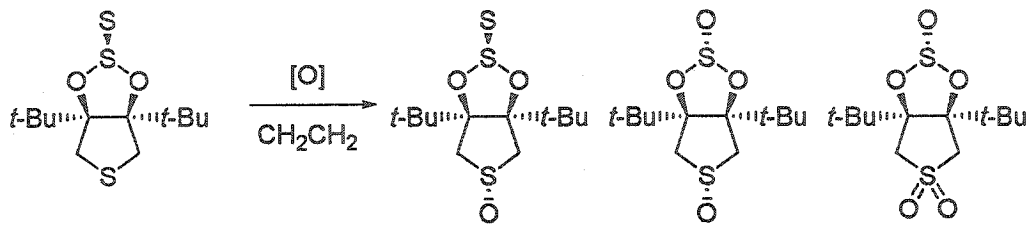

5m	146		147		148
MCPBA (1.1 equiv)	94	:	6		
MCPBA (3.3 equiv)			90	:	10

Scheme 40.

2.7 Concluding Remarks

The previous extensive introduction was necessary to provide important insight not only into the potential usefulness of alkoxy disulfides but also to introduce important concepts in conformational analysis and isomerization. It was also necessary to introduce a comparison of theoretical calculations with experimental results because a fundamental facet of this project is the use of theoretical modeling as a tool for the investigation of physical properties of these compounds. In much of this thesis, argument by analogy is intrinsic to our conclusions. It is for this reason that the physical properties of so many related systems were explored herein.

2.8 References

(1) Lengfeld, F. *Ber.* **1895**, *28*, 449.

(2) Thompson, Q. E.; Crutchfield, M. M.; Dietrich, M. W. *J. Am. Chem. Soc.* **1964**, *86*, 3891.

(3) Thompson, Q. E.; Crutchfield, M. M.; Dietrich, M. W.; Pierron, E. *J. Org. Chem.* **1965**, *30*, 2692.

(4) For a review of Thompson's work on alkoxy disulfides see: Thompson, Q. E. *Quarterly Reports on Sulfur Chemistry* **1970**, *5*, 245

(5) Zinner, G. *Angew. Chem.* **1957**, *69*, 508.

(6) Meuwsen, A. *Ber.* **1935**, *68*, 121.

(7) Clow, A.; Kirton, H. M.; Thompson, J. M. C. *Trans. Farady Soc.* **1940**, *36*, 1029.

(8) Meuwsen, A. *Ber.* **1936**, *69*, 935.

(9) Goehring, M.; Stamm, H. *Angew. Chem.* **1948**, *A60*, 147.

(10) Stoll, O.; Scheibe, G. *Ber.* **1938**, *71*, 1571.

(11) Goehring, M. *Chem. Ber.* **1947**, *80*, 219.

(12) For a background on the causes of pyramidal inversion see: Mislow, K.; Rauk, A.; Allen, L. C. *Angew. Chem. Int. Ed. Engl.* **1970**, *9*, 400

(13) For a review on linear free energy correlations of barriers to pyramidal inversion see: Mislow, K.; Baechler, R. D.; Andose, J. D.; Stackhouse, J. *J. Am. Chem. Soc.* **1972**, *94*, 8060

(14) For a review on calculated and experimental barriers to pyramidal inversion for first- and second-row elements see: Mislow, K.; Rauk, A.; Andose, J. D.; Frick, W. G.; Tang, R. *J. Am. Chem. Soc.* **1971**, *93*, 6507

(15) Pritchard, J. G.; Lauterbur, P. C. *J. Am. Chem. Soc.* **1961**, *83*, 2105.

(16) Faucher, H.; Guimaraes, A. C.; Robert, J. B.; Sauriol, F.; St-Jacques, M. *Tetrahedron* **1981**, *37*, 689.

(17) Lauterber, P. C.; Pritchard, J. G.; Vollmer, R. L. *J. Chem. Soc.* **1963**, 5307.

(18) Baw, H.; Bennett, G. M.; Dearns, P. *J. Chem. Soc.* **1934**, 680.

(19) Fries, K.; Vogt, W. *Ber.* **1911**, *44*, 756.

(20) Johnson, C. R.; McCants Jr., D. *J. Am. Chem. Soc.* **1965**, *87*, 1109.

(21) Johnson, C. R.; McCants Jr., D. *J. Am. Chem. Soc.* **1964**, *86*, 2935.

(22) Mislow, K. *Int J. Sulfur Chem. A.* **1971**, *1*, 66.

(23) Mislow, K.; Schneider, P.; Ternay Jr., A. L. *J. Am. Chem. Soc.* **1964**, *86*, 2957.

(24) Farina, G.; Montanari, F.; Negrini, A. *Gazz. Chim. Ital.* **1959**, *89*, 1548.

(25) Henbest, H. B.; Khan, S. A. *Proc. Chem. Soc.* **1964**, 56.

(26) Mislow, K.; Rayner, D. R.; Miller, E. G.; Bickart, P.; Gordon, A. J. *J. Am. Chem. Soc.* **1966**, *88*, 3138.

(27) For a detailed investigation into the mechanism and activation parameters of pyramidal inversion of sulfoxides see: Mislow, K.; Rayner, D. R.; Gordon, A. J. *J. Am. Chem. Soc.* **1968**, *90*, 4854

(28) Thompson, Q. E. *J. Org. Chem.* **1965**, *30*, 2703.

(29) Claeson, G.; Androes, G.; Calvin, M. *J. Am. Chem. Soc.* **1961**, *83*, 4357.

(30) Steudel, R.; Miaskiewicz, K. *J. Chem. Soc. Dalton Trans.* **1991**, 2395.

(31) Steudel, R.; Schmidt, H.; Baumeister, E.; Oberhammer, H.; Koritsanszky, T. *J. Phys. Chem.* **1995**, *99*, 8987.

(32) Koritsanszky, T.; Buschmann, J.; Schmidt, H.; Steudel, R. *J. Phys. Chem.* **1994**, *98*, 5416.

(33) Borghi, R.; Lunazzi, L.; Placucci, G.; Cerioni, G.; Foresti, E.; Plumitallo, A. *J. Org. Chem.* **1997**, *62*, 4924.

(34) Cerioni, G.; Plumitallo, A. *OMR. Organic Magnetic Resonance* **1998**, *36*, 461.

(35) Harpp, D. N.; Tardif, S. L.; Williams, C. R. *J. Am. Chem. Soc.* **1995**, *117*, 9067.

(36) Snyder, J. P.; Nevins, N.; Tardif, S. L.; Harpp, D. N. *J. Am. Chem. Soc.* **1997**, *119*, 12685.

(37) Chapman, J. S.; Ghosh, T. *Patent # EP 1008 296 A1* Europe, **1999**, 10

(38) For a review on compounds containing the S=S bond see: Turnbull, K.; Kutney, G. W. *Chem. Rev.* **1982**, *82*, 333

(39) Foss, O. *Acta Chem. Scand.* **1950**, *4*, 404.

(40) Harpp, D. N.; Steliou, K.; Cheer, C. J. *J. Chem. Soc. Chem. Commun.* **1980**, 825.

(41) Harpp, D. N.; Zysman-Colman, E.; Abrams, C. B. *J. Org. Chem.* **2003**, *68*, 7059.

(42) Tanaka, S.; Sugihara, Y.; Sakamoto, A.; Ishii, A.; Nakayama, J. *J. Am. Chem. Soc.* **2003**, *ASAP*.

(43) Ligroin is any petroleum distillate fraction wherein its boiling point is below 150 °C. Common names for Ligroin include benzine, mineral spirits, and VM&P naphtha though the term ligroin has been used as a substitute for petroleum ether and naphtha.

(44) Stamm, H.; Wintzer, H. *Ber.* **1937**, *70*, 2058.

(45) Hacklin, H.; Baltruschat, E.; Röschenthaler, G.-V. *Z. Anorg. Allg. Chem.* **1985**, *522*, 155.

(46) Wang, C. S.; Pullen, K. E.; Shreeve, J. n. M. *Inorg. Chem.* **1970**, *9*, 90.

(47) Denham, W. S.; Woodhouse, H. *J. Chem. Soc.* **1913**, 1861.

(48) Thompson, Q. E. *Patent # 3,376,322* United States, **1968**, 8

(49) Borghi, R.; Lunazzi, L.; Placucci, G.; Cerioni, G.; Plumitallo, A. *J. Org. Chem.* **1996**, *61*, 3327.

(50) Harpp, D. N.; Priefer, R.; Farrell, P. G. *Tetrahedron Lett.* **2002**, *43*, 8781.

(51) Tardif, S. Ph.D. thesis, McGill University, **1997**.

(52) Braverman, S.; Pechenick, T. *Tetrahedron Lett.* **2002**, *43*, 499.

(53) Braverman, S.; Pechenick, T.; Gottlieb, H. E. *Tetrahedron Lett.* **2003**, *44*, 777.

(54) Su, Y. Z.; Gong, K. C. *Mat. Res. Soc. Symp. Proc.* **2000**, *600*, 215.

(55) Röschenthaler, G.-V.; Storzer, W. *Phosphorus and Sulfur* **1978**, *4*, 373.

(56) Steudel, R.; Göbel, T.; Schmidt, H.; Holdt, G. *Fresenius Z. Anal. Chem.* **1989**, *334*, 266.

(57) Möckel, H. J.; Singer, E. *Chromatographia* **1989**, *27*, 27.

(58) Möckel, H. J.; Singer, E. *Journal of Liquid Chromatography* **1990**, *13*, 1499.

(59) Blaschette, A.; Näveke, M.; Jones, P. G. *Z. Naturforsch. B* **1991**, *46*, 5.

(60) Harpp, D. N.; Steliou, K.; Chan, T. H. *J. Am. Chem. Soc.* **1978**, *100*, 1222.

(61) Wenschun, E.; Ritzel, R. *Sulfur Letters* **1986**, *4(5)*, 161.

(62) Thompson, Q. E.; Crutchfield, M. M.; Dietrich, M. W. *J. Org. Chem.* **1965**, *30*, 2696.

(63) Price, C. C.; Berti, G. *J. Am. Chem. Soc.* **1954**, *76*, 1211.

(64) Langs, D. A.; Smith, G. D.; Stezowski, J. J.; Hughes, R. E. *Science* **1986**, *232*, 1240.

(65) The structure of oxytocin is Cys^1-Tyr^2-Ile^3-Gln^4-Asn^5-Cys^6-Pro^7-Leu^8-Gly^9-NH_2 containing a disulfide bridge between the two cysteine amino acids forming a

hexapeptide ring. The structure of vasopressin differs in two positions: Phe^3 and Arg^8. Both are neurohypophyseal hormones.

(66) Garrett, R. H.; Grisham, C. M. *Biochemistry*; 2 ed.; Saunders College Publishing: New York, **1995**; p.189.

(67) The H-H BDE = 104 kcal/mol; the C-C BDE = 79 kcal/mol.

(68) Oae, S. *Main Group Chemistry News* **1996**, *4*.

(69) Poisel, H.; Schmidt, U. *Angew. Chem., Int. Ed. Engl.* **1971**, *10*, 130.

(70) Hald, J.; Jacobsen, E.; Larsen, V. *Acta Pharmacol. Toxicol.* **1948**, *4*, 285.

(71) Nieuwenhuizen, P. J.; Ehlera, A. W.; Hofstraat, J. W.; Janse, S. R.; Nielsen, M. W. F.; Reedijk, J.; Barends, E. J. *Eur. J. Chem.* **1998**, *4*, 1816.

(72) Kato, S.; Hamada, Y.; Shiroji, T. *Tetrahedron Lett.* **1986**, *27*, 2653.

(73) Menger, F. M.; Caran, K. L. *J. Am. Chem. Soc.* **2000**, *122*, 11679.

(74) Winnewisser, G.; Haase, J. *Z. Naturforsch. A* **1968**, *23A*, 56.

(75) Winnewisser, G.; Winnewisser, M.; Gordy, W. *J. Chem. Phys.* **1968**, *49*, 3465.

(76) Winnewisser, G. *J. Mol. Spectrosc.* **1972**, *41*, 534.

(77) Redington, R. L. *J. Mol. Spectrosc.* **1962**, *9*, 469.

(78) Aida, M.; Nagata, C. *Theor. Chim. Acta* **1986**, *70*, 73.

(79) Winnewisser, G. *J. Chem. Phys.* **1972**, *56*, 2944.

(80) Winnewisser, G.; Helminger, P. *J. Chem. Phys.* **1972**, *56*, 2967.

(81) Hahn, J.; Schmidt, P.; Reinartz, K.; Behrend, J.; Winnewisser, G.; Yamada, K. M. T. *Z. Naturforsch.* **1991**, *46B*, 1338.

(82) Marsden, C. J.; Smith, B. J. *J. Phys. Chem.* **1988**, *92*, 347.

(83) Harmony, M. D.; Laurie, V. W.; Kuczkowski, R. L.; Schwendeman, R. H.; Ramsay, D. A.; Lovas, F. J.; Lafferty, W. J.; Maki, A. G. *J. Phys. Chem. Ref. Data* **1979**, *8*, 619.

(84) Herbst, E.; Winnewisser, G. *Chem. Phys. Lett.* **1989**, *155*, 572.

(85) Allen, H. C.; Plyler, E. K. *J. Chem. Phys.* **1956**, *25*, 1132.

(86) Ha, T.-K.; Nguyen, M. T.; Vanquickenborne, L. G. *J. Mol. Str. (THEOCHEM)* **1982**, *90*, 107.

(87) Ha, T.-K.; Nguyen, M. T.; Vanquickenborne, L. G. *J. Mol. Str. (THEOCHEM)* **1982**, *90*, 99.

(88) Cremer, D. *J. Chem. Phys.* **1978**, *82*, 3322.

(89) Blair, R. A.; Goddard III, W. A. *J. Am. Chem. Soc.* **1982**, *104*, 2719.

(90) Cárdenas-Jirón, G. I.; Cárdenas-Lailhacar, C.; Toro-Labbé, A. *J. Mol. Str. (THEOCHEM)* **1993**, *282*, 113.

(91) Hinchliffe, A. *J. Mol. Struct.* **1979**, *55*, 127.

(92) Ha, T.-K. *J. Mol. Str. (THEOCHEM)* **1985**, *122*, 225.

(93) Boyd, R. J.; Perkyns, J. S.; Ramani, R. *Can. J. Chem.* **1983**, *61*, 1082.

(94) Dixon, D. A.; Zeroka, D.; Wendoloski, J. J.; Wasserman, Z. R. *J. Phys. Chem.* **1985**, *89*, 5334.

(95) Steudel, R.; Laitinen, R. S.; Pakkanen, T. A. *J. Am. Chem. Soc.* **1987**, *109*, 710.

(96) Samdal, S.; Mastryukov, V. S.; Boggs, J. E. *J. Mol. Struct. (THEOCHEM)* **1994**, *309*, 21.

(97) Bickelhaupt, F. M.; Solà, M.; Schleyer, P. v. R. *J. Comput. Chem.* **1995**, *16*, 465.

(98) Steudel, R.; Drozdova, Y.; Miaskiewicz, K.; Hertwig, R. H.; Koch, W. *J. Am. Chem. Soc.* **1997**, *119*, 1900.

(99) Koput, J. *Chem. Phys. Lett.* **1996**, *259*, 146.

(100) The average structural parameters represents a virtual structure and is placed solely for the reader's convenience.

(101) Flemming, I. *Frontier Orbitals and Organic Chemical Reactions*; John Wiley & Sons, **1996**.

(102) Mulliken, R. S. *J. Chem. Phys.* **1955**, *23*, 1833.

(103) Boyd, D. B. *J. Am. Chem. Soc.* **1972**, *94*, 8799.

(104) Steudel, R. *Top. Curr. Chem.* **1982**, *102*, 149.

(105) Freed, K. *Chem. Phys. Lett.* **1968**, *2*, 255.

(106) Laitinen, R.; Pakkanen, T. *J. Mol. Struct. (THEOCHEM)* **1985**, *124*, 293.

(107) Veillard, A.; Demuynck, J. *Chem. Phys. Lett.* **1970**, *4*, 476.

(108) Rauk, A. *J. Am. Chem. Soc.* **1984**, *106*, 6517.

(109) Lowe, J. P. *J. Am. Chem. Soc.* **1970**, *92*, 3799.

(110) Schleyer, P. v. R.; Kaupp, M.; Hampel, F.; Bremer, M.; Mislow, K. *J. Am. Chem. Soc.* **1992**, *114*, 6791.

(111) Pophristic, V.; Goodman, L. *Nature* **2001**, *411*, 565.

(112) Schreiner, P. R. *Angew. Chem. Int. Ed. Engl.* **2002**, *41*, 3579.

(113) The most stabilizing hyperconjugative interaction occurs in the ground state (n_S to $\sigma^*_{S\text{-}H}$) *vide supra.*

(114) Lowe, J. P. *J. Chem. Phys.* **1969**, *51*, 832.

(115) Veillard, A. *Chem. Phys. Lett.* **1969**, *4*, 51.

(116) The potential energy function $V(\tau)$ can be expanded as a trigonometric series of the form $V(\tau) = V_1\cos\tau + V_2\cos2\tau + V_3\cos3\tau + \ldots$ where V_n represents the *n*-fold torsional component. See: Koput, J. *Chem. Phys. Lett.* **1996**, *259*, 146

(117) Hunt, R. H.; Leacock, R. A.; Peters, C. W.; Hecht, K. T. *J. Chem. Phys.* **1965**, *42*, 1931.

(118) Smyth, C. P.; Lewis, G. L.; Grossman, A. J.; Jennings III, F. B. *J. Am. Chem. Soc.* **1940**, *62*, 1219.

(119) Sutter, D.; Dreizler, H.; Rudolph, H. D. *Z. Naturforsch.* **1965**, *20a*, 1676.

(120) Beagley, B.; McAloon, K. T. *Trans. Farady Soc.* **1971**, *67*, 3216.

(121) Yokozeki, A.; Bauer, S. H. *J. Phys. Chem.* **1976**, *80*, 618.

(122) Van Wart, H. E.; Shipman, L. L.; Scheraga, H. A. *J. Phys. Chem.* **1974**, *78*, 1848.

(123) Allinger, N. L.; Hickey, M. J.; Kao, J. *J. Am. Chem. Soc.* **1976**, *98*, 2741.

(124) Donohue, J.; Caron, A.; E., G. *J. Am. Chem. Soc.* **1961**, *83*, 3948.

(125) Abrahams, S. C. *Acta Cryst.* **1955**, *8*, 661.

(126) Scott, D. W.; Finke, H. L.; Gross, M. E.; Guthrie, G. B.; Huffman, H. M. *J. Am. Chem. Soc.* **1950**, *72*, 2424.

(127) Hubbard, W. N.; Douslin, D. R.; McCullough, J. P.; Scott, D. W.; Todd, S. S.; Messerly, J. F.; Hossenlopp, I. A.; George, A.; Waddington, G. *J. Am. Chem. Soc.* **1958**, *80*, 3547.

(128) El-Sabban, M. Z.; Scott, D. W. *U.S. Bur. Mines, Bull.* **1970**, *654*.

(129) Senning, A. *Sulfur in Organic and Inorganic Chemistry*; M. Dekker: New York, **1971**.

(130) Perahia, D.; Pullman, B. *Biochem. Biophys. Res. Commun.* **1971**, *43*, 65.

(131) Yamabe, H.; Kato, H.; Yonezawa, T. *Bull. Chem. Soc. Japan* **1971**, *44*, 604.

(132) Jiao, D.; Barfield, M.; Combariza, J. E.; Hruby, V. J. *J. Am. Chem. Soc.* **1992**, *114*, 3639.

(133) Reinhardt, L. A. Ph.D. thesis, University of Wisconsin-Madison, **1994**.

(134) The V_1 term is associated with dipole-dipole interactions. The V_2 term is associated with hyperconjugation. The V_3 term is associated with steric repulsion.

(135) Radom, L.; Hehre , W. J.; Pople, J. A. *J. Am. Chem. Soc.* **1972**, *94*, 2371.

(136) For an extensive survey of structural parameters of and empirical geometric relations in organic disulfides see: Higashi, L.; Lundeen, M.; Seff, K. *J. Am. Chem. Soc.* **1978**, *100*, 8101

(137) For a expansive survey of Raman spectra and structural parameters of cystine-related disulfides see: Van Wart, H. E.; Scheraga, H. A. *J. Phys. Chem.* **1976**, *80*, 1812

(138) For a review on the chiroptical properties of disulfides see: Rauk, A. *J. Am. Chem. Soc.* **1984**, *106*, 6517

(139) Ranganathan, D.; Haridas, V.; Nagaraj, R.; Karle, I. L. *J. Org. Chem.* **2000**, *65*, 4415.

(140) Extremely compressed disulfides with r(S-S) shorter than the shortest reported S-S bond (FSSF *vide infra*) should be regarded with great skepticism and may solely be the result of crystal packing forces.

(141) Van Wart, H. E.; Shipman, L. L.; Scheraga, H. A. *J. Phys. Chem.* **1975**, *79*, 1428.

(142) Snyder, James P.; Jørgensen, F. S. *Tetrahedron* **1979**, *35*, 1399.

(143) Karle, I. L.; Estlin, J. A.; Britts, K. *Acta Crystallogr. Sect. A* **1967**, *22*, 273.

(144) Harpp, D. N.; Priefer, R.; Lee, Y. J.; Barrios, F.; Wosnick, J. H.; Lebuis, A.-M.; Farrell, P. G.; Sun, A.; Wu, S.; Snyder, J. P. *J. Am. Chem. Soc.* **2002**, *124*, 5626.

(145) Snyder, J. P.; Jørgensen, F. S.; Rindorf, G. *J. Org. Chem.* **1980**, *45*, 5343.

(146) Snyder, J. P.; Jørgensen, F. S. *J. Org. Chem.* **1980**, *45*, 1015.

(147) Lee, J. D.; Bryant, M. W. R. *Acta Crystallogr. Sect. B* **1969**, *25*, 2497.

(148) Bernal, I.; Ricci, J. S. *Acta Crystallogr. Sect. A* **1966**, *21*, S104.

(149) Ostrowski, M.; Jeske, J.; Jones, P. G.; du Mont, W.-W. *Chem. Ber.* **1993**, *126*, 1355.

(150) Raghavan, N. V.; Seff, K. *Acta Crystallogr. Sect. B* **1977**, *33*, 386.

(151) Ricci, J. S.; Bernal, I. *Acta Crystallogr. Sect. A* **1969**, *25*, S149.

(152) Shefter, E.; Kalman, T. I. *Chem. Commun.* **1969**, 1027.

(153) Ricci, J. S.; Bernal, I. *J. Am. Chem. Soc.* **1969**, *91*, 4078.

(154) Woodard, C. M.; Brown, D. S.; Lee, J. D.; Massey, A. G. *J. Organomet. Chem.* **1976**, *12*, 333.

(155) Lee, J. D.; Bryant, M. W. R. *Acta Crystallogr. Sect. B* **1970**, *26*, 1729.

(156) Furberg, S.; Solbakk, J. *Acta Chem. Scand.* **1973**, *27*, 2536.

(157) Higashi, L.; Lundeen, M.; Seff, K. *J. Am. Chem. Soc.* **1978**, *100*, 8101.

(158) Shefter, E.; Kotick, M. P.; Bardos, T. J. *J. Pharm. Sci.* **1967**, *56*, 1293.

(159) Shefter, E.; Kalman, T. I. *Biochem. Biophys. Res. Commun.* **1968**, *30*, 878.

(160) Shefter, E. *J. Chem. Soc. B* **1970**, 903.

(161) Rosenfield Jr., R. E.; Parthasarathy, R. *Acta Crystallogr. Sect. B* **1975**, *31*, 462.

(162) Oughton, B. M.; Harrison, P. M. *Acta Crystallogr.* **1959**, *12*, 396.

(163) Foss, O.; Hordvik, A.; Sletten, J. *Acta Chem. Scand.* **1966**, *20*, 1169.

(164) Hordvik, A. *Acta Chem. Scand.* **1966**, *20*, 1885.

(165) Snyder, J. P.; Carlsen, L. *J. Am. Chem. Soc.* **1977**, *99*, 2931.

(166) Fraser, R. R.; Boussard, G.; Saunders, J. K.; Lambert, J. B. *J. Am. Chem. Soc.* **1971**, *93*, 3822.

(167) Benassi, R.; Fiandi, G. L.; Taddei, F. *J. Mol. Struct. (THEOCHEM)* **1997**, *418*, 127.

(168) Kessler, H.; Rundel, W. *Chem. Ber.* **1968**, *101*, 3350.

(169) The trend for calculated torsional barriers especially shows an increase in the *cis* barrier height.

(170) Hirota, E. *Bull. Chem. Soc. Japan* **1958**, *31*, 130.

(171) Kniep, R.; Korte, L.; Mootz, D. *Z. Naturforsch. B* **1983**, *38*, 1.

(172) Ackermann, P. G.; Mayer, J. E. *J. Chem. Phys.* **1936**, *4*, 377.

(173) Palmer, K. J. *J. Am. Chem. Soc.* **1938**, *60*, 2360.

(174) Beagley, B.; Eckersley, G. H.; Brown, D. P.; Tomlinson, D. *Trans. Farady Soc.* **1969**, *165*, 2300.

(175) Bock, H.; Solouki, B. *Inorg. Chem.* **1977**, *16*, 665.

(176) Brown, R. D.; Marsden, C. J.; Godfrey, P. D. *J. Chem. Soc. Chem. Commun.* **1979**, 399.

(177) Kuczkowski, R. L. *J. Am. Chem. Soc.* **1964**, *86*, 3617.

(178) Marsden, C. J.; Oberhammer, H.; Losking, O.; Willner, H. *J. Mol. Struct.* **1989**, *193*, 233.

(179) Solà, M.; Mestres, J.; Carbó, R.; Duran, M. *J. Am. Chem. Soc.* **1994**, *116*, 5909.

(180) Torrent, M.; Duran, M.; Sola, M. *J. Mol. Struct. (THEOCHEM)* **1996**, *362*, 163.

(181) Bowen, H. J. M. *Trans. Farady Soc.* **1954**, *50*, 432.

(182) Steudel, R. *Z. Naturforsch. B* **1971**, *26*, 750.

(183) Das, D.; Whittenburg, S. L. *J. Phys. Chem. A.* **1999**, *103*, 2134.

(184) Jursic, B. S. *J. Comput. Chem.* **1996**, *17*, 835.

(185) Alleres, D. R.; Cooper, D. L.; Cunningham, T. P.; Gerratt, J.; Karadakov, P. B. *J. Chem. Soc. Faraday Trans.* **1995**, *91*, 3357.

(186) Jursic, B. S. *J. Mol. Struct. (THEOCHEM)* **1996**, *366*, 97.

(187) Kuczkowski, R. L.; Wilson Jr., E. B. *J. Am. Chem. Soc.* **1963**, *85*, 2028.

(188) Myers, R. J.; Meschi, D. J. *J. Mol. Spectrosc.* **1959**, *3*, 405.

(189) Meyer, B.; Jensen, D.; Oommen, T. In *Sulfur in Organic and Inorganic Chemistry*; Senning, A., Ed.; Dekker: New York, 1972; Vol. 2, p 13.

(190) Iwasaki, F. *Acta Crystallogr. Sect. B* **1979**, *35*, 2099.

(191) Chivers, T.; Oakley, R. T.; Cordes, A. W.; Swepston, P. *J. Chem. Soc. Chem. Commun.* **1980**, *1*, 35.

(192) Lovas, F. J.; Tiemann, E.; Johnson, D. *J. Chem. Phys.* **1974**, *60*, 5005.

(193) Eliel, E. L.; Wilen, S. H. *Stereochemistry of Organic Compounds*; John Wiley & Sons, Inc.: Toronto, **1994**.

(194) Van Tamelen, E. E. *Acc. Chem. Res.* **1972**, *5*, 186.

(195) Wilzbach, K. E.; Kaplan, L. *J. Am. Chem. Soc.* **1965**, *87*, 4004.

(196) Den Besten, I. E.; Kaplan, L.; Wilzbach, K. E. *J. Am. Chem. Soc.* **1968**, *90*, 5868.

(197) Dabbagh, A.-M. M.; Flowers, W. T.; NHaszeldine, R. N.; Robinson, P. J. *J. Chem. Soc. Perkin. Trans. 2* **1979**, 1407.

(198) Mandella, W. L.; Franck, R. W. *J. Am. Chem. Soc.* **1973**, *95*, 971.

(199) Goldberg, I. B.; Crowe, H. R.; Franck, R. W. *J. Am. Chem. Soc.* **1976**, *98*, 7641.

(200) Dewar, M. J. S.; Kirschner, S.; Kollmar, H. W. *J. Am. Chem. Soc.* **1974**, *96*, 5240.

(201) Laerum, T.; Undheim, K. *J. Chem. Soc. Perkin. Trans. 1* **1979**, *5*, 1150.

(202) Kurita, J.; Iwata, K.; Sakai, H.; Tsuchiya, T. *Chem. Pharm. Bull.* **1985**, *33*, 4572.

(203) Messmer, A.; Hajós, G.; Giber, J.; Holly, S. *J. Heterocyclic Chem.* **1987**, *24*, 1133.

(204) Béres, M.; Hajós, G.; Riedl, Z.; Soós, T.; Timári, G.; Messmer, A. *J. Org. Chem.* **1999**, *64*, 5499.

(205) Kövér, P.; Hajós, G.; Riedl, Z.; Párkányi, L.; Kollenz, G. *Chem. Commun.* **2000**, *18*, 1785.

(206) Turnbull, K.; Kutney, G. W. *Chem. Rev.* **1982**, *82*, 333.

(207) Kutzelnigg, W. *Angew. Chem. Int. Ed. Engl.* **1984**, *23*, 272.

(208) Foss, O. In *Organic Sulfur Compounds*; Kharasch, N., Ed.; Pergammon Press Inc.: New York, 1961; Vol. 1, p 75.

(209) Kuczkowski, R. L. *J. Am. Chem. Soc.* **1963**, *85*, 3047.

(210) Seel, F.; Budenz, R. *Chem. Ber.* **1965**, *98*, 251.

(211) Seel, F.; Gombler, W.; Budenz, R. *Liebigs Ann. Chem.* **1970**, *735*, 1.

(212) Pez, G. P.; Brown, R. D. *Aust. J. Chem.* **1967**, *20*, 2305.

(213) Brown, R. D.; Burden, F. R.; Pez, G. P. *J. Chem. Soc. Chem. Commun.* **1965**, 277.

(214) Gombler, W.; Schaebs, J.; Willner, H. *Inorg. Chem.* **1990**, *29*, 2697.

(215) Davis, R. W.; Firth, S. *J. Mol. Spectrosc.* **1991**, *145*, 225.

(216) Seel, F.; Budenz, R. *Chimia* **1963**, *17*, 355.

(217) Seel, F.; Gölitz, D. *Z. Anorg. Allg. Chem.* **1964**, *327*, 32.

(218) Cao, X.; Qiao, C.; Wang, D. *Chem. Phys. Lett.* **1998**, *290*, 405.

(219) Lösking, O.; Willner, H.; Baumgärtel, H.; Jochims, H. W.; Rühl, E. *Z. Anorg. Allg. Chem.* **1985**, *530*, 169.

(220) Cao, X.; Qian, X.; Qiao, C.; Wang, D. *Chem. Phys. Lett.* **1999**, *299*, 322.

(221) A barrier of 36.7 kcal/mol for this same isomerization mechanism has been calculated at the MP2/6-31+G* level Snyder, J. P.; Harpp, D. N. unpublished results

(222) Allred, A. L.; Rochow, E. *J. Inorg. Nucl. Chem.* **1950**, *5*, 264.

(223) Reid, E. E.; Macy, R.; Jarman, G. N.; Morrison, A. *Science* **1947**, 355.

(224) Spong, A. H. *J. Chem. Soc.* **1934**, 485. and references cited therein

(225) Amaresh, R. R.; Lakshmikantham, M. V.; Baldwin, J. W.; Cava, M. P.; Metzger, R. M.; Rogers, R. D. *J. Org. Chem.* **2002**, *67*, 2453.

(226) Gerding, H. *J. Chim. Phys.* **1948**, *46*, 118.

(227) Bradley, E. B.; Mathur, M. S.; Frenzel, C. A. *J. Chem. Phys.* **1967**, *47*, 4325.

(228) Frankiss, S. G. *J. Mol. Struct.* **1968**, *2*, 271.

(229) Steudel, R.; Jensen, D.; Plinke, B. *Z. Naturforsch. B* **1987**, *42*, 163.

(230) Frenzel, C. A.; Blick, K. E. *J. Chem. Phys.* **1971**, *55*, 2715.

(231) Colton, R. J.; Rabalais, J. W. *Journal of Electron Spectroscopy and Related Phenomena* **1974**, *3*, 345.

(232) Yao, M.; Kawakita, Y.; Takahiro, S.; Yamamoto, I.; Endo, H. *J. Phys. Soc. Japan* **1997**, *66*, 3115.

(233) Chadwick, B. M.; Grzybowski, J. M.; Long, D. A. *J. Mol. Struct.* **1978**, *48*, 139.

(234) Feuerhahn, M.; Vahl, G. *Chem. Phys. Lett.* **1979**, *65*, 322.

(235) Das, D.; Whittenburg, S. L. *J. Phys. Chem. A.* **1993**, *103*, 2134.

(236) Steudel, R.; Schmidt, H.; Sülzle, D.; Schwarz, H. *Inorg. Chem.* **1992**, *31*, 941.

(237) Using NRMS, HOSSOH is stable for only 10^{-5} s under highly dilute conditions in the gas phase.

(238) Steudel, R.; Schmidt, H. *Z. Naturforsch.* **1990**, *45B*, 557.

(239) HSOH is significantly more stable than $H_2S{=}O$. See: Wallmeier, H.; Kutzelnigg, W. *J. Am. Chem. Soc.* **1979**, *101*, 2804

(240) Steudel, R.; Gleiter, R.; Hyla-Kryspin, I.; Schmidt, H. *Chem. Ber.* **1993**, *126*, 2363.

(241) A'Hearn, M. F.; Feldman, P. D.; Schleicher, D. G. *Astrophys. J.* **1983**, *274*, L99.

(242) Greenwood, N. N.; Earnshaw, A. *Chemistry of the Elements*; Pergamon Press: New York, **1984**; p.775.

(243) Spencer, J. R.; Jessup, K. L.; McGrath, M. A.; Ballester, G. E.; Yelle, R. *Science* **2000**, *288*, 1208.

(244) Spencer, J. R.; Rathbun, J. A.; Travis, L. D.; Tamppari, L. K.; Barnard, L.; Martin, T. Z.; McEwen, A. S. *Science* **2000**, *288*, 1198.

(245) Spencer, J. R.; McEwen, A. S.; McGrath, M. A.; Sartoretti, P.; Nash, D. B.; Noll, K. S.; Gilmore, D. *Icarus* **1997**, *127*, 221.

(246) Geissler, P. E.; McEwen, A. S.; Keszthelyi, L.; Lopes-Gautier, R.; Granahan, J.; Simonelli, D. P. *Icarus* **1999**, *140*, 265.

(247) Noll, K. S.; McGrath, M. A.; Trafton, L. M.; Atreya, S. K.; Caldwell, J. J.; Weaver, H. A.; Yelle, R. V.; Barnet, C.; Edgington, S. *Science* **1995**, *267*, 1307.

(248) Meyer, B.; Stroyer-Hansen, T. *J. Phys. Chem.* **1972**, *76*, 3968.

(249) Gilchrist, T. L.; Wood, J. E. *J. Chem. Soc. Chem. Commun.* **1992**, 1460.

(250) Steliou, K. *Acc. Chem. Res.* **1991**, *24*, 341.

(251) Harpp, D. N.; Tardif, S. L.; Rys, A. Z.; Abrams, C. B.; Abu-Yousef, I. A.; Lesté-Lassere, P.; Schultz, E. K. V. *Tetrahedron* **1997**, *53*, 12225.

(252) Harpp, D. N. *Phosphorus, Sulfur and Silicon* **1997**, *120 & 121*, 41.

(253) Lesté-Lassere, P. Ph.D. thesis, McGill, **2001**.

(254) Steliou, K.; Gareau, Y.; Milot, G.; Salama, P. *J. Am. Chem. Soc.* **1990**, *112*, 7819.

(255) Wasserman, H. H.; Murray, R. W. *Singlet Oxygen*; Academic Press: New York, **1989**.

(256) Harpp, D. N.; Steliou, K.; Gareau, Y. *J. Am. Chem. Soc.* **1984**, *106*, 799. and references cited therein.

(257) Miscallef, A. S.; Bottle, S. E. *Tetrahedron Lett.* **1997**, *38*, 2303.

(258) Borghi, R.; Guidi, B.; Placucci, G.; Lunazzi, L. *J. Org. Chem.* **1996**, *61a*, 5667.

(259) Braverman, S.; Stabinsky, Y. *J. Chem. Soc. Chem. Commun.* **1967**, 270.

(260) Block, E. *Angew. Chem. Int. Ed. Engl.* **1992**, *31*, 1135.

(261) Kobayashi, M.; Minato, H.; Shimada, K. *Int. J. Sulfur Chem., A* **1971**, *1*, 105.

(262) Radiolabelling H_2O^{18} experiments indicate that the oxygen in sulfite **101** did not arise from thus source.

(263) Motoki, S.; Kagami, H.; Satsumabayashi, H. *J. Org. Chem.* **1977**, *42*, 958.

(264) Motoki, S.; Kagami, H. *J. Org. Chem.* **1977**, *42*, 4139.

(265) Steudel, R.; Schmidt, H. *Chem. Ber.* **1994**, *127*, 1219.

(266) Motoki, S.; Kagami, H. *Bull. Chem. Soc. Japan* **1979**, *52*, 3463.

(267) Hey, D. H.; Waters, W. A. *J. Chem. Soc.* **1948**, 882.

(268) Motoki, S.; Kagami, H.; Hanzawa, T.; Suzuki, N.; Yamaguchi, S.; Saito, M. *Bull. Chem. Soc. Japan* **1980**, *53*, 3658.

(269) Hoepping, A.; Mayer, R. *Bull. Soc. Chim. Belg.* **1994**, *103*, 389.

(270) Hoepping, A.; Mayer, R. *Phosphorus, Sulfur and Silicon* **1995**, *1-7*, 285.

(271) Smith, J. D.; O'Hair, R. A. J. *Phosphorus, Sulfur and Silicon And The Related Elements* **1997**, *126*, 257.

(272) Meuwsen, A.; Gebhardt, H. *Ber.* **1936**, *69*, 937.

(273) Meuwsen, A.; Gebhardt, H. *Ber.* **1935**, *68*, 1011.

(274) Matsuyama, H.; Minato, H.; Kobayashi, M. *Bull. Chem. Soc. Japan* **1973**, *46*, 2845.

(275) Matsuyama, H.; Minato, H.; Kobayashi, M. *Bull. Chem. Soc. Japan* 1973, *46*, 3158.

(276) Matsuyama, H.; Minato, H.; Kobayashi, M. *Bull. Chem. Soc. Japan* 1973, *46*, 3828.

(277) Trost, B. M. *J. Am. Chem. Soc.* 1967, *89*, 138.

Chapter 3

Theoretical Modeling of Alkoxy Disulfides and Thionosulfites

3.1 Introduction

As was detailed in Chapter 2, the dialkyl disulfide moiety exists as a chiral, four atom fragment (R-S-S-R) containing two S-C bonds and a torsional barrier to racemization of *ca.* 7 kcal/mol (as in **71a**). Recently, it was shown[1] that the alkoxy disulfides **1** sustain a barrier to rotation *ca.* 10 kcal/mol higher than that of dialkyl disulfides (our own current work in this area is detailed in Chapter 4). Furthermore unlike disulfides, alkoxy disulfides have the capacity to exist as stable entities in their branch-bonded isomeric thionosulfite form **2**. At present, only a single general substitution pattern for **2** has been observed (wherein the carbon atoms in **2** are bound to form a 5-membered ring as in **5**).

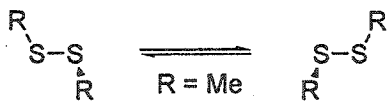

71a

Part of our focus in this area is to understand the factors that affect the stability of each isomer, the isomerization mechanism and the torsional barriers of alkoxy disulfides. In this way, we hope to identify and synthesize alkoxy disulfides with rotational barriers that exceed 18 kcal/mol sufficiently so that the chiral atropisomers can be isolated as stable entities under ambient temperature conditions. Enantiomeric resolution has already been achieved for sulfenamides ($RS\text{-}NR_2$) at 0 °C.[2] In addition, we seek to identify stable classes of branch-bonded thionosulfite structures that permit an exploration of their chemistry beyond the single ring type. As will be seen, much of this work has come to fruition and the synthetic results are highlighted in Chapters 4-6.

One approach to achieve these goals is to learn which levels of quantum theory provide accurate predictions of molecular geometry and torsional energy barriers at modest computational cost. The motive for such an examination is the unusual contiguity of multiple lone pair bearing atoms in both **1** and **2**. With such protocols in hand, we can apply the theory to molecules of sufficient complexity that it will be able to partner and pace our active synthetic program. Accordingly, we have examined the equilibrium geometric structure, torsional potential and isomerization for a model system of **1** and **2**. We conclude with recommendations for an efficient approach to treat systems such as **1** and **2**.[§]

3.2 Computational Methodology

All *ab initio* calculations were carried out with the GAUSSIAN 94[3] and GAUSSIAN 98[4] series of programs as well as the Natural Bond Order (NBO) program.[5-10] Geometries for dialkoxy disulfides **1** and branch-bonded thionosulfites **2** were evaluated computationally using both Restricted Hartree-Fock (RHF)[11] self-consistent field (SCF) and second-order Møller-Plesset (MP2)[12,13] pertubation theories. In addition, density

---

[§] It should be noted that the work contained within this Chapter is the result of a collaborative effort. Drs. Neysa Nevins of Glaxo-Smith Kline (formerly of Emory University) and Dr. James Snyder of Emory Univeristy contributed to the calculations as well as the analysis.

functionals[14,15] were used as they often yield superior results in a shorter amount of time. Becke's three-parameter exchange function (B3)[15] was used in conjunction with each of three sets of correlation functionals: The Lee, Yang and Parr (LYP)[16,17] non-local functional, the Perdew (P86)[18,19] gradient-corrected functional and the Perdew and Wang (PW91)[20,21] gradient-corrected functional. These combined exchange and correlation functionals are commonly referred to as B3LYP, B3P86 and B3PW91. In addition, the Slater exchange functional with the Vosko, Wilk and Nusair correlational functional (SVWN)[22,23] was used. The effects of systematic increase in basis set size along with the addition of diffuse and polarization functions was investigated for ground state geometries. The following Pople double split valence basis sets[24-28] were employed: 6-31G(d), 6-31G(2d), 6-31G(df), 6-31G(2df), 6-31G(3d), 6-31G(3df), and 6-31G(3d2f). Triple split valence basis sets[29,30] with the same series of polarization functions were also used at the MP2 level. The role of diffuse functions was also examined. Geometries were also calculated based on Allinger's MM3(94)[31] and our[32] modified[§] MM3* force fields (see Chapter **1.4** for an overview of the different classes of computational methods).

Ground state and transition state energy differences for conformers of MeOSSOMe **6** were determined by carrying out single point calculations at the HF, B3LYP, MP2, and MP3[33,34] levels of theory with the aforementioned basis sets. Geometry optimization and zero point vibrational energies (ZPVEs) were also performed with the B3LYP and B3P86

[§] Details on our modifications of the MM3* force field may be obtained from Dr. James P. Snyder, Emory University (snyder@heisenbug.chem.emory.edu).

functionals. Vibrational frequencies were calculated to confirm the existence of ground ($N_{imag} = 0$) and transition states ($N_{imag} = 1$).

3.3 Results and Discussion

3.3.1 Geometries of MeOSSOMe – Literature Review

The equilibrium geometry of MeOSSOMe **6** has been studied. This compound is the dimethyl ester of thiosulfurous acid $H_2S_2O_2$. *Ab initio* calculations on this parent compound indicate that three isomeric forms exist which are of comparable energies (*cf.* Chapter **2.5.4**, Table **25**) with their relative stabilities dependent on the sophistication of the calculation.[35] The unbranched isomer HOSSOH **95a** has been generated in the gas phase[36] and two stable conformers have been calculated;[35] one possesses C_1 symmetry while the other displays C_2 symmetry.

Steudel and co-workers reported the photoelectron spectrum of **6**.[37] Their initial low level *ab initio* (HF-SCF/3-21G*) and semiempirical (MNDO) calculations indicated that **6** exists as a mixture of three rotamers **6a-6c**.

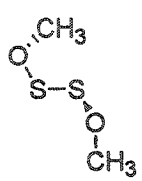

6a

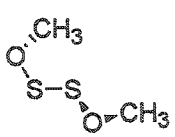

6b

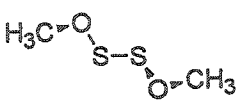

6c

A common τ(S-S) angle of *ca.* 83-95° was recorded, similar to that observed for most XSSX systems (*cf.* Chapter 2.4). The preference for this *gauche* conformation is usually attributed to a minimization of lone pair interactions.[38] The three conformers differ mainly in their two τ(S-O) angles α and β. A summary of the observed torsional angles is shown in Table 26.

Table 26. Observed dihedral angles deduced from the PE spectrum for three conformers of MeOSSOMe **6**

torsional angles (°)	**6a**	**6b**	**6c**
τ(S-S)	83.1	83.5	95.1
τ(S-O) α	76.1	81.3	-98.1
τ(S-O) β	76.1	-75.4	-98.1

Steudel and co-workers' calculations in combination with PE spectra permitted an estimate of the torsional parameters of conformers **6a** and **6b** but not **6c**. They thus determined that the order of stability was **6a** > **6b** > **6c**. Theoretically, one would expect that three enantiometric pairs of conformers should exist for both **6** and **95a**, corresponding to rotation about each of the two S-O bonds and the one S-S bond. Thus, torsional angles about chalcogen-chalcogen bonds can be represented in terms of their helical twist (using Cahn-Ingold-Prelog (CIP) nomenclature, a positive dihedral angle is denoted by a P conformation while a negative dihedral angle is denoted by an M conformation). The combinations are shown in Table 27.

Table 27. Different expected rotomers for **6**.

rotamer	Cmpd	Symmetry
P,P,P (+/+/+)	**6a**	C_2
P,P,M (+/+/-)	**6b**	C_1
M,P,M (-/+/-)	**6c**	C_2

Whereas in the solid state[39] **6a** was found as the sole conformer by low temperature (-158 °C) X-ray crystallography where its geometry deviates slightly from an idealized C_2 symmetry,[40] **6b** dominates in the gas phase.[39] The main difference in the parameters of **6** between the two experimental methods is that the observed τ(S-S) in the ED data is 10° larger than that of the crystal structure (*c.f.* for *e.g.* Table **28**). In addition, the nonbonding O···H distances are all larger than their respective van der Waals radii,[41] indicating that hydrogen bonding can be excluded as an attractive force.

The initial calculational work by Steudel and co-workers at the HF/3-21G* and HF/6-311G** level, did not accurately predict the structural parameters of **6**, though **6b** was predicted to be the most stable conformer (4.2 kcal/mol more stable than **6a** and 11.4 kcal/mol more stable than **6c**). To date, no theoretical modeling on the structures of thionosulfites has been performed.

3.3.2 Geometries of MeOSSOMe – Current Work

An extensive series of calculations for unbranched **6** and branch-bonded **5a** and **5d** (*cf.* Chapter **2.1** for structures) were carried out at the HF, density functional (SVWN, B3LYP, B3P86, B3PW91), and MP2 levels of theory with the aforementioned basis sets. Calculated structural parameters were then compared to both the solid state[39] and gas phase[42] geometries.[43] These results are summarized in Tables **28-33** with a numbering scheme consistent with that defined in the X-ray structure (Figure **4**).

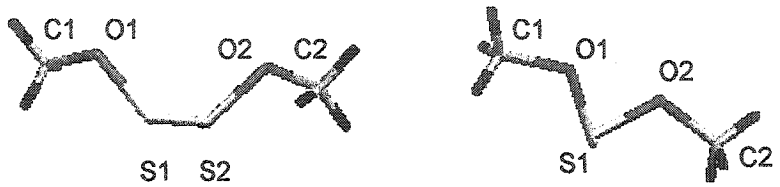

A B

Figure 4. A) Stick representation of MeOSSOMe **6**. B) Newman Projection of **6** along S-S bond

Both the HF (Tables **28** and **29**) and B3LYP (Tables **30** and **31**) methods overestimate the S-S bond length even with the use of large basis sets (0.03-0.05 Å and 0.02-0.04 Å, respectively). Although the geometry did not converge, the inclusion of polarization functions was necessary in order to predict a r(S-S) < 2 Å. In fact, the predicted S-S bond length approached that of the experimental parameters, albeit only asymptotically. The use of triple split valence basis sets or the inclusion of diffuse functions while using the B3LYP method did not significantly alter the predicted S-S bond length (Table **31**). These result are not surprising considering that these methods similarly overestimated the r(S-S) in S_2Cl_2 **77a** and S_2F_2 **75a** (Chapter **2.4.4**, Table **20**).

While HF slightly underestimated the S-O bond lengths (by 0.02-0.04 Å), B3LYP consistently overestimated them by 0.01-0.03 Å (*cf.* Tables **28-31**). In fact, as a general rule, the inclusion of polarization functions shortened the chalcogen-chalcogen bond length. In the case of the S-O bond lengths, this led to a divergence from both experimentally determined geometries. For instance, the calculated r(S-O) at the HF/6-31G(2df) level were shorter by greater than 0.03 Å.

B3LYP was able to consistently reproduce the r(C-O) separation, though HF underestimated this bond length as well. Both methods were able to accurately predict both the bond and dihedral angles. In general, bond and dihedral angles differed from experiment by approximately 1-2° and 5-8°, respectively. The errors for the τ(S-S) and τ(S-O) dihedral angles are reasonable, due to the shallow potential of each minimum (*vide infra*, Figure 6). Even with increasing basis set size, convergence to experiment was never fully realized using either HF or B3LYP. These two methods proved insufficient[44] to accurately predict the alkoxy disulfide system with the HF method being the worst predictor of the methods tried.

Interestingly, the 3-21G* basis set reproduced the bond lengths overall more accurately than the 6-31G* basis set using the HF method (*cf.* Tables **28-29**). This is most likely due to a cancellation of errors.

Table **28**. Geometry optimization of **6** using the HF method with small basis sets.

	ED[42]	X-ray[39]	HF/	
			3-21G*	3-21+G*
Bond Lengths (Å)				
S1–S2	1.960	1.972	1.991	1.994
S1–O5	1.653	1.658	1.654	1.659
S2–O3	1.653	1.658	1.646	1.65
O3–C4	1.432	1.435	1.461	1.467
O5–C6	1.432	1.435	1.456	1.465
Bond Angles (°)				
S1–S2–O3	108.2	108.2	104.8	105.2
S1–O5–C6	114.5	114.5	117.6	119.4
S2–S1–O5	108.2	108.2	104.8	105.1
S2–O3–C4	114.5	114.5	116.3	119.7
Dihedral Angles (°)				
S1–S2–O3–C4	-74	-75	-76	-79.3
S2–S1–O5–C6	74	75	81	84.2
O3–S2–S1–O5	91	82	84	86.2

Table 29. Geometry optimization of 6 using the HF method with different basis sets.

	ED[42]	X-ray[39]	HF/							
			6-31G*	6-31+G*	6-31G(2d)	6-31G(df)	6-31G(3d)	6-31G(2df)	6-31G(3df)	6-31G(3d2f)
Bond Lengths (Å)										
S1–S2	1.960	1.972	2.007	2.011	2.008	2.003	1.997	1.997	1.990	1.991
S1–O5	1.653	1.658	1.645	1.644	1.647	1.631	1.633	1.625	1.619	1.618
S2–O3	1.653	1.658	1.638	1.636	1.640	1.624	1.626	1.619	1.612	1.612
O3–C4	1.432	1.435	1.414	1.415	1.411	1.411	1.413	1.409	1.410	1.410
O5–C6	1.432	1.435	1.412	1.413	1.409	1.409	1.411	1.408	1.409	1.409
Bond Angles (°)										
S1–S2–O3	108.2	108.2	105.5	105.6	106.3	106.0	106.3	106.5	106.8	106.7
S1–O5–C6	114.5	114.5	116.5	117.1	116.3	117.1	117.1	117.4	117.7	117.7
S2–S1–O5	108.2	108.2	105.6	105.7	106.5	106.1	106.5	106.7	106.9	106.9
S2–O3–C4	114.5	114.5	116.5	117.5	116.3	117.1	117.2	117.4	117.9	117.9
Dihedral Angles (°)										
S1–S2–O3–C4	-74	-75	-83	-83	-82	-82	-81	-82	-82	-82
S2–S1–O5–C6	74	75	85	85	82	85	82	82	82	82
O3–S2–S1–O5	91	82	87	87	86	87	86	86	86	86

Table 30. Geometry optimization of 6 using the B3LYP hybrid method with different double split basis sets.

	ED[42]	X-ray[39]	B3LYP/						
			6-31G*	6-31G(2d)	6-31G(df)	6-31G(3d)	6-31G(2df)	6-31G(3df)	6-31G(3d2f)
Bond Lengths (Å)									
S1–S2	1.960	1.972	2.028	2.015	2.024	2.000	2.008	1.994	1.994
S1–O5	1.653	1.658	1.695	1.694	1.682	1.684	1.673	1.669	1.669
S2–O3	1.653	1.658	1.688	1.687	1.674	1.677	1.666	1.662	1.661
O3–C4	1.432	1.435	1.435	1.431	1.434	1.434	1.431	1.434	1.433
O5–C6	1.432	1.435	1.433	1.429	1.432	1.433	1.429	1.432	1.432
Bond Angles (°)									
S1–S2–O3	108.2	108.2	107.4	108	107.7	108.1	108.0	108.3	108.3
S1–O5–C6	114.5	114.5	114.7	115	115	115.6	115.6	115.9	115.8
S2–S1–O5	108.2	108.2	107.7	108.3	107.9	108.4	108.3	108.5	108.5
S2–O3–C4	114.5	114.5	114.4	114.8	114.8	115.6	115.4	116	115.8
Dihedral Angles (°)									
S1–S2–O3–C4	-74	-75	-81	-81	-81	-81	-81	-81	-81
S2–S1–O5–C6	74	75	81	78	81	79	79	80	80
O3–S2–S1–O5	91	82	87	87	87	87	87	87	87

Table 31. Geometry optimization of 6 using the B3LYP hybrid method with different triple split basis sets.

	ED[42]	X-ray[39]	B3LYP/				
			6-311G*	6-311G(2d)	6-311G(3d)	6-311G(2df)	6-311+G(2df)
Bond Lengths (Å)							
S1–S2	1.960	1.972	2.034	2.018	2.002	2.003	2.003
S1–O5	1.653	1.658	1.695	1.687	1.681	1.675	1.677
S2–O3	1.653	1.658	1.687	1.679	1.673	1.667	1.669
O3–C4	1.432	1.435					
O5–C6	1.432	1.435					
Bond Angles (°)							
S1–S2–O3	108.2	108.2	107.0	107.7	108.2	107.5	108.2
S1–O5–C6	114.5	114.5	115.3	115.0	115.7	115.7	115.9
S2–S1–O5	108.2	108.2	107.3	108.1	108.5	108.0	108.4
S2–O3–C4	114.5	114.5	115.0	114.7	115.6	115.4	116.2
Dihedral Angles (°)							
S1–S2–O3–C4	-74	-75					
S2–S1–O5–C6	74	75					
O3–S2–S1–O5	91	82					

The SVWN method with the Slater exchange term (local spin density exchange contrasted with the non-local Becke3 exchange term) and VWN correlation term, reproduced experimental results closely when the basis set included three d and one f polarization functions (*cf.* Table **32**). The inclusion of diffuse functions did not appreciably influence the predicted geometry. This was expected as diffuse functions describe the shape of the wave function far from the nucleus and are used to model charged compounds such as anions. Only the C-O bond lengths were not within experimental error as they were overestimated by *ca.* 0.02 Å. Results using the SVWN method for the analogous FOOF[45] and FSSF[46] systems have been reported by Jursic. He determined that the SVWN method, with a sufficiently large basis set, reproduced the microwave geometries of both FOOF[47] and FSSF[48] with great accuracy. Thus it should not be surprising that this DFT method performs well for the dialkoxy disulfide system.

Probing the inclusion of polarization functions in greater detail, we observe that as d functions are included in the calculation, the S-S bond length converges to experiment. However, full convergence is not achieved, even with three d functions. The addition of an f function is also required for both accurate r(S-S) and r(S-O) (*cf.* Table **32**). In fact it is the contribution of the f polarization function that seems to have the greatest impact upon this convergence. This is most evident by comparing the increase in accuracy of the r(S-O) predictions at the 6-311G(1d) level to that at the 6-311G(df) level *versus* at the 6-311G(2d) level.

The Becke3 exchange term with either the P86 or PW91 dynamic correlation terms (B3P86 and B3PW91) resulted in geometries that were reasonably close to experiment (*cf.* Tables **33** and **34**) though these two methods also underestimated the r(C-O) distance. A large basis set containing three d and one f polarization functions was required to accurately predict the experimental structural parameters. It has been reported that large basis sets are required with DFT methods for calculating bond lengths involving second-row atoms, as is the case here.[49] The inclusion of diffuse functions did not appreciably improve the geometry as evidenced in Table **35**. It would seem that the good predictions using the aforementioned DFT methods result from the inclusion of correlation inherent in DFT calculations.

It is not clear why the LYP dynamic correlation term is insufficient to reproduce the experimental geometries for this particular system even though the B3LYP method is widely used in the literature to accurately reproduce geometries of small organic molecules including the analogous FSSF system.[46]

Table 32. Geometry optimization of **6** using the SVWN method with different basis sets.

	ED[42]	X-ray[39]	SVWN/									
			6-31G*	6-31+G*	6-311+G*	6-31G(2d)	6-31G(df)	6-31G(3d)	6-31G(2df)	6-31G(3df)	6-31G(3d2f)	6-311+G(2df)
Bond Lengths (Å)												
S1–S2	1.960	1.972	1.994	1.992	1.992	1.974	1.990	1.961	1.970	1.958	1.954	1.963
S1–O5	1.653	1.658	1.684	1.688	1.690	1.683	1.672	1.674	1.662	1.659	1.658	1.666
S2–O3	1.653	1.658	1.676	1.679	1.680	1.673	1.664	1.665	1.654	1.651	1.650	1.658
O3–C4	1.432	1.435	1.415	1.417	1.412	1.410	1.414	1.413	1.410	1.413	1.413	
O5–C6	1.432	1.435	1.412	1.415	1.410	1.407	1.412	1.411	1.408	1.411	1.411	
Bond Angles (°)												
S1–S2–O3	108.2	108.2	107.8	107.7	107.6	108.4	108.0	108.6	108.2	108.6	108.6	108.1
S1–O5–C6	114.5	114.5	113.3	114.0	114.3	113.6	113.5	114.1	114.3	114.3	114.1	114.2
S2–S1–O5	108.2	108.2	107.7	107.7	107.5	108.2	107.9	108.2	108.1	108.3	108.3	108.0
S2–O3–C4	114.5	114.5	112.5	113.9	114.1	112.9	112.8	113.7	114.3	114.0	113.8	114.2
Dihedral Angles (°)												
S1–S2–O3–C4	-74	-75	-74	-74	-73	-73	-74	-72	-73	-72	-72	
S2–S1–O5–C6	74	75	73	76	75	67	73	68	73	69	70	
O3–S2–S1–O5	91	82	86	88	87	86	86	87	88	87	87	

Table 33. Geometry optimization of 6 using the B3P86 hybrid method with different basis sets.

	ED[42]	X-ray[39]	B3P86/						
			6-31G*	6-31G(2d)	6-31G(df)	6-31G(3d)	6-31G(2df)	6-31G(3df)	6-311+G(2df)
Bond Lengths (Å)									
S1–S2	1.960	1.972	2.006	1.993	2.002	1.980	1.986	1.975	1.980
S1–O5	1.653	1.658	1.683	1.683	1.670	1.672	1.663	1.658	1.664
S2–O3	1.653	1.658	1.676	1.676	1.663	1.665	1.656	1.651	1.657
O3–C4	1.432	1.435	1.427	1.423	1.425	1.426	1.422	1.425	
O5–C6	1.432	1.435	1.425	1.421	1.424	1.424	1.421	1.423	
Bond Angles (°)									
S1–S2–O3	108.2	108.2	107.5	108.1	107.8	108.8	108.1	108.4	108.2
S1–O5–C6	114.5	114.5	114.2	114.4	114.5	115.0	115.1	115.3	115.3
S2–S1–O5	108.2	108.2	107.6	108.3	107.9	108.4	108.3	108.5	108.4
S2–O3–C4	114.5	114.5	114.0	114.3	114.4	115.0	114.9	115.4	115.6
Dihedral Angles (°)									
S1–S2–O3–C4	-74	-75	-80	-80	-80	-79	-79	-79	
S2–S1–O5–C6	74	75	80	77	80	77	78	78	
O3–S2–S1–O5	91	82	88	88	88	87	87	87	

Table 34. Geometry optimization of 6 using the B3PW91 hybrid method with different basis sets.

	ED[42]	X-ray[39]	B3PW91/					
			6-31G*	6-31G(2d)	6-31G(df)	6-31G(3d)	6-31G(2df)	6-31G(3df)
Bond Lengths (Å)								
S1–S2	1.960	1.972	2.008	1.995	2.004	1.982	1.988	1.977
S1–O5	1.653	1.658	1.686	1.686	1.673	1.675	1.666	1.661
S2–O3	1.653	1.658	1.679	1.679	1.666	1.668	1.659	1.654
O3–C4	1.432	1.435	1.428	1.425	1.427	1.427	1.424	1.426
O5–C6	1.432	1.435	1.427	1.423	1.426	1.426	1.423	1.425
Bond Angles (°)								
S1–S2–O3	108.2	108.2	107.7	108.3	108.0	108.4	108.3	108.5
S1–O5–C6	114.5	114.5	114.4	114.5	114.7	115.1	115.2	115.4
S2–S1–O5	108.2	108.2	107.8	108.6	108.1	108.5	108.5	108.7
S2–O3–C4	114.5	114.5	114.2	114.4	114.5	115.2	115.1	115.6
Dihedral Angles (°)								
S1–S2–O3–C4	-74	-75	-82	-81	-81	-80	-81	-80
S2–S1–O5–C6	74	75	81	78	81	78	79	79
O3–S2–S1–O5	91	82	88	88	88	88	88	87

Table 35. Comparison of optimized geometries of **6** using DFT methods with and without diffuse functions.

	B3LYP/				B3P86/			
	6-31+G(2d)	Δ[a]	6-31+G(3df)	Δ[a]	6-31+G(2d)	Δ[a]	6-31+G(3df)	Δ[a]
Bond Lengths (Å)								
S1–S2	2.010	-0.005	1.993	-0.001	1.989	-0.004	1.973	-0.002
S1–O5	1.699	0.005	1.672	0.003	1.687	0.004	1.660	0.002
S2–O3	1.692	0.005	1.664	0.002	1.679	0.003	1.653	0.002
O3–C4	1.433	0.002	1.436	0.002	1.424	0.001	1.426	0.001
O5–C6	1.432	0.003	1.435	0.003	1.423	0.002	1.425	0.002
Bond Angles (°)								
S1–S2–O3	108.5	0.5	108.8	0.5	108.4	0.3	108.7	0.3
S1–O5–C6	115.5	0.5	116.2	0.3	115.0	0.6	115.6	0.3
S2–S1–O5	108.3	0.0	108.5	0.0	108.4	0.1	108.6	0.1
S2–O3–C4	115.3	0.5	115.9	-0.1	114.7	0.4	115.3	-0.1
Dihedral Angles (°)								
S1–S2–O3–C4	-81	0	-82	-1	-80	0	-80	-1
S2–S1–O5–C6	80	2	81	1	78	1	79	1
O3–S2–S1–O5	88	1	88	1	88	0	88	1

a) Difference from geometry optimized at the same level of theory except without a set of diffuse functions.

Table 36. Geometry optimization of 6 using the MP2 method with different triple split basis sets.

	ED[42]	X-ray[39]	MP2/					
			6-311G*	6-311G(2d)	6-311G(df)	6-311G(3d)	6-311G(2df)	6-311G(3df)
Bond Lengths (Å)								
S1–S2	1.960	1.972	2.003	2.008	1.980	1.991	1.979	1.965
S1–O5	1.653	1.658	1.682	1.682	1.656	1.678	1.665	1.660
S2–O3	1.653	1.658	1.673	1.673	1.648	1.669	1.657	1.651
O3–C4	1.432	1.435	1.434	1.439	1.426	1.437	1.434	1.432
O5–C6	1.432	1.435	1.432	1.437	1.424	1.435	1.432	1.430
Bond Angles (°)								
S1–S2–O3	108.2	108.2	106.0	106.9	106.8	107.1	106.9	107.5
S1–O5–C6	114.5	114.5	113.7	113.1	113.6	113.9	113.5	114.2
S2–S1–O5	108.2	108.2	106.2	107.1	107.0	107.2	107.2	107.6
S2–O3–C4	114.5	114.5	113.3	112.6	113.2	113.6	113.0	114.0
Dihedral Angles (°)								
S1–S2–O3–C4	-74	-75	-78	-77	-77	-76	-76	-76
S2–S1–O5–C6	74	75	79	76	78	77	76	77
O3–S2–S1–O5	91	82	87	86	87	86	86	86

Second order Møller-Plesset perturbation theory was better at predicting the geometry of **6**. As d functions are included in the calculations, the S-S bond converges to experiment. However, complete convergence to experiment is only achieved when at least three d and one f polarization functions were included in the basis set. The addition of the f polarization function seems to have the greatest impact upon prediction of accurate bond lengths. This is most evidence in Table **36** by comparing the 6-311G(2d) and 6-311G(df) basis sets. MP2-type correlation, although not sufficient, is necessary for predicting experimental geometry. The addition of electron correlation results in an increased rate of convergence. This is best exemplified by comparing the r(S-S) predictions made at the HF and MP2 levels (*cf.* Tables **29** and **36**). As polarization functions were included, HF provides a convergence in the S-S bond length of only 0.016 Å. However, MP2 converges it 0.038 Å to experiment. Conversely, it would seem that polarization functions too were also necessary though not sufficient for geometry convergence. Thus electron correlation and basis set size seem to have a multiplicative effect on geometry convergence for this class of compounds.

The use of either Allinger's original MM3[31] force field or our own modified (MM3*)[32] force field implemented in Macromodel® proved quite effective at modeling **6** (Δ_{ED} and $\Delta_{X\text{-}ray}$, Table **37**).

Table 37. Geometry optimization of **6** using the MM3 and MM3* force fields.

	ED[42]	X-ray[39]	MM3	Δ_{ED}	$\Delta_{X\text{-ray}}$	MM3*	Δ_{ED}	$\Delta_{X\text{-ray}}$
Bond Lengths (Å)								
S1–S2	1.960	1.972	1.966	0.006	-0.006	1.966	0.006	-0.006
S1–O5	1.653	1.658	1.656	0.003	-0.002	1.656	0.003	-0.002
S2–O3	1.653	1.658	1.656	0.003	-0.002	1.655	0.002	-0.003
O3–C4	1.432	1.435	1.435	0.003	0	1.437	0.005	0.002
O5–C6	1.432	1.435	1.435	0.003	0	1.436	0.004	0.001
Bond Angles (°)								
S1–S2–O3	108.2	108.2	108.1	-0.1	-0.1	108.0	-0.2	-0.2
S1–O5–C6	114.5	114.5	114.4	0.2	0.2	114.4	0.1	0.1
S2–S1–O5	108.2	108.2	108.4	-0.1	-0.1	108.3	-0.1	-0.1
S2–O3–C4	114.5	114.5	114.5	0	0	114.5	0	0
Dihedral Angles (°)								
S1–S2–O3–C4	-74	-75	-81	-7	-6	-81	-7	-6
S2–S1–O5–C6	74	75	82	8	7	82	8	7
O3–S2–S1–O5	91	82	84	-7	2	84	-7	3

Molecular mechanics has the advantage of modeling larger molecular weight compounds which DFT and *ab initio* calculations could not handle. We were able to accurately model bis(*p*-nitrobenzyloxy) disulfide **49** (Table **38**).

Table 38. Geometry optimization of 49 using the MM3 and MM3* force fields.

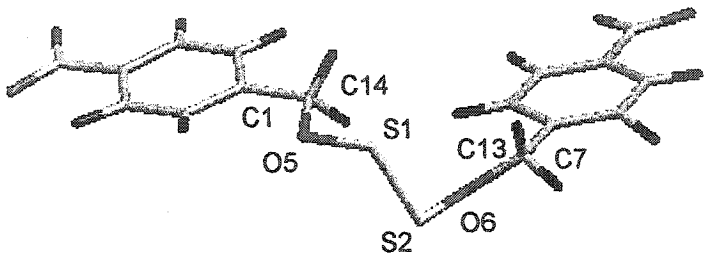

	X-ray[50]	MM3	Δ	MM3*	Δ
Bond Lengths (Å)					
S1-S2	1.968	1.965	-0.003	1.965	-0.003
S1-O5	1.648	1.655	0.006	1.654	0.006
S2-O6	1.659	1.654	-0.005	1.655	-0.004
Bond Angles (°)					
S2-S1-O5	107.3	107.6	0.3	107.9	0.6
S1-S2-O6	107.8	107.4	-0.4	107.4	-0.4
S1-O5-C14	114.6	114.6	-0.1	114.5	-0.1
S2-O6-C13	115.5	114.9	-0.6	114.7	-0.8
O6-C13-C7	109.7	109.9	0.1	110.0	0.3
O5-C14-C1	110.0	110.3	0.3	110.0	0.0
Dihedral Angles (°)					
S1-S2-O6-C13	-74	-83	-9	-83	-9
S1-O5-C14-C1	175	-178	3	178	3
S2-S1-O5-C14	87	82	-4	81	-6
S2-O6-C13-C7	171	177	7	179	8
O5-S1-S2-O6	-86	-83	3	-83	2

Overall, the 6-31G(3df) and 6-311G(3df) basis sets produced the best agreement. The use of MP2 most closely reproduced the experimental geometries. Less computationally demanding density functionals (SVWN, B3P86, B3PW91) do reasonably well as predictive tools with SVWN showing the closest agreement (using the 6-31G(2df) basis set). Surprisingly this was not the case for B3LYP. HF proved woefully incapable of accurately predicting the geometry of the experiment within the three standard deviation (3σ) tolerance criterion used in this study. For these classes of compounds, molecular

mechanics seems to be an effective alternative to both *ab initio* and density functional theory. This may be due to the ability of the force field to handle hyperconjugation.

3.3.3 Geometries of a Model Thionosulfite

The first experimental evidence for the existence of isomeric thionosulfites occurred in the mid 1960s.[51-53] Currently, four crystal structures (**5g**, **5i**, **5m**, **5n**)[54-56] exist with which we could reference our modeling work (Figure 5).[57] As these all contained a 5-membered cyclic core, we chose as our model the parent thionosulfite **5a** as well as the tetramethyl-substituted derivative **5d**. Our predictive work for **5a** is shown in Tables **39-41** while for **5d** is shown in Table **42**.

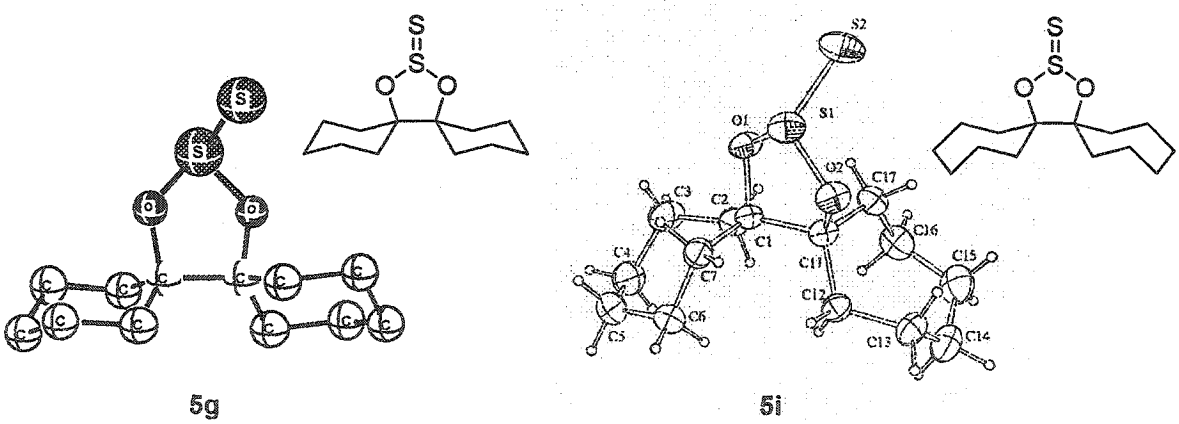

5g **5i**

Figure 5. Ortep representations of **5g** and **5i**, the two reference thionosulfites.

Table 39. Geometry optimization of 5a using the HF and B3LYP methods with different basis sets.

	X-ray[54]	X-ray[55]	HF/	B3LYP/				
	5g	5i	6-31G*	6-31G*	6-31G(2d)	6-31G(df)	6-31G(3d)	6-31G(2df)
Bond Lengths (Å)								
C1-C2	1.553	1.556	1.543	1.525	1.527	1.531	1.527	1.529
O3-S4	1.639	1.644	1.615	1.703	1.692	1.681	1.675	1.666
C1-O5	1.485	1.491	1.426	1.440	1.436	1.441	1.441	1.442
S4-O5	1.643	1.626	1.615	1.715	1.704	1.690	1.685	1.672
C2-O3	1.488	1.483	1.426	1.438	1.434	1.438	1.436	1.436
S4-S6	1.900	1.911	1.938	1.934	1.930	1.934	1.919	1.923
Bond Angles (°)								
C1-C2-O3	101.6	101.3	105.7	103.9	104.3	103.9	104.4	104.6
C2-C1-O5	102.3	105.9	105.7	106.1	106.5	106.2	106.4	106.6
O3-S4-O5	94.3	94.2	91.6	91.7	91.6	91.8	91.6	91.7
O5-S4-S6	106.4	106.1	109.0	107.6	108.0	108.4	108.5	108.6
C1-O5-S4	111.6	112.7	110.9	111.8	112.1	112.3	112.7	112.6
C2-O3-S4	112.2	109.8	110.9	108.2	108.2	108.0	108.7	108.5
O3-S4-S6	110.6	111.4	109.0	111.2	110.9	111.0	110.8	110.2
Dihedral Angles (°)								
C1-C2-O3-S4	35	-34	25	45	44	45	43	42
C1-O5-S4-S6	-127	135	-75	-107	-102	-101	-99	-94
C2-O3-S4-O5	-14	9	-36	-31	-33	-34	-34	-36
O3-C2-C1-O5	-42	45	0	-39	-35	-35	-31	-28
C1-O5-S4-O3	-14	21	36	6	11	12	14	18
C2-C1-O5-S4	36	-42	-25	18	13	11	8	4
C2-O3-S4-S6	96	-100	75	79	78	76	77	75

Table 40. Geometry optimization of 5a using the B3P86 method with different triple split basis sets.

	X-ray[54]	X-ray[55]	B3P86/					
	5g	5i	6-311G*	6-311G(2d)	6-311G(df)	6-311G(3d)	6-311G(2df)	6-311G(3df)
Bond Lengths (Å)								
C1-C2	1.553	1.556	1.521	1.529	1.533	1.544	1.547	1.546
O3-S4	1.639	1.644	1.686	1.674	1.665	1.660	1.647	1.644
C1-O5	1.485	1.491	1.433	1.432	1.435	1.431	1.429	1.431
S4-O5	1.643	1.626	1.696	1.677	1.667	1.660	1.647	1.644
C2-O3	1.488	1.483	1.430	1.426	1.429	1.432	1.429	1.431
S4-S6	1.900	1.911	1.922	1.920	1.923	1.911	1.917	1.907
Bond Angles (°)								
C1-C2-O3	101.6	101.3	103.8	105.0	104.5	106.5	106.3	106.2
C2-C1-O5	102.3	105.9	106.2	106.9	106.5	106.4	106.3	106.2
O3-S4-O5	94.3	94.2	91.5	91.1	91.3	90.4	90.9	90.9
O5-S4-S6	106.4	106.1	108.1	109.1	109.5	109.5	109.5	109.5
C1-O5-S4	111.6	112.7	111.9	111.8	111.9	109.2	109.2	109.3
C2-O3-S4	112.2	109.8	107.4	107.3	107.2	109.2	109.2	109.4
O3-S4-S6	110.6	111.4	110.7	110.2	110.5	109.5	109.5	109.5
Dihedral Angles (°)								
C1-C2-O3-S4	35	-34	46	43	44	27	27	27
C1-O5-S4-S6	-127	135	-101	-89	-89	-72	-72	-72
C2-O3-S4-O5	-14	9	-34	-39	-40	-39	-39	-39
O3-C2-C1-O5	-42	45	-37	-26	-26	0	0	0
C1-O5-S4-O3	-14	21	11	23	23	39	39	39
C2-C1-O5-S4	36	-42	13	-2	-1	-28	-28	-28
C2-O3-S4-S6	96	-100	76	72	71	72	72	72

Table 41. Geometry optimization of 5a using the MP2 method with different triple split basis sets.

	X-ray[54]	X-ray[55]	MP2/						
	5g	5i	6-311G*	6-311G(2d)	6-311G(df)	6-311G(3d)	6-311G(2df)[a]	6-311G(2df)[b]	6-311G(3df)[b]
Bond Lengths (Å)									
C1-C2	1.553	1.556	1.551	1.541	1.549	1.524	1.543	1.522	1.523
O3-S4	1.639	1.644	1.676	1.665	1.644	1.670	1.645	1.655	1.650
C1-O5	1.485	1.491	1.439	1.446	1.432	1.446	1.440	1.443	1.441
S4-O5	1.643	1.626	1.676	1.665	1.643	1.677	1.646	1.659	1.654
C2-O3	1.488	1.483	1.439	1.446	1.432	1.439	1.440	1.437	1.435
S4-S6	1.900	1.911	1.905	1.923	1.897	1.904	1.905	1.900	1.891
Bond Angles (°)									
C1-C2-O3	101.6	101.3	106.3	106.5	105.8	103.9	106.2	103.7	103.6
C2-C1-O5	102.3	105.9	106.3	106.5	105.8	106.3	106.2	106.4	106.0
O3-S4-O5	94.3	94.2	89.4	90.4	107.2	91.2	91.0	92.0	91.8
O5-S4-S6	106.4	106.1	109.3	109.3	109.7	108.6	108.9	108.2	108.5
C1-O5-S4	111.6	112.7	107.5	107.5	107.2	111.8	107.8	111.4	112.0
C2-O3-S4	112.2	109.8	107.5	107.5	107.2	106.9	107.8	106.4	107.0
O3-S4-S6	110.6	111.4	109.3	109.3	109.7	110.3	108.9	109.9	110.2
Dihedral Angles (°)									
C1-C2-O3-S4	35	-34	31	30	31	46	29	46	46
C1-O5-S4-S6	-127	135	-67	-69	-67	-92	-69	-91	-92
C2-O3-S4-O5	-14	9	-43	-42	-44	-39	-42	-40	-39
O3-C2-C1-O5	-42	45	0	0	0	-31	0	-31	-31
C1-O5-S4-O3	-14	21	43	42	44	20	42	21	20
C2-C1-O5-S4	36	-42	-31	-30	-31	3	-29	3	4
C2-O3-S4-S6	96	-100	67	69	67	71	69	70	71

a) τ(O3-C2-C1-O5) fixed at 0°. b) τ(O3-C2-C1-O5) fixed at -33°.

Table 42. Geometry optimization of 5d using HF, density functionals, MP2 with different basis sets as well as MM3*.

	X-ray[54]	X-ray[55]	HF/		B3LYP/				B3P86/			MP2/	MM3*
	5g	5i	6-31G*	6-31G(2d)	6-31G*	6-31G(2d)	6-31G(2df)	6-31G(3df)	6-31G(2d)	6-31G(2df)	6-31G(3df)	6-311G*	
Bond Lengths (Å)													
C1-C2	1.553	1.556	1.552	1.550	1.563	1.562	1.563	1.562	1.552	1.553	1.553	1.546	1.532
O3-S4	1.639	1.644	1.624	1.620	1.704	1.696	1.672	1.670	1.681	1.659	1.656	1.706	1.649
C1-O5	1.485	1.491	1.442	1.438	1.458	1.454	1.454	1.455	1.445	1.444	1.445	1.449	1.485
S4-O5	1.643	1.626	1.628	1.625	1.709	1.701	1.678	1.676	1.686	1.665	1.663	1.710	1.648
C2-O3	1.488	1.483	1.445	1.441	1.463	1.458	1.459	1.459	1.449	1.449	1.449	1.453	1.485
S4-S6	1.900	1.911	1.931	1.927	1.936	1.931	1.925	1.913	1.918	1.912	1.901	1.895	1.903
Bond Angles (°)													
C1-C2-O3	101.6	101.3	101.8	101.9	102.7	102.7	102.4	102.3	102.5	102.2	102.1	102.7	101.9
C2-C1-O5	102.3	105.9	102.4	102.3	103.1	103.0	102.8	102.6	102.9	102.7	102.5	102.9	102.4
O3-S4-O5	94.3	94.2	93.2	93.2	92.1	92.0	92.5	92.3	92.3	92.7	92.5	91.7	94.1
O5-S4-S6	106.4	106.1	107.5	107.4	106.6	106.7	106.8	106.8	106.6	106.6	106.7	106.4	108.8
C1-O5-S4	111.6	112.7	112.8	112.7	111.3	111.6	112.1	112.2	111.4	111.8	112.0	110.8	111.1
C2-O3-S4	112.2	109.8	113.6	113.7	112.1	112.4	112.8	113.2	112.1	112.5	112.8	111.4	111.3
O3-S4-S6	110.6	111.4	111.1	111.4	112.6	112.5	112.3	112.3	112.4	112.2	112.3	112.5	108.3
Dihedral Angles (°)													
C1-C2-O3-S4	35	-34	33	35	35	34	34	33	35	35	34	37	37
C1-O5-S4-S6	-127	135	-132	-129	-128	-130	-130	-130	-130	-129	-130	-130	-125
C2-O3-S4-O5	-14	9	-13	-13	-13	-15	-13	-12	-13	-13	-13	-14	-15
O3-C2-C1-O5	-42	45	-40	-40	-44	-43	-42	-42	-44	-43	-43	-46	-44
C1-O5-S4-O3	-14	21	-15	-16	-16	-16	-15	-16	-16	-15	-15	-16	-14
C2-C1-O5-S4	36	-42	35	37	37	37	36	37	37	36	37	39	37
C2-O3-S4-S6	96	-100	98	96	96	97	97	97	96	96	96	95	97

Salient structural features in both X-rays include the extremely short S-S bond, the pseudo-axial orientation of the branched bond with respect to the five-membered ring and the inherent twist in the ring with a τ(O-C-C-O) of *ca.* 40°. A representative set of structural parameters is provided for HF (Table **39**). For all basis sets, the 1,3,2-dioxathiolane ring flattened out and thus could not reproduce the twist present in the X-ray structures. This proved not to be the case using B3LYP (Table **40**) where the conformation remained twisted regardless of basis set size, though less so by *ca.* 12°. Interestingly, the use of larger basis sets with B3P86 (Table **41**) resulted in the same observed ring flattening. The MP2 level with 3 d polarization functions is able to reproduce the twist however the subsequent addition of f polarization functions re-flattens the geometry into the undesired envelope conformation (Table **41**).

All methods predict the expected pseudo-axial orientation of the S-S bond with respect to the 5-membered ring core. This preferred conformation is most likely due to the optimal orbital overlap engendered in $n_O \rightarrow \sigma^*_{S-S}$. This negative hyperconjugation has been found to be the principle factor responsible for the stabilization of hypervalent[58,59] chalcogen atoms.[60] Inductive removal of electronic charge by oxygen from the branched sulfur leading to a lowering of the energy of the d-AO ((p-d)π bonding) and to a reinforcement of the backbonding has also been proposed to explain the stability of hypervalent sulfur species but this is the subject of much debate.[61,62] In general the θ(O3-S4-O5) is underestimated by *ca.* 3° no matter the level of theory or the basis set used. All methods faithfully predict the θ(O3-S4-S6) bond angle but overestimate the θ(O5-S4-S6)

by *ca.* 3°. Interestingly, the presence of 4 methyl substituents forced the twist when using DFT and MP2 methods (Table **42**). As well, bond angles were more faithfully reproduced with errors less than 2°.

HF respectively overestimates and underestimates the r(S-S) and r(S-O) bond lengths by greater than 0.02 Å. The predicted B3LYP r(S-S) approaches the experiment the most when using the 6-31G(3d) basis set. The B3P86 method also accurately predicts this key structural identifier at this basis set (Table **40**). Interestingly, the inclusion of an f polarization function to this basis set resulted in a net increase in accuracy. Though one does observe a slight convergence with increasing basis set size, B3LYP consistently overestimates the r(S-O). The B3P86 method with a minimum of two d and one f polarization functions does converge to experiment. MP2 predicts bond lengths within experimental error using large basis sets (Table **41**) if we artificially lock the τ(O-C-C-O) into a twist conformation.[63] Using the 6-31G(3d) basis set, we get a good r(S-S) prediction but the r(S-O) values are larger by *ca.* 0.03 Å.

Bond length predictions in **5d** (Table **42**) still required the addition of polarization functions to approach the crystal structure geometries. For instance, MP2/6-311G* underestimates the r(S-S) and overestimates by 0.4 Å the r(S-O). As with Jursic's work on the related $F_2S{=}S$ **75b** system where his best method was B3P86/6-311++G(3df), our most predictive method for **5d** was the B3P86/6-311G(3df). It should not be surprising that larger basis sets containing polarization functions were necessary to afford accurate

predictions of thionosulfites as the use of d functions has been shown to stabilize hypervalent sulfur species.[62,64] The role of these functions is to provide "orbital space" at the branched sulfur to allow for back bonding. That is, these orbitals act as true valence orbitals.[65]

Using our hybrid force field parameters, the predicted structure for **5d** (Table **42**) converged to experiment. The ability to accurately model branched sulfur compounds is a primary goal of ours and the use of the MM3* force field seems to be a low-cost alternative to the *ab initio* and DFT methods tested. More telling is the accurate structural predictions when **5g** and **5i** were modeled using MM3* (Table **43**).

Table 43. Geometry optimization of **5g** and **5i** using MM3*

	X-ray[54] **5g**	MM3*	Δ[a]	X-ray[55] **5i**	MM3*	Δ[a]
Bond Lengths (Å)						
C1-C2	1.553	1.554	-0.001	1.556	1.556	0.000
O3-S4	1.639	1.648	-0.009	1.644	1.647	-0.003
C1-O5	1.485	1.485	0.000	1.491	1.491	0.000
S4-O5	1.643	1.646	-0.003	1.626	1.648	-0.022
C2-O3	1.488	1.487	0.001	1.483	1.489	-0.006
S4-S6	1.900	1.903	-0.003	1.911	1.903	0.008
Bond Angles (°)						
C1-C2-O3	101.6	101.7	-0.1	101.3	101.2	0.1
C2-C1-O5	102.3	101.9	0.4	105.9	107.5	-1.6
O3-S4-O5	94.3	93.9	0.4	94.2	93.6	0.6
O5-S4-S6	106.4	108.8	-2.4	106.1	108.7	-2.6
C1-O5-S4	111.6	111.2	0.4	112.7	111.5	1.2
C2-O3-S4	112.2	111.7	0.5	109.8	111.1	-1.3
O3-S4-S6	110.6	108.3	2.3	111.4	108.4	3.0
Dihedral Angles (°)						
C1-C2-O3-S4	35	36	-1	-34	35	-1
C1-O5-S4-S6	-127	-127	0	135	127	8
C2-O3-S4-O5	-14	-13	-1	9	14	-5
O3-C2-C1-O5	-42	-44	2	45	46	-1
C1-O5-S4-O3	-14	-16	2	21	16	5
C2-C1-O5-S4	36	38	-2	-42	-40	2
C2-O3-S4-S6	96	98	-2	-100	96	4

a) Δ = X-ray - MM3*; where the difference in dihedral angles is defined as Δ = |X-ray| - |MM3*|.

3.3.4 Vibrational Frequencies of MeOSSOMe

The vibrational frequencies of **6** have been determined at the B3LYP level using the 6-311G* basis set. The calculated frequencies have been scaled with respect to the experimental IR.[42] These are shown in Table **44**. The calculated and experimental frequencies match excellently though some CH_3 modes are grossly underestimated.

Table 44. Vibrational fequencies (cm^{-1}) for MeOSSOMe **6**

Mode	IR[a]	B3LYP[b]	Scaling Factor (IR/Calc.)[c]	Scaled B3LYP[b,c]	Δ[d]
$\nu(CH_3)$	3002	3132	0.959	3003	1
	3002	3129	0.959	3001	-1
	2964	3093	0.959	2967	3
	2964	3087	0.959	2961	-3
	2940	3022	0.959	2898	-42
	2940	3019	0.959	2896	-44
$\delta(CH_3)$	1453	1519	0.969	1472	19
	1453	1518	0.969	1471	18
	1453	1502	0.969	1455	2
	1453	1501	0.969	1454	1
	1453	1479	0.969	1434	-19
	1453	1478	0.969	1432	-21
(CH_3) rock	1160	1201	0.975	1171	11
	1160	1197	0.975	1167	7
	1160	1181	0.975	1152	-8
	1160	1178	0.975	1149	-11
ν(C-O)	1000	1016	0.988	1004	4
	1000	1009	0.988	997	-3
ν(S-O) in the plane	688	655	1.051	688	0
ν(S-O) out of plane	662	630	1.05	662	0
ν(S-S)	527	468	1.126	527	0
δ(C-O-S)	423	410	1.032	423	0
δ(C-O-S)	385	381	1.009	385	0
δ(O-S-S)	248	309	0.802	248	0
δ(O-S-S)	209	257	0.815	209	0
τ(C-O)	-	178	-	178	-
τ(C-O)	-	173	-	173	-
τ(O-S)	-	114	-	114	-
τ(O-S)	-	94	-	94	-
τ(S-S)	-	75	-	75	-

a) IR in the gas phase measured at 25 °C. b) 6-311G* Basis set. c) Scaling factors for stretching and deformation frequencies were determined by scaling to experiment. No scaling was applied to the torsional modes, since B3LYP and experimental low-frequency vibrations have been shown to be close to each other. d) $\Delta = \nu_{scaled} - \nu_{expt.}$

3.3.5 Dipole Moment of MeOSSOMe

The calculated dipole moments of **6** at HF, B3LYP and MP2 at different basis sets are given in Table 45.

Table 45. Calculated dipole moments (debyes)

basis set	HF	B3LYP	MP2
6-31G*	2.546	2.548	
6-31+G*	2.560		
6-31G(2d)	2.322	2.123	
6-31G(3d)	2.376	2.168	
6-31G(2df)	2.361	2.163	
6-31G(3df)	2.407	2.196	
6-31G(3d2f)	2.407	2.195	
6-311G*		2.434	2.655
6-311G(2d)		2.266	
6-311G(3d)		2.204	2.392
6-311G(2df)		2.248	
6-311+G(2df)			2.458
6-311G(3df)			2.395

There is a wide range of values which are both method and basis set dependent. To our knowledge, no one has measured the dipole moment of any alkoxy disulfide. However, dipole moment calculations were very sensitive to the quality of the basis set in S_2Cl_2 **77a**.[66] The experimental dipole moments (in debyes) for HSSH **69a**[67] (1.17 ± 0.02) and FSSF **75a** [68] (1.45 ± 0.02) are much smaller than those calculated for **6**.

3.3.6 Rotational Barriers

We next determined the torsional potential of **6a**. It is important to understand that internal rotation is not pure rotation. It involves simultaneous structural changes (*i.e.* in

bond lengths and angles). Single point calculations were carried out on MP2/6-311G(2df) optimized geometries for the τ(O-S-S-O) barrier (τ = 86.7 for the global minimum and 180° for the transition state) using HF, SVWN, MP2, MP3, B3LYP and

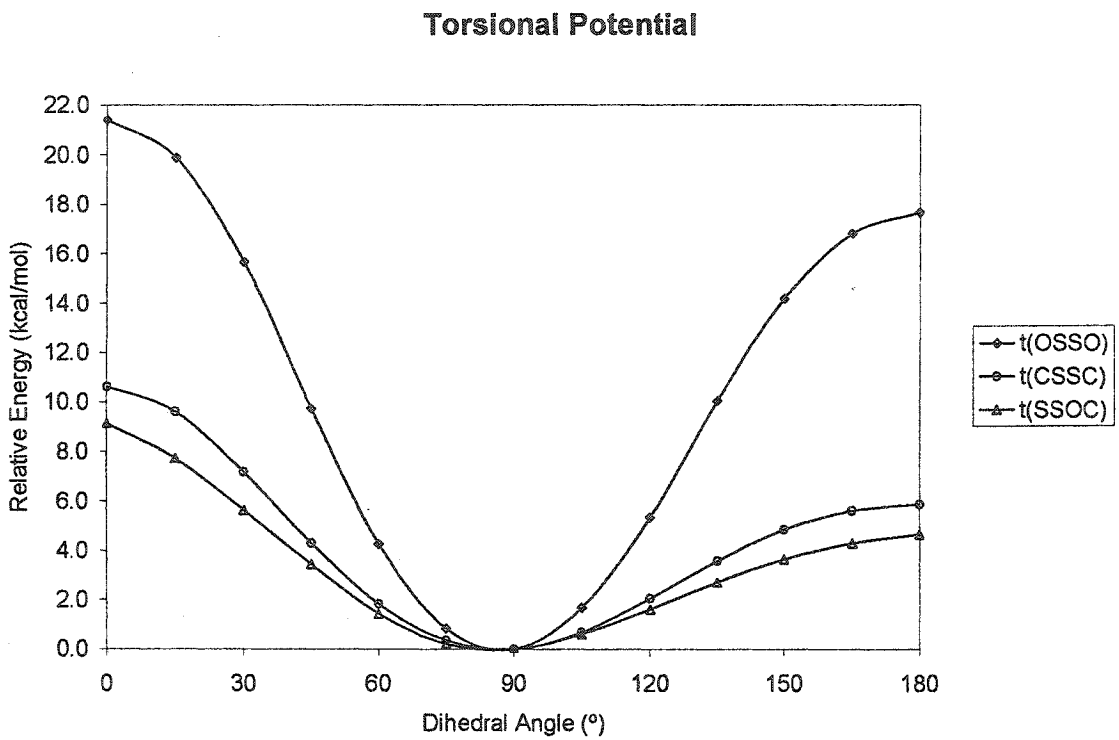

Figure 6. Change in Energy with τ(O-S-S-O) and τ(S-S-O-C) in **6** and with τ(C-S-S-C) in MeSSMe **71a** at B3LYP/6-31G(2d).

B3P86 levels with the basis sets listed in Chapter **3.2**.[69] The rotational barrier about the S-S bond (Figure 6) was calculated to be 17.7 kcal/mol (17.4 kcal/mol including zero point vibrational energy ZPVE and thermal corrections at 298.15 K) at the B3LYP/6-31G(2d) level of theory (Figure 6, Table 47), which is in good agreement with a recent experimental measurement ($\Delta G^{\ddagger}$ = 18.4 ± 0.15 kcal/mol).[1] Our experimentally determined barrier heights, profiled in Chapter 4, are also in agreement. This represents the best method at minimum computational cost to accurately reproduce the barrier

height. It should be noted that our single point energy calculations were carried out on structures where the geometry did not converge to experiment; nonetheless these geometries did reproduce experimental energies.[70] In general both DFT methods with basis sets larger than 6-31G* were able to accurately reproduce the observed barrier height (Table 47). The HF and MP3 methods underestimated this barrier while SVWN overestimated it (Table **46**). The MP2 level (Table **46**) however also was able to approach it. The presence of such a large S-S torsional barrier in essence renders the alkoxy disulfide functional group an element of axial chirality.[71]

Table **46**. Calculated *trans* barrier heights for **6a** with a geometry optimized at MP2/6-311G(2df)

Level	Basis Set	$\Delta E^{\ddagger}$	Level	Basis Set	$\Delta E^{\ddagger}$
HF/	6-31G*	12.8	SVWN/	6-31G*	21.0
	6-31G(2d)	14.0		6-31G(2d)	22.5
	6-31G(df)	13.1		6-31G(df)	21.0
	6-31G(3d)	14.8		6-31G(3d)	23.5
	6-31G(2df)	14.7		6-31G(2df)	22.6
	6-31G(3df)	15.2		6-31G(3df)	23.5
MP2/	6-311G*	17.0	MP3/	6-311G*	14.7
	6-311G(2d)	17.9		6-311G(2d)	15.5
	6-311G(df)	18.7		6-311G(df)	16.3
	6-311G(3d)	18.8		6-311G(3d)	16.3
	6-311G(2df)	19.3			

Table 47. Calculated *trans* barrier heights for **6a**. Except where stated, geometry of **6a** has been optimized at MP2/6-311G(2df)

Level	Basis Set	$\Delta E^{\ddagger}$	$\Delta E^{\ddagger a,b}$	Level	Basis Set	$\Delta E^{\ddagger}$	$\Delta E^{\ddagger a,b}$
B3LYP/	6-31G*	15.9	17.4	B3P86/	6-31G*	17.2	17.4
	6-31G(2d)	17.5	17.7		6-31G(2d)	18.8	19.0
	6-31G(df)	16.0	16.2		6-31G(df)	17.3	17.5
	6-31G(3d)	18.4	18.5		6-31G(3d)	19.7	19.9
	6-31G(2df)	17.8	17.8		6-31G(2df)	19.1	19.2
	6-31G(3df)	18.5	18.7		6-31G(3df)	19.9	20.0

a) Geometry is optimized at the same level of theory. b) Subtract 0.3 kcal/mol from $\Delta E^{\ddagger}$ to include ZPE correction.

The *trans* barrier height was *ca.* 3 kcal/mol smaller than that of the *cis* (Figure 5). The substitution of alkoxyl groups from alkyl groups resulted in a significantly greater S–S barrier where the average barrier for a dialkyl disulfide is reported to be *ca.* 7 kcal/mol (*cf.* Chapter **2.4.2**).[72] The existence of a four-electron interaction (lone pair–lone pair repulsion) cannot solely account for the barrier height. The origins of this barrier are discussed in Chapter **3.3.7**. The SS-OC *trans* barrier was calculated to be *ca.* 4.5 kcal/mol (Figure 6) indicating that torsional hindrance about the S-O bond is not a major contributor to the overall barrier height. This is in accord with the literature.[37]

3.3.7 Natural Bond Order Analysis

Natural bond order (NBO) analysis[10] was undertaken in order to ascertain the origin of the stability of the 90° τ(S-S) conformer. Second order perturbation NBO analysis can measure and attribute this stabilization to specific individual orbital interactions *i.e.* it can separate energy contributions due to hyperconjugation from those caused by electrostatic or steric interactions. The S-S bonding orbitals appear to be σ_p, with increasing p

character upon rotation about the S-S bond from the minimum (*ca.* 90°) to the *trans* transition state (180° where there exists *ca.* sp^{11} mixing). This trend is illustrated in Figure 8. The Wiberg S-S bond order index (WBI) also decreases slightly upon rotation away from the energy minimum (Figure 7, Table 48) whereas the two S-O WBI increase slightly.[73] The S-S bond order of 1.13 is similar to that obtained for the FSSF and FSSCl systems.[74]

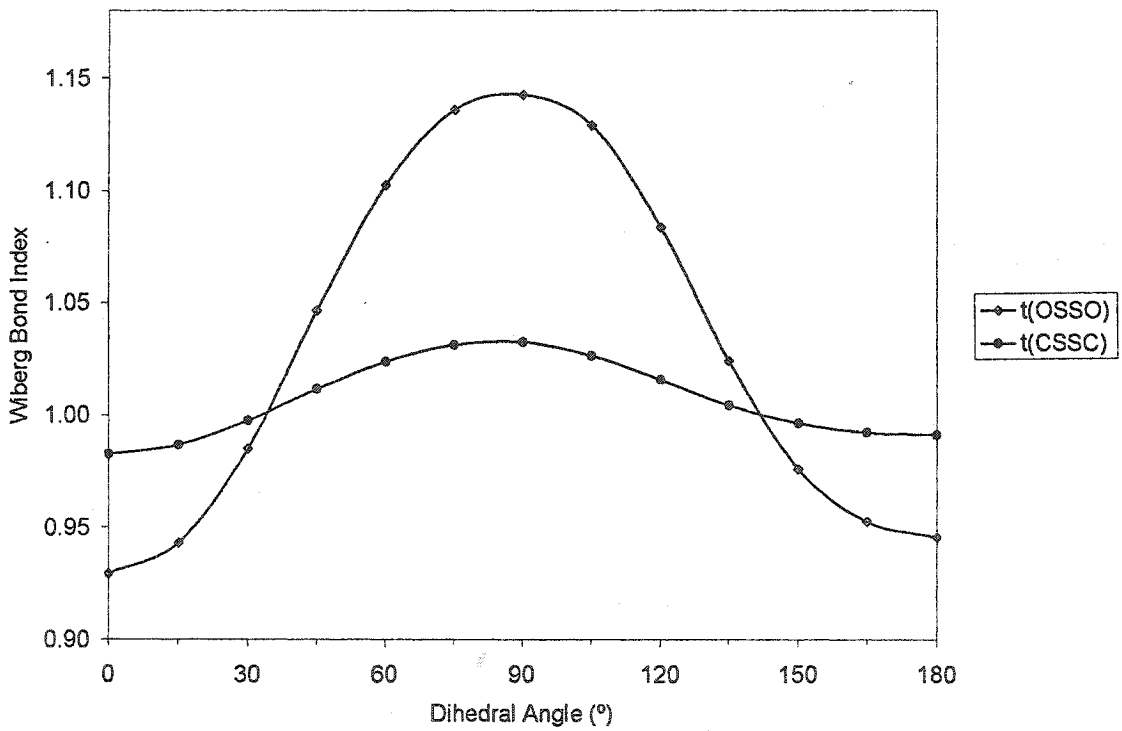

Figure 7. Wiberg bond order index (WBI) as a function of τ(S-S) in **6** and MeSSMe **71a**.

Energy corresponding to delocalization (E_{del}) can be assessed by the NBO deletion procedure. According to the NBO method,[5,6,10,75] delocalization effects (hyperconjugation) are due to the interactions between occupied orbitals and anti-bonding and Rydberg[76] orbitals and are represented by off-diagonal terms in the Fock matrix.[77]

To evaluate these contributions, the off-diagonal elements in the Fock matrix are zeroed (*i.e.* the contributions are deleted) and a single SCF cycle is carried out at the HF/6-31G* level[78] based on B3LYP/6-31G(2d) optimized geometries. Evaluation of the energy of this altered Fock matrix results in the Lewis energy (E_{Lew}). E_{Lew} is the energy due to localized bonds, steric and dipole effects, none of which can be separated by means of the NBO procedure. The difference between total SCF (E_{tot}) and E_{Lew} energies corresponds to the delocalization energy (E_{del}), the energetic contribution arising from all the possible interactions between orbitals, equation (1).[10,79]

$$E_{del} = E_{tot} - E_{Lew} \quad (1)$$

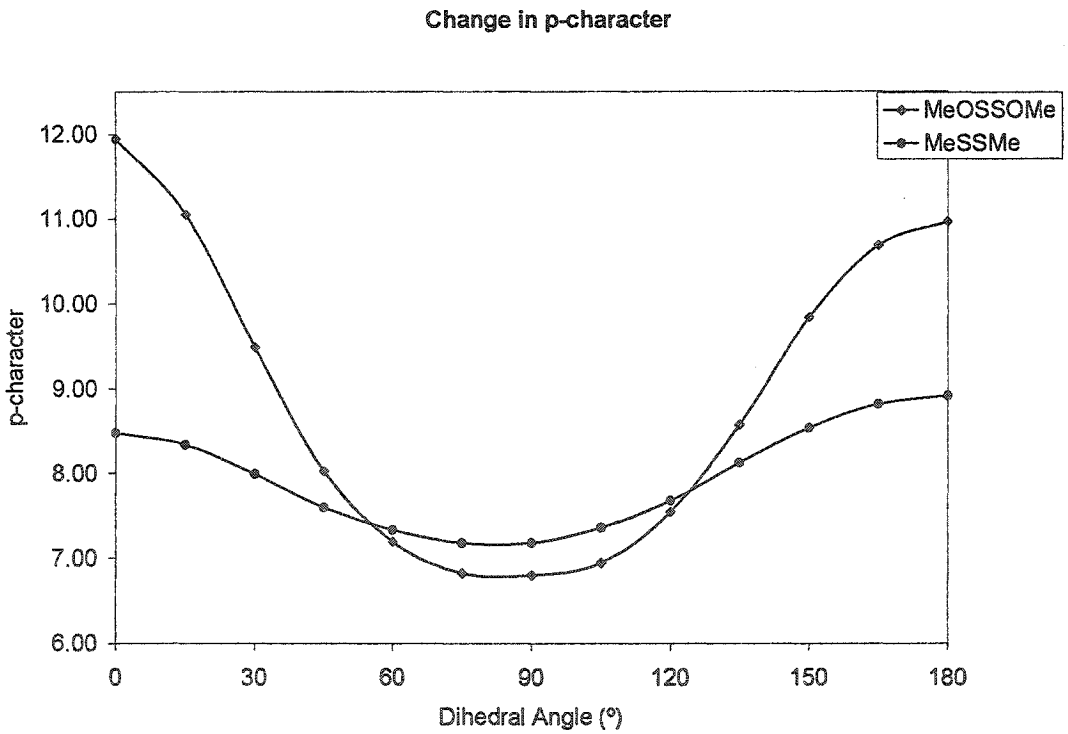

Figure 8. Change in p-character with τ(S-S) in **6** compared with τ(S-S) in **71a**.

Table 48. Wiberg bond order index (WBI) as a function of τ(S-S) in **6**. For comparison, the calculated MP2/6-311g(2df) S-S bond lengths are also included.

	τ(O-S-S-O)												
	0	15	30	45	60	75	90	105	120	135	150	165	180
r(S-S) (Å)	2.143	2.128	2.092	2.054	2.026	2.011	2.008	2.017	2.039	2.068	2.091	2.103	2.106
S-S WBI	0.939	0.954	0.994	1.046	1.094	1.123	1.129	1.111	1.072	1.024	0.986	0.965	0.959
S1-O5 WBI	0.860	0.854	0.844	0.829	0.814	0.807	0.806	0.811	0.821	0.830	0.837	0.839	0.840
S2-O3 WBI	0.860	0.858	0.847	0.835	0.825	0.819	0.818	0.822	0.831	0.839	0.843	0.842	0.840

In order to assess trends in the structure of **6**, each point on the rotational profiles was compared with the S-S and S-O bond lengths (Figure **9** and **10**), S-S-O and S-O-C bond angles (Figures **11** and **12**). In addition, in order to understand the origin of the stabilization of the equilibrium geometry, the total SCF (E_{tot}), Lewis (E_{Lew}), and delocalization (E_{del}) energies (Figure **12**) were also ascertained.

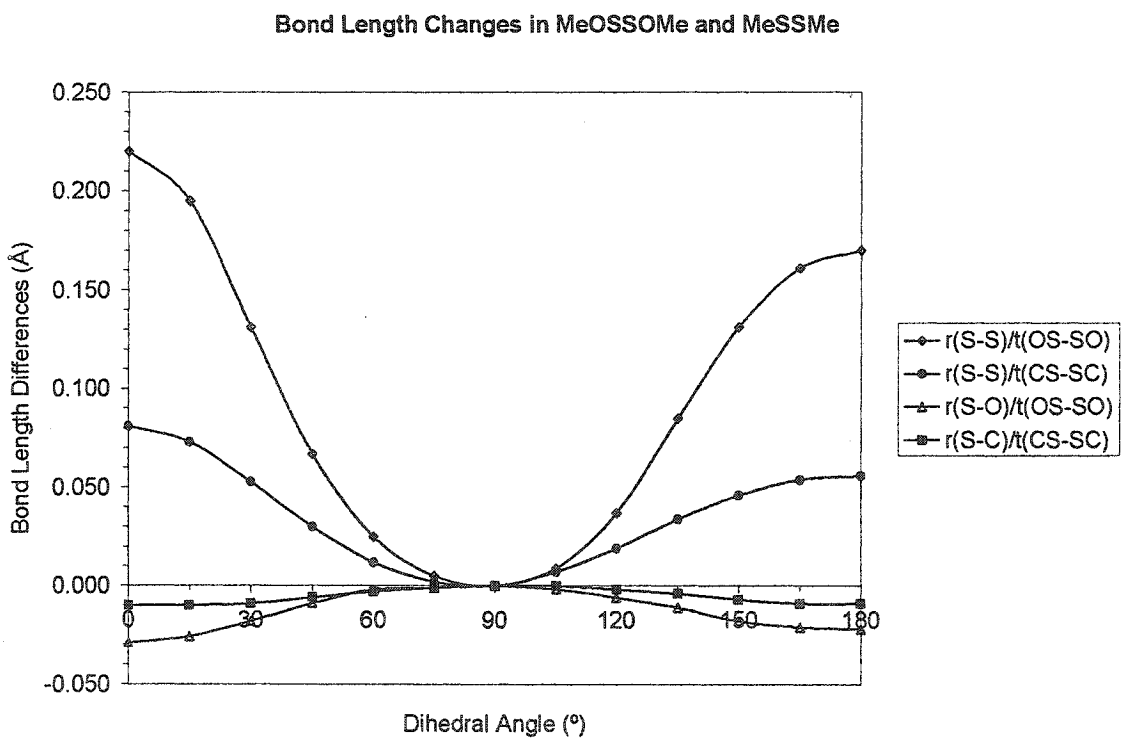

Figure **9**. Changes in Δr(S-S) and Δr(S-O) with τ(S-S) in **6**. The corresponding changes in Δr(S-S) and Δr(S-C) as a function of τ(S-S) for **71a** are also shown.

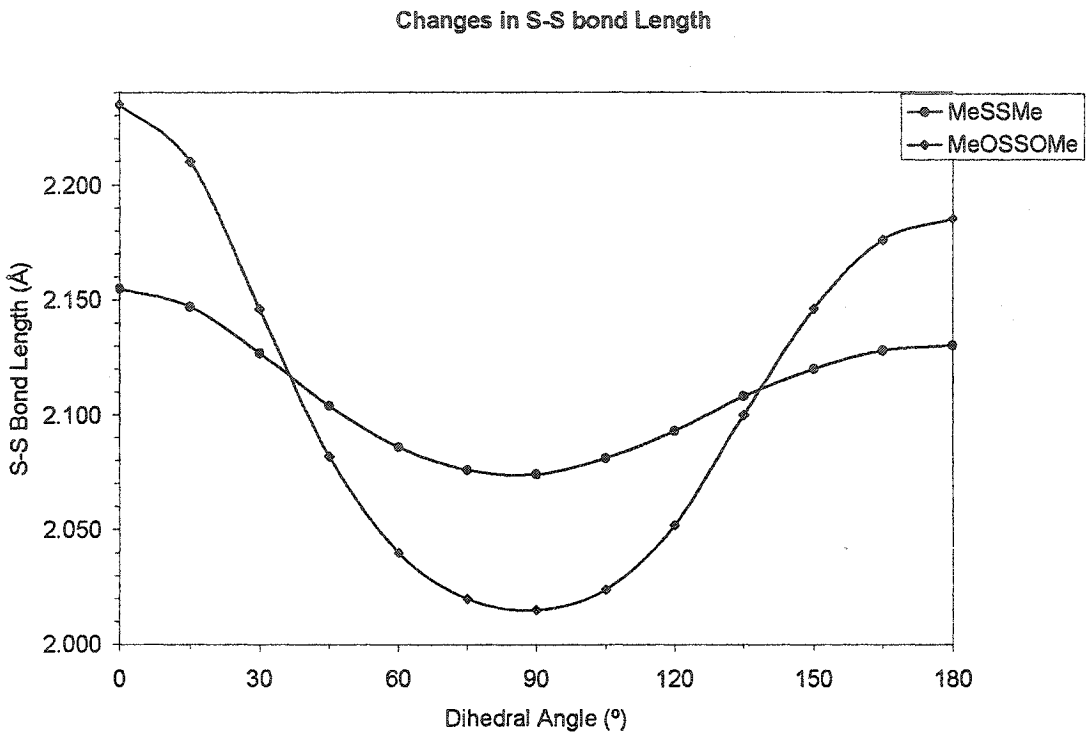

Figure **10**. Changes in r(S-S) with τ(S-S) in **6**. The corresponding changes in r(S-S) as a function of τ(S-S) for **71a** is also shown.

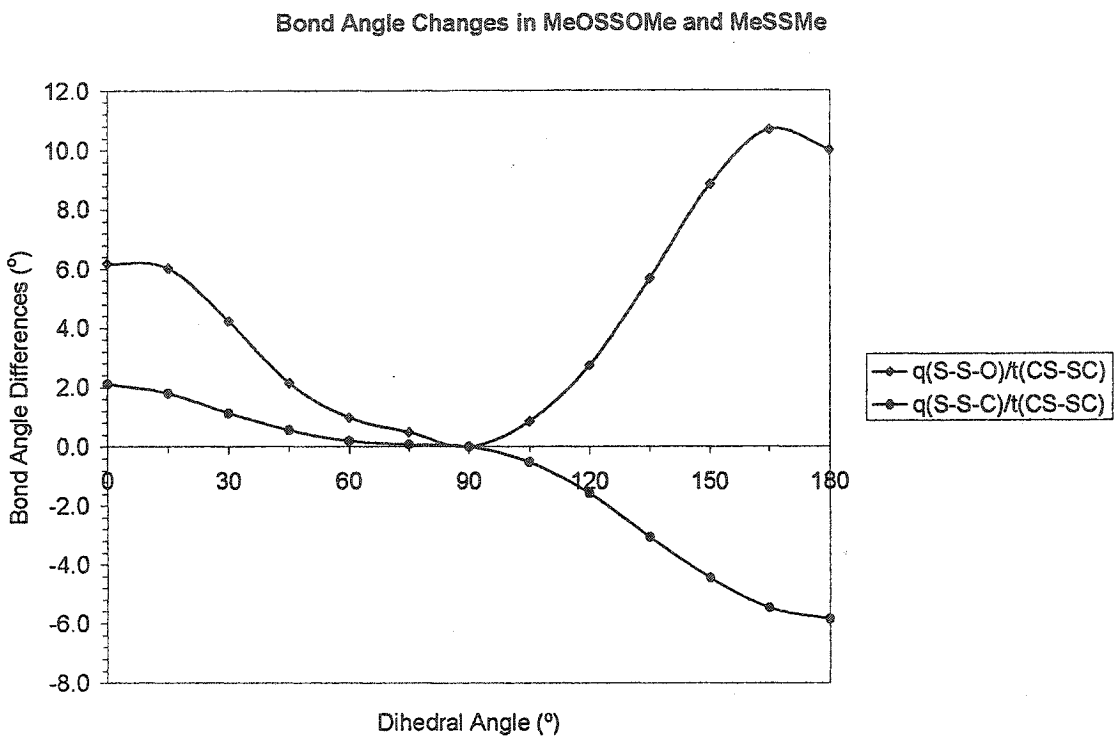

Figure 11. Changes in $\Delta\theta$(S-S-O) with τ(S-S) in **6**. The corresponding changes in θ, $\Delta\theta$(S-S-C), as a function of τ(S-S) for **71a** are also shown.

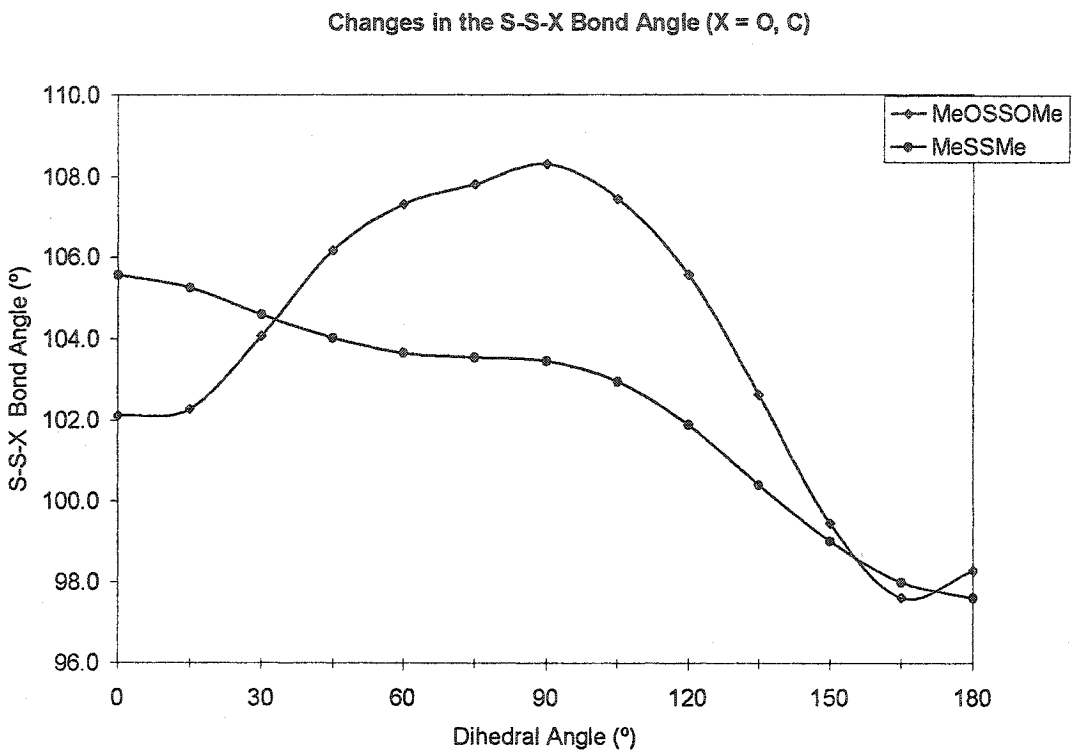

Figure 12. Changes in θ(S-S-O) with τ(S-S) in **6**. The corresponding changes in θ(S-S-C) as a function of τ(S-S) for **71a** are also shown.

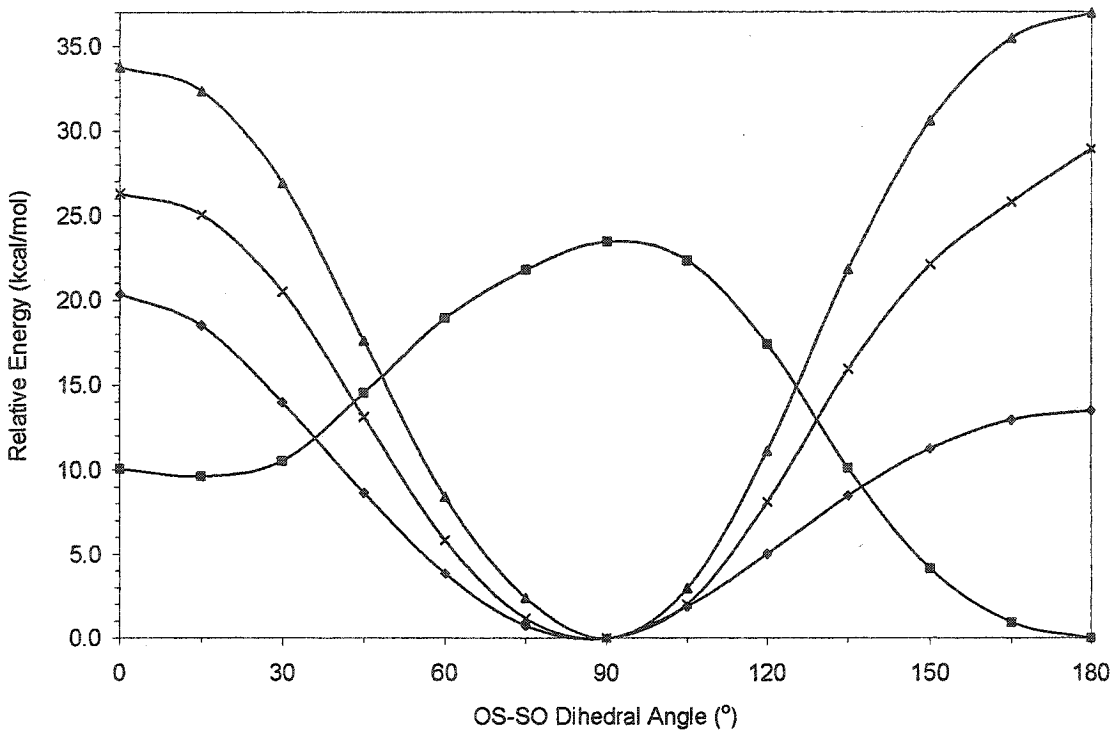

Figure 13. Energy comparisons for the OS-SO dihedral angle in **6**; ΔE_{tot} (◆), ΔE_{Lew} (■), ΔE_{del} (▲), $\Delta E_{nS\rightarrow\sigma^*S\text{-}O}$ (✕).

The results displayed in Figures **8-13** indicate the importance of negative hyperconjugation[80] which accounts for the observed "generalized anomeric effect"[81-86] in stabilizing the 90° τ(S-S) conformation (Figure **14**).[87] In fact, if only covalent interactions were present, the 180 degree conformer would have the lowest energy (*cf.* Figure **13**, ΔE_{Lew}). Analogously, delocalization would favour a τ(S-S-O-C) of 0° but steric hindrance of the adjacent substituents would disfavour this conformer. These effects can be seen in Figure **6**.

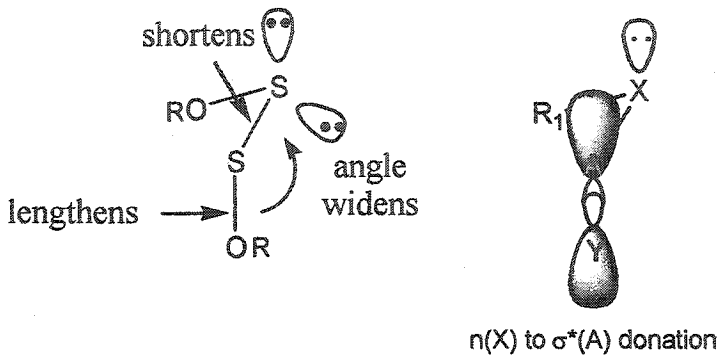

Figure **14**. a) Geometric consequences of negative hyperconjugation on the ground state equilibrium geometry of **6** (R = Me); b) molecular orbit representation of the stabilization resulting from negative hyperconjugation.

The basis for the "generalized anomeric effect" as we know it today was originated by J.T. Edward to denote the axial preference of electronegative substituents at the anomeric position of pyranoses. In this conformation, the C-X bond is gauche to the adjacent O-C bond (Figure **15**).[88-91]

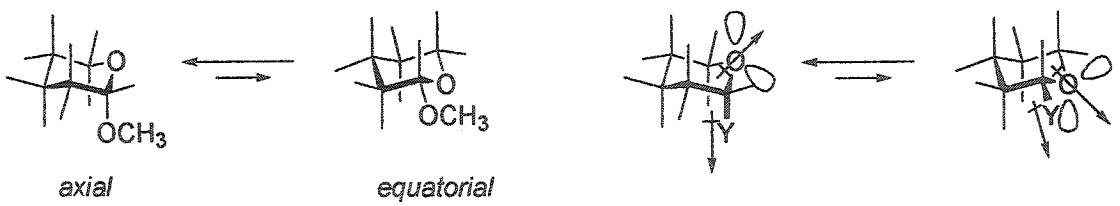

Figure **15**. a) Axial *vs.* equatorial preference in pyranose rings; b) Electrostatic repulsion model to account for the observed anomeric effect. The negative hyperconjugation model is shown in Figure **13**.

Generally this term refers to the preference of a conformer with a bond that is centered on an atom (A) attached to an electronegative substituent (Y) to lengthen, if a lone pair

on X is antiperiplanar to that bond (Figure 14).[92] This effect is well documented in the literature[86,93-109] and is specifically demonstrated in S_2X_2 where X is a halogen (*cf.* Chapter 2.4). In the case of these particular systems, the A–X bond of the donor group shortens as a consequence of the increased π-character, the A–Y bond of the acceptor group lengthens due to a weakening of the σ bonds through the population of σ* orbitals, and the X–A–Y (S-S-O) bond angle widens. For example, in FSSF 75a the r(S-S) increased by *ca.* 10% and θ(S-S-F) decreased by 14% upon rotating about the S-S bond from the ground state to the transition state.[110]

The inclusion of d and f functions on the sulfur atoms in alkoxy disulfides are critical in order to polarize the S-O σ* orbital.[111] However in nonhypervalent species such as these, n → σ* negative hyperconjugation is much more important than (d-p)π bonding.[111-113] If (d-p)π interactions were responsible for the rotational barrier then we would observe a considerable increase in that barrier with the inclusions of d and f polarization functions. This is not observed (there is *ca.* 2 kcal/mol increase in the barrier height with the inclusion of these functions - *cf.* Tables 46 and 47).

In 6, the r(S-S) (Figure 9) and the barrier (Figure 6) both increase when going from the ground state to the transition state. This is in part due to lone pair–lone pair repulsion. This four-electron interaction is largest in the two transition states where both sulfur lone pairs are in the correct geometry for a destabilizing π-π* ovelap.[114] The main contribution to the increased barrier results from the $n_S \rightarrow \sigma^*_{S\text{-}O}$ interaction (note ΔE_{del} (▲) and $\Delta E_{nS\rightarrow\sigma^*S\text{-}O}$ (✕) in Figure 13).[115] Inspection of the MP2/6-311G(2df) minimum

and transition state geometries show the existence of the anomeric effect (Figure 14 and Table 49).[116] For the ground state conformation, the S-S bond is shortened (Figures 9 and 7), the S-O is elongated (Figure 8), and the S-S-O angle is widened (Figures 11 and 12) compared with the *trans* conformation. This is a result of the negative hyperconjugation. As there are two sulfur atoms and two S-O bonds, this results in the formation of two orthogonal π-type bonds. This is evidenced in the decrease in p-character of the S-S bond at the equilibrium geometry (Figure 8). The decrease in p-character in each of the sulfur atoms indicates that at the equilibrium geometry, a significant portion of the 3p electrons are involved in $\pi_{S\text{-}S}$, rather than $\sigma_{S\text{-}S}$ bonding. Interestingly, microwave discharge experiments[117] for S_2O_2 show a *cis*-planar geometry while theoretical calculations reveal a trigonal planar geometry.[118] Thus in these two latter cases, the stabilizing interactions highlighted above do not seem to be applicable to this problem.

Table 49. MP2/6-311G(2df) geometries for the ground and *trans* transition state (TS). The barrier height calculated at the same level is 19.3 kcal/mol.

	MP2/	
	6-311G(2df)	6-311G(2df)[a]
	Minimum	TS
Bond Lengths Å		
S1–S2	1.979	2.130
S1–O5	1.665	1.650
S2–O3	1.657	1.651
Bond Angles °		
S1–S2–O3	106.9	96.9
S1–O5–C6	107.2	97.0
S2–S1–O5	113.5	113.1
S2–O3–C4	113.0	113.1
Dihedral Angles °		
S1–S2–O3–C4	-76	-89
S2–S1–O5–C6	76	89
O3–S2–S1–O5	86	180

a) τ(O3-S2-S1-O5) fixed at 180 for *trans* TS.

3.4 Concluding Remarks

We have demonstrated that the geometries of alkoxy disulfides **1** and thionosulfites **2** can be accurately predicted assuming the inclusion of both d and f polarization functions. Electron correlation (DFT and MP2 methods) is essential in order to account for hyperconjugation which is the major source of the S-O bond lengthening, the S-S bond contraction due to decreased p-character and the S-S-O bond angle widening. This is most evident in the complete inability of HF to predict the geometries for **6**. This work represents the first series of high level calculations reported on these two related classes of compounds.

The use of our hybrid force field parameters ably predicts the geometries of both alkoxy disulfides and thionosulfites. An attractive feature of MM3* is its ability to model larger, more complex molecules.

The large S-S barrier height in **6** is calculated within experimental error using either B3LYP or MP2 methods. The inclusion of ZPVE corrections had little effect on the magnitude of the barrier, lowering it by 0.3 kcal/mol. With the aid of NBO energetic analysis, we have derived a refined relationship between the energetic and geometric effects and the molecular wave functions. We have found a direct correlation between the presence of two $n_S \rightarrow \sigma^*_{S\text{-}O}$ stabilizing orbital interactions and the generalized anomeric effect. This effect is maximized when the atoms adjacent to the S-S moiety are strongly electronegative.[119] Moreover the ground state geometry is optimally aligned for maximum delocalization. Thus the increased barrier is mainly due to ground state stabilization It is for these reasons that we observe such a significant (*ca.* 10 kcal/mol) stabilization of the ground state of alkoxy disulfides with respect to its transition state as compared to dialkyl disulfides.

The isomerization of and relative stabilities between alkoxy disulfides and thionosulfites will be discussed in detail in Chapter 6. It should be noted that **6** is calculated at B3LYP/6-31G(2d) and B3LYP/6-31G(3df) levels to be 2.5-3.0 kcal/mol more stable than branch-bonded analog $(MeO)_2S{=}S$. This is in accord with the related S_2F_2 **75** system (*cf.* Chapter **2.5.2**).[74]

3.5 References

(1) Borghi, R.; Lunazzi, L.; Placucci, G.; Cerioni, G.; Foresti, E.; Plumitallo, A. *J. Org. Chem.* **1997**, *62*, 4924.

(2) The enantiomers were resolved at 0 °C by HPLC on a chiral column. Blanca, M. B.-D.; Maimon, E.; Kost, D. *Angew. Chem. Int. Ed. Engl.* **1997**, *36*, 2216.

(3) Frisch, M. J.; Trucks, G. W.; Sclegel, H. B.; Gill, P. M. W.; Johnson, B. G.; Robb, M. A.; Cheeseman, J. R.; Keith, T.; Petersson, G. A.; Montgomery, J. A.; Raghavachari, K.; Al-Laham, M. A.; Zakrzewski, V. G.; Ortiz, J. V.; Foresman, J. B.; Cioslowski, J.; Stefanov, B. B.; Nanayakkara, A.; Challacombe, M.; Peng, C. Y.; Ayala, P. Y.; Chen, W.; Wong, M. W.; Andres, J. L.; Replogle, E. S.; Gomperts, R.; Martin, R. L.; Fox, D. J.; Binkley, J. S.; Defrees, D. J.; Baker, J.; Stewart, J. P.; Head-Gordon, M.; Gonzalez, C.; Pople, J. A. *Gaussian 94*; Gaussian Inc.: Pittsburgh, PA, **1995**; Vol. revision D.4.

(4) Frisch, M. J.; Trucks, G. W.; Sclegel, H. B.; Scuseria, G. E.; Robb, M. A.; Cheeseman, J. R.; Zakrzewski, V. G.; Montgomery, J. A.; Stratmann, R. E.; Burant, J. C.; Dapprich, S.; Millam, J. M.; Daniels, A. D.; Kudin, K. N.; Strain, M. C.; Farkas, O.;

Tomasi, J.; Barone, V.; Cossi, M.; Cammi, R.; Mennucci, B.; Pomelli, C.; Adamo, C.; Clifford, S.; Ochterski, J.; Petersson, G. A.; Ayala, P. Y.; Cui, Q.; Morokuma, K.; Malick, D. K.; Rabuck, A. D.; Raghavachari, K.; Foresman, J. B.; Cioslowski, J.; Ortiz, J. V.; Baboul, A. G.; Stefanov, B. B.; Liu, G.; Liashenko, A.; Piskorz, P.; Komaromi, I.; Gomperts, R.; Martin, R. L.; Fox, D. J.; Keith, T. A.; Al-Laham, M. A.; Peng, C. Y.; Nanayakkara, A.; Gonzalez, C.; Challacombe, M.; Gill, P. M. W.; Johnson, B.; Chen, W.; Wong, M. W.; Andres, J. L.; Gonzalez, C.; Head-Gordon, M.; Replogle, E. S.; Pople, J. A. *Gaussian 98*; Gaussian Inc.: Pittsburgh, PA, **1995**.

(5) Carpenter, J. E. *J. Mol. Struct. (THEOCHEM)* **1988**, *169*, 41.

(6) Curtiss, L. A.; Pochatko, D. J.; Reed, A. E.; Weinhold, F. *J. Chem. Phys.* **1983**, *82*, 2679.

(7) Foster, J. P.; Weinhold, F. *J. Am. Chem. Soc.* **1980**, *102*, 7211.

(8) Glendening, E. D.; Reed, A. E.; Carpenter, J. E.; Weinhold, F. *NBO ver. 3.1*.

(9) Reed, A. E.; Weinstock, R. B.; Weinhold, F. *J. Chem. Phys.* **1985**, *83*, 735.

(10) Reed, A. E.; Curtiss, L. A.; Weinhold, F. *Chem. Rev.* **1988**, *88*, 899.

(11) Roothaan, C. C. J. *Rev. Mod. Phys.* **1951**, *23*, 69.

(12) Møller, C.; Plesset, M. S. *Phys. Rev.* **1934**, *46*, 618.

(13) Head-Gordon, M.; Pople, J. A.; Frisch, M. J. *Chem. Phys. Lett.* **1988**, *153*, 503.

(14) Becke, A. D. *Int. J. Quantum Chem.* **1994**, *S28*, 625.

(15) Becke, A. D. *J. Chem. Phys.* **1993**, *98*, 5648.

(16) Lee, C.; Yang, W.; Parr, R. G. *Phys. Rev. B* **1988**, *37*, 785.

(17) Miehlich, B.; Savin, A.; Stoll, H.; Preuss, H. *Chem. Phys. Lett.* **1989**, *157*, 200.

(18) Perdew, J. P. *Phys. Rev. B* **1987**, *34*, 7046.

(19) Perdew, J. P. *Phys. Rev. B* **1986**, *33*, 8822.

(20) Perdew, J. P.; Wang, Y. *Phys. Rev.* **1992**, *B45*, 13244.

(21) Perdew, J. P.; Chevary, J. A.; Vosko, S. H.; Jackson, K. A.; Pederson, M. R.; Singh, D. J.; Fiolhais, C. *Phys. Rev. B* **1993**, *48*, 4979(E).

(22) Slater, J. C. *The Self-Consistent Field for Molecular and Solids*; McGraw-Hill: New York, **1974**; Vol. 4.

(23) Vosko, S. H.; Wilk, L.; Nusair, M. *Can. J. Phys.* **1980**, *58*, 1200.

(24) Ditchfield, R.; Hehre , W. J.; Pople, J. A. *J. Chem. Phys.* **1971**, *54*, 724.

(25) Hehre, W. J.; Ditchfield, R.; Pople, J. A. *J. Chem. Phys.* **1972**, *56*, 2257.

(26) Hariharan, P. C.; Pople, J. A. *Mol. Phys.* **1974**, *27*, 209.

(27) Gordon, M. S. *Chem. Phys. Lett.* **1980**, *76*, 163.

(28) Hariharan, P. C.; Pople, J. A. *Theo. Chim. Acta.* **1973**, *28*, 213.

(29) Krishnan, R.; Binkley, J. S.; Seeger, R.; Pople, J. A. *J. Chem. Phys.* **1980**, *72*, 650.

(30) McLean, A. D.; Chandler, G. S. *J. Chem. Phys.* **1980**, *72*, 5639.

(31) Allinger, N. L.; Yuh, Y. H.; Lii, J.-H. *J. Am. Chem. Soc.* **1989**, *111*, 8551.

(32) Mohamadi, F.; Richards, N. G. J.; Guida, W. C.; Liskamp, R.; Lipton, M.; Caufield, C.; Chang, G.; Hendrickson, T.; Still, W. C. *J. Comput. Chem.* **1990**, *4*, 440.

We have modified the MM3* force field to include new atom types and parameters to better handle the OSSO and OS(S)O functionalities.

(33) Pople, J. A.; Binkley, J. S.; Seeger, R. *Int. J. Quant. Chem. Symp.* **1976**, *10*, 1.

(34) Pople, J. A.; Seeger, R.; Krishnan, R. *Int. J. Quant. Chem. Symp.* **1977**, *11*, 149.

(35) Steudel, R.; Miaskiewicz, K. *J. Chem. Soc. Dalton Trans.* **1991**, 2395.

(36) Steudel, R.; Schmidt, H.; Sülzle, D.; Schwarz, H. *Inorg. Chem.* **1992**, *31*, 941.

(37) Gleiter, R.; Hyla-Kryspin, I.; Schmidt, H.; Steudel, R. *Chem. Ber.* **1993**, *126*, 2363.

(38) Snyder, J. P.; Carlsen, L. *J. Am. Chem. Soc.* **1977**, *99*, 2931.

(39) Koritsanszky, T.; Buschmann, J.; Schmidt, H.; Steudel, R. *J. Phys. Chem.* **1994**, *98*, 5416.

(40) The deviation in geometry for MeOSSOMe in the solid state is due to crystal packing forces.

(41) The sum of the van der Waals radii for oxygen and hydrogen is 2.700 Å. See: Bondi, A. *J. Phys. Chem.* **1964**, *68*, 441.

(42) Steudel, R.; Schmidt, H.; Baumeister, E.; Oberhammer, H.; Koritsanszky, T. *J. Phys. Chem.* **1995**, *99*, 8987.

(43) It is important to note the differences in structural measurement techniques. X-ray crystallography is carried out on crystals. X-Ray bond lengths are the distances measured between the mean positions of atoms. Electron diffraction (ED) and microwave spectroscopy (MW) are carried out in the gas phase. In ED, bond lengths are the average distances between atoms. For greater details concerning the differences in measurement techniques see: Burkert, U.; Alliner, N. L. *ACS Monograph 177*; American Chemical Society: Washington D.C., **1982**.

(44) Predictive geometries are deemed accurate if the structural parameters fall within three standard deviations of the experiment.

(45) Jursic, B. S. *J. Mol. Struct. (THEOCHEM)* **1996**, *366*, 97.

(46) Jursic, B. S. *J. Comput. Chem.* **1996**, *17*, 835.

(47) Jackson, R. H. *J. Chem. Soc.* **1962**, 4585.

(48) Kuczkowski, R. L. *J. Am. Chem. Soc.* **1963**, *85*, 3047.

(49) Ma, B.; Lii, J.-H.; Schaefer, H. L. I.; Allinger, N. L. *J. Phys. Chem.* **1996**, *100*, 8763.

(50) Structural parameters from X-Ray reported in the Ph.D. thesis of S. Tardif, 1997.

(51) Thompson, Q. E.; Crutchfield, M. M.; Dietrich, M. W. *J. Am. Chem. Soc.* **1964**, *86*, 3891.

(52) Thompson, Q. E.; Crutchfield, M. M.; Dietrich, M. W. *J. Org. Chem.* **1965**, *30*, 2696.

(53) Thompson, Q. E. *3,357,993*; United States Patent Office: United States of America, **1967**, 4.

(54) Harpp, D. N.; Steliou, K.; Cheer, C. J. *J. Chem. Soc. Chem. Commun.* **1980**, 825.

(55) Harpp, D. N.; Zysman-Colman, E.; Abrams, C. B. *J. Org. Chem.* **2003**, *68*, 7059.

(56) Tanaka, S.; Sugihara, Y.; Sakamoto, A.; Ishii, A.; Nakayama, J. *J. Am. Chem. Soc.* **2003**, *125*, 9024.

(57) We compared our calculated work solely to our own two crystal structures.

(58) Cioslowski, J.; Mixon, S. T. *Inorg. Chem.* **1993**, *32*, 3209.

(59) Hypervalent molecules are defined as those which contain atoms which have violated the octet rule (*i.e.* there are more than four pairs of electrons in a traditional Lewis structure of the molecule). Gillespie, R. J.; Robinson, E. A. *Inorg. Chem.* **1995**, *34*, 978.

(60) Minyaev, R. M.; Minkin, V. I. *Can. J. Chem.* **1998**, *76*, 776.

(61) Kutzelnigg, W. *Angew. Chem. Int. Ed. Engl.* **1984**, *23*, 272.

(62) Reed, A. E.; Schleyer, P. v. R. *J. Am. Chem. Soc.* **1990**, *112*, 1434.

(63) Using **5a** as the model thionosulfite, the S-S bond length was adequately reproduced without an f function (MP2/6-311G*) though the S-O bond lengths were dependent upon polarization functions, with at least 1 d and 1 f functions required to accurately reproduce the X-ray results.

(64) Patterson, C. H.; Messmer, R. P. *J. Am. Chem. Soc.* **1989**, *111*, 8059.

(65) Mayer, I. *J. Mol. Str. (THEOCHEM)* **1987**, *149*, 81.

(66) Das, D.; Whittenburg, S. L. *J. Phys. Chem. A.* **1999**, *103*, 2134.

(67) Winnewisser, G.; Winnewisser, M.; Gordy, W. *J. Chem. Phys.* **1968**, *49*, 3465.

(68) Surjan, P. R.; Mayer, I.; Kertész, M. *J. Chem. Phys.* **1982**, *77*, 2454.

(69) Single point energy calculations were performed in an iterative process on optimized geometries of MeOSSOMe **6** at the MP2/6-311G(2df) level given a constrained τ(O-S-S-O). This dihderal angle was altered by 15° each time and the geometry was reoptimized prior to each single point calculation.

(70) This is perhaps not too surprising given the large rotational barrier in **6**. Small perturbations in the ground state geometry of **6** would not be expected adversely influence the overall rotational profile.

(71) Raban, M.; Kenney Jr., G. W. J.; Jones Jr., F. B. *J. Am. Chem. Soc.* **1969**, *91*, 6677.

(72) Hubbard, W. N.; Douslin, D. R.; McCullough, J. P.; Scott, D. W.; Todd, S. S.; Messerly, J. F.; Hossenlopp, I. A.; George, A.; Waddington, G. *J. Am. Chem. Soc.* **1958**, *80*, 3547.

(73) Wiberg, K. *Tetrahedron* **1968**, *24*, 1083.

(74) Bickelhaupt, F. M.; Solà, M.; Schleyer, P. v. R. *J. Comput. Chem.* **1995**, *16*, 465.

(75) Tyrell, J.; Weinstock, R. B.; Weinhold, F. *Int. J. Quant. Chem.* **1981**, *19*, 781.

(76) For a molecule, a Rydberg orbital is a molecular orbital (MO) which correlates with a Rydberg atomic orbital in an atomic fragment produced by dissociation. A Rydberg atomic orbital is an orbital whose principal quantum number is greater than that of any occupied orbital of the ground state. Goodman, L.; Pophristic, V. *Encyclopedia of Computational Chemistry*; John Wiley and Sons: **1998**, 2525.

(77) In NBO, the molecular wave function is described by a set of optimum localized bond and lone pair orbitals. See: Reed, A. E.; Schleyer, P. v. R. **1987**, *109*, 7362.

(78) The HF/6-31G* level of theory was employed as the authors of the NBO program warn that DFT methods are not suitable for evaluating deletion energies. See: Glendening, E. D.; Badenhoop, J. K.; Reed, A. E.; Carpenter, J. E.; Weinhold, F. *Natural Bond Order Analysis Programs*; University of Wisconsin: Madison, **1999**.

(79) Salzner, U.; Schleyer, P. v. R. *J. Am. Chem. Soc.* **1993**, *115*, 10231.

(80) Schleyer, P. v. R.; Kos, A. J. *Tetrahedron* **1983**, *39*, 1141. Negative hyperconjugation is equivalent to double bond-no-bond resonance in terms of valence bond theory.

(81) Thatcher, G. R. J. *The Anomeric Effect and Associated Stereoelectronic Effects*; American Chemical Society: Washington, D. C., **1992**; Vol. 539.

(82) Lemieux, R. U. *Pure Appl. Chem.* **1971**, *25*, 527.

(83) Eliel, E. L. *Angew. Chem. Int. Ed. Engl.* **1972**, *11*, 739.

(84) *The Anomeric Effect*; Juaristi, E., Ed.; CRC Press: Boca Raton, **1995**.

(85) Deslongchamps, P. *Stereoelectronic Effects in Organic Chemistry*; Wiley: New York, **1983**.

(86) The use of the electrostatic model of dipole interactions to account for the generalized anomeric effect has been the subject of much debate and detailed discussion. For a history on the origin of the anomeric effect see: Omoto, K.; Marusaki, K.; Hirao, H.; Imade, M.; Fujimoto, H. *J. Phys. Chem. A* **2000**, *104*, 6499. and references cited therein.

(87) The term "*gauche* effect" would also accurately describe the phenomenon studied. It is defined as the tendency to adopt that structure which has the maximum number of *gauche* interactions between the adjacent electron pairs and/or polar bonds. See: Wolfe, S. *Acc. Chem. Res.* **1970**, 102.

(88) Edward, J. T. *Chem. Ind.* **1955**, 1102.

(89) Lemieux, R. U.; Chü, N. J. *Abstr. Pap. - Am. Chem. Soc.* **1958**, *133*, 31N.

(90) Kirby, A. J. The Anomeric Effect and Related Stereoelectronic Effects at Oxygen; Springer Verlag: Berlin, **1983**.

(91) Salzner, U.; Schleyer, P. v. R. *J. Org. Chem.* **1994**, *59*, 2138.

(92) Zefirov, N. S.; Shekhtman, N. M. *Russ. Chem. Rev.* **1971**, *40*, 315.

(93) Booth, G. E.; Ouellette, R. J. *J. Org. Chem.* **1965**, *31*, 544. For 2-Chloro- and 2-Bromotetrahydropyrans.

(94) Eliel, E. L.; Giza, C. A. *J. Org. Chem.* **1968**, *33*, 3754. For 2-Alkoxy- and 2-Alkylthiotetrahydropyrans and 2-Alkoxy-1,3-dioxanes.

(95) Pierson, G. O.; Runquist, O. A. *J. Org. Chem.* **1968**, *33*, 2572. For 2-alkoxytetrahydropyrans.

(96) Raban, M.; Yamamoto, G. *J. Am. Chem. Soc.* **1979**, *101*, 5890. For sulfenamides (R_2N-SR).

(97) Riddeli, F. G. *Tetrahedron* **1981**, *37*, 849. For hydroxylamine derivatives (R_2N-OR).

(98) Reed, A. E.; Schleyer, P. v. R. *J. Am. Chem. Soc.* **1987**, *109*, 7362. For polyfuorinated 1st and 2nd row hydrides.

(99) Kost, D.; Egozy, H. *J. Org. Chem.* **1989**, *54*, 4909. For Methyl *N*-Benzyl-*N*-(trihalomethanesulfenyl)carbamates.

(100) Wiberg, K. B.; Murcko, M. A. *J. Am. Chem. Soc.* **1989**, *111*, 4821. For dimethoxymethane ($(MeO)_2CH_2$).

(101) Salzner, U.; Schleyer, P. v. R. *J. Am. Chem. Soc.* **1993**, *115*, 10231. For $CH_2(XH)_2$ where X = O, S, Se, Te.

(102) BelBruno, J. J. *Heteroatom Chemistry* **1997**, *8*, 199. For H_2Te_2 and Me_2Te_2.

(103) Gobbato, K. I.; Mack, H.-G.; Oberhammer, H.; Della Védova, C. O. *J. Am. Chem. Soc.* **1997**, *119*, 803. For bis(fluorooxy)difluoromethanes ($(FO)_2CF_2$).

(104) Cárdenas-Jirón, G. I.; Letelier, J. R.; Toro-Labbe, A. *J. Phys. Chem. A* **1998**, *102*, 7864. For thioperoxide (HS-OH).

(105) Moudgil, R.; Kaur, D.; Vashisht, R.; Bharatam, P. *Proc. Indian Acad. Sci. (Chem. Sci.)* **2000**, *112*, 623. For selenamides (R_2N-SeR).

(106) Carballeira, L.; Pérez-Juste, I. *J. Phys. Chem. A* **2000**, *104*, 9362. For $CH_2(XH_2)_2$ (X = N, P, As).

(107) Anderson, J. E. *J. Org. Chem.* **2000**, *65*, 748. For acyclic acetals ($ROCH_2OR$).

(108) Carballeira, L.; Pérez-Juste, I. *J. Comput. Chem.* **2000**, *21*, 462. For R-O-CR_2-NR_2 (R = H, Me).

(109) Pophristic, V.; Goodman, L. *J. Phys. Chem. A* **2002**, *106*, 1642. For methanol (CH_3-OH).

(110) Reinhardt, L. A. Ph.D. thesis, University of Wisconsin-Madison, **1994**.

(111) Reed, A. E.; Schleyer, P. v. R. *Inorg. Chem.* **1988**, *27*, 3969.

(112) Reed, A. E.; Schade, C.; Schleyer, P. v. R.; Kamath, P. V.; Chandrasekhar, J. *J. Chem. Soc. Chem. Commun.* **1988**, 67.

(113) Kost, D.; Stacer, W. A.; Raban, M. *J. Am. Chem. Soc.* **1972**, *94*, 3233. and references cited therein.

(114) As both atomic orbitals are filled, the resulting π and π^* molecular orbitals are also filled and thus no net bonding occurs.

(115) The generalized anomeric effect is a combination of several factors: stereoelectronic, electrostatic and steric. Delocalization due to negative hyperconjugation is but one of these components.

(116) Tvaroska, I.; Bleha, T. *Chem. Pap.* **1985**, *39*, 805.

(117) Lovas, F. J.; Tiemann, E.; Johnson, D. *J. Chem. Phys.* **1974**, *60*, 5005.

(118) Marsden, C. J.; Smith, B. J. *J. Chem. Phys.* **1990**, *141*, 335.

(119) For a review of σ acceptor properties of analogous C-X bonds see: Alabugin, I. V.; Zeidan, T. A. *J. Am. Chem. Soc.* **2002**, *124*, 3175. and references cited therein.

Chapter 4

The Chemistry and Physical Properties of Acyclic Alkoxy Disulfides

4.1 Introduction

As was shown in Chapter 3, the origin of the barrier to rotation of the dialkoxy disulfides, **1**, appears to arise entirely from an electronic modulation of the S-S σ-bond. Indeed, the degree of this electronic effect manifests itself through electron-withdrawing elements immediately adjacent to the S-S bond (Table **50**). Restricted rotation about single bonds[1] is not usually influenced solely through stereoelectronic interactions. For instance, well-documented high torsional barriers in amides,[2-15] thioamides,[12,16,17] sulfenamides,[18] acrylonitriles (DMAAN)[19] and carbamates[20,21] are due in part to resonance-induced double bond character in these systems.[22] In biphenyls[23,24] and related compounds[25-28] however, they are due to steric interactions about either an sp^2-sp^2 or an sp^2-sp^3 carbon-carbon bond.[29,30]

Table **50**. S-S torsional barrier of some related polychalcogens

Compound		Barrier[a]	Ref
MeS-SMe	**71a**	6.8	[31]
$MeOS\text{-}SN(Me)_2$	**149**	14.5	[32]
EtOS-SOEt	**7**	18.4	[33]

a) In kcal/mol.

Thompson[34] observed that upon heating, **1** decomposed to afford the corresponding aldehyde **100** and alcohol **13** and elemental sulfur. He hypothesized a six-membered cyclic transition state, similar to that shown in Scheme **41**, to account for the product formation. We have shown that diatomic sulfur can indeed be trapped by dienes in good yield (61-79%) in what was similarly suggested to be a thermal pseudo-pericyclic reaction; in the absence of a diene trap[35] S_2 condenses to S_8 (*cf.* Chapter **2.6.1**).[35]

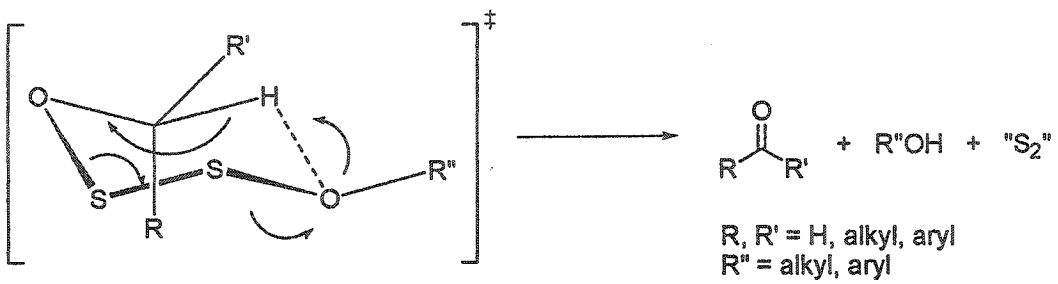

Scheme 41. 3-D representation of original concerted mechanism

In this Chapter we examine the diasterotopic coalescence phenomenon as a function of the substituent as well as the solvent. We also investigate the nature of the thermal decomposition pathway. We used the relatively stable bis(*p*-nitrobenzyloxy) disulfide **49** as a representative alkoxy disulfide in most of these studies.

4.2 Preparation of Acyclic Alkoxy Disulfides

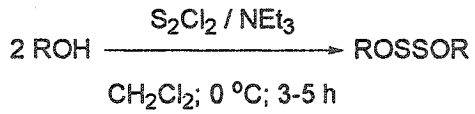

Scheme 42.

As part of our wider interests in the physical properties of alkoxy disulfides, we synthesized and characterized several alkoxy disulfides (derived from the corresponding alcohols **13**) according to a modification of the procedure used by Thompson[34] (Scheme 42, Table 51). Dilute conditions and freshly distilled sulfur monochloride (S_2Cl_2) are key in attaining high yields and purity. This is due to the photolytic instability of S_2Cl_2 over a

wider range of wavelengths.[36] Our[§] current synthetic method is effective, with addition times reduced by *ca.* 90% from earlier preparative methods.[35] Longer reaction times were sometimes necessary (5 h instead of 3 h), in particular for **150**, **51** and **48**, wherein the para-substituted group was not electron-withdrawing. Initial purification attempts with **51** resulted in lower yields as this product was unstable to chromatographic conditions.[35] Increasing the steric bulk of the alcohol decreased the yield of the resulting alkoxy dilsufide. In fact, with R = trityl, **153**, only starting alcohol was obtained.

Table **51**. Yields of alkoxy disulfides

Cmpd	R	Yield (%)	Cmpd	R	Yield (%)
49	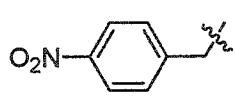	97			
			153	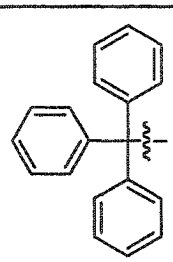	0[b]
150	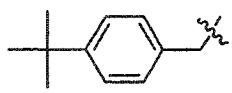	90			
51	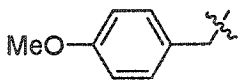	93	**24**		69
48	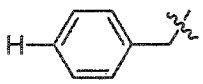	86	**34**	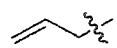	82
151		0[a]	**42**		57
152	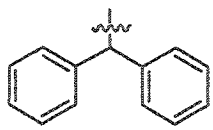	86	**154**		0[b]

a) Complex mixture of products. b) Only Starting Material detected.

[§] This work has been submitted: Zysman-Colman, E.; Harpp, D.N. *J. Org. Chem.* 2003

This series represents a varied substrate study in the synthesis of alkoxy disulfides, although Thompson prepared several aliphatic examples in his original paper.[34] The coupling of *p*-cresol to form alkoxy disulfide **154** and 4-*N,N*-dimethylaminobenzyl alcohol to form alkoxy disulfide **151** proved unsuccessful. Interestingly, only one aromatic alkoxy disulfide has ever been reported (R = 2,2'diaminophenoxy).[37,38] Here, there are strong electron-donating groups in the *ortho* positions which apparently increase the nucleophilicity of the phenolic oxygens enough to drive the reaction forward. It is unclear why **151** could not form given that alkoxy disulfides with electron-donating groups such as **51** can be synthesized and are stable. During the reaction with **154**, the mixture turns a bright green color. This is in contrast to the yellow solutions that are usually observed. Direct electrophilic substitution of sulfur monochloride is not unprecedented[37-39] and the benzene ring may act as a competing nucleophile in this particular case.

Compounds **24**, **34**, **42**, **48**, **49**, **51**, **150**, and **152** were conveniently stored at -10 °C for months with only minor decomposition to the corresponding alcohol. Compound **42** decomposed to a brown solid upon reduced pressure solvent removal but could be stored in CH_2Cl_2 for weeks. Braverman and co-workers also observed the same solution stability.[40] All the alkoxy disulfides synthesized possess a sweet-fruity aroma and its presence is indicative of the successive coupling of the starting alcohol with S_2Cl_2.

It should be noted that the synthesis of **24**, **48**, **49** and **51** were all optimized. The preparation of **150** and **152** had previously not been reported. Compound **42** was coincidently reported[40] during our synthesis survey.

4.3 Synthesis of Some Related Acylic Chalcogenic Compounds

As part of our study of the chemistry of alkoxy disulfides, we required pure samples of related compounds **155-160** such that we could compare the ^{1}H NMR spectra of these authentic samples to that of the photolyzed and thermalized alkoxy disulfide **49** (*vide infra*). Commentary on the individual synthesis of these compounds is worthwhile due to the potential synthetic difficulty in dealing with *p*-nitrobenzyl derivatives.

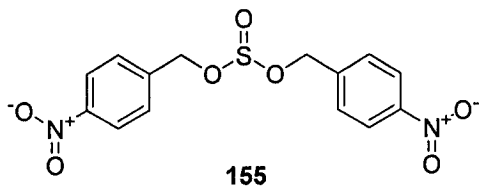

155

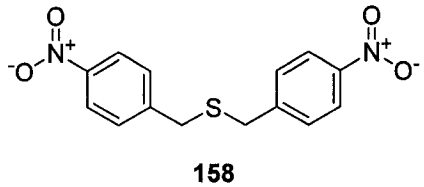

158

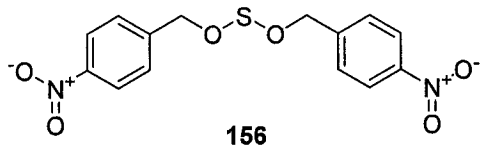

156

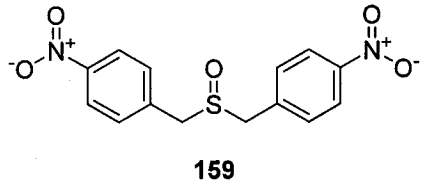

159

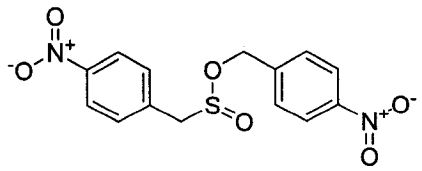

157

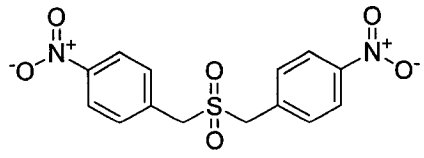

160

4.3.1 Preparation of bis(4-nitrobenzyl) sulfite 155

The coupling of alcohols with thionyl chloride ($SOCl_2$) to form the corresponding sulfite has been known for over 60 years.[41] The use of triethylamine (NEt_3) as the amine base and HCl sink has recently become popular[42,43] although other amine bases such as pyridine[44] have also been used.

Although Tardif[45] had previously synthesized **155** in moderate yield using pyridine as the base (66%), we decided to use triethylamine (Scheme **43**) given our success in the synthesis of related alkoxy disulfide **49**. This method proved equally effective affording a light yellow crystalline solid (Mp. 84-86 °C) in 62% yield.

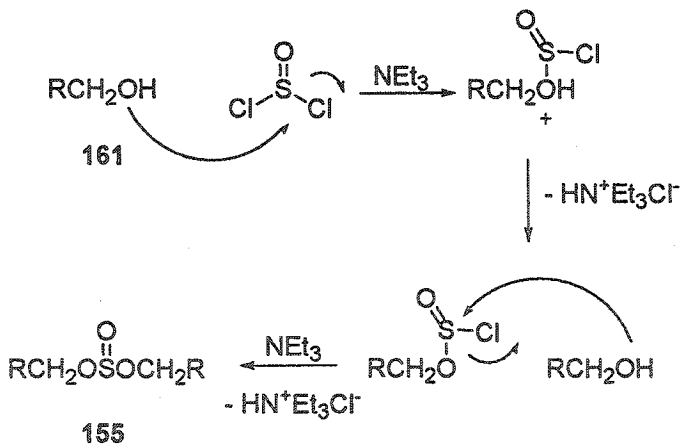

Scheme **43**.

4.3.2 Preparation of bis(4-nitrobenzyl) sulfoxylate 156

As with **155**, Tardif[45] had previously prepared sulfoxylate **156** through the coupling of **161** with SCl_2 in CH_2Cl_2 using NEt_3 as the base. She reported an overall yield of 50% as light orange crystals; curiously, no melting point was recorded. In our hands, using freshly distilled SCl_2 and NEt_3, we were able to isolate **156** in near quantitative yield (98%) after a standard work-up and flash chromatography. The sulfoxylate **156**, with a melting point of 86-87 °C, was isolated as a light orange solid with a fruity aroma that could then be recrystallized in CH_2Cl_2 as white crystals (confirmed as the sulfoxylate by X-Ray analysis). The increased yield may in part be due to longer reaction times (3 h instead of 2 h) and warmer temperatures (0 °C instead of -78 °C). Interestingly, Tardif[46] reported poor yields (10%) at similar temperatures to ours.

We observed little (< 1% by ^{1}H NMR) to no isomerization of **156** to the corresponding *p*-nitrobenzyl *p*-nitrobenzyl sulfinate **157** during either the reaction or the work-up. This is contrary to Thompson's original work on sulfoxylate synthesis.[47] However after 24 h in $CDCl_3$ at RT, **156** had isomerized in part to **157**. It was not possible to isolate **157** but its ^{1}H NMR and ^{13}C NMR agreed with the literature.[45] After 48 h, both **156** and **157** had completely decomposed even though the sample was not exposed to light, the products of which were not isolable. Attempts to synthesize **157** *via* complete isomerization of **156** proved unsuccessful.

4.3.3 Preparation of bis(4-nitrobenzyl) sulfide 158

We decided to adapt an effective procedure developed by Yoon[48] for the formation of **158** (Scheme 44).

158

Scheme **44**.

The coupling of Na_2S with *p*-nitrobenzyl bromide in refluxing methanol is facilitated by a phase transfer catalyst (PTC) in Amberlite-IRA 400(Cl). The work-up involves a two-step filtration. Compound **158** is only slightly soluble in methanol and as we were uninterested in optimizing the yield, the filtrate was discarded. The solute was then dissolved in CH_2Cl_2 and then concentrated to afford an orange-yellow solid (88%) with a melting point of 144-148 °C.

4.3.4 Preparation of bis(4-nitrobenzyl) sulfoxide 159

Selective oxidation to the sulfoxide without overoxidation to the sulfone is always a synthetic challenge. We initially hoped that we could access **159** through a facile MCPBA oxidation of the sulfide **158** (Scheme **45**).[49,50]

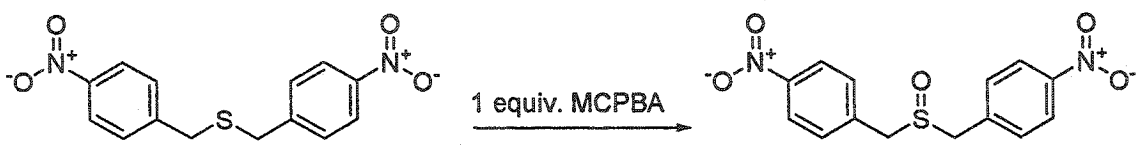

158 **159**

Scheme **45**.

This method proved to be unsuccessful resulting in a mixture of **158**, **159** and **160**. Modification of the reaction time and addition temperature had little effect in improving the overall yield. Moreover, in a solvent survey (13 common solvents) it was found that both **159** and **160** were only soluble to an appreciable extent in DMSO; they were found to be slightly soluble in $CHCl_3$ and CH_3CN. This made the work-up problematic in both syntheses.

Many other synthetic techniques for this procedure exist in the literature.[51] Methods include the pollution-free oxidation by H_2O_2,[52-59] oxidation through the use of polymer supported periodate ions[60,61] or IBX,[62] the use of heterogenous photochemical systems,[63] and oxidation using hydroperoxy sultams.[64]

Recently, solid-state oxidation of sulfides and sulfones using the urea-hydrogen peroxide adduct had been reported.[54] Different oxidation states could be accessed

depending on the reaction time. In our hands, this reagent proved ineffective. Even after 24 h, incomplete oxidation to **159** with concomitant over-oxidation to **160** was observed.

We therefore tried a recently published selective oxidation of **158** using excess H_2O_2 in 1,1,1,3,3,3-hexafluoroisopropanol HFIP (Scheme **46**).[65] Ravikumar reported decreased reaction times in fluorinated solvents. HFIP had the added benefit of readily solubilizing both **158** and **159**, which most likely resulted in the increased yield as compared to other methods tested. In our hands, this method proved to be extremely successful, affording the desired sulfoxide in quantitative yield (>99%) as a yellow solid with a melting point of 202-206 °C.

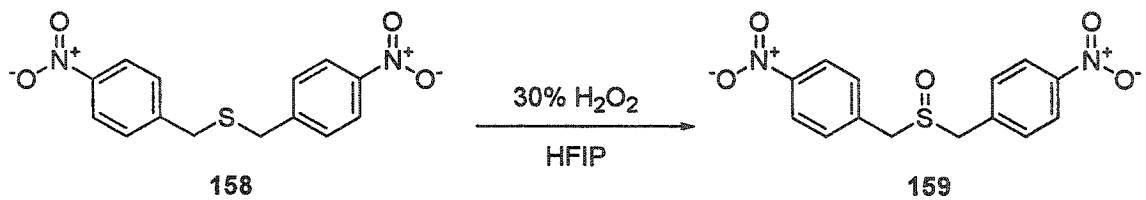

158 **159**

Scheme **46**.

4.3.5 Preparation of bis(4-nitrobenzyl) sulfone 160

We were able to obtain analytically pure samples of **160** from **158** using excess MCPBA (Scheme **47**). This method is not synthetically useful for this particular sulfone but nevertheless we isolated **160** in 22% yield as a white solid with a melting point of 235-239 °C.

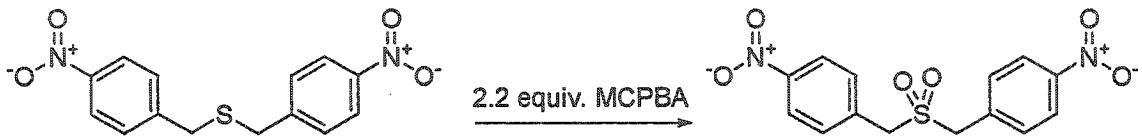

158 160

Scheme 47.

4.3.6 General Commentary on 155-160

All compounds in Chapter **4.3** were identified by Mp, ^{1}H NMR, ^{13}C NMR, MS and HRMS. The syntheses of **155** and **156** were optimized. In addition, three new *p*-nitrobenzyl derivatives **158-160** were prepared. The thermal stability increased markedly with increasing oxidation of the sulfur atom (**158-160**).

4.4 Evaluation of Rate Parameters

Although Thompson first concluded that the barrier to rotation was close to that of disulfides (E_a = 8.6 ± 1.7 kcal/mol),[34] such a low value would require an unexpected[66] large negative $\Delta S^{\ddagger}$. Subsequent work has shown that the reported value (8.6 kcal/mol) is erroneous.[67]

Seel[67] demonstrated that such a barrier for **6** (MeOSSOMe) was much higher ($\Delta G^{\ddagger}$ = 17.8 ± 0.1 kcal/mol). Lunazzi and co-wrokers[33] determined the thermodynamic properties for **49** in perchloroethene (C_2Cl_4) at 105 °C ($\Delta G^{\ddagger}$ = 19.0 ± 0.2 kcal/mol, $\Delta H^{\ddagger}$ =

20 ± 1 kcal/mol, $\Delta S^{\ddagger} = 2 \pm 5$ eu). In Chapter 3 we showed *via* gas phase calculations and others[33] have suggested that the origin of the large barrier is due to two n_S to $\sigma^*_{S\text{-}O}$ MO interactions. We now report our own experimentally determined barriers to rotation.

4.4.1 The S-S Torsional Barrier as a Function of Substituent

We were first interested in determining whether the barrier height could be modulated by altering the substituent R group of an alkoxy disulfide.

Table 52 Chemical shift and coupling constant data for related ROSSOR

Entry	Cmpd	J_{AB}	ν_z	$\delta\Delta\nu/J_{AB}$	R
1	49	12.40	4.94	3.84	*p*-NO_2-Bn
2	48	11.25	4.84	4.67	Bn
3	150	11.50	4.82	4.81	*p*-t-butyl-Bn
4	51	11.25	4.77	4.54	*p*-MeO-Bn

A substituent study (Table 52) of compounds 48, 49, 51 and 150 reveals a measurable electronic effect on the benzyl proton signals. As the para-substituent is altered from an electron-donating to an electron-withdrawing group, the coupling constant, J_{AB}, increases and the chemical shift of the AB-quartet, ν_z, moves downfield. These two parameters do not change uniformly as noted in their relative ratio (which is a marker of the magnetic environment of the diastereotopic benzyl protons).

Studies of the mutual-site exchange kinetics provide the torsional barrier about the S-S bond in **49** in DMSO-d_6 by a complete line-shape analysis (LSA) of the exchange-broadened benzyl signals by fitting the experimental data with the computer program WINDNMR[68] (Table **53**).[69] The program was provided with the proton chemical shifts at slow exchange, the coupling constant, the FWHH and the digitized NMR spectrum. Standard activation parameters were obtained from the linear least squares fit of the experimental rate data to both the Eyring and Arrhenius equations assuming a transmission coefficient of unity. The Pearson regression factor (R^2) for these fits was greater than 0.98 as exemplified in Figure **16**. The error limits in Table **54** assume only random errors. It is unclear why **49** decomposed in previous studies[35,70] though the cleavage of alkoxy disulfides is both acid and base sensitive (*cf.* Chapter **2.6**).

Clearly the electronic effect shown in Table **51** did not affect the barrier to rotation (see $\Delta G^{\ddagger}_{298}$, Table **53**). Thus the high barrier in alkoxy disulfides is a function not of the electronics of the R group but intrinsically that of the OS-SO moiety.

Table **53**. Substrate study of the activation parameters for **49**, **51** and **150**.

Cmpd	Activation Parameters[a]					
	$\Delta H^{\ddagger}$ (kcal/mol)	$\Delta S^{\ddagger}$ (eu)	$\Delta G^{\ddagger}_{298}$ (kcal/mol)	$\Delta G^{\ddagger}_{Tc}$[b] (kcal/mol)	E_A (kcal/mol)	log A (/s)	T_c (K) ± 0.5
49	13.0 ± 0.9	-14.7 ± 2.7	17.4 ± 1.2	18.3 ± 1.3	13.6 ± 0.9	23.1 ± 1.4	360.7
150	16.6 ± 1.0	-4.9 ± 2.9	18.1 ± 1.3	18.4 ± 1.4	17.2 ± 1.0	28.0 ± 1.5	362.7
51	13.7 ± 0.6	-12.4 ± 1.8	17.4 ± 0.8	18.2 ± 0.9	14.3 ± 0.6	24.2 ± 0.9	362.7

a) The errors, as given here, represent a 68% confidence interval in the least squares deviation calculation. b) $\Delta G^{\ddagger}$ determined at the T_c for each compound.

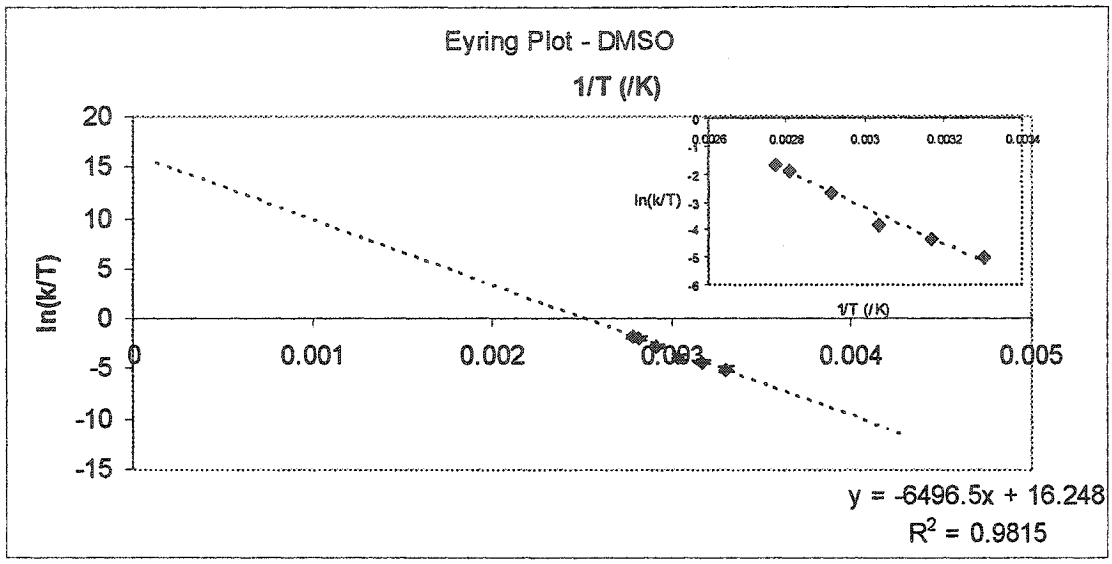

Figure **16**. Eyring plot of the rotation about the S-S bond in **49** in DMSO-d_6

4.4.2 The S-S Torsional Barrier as a Function of Solvent

The soluble, crystalline and stable **49** is nicely suited for the evaluation of the influence of solvent polarity on the torsional barrer. The MP2/6-311G(3d) dipole moments of the optimized *gauche* ground state and the *trans*-transition state for MeOSSOMe **6** (2.4 and 0 D, respectively – *cf.* Chapter **3** for GS value) suggest a siginificant difference potentially responsive to a substantial variation in solvent polarity. Examination of the torsional potential of **49** in different solvents complements the work by Lunazzi[33] and co-workers who evaluated simple alkoxy disulfides to reveal little or no influence on barrier height.

The rate of exchange of the benzyl protons during rotation about the S-S bond in **49** was determined in a similar manner to that detailed in Chapter **4.4.1**. As shown in Figure **17**, the two doublets of the AB system eventually coalesce into a single line since fast

rotation about the S-S creates a dynamic plane of symmetry that makes the benzyl protons enantiotopic. The Pearson regression factor (R^2) for the linear fits to the Eyring and Arrhenius equations ranged from 0.96-0.99, indicating that the simulations are in good agreement with the obtained spectra. The free energies of activation scaled to a common temperature (298 K) for six solvents with empirical solvent polarity parameter E_T values[71] ranging from 33-45 exhibit no apparent medium effect (Table **54**). The spread of $\Delta G^{\ddagger}_{298}$ is a diminutive 0.7 kcal/mol that is essentially flat with respect to solvent polarity as illustrated by plots of activation free energy against the empirical solvent polarity parameter, E_T and the Onsager[72,73] dielectric constant function, defined as $(\varepsilon-1)/(2\varepsilon+1)$ where ε is the dielectric constant (Figures **18** and **19**). The lack of solvent correlation with the Onsager reaction field model is at first surprising as energy differences[74] in *gauche* and *trans* conformers and the rotational barriers[75] of 1,2-dichloroethane are well correlated. Recall that there exist similar stereoelectronic interactions in **49** and 1,2-dichloroethane (*cf.* Chapter **3**). This lack in correlation may be due to the limited choice of solvents, most of which are aromatic; solvents needed to be high boiling for this study.

The H-C-H bond angles, θ, have been determined by X-ray crystallography[46] to be 93.57° and 113.52° for each of the sets of H-C-H angles. These bond angles are not unusual for sp^3 carbons and this is reflected in the ^2J values.

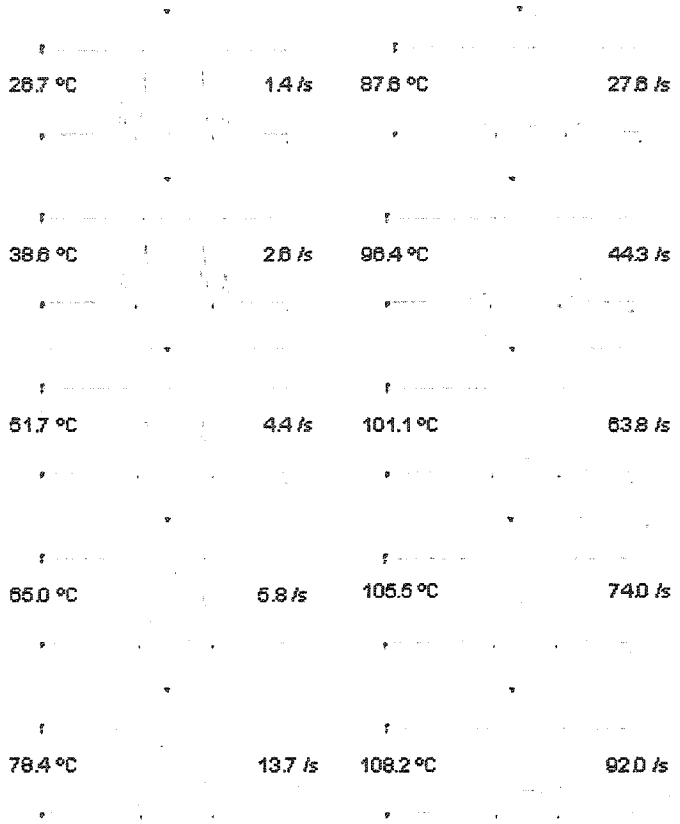

Figure 17. Temperature dependence of the benzyl CH_2 signal of **49** (500 MHz in DMF-d_7). Superimposed on each spectrum is the display of each computer simulation obtained with the rate constants (in s^{-1}) indicated. Above each spectrum is a difference spectrum indicating the goodness of fit of the simulation.

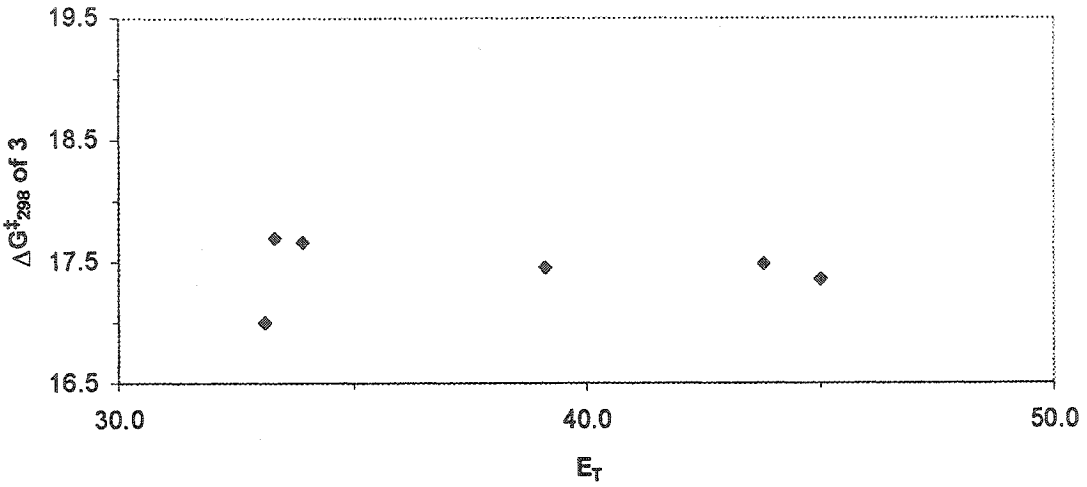

Figure 18. Relationship between the observed rotational barriers of 49 and the Dimroth-Reichardt solvent polarity parameter, E_T.[71]

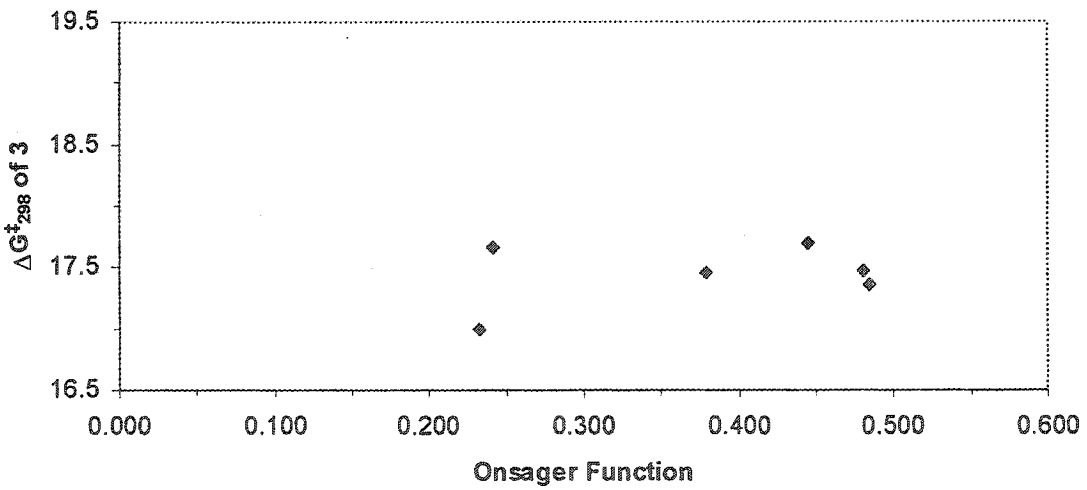

Figure 19. Relationship between the observed rotational barriers of 49 and the Onsager function $(\varepsilon-1)/(2\varepsilon+1)$, where ε is the dielectric constant.[73]

Table 54. NMR-derived activation parameters for coalescence of the diastereotopic methylene protons of **49** obtained by line shape analysis; S-S bond rotation, 298 K.[a]

Solvent	$\Delta H^{\ddagger}$ (kcal/mol)	$\Delta S^{\ddagger}$ (eu)	$\Delta G^{\ddagger}_{298}$ (kcal/mol)	E_A (kcal/mol)	log A (/s)	k_c (s^{-1}) ± 10	$E_T(30)$[b] (kcal/mol)	J_{AB}[c] (Hz)	$\Delta\nu$[d] (Hz)	T_c (K) ± 0.5
C_2Cl_4[e]	20.0 ± 1	2 ± 5					32.1	-12.5	37.5	378.2
p-xylene	8.6 ± 0.5	-28.1 ± 1.4	17.0 ± 0.7	9.3 ± 0.5	16.4 ± 0.7	87	33.1	-12.5	75.0	383.2
pyridine	15.4 ± 1.3	-7.7 ± 4.0	17.7 ± 1.8	16.1 ± 1.3	26.7 ± 2.0	103	33.3	-13.0	54.5	365.1
toluene	13.1 ± 0.5	-15.4 ± 1.4	17.7 ± 0.6	13.7 ± 0.5	22.8 ± 0.7	127	33.9	-12.3	69.7	378.6
chlorobenzene	10.4 ± 0.7	-23.5 ± 2.1	17.5 ± 1.0	11.1 ± 0.8	18.8 ± 1.1	145	39.1	-12.7	67.6	394.7
DMF	11.1 ± 0.7	-21.5 ± 2.1	17.5 ± 1.0	11.7 ± 0.7	19.7 ± 1.1	92	43.8	-12.5	45.8	381.3
DMSO	12.9 ± 0.9	-14.9 ± 2.7	17.4 ± 1.2	13.6 ± 0.9	23.1 ± 1.4	68	45.0	-13.0	39.9	360.7

a) The errors, as given here are assumed to be only random and represent a 68% confidence interval in the least squares deviation calculation. b) From ref [71]. c) Two bond couplings assigned a negative value consistent with the general rule for geminal couplings. d) Chemical shift difference at no exchange (500 MHz at 23 °C) except for C_2Cl_4 (300 MHz at 22 °C). e) From ref [33], $\Delta G^{\ddagger}$ determined at 105 °C.

Rate constants, k_c, and free energies of activation, $\Delta G^{\ddagger}$, at coalescence temperature, T_c, were also calculated using approximation equations (2) and (3) following Raban and co-workers,[76] where R, k_B and h are the universal gas constant (8.314 J/mol K), Boltzmann's constant (1.381×10^{-31} J/K) and Planck's constant (6.626×10^{-34} J*s), respectively.[77] The coalescence temperature is defined as the temperature at which the appearance of the spectrum is that of a single, flat-topped peak. For each solvent, the coupling constant, J_{AB}, the chemical shift difference, $\Delta\nu$, and the full-width-at-half-height (FWHH) were obtained directly from the frequency separation of the appropriate peaks in the slow exchange region ($k_c << \Delta\nu$), in the present cases at least 70 °C below each individual T_c.

$$k_c = \frac{\pi}{\sqrt{2}}\sqrt{\Delta\nu^2 + 6J_{AB}^2} \qquad (2)$$

$$\Delta G^{\ddagger} = RT_c\left[\ln\left(\frac{k_B}{h}\right) - \ln\left(\frac{k_c}{T_c}\right)\right] \qquad (3)$$

Table 55. Comparison of S-S torsion barriers for **49** derived from complete line shape analysis (LSA) and the T_c method of eqs. (2) and (3) at T_c.

Solvent	LSA[a] $\Delta G^{\ddagger}_{Tc}$[c] (kcal/mol)	T_c method[b] k_c (s^{-1}) ± 60	T_c method[b] $\Delta G^{\ddagger}_{Tc}$[c] (kcal/mol)	Discrepancy k_c (s^{-1}) ± 61	Discrepancy $\Delta G^{\ddagger}$ (kcal/mol)	$E_T(30)$[d] (kcal/mol)
C_2Cl_4[e]	19.0 ± 0.2					32.1
p-xylene	19.4 ± 0.7	180	18.7 ± 0.3	-93	0.7 ± 0.8	33.1
pyridine	18.2 ± 2.0	140	17.9 ± 0.3	-37	0.3 ± 2.0	33.3
toluene	18.9 ± 0.7	169	18.5 ± 0.3	-41	0.4 ± 0.8	33.9
chlorobenzene	19.7 ± 1.1	165	19.3 ± 0.3	-20	0.4 ± 1.2	39.1
DMF	19.3 ± 1.1	122	18.9 ± 0.4	-30	0.4 ± 1.2	43.8
DMSO	18.3 ± 1.3	113	17.9 ± 0.4	-45	0.4 ± 1.4	45.0

a) $\Delta G^{\ddagger}$ was determined using LSA. b) Comparison of $\Delta G^{\ddagger}$ was made at T_c for each of the solvents. c) $\Delta G^{\ddagger}$ determined at the T_c of **49** in each respective solvent. d) From ref [71]. e) From ref [33], $\Delta G^{\ddagger}$ determined at 105 °C.

The LSA free energies from Table **54** recalculated at the corresponding coalescence temperatures (Table **55**) are within 0.4 kcal/mol on average from those derived from T_c, indicating that both free energy assessment methods provide comparable values. In this context, the $\Delta G^{\ddagger}_{Tc}$'s span the slightly larger range of 1.5 kcal/mol, but once again show no correlation with solvent polarity. Unlike amides,[10,11,13] acrylonitriles,[19] 2-alkoxy-3-halobutanes and 2-acetoxy-3-halobutanes,[78] which all exhibit a detectable solvent dependence on the barrier to rotation, rotation in **49** appears to be indifferent to medium influences (Scheme **48**).

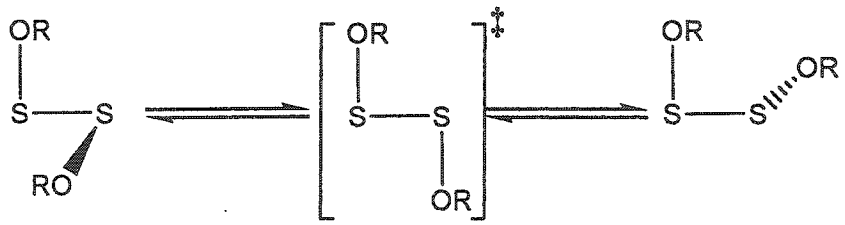

gauche P TS *gauche* M

Scheme **48**. Interconversion of enantiomers of **1**

The solvent effects observed for amide rotation[79] for instance depend on a reduction in dipole moment during the dynamic process.[80] For amides, the decrease amounts to *ca.* 0.2 or 1.8 D, depending on the nature of the torsional transition state (DMA, Figure **20**).[6,7,11,13,15]

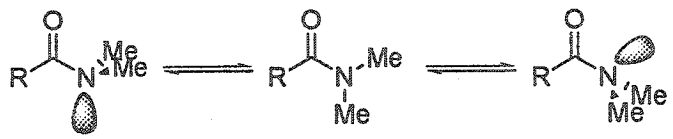

	TS1	*GS*	*TS2*
R = H[a]	1.66	4.22	4.14
R = Me[b]	2.12	3.93	3.75
R = OMe[c]	0.88	2.50	2.96

Figure 20. Gas phase ground and transition state dipoles (D) for amide and carbamate isomerization. a) Dipole moments calculated at HF/6-31++G**. Here rotation through TS1 is preferred by 3.5 kcal/mol.[13] b) Dipole moments calculated at HF/6-31G*. Here TS1 is more stable than TS2 by 4.1 kcal/mol.[15] c) Dipole moments calculated at HF/6-311G**. Here TS1 is more stable than TS2 by 0.6 kcal/mol.[20]

A polar solvent preferentially stabilizes the charge separation in the more polar ground state relative to the less polar transition states;[10] the lack of a solvent effect in carbamates has been attributed in part to the presence of increased charge separation in the transition state[20] and the relatively smaller dipole moments of carbamates as compared to analogous amides.[21] As implied above for MeOSSOMe **6**, the dipole moment difference for dialkoxy disulfides is significant. To evaluate the situation for **49**, the X-Ray[33] structure and the corresponding *trans*-transition state were optimized with the MM3* force field (Chapter **3.1.1**, Table **38**) and subsequently subjected to single point calculations with density functional theory using the B3LYP/6-311G* method. While the transition state model is essentially nonpolar (μ_{calc} = 0.03 D), the enantiomeric ground states are estimated to sustain a substantial dipole moment (μ_{calc} = 5.9 D). Since the ground state–transition state difference is of the same order of magnitude as that for amides a solvent

dependence is expected; recall that solvation energy is also proportional to the square of the dipole moment of the equilibrium geometry. It should be noted however that for non-hydrogen bonding solvents similar to those used in the present work, the solvent-induced activation free energy variation for amides is a diminutive 0.5-1.5 kcal/mol. If the NMR measurements incorporate an error of ± 0.5 kcal/mol, such an effect would therefore not be observed. While the random errors for **49** are only of the order of ± 0.3 kcal/mol, complementary errors due in part to temperature control and acquisition procedures appear to have raised the accumulated errors beyond the threshold where a small medium effect can be observed (*cf.* Chapter **4.4.3** for details).

The thermodynamic data is in general good agreement with the literature[33,70] as well as our own calculated work (*cf.* Chapter **3**). Lunazzi[33] and co-workers report $\Delta G^{\ddagger}$ to be 18-19 kcal/mol for a series of 7 alkoxy disulfides with both small and large R substitutents. Both the absolute values and the 1 kcal/mol range are entirely compatible with the data of Tables **53-55**. Clearly, neither substituent size nor electronics nor medium effects significantly perturb the energetics of the S-S rotation barrier. The magnitude of the S-S rotation barrier for dialkoxy disulfides is of interest as it is related to the barrier of thermal cleavage outlined in Chapter **4.5**.

4.4.3 A Closer Investigation of the Activation Parameters in Chapters 4.4.1 and 4.4.2

As stated in the previous section, the activation parameters are generally in close agreement with the literature.[33] The $\Delta H^{\ddagger}$ values are smaller than those cited by Lunazzi

and co-workers,[33] whereas $\Delta S^{\ddagger}$ values are much larger and negative. Though rotation about single bonds is usually characterized by $\Delta S^{\ddagger}$ values of *ca.* 0 eu,[81-83] large negative

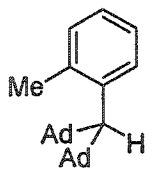

$\Delta G^{\ddagger}$ = 45.1 kcal/mol
$\Delta S^{\ddagger}$ = -11 eu

161

$\Delta S^{\ddagger}$ of the same order of magnitude as our experimentally determined activation entropies are not unprecedented as with *anti-o*-tolyldi(1-adamantyl)methane[84] **161** and related alcohols[85,86] and hydrocarbons.[85] Unimolecular isomerization of carbamates in protic solvents also display a significant negative $\Delta S^{\ddagger}$.[20] In this case, the negative $\Delta S^{\ddagger}$ observed may be associated with stronger solvation of the more polar transition state

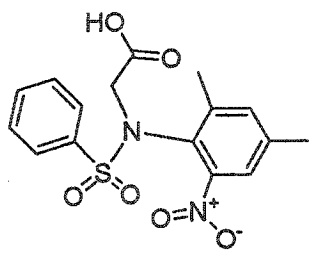

162

(TS2 in Figure 20) as compared to the ground state, resulting in it being the more favoured transition state in water. The racemization of *N*-benzenesulfonyl-*N*-carboxymethyl-2,4-dimethyl-6-nitroanaline **162** in 26 different solvents consistently displays a large negative entropy of activation.[87] Systems where torsional motion is severely restricted are inherently entropically unfavourable.[88,89] This is the case with **49**. A possible interpretation of our observed large $\Delta S^{\ddagger}$ is simply a reflection of degree of rigidity afforded by the OSSO functionality, though this only accounts for the magnitude

not the sign of $\Delta S^{\ddagger}$. The observed decrease in entropy indicates that the transition state is being preferentially solvated. This is quite surprising given that the ground state has the larger net dipole. It should be pointed out that restricted rotation about single bonds does not necessitate large entropies. Rotation in secondary amides ($k \sim 1\ s^{-1}$) is restricted with a high energy barrier (*ca.* 17.9 kcal/mol) but possessing small entropies of activation.[90]

Another interpretation of our discrepant entropic and enthalpic data is in terms of enthalpy-entropy compensation, wherein perturbations in $\Delta H^{\ddagger}$ are accompanied by compensatory perturbations in $\Delta S^{\ddagger}$ such that $\Delta G^{\ddagger}$ remains the same.[91] This thermodynamic relationship (Figure **21**), wherein a correlation exists between $\Delta H^{\ddagger}$ and $\Delta S^{\ddagger}$, has widely been employed to explain an observed isokinetic relationship in both biological[92-95] and non-biological systems.[96-106] However, of late, many[107-111] have questioned the validity of this relationship, attributing the correlation to a statistical compensation pattern that is independent of the chemistry observed, reactions and

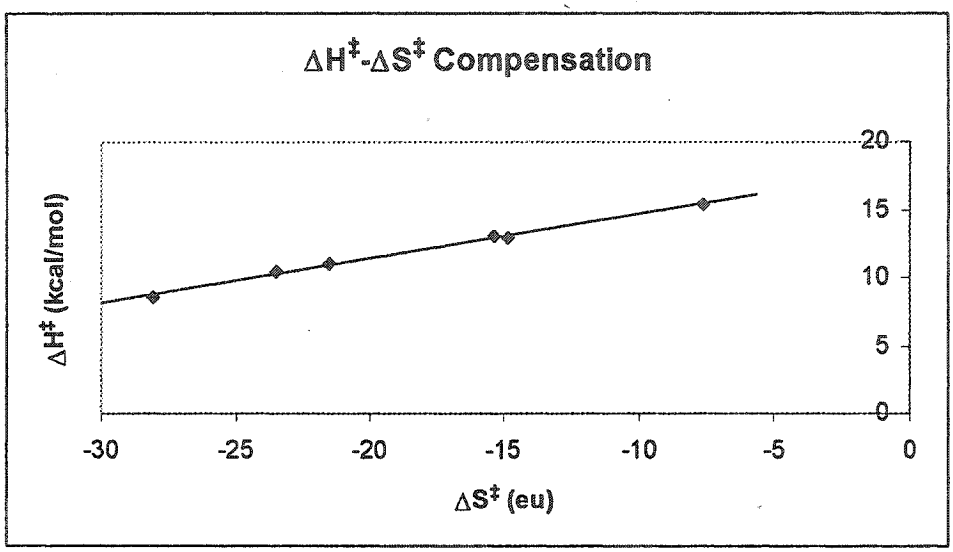

Figure 21. Entropy-enthalpy compensation plot ($\Delta H^{\ddagger} = \beta\Delta S^{\ddagger} + \Delta H^{\ddagger}_{o}$) of **49**. The slope normally represents the isokinetic temperature, β, which in this case would be 325.4 K.

equilibria.[108] Inferring $\Delta H^{\ddagger}$ and $\Delta S^{\ddagger}$ from either the Eyring or Arrhenius equations would be misleading and erroneous as both parameters would have been derived from only one independent variable, temperature. Thus, the calculated $\Delta H^{\ddagger}$ and $\Delta S^{\ddagger}$ parameters are really one and the same. In order to gain more thermodynamic information, one would have to perform independent calorimetry experiments to ascertain accurate $\Delta H^{\ddagger}$ and $\Delta S^{\ddagger}$.

If we acknowledge that the derived $\Delta H^{\ddagger}$ and $\Delta S^{\ddagger}$ parameters from the Eyring equation are valid, then other potential sources of error need to be assigned. As detailed in the following section (Chapter 4.4.4), $\Delta H^{\ddagger}$ is a function of the slope and $\Delta S^{\ddagger}$ is a function of the y-intercept of the Eyring equation. As stated earlier, these two values are extrapolated from a linear least squares fit of the rate data. Thus, minor errors in rate constant determination can lead to much larger errors in the activation parameters; $\Delta G^{\ddagger}$

seems to be reliable (*vide supra*). The fitting of each spectrum to the computer simulation affords the rotational rate constant, k_c. This parameter is not only temperature sensitive but also is a function of the FWHH (full width at high height) and the relative chemical shifts of each doublet of the AB system being modeled. Thus errors in one of these latter two parameters will result in errors in the final activation parameters. In particular, the rate constant, k_c, is derived from the difference of an aggregate rate constant and the FWHH. In the region of slow exchange, where k_c is small, large errors in the FWHH lead to large errors in the rate constant. Errors in the true FWHH can result from an inability to account for other sources of line broadening; the determination of the rate constant is predicated upon the assumption that the sole source of line broadening is due to temperature. The benzyl protons being modeled couple to the aromatic ring and are thus always broader. In our system, we did not have an internal standard containing non-coupled protons to gauge and compensate for this source of broadening; bibenzyl or dibenzyl ether would have been appropriate choices. Thus we did not take this source of error into account at the time of data acquisition.

To gauge whether the broadened peaks were really a potential source of error in our activation parameters, we introduced an artificially small FWHH (corresponding to an uncertainty of as large as ± 50%), and redid the LSA. This produced nearly identical activation parameters to those reported so this source of error was discounted as a major contributor to the overall error in the activation parameters. We also did not use an internal standard to ascertain the degree of magnetic field inhomogeneity contribution to the line width. Other sources of line broadening also include non-optimal tuning of the

spectrometer, which is also temperature sensitive; the spectrometer was tuned prior to each acquisition. It is also important to handle the chemical shifts of each doublet of the AB system correctly if they vary at all from their slow exchange values. Though it is easy to determine them in the region of slow exchange, extrapolating them at higher temperatures is more problematic due to the difficulty in fitting the spectrum; for instance, the four peaks of the AB system may not be resolvable at higher temperatures. Thus small errors in chemical shifts (at high temperatures) and natural line width (at low temperatures) make the biggest difference in ascertaining correct $\Delta S^{\ddagger}$.

4.4.4 Experimental Details For Dynamic NMR Spectroscopy and the Determination of the Rotational Activation Parameters

The variable-temperature ^{1}H NMR spectra were recorded on a 500 MHZ machine using a 5 mm triple resonance probe. Spectra were recorded in deuteratured *p*-xylene, toluene, chlorobenzene, pyridine, DMF and DMSO. The calibration of the probe's temperature controller was established against a vacuum-sealed ethylene glycol standard. The difference in chemical shifts of the two ethylene glycol peaks was measured in a series of seven temperatures separated by 20 °C over a 120 °C range. The calibrated temperatures were determined after *ca.* 40 min of temperature equilibration time (Figure 22).

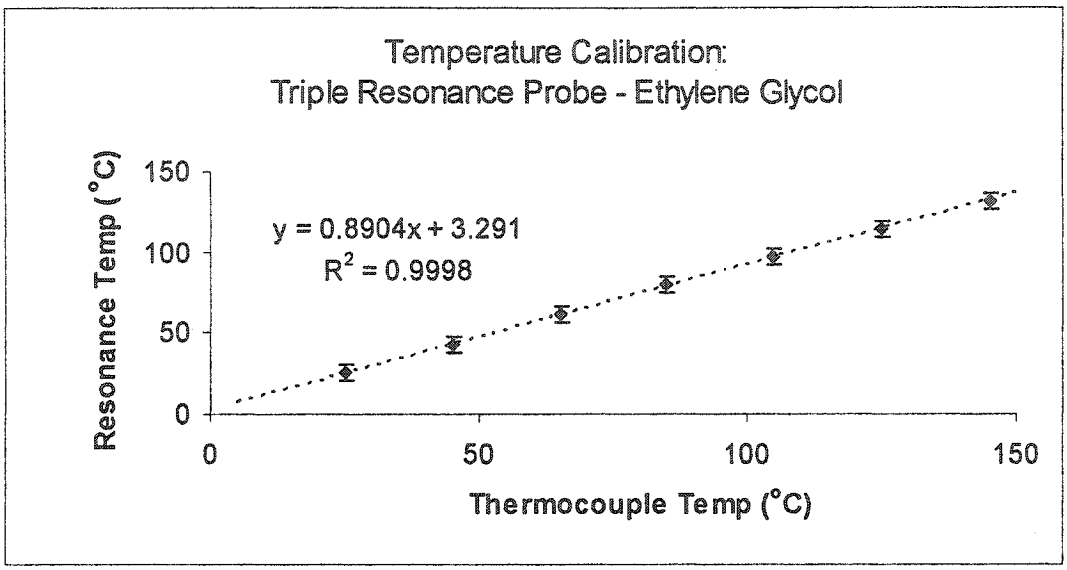

Figure 22. Ethylene glycol temperature calibration of the 5 mm triple resonance probe for the 500 MHz spectrometer

An NMR tube containing either **49**, **51** or **150** and the appropriate solvent was filled to *ca.* 600 μl and isolated from the ambient light. The spectra were acquired over a temperature range of *ca.* 100 °C in approximately 20° intervals (smaller intervals were used near T_c). The spectra were simulated by means of a computer program[68] which solves the Kubo-Sack exchange matrix in an iterative fashion. The program was provided with the coupling constant, J_{AB}, and the effective line width parameter (FWHH) as measured at the limit of slow exchange, and the digitized NMR spectrum. The coupling constant, J_{AB}, and the FWHH remained constant throughout each of the simulations. The best fit was visually judged by overlapping the spectrum with the simulated trace as well as by observing the difference spectrum.

As this internal rotation about the S-S bond is an equilibrium process, thermodynamic rate theory can be used to evaluate activation parameters involved in this process. The

rate of mutual site-exchange can be expressed in terms of both the Eyring equation (4)

$$k = \kappa \frac{k_B T}{h} e^{-\Delta G^{\ddagger}/RT} \qquad (4)$$

$$k = A e^{-E_A^{\ddagger}/RT} \qquad (5)$$

and the Arrhenius equation (5).

Here, κ is the transmission coefficient, assumed to be unity, which is defined as the fraction of the reactant reaching the transition state that proceeds to the product; A is the preexponential factor; $E_A^{\ddagger}$ is the activation energy; the remaining constants are defined as in Chapter **4.4.2**. Substituting $\Delta G^{\ddagger} = \Delta H^{\ddagger} - T\,\Delta S^{\ddagger}$, eq (4) becomes eq (6):

$$k = \frac{k_B T}{h} e^{\frac{-\Delta H^{\ddagger}}{RT}} e^{\frac{\Delta S^{\ddagger}}{R}} \qquad (6)$$

Linearizing equation (5) and dividing eq (6) by T then linearizing it affords equations (7) and (8), respectively.

$$\ln(k) = \ln(A) - \frac{E_A^{\ddagger}}{RT} \qquad (7)$$

$$\ln\left(\frac{k}{T}\right) = -\frac{\Delta H^{\ddagger}}{RT} + \frac{\Delta S^{\ddagger}}{R} + \ln\left(\frac{k_B}{h}\right) \qquad (8)$$

These two equations can now be linearly fitted, whence the activation parameters are related to the slope, m, and y-intercept, b, by the following; equations (9) and (10) relate to eq (7) whereas equations (11) and (12) relate to eq (8):

$$m = \frac{-E_A^{\ddagger}}{R} \qquad (9)$$

$$b = \ln(A) \qquad (10)$$

$$m = \frac{-\Delta H^{\ddagger}}{R} \qquad (11)$$

$$b = \frac{\Delta S^{\ddagger}}{R} + \ln\left(\frac{k_B}{h}\right) \qquad (12)$$

The activation energy, $E^{\ddagger}_{A}$, and enthalpy, $\Delta H^{\ddagger}$, are related by eq (13):

$$E_A^{\ddagger} = \Delta H^{\ddagger} + RT \qquad (13)$$

Using eqs (9)-(13) the activation parameters cited in Tables 53 and 54 were obtained.

The error in a function q(x,...,z), assuming that the uncertainties in x,...,z are themselves independent and random, is defined as eq (14):[112]

$$\sigma(q) = \sqrt{\left(\frac{\delta q}{\delta x}\sigma(x)\right)^2 + \cdots + \left(\frac{\delta q}{\delta z}\sigma(z)\right)^2} \qquad (14)$$

Where σ(q), σ(x) and σ(z) are the respective errors on q, x and z.

The errors on $\Delta H^{\ddagger}$, $\Delta S^{\ddagger}$, $\Delta G^{\ddagger}$, $E_A^{\ddagger}$ and ln(A) can now be defined as follows:

$$\sigma(\Delta H^{\ddagger}) = R\sigma(m) \qquad (15)$$

$$\sigma(\Delta S^{\ddagger}) = R\sigma(b) \qquad (16)$$

$$\sigma(\Delta G^{\ddagger}) = \sqrt{\sigma(\Delta H^{\ddagger})^2 + \left[-\Delta S^{\ddagger}\sigma(T)\right]^2 + \left[-T\sigma(\Delta S^{\ddagger})\right]^2} \qquad (17)$$

$$\sigma(E_A^{\ddagger}) = R\sigma(m) \qquad (18)$$

$$\sigma(\ln A) = \sigma(b) \qquad (19)$$

The errors on m and b, σ(m) and σ(b), are derived from the linear least squares fit of the data to either the Eyring or Arrhenius function. Errors on k_B, h and R are assumed to be 0 and σ(T) was conservatively estimated to be 0.5 K.

4.5 Evaluation of the Thermal and Photolytic Stability of Alkoxy Disulfides

Although acid- and base-catalyzed[34,113] decomposition of alkoxy disulfides has been briefly investigated, only one report exists on their photochemistry.[114] The authors were

able to detect the presence of radicals both at high temperatures as well as under photolytic conditions. We initially examined the photolytic decomposition of **49** both in the solid state as well as in solution ($CDCl_3$), in air and under an inert atmosphere. In addition, we probed the effect of silica on the decomposition mechanism after observing that the corresponding sulfite by-product **155** is produced during flash chromatography. The results are summarized in Table **56**.

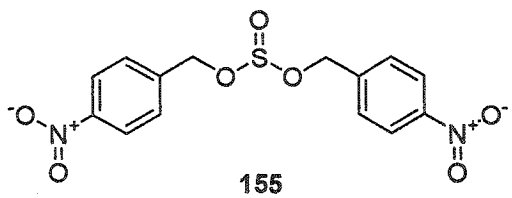

155

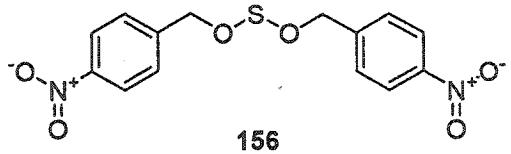

156

Table **56**. Photolytic and thermolytic activity experiments for **49**

Entry[b]	Conditions							^{1}H NMR Product Yield Distribution (%)[d]			
	dark	UV	air	N_2	solid state	$CDCl_3$	Temp (°C)[c]	**49**	**163**	**164**	**155**
1	x		x		x		27	86	10	0	4
2		x	x			x	27	87	9	1	3
3		x		x		x	27	89	8	0	3
4[a]		x	x			x	27	74	21	1	3
5[a]		x		x		x	27	83	14	1	2
6		x	x		x		27	85	10	0	4
7		x		x	x		27	88	9	0	3
8		x	x		x		60	21	45	1	10
9		x		x	x		50	0	85	0	0
10		x	x			x	60	81	15	1	3
11		x		x		x	50	85	15	0	0

a) Silica added. b) Reaction time 20-26 h. c) No change in relative integrations at 37 °C. d) ^{1}H NMR yields ± 5%.

After *ca.* 24 h at 27 °C, no matter whether in solution (Entries 2-4) or not (Entries 6, 7) or under an inert atmosphere (Entries 2, 6) or not (Entries 3, 7), little change was detected in the product ratios of **49** as compared to a control sample (Entry 1) that was left at room temperature exposed to the atmosphere (but shielded from light). The addition of silica

catalyzed a slight decomposition to the corresponding alcohol **163** while exposed to air (Entry 4) or under an inert atmosphere (Entry 5). However, when **49** was heated to temperatures greater than 37 °C under an inert atmosphere while in the solid state (Entry 9), it decomposed completely to form the alcohol **163** with concomitant formation of a small amount of an as yet unknown compound containing a singlet in the ^{1}H NMR spectrum in the benzylic region.

Upon heating **49** in the solid state (exposed to the atmosphere (Entry 8)), the corresponding aldehyde **164** as well as the sulfite **155** were observed as decomposition products. Except for this particular case, only trace sulfite **155** and no sulfoxylate **156** were ever detected. The decomposition observed in the solid state at elevated temperatures did not translate to the solution state (Entries 10 and 11). In fact, decomposition in solution was only observed at much higher temperatures (*ca.* 100-140 °C). It should be noted that in all thermolysis experiments, there was consistently detected a greater amount of alcohol **163** than aldehyde **164**. Such a product distribution inequality argues against a concerted mechanism; these results suggest that these compounds are much more UV stable than previously reported.[114] No rearrangement products such as those observed by Braverman[40,115] were observed owing to the fact that the *p*-nitrobenzyl group is not prone to undergo such [2,3]-sigmatropic rearrangements. In addition, no isomerization to the thionosulfite was observed.

Decomposition to the corresponding alcohol and aldehyde was also observed at elevated temperatures in all the solvents used in the determination of the rotational

barrier. Qualitative observations revealed that **49** was much less stable and decomposed much more readily in pyridine relative to the other solvents tested. This is most likely due to the nucleophilic nitrogen of the solvent catalyzing the process.[116,117] We undertook a quantitative solvent study in order to elucidate this decomposition pathway. The rate constant of decomposition of **49**, over a temperature range of 40 °C, was extrapolated from a series of ^{1}H NMR spectra taken at regular intervals, each containing an internal standard.

We chose three solvents which span a large polarity range. Upon least squares fitting of the resulting data, we determined that the rate of decomposition of the reaction was 1st order in **49** – Rate=k_d[**49**] (*e.g.* Figure **23**).[118]

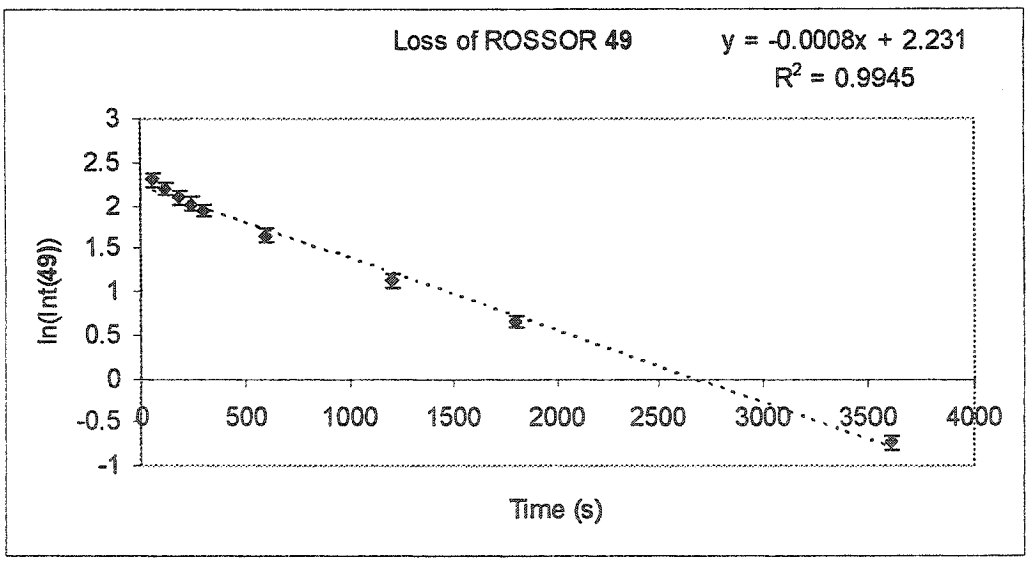

Figure **23**. First order rate plot of the decomposition of **49** at 105.7 °C in DMSO-d_6. Errors as shown here represent a 68% confidence interval in the linear fit of the data.

From this data, through the use of Eyring transition state theory, the following activation parameters were obtained (Table **57**). It should be noted that although the

individual decomposition kinetics were good, the corresponding Eyring plots yielded poor linear fits (R^2 ranged from 0.47-0.67), which is reflected in the large errors in Table 57. The estimation of these errors was performed in a similar manner to that described in Chapter **4.4.4**. The large $\Delta S^{\ddagger}$ values indicate a highly ordered and associative mechanism. The negative entropies are also comparable with other processes which have non-polar transition states, though these examples relate to concerted reactions.[45,119-124] However, we would have expected positive entropies to account for the dissociative mechanism implied by our data (*vide infra*).

Table **57**. Activation parameters for the decomposition of **49**.[a]

Solvent	$\Delta H^{\ddagger}$ (kcal/mol)	$\Delta S^{\ddagger}$ (eu)	$\Delta G^{\ddagger}_{298}$ (kcal/mol)	$E_T(30)^b$ (kcal/mol)
p-xylene	10 ± 4	-46 ± 10	24 ± 5	33.1
chlorobenzene	11 ± 6	-45 ± 15	24 ± 7	39.1
DMSO	13 ± 5	-38 ± 12	25 ± 6	45.0

a) The errors, as given here, represent a 68% confidence interval in the least squares deviation calculation. b) From ref [71].

A non-polar transition state is suggested as there seems to be little solvent dependency ($\Delta G^{\ddagger}$ ranges by *ca.* 1 kcal/mol over the three solvents). Although a stepwise mechanism, containing either a tight ion-pair or one which was pseudo-pericyclic is possible, calculations have shown that these are too energetically disfavoured.

Lunazzi[114] and co-workers demonstrated the trapping of aliphatic sulfenyl and sulfonyl radicals in the photolysis (-20 °C) of the corresponding alkoxy disulfide (EtOSSOEt 7), the latter of these two radicals resulting from oxidation of the former, ostensibly in the presence of the radical trap. They attributed the formation of the sulfenyl radical through

S-S scission. GC-MS analysis of the products derived from the photolysis of 7 in benzene resulted in the corresponding sulfite (EtOS(O)OEt **165**) and sulfoxylate (EtOSOEt **166**), as well as elemental sulfur. Such a product distribution could be

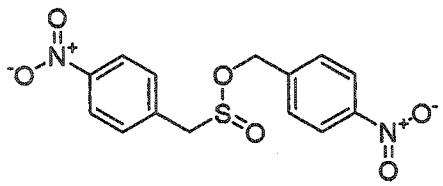

157

envisioned to occur from the coupling of alkoxyl radicals with the sulfur-centered radicals; these alkoxyl radicals could originate from S-O scission. There were only trace amounts of the analogous sulfite **155**, and no sulfoxylate **156** or sulfinate **157** was detected in the photolysis of **49**; the latter compound likely resulting from the room temperature isomerization of **156**. Interestingly, room temperature photolysis of di-*t*-butyloxy disulfide **18** in the presence of DMPO (4-*N,N* dimethylpyridine-*N*-oxide) yielded an ESR spectrum[125] characteristic of solely the presence of the *t*-butoxyl radical (*t*-BuO$^{\bullet}$). Photolysis of **48** in the presence of C_{60}-fullerene yielded a sole adduct indicating benzyloxyl radical formation.

The Lunazzi group also trapped an alkoxyl radical under moderately elevated temperatures (50-70 °C). Their thermolysis of **48** yielded a similar spectrum to that of its photolysis; in addition, formation of the corresponding benzyl adduct was detected.

In order to account for our results, we propose the following unsymmetric diradical decomposition mechanism, Scheme **49**. This pathway is consistent not only with the radical trapping experiments summarized above but also with the decomposition kinetics

and product decomposition ratios obtained during the thermally induced homolysis of alkoxy disulfides (*vide supra*), Tables 56 and 57. Diradical pathways have also been implicated in the photolysis[126-128] and thermolysis of cinnamyl-4-nitrobenzene sulfenate and related compounds to their corresponding sulfoxides.[129-131] It should be noted that the concerted mechanism originally proposed by Thompson (Scheme 17, Chapter 2.6.1) is incongruous with the data.

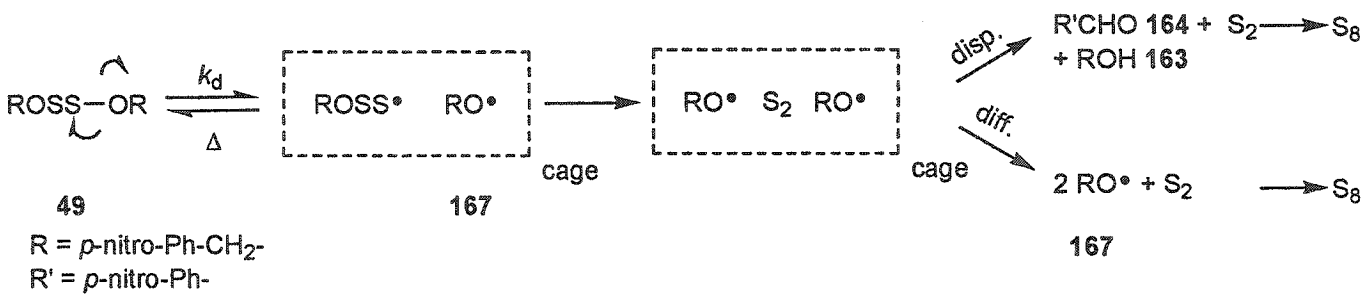

A

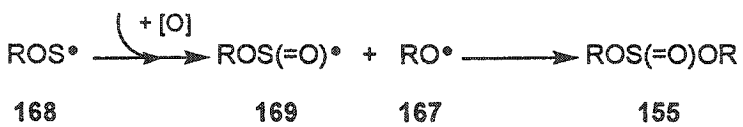

B

Scheme 49. Thermally-induced radical decomposition mechanism of ROSSOR (R = *p*-NO_2-Ph-CH_2) **49** – disp. = disproportionation; diff. = diffusion.

It is reasonable that the benzylic radicals that Lunazzi observed might arise from C-O scission to form highly chalcogenated radical $RCH_2OSSO^•$ followed by SO loss to afford the sulfenyl radical **168**. This mechanism is supported (in part) through the HRMS of decomposition products of bis(*p*-MeO-benzyloxy) disulfide **51** wherein SO was lost (HRMS of a second decomposition product wherein SO_2 was lost was also observed). Indeed, the loss of SO was noted in the MS of all of the alkoxy disulfides. Of

significance is that no decomposition products of the form **49** – SO or **49** – SO_2 were ever detected by ^{1}H NMR during either photolysis or thermolysis experiments as compared with authentic samples such as sulfide **158** or sulfoxide **159**; related sulfone **160** was also never detected. Though we did not detect any benzyl-derived products resulting from C-O cleavage such as *p*-nitrobibenzyl, we nevertheless detected benzyl radical cations by EI MS. C-O homolysis in **49** might have been expected given the origin of the para-nitro group. The presence of this electron-withdrawing group effectively raises the benzylic carbon's electronegativity, thus decreasing the electronegativity difference and thus the BDE between it and the adjoining oxygen atom.[132]

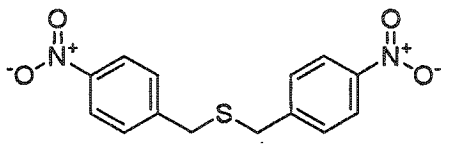

158

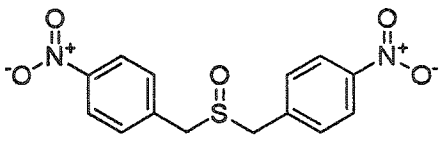

159

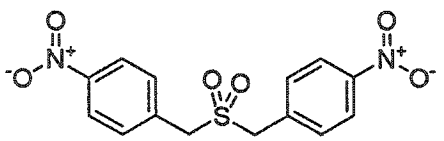

160

In our scheme, alkoxyl radicals, **167**, would arise from initial caged S-O bond scission; a second caged S-O bond cleavage is also possible. Pasto[133] has shown in a related H-S-S-O-H system that S-S cleavage is only slightly more favoured than S-O cleavage. The preference for S-S cleavage over S-O cleavage was shown to be highly dependent on the stabilities of the radicals formed. Additionally, for non-diaryl disulfides, C-S homolysis is slightly more favourable than symmetric S-S bond breakage.[134] The presence of the benzyl group, a group which contains conjugated π electrons, exerts a bond weakening effect upon the S-O bond.[135]

Finally, the cage could then disproportionate (*via* a remote hydrogen abstraction[128] of either of the alkoxyl radicals **167** or the solvent by the other alkoxyl radical) to yield the alcohol **163** that was the major product observed in our thermolysis experiments. If the source of the hydrogen atom abstraction is another alkoxyl radical or if β-scission of **167** occurs, then this would afford observed aldehyde **164**. Diatomic sulfur is the final disproportionation product which would immediately concatenate to form the more stable S_8 allotrope in the absence of a diene trap. This step-wise type of decomposition mechanism is not unprecedented. Indeed tetroxides[136-139] (some have suggested symmetric homolytic cleavage as the first step[140,141] but it is only the asymmetric cleavage of tetroxides that leads to product formation) and hyponitrites[142-146] have been shown to decompose by analogous mechanisms. Formation of minor amounts of sulfite **155** is outlined in Scheme **9B**.[147] The presence of only small amounts of sulfite **155** suggests that in our system, the propensity for *in situ* oxidation of radical species such as **168** is low.

The observed product ratios during the high temperature decomposition kinetics experiments are shown in Figure **24**.

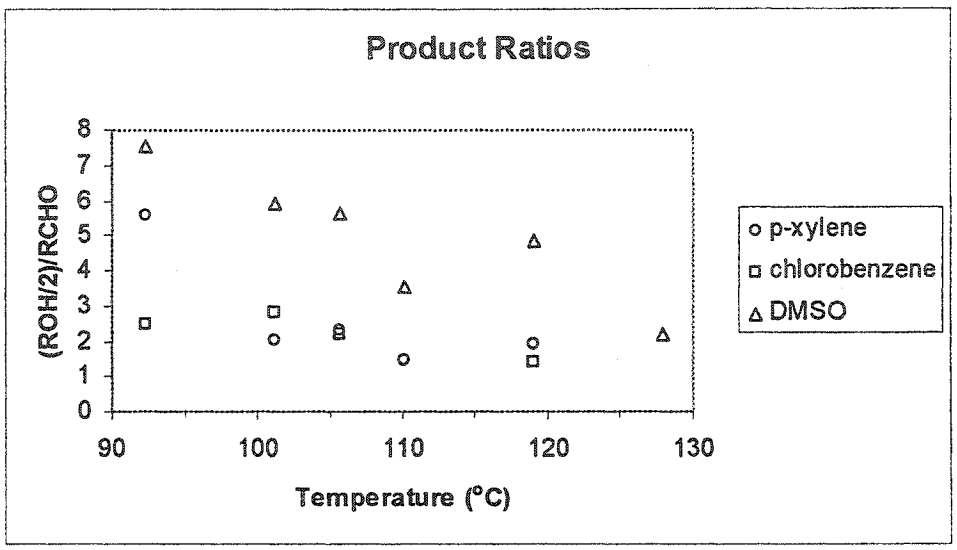

Figure 24. Ratio of the integration of alcohol **163** to aldehyde **164** per mole of integratrable protons.

The average **163**:**164** (ROH:RCHO) ratio is *ca.* 2:1 for chlorobenzene and *p*-xylene. There is consistently considerably more alcohol formed in DMSO. The non 1:1 ratio of decomposition products can usually[144,145] be ascribed to alkoxyl radicals **167** diffusing from the cage and subsequently abstracting hydrogens from the environment. In hydroxylic solvents a 1,2-H shift from carbon to oxygen has also been suggested as a viable possibility;[148] this shift is solvent-assisted and would occur due to increased radical stabilization (benzylic radical formation).[149] The relative excess of alcohol observed in DMSO may be due to the presence of water in the solvent, which might promote the fast 1,2-H shift.[146]

To our knowledge, the S-O and S-S bond dissociation energies for alkoxy disulfides have not been reported. Estimating them is problematic due to the formation of highly chalcogenated radicals. Nevertheless, the BDEs are related by equation (**20**).

$$BDE(ROSS\text{-}OR) = \Delta H_f^\circ(ROSS^\bullet) + \Delta H_f^\circ(RO^\bullet) - 2\,\Delta H_f^\circ(ROS^\bullet) + BDE(ROS\text{-}SOR) \quad (20)$$

In peroxides (RO-OR), the lone pair repulsion between oxygen atoms is believed to be responsible for the weakening of the O-O bond.[150] In disulfides, the lone pairs are more diffuse and therefore the S-S bond is stronger. The BDE of sulfenates (RO-SR) is intermediate between peroxides and disulfides. This is evidenced by their relative BDEs: BDE(MeO-OMe) = 38 ± 2 kcal/mol,[151] BDE(MeS-OMe) = 53 ± 10 kcal/mol,[129] BDE(MeS-SMe) = 65 ± 1 kcal/mol.[152] Analogously, we would expect S-O bond cleavage to be easier than S-S bond cleavage in alkoxy disulfides **1**. Additionally, the formed ROSS$^\bullet$ radical is able to be better stabilized through a three-electron π system with enhanced hyperconjugation compared to ROS$^\bullet$,[153] which would result from S-S scission. This is qualitatively shown in Figure **25**. As oxygen is more electronegative than sulfur,

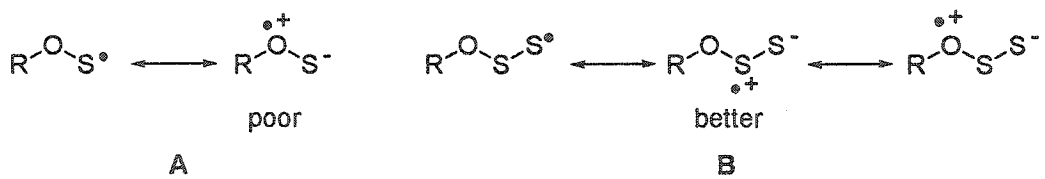

Figure **25**. Resonance form of ROS$^\bullet$ *vs.* ROSS$^\bullet$

the dipolar structure in Figure **10A** would be expected to be a poor contributor to the overall stability of the sulfenyl radical. Sulfur is also more polarizable than oxygen so charge separated species as in Figure **10B** would be seen as more viable resonance contributors. In fact, quantitively, Gregory and Jenks[154] have shown the ROS$^\bullet$ radical to be quite unstable: ΔH_f° = 1.4 kcal/mol for MeOS$^\bullet$ at the G2(MP2,SVP) level. The bond

dissociation energy for FS-SF **75a** is 61 ± 4 kcal/mol,[135] which is slightly less than that reported for MeS-SMe **71a**. So it is also reasonable to conclude that the BDE(ROS-SOR) would approximate to this value. The ΔH_f° for *t*-BuO$^\bullet$ = -22.8 kcal/mol[155] and is a good estimate for other alkoxyl radicals. So, in order for the BDE(ROSS-OR) < BDE(ROS-SOR), the contribution of ΔH_f°(ROSS$^\bullet$) + ΔH_f°(RO$^\bullet$) – 2 ΔH_f°(ROS$^\bullet$) has to be negative in magnitude. Given a large negative value for ΔH_f°(RO$^\bullet$) and a small positive value for ΔH_f°(ROS$^\bullet$) as well as rationales in the stabilization of ROSS$^\bullet$ (*vide supra*), it is reasonable to expect that the S-O bond would be the weaker bond and thus more prone to homolysis than the S-S bond in ROSSOR **1**.

It seems that there are two observable processes, both a decomposition pathway and a coalescence pathway that are each *solvent-insensitive*. Moreover, the decomposition phenomenon is *ca.* 6-8 kcal/mol higher. This is in accordance with our qualitative observations; if the decomposition phenomenon were more energetically favoured then one would not be able to observe coalescence.

4.5.1 Experimental Details for Thermal and Photolytic Decomposition Reactions of Alkoxy Disulfides

The decomposition ^{1}H NMR spectra were recorded on a 500 MHz machine using a 5 mm triple resonance probe. An NMR tube containing **49** and 1,3,5-tri-*t*-butylbezene, which acted as the internal standard, was filled to *ca.* 600 μL of either deuterated *p*-xylene, chlorobenzene or DMSO. The decomposition was followed each minute over the first 5 minutes and then at 10, 20, 30 and 60 minute intervals. A delay time of 5 s was

used. The reaction was performed at 92.3, 101.2, 105.7, 110.1, 119.0 and 127.9 °C. As **49** was only slightly soluble at room temperature in these solvents yet became fully soluble at elevated temperatures, the first couple of data points were usually discarded as they would not truly reflect the concentration of **49**. In addition, the last 1-3 data points may also have been discarded if **49** decomposed too rapidly. In this case, poor a signal to noise ratio would became a factor in the integration of the benzyl protons. For all experiments, at least 6 data points were used in the linear least squares fitting of the 1st order rate plots. Each decomposition experiment was repeated at least twice and the average rate constant was used in the determination of the activation parameters. In all cases the reaction was found to be 1st order in starting material with good correlation coefficients.

Under the conditions outlined in Table **56**, **49** was subjected to UV radiation by the use of a GE ultraviolet sun lamp (275 W; 110-125 V AC). All experiments were performed in 1 dram pyrex vials. Those reactions which were carried out under an inert atmosphere were degassed prior to being placed under a nitrogen (N_2) stream. The temperature of the reaction was mediated by the use of a water bath and the temperature was monitored at intervals throughout the reaction. ^{1}H NMR spectra ($CDCl_3$) of the reaction mixture were taken and products were identified through comparison with authentic samples.

4.6 Concluding Remarks

We have optimized a generalized synthetic procedure for the synthesis of acyclic alkoxy disulfides. We embarked on a substituent and solvent study on their ability to influence the S-S torsional barrier. Our data indicates that there exists no significant substituent or solvent effect. The latter point may seem incongruent given our calculated dipoles for the ground and *trans* transition states, but the errors on the measurements are sufficiently significant to cloud any possible solvent effect. In addition, we propose a mechanism to account for the observed thermal decomposition of **49**. Our experimentally determined activation parameters for this process indicate that **49** decomposes under first order kinetics and that there also does not seem to exist any appreciable solvent effect. Decomposition appears to proceed *via* initial S-O bond homolysis and is *ca.* 6-8 kcal/mol more thermally demanding than overcoming the internal S-S rotation barrier. To our knowledge, this represents the first study to account for the mechanism of decomposition of these highly unusual compounds.

4.7 Synthetic Experimental Section

The large scale synthesis of **15a** and **15b** was adapted from the literature according to Scheme **50**.[156]

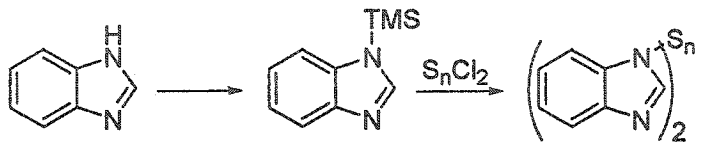

n = 1 **15a**
n = 2 **15b**

Scheme 50.

1-Trimethylsilylbenzimidazole: Yield: 69%; This intermediate was used immediately in the following reactions. ^{1}H NMR ($CDCl_3$) δ 8.12 (s, 1H), 7.45 (m, 4H), 0.06 (s, 9H). ^{13}C NMR δ 145.6, 136.8, 122.8, 122.2, 120.2, 112.5, 97.5, -0.6. MS (EI) *m/z*: 190 ($M^{+\bullet}$), 175, 118, 91; HRMS Calc'd for $C_{10}H_{14}N_2Si$: 190.0926. Found: 190.092(9).

1,1'-thiobisbenzimidazole, 15a: White powder; Yield: 79%; Recrystallized from CH_2Cl_2/hexanes. Mp. 187-190 °C (lit. Mp.[156] 180-185 °C). ^{1}HNMR ($CDCl_3$) δ 8.18 (s, 2H), 7.90 (d_{obs}, 2H, J = 7.90 Hz), 7.75 (d_{obs}, 2H, J = 7.90 Hz), 7.47 (td, 2H, J_{AB} = 7.60 Hz, J_{BC} = 1.20 Hz), 7.34 (td, 2H, J_{AB} = 7.60 Hz, J_{BC} = 0.93 Hz). MS (EI) *m/z*: 266 ($M^{+\bullet}$), 118, 91; HRMS Calc'd for $C_{10}H_{10}N_4S$: 266.0626. Found: 266.063(2).

1,1'-dithiobisbenzimidazole, 15b: White powder; Yield: 100%; Mp. 142-148 °C (lit. Mp.[156] 138-145 °C). ^{1}HNMR ($CDCl_3$) δ 7.80 (d, 2H, J_{AB} = 8.10 Hz), 7.77 (s, 2H), 7.31, (t_{obs}, 2H, J = 7.65 Hz), 7.20 (t_{obs}, 2H, J = 7.65 Hz), 7.06 (d, 2H, J_{AB} = 8.10 Hz). MS (EI) *m/z*: 298 ($M^{+\bullet}$), 181, 118; HRMS Calc'd for $C_{10}H_{10}N_4S_2$: 298.0347. Found: 298.035(5).

General methodology for the synthesis of alkoxy disulfides. These were synthesized by a modification of a procedure from Thompson and co-workers.[34] The synthesis of

151, 153 and 154 proved unsuccessful under the reaction conditions. The following is a representative example of the synthetic procedure used:

A solution of *p*-nitrobenzyl alcohol, **161**, (10 mmol, 2 equiv) and NEt_3 (10 mmol, 2 equiv) in 10 mL of CH_2Cl_2 was allowed to stir under nitrogen at 0 °C. A solution of S_2Cl_2 (5.0 mmol, 1 equiv) in 10 mL of CH_2Cl_2 was added dropwise over *ca.* 5-10 min. The reaction mixture was allowed to stir for a further 3 h. The reaction mixture was quenched with 15 mL of H_2O. The organic phase was washed 3x 33 mL of H_2O. The organic phase was washed 1x 25 mL brine. The organic phase was dried over $MgSO_4$. This mixture was vacuum filtered, and the solvent was removed first under reduced pressure and then *in vacuo*. Frequently, it was not necessary to chromatograph the product as there was quantitative conversion as detected by TLC and ^1H NMR. The product was usually pure enough for HRMS acquisition.

Bis(*p*-nitrobenzyloxy) disulfide, 49:

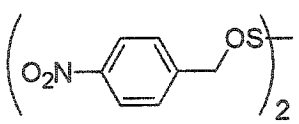

Light yellow solid R*f* (25% EtOAc/hexanes) 0.31. Yield: 97 %. Mp. 95-96 °C (lit Mp.[35] 92-93 °C); ^1H NMR δ 8.20 (d, 4H, J = 8.40 Hz), 7.48 (d, 4H, J = 8.40 Hz), 5.00 (d, 2H, J_{AB} = 12.40 Hz), 4.88 (d, 2H, J_{AB} = 12.40 Hz); ^{13}C NMR δ 75.1, 123.8, 128.7, 143.5, 149.7; MS (CI) *m/z* 386 ($M^{+\bullet}$ + NH_4^+), 338 ($M^{+\bullet}$ – SO); HRMS. Calcd for $C_{14}H_{16}N_3S_2O_6$: 386.0480. Found: 386.048(7).

Bis(*p*-*t*-butylbenzyloxy) disulfide, 150:

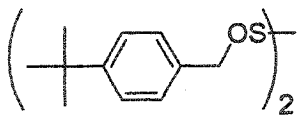

Light yellow oil. The crude was purified by chromatographed in 20% EtOAc/hexanes - R*f* 0.73. Yield: 90%. Mp. *ca* -10 °C; ^{1}H NMR δ 7.37 (d, 4H, J_{AB} = 8.25 Hz), 7.27 (d, 4H, J_{AB} = 8.25 Hz), 4.87 (d, 2H, J_{AB} = 11.50 Hz), 4.76 (d, 2H, J_{AB} = 11.50 Hz), 1.30 (s, 18H); ^{13}C NMR δ 31.3 (CH_3), 34.6 (C-quat), 76.8, 125.5, 128.5, 133.6 (C-quat), 151.6 (C-quat); MS (EI) *m/z* 390($M^{+\bullet}$), 375 ($M^{+\bullet}$ - CH_3), 342 ($M^{+\bullet}$ – SO), 326 ($M^{+\bullet}$ – SO_2), 294 ($M^{+\bullet}$ – S_2O_2), 279 ($M^{+\bullet}$ – $S_2O_2CH_3$), 259 ($M^{+\bullet}$ – $S_2O_2(CH_3)_2$), 164 ($C_{11}H_{16}O$), 147 ($C_{11}H_{15}$); HRMS. Calcd for $C_{22}H_{30}S_2O_2$: 390.1687. Found: 390.169(0).

Bis(*p*-methoxybenzyloxy) disulfide, 51:

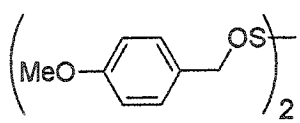

Light yellow solid. The crude can be chromatographed in 20% EtOAc/hexanes - R*f* 0.57 - but is unstable to these conditions. Yield: 93%. Mp. 37-38 °C (lit Mp.[35] 34-36 °C) ^{1}H NMR δ 7.26 (d, 4H, *J* = 8.25 Hz), 6.87 (d, 4H, *J* = 8.25 Hz), 4.82 (d, 2H, J_{AB}=11.25 Hz), 4.72 (d, 2H, J_{AB}=11.25 Hz), 3.79 (s, 6H) ; ^{13}C NMR δ 55.6; 76.8, 114.1, 130.7, 160.0, 183.2; MS (EI) *m/z* 338 ($M^{+\bullet}$), 290 ($M^{+\bullet}$ – SO), 274 ($M^{+\bullet}$ – SO_2); HRMS. Calcd for $C_{16}H_{18}S_2O_4$: 338.0646. Found: 338.06(3)5; HRMS. Calcd for $C_{16}H_{18}S_2O_4$ – SO:

290.0977. Found: 290.098(6); HRMS. Calcd for $C_{16}H_{18}S_2O_4 - SO_2$: 274.1027. Found: 274.103(3)

Bis(benzyloxy) disulfide, 48:

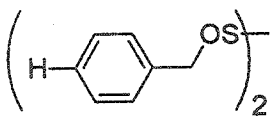

Light yellow solid. Yield: 86%. Mp. 47-52 °C (lit Mp.[35] 50-51 °C). ^{1}H NMR δ 7.39 (m, 15 H), 4.89 (d, 2H, J_{AB} = 11.25 Hz), 4.79 (d, 2H, J_{AB} = 11.25 Hz); ^{13}C NMR δ 76.7, 109.7, 128.4, 128.6, 136.4; MS (FAB) *m/z* 278 ($M^{+\bullet}$), 230 ($M^{+\bullet}$ – SO); HRMS. Calcd for $C_{14}H_{14}S_2O_2$: 278.0435. Found: 278.043(1)

Bis(benzhydroloxy) disulfide, 152:

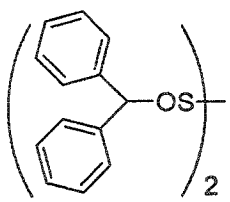

White solid that crystallized from CH_3CN at -10 °C. Yield: 86 %. Mp. 42-46 °C; R*f*. (10% EtOAc/hexanes) 0.50. ^{1}H NMR δ 7.23-7.29 (m, 20H), 5.82 (s, 2H); ^{13}C NMR δ 87.7, 127.3, 127.5, 127.9, 128.3, 129.3, 140.4; MS (CI) *m/z* 448 ($M^{+\bullet}$ + NH_4^+), 184 ($C_{13}H_{12}O$), 183 ($C_{13}H_{11}O$), 182 ($C_{13}H_{10}O$), 167 ($C_{13}H_{11}$), 105, 77 (C_6H_5); HRMS Calcd for $C_{26}H_{22}S_2O_2 + NH_4^+$: 448.1405. Found: 448.139(7).

Bis(cyclohexyloxy) disulfide, 24:

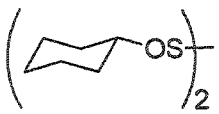

Clear orange oil. The crude was purified by chromatographed in 10% EtOAc/hexanes. Yield: 69 %. R*f* (10% EtOAc/hexanes) 0.70. ^{1}H NMR δ 1.15-1.60 (m, 14H), 1.73 (d, 4H), 2.00 (s, 4H); ^{13}C NMR δ 84.5, 32.9, 32.1, 25.4, 24.0, 23.9; MS (EI) *m/z* 262 ($M^{+\bullet}$), 214 ($M^{+\bullet}$ – SO), 180 ($M^{+\bullet}$ – H_2S_2O) 162 ($M^{+\bullet}$ – $H_3S_2O_2$), 132 ($C_6H_{12}SO$), 99 ($C_6H_{11}O$), 83 (C_6H_{11}); HRMS. Calcd for $C_{12}H_{22}S_2O_2$: 262.1061. Found: 262.106(6).

Bis(allyloxy) disulfide, 34:

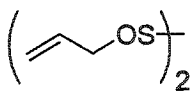

Orange oil. Yield: 82 %. ^{1}H NMR δ 5.92 (m, 2H); 5.27 (m, 4H), ABq system: 4.27 (dd, *J* = 12.25, 6.00 Hz, 2H); 4.38 (dd, *J* = 12.25, 6.00 Hz, 2H); ^{13}C NMR δ 75.7 (-CH_2-), 119.2 (=CH_2), 133.2 (=CH-); MS (EI) *m/z* 178 ($M^{+\bullet}$), 146 ($M^{+\bullet}$ – S), 137, 113, 105; HRMS. Calcd for $C_6H_{10}S_2O_2$: 177.9945. Found: 177.995(6). ^{1}HNMR, ^{13}CNMR, MS similar to literature.[115]

Bis(propargyloxy) disulfide, 42:

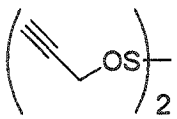

Stored as a yellow solution in CH_2Cl_2. Yield: 57 %. ^{1}H NMR δ ABX system: 4.50 (dd, 2H, J_{AB} = 15.45 Hz, J_{BC}=2.40 Hz), 4.45 (d, 2H, J_{AB} = 15.45 Hz, J_{BC} = 2.40 Hz), 2.55 (t, 2H, J_{BC} = 2.40 Hz); ^{13}C NMR δ 17.4, 61.3, 76.3; MS (EI) *m/z* 174 ($M^{+\bullet}$), 126 ($M^{+\bullet}$ – SO); HRMS. Calcd for $C_6H_6S_2O_2$: 173.9809. Found: 173.980(6). ^{1}HNMR, ^{13}CNMR, MS similar to literature.[40]

Synthesis of bis(*p*-nitrobenzyl) sulfite, 155:

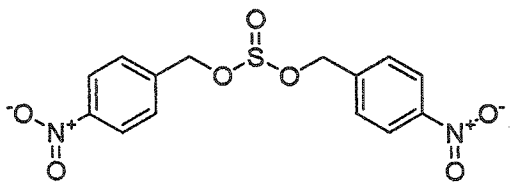

To a solution of **161** (300.0 mg, 2 mmol, 2 equiv) and NEt_3 (280 μL, 2 mmol, 2 equiv) in 10 mL CH_2Cl_2 was added dropwise a solution of 75 μL of $SOCl_2$ in 10 mL CH_2Cl_2 at 0 °C under N_2. The reaction was stirred for 1.5 h. The reaction was quenched with 20 mL H_2O. The organic phase was washed 3x 30 mL H_2O. The solution was dried over $MgSO_4$. The solvent was removed first under reduced pressure and then *in vacuo*. Column chromatography using 50% EtOAc in hexanes gave sulfite. Light yellow crystalline solid. R*f* (30% EtOAc/hexanes) 0.30. Yield: 62 %. Mp. 84-86 °C (lit Mp.[45] 81-82 °C); ^{1}H NMR δ 8.21 (d, 4H, *J* = 8.75 Hz), 7.48 (d, 4H, *J* = 8.75 Hz), 5.17 (d, 2H, J_{AB} = 12.75 Hz), 5.02 (d, 2H, J_{AB} = 12.75 Hz); ^{13}C NMR δ 62.6, 123.9, 128.5, 142.0,

147.9; MS (CI) *m/z* 370 ($M^{+\bullet}$), 153 ($C_7H_7NO_3$); HRMS. Calcd for $C_{14}H_{12}N_2SO_7 + NH_4^+$: 370.0709. Found: 370.07(0)0.

Synthesis of bis(*p*-nitrobenzyl) sulfoxylate, 156:

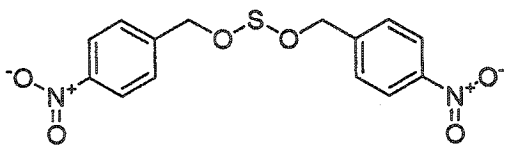

A solution of *p*-nitrobenzyl alcohol, **161**, (309.3 mg, 1 mmol, 2 equiv) and NEt_3 (280 μL, 2 mmol, 2 equiv) in 10 mL of CH_2Cl_2 was allowed to stir under nitrogen at 0 °C. A solution of sulfur dichloride (64 μL, 1.0 mmol, 1 equiv) in 10 mL of CH_2Cl_2 was added dropwise over *ca.* 5-10 min. The reaction mixture was allowed to stir for a further 3 h. The reaction mixture was quenched with 15 mL of H_2O. The organic phase was washed 3x 33 mL of H_2O. The organic phase was dried over $MgSO_4$. This mixture was vacuum filtered, and the solvent was removed first under reduced pressure and then *in vacuo*. Light orange solid with a fruity aroma. R*f* (25% EtOAc/hexanes) 0.25. Yield: 98 %. Mp. 86-87 °C; ^{1}H NMR δ 8.20 (d, 4H, *J* = 8.24 Hz), 7.46 (d, 4H, *J* = 8.25 Hz), 5.17 (s, 4H); ^{13}C NMR δ 80.3, 123.6, 128.4, 143.6, 147.6; MS (CI) *m/z* 354 ($M^{+\bullet} + NH_4^+$), 294, 243, 211, 171, 155, 122, 108; HRMS. Calcd for $C_{14}H_{16}N_3SO_6 + NH_4^+$: 354.0760. Found: 354.07(6)7. Upon standing in solution, **156** isomerizes to sulfinate **157**.[45] ^{1}H NMR δ 7.38-7.53 (m, 4H), 4.19 (d, 2H, *J* = 5.50 Hz), ABq system: 4.88 (d, 2H, *J* = 12.45 Hz), 5.00 (d, 2H, *J* = 12.45 Hz); ^{13}C NMR δ 63.3, 68.9, 123.7, 126.8, 128.5, 131.5, 135.3, 143.4, 147.8, 147.9.

Synthesis of bis(*p*-nitrobenzyl) sulfide, 158:

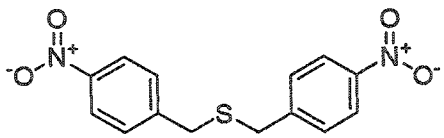

The synthesis was adapted from the literature.[48] A solution of *p*-nitrobenzyl alcohol, **161**, (2.16 g, 10.00 mmol, 1 equiv), sodium sulfide, Na_2S (418 mg, 5.35 mmol, 0.54 equiv), and activated Amberlite-IRA-400(Cl) (237 mg, 1.10 mmol, 0.11 equiv) was refluxed in 50 mL of methanol (MeOH) under a nitrogen atmosphere for 90 min. The solution was vacuum-filtered and the solute, which contained the precipitated product, was washed with methanol. This was then discarded and the solute was then washed with CH_2Cl_2. The solvent was removed first under reduced pressure and then *in vacuo*. Yellow solid. Yield: 88%. Mp. 153-157 °C; ^{1}H NMR δ 8.17 (d, 4H, J= 7.95 Hz), 7.42 (d, 4H, J= 7.95 Hz), 3.66 (s, 4H); ^{13}C NMR δ 35.3, 123.8, 129.6, 145.0, 147.0; MS (EI) *m/z* 304 ($M^{+\bullet}$), 136 ($C_7H_6NO_2$), 106; HRMS. Calcd for $C_{14}H_{12}N_2SO_4$: 304.0518. Found: 304.052(8).

Synthesis of bis(*p*-nitrobenzyl) sulfoxide, 159:

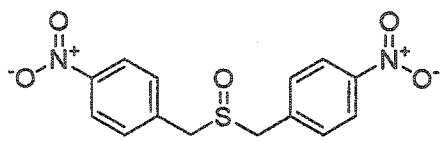

This was synthesized as an adaptation of the literature.[65] To a solution of *p*-nitrobenzyl sulfide, **158**, (304 mg, 1.00 mmol, 1 equiv) in 5 ml of HFIP (1,1,1,3,3,3-hexafluoroisopropanol) at 0 °C was added dropwise 30% H_2O_2 (130 μL, 1.15 mmol, 1.15

equiv). After the addition, the solution was stirred for 40 min at RT. The excess H_2O_2 was decomposed through the addition of Na_2SO_3 (54.3 mg, 0.43 mmol, 0.4 equiv). This was stirred for 30 min at 50 °C using a water bath a heating medium. The fluorinated solvent was removed under reduced pressure. Upon addition of *ca.* 20 mL of Et_2O, a yellow solid precipitated out of solution. The solution was then decanted and the solute was washed 3x 10 ml Et_2O and then dried *in vacuo*. This afforded a yellow solid. Yield: >99%. Mp. 202-206 °C. ^{1}H NMR δ 8.25 (d, 4H, J= 8.55 Hz), 7.47 (d, 4H, J= 8.45 Hz), ABq system: 4.05 (d, 2H, J_{AB} = 12.90 Hz), 3.94 (d, 2H, J_{AB} = 12.90 Hz); ^{13}C NMR δ 57.02, 124.08, 130.99, 136.81, 148.01; MS (EI) *m/z* 320 ($M^{+\bullet}$), 167, 136 ($C_7H_6NO_2$), 106, 90, 78; HRMS. Calcd for $C_{14}H_{12}N_2SO_5$: 320.0467. Found: 320.04(7)2.

Synthesis of bis(*p*-nitrobenzyl) sulfone, 160:

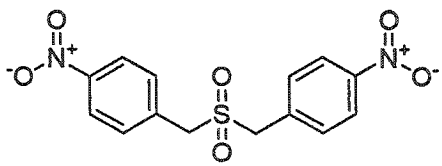

A solution of *p*-nitrobenzyl sulfide, **158**, (304 mg, 1.00 mmol, 1 equiv) and MCPBA (345 mg, 2.00 mmol, 2 equiv) was stirred in 20 mL CH_2Cl_2 under a nitrogen atmosphere for 24 hours. The solution was filtered. The filtrate was discarded and the solute was dissolved in a minimum volume of DMSO. To this, H_2O was added and a white precipitate formed. This was filtered, collected and dried on top of the oven. This afforded a white solid, 69.7 mg. Yield: 21%. Mp. 235-239 °C, after which the liquid turned bright orange; ^{1}H NMR δ 8.27 (d, 4H, J= 8.70 Hz), 7.57 (d, 4H, J= 8.70 Hz), 4.28 (s, 4 Hz); ^{13}C NMR δ 58.3, 124.1, 131.8, 133.6, 136.8; MS (EI) *m/z* 336 ($M^{+\bullet}$), 320 ($M^{+\bullet}$

– O), 272 ($M^{+\bullet}$ – SO_2), 226 ($M^{+\bullet}$ – SO_2 – NO_2), 166, 136 ($C_7H_6NO_2$), 120, 106, 90, 78; HRMS. Calcd for $C_{14}H_{12}N_2SO_4$: 336.0416. Found: 336.04(1)9.

4.8 References

(1) For a review on rotation about single bonds see: Sternhell, S. *Dynamic Nuclear Magnetic Resonance Spectroscopy*; Jackman, L. M., Cotton, F. A., Eds.; Academic Press: New York, **1975**, *6*.

(2) Schnur, D. M.; Yuh, Y. H.; Dalton, D. R. *J. Org. Chem.* **1989**, *54*, 3779.

(3) Li, P.; Chen, X. G.; Shulin, E.; Asher, S. A. *J. Am. Chem. Soc.* **1997**, *119*, 1116.

(4) Bushweller, C. H.; O'Neil, J. W.; Halford, M. H.; Bissett, F. H. *J. Am. Chem. Soc.* **1971**, *93*, 1471.

(5) Scherer, G.; Kramer, M. L.; Schutkoxski, M.; Reimer, U.; Fisher, G. *J. Am. Chem. Soc.* **1998**, *120*, 5568.

(6) Suarez, C.; Tafazzoli, M.; True, N. S.; Gerrard, S.; Lemaster, C. B.; Lemaster, C. L. *J. Phys. Chem.* **1995**, *99*, 8170.

(7) Suarez, C.; Lemaster, C. B.; Lemaster, C. L.; Tafazzoli, M.; True, N. S. *J. Phys. Chem.* **1990**, *94*, 6679.

(8) Stewart, W. E.; Siddall III, T. H. *Chem. Rev.* **1970**, *70*, 517.

(9) Ross, B. D.; True, N. S.; Decker, D. L. *J. Phys. Chem.* **1983**, *87*, 89.

(10) Drakenberg, T.; Dahlqvist, K.-I.; Forsén, S. *J. Phys. Chem.* **1972**, *76*, 2178.

(11) Wiberg, K. B.; Rablen, P. R.; Rush, D. J.; Keith, T. A. *J. Am. Chem. Soc.* **1995**, *117*, 4261.

(12) Taha, A. N.; Neugebauer-Crawford, S. M.; True, N. S. *J. Phys. Chem. A* **1998**, *102*, 1425.

(13) Taha, A. N.; True, N. S. *J. Phys. Chem. A* **2000**, *104*, 2985.

(14) Gao, J. *J. Am. Chem. Soc.* **1993**, *115*, 2930.

(15) Duffy, E. M.; Severance, D. L.; Jorgensen, W. L. *J. Am. Chem. Soc.* **1992**, *114*, 7535.

(16) Laidig, K. E.; Cameron, L. M. *J. Am. Chem. Soc.* **1996**, *118*, 1737.

(17) Wilson, N. K. *J. Phys. Chem.* **1971**, *75*, 1067.

(18) Raban, M.; Yamamoto, G. *J. Am. Chem. Soc.* **1979**, *101*, 5890.

(19) Rablen, P. R.; Miller, D. A.; Bullock, V. R.; Hutchinson, P. H.; Gorman, J. A. *J. Am. Chem. Soc.* **1999**, *121*, 218.

(20) Cox, C.; Lectka, T. *J. Org. Chem.* **1998**, *63*, 2426.

(21) Rablen, P. R. *J. Org. Chem.* **2000**, *65*, 7930.

(22) Some have argued that the high observed barrier in amides is due to the inherent preference for nitrogen planarity, resulting in its effective increase in electronegativity and thus better able to stabilize itself. See for instance: Wiberg, K. B.; Breneman, C. M. *J. Am. Chem. Soc.* **1992**, *114*, 831.

(23) Meyer, W. L.; Meyer, R. B. *J. Am. Chem. Soc.* **1963**, *85*, 2170.

(24) Grein, F. *J. Phys. Chem. A.* **2002**, *106*, 3823.

(25) Gust, D.; Mislow, K. *J. Am. Chem. Soc.* **1973**, *95*, 1535.

(26) Mislow, K.; Glass, M. A. W.; Hopps, H. B.; Simon, E.; Wahl Jr., G. H. *J. Am. Chem. Soc.* **1963**, *86*, 1710.

(27) Casarini, D.; Rosini, C.; Grilli, S.; Lunazzi, L.; Mazzanti, A. *J. Org. Chem.* **2003**, *68*, 1815.

(28) Casarini, D.; Lunazzi, L.; Mazzanti, A. *J. Org. Chem.* **1997**, *62*, 3315.

(29) Sterically induced high torsional barriers are not limited to rotation about carbon-carbon bonds. See for instance: Beatriz Garcia, M.; Grilli, S.; Lunazzi, L.; Mazzanti, A.; Orelli, L. R. *J. Org. Chem.* **2001**, *66*, 6679. for rotation about the sp^2-sp^2 carbon-nitrogen bond in *N*-aryl-tetrahydropyrimidines.

(30) For another example of a sterically induced high barrier to rotation see: Gasparrini, F.; Lunazzi, L.; Mazzanti, A.; Pierini, M.; Pietrusiewicz, K. M.; Villani, C. *J. Am. Chem. Soc.* **2000**, *122*, 4776. for rotation about the sp^2-carbon-phosphorus bond in secondary phosphine oxides.

(31) Hubbard, W. N.; Douslin, D. R.; McCullough, J. P.; Scott, D. W.; Todd, S. S.; Messerly, J. F.; Hossenlopp, I. A.; George, A.; Waddington, G. *J. Am. Chem. Soc.* **1958**, *80*, 3547.

(32) Cerioni, G.; Cremonini, M. A.; Lunazzi, L.; Placucci, G.; Plumitallo, A. *J. Org. Chem.* **1998**, *63*, 3933.

(33) Borghi, R.; Lunazzi, L.; Placucci, G.; Cerioni, G.; Foresti, E.; Plumitallo, A. *J. Org. Chem.* **1997**, *62*, 4924.

(34) Thompson, Q. E.; Crutchfield, M. M.; Dietrich, M. W.; Pierron, E. *J. Org. Chem.* **1965**, *30*, 2692.

(35) Harpp, D. N.; Tardif, S. L.; Williams, C. R. *J. Am. Chem. Soc.* **1995**, *117*, 9067.

(36) Einfeld, T. S.; Maul, C.; Gericke, K.-H. *J. Chem. Phys.* **2002**, *117*, 4214. and references cited therein.

(37) Su, Y. Z.; Ma, W. S.; Gong, K. C. *Mat. Res. Soc. Symp. Proc.* **2000**, *575*, 403.

(38) Su, Y. Z.; Gong, K. C. *Mat. Res. Soc. Symp. Proc.* **2000**, *600*, 215.

(39) Yamomoto, K.; Jikei, M.; Miyatake, K.; Katoh, J.; Nishide, H.; Tsuchida, E. *Macromolecules* **1994**, *27*, 4312.

(40) Braverman, S.; Pechenick, T.; Gottlieb, H. E. *Tetrahedron Lett.* **2003**, *44*, 777.

(41) Suter, C. M.; Gerhart, H. L. *Org. Syn. Coll.* **1943**, *2*, 112.

(42) Suh, J.; Koh, D.; Min, C. *J. Org. Chem.* **1988**, *53*, 1147.

(43) Lachapelle, A.; St-Jacques, M. *Can. J. Chem.* **1985**, *63*, 2185.

(44) Lowe, G.; Parratt, M. J. *J. Chem. Soc. Chem. Commun.* **1985**, *16*, 1075.

(45) Harpp, D. N.; Tardif, S. *J. Org. Chem.* **2000**, *65*, 4791.

(46) Tardif, S. Ph.D. thesis, McGill University, **1997**.

(47) Thompson, Q. E. *J. Org. Chem.* **1965**, *30*, 2703.

(48) Choi, J.; Lee, D. W.; Yoon, N. M. *Bull. Korean Chem. Soc.* **1995**, *16*, 189.

(49) Paquette, L. A. *J. Am. Chem. Soc.* **1964**, *86*, 4085.

(50) Russell, G. A.; Ochrymowycz, L. A. *J. Org. Chem.* **1970**, *35*, 2106.

(51) For a review on sulfoxide synthesis see: Montanari, F.; Cinuini, M. *Mechanisms of Reactions of Sulfur Compounds* **1968**, *3*, 121.

(52) Schultz, H. S.; Freyermuth, H. B.; Buc, S. R. *J. Org. Chem.* **1963**, *28*, 1140.

(53) Russell, G. A.; Pecoraro, J. M. *J. Am. Chem. Soc.* **1979**, *101*, 3331.

(54) Varma, R. S.; Naicker, K. P. *Org. Lett.* **1999**, *1*, 189.

(55) Choi, S.; Yang, J.-D.; Ji, M.; Choi, H.; Kee, M.; Ahn, K.-H.; Byeon, S.-H.; Baik, W.; Koo, S. *J. Org. Chem.* **2001**, *66*, 8192.

(56) Brinksma, J.; La Crois, R.; Feringa, B. L.; Donnoli, M. I.; Rosini, C. *Tetrahedron Lett.* **2001**, *42*, 4049.

(57) Sato, K.; Hyodo, M.; Aoki, M.; Zheng, X.-Q.; Noyori, R. *Tetrahedron* **2001**, *57*, 2469.

(58) Reddy, T. I.; Varma, R. S. *Chem. Commun.* **1997**, 471

(59) Fraile, J. M.; García, J. I.; Lázaro, B.; Mayoral, J. A. *Chem. Commun.* **1998**.

(60) Leonard, N. J.; Johnson, C. R. *J. Org. Chem.* **1962**, *27*, 282.

(61) Karalkar, N. B.; Salunkhe, M. M.; Talekar, K. P.; Maldar, N. N. *Indian J. Chem.* **1998**, *37B*, 1184.

(62) Shukla, V. G.; Salgaibkar, P. D.; Akamanchi, K. G. *J. Org. Chem.* **2003**, ASAP.

(63) Zen, J.-M.; Liou, S.-L.; Kumar, A. S.; Hsia, M.-S. *Angew. Chem. Int. Ed. Engl.* **2003**, *42*, 577.

(64) Gelalcha, F. G.; Bärbel, S. *J. Org. Chem.* **2002**, *57*, 8400.

(65) Ravikumar, K. S.; Kesavan, V.; Crousse, B.; Bonnet-Delpon, D.; Bégué, J.-P. *Organic Syntheses* **2003**, *80*, 184.

(66) Fraser, R. R.; Boussard, G.; Saunders, J. K.; Lambert, J. B. *J. Am. Chem. Soc.* **1971**, *93*, 3822.

(67) Seel, F.; Gombler, W.; Budenz, R. *Liebigs Ann. Chem.* **1970**, *735*, 1.

(68) Reich, H. J.; WINDNMR 7.1.5 ed. **2000**.

(69) For an excellent reference on DNMR spectroscopy see: Sandström, J. *Dynamic NMR Spectroscopy*; Academic Press: Toronto, **1982**.

(70) Snyder, J. P.; Nevins, N.; Tardif, S. L.; Harpp, D. N. *J. Am. Chem. Soc.* **1997**, *119*, 12685.

(71) Reichardt, C. *Chem. Rev.* **1994**, *94*, 2319.

(72) Onsager, L. *J. Am. Chem. Soc.* **1936**, *58*, 1486.

(73) 3rd electronic ed.; CRC Press LLC: **2001**.

(74) Wiberg, K. B.; Murcko, M. A. *J. Phys. Chem.* **1987**, *91*, 3616.

(75) Wong, M. W.; Frisch, M., J.; Wiberg, K. B. *J. Am. Chem. Soc.* **1991**, *113*, 4776.

(76) Kost, D.; Carlson, E. H.; Raban, M. *Chem. Commun.* **1971**, 656.

(77) For a review on intramolecular exchange rates from complex NMR see: Dahlqvist, K.-I.; Forsén, S. *Acta Chem. Scand.* **1970**, *24*, 651.

(78) $\Delta G^{\ddagger}$ varies by *ca.* 0.2 kcal/mol over two solvents (CH_2CHCl and $CBrF_3$) for a series of 2-alkoxy-3-halobutanes and 2-acetoxy-3-halobutanes. See: Wang, C. Y.; Bushweller, C. H. *J. Am. Chem. Soc.* **1977**, *99*, 313.

(79) $\Delta G^{\ddagger}$ can increase by as much as 3 kcal/mol upon changing from an apolar solvent to water. Drakenberg, T.; Dahlqvist, K.-I.; Forsén, S. *J. Phys. Chem.* **1972**, *76*, 2178.

(80) Some have attributed the observed solvent effect in the rotation about the C-N amide bond to internal pressure and the increased volume requirements of the transition state structure in comparison to the ground state structure. See for instance: Suarez, C.; Lemaster, C. B.; Lemaster, C. L.; Tafazzoli, M.; True, N. S. *J. Phys. Chem.* **1990**, *94*, 6679. It should be noted that in the case of alkoxy disulfides, the transition state does not require greater steric requirements compared to the ground state. Thus any increase in the barrier in the liquid phase compared to the gas phase cannot be due to this reasoning.

(81) Experimentally determined $\Delta S^{\ddagger}$ for the rotation about the carbon-nitrogen single bond in *tert*-butylamine is 1.3 eu. See: Bushweller, C. H.; O'Neil, J. W.; Bilofsky, H. S. *J. Am. Chem. Soc.* **1970**, *92*, 6349.

(82) Experimentally determined $\Delta S^{\ddagger}$ values ranged from -1 to -5 eu for a series of polyhalogenated ethane derivatives. See: Brunelle, J. A.; Letendre, L. J.; Weltin, E. E.; Brown, J. H.; Bushweller, C. H. *J. Phys. Chem.* **1992**, *96*, 9225.

(83) Though not strictly rotation about a single bond, due to resonance stabilization afforded by the benzene ring, $\Delta S^{\ddagger}$ ranges between 0 and -3 eu in three aprotic solvents for

p-trifluoromethanesulfonylbenzyltriflone carbanion. See: Gromova, M.; Béguin, C. G.; Goumont, R.; Faucher, N.; Tordeux, M.; Terrier, F. *Magn. Reson. Chem.* **2000**, *38*, 655.

(84) Lomas, J. S.; Anderson, J. E. *J. Org. Chem.* **1995**, *60*, 3246.

(85) Lomas, J. S.; Bru-Caodeville, V. *J. Chem. Soc. Perkin. Trans. 2* **1994**, 459.

(86) Lomas, J. S.; Dubois, J. E. *Tetrahedron* **1981**, *37*, 2273.

(87) McKelvey, D. R.; Kraig, R. P.; Zimmerman, K.; Ault, A.; Perfetti, R. *J. Org. Chem.* **1973**, *38*, 3610.

(88) For a review on methodology that estimates, and trends concerning torsional entropy about single bonds see: Mammen, M.; Shakhnovich, E. I.; Whitesides, G. M. *J. Org. Chem.* **1998**, *63*, 3168. and references cited therein.

(89) For a commentary on the definition of torsional entropy see: Ercolani, G. *J. Org. Chem.* **1999**, *64*, 3350.

(90) *Physical Chemistry*; Laidler, K. J.; Meiser, J. H., Eds.; Benjamin/Cummings Publishing Co. Inc.: Toronto, **1982**.

(91) For a review on enthalpy-entropy compensation see: Liu, L.; Guo, Q.-X. *Chem. Rev.* **2001**, *101*, 673.

(92) Gilli, P.; Ferretti, V.; Gilli, G. *J. Phys. Chem.* **1994**, *98*, 1515.

(93) Grunwald, E.; Steel, C. *J. Am. Chem. Soc.* **1995**, *117*, 5687.

(94) Dunitz, J. D. *Chemistry and Biology* **1995**, *2*, 709.

(95) Stein, R. *Adv. Protein Chem.* **1993**, *44*, 1. and references therein.

(96) Cohen, M. D.; Leffler, J. E.; Barbato, L. M. *J. Am. Chem. Soc.* **1954**, *76*, 4169.

(97) Adler, M. G.; Leffler, J. E. *J. Am. Chem. Soc.* **1954**, *76*, 1425.

(98) Leffler, J. E. *J. Org. Chem.* **1955**, *20*, 3019.

(99) Boots, H. M. J.; de Bokx, P. K. *J. Phys. Chem.* **1989**, *93*, 8240.

(100) Harpp, D. N.; Chew, W. *J. Org. Chem.* **1993**, *58*, 4405.

(101) Bartlett, P. D.; Hiatt, R. R. *J. Am. Chem. Soc.* **1958**, *80*, 1398.

(102) Cook, C. D.; Norcross, B. E. *J. Am. Chem. Soc.* **1959**, *81*, 1176.

(103) Huyser, E. S.; VanScoy, R. M. *J. Org. Chem.* **1968**, *33*, 3524.

(104) Matsumoto, Y.; Ueoka, R. *J. Org. Chem.* **1990**, *55*, 5797.

(105) Hassan, R. M. *Can. J. Chem.* **1991**, *69*, 2018.

(106) Inoue, Y.; Yamasaki, N.; Yokoyama, T.; Tai, A. *J. Org. Chem.* **1992**, *57*, 1332.

(107) Krug, R. R.; Hunter, W. G.; Grieger, R. A. *J. Phys. Chem.* **1976**, *80*, 2335.

(108) Krug, R. R.; Hunter, W. G.; Grieger, R. A. *J. Phys. Chem.* **1976**, *80*, 2341.

(109) McBane, G. C. *J. Chem. Ed.* **1998**, *75*, 919.

(110) Sharp, K. *Protein Science* **2001**, *10*, 661.

(111) Cornish-Bowden, A. *J. Biosci.* **2002**, *27*, 121.

(112) Taylor, J. R. An Introduction to Error Analysis: The Study of Uncertainties in Physical Measurements. Second Edition; University Science Books: Sausalito, California, **1997**.

(113) Kobayashi, M.; Minato, H.; Shimada, K. *Int. J. Sulfur Chem., A* **1971**, *1*, 105.

(114) Borghi, R.; Lunazzi, L.; Placucci, G.; Cerioni, G.; Plumitallo, A. *J. Org. Chem.* **1996**, *61*, 3327.

(115) Braverman, S.; Pechenick, T. *Tetrahedron Lett.* **2002**, *43*, 499.

(116) Smith, J. D.; O'Hair, R. A. J. Phosphorus, Sulfur and Silicon And The Related Elements **1997**, 126, 257.

(117) Motoki, S.; Kagami, H. *J. Org. Chem.* **1977**, *42*, 4139.

(118) The average R^2 value for the linear fits was *ca.* 0.97.

(119) Harpp, D. N.; Snyder, J. P. *J. Am. Chem. Soc.* **1976**, *98*, 7821.

(120) Jorgensen, W. L.; Blake, J. F. *J. Am. Chem. Soc.* **1991**, *113*, 7430.

(121) Ruiz-López, M. F.; Assfeld, X.; García, J. I.; Mayoral, J. A.; Salvatella, L. *J. Am. Chem. Soc.* **1993**, *115*, 8780.

(122) Doorakian, G. A.; Freedman, H. H. *J. Am. Chem. Soc.* **1968**, *90*, 3582.

(123) von E. Doering, W.; Toscano, V. G.; Beaseley, G. H. *Tetrahedron* **1971**, *27*, 5299.

(124) Schuler, F. W.; Murphy, G. W.; 1950 *J. Am. Chem. Soc.* **1950**, *72*, 3155.

(125) It should be noted that the sensitivity of ESR spectroscopy is much higher than that of ^{1}H NMR. Thus radical concentrations of 10^{-6} can easily be detected by this method. The ESR photolytic method thus produces radicals in such small concentrations as to not contribute to the decomposition of alkoxy disulfides as detected by ^{1}H NMR spectroscopy.

(126) Guo, Y.; Jenks, W. S. *J. Org. Chem.* **1995**, *60*, 5480.

(127) Guo, Y.; Jenks, W. S. *J. Org. Chem.* **1997**, *62*, 857.

(128) Pasto, D. J.; Cottard, F. *Tetrahedron Lett.* **1994**, *35*, 4303.

(129) Amaudrut, J.; Wiest, O. *J. Am. Chem. Soc.* **2000**, *122*, 3367.

(130) Miller, E. G.; Rayner, D. R.; Mislow, K. *J. Am. Chem. Soc.* **1966**, *88*, 3139.

(131) Amaudrut, J.; Pasto, D. J.; Wiest, O. *J. Org. Chem.* **1998**, *63*, 6061.

(132) Nau, W. M. *J. Phys. Org. Chem.* **1997**, *10*, 445.

(133) Pasto, D. J. *J. Mol. Struct.* **1998**, *446*, 75.

(134) Benassi, R.; Taddei, F. *J. Comput. Chem.* **2000**, *21*, 1405.

(135) Benson, S. W. *Chem. Rev.* **1978**, *78*, 23.

(136) Russell, G. A. *J. Am. Chem. Soc.* **1957**, *79*, 3871.

(137) Fessenden, R. W. *J. Chem. Phys.* **1968**, *48*, 3725.

(138) Ingold, K. U.; Adamic, K.; Howard, J. A. *Can. J. Chem.* **1969**, *47*, 3803.

(139) Francisco, J. S.; Williams, I. H. *Int. Journal of Chemical Kinetics* **1988**, *20*, 455.

(140) Howard, J. A.; Bennet, J. E. *Can. J. Chem.* **1972**, *50*, 2374.

(141) Minato, T.; Yamabe, S.; Fujimoto, H.; Fukui, K. *Bull. Chem. Soc. Japan* **1978**, *51*, 682.

(142) Neumann, W. P.; Lind, H. *Chem. Ber.* **1968**, *101*, 2837.

(143) Mendenhall, G. D.; Ogle, C. A.; Martin, S. W.; Dziobak, M. P.; Urban, M. W. *J. Org. Chem.* **1983**, *48*, 3728.

(144) Mendenhall, G. D.; Quinga, E. M. Y. *Int. Journal of Chemical Kinetics* **1985**, *17*, 1187.

(145) Ingold, K. U.; Paul, T.; Young, M. J.; Doiron, L. *J. Am. Chem. Soc.* **1997**, *119*, 12364.

(146) Ingold, K. U.; Konya, K. G.; Paul, T.; Lin, S.; Lusztyk, J. *J. Am. Chem. Soc.* **2000**, *122*, 7518.

(147) Formation of sulfenyl radical **168** *via* homolysis of the S-S bond cannot be ruled out.

(148) Gilbert, B. C.; Holmes, R. G. G.; Laue, H. A. H.; Norman, R. O. C. *J. Chem. Soc. Perkin. Trans. 2* **1976**, 1047.

(149) Elford, P. E.; Roberts, B. P. *J. Chem. Soc. Perkin. Trans. 2* **1996**, 2247.

(150) Bach, R. D.; Ayala, P. Y.; Schlegel, H. B. *J. Am. Chem. Soc.* **1996**, *118*, 12758.

(151) McMillen, D. F.; Golden, D. M. *Annu. Rev. Phys. Chem.* **1982**, *33*, 493.

(152) Nicovich, J. M.; Kreuter, K. D.; van Dijk, C. A.; Wine, P. H. *J. Phys. Chem.* **1992**, *96*, 2518.

(153) The three electrons would be placed in a new set of π and π^* orbitals.

(154) Gregory, D. D.; Jenks, W. S. *J. Org. Chem.* **1998**, *63*, 3859.

(155) Nangia, P. S.; Benson, S. W. *J. Phys. Chem.* **1979**, *83*, 1138.

(156) Harpp, D. N.; Steliou, K.; Chan, T. H. *J. Am. Chem. Soc.* **1978**, *100*, 1222.

Chapter 5

Synthesis, Characterization and Conformational Analysis of an 8-Membered Ring Alkoxy Disulfide, Its 7-Membered Isomeric Thionosulfite And Related Compounds

5.1 Introduction

As was detailed in Chapter 2, to our knowledge there are no examples in the literature of a cyclic alkoxy disulfide. Common to all the known thionosulfites, **5**, is the presence of a 5-membered ring core. In this Chapter we report the synthesis of the first cyclic alkoxy disulfide and its thionosulfite isomer. This latter compound represents the first medium-sized (7-membered ring) thionosulfite. We have also synthesized a 16-membered macrocycle containing two OSSO moieties. In addition, we report the synthesis of the related sulfite and sulfoxylate compounds. A discussion as to the solution and solid state conformational analysis of these interesting molecules is also provided. Chapter **6** provides an investigation as to the relative stabilities of alkoxy disulfides and thionosulfites as well as the isomerization between the two.

5.2 Synthesis

In Chapter **4** we reported the optimization of the preparation of acyclic alkoxy disulfides. Using these reaction conditions as a starting point, we investigated the S_2Cl_2 coupling to a model diol, 1,2-benzenedimethanol **170**. The results are summarized in Table **58**.

Table 58. S_2Cl_2 coupling of diol 170

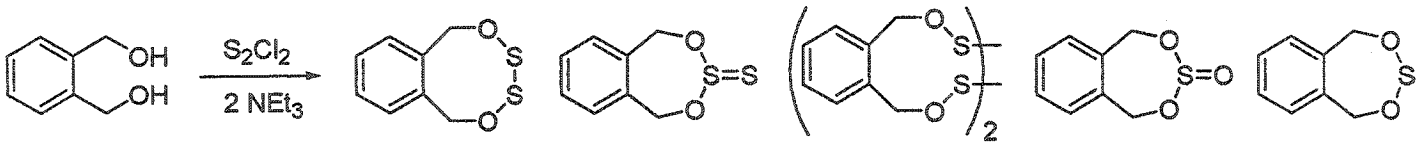

170 171 172 173 174 175

Entry[a]	$[S_2Cl_2]$ (M)	equiv. S_2Cl_2	Addn time (min)	time (h)	Solvent	temp[c] (°C)	yield[d] (%) 171		172		173		174	175
1	0.1	1	5	5	CH_2Cl_2	0	93	(94)	0		7		0	0
2[b]	0.1	1	9	5.5	CH_2Cl_2	0	96	(96)	0		4		0	0
3	0.1	1	35	6	CH_2Cl_2	-78	94		0		4		2	0
4	0.1	1	12	5	CH_2Cl_2	23	58		33	(22)	5	(>1)	2	1
5	0.02	1	50	5	CH_2Cl_2	0	96	(79)	0		4		0	0
6	1.0	1	2	5	CH_2Cl_2	0	92		0		8		0	0
7	0.2	2	13	5.3	CH_2Cl_2	0	13		0		0		87	0
8	0.1	1	3	5	THF	0	88		1		10	(9)	2	0
9	0.1	1	3	5	CH_3CN	0	0		9		0		87	4

a) The concentration of 170 was 0.1 M in all cases. b) 170 and S_2Cl_2 were simultaneously added to 10 mL of CH_2Cl_2. c) Refers to the temperature maintained during the addition of S_2Cl_2. d) By ^1H NMR with isolated yields in parentheses.

In most cases, alkoxy disulfide 171 was the major product formed and isolated. To our knowledge, this represents the *first* example of a cyclic alkoxy disulfide. We were able to influence the ratio of 171:172 by increasing the S_2Cl_2 addition temperature to 23 °C (Entry 4). Thompson indicated in his patent[1] that thionosulfites could be preferentially formed with simultaneous diol and S_2Cl_2 addition. In our hands, these conditions (Entry 2) produced the same ratio of products and isolated yield of 171 as addition of S_2Cl_2 solution to 170 (Entry 1). Moreover, no thionosulfite 172 was detected. It was believed that by decreasing the temperature to -78 °C and lengthening the addition

time we could promote the formation of dimer **173** over monomer **171**. Although there is evidence to suggest that by lowering the temperature, we could stabilize the highly chalcogenated intermediate **176**,[2] this did not translate into an increased yield of **173**. Changing the solvent to THF (Entry 8) or increasing the concentration of the S_2Cl_2 solution (Entry 6) promoted an increase in the yield of **173** relative to **171**, whereas changing the solvent to the more polar CH_3CN (Entry 9) resulted in formation of unwanted sulfite **174**. Similar results were observed with the use of 2 equivalents of S_2Cl_2. Apparently, under these conditions, 7-*exo-tet* ring closure to form sulfoxylate **175** and subsequent oxidation in the work-up to the sulfite **174** is preferred over 8-*exo-tet* ring closure to give alkoxy disulfide **171**. Trace acid- or base-catalyzed decomposition of **171** to **174** cannot be ruled out. Decreasing the concentration of the S_2Cl_2 solution from 1 M to 0.02 M while increasing the addition time from 2 to 50 min slightly increased the yield of **171** over dimer **173** (Entries 5 and 6). Thus, given that **172** could only be synthesized at RT (Entry 4) while **171** could be synthesized at lower temperatures (*e.g.* Entry 3) and given that **171** slowly isomerized to **172** (*vide infra*) but the reverse isomerization was not observed, it would appear that **171** is the kinetic product whereas **172** is the thermodynamic product. The isolation of **172** represents the *first* synthesis of a non 5-membered-ringed thionosulfite.

Altering the base from NEt_3 to pyridine resulted in decreased yields and product purity. Altering the sulfur transfer reagent from S_2Cl_2 to **15a** and **15b**, compounds which had been shown as useful sulfur transfer reagents in the formation of 5-membered

thionosulfites[3] (*cf.* Chapter 2.3), proved ineffective in the formation of 171-175, as they provided complex mixtures of products.

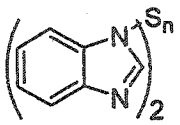

n = 1 **15a**
n = 2 **15b**

We were interested in the factors that determined formation of 171 and 172. Initially, it was not clear whether 172 was the result of an isomerization process from 171 or whether 172 formed independently from 171. We propose the following synthetic scheme (Scheme 51).

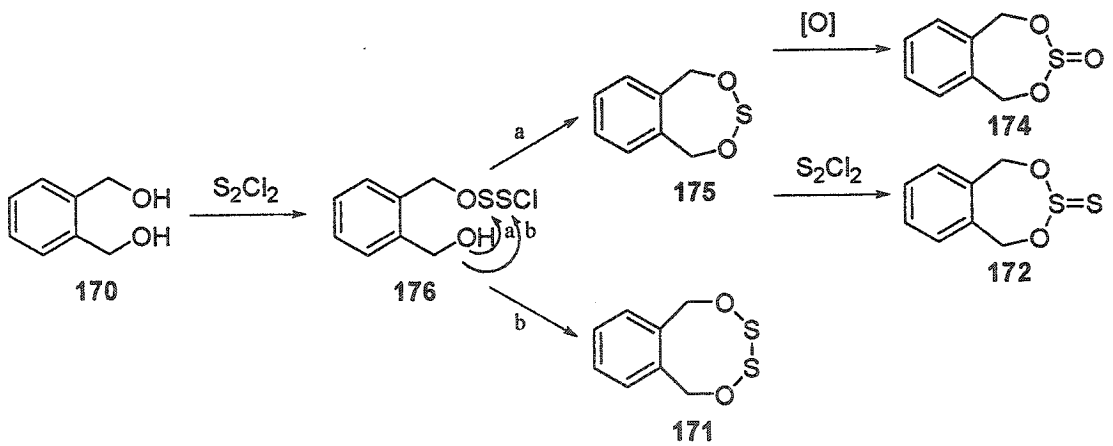

Scheme 51. Different cylization routes in the formation of either 171 or 172.

The ^{1}H NMR of pure 171 stored at 0 °C showed a slow isomerization to 172 wherein after *ca.* 2 weeks, there was a 95:5 ratio of 171:172. Such a slow isomerization process would argue against the *in situ* pre-formation then interconversion of 171 to 172; the reverse isomerization of 172 to 171 at 0 °C was not observed. Although the possibility of an S_N2'-type of ring closure to form 172 using only one equivalent of S_2Cl_2 could not be

discounted, the presence of trace **174** and **175** would support the contention for the current mechanism. Moreover, we were never able to promote the formation of >33% of **172**. This low yield would also seem to suggest that 2 equivalents of S_2Cl_2 are used in its formation. Although some have suggested[4] that branch-bonded products using S_2Cl_2 emanate from the fact that trace S_2Cl_2 may exists in its branch-bonded form $Cl_2S{=}S$, there is little evidence to suggest at the addition temperatures, that this is true[5-10] (*cf.* also Chapter **2.5.3**).

5.3 Thermal Stability Investigations

We investigated the thermal stability of **171** and **172**. Whereas **172** was stable at 120 °C for >3 h, **171** decomposed within minutes under the same conditions to afford **172**, **174**, and **175** amongst other products as detected by ^{1}H NMR. The lack of observable coalescence of the AX signal in **172** is due to the contribution of two distinct barriers: (1) the pyramidal sulfur inversion barrier; (2) the H/C_{SP2} eclipsing interactions ($A^{1,3}$ strain), similar to those found in toluene that exist given the chair conformation of the 7-membered ring (*vide infra*). Differential scanning calorimetry (DSC) also provides insight into the relative stabilities of **171**-**173**. Although phase transitions in both **171** and **172** were observed, the thermodynamic profiles of **171** and **173** were unique in that they also present an exotherm at higher temperatures (*ca.* 140 °C), indicating decomposition. The barrier to rotation of **171** was also calculated to be 18.8 ± 0.2 kcal/mol using approximations developed by Raban.[11] The ABq splitting of the benzyl protons coalesced at 114.6 °C in *p*-xylene-d_{10}. This barrier is comparable to those

measured[12,13] and calculated[14,15] for acyclic alkoxy disulfide analogues (*cf.* also Chapters 3 and 4). This indicates that the major contributor to the barrier in **171** is that of the rotation about the S-S bond; 8-membered ring inversion is much less energetically demanding. Dimer **173** was also heated in *p*-xylene-d_{10}, but full coalescence could not be achieved even at 140 °C. Here the two ABq systems (*vide infra*) only coalesced into a single doublet.

5.4 Conformational Analysis

5.4.1 IR and Raman data

The infrared spectra (IRs) of **171** and **172** were similar except that in **172** there were strong bands at 688 and 696 cm^{-1}. These bands are assigned as the ν(S=S) stretch of the thionosulfite and have a similar energy with respect to both experimental[3,16] and theoretical calculations.[15] The predicted S-S bond stretch of *ca.* 525 cm^{-1} for **171** was not observed in this case. It is probable that this stretching mode is too weak to be detected by IR. We thus measured the Raman spectra of **171** and **172**. Here we were able to detect the S-S stretch at 518 cm^{-1} as well as the S-O stretch at 676 cm^{-1} for **171**; these are consistent with the literature values.[15] We assigned the corresponding S-O stretch in **172** at 633 cm^{-1}. Interestingly, the major peak, which was assigned as the S=S stretching mode at 540 cm^{-1} is at a lower energy than that of the predicted value (640-665 cm^{-1}).[15]

We ascribe this difference in stretching frequency to the 2 oxygen lone pair backdonations into the σ* antibonding orbital of the S=S bond.[17] This is a classic example of the anomeric effect, similar to that observed in cyclic sulfites[18-21] and would result in a shortening of the S-O bonds and a lengthening of the S=S bond, the latter resulting in a lower energy stretching mode. The S=S bond distance in the crystal structure, as will be discussed in detail later, is 1.9361(8) Å. Although this is a very short S-S bond as compared to other S-S single bonds (*cf.* Chapter **2.4**), it is longer than other S=S double bond system: S_2 (1.890 Å)[22], S_2O (1.884 Å)[23], S_2F_2 (1.860 Å)[24] and S_2NR_2 (1.898 Å)[25] (*cf.* also Chapter **2.4.5**). There may also be a delocalization interaction between the parallel S=S bond with the π-system of the benzene ring which may contribute to the lower energy Raman signal of 518 cm^{-1}.

5.4.2 ^{1}H NMR and ^{13}C NMR data

The ^{1}H NMR spectra of the benzyl protons of **171-175** are distinct from one another (the ^{1}H NMR spectrum of the benzyl protons of **175** is a singlet at 5.54 ppm), Figure **26**. Selected NMR parameters are shown in Table **59**.

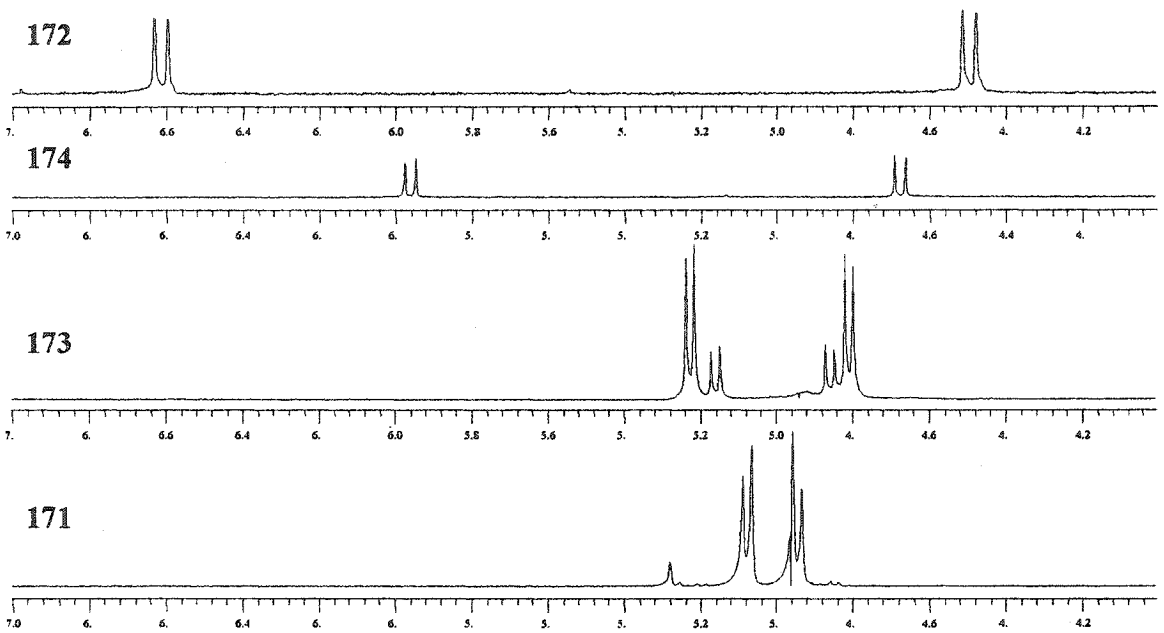

Figure **26**. The ^{1}H NMR spectra of the benzyl protons of **171-174**.

Table 59. Selected ^{1}H and ^{13}C parameters for 170-175.

Compounds		Chemical Shifts,[a]			^{2}J (Hz)
		^{1}H NMR		^{13}C NMR	
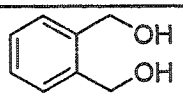	170	4.65	-	64.01	-
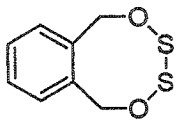	171	4.94	5.07	72.27	-12.00
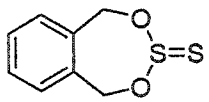	172	4.49	6.61	62.92	-14.25
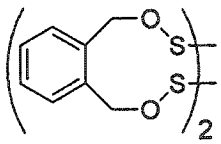	173	4.84	5.26	75.31	-11.00[b]
		4.89	5.20	75.35	-12.00[c]
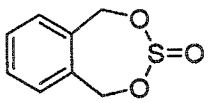	174	4.68	5.96	62.72	-14.00
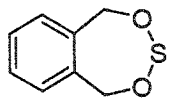	175	5.54	-	88.73	-

a) The ^{1}H NMR and ^{13}C NMR were recorded in $CDCl_3$. The chemical shifts are in ppm downfield from TMS. The chemical shifts have been referenced to the solvent peak at 7.24 ppm. The chemical shifts refer to the benzyl protons and carbons respectively. b) Outer doublet of 173. c) Inner doublet of 173.

The ^{1}H NMR of 171 is characteristic of alkoxy disulfides in that the two benzyl protons are anisochronous. This diastereotopicity results from the high barrier to rotation about the chiral axis that is the OS-SO moiety. This indicates that in solution, 171 is a racemic mixture of two enantiomeric atropisomers;[26] the sense of helicity defined by viewing down the S-S bond. Recall that a clockwise rotation is designated P (+), and a

counterclockwise rotation is designated M (-). The conformation of **171** is quite similar to that of tetrasulfide **177**.[27] This is evidenced in the small differences in related dihedral angles (Table **60**). Of note between the two structures are the slightly larger θ_{av}(O-S-S) = 108.3° as compared with θ_{av}(S-S-S) = 106.2°. This increase is due to a relatively larger anomeric effect present in **171** (*cf.* Chapter **3** for details on the anomeric effect). The θ_{av}(C-O-S) = 116.9° is 12.5° larger than that of θ_{av}(C-S-S). This is most likely due to a compensatory alleviation of steric strain owing to the shorter r_{av}(C-O) = 1.456 Å *vs.* r_{av}(C-S) = 1.829 Å.

Table **60**. Comparison of the conformations of **171** and **177**

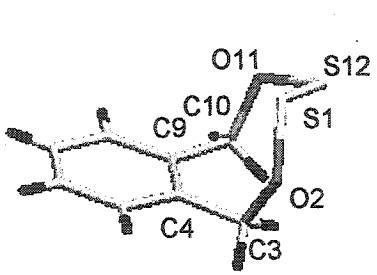

171

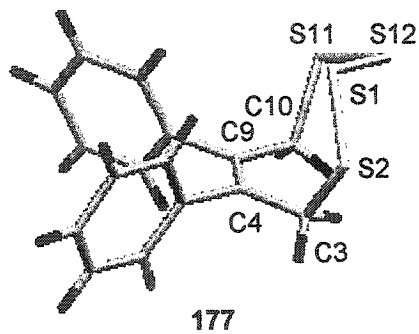

177

Dihedral Angle[a]	**171**[b,c]	**177**[b,d]	Δ(171-177) (°)
C3-C4-C9-C10	-3.4	-3.1	-0.3
C4-C9-C10-X11	-86.7	-101.2	14.4
C9-C10-X11-S12	90.2	88.1	-2.2
C10-X11-S12-S1	-77.9	-72.6	-5.3
X11-S12-S1-X2	93.2	103.6	10.4
S12-S1-X2-C3	-53.9	-65.1	11.2
S1-X2-C3-C4	-46.6	-41.9	-4.8
X2-C3-C4-C9	99.1	105.0	6.0

a) X = O in **171**, X = S in **177**. b) Dihedral angles in degrees. c) Numbering as that of X-Ray. d) Numbering altered from X-Ray to facilitate comparisons with **171**.

The observed ^{1}H NMR of dimer **173** indicates the presence 2 ABq in a *ca.* 2:1 ratio. The connectivity of **173** is that of a 16-membered ring containing two chiral axes in the two OSSO functional groups (*vide infra*). This would imply that **173** could exist in one of three conformations: (M,M), (P,P), (M,P). The latter conformation is a meso form. A reasonable explanation for the observed ^{1}H NMR is that of a statistical average of the three conformations. The (M,M) and (P,P) conformations would have the same ^{1}H NMR spectrum, hence the observed *ca.* 2:1 ratio of integrations of the two ABq, each of which has a slightly different coupling constant (Table **59**). Based on the ratios of ^{1}H NMR intensities and assuming a Boltzmann population distribution at 296 K, the (M,P) conformer is disfavored over the other two by 0.30 kcal/mol (Table **61**). The ^{13}C NMR of **173** as compared to **171** indicates that the relief in strain afforded by the larger macrocycle did not translate locally into a different magnetic environment for the benzyl carbon. The two different conformers of **173** were also detected by ^{13}C NMR. The ^{13}C NMR ratio of the benzyl carbons of the two conformers was also observed to be 2:1.

Table **61**. Observed population distributions and calculated energies for the three conformers of **173**

Conformers of **173**	Calcd.ΔΔG (kcal)[a]	Observed Population Distribution[b,c] (%)
(M,M) + (P,P)	0	62
(M,P)	0.30	38

a) ΔΔG with respect to (M,M) + (P,P) conformers. b) According to the Boltzmann relationship: $n_2/n_1 = exp(-\Delta G/RT)$, T = 296 K. c) Based on ^{1}H NMR integrals in $CDCl_3$.

Thionosulfite **172** and sulfite analog **174** each contain a chiral centre in the branch-bonded pyramidalized sulfur. This results in a splitting of the benzyl protons as two sets of doublets (each with an AX pattern). The large separation of the chemical shifts of the geminal protons is induced by the electronic effects resulting from the relative *syn*-orientation of a benzyl proton with respect to the deshielding zones of the axial S=O or S=S bond (Figure 27).

Figure 27. Shielding (+) and deshielding (-) zones of sulfites (X = O) and thionosulfites (X = S)

It is well known in the literature that the S=O bond in sulfites strongly differentiates between axial and equatorial protons attached to carbons adjacent to the sulfite moiety.[28-30] This would imply that the major conformation in each of **172** and **174** contain two *syn*-axial benzylic protons. The large observed geminal coupling constants for **172** and **174** (Table **59**) is also consistent with the presence of a respective axial S=S or S=O bond (13.7 Hz in **178**; 13.2 Hz in **179**).[31] In the solid state, the chair conformation is the respective major or sole conformation of both of these compounds (*vide infra*). The relative downfield shift of 0.5 ppm of the downfield doublet in **172** with respect to **174** is an indicator of the increased polarization and polarizability of the S=S bond as S^{+}–S^{-}, similar to that found in the S=O bond of sulfites.[32] Steudel had previously calculated that such thionosulfite bonds would be polarized in this fashion.[33] This would imply that there exists a larger polarizability within the S=S bond of **172** *vs.* that of S=O bond of **174**.

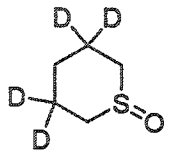

178

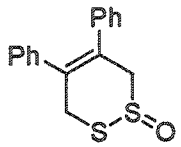

179

Interestingly, the ^{13}C NMR of the benzyl carbons of **171** and **173** are *ca.* 10 ppm more downfield than those of **172** and **174**. This is a result of the 'γ' shift, which is normally an indicator of the interaction of an axial S=O bond with *syn*-axial H's, and results in the shielding of, in this case, the benzyl carbon (*ca.* 9 ppm) relative to a conformation wherein the S=O bond is equatorial. It is assumed that the 'γ' shift would also apply to the analogous thionosulfite system. Moreover, the benzyl carbons of **175** resonate *ca.* 10 ppm further downfield from **171** and **173**. In this case, the relative downfield position of benzyl carbons would support the contention that the sulfur is negatively polarized and thus can act as a suitable nucleophile, as suggested in the mechanism in Scheme **51**.

Much work has been published on the conformation of 5-[34,35] and 6-membered[28,29,36-38] cyclic sulfites but few have investigated larger rings.[39-41] Spectroscopic studies on the conformation of **174** had previously been carried out by Faucher and co-workers.[42,43] It was shown *via* low temperature ^{1}H NMR and ^{13}C NMR that **174** existed in at least two conformations. They inferred from the IR spectrum (CCl_4) that the major conformation was that of the chair at room temperature, which possesses an axial S=O bond ν(S=O) = 1184 cm^{-1} whereas the minor conformation was that of the twist-boat, which possesses no axial S=O bond ν(S=O) = 1220 cm^{-1}. The authors also reported that the conformational equilibrium can be influenced by solvent with more polar solvents favouring the twist-

boat conformation; at -100 °C in CHF_2Cl, there was a 1:1 conformational equilibrium between the two conformers. Substitution at the benzylic position influenced the conformational equilibrium between the twist-boat and the chair.[44] In fact, St.-Jacques[45] showed in a related sulfite wherein the *ortho*-H's of **174** were replaced by methyl groups, that in an 80:20 solution of CHF_2Cl/CD_2Cl_2, the most stable conformer is that of the twist-boat (83%); the chair with the axial S=O was 17%. The reported[43] ^1H NMR was that of an AB spectrum for the benzyl protons at RT in CHF_2Cl. Our RT spectrum obtained in $CDCl_3$ has an AX pattern with a $\delta\Delta\nu/J = 45.88$, an indicator that the spectrum is indeed first order.

5.4.3 NOE data

NOE experiments on **171**, **172**, and **174** were carried out in $CDCl_3$ at 23 °C in order to further define their solution state conformations. Intraproton distances were assigned by standard 1DNOESY experiments on a 400 MHz spectrometer. 1DNOESY spectra were recorded at five mixing times (0.2 s, 0.5 s, 0.8 s, 1.0 s, 1.2 s) to check the linearity of the cross-relaxation buildup. Intraproton distances were calculated using the initial rate approximation according to the internal calibration distances of the weighted average of each of the average intraproton distances per conformer of **174**: (1) between geminal benzyl protons, (2) between the highfield benzyl proton and the *ortho*-benzene proton, (3) between the lowfield benzyl proton and the *ortho*-benzene proton. For all 1DNOESY experiments, the acquisition time was 2.0 s (spectral width 6410 Hz) and the relaxation delay time was 1.0 s.

In the cases of **172** and **174**, irradiation of either benzylic proton resulted in a positive NOE to the other benzylic proton as well as a positive NOE to the *ortho*-protons of the benzene ring. A similar positive enhancement was observed for **171** however a negative NOE was observed between the two benzylic protons. The negative NOE results from the fact that the benzyl protons in **171** are exchangeable, a property that was confirmed in dynamic NMR experiments (*vide supra*). Intratomic separations are summarized in Table **5**.

The relatively small differences in solution intraproton distances to extrapolated X-Ray intraproton distances in **172** would seem to indicate that both **172** and **174** possess similar conformations in solution. Moreover as the conformation of **172** in the solid state is that of a 7-membered chair possessing an axially oriented S=S bond (*vide infra*), we can infer that the solution conformations of **172** and **174** mirror this as well.

Table 62. Intraproton distances of 171 and 172

Compound		NOE(Ha,Hb)	NOE distance[a] (Å)	X-Ray distance (Å)	Δ (Å)	type of coupling
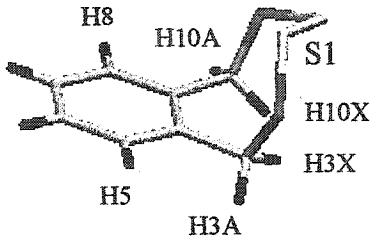	171	H10A H8		2.4		
		H3A H5		2.4		
		average	2.45	2.4	0.05	
		H10X H8		3.5		
		H3X H5		3.5		
		average	3.1	3.5	-0.4	
		H10A H10X		1.6		
		H3A H3X		1.6		
		average	-[b]	1.6		AB
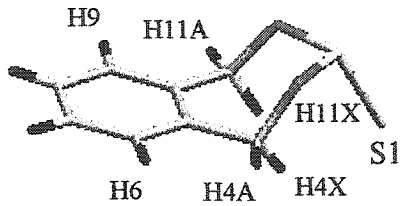	172	H6 H4A		2.2		
		H9 H11A		2.3		
		average	2.2	2.3	-0.04	
		H6 H4X		3.3		
		H9 H11X		3.4		
		average	3.6	3.4	0.2	
		H4A H4X		1.6		
		H11A H11X		1.6		
		average	1.60	1.6	-0.005	AX

a) The intraproton distances were calculated using the initial rate approximation according to a two-spin model and were referenced with respect to a weighted average of the two conformers of =174 [Avg(H6-H4A, H9-H11A = 2.3 Å); Avg(H6-H4X,H9-H11X = 3.3 Å); Avg(H4A-H4X, H11A-H11X = 1.59 Å]. b) Not ascertainable as the geminal protons of 171 are exchangeable.

5.4.4 Solid State and Structure Analysis

The stick representation of **171** is shown in Figure **28**. The r(S-S) of 1.959 Å is intermediate between the three other published crystal structures for dialkoxy disulfides (for MeOS-SOMe **6** r(S-S) = 1.972 Å;[46] for *p*-NO_2-BnOS-SOBn-*p*-NO_2 **49** r(S-S) = 1.968 Å;[15] for *p*-Cl-BnOS-SOBn-*p*-Cl **50** r(S-S) = 1.933 Å[47]). The r_{av}(S-O) of 1.653 Å

and θ_{av}(O-S-S) of 108.4° are unremarkable with respect to the respective average reported crystal structure values of 1.651 Å and 108.2°. The τ(OS-SO) of 93.2° is larger than the normal dihedral angle for this class of compounds (τ_{av}(OS-SO) = 81.3°), but not

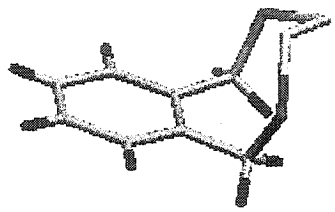

Figure **28**. Stick representation of the crystal structure of **171**.

unusually so for XSSX systems (*cf.* Chapter **2.4**). This perturbation may be due to the fact that **171** is cyclic and cannot adopt an ideal OS-SO dihedral angle. In the solid state **171** possesses no symmetry (C_1). This 8-membered ring seems to adopt a pseudo-saddle type geometry[48] with limited conformational flexibility in that it contains both a second degree of unsaturation in the fused benzene ring as well as the OS-SO moiety. Most 8-membered rings adopt either a boat-chair or a twist-boat-chair conformation in the solid state, with potential interconversion into the higher energy crown conformation.[26,48,49] The r(H3X-H10X) intraproton distance of 2.02 Å is smaller than that of the sum of the two respective proton van der Waals radii (2.4 Å). Crystal structure intra-atom distances which are smaller than their respective van der Waals radii are not unknown in the literature,[50] however the magnitude of the crowding is quite unusual. To our knowledge only pyrene has a comparable H-H distance (2.03 Å).[50]

The stick representation of **173** is shown in Figure **29**. This dimeric by-product of the formation of **171** is a novel 16-membered macrocycle possessing C_2 symmetry and

containing two OS-SO functional groups. These two chiral units offer the potential of isolable diastereomeric conformers. The conformation of **173** is that of (M,M / P,P),

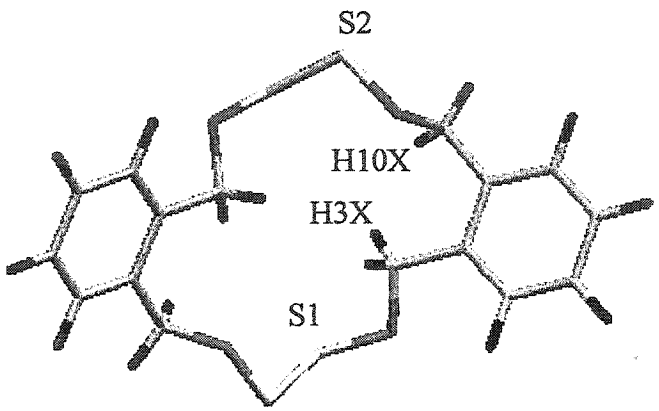

Figure **29**. Stick representation of the crystal structure of **173**.

which is the major predicted solution conformation. The r(S-S) of 1.964 Å, r_{av}(S-O) of 1.660 Å and θ_{av}(O-S-S) of 108.4° are all consistent not only with that of **171** but with the literature.[15,46,47] The τ(OS-SO) of 87.6° is also unremarkable. In the crystal structure, there are two distinct benzylic-CH_2 groups. However, in solution, we observe a *ca.* 2:1 ratio of two ABqs. This suggests that in solution, there is a dynamic conformational equilibrium occurring to average out the signals between these two CH_2-groups to account for the larger of the ABq. The smaller ABq is assigned to the (M,P) conformer. The r(H3X-H10X) intraproton distance of 2.11 Å is slightly larger than the corresponding intraproton distance found in **171** but nevertheless is still smaller than that of the sum of the two respective proton van der Waals radii (2.4 Å).

We believe that the conformation of both **172** and **174** would be similar and that the large downfield shift observed in one of the doublets would argue for an axial

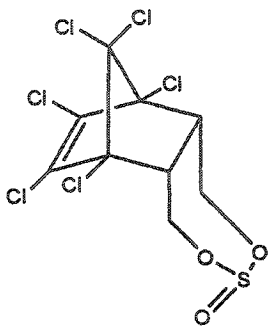

mp. 108-110

180a

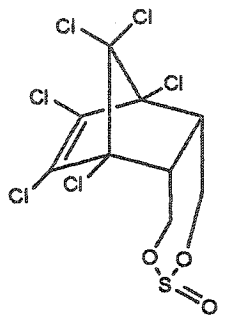

mp. 208-210

180b

configuration for that corresponding benzyl proton. The chair conformation contains an axial benzyl proton whereas the twist-chair does not. The chair conformation is stabilized over the two $n_O \rightarrow \sigma^*_{S=O}$ stereoelectronic donations present (*vide supra*). There exists also a favorable dipolar interaction in the chair conformation as compared to that of the twist.[51,52] Moreover, in the solid state, **172** (Figure **30**) is exclusively found in the chair conformation whereas **174** (Figure **31**) is found as a 9:1 mixture of chair:twist-boat. The conformation of **172** and that of the chair conformation of **174** are nearly superimposable. Unsaturation in 7-membered rings, as exists in **172** and **174**, favours the chair conformation over that of the twist.[49] Thus it would seem most likely that the preferred conformation of **174** in solution at room temperature mirrors that found in the solid state (chair) and not, as the authors[42] had contended, that of a 1:1 mixture of chair:twist-boat. Interestingly, the two major conformations for a related sulfite, insecticide thiodan **180a** and **180b** exist as chairs with axial S=O bonds. Related disulfides[53] **181a** and **181b** also exists exclusively as the chair and trisulfide **182** exists as an 85:15 ratio of chair:twist-boat conformations.[54]

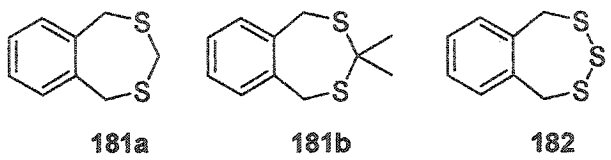

181a 181b 182

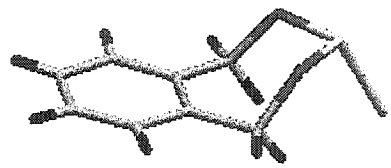

Figure **30**. Stick representation of the crystal structure of **172**.

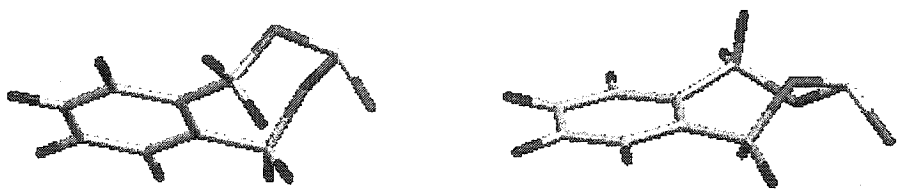

A B

Figure **31**. Stick representation of the deconvoluted crystal structure **174**. A) The major chair conformation. B) The minor twist conformation

The sum of the two θ(O-S-S) and one θ(O-S-O) of **172** is 319.2° is comparable to the sum of the three θ(O-S-O) found in the **174A** (317.1°) and indicates the pyramidal nature of the branch-bonded sulfur. The two $n_O \rightarrow \sigma^*_{S=O}$ stereoelectronic donations present in **174** and two $n_O \rightarrow \sigma^*_{S=S}$ stereoelectronic donations present in **172** contribute to a lengthening of the respective S=O and S=S bonds. The S=S bond length in **172** is 1.9361(8) Å and is slightly longer than that found in **5g** (1.901(2) Å).[55] Similarly, the S=O bond in **174A** is 1.595(2) Å which also is much longer than that found in **183** (1.45 Å).[56]

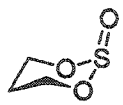

183

5.5 Concluding Remarks

In this Chapter we have shown that it is indeed possible to synthesize cyclic alkoxy disulfides as well as larger ringed thionosulfites. We have investigated the solution and solid state conformations of **171-174** and have compared these to other medium sized chalcogen-containing rings. In the next chapter, we will explore the factors which govern which isomer should be the more stable.

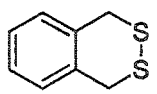

184

Recently, benzodithiin derivatives such as **184** were found to be highly potent and specific inhibitors of *in vitro* replication of the respiratory syncytial virus (RSV), possessing an EC_{50} of 4.5 μM.[57] The partial parallel in structure with **171** may imply that it too may be a good inhibitor again RSV replication activity. A study into the biological activity of **171** may be warranted.

5.6 Synthetic Experimental Section

DSC Spectra of **171-173** are available in Appendix III. IR Spectra of **171-173** are available in Appendix IV, including zoomed spectra highlighting the region < 1500 cm^{-1}. In addition, a composite IR plot of isomers **171** and **172** is provided to aid in the comparison of the spectra. Raman spectra for **171** and **172** are available in Appendix V.

5.6.1 Synthesis of 1,2-benzenedimethanol 170:

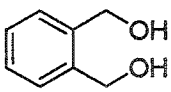

To a slurry of $LiAlH_4$ (19.3 g, 0.5 mol, 2.5 equiv) in 315 mL THF was slowly added a solution of *o*-phthalic acid (33.5 g, 0.2 mol, 1 equiv) in 215 ml THF at 0 °C under N_2. The flask was equipped with an exit to monitor the production of H_2 gas during the addition. The solution was stirred for 18 h and then quenched according to the literature procedure.[58] This was then stirred for an additional 3 h. The whitish slurry was then vacuum-filtered and washed with excess THF. The organic section was extracted with Et_2O. The solution was dried over $MgSO_4$. The solvent was removed first under reduced pressure and then *in vacuo*. White crystalline solid. If need be, this can be recrystallized in EtOAc as the solvent and hexanes as the co-solvent. R*f* (50% EtOAc/hexanes) 0.35. Yield: 84 %. Mp. 68-69 °C (lit Mp. 62-63 °C,[59] 63-65 °C[60]) ^1H NMR δ 3.44 (s, 2H), 4.65 (s, 4H), 7.30 (m, 4H); ^{13}C NMR δ 64.0, 128.5, 129.7, 139.3; MS (CI) *m/z* 156 ($M^{+\bullet}$ + NH_4^+), 139 ($M^{+\bullet}$ + H^+), 120, 91; HRMS. Calcd for $C_8H_{11}O_2$ ($M^{+\bullet}$ + H^+): 139.0759. Found: 139.075(3).

5.6.2 Synthesis of 8-membered ring alkoxy disulfide 171:

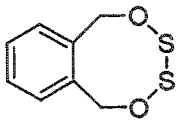

This was synthesized as a modification of the literature procedure for the synthesis of acyclic alkoxy disulfides.[61] A solution of diol, **170**, (138 mg, 1 mmol, 1 equiv) and NEt_3 (280 μL, 2 mmol, 2 equiv) in 10 mL of CH_2Cl_2 was allowed to stir under nitrogen at 0 °C. A solution of S_2Cl_2 (80 μL, 1.0 mmol, 1 equiv) in 50 mL of CH_2Cl_2 was added dropwise over *ca.* 60 min. The reaction mixture was allowed to stir for a further 4 h. The reaction mixture was quenched with 20 mL of H_2O. The organic phase was washed 3x 33 mL of H_2O. The organic phase was dried over $MgSO_4$. This mixture was vacuum filtered, and the solvent was removed first under reduced pressure and then *in vacuo*. Frequently, it was not necessary to chromatograph the product as there was quantitative conversion as detected by TLC and ^1H NMR. Fruity-smelling white crystalline solid. R*f* (25% EtOAc/hexanes) 0.47, (25% CH_2Cl_2/hexanes) 0.17. Yield: 94 %. Mp. 59-60 °C; DSC. T_{onset}: 61.11, T_{max}: 64.63, ΔH = 476.2 J/g; T_{onset}: 117.98, T_{max}: 125.36, ΔH = -404.5 J/g. ^1H NMR δ 7.43 (m, 4H), ABq system 4.94 (d, 2H, J_{AB} = 12.00 Hz), 5.07 (d, 2H, J_{AB} = 12.00 Hz); ^{13}C NMR δ 72.3, 130.1, 132.1, 136.1; ^{13}C NMR indirectly detected by HMQC(500 MHz, 125 MHz) δ 72.6, 131.0, 133.0; IR ($CDCl_3$) 531 cm^{-1} (S-S stretch); MS (EI) *m/z* 200 ($M^{+\bullet}$), 152 ($M^{+\bullet}$ – SO); 119 ($M^{+\bullet}$ – S_2OH), 104 ($M^{+\bullet}$ – S_2O_2) HRMS. Calcd for $C_8H_8S_2O_2$: 199.9966. Found: 199.997(0). Calcd for $C_8H_8S_2O_2$ - SO: 152.0296. Found: 152.030(0). IR – KBr (cm^{-1}) 1471(w), 1452(w), 1384(w), 1352(w), 1306(w), 1209(w), 1188(w), 1117(w), 956(m), 932(s), 874(w), 848(w), 816(w), 789(w), 760(m),

743(s), 698(w), 676(w), 647(s), 619(m), 590(w), 531(w). Raman (powder – 5000 scans) 3046, 2966, 2920, 1604, 1051, 676 ν(S-O), 518 ν(S-S), 355, 196, 137, 122, 84.

5.6.3 Synthesis of 7-membered ring thionosulfite 172:

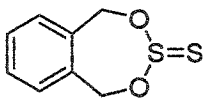

The following conditions appear to be optimal for the procedure of **172**. A solution of diol, **170**, (138 mg, 1 mmol, 1 equiv) and NEt_3 (280 μL, 2 mmol, 2 equiv) in 10 mL of CH_2Cl_2 was allowed to stir under N_2 at RT. A solution of S_2Cl_2 (80 μL, 1.0 mmol, 1 equiv) in 10 mL of CH_2Cl_2 was added dropwise over *ca.* 60 min. The reaction mixture was allowed to stir for a further 4 h. The reaction mixture was quenched with 10 mL of H_2O. The organic phase was washed 3x 33 mL of H_2O. The organic phase was dried over $MgSO_4$. This mixture was vacuum filtered, and the solvent was removed first under reduced pressure and then *in vacuo*. The crude solid, which contained a 2:1 mixture of **171**:**172**, was flash chromatographed[62] in 25% CH_2Cl_2/hexanes as the eluant to afford a slightly aromatic white crystalline solid. R*f* (25% CH_2Cl_2/hexanes) 0.31. Yield: 22 %. Mp. 73-74 °C; DSC. T_{onset}: 79.93, T_{max}: 80.69, ΔH = 78.10 J/g; ^1H NMR δ 7.32 (m, 4H), 6.61 (d, 2H, *J* = 14.25 Hz), 4.49 (d, 2H, *J* = 14.25 Hz); ^{13}C NMR δ 62.9, 128.4, 129.5, 136.9; MS (EI) *m/z* 200 ($M^{+\bullet}$), 170, 135, 119, 90, 78; HRMS. Calcd for $C_8H_8S_2O_2$: 199.9966. Found: 199.995(9); Calcd for $C_8H_8S_2O_2$ – O: 184.0017. Found: 184.001(6); Calcd for $C_8H_8S_2O_2$ – O_2: 168.0067. Found: 184.005(9); Calcd for $C_8H_8S_2O_2$ - SO: 152.0296. Found: 152.029(4); IR – KBr (cm^{-1}) 1496(w), 1455(m), 1442(w), 1384(w),

1352(w), 1306(w), 1242(w), 1219(w), 1209(w), 1186(w), 1118(w), 956(w), 947(m), 932(s), 893(m), 874(w), 853(w), 848(w), 816(w), 789(w), 774(m), 760(w), 743(w), 739(m), 696(m), 685(m), 676(m), 669(m), 647(w), 632(s), 619(m), 595(m), 590(w), 540(w), 531(w). Raman (powder – 1000 scans) 3047, 2983, 1606, 1220, 1160, 1048, 745, 633 ν(S-O), 540 ν(S=S), 337, 304, 179, 135, 87, 58.

5.6.4 Synthesis of 16-membered ring dimer 173:

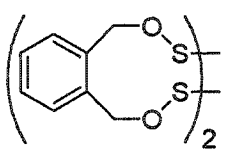

The following conditions appear to be optimal for the procedure of **173**. A solution of diol, **170**, (138 mg, 1 mmol, 1 equiv) and NEt_3 (280 μL, 2 mmol, 2 equiv) in 10 mL of THF was allowed to stir under nitrogen at 0 °C. A solution of S_2Cl_2 (80 μL, 1.0 mmol, 1 equiv) in 10 mL of THF was added dropwise over *ca.* 3 min. The reaction mixture was allowed to stir for a further 5 h. The reaction mixture was quenched with 10 mL of H_2O. The organic phase was extracted in 20 mL Et_2O. The organic phase was washed 3x 33 mL of H_2O. The organic phase was dried over $MgSO_4$. This mixture was vacuum filtered, and the solvent was removed first under reduced pressure and then *in vacuo*. The crude solid, which contained a 10:1 mixture of **171**:**173**, was flash chromatographed[62] in 25% CH_2Cl_2/hexanes as the eluant to afford a slightly aromatic white crystalline solid. *Rf* (25% CH_2Cl_2/hexanes) 0.13. Yield: 9 %. Mp. 153-155 °C; DSC. T_{onset}: 92.18, T_{max}: 95.80, ΔH = 11.99 J/g; T_{onset}: 139.88, T_{max}: 143.19, ΔH = -

124.70 J/g; T_{onset}: 153.75, T_{max}: 156.76, ΔH = -42.52 J/g. ^{1}H NMR δ 7.36 (m, 8H), AX system: 5.26 (d, 4H, *J* = 11.00 Hz), 5.20 (d, 2H, *J* = 12.00 Hz), 4.89 (d, 2H, *J* = 12.00 Hz), 4.84 (d, 4H, *J* = 11.00 Hz); ^{13}C NMR δ 75.3, 75.4, 128.7, 129.0, 129.7, 134.7, 134.9; ^{13}C NMR indirectly detected by HMQC(600 MHz, 151 MHz) δ 75.2, 129.0, 129.7; MS (EI) *m/z* 400 ($M^{+\bullet}$), 352 ($M^{+\bullet}$ – SO), 272 ($C_{12}H_{16}O_3S_2$), 255, 200 ($C_8H_8O_2S_2$), 152 (C_8H_8OS), 135, 121, 120 (C_8H_8O), 105, 104 (C_8H_8); HRMS. Calcd for $C_{16}H_{16}S_4O_4$: 399.9931. Found: 399.99(3)4. IR – KBr (cm^{-1}) 1481(w), 1456(w), 1447(w), 1384(w), 1367(w), 1360(w), 1300(w), 1262(w), 1232(w), 1205(w), 1189(w), 1112(w), 984(m), 974(m), 953(m), 926(s), 874(m), 855(w), 816(m), 763(s), 736(m), 723(m), 697(s), 639(w), 602(w), 514(w).

5.6.5 Synthesis of sulfite 174:

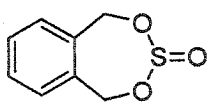

To a solution of **170** (141.5 mg, 1 mmol, 1 equiv) and NEt_3 (280 μL, 2 mmol, 2 equiv) in 10 mL CH_2Cl_2 was added dropwise a solution of 75 μL of $SOCl_2$ in 10 mL CH_2Cl_2 at 0 °C under N_2. The reaction was stirred for 2.3 h. The reaction was quenched with 20 mL H_2O. The organic phase was washed 3x 30 mL H_2O. The solution was dried over $MgSO_4$. The solvent was removed first under reduced pressure and then *in vacuo*. Brownish crystals. R*f* (25% EtOAc/hexanes) 0.38; (25% CH_2Cl_2/hexanes) baseline. Yield: 74 %. Mp. 33-36 °C; Recrystallized as clear crystals from CH_2Cl_2/hexanes: Mp 34-35 °C; ^{1}H NMR δ 7.27 (m, 4H), 5.96 (d, 2H, *J* = 14.00 Hz), 4.68 (d, 2H, *J* = 14.00

Hz); ^{13}C NMR δ 62.7, 128.3, 128.3, 136.1; MS (EI) *m/z* 184 ($M^{+\bullet}$), 119, 91; HRMS. Calcd for $C_8H_8SO_3$: 184.0194. Found: 184.019(8).

5.6.6 Synthesis of sulfoxylate 175:

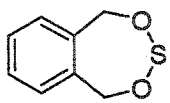

A solution of diol, **170**, (138 mg, 1 mmol, 1 equiv) and NEt_3 (280 μL, 2 mmol, 2 equiv) in 10 mL of CH_2Cl_2 was allowed to stir under nitrogen at 0 °C. A solution of SCl_2 (64 μL, 1.0 mmol, 1 equiv) in 10 mL of CH_2Cl_2 was added dropwise over *ca.* 10 min. The reaction mixture was allowed to stir for a further 3 h. The reaction mixture was quenched with 20 mL of H_2O. The organic phase was washed 3x 33 mL of H_2O. The organic phase was dried over $MgSO_4$. This mixture was vacuum filtered, and the solvent was removed first under reduced pressure and then *in vacuo*. Aromatic light-brown solid. R*f* (25% CH_2Cl_2/hexanes) 0.18. Yield: 92 %. ^1H NMR δ 7.28 (m, 4H), 5.54 (s, 4H); ^{13}C NMR δ 88.7, 128.4, 129.8, 138.6; MS (EI) *m/z* 168 ($M^{+\bullet}$), 160, 138, 135, 119, 104, 78 HRMS. Calcd for $C_8H_8SO_2$: 168.0245. Found: 168.024(0).

5.7 References

(1) Thompson, Q. E. *3,357,993*; United States Patent Office: United States of America, **1967**, 4.

(2) Steudel, R.; Schmidt, H. *Z. Naturforsch.* **1990**, *45B*, 557.

(3) Harpp, D. N.; Zysman-Colman, E.; Abrams, C. B. *J. Org. Chem.* **2003**, *68*, 7059.

(4) Amaresh, R. R.; Lakshmikantham, M. V.; Baldwin, J. W.; Cava, M. P.; Metzger, R. M.; Rogers, R. D. *J. Org. Chem.* **2002**, *67*, 2453.

(5) Spong, A. H. *J. Chem. Soc.* **1934**, 485.

(6) Palmer, K. J. *J. Am. Chem. Soc.* **1938**, *60*, 2360.

(7) Beagley, B.; Eckersley, G. H.; Brown, D. P.; Tomlinson, D. *Trans. Farady Soc.* **1969**, *165*, 2300.

(8) Hirota, E. *Bull. Chem. Soc. Japan* **1958**, *31*, 130.

(9) Chadwick, B. M.; Grzybowski, J. M.; Long, D. A. *J. Mol. Struct.* **1978**, *48*, 139.

(10) Bock, H.; Solouki, B. *Inorg. Chem.* **1977**, *16*, 665.

(11) Kost, D.; Carlson, E. H.; Raban, M. *Chem. Commun.* **1971**, 656.

(12) Seel, F.; Gombler, W.; Budenz, R. *Liebigs Ann. Chem.* **1970**, *735*, 1.

(13) Borghi, R.; Lunazzi, L.; Placucci, G.; Cerioni, G.; Foresti, E.; Plumitallo, A. *J. Org. Chem.* **1997**, *62*, 4924.

(14) Snyder, J. P.; Carlsen, L. *J. Am. Chem. Soc.* **1977**, *99*, 2931.

(15) Snyder, J. P.; Nevins, N.; Tardif, S. L.; Harpp, D. N. *J. Am. Chem. Soc.* **1997**, *119*, 12685.

(16) Tanaka, S.; Sugihara, Y.; Sakamoto, A.; Ishii, A.; Nakayama, J. *J. Am. Chem. Soc.* **2003**, *125*, 9024.

(17) Gillespie, R. J.; Robinson, E. A. *Can. J. Chem.* **1963**, *41*, 2074.

(18) Lehn, J.-M.; Wipff, G.; Bürghi, H.-B. *Helv. Chim. Acta* **1974**, *57*, 493.

(19) Lehn, J.-M.; Wipff, G. *J. Chem. Soc. Chem. Commun.* **1975**, 800.

(20) Jeffrey, G. A.; Pople, J. A.; Binkley, J. S.; Vishveshwara, S. *J. Am. Chem. Soc.* **1978**, *100*, 373.

(21) Bürghi, H.-B.; Dunitz, J. D.; Lehn, J.-M.; Wipff, G. *Tetrahedron* **1974**, *30*, 1563.

(22) Abrahams, S. C. *Acta Cryst.* **1955**, *8*, 661.

(23) Myers, R. J.; Meschi, D. J. *Journal of Molecular Spectroscopy* **1959**, *3*, 405.

(24) Kuczkowski, R. L. *J. Am. Chem. Soc.* **1964**, *86*, 3617.

(25) Iwasaki, F. *Acta Cryst. Sect. B* **1979**, *35*, 2099.

(26) Eliel, E. L.; Wilen, S. H. *Stereochemistry of Organic Compounds*; John Wiley & Sons, Inc.: Toronto, **1994**.

(27) This tetrasulfide was isolated in a trapping experiment between dithiatopazine and 2,3-diphenylbutadiene. See: Nicolaou, K. C.; DeFrees, S. A.; Hwang, C.-K.; Stylianides, N.; Carroll, P. J.; Snyder, J. P. *J. Am. Chem. Soc.* **1990**, *112*, 3029.

(28) Green, C. H.; Hellier, D. G. *J. Chem. Soc. Perkin. Trans. 2* **1972**, 458.

(29) Albriktsen, P. *Acta Chem. Scand.* **1972**, *26*, 3678.

(30) Maroni, P.; Cazaux, L.; Gorrichon, J. P.; Tisnes, P.; Wolf, J. G. *Bull. Soc. Chim. Fr.* **1975**, 1253.

(31) Dodson, R. M.; Srinivasan, V.; Sharma, K. S.; Sauers, R. F. *J. Org. Chem.* **1972**, *37*, 2367.

(32) Pritchard, J. G.; Lauterber, P. C. *J. Am. Chem. Soc.* **1961**, *83*, 2105.

(33) Steudel, R.; Laitinen, R. S.; Pakkanen, T. A. *J. Am. Chem. Soc.* **1987**, *109*, 710.

(34) Buchanan, G. W.; Hellier, D. G. *Can. J. Chem.* **1976**, *54*, 1428.

(35) Green, C. H.; Hellier, D. G. *J. Chem. Soc. Perkin. Trans. 2* **1975**, 190.

(36) Hellier, D. G.; Tillett, J. G.; Van Woerden, H. F.; White, R. F. M. *Chem. and Ind.* **1963**, 1956.

(37) Wood, G.; McIntosh, J. M.; Miskow, M. H. *Can. J. Chem.* **1971**, *49*, 1202.

(38) Buchanan, G. W.; Cousineau, C. M. E.; Mundell, T. C. *Can. J. Chem.* **1978**, *56*, 2019.

(39) Riemschneider, R.; Wuscherpfennig, V. *Z. Naturforsch.* **1962**, *17B*, 516.

(40) Riemschneider, R.; Wuscherpfennig, V. *Z. Naturforsch.* **1962**, *17B*, 585.

(41) Forman, S. E.; Durbetaki, A. J.; Cohen, M. V.; Olofson, R. A. *J. Org. Chem.* **1965**, *30*, 169.

(42) Faucher, H.; Guimaraes, A.; Robert, J. B. *Tetrahedron Lett.* **1977**, *20*, 1743.

(43) Faucher, H.; Guimaraes, A. C.; Robert, J. B.; Sauriol, F.; St-Jacques, M. *Tetrahedron* **1981**, *37*, 689.

(44) Lachapelle, A.; St-Jacques, M.; Guimaraes, A.; De Almeda, P. *Can. J. Chem.* **1983**, *61*, 2244.

(45) Lachapelle, A.; St-Jacques, M. *Can. J. Chem.* **1985**, *63*, 2185.

(46) Koritsanszky, T.; Buschmann, J.; Schmidt, H.; Steudel, R. *J. Phys. Chem.* **1994**, *98*, 5416.

(47) Tardif, S. Ph.D. thesis, McGill University, **1997**.

(48) Evans, D. G.; Boeyens, J. C. A. *Acta Cryst. B* **1988**, *44*, 663.

(49) Setzer, W., N.; Glass, R. S. In *Conformational Analysis of Medium-Sized Heterocycles*; VCH: **1988**, p 151.

(50) Dunitz, J. D.; Gavezzotti, A. *Acc. Chem. Res.* **1999**, *32*, 677.

(51) Lemieux, R. U.; Koto, S. *Tetrahedron* **1974**, *30*, 1933.

(52) Harpp, D. N.; Gleason, J. G. *J. Org. Chem.* **1971**, *36*, 1314.

(53) Friebolin, H.; Mecke, R.; Kabuss, S.; Lüttringhaus, A. *Tetrahedron Lett.* **1964**, *29*, 1929.

(54) Kabuss, S.; Lüttringhaus, A.; Friebolin, H.; Mecke, R. *Z. Naturforsch.* **1966**, *21*, 320.

(55) Harpp, D. N.; Steliou, K.; Cheer, C. J. *J. Chem. Soc. Chem. Commun.* **1980**, 825.

(56) Altona, C.; Geise, H. J.; Romers, C. *Rec. Trav. Chim.* **1966**, *85*, 1197.

(57) Watanabe, W.; Sudo, K.; Sato, R.; Kajiyashiki, T.; Konno, K.; Shigeta, S.; Yokota, T. *Biochem. Biophys. Res. Commun.* **1998**, *249*, 922. Human RSV is a member of the family Paramyxoviridae and is the most prevalent infectious agent of acute respiratory illness in infants and young children.

(58) Fieser, L. F.; Fieser, M. *Reagents for Organic Synthesis*; John Wiley and Sons, Inc.: New York, **1967**; Vol. 1; p.583.

(59) Anderson, W. K.; Kinder Jr., F. R. *J. Heterocyclic Chem.* **1990**, *27*, 975.

(60) *Aldrich Catalog Handbook of Fine Chemicals*; Aldrich Chemical Company, Inc., **2003**.

(61) Harpp, D. N.; Zysman-Colman, E. *J. Org. Chem.* **2003**, Submitted.

(62) Still, W. C.; Kahn, M.; Mitra, A. *J. Org. Chem.* **1978**, *43*, 2923.

Chapter 6

Understanding the Relative Ground State Energies and Isomerization Between Alkoxy Disulfides and Thionosulfites

6.1 Introduction

In Chapter 5, we showed for the first time the existence of both the alkoxy disulfide and the thionosulfite isomers in a single system. We have not yet unequivocally established whether these isomers exist in equilibrium and if they do, what factors govern such an equilibrium nor have we explored possible mechanisms by which interconvertion between the two isomers could occur. Herein we report our initial calculational results as pertains to isomer ground state stability and relate our predictions to both our experimental results (in part detailed in Chapters 4 and 5) as well as the literature.

6.2 Computational Methodology

All *ab initio* calculations were carried out with the GAUSSIAN 94[1] suite. Geometries for the dialkoxy disulfides and their branch-bonded thionosulfites isomers **185-212** were calculated using the B3LYP density functional[2-5] with the 6-31G(d) Pople double ζ (zeta) split valence basis set.[6-10] Additionally, geometries were also calculated based on our hybrid MM3* force field.[11] Single point energy calculations using either B3LYP or second- (MP2) and third-order Møller-Plesset (MP3) pertubation theories[12,13] were calculated. The following basis sets were employed: 6-31G(d), 6-31G(2d), 6-31G(df), 6-31G(2df), 6-31G(3d), 6-31G(3df), and 6-31G(3d2f). Triple ζ split valence basis sets[14,15] with the same series of polarization functions were also used at the B3LYP, MP2 and MP3 levels. The role of diffuse functions was also examined.

6.3 Results and Discussion

Our results are discussed in three sections. We first present our calculations and discuss the predictions that these entail. Next, our experimental evidence in the context of the relative ground state energies of alkoxy disulfides and their isomeric thionosulfites is summarized. Finally we comment on the validity of the predictions in light of the experimental evidence.

6.3.1 Computational Predictions

A fascinating property of alkoxy disulfides **1** (ROSSOR) is that they can potentially exist in their constitutionally isomeric thionosulfite **2** (ROS(S)OR) form. It has been experimentally shown in similar systems such as S_2F_2 **75** that the two isomers exist in equilibrium (Chapter **2.5.2**); however to our knowledge no one has experimentally investigated a similar equilibrium in the ROSSOR system.[16] As a first step, we were interested in determining the relative ground state stabilities of isomers of forms **1** and **2**. We noted that all thionosulfides **5** in the literature contained 5-membered ring cores and that an intrinsic conformational feature in the two crystal structures which we possessed (**5g** and **5i**) was the presence of a twist in the τ(O-C-C-O). We hypothesized that forcing the ring to adopt another geometry may influence the relative ground state stabilities of the two isomers. We thus set out to model compounds which influenced the initial thionosulfite geometry in one of two fashions: (1) modification of the substituents pattern

along the carbon backbone to flatten the observed puckering of the ring; (2) altering the core ring size as a means of relieving ring strain. We optimized the geometries of each isomer per system and then computed their respective single point energies. Model compounds **185-204** were used to determine the validity of hypothesis (1) that substitution pattern could affect isomer stability. Model compounds **185**, **186** and **205-212** were developed to test whether ring size affects the relative ground state energies of the two isomeric forms as in hypothesis (2).

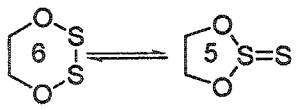

185 **186**

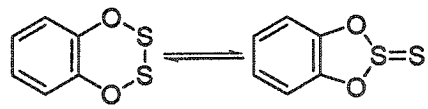

187 **188**

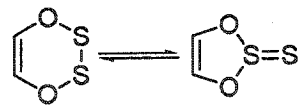

189 **190**

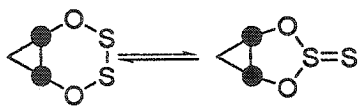

191 **192**

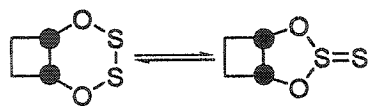

193 **194**

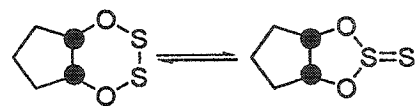

195 **196**

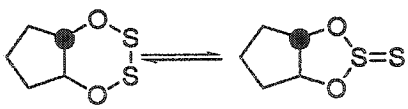

197 **198**

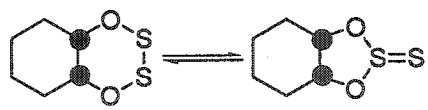

199 **200**

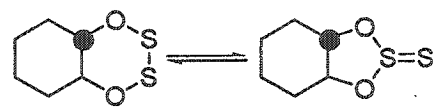

201 **202**

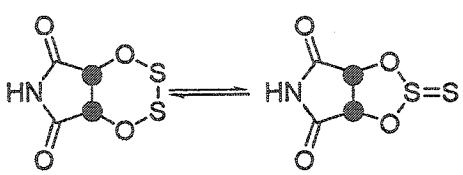

203 **204**

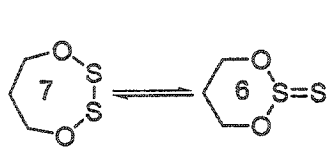

205 **206**

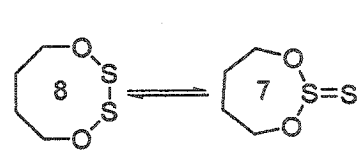

207 **208**

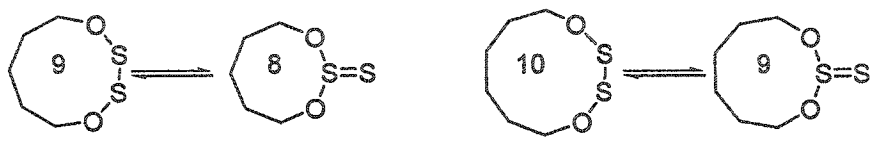

209 210 211 212

We first needed to determine which method and basis set were sufficient to accurately model the energies of these systems. Though we had previously shown that B3LYP/6-31G* was a poor predictor of the geometries of a more simple model alkoxy disulfide in MeOSSOMe **6** and simple model thionosulfites **5a** and **5d**, energies derived from the predicted geometries for **6** nevertheless were deemed accurate, assuming that the basis set contained more than one d-type polarization functions (*cf.* Chapter **3**). A basis set survey of the energies of **185** and **186** using the B3LYP method is shown in Table **63**.

Using either double ζ split or triple ζ split basis sets, the calculations predict that thionosulfite **186** is the preferred isomer by *ca.* 3.5 kcal/mol, assuming that a minimum of 2 d-type polarization functions are incorporated into the basis set. The use of smaller basis sets results in nearly isoenergetic isomers which is neither consistent with the results obtained using larger basis sets nor with the available experimental evidence (*vide infra*). This is perhaps not too surprising given that the inclusion of polarization functions was deemed necessary in order to accurately reproduce the energy difference in the S_2F_2 **75** system.[17] Miaskiewicz and Steudel[18] however were able to correctly show at the MP2/6-311G**//HF/6-31G** + ZPVE that HOSSOH **95a** was more stable than HOS(S)OH **95c** by 3.35 kcal/mol. Though the identity of the more stable isomer is correct (in **95a**), the choice of a small basis set results in a magnitude that should be questioned. The addition of the extra Gaussian primitive further stabilizes **186** by *ca.* 0.8

kcal/mol (*cf.* ΔΔE, Table **63**), though this was not universally observed to be the case. The existence of such a large energy difference between the two isomers would seem to indicate that **186** would be the sole observable isomer (>99.99:1).

Interestingly, Jursic[19] determined that of all the DFT methods tested, SVWN/6-311++G(3df)//SVWN/6-311++G(3df) proved to be most accurate in predicting both the magnitude and identity of the most stable isomeric form for the S_2F_2 **75** system (experimentally[20] determined to be 2.7 kcal/mol in favour of $F_2S{=}S$ **75b**); B3LYP, even using large basis sets, could not reproduce the experiment. Using extended polarized basis sets and conventional correlated *ab initio* theory, Bickelhaupt and co-workers[17] could not unequivocally determine that **75b** was the most stable though their results indicated that the $\Delta E_{75a/75b}$ was miniscule; QCISD(T)/6-31G(df)//MP2/6-31G* most accurately reproduced experiment in their computational survey. It would seem that the choice of basis sets size and computational method is important in obtaining accurately predictive and consistent results for our related systems.

Table 63. Comparison of the relative ground state energies of **185** and **186** with different basis sets

B3LYP/[a]	Energy of **185**[b]	Energy of **186**[b]	ΔE(185-186)[c,d]	B3LYP/[a]	Energy of **185**[b]	Energy of **186**[b]	ΔE(185-186)[c,d]	ΔΔE[c,e]
6-31G*	-1025.37587	-1025.37750	1.0	6-311G*	-1025.48243	-1025.48280	0.2	-0.8
6-31+G*	-1025.39029	-1025.39027	0.0	6-311+G*	-1025.49412	-1025.49293	-0.7	-0.7
6-31++G*	-1025.39043	-1025.39045	0.0	6-311++G*	-1025.49442	-1025.49315	-0.8	-0.8
6-31G(2d)	-1025.39123	-1025.39741	3.9	6-311G(2d)	-1025.50576	-1025.51116	3.4	-0.5
6-31+G(2d)	-1025.40645	-1025.41028	2.4	6-311+G(2d)	-1025.51574	-1025.51894	2.0	-0.4
6-31G(df)	-1025.39144	-1025.39472	2.1	-	-	-	-	-
6-31G(2df)	-1025.41019	-1025.41610	3.7	6-311G(2df)	-1025.52284	-1025.52986	4.4	0.7
6-31+G(2df)	-1025.42472	-1025.42935	2.9	6-311+G(2df)	-1025.53338	-1025.53823	3.0	0.1
6-31G(3d)	-1025.41123	-1025.41636	3.2	6-311G(3d)	-1025.51699	-1025.52326	3.9	0.7
6-31+G(3d)	-1025.42092	-1025.42618	3.3	6-311+G(3d)	-1025.52371	-1025.52859	3.1	-0.2
6-31G(3df)	-1025.42735	-1025.43322	3.7	6-311G(3df)	-1025.53268	-1025.54028	4.8	1.1
6-31+G(3df)	-1025.43569	-1025.44190	3.9	6-311+G(3df)	-1025.53928	-1025.54517	3.7	-0.2
6-31G(3d2f)	-1025.42885	-1025.43479	3.7	6-311G(3d2f)	-1025.53461	-1025.54211	4.7	1.0

a) All single point energies based on B3LYP/6-31G* optimized geometries. b) In Hartrees. c) In kcal/mol. d) A negative value denotes that **185** is the preferred isomer. e) Energy Difference between triple ζ split and double ζ split basis sets.

In Chapter 3 we demonstrated that molecular mechanics geometries could accurately predict experimental structures of both alkoxy disulfides and thionosulfites. We thus also calculated the energies of **185** and **186** based on their MM3* optimized geometries. The results are shown in Table **64.**

Table **64.** Ground state energies of **185** and **186** at different basis sets using B3LYP, MP2 and MP3 methods based on MM3* optimized geometries

//MM3*	Energy of **185**[a]	Energy of **186**[a]	ΔE(**185-186**)[b,c]
B3LYP/6-31G*	-1025.36518	-1025.37151	4.0
B3LYP/6-31G(2d)	-1025.38263	-1025.39259	6.3
B3LYP/6-31G(df)	-1025.38225	-1025.39030	5.1
B3LYP/6-31G(2df)	-1025.40309	-1025.41366	6.6
B3LYP/6-31G(df)	-1025.38225	-1025.39030	5.1
B3LYP/6-31G(3d)	-1025.40363	-1025.41260	5.6
B3LYP/6-31G(3df)	-1025.42146	-1025.43135	6.2
B3LYP/6-31G(3d2f)	-1025.42325	-1025.43303	6.1
MP2/6-311G*	-1023.72865	-1023.73457	3.7
MP2/6-311G(2d)	-1023.83176	-1023.84749	9.9
MP2/6-311G(df)	-1023.89289	-1023.89508	1.4
MP2/6-311G(2df)	-1023.97337	-1023.99051	10.8
MP2/6-311G(3d)	-1023.86209	-1023.87779	9.9
MP2/6-311G(3df)	-1024.00125	-1024.01859	10.9
MP2/6-311G(3d2f)	-1024.02336	-1024.04093	11.0
MP3/6-311G*	-1023.75512	-1023.75433	-0.5
MP3/6-311G(2d)	-1023.85451	-1023.86344	5.6
MP3/6-311G(df)	1023.92153	1023.92369	-1.4
MP3/6-311G(3d)	-1023.88493	-1023.89375	5.5
MP3/6-311G(2df)	-1024.00460	-1024.01475	6.4

a) In Hartrees. b) In kcal/mol. c) A negative value denotes that **185** is the preferred isomer.

Provided with a more accurate MM3*-optimized geometry, B3LYP at all basis sets now predicts that **186** is the more stable isomer. MP2 energies generally mirror this result with the notable exception of the 6-311G(df) basis set. It is not clear why the use of this basis set provides a divergent result. MP3 energies however do not seem to

converge so uniformly. It would seem that when using this method, at least 2 d-type polarization functions must be used in order to obtain results comparable with the other computational methods in Tables **63** and **64**.

With an understanding of the minimum basis sets required to obtain reasonable energies, we then proceeded to model **185-204**. We derived single point energies using both the B3LYP/6-31G(2d) and MP2/6-311G(2df) basis sets, basis sets which we had previously shown (Chapter **3** and Chapter **6**) to be effective in accurately calculating energies of these systems. These results are summarized in Table **65**.

Table **65**. B3LYP/6-31G(2d)//MM3* and MP2/6-311G(2df)/B3LYP/6-31G* single point energies of **185-204**

	E(185)[a]	E(186)[a]	ΔE(185-186)[d]	E(195)[a]	E(196)[a]	ΔE(195-196)[d]
B3LYP/6-31G(2d)[b]	-1025.38263	-1025.39260	6.3	-1142.11479	-1142.12997	9.5
MP2/6-311G(2df)[c]	-1023.97818	-1023.99004	7.4	-1140.42264	-1140.43962	10.7
	E(187)[a]	E(188)[a]	ΔE(187-188)[d]	E(197)[a]	E(198)[a]	ΔE(197-198)[d]
B3LYP/6-31G(2d)[b]	-1178.97808	-1178.98928	7.0	-1142.11721	-1142.10873	-5.3
MP2/6-311G(2df)[c]	-1177.22484	-1177.23995	9.5	-1140.42345	-1140.41862	-3.0
	E(189)[a]	E(190)[a]	ΔE(189-190)[d]	E(199)[a]	E(200)[a]	ΔE(199-200)[d]
B3LYP/6-31G(2d)[b]	-1024.14807	-1024.15293	3.1	-1181.43771	-1181.45092	8.3
MP2/6-311G(2df)[c]	-1022.77551	-1022.78476	5.8	-1179.64927	-1179.65218	1.8
	E(191)[a]	E(192)[a]	ΔE(191-192)[d]	E(201)[a]	E(202)[a]	ΔE(201-202)[d]
B3LYP/6-31G(2d)[b]	-	-	-	-1181.43122	-1181.44786	10.4
MP2/6-311G(2df)[c]	-1061.95995	-1061.97816	11.4	-1179.63098	-1179.64927	11.5
	E(193)[a]	E(194)[a]	ΔE(193-194)[d]	E(203)[a]	E(204)[a]	ΔE(203-204)[d]
B3LYP/6-31G(2d)[b]	-1102.76411	-1102.77341	5.8	-1268.10170	-1268.11623	9.1
MP2/6-311G(2df)[c]	-1101.18645	-1101.19944	8.2	-1266.33226	-1266.35041	11.4

a) In Hartrees. b) Based on MM3* optimized geometries. c) Based on B3LYP/6-31G* optimized geometries. d) In kcal/mol.

Given the known existence of **5g** and **5i** at the time of these calculations, it seemed that the inclusion of sterically demanding substituents has little effect on the relative energies of thionosulfites *vis a vis* their isomeric alkoxy disulfides. As stated earlier, we chose model compounds with substitution patterns that were designed to flatten the O-C-C-O torsional angle. Except for the relative energies of **197** and **198**, the overwhelming conclusion is that the thionosulfite isomer is preferred in each case. In fact, the ΔE's are generally such that we would expect to observe only the thionosulfite isomer. So it would seem that the introduction of substituents designed to flatten the compounds has little effect in altering the relative ground state stabilities between the two isomeric forms. We believe that the reversal in expected isomeric stability for **197** and **198** results from the fact that 5,5-fused bicycles prefer to be *cis*-fused and that the overwhelming steric strain imparted in the *trans*-fused bicycle in **197** destabilizes to such an extent that 5,6-fused bicycle **198** would become the more favoured isomer. Similarly, at the MP2/6-311G(2df) level the *cis*-fused 5,6-bicycle **200** is destabilized relative to the *cis*-fused 6,6-bicycle **199** though not to such an extent where it is no longer the most stable isomer. In general, the lack of stability in 6-membered alkoxy disulfides is most likely due to the increased strain afforded by a reduced τ(O-S-S-O) from its ideal *ca.* 90°.

We next looked at model compounds **185-186** and **205-212**. It was necessary to determine the lowest energy conformation for each compound. Whereas **185-204** possess little conformational flexibility due to their small ring size, this is not the case for **205-212**. We thus performed 3000-iteration Monte-Carlo simulations based on MM3* optimized input structures for each compound in this series. All conformations within a 3

kcal/mol window were then submitted for single point energy analysis at the B3LYP/6-31G(2d) level of theory. Frequently, the lowest energy conformation obtained by the Monte-Carlo simulation did not translate into the lowest energy conformation by *ab initio* methods though the ΔE between the two methods was no greater than 1.5 kcal/mol. The results relating the relative energy difference between isomeric forms as a function of core ring-size are graphically summarized in Figure 32.

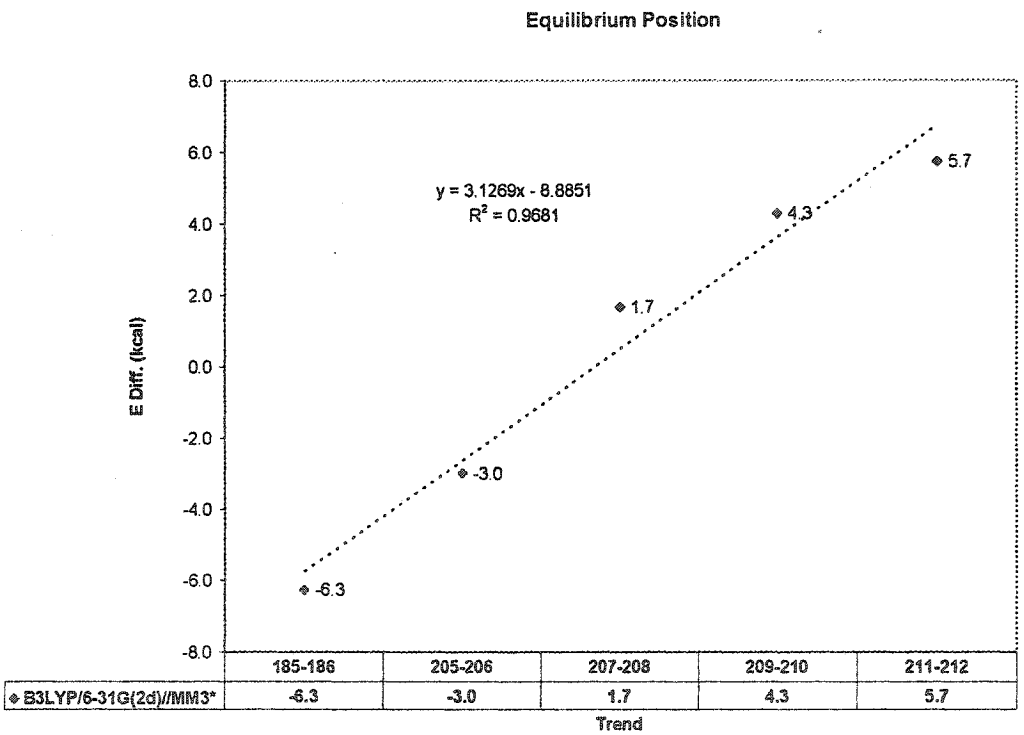

Figure 32. Ring-size trend in ΔE of **185-186, 205-212**. A positive value indicates that the alkoxy disulfide isomer is the more stable.

As is graphically evident, modifying the ring size influences the relative ground state stabilities between form 1 and form 2. There is a monotonically increasing relationship

which seems to be linear based on ring size; small ringed compounds are predicted to be thionosulfites whereas large ringed and acyclic compounds (the latter being considered an infinitely large ring) are predicted to adopt the alkoxy disulfide form. The trend would seem to indicate that the cross-over point in isomeric stability occurs with the 7-membered thionosulfite **207** and 8-membered alkoxy disulfide **208** system. It would not be unreasonable to predict that analogues of **205/206** might also exist as a mixture at RT.

Table 66. Boltzmann population analysis of the **207/208** system at 298 K.

		B3LYP/6-31G(2d)//MM3*	$\Delta E^{a,b}$	Weight	Pop (%)^{c,d}	$\Delta E^{a,e}$	Total Pop (%)^{c,f}	Weighted Total Pop (%)^{c,f}
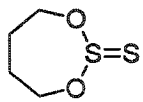	**208a**	-1104.01920	0.4	2	22.9	2.1	2.2	4.4
	208b	-1104.01982	0.0	2	44.9	1.7	4.3	8.6
	208c	-1104.01943	0.2	2	32.1	1.9	3	6.0
								19.0
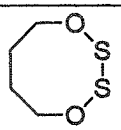	**207a**	-1104.02248	0.0	1	92.8	0.0	75.1	75.1
	207b	-1104.01982	1.7	1	5.3	1.7	4.3	4.3
	207c	-1104.01822	2.7	2	1	2.7	0.8	1.6
								81.1

a) In kcal/mol. b) Relative energy difference to the MM3* lowest energy conformer. c) Boltzmann population distribution. d) Population distribution per isomer. e) Relative energy difference to **207a**. f) Combined population distribution.

A closer analysis of this data point reveals that **207** and **208** should co-exist in an 81:19 ratio at RT (Table 66). It remained to be seen whether the results summarized in Figure 32, though compellingly simple, actually mirror and/or predict experimental findings. The experimental data is summarized in Chapter **6.3.2**.

6.3.2 Experimental Data

In Chapter 2, we saw that coupling of 1,2-diols with a sulfur transfer reagents such as **15a** or **15b** formed exclusively 5-membered thionosulfites **5a-5l**. In Chapter 4, a series of acyclic alkoxy disulfides were synthesized. Here too, only one isomeric form of ROSSOR 1 was ever isolated; the identity of the isomer was confirmed by DNMR studies as well as inferred given the resolution of the crystal structures of three representative alkoxy disulfides (**6**, **49** and **50**).

Given the potential to isolate both isomers in a 7/8-ring system such as **207** and **208**, we decided to use 1,2-benzenedimethanol **170** as our starting diol in order to ascertain whether this analogous system would afford the predicted two isomer products. We hypothesized that the extra degree of unsaturation would have a minimal impact on the relative ground state energies of this system given that in the analogous 5/6-ring systems **185-188** there was no effect in altering the isomer preference and but a small effect in energies at the B3LYP/6-31G(2d) level. In Chapter 5, we were able to synthesize and isolate both the 7-membered thionosulfite **172** as well as the 8-membered ring alkoxy disulfide **171**. Moreover under all the experimental conditions used, **171** was found to be the major product formed (58% NMR yield under the same thermodynamically controlled reaction conditions – Chapter 5.2, Table 58); thionosulfite **172** could only be isolated in maximum of 22 % yield.

Besides the heavily studied system in Chapter 5, we were also interested in synthesizing other ring-sized alkoxy disulfides (and/or their thionosulfite isomers). We next turned our attention to the S_2Cl_2 coupling of 2,2'-biphenyldimethanol **213**.

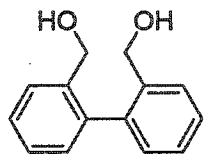

213

Reaction conditions were similar to those used in the synthesis of acyclic alkoxy disulfides (Chapter 4). The crude solution yielded a complex mixture of products where, upon chromatographic isolation, alkoxy disulfide **214** was isolated in 25% yield as a clear oil which subsequently solidified in the freezer.

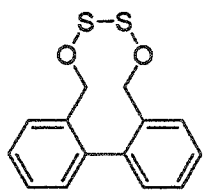

214

Interestingly, this compound possesses two chiral axes: (1) the OS-SO functionality; (2) the C_{sp2}-C_{sp2} bond of the biphenyl moiety. Potentially this implies that **214** could exist in diastereomeric conformations, which may themselves be isolable. Diagnostic of this claim is the ^{1}H NMR of **214** (Figure **33**). From the inset, it is possible to observe two ABq systems in a *ca.* 5:2 ratio, ostensibly related to two distinct conformations. The ^{13}C NMR ratio of the benzyl carbon signals corroborates this analysis as well.

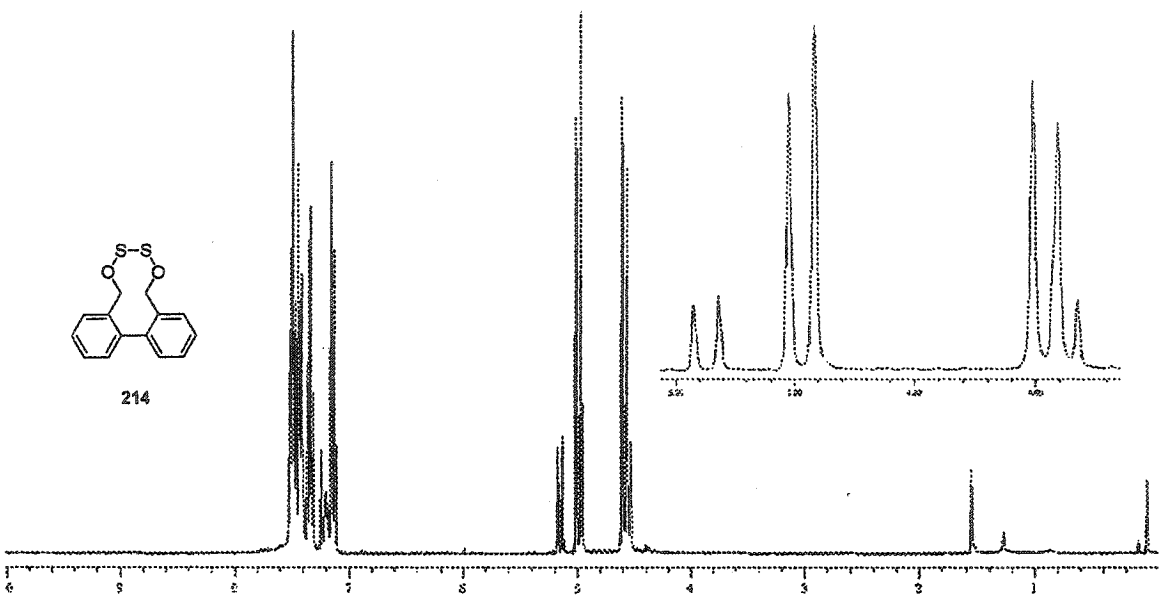

Figure 33. The ^{1}H NMR (300 MHz) of **214**. The inset displays an expansion of the benzyl proton region.

6.3.3 How Do The Calculations Relate To The Experimental Results?

A generous qualitative reading of the combined set of experimental data on alkoxy disulfide systems (Summarized in Chapter **6.3.2**) implies that the relative ground state energies of thionosulfites **2** and alkoxy disulfides **1** are influenced by a relief of ring strain (Figure **32**). Moreover, the relative experimental yields of **171** and **172** under thermodynamic control are similar to those predicted by the Boltzmann population analysis (Table **66**). This suggests that the predicted energies accurately reflect the physical system. As **171** slowly isomerizes to **172** at *ca.* 0 °C but unidirectionally (Chapter **5** – the isomerization was also observed at elevated temperatures with concomitant decomposition of **171**) implies that the relative energy difference between

171 and 172 is mirrored in the relative energy difference of their respective transition states. A corollary to this supposition implies that the transition states are themselves late, with minimal bond reorganization in the formation of the products. Though the calculations presented do not specifically address a mechanism of isomerization between 171 and 172, and more generally 1 and 2, it may be inferred that the barrier to isomerization is significant given that the ground state energy calculations mirror the experimental isolated yields and the observed isomerization is exceedingly slow.

6.4 Synthetic Experimental Section

6.4.1 Synthesis of 10-membered ring alkoxy disulfide, 214:

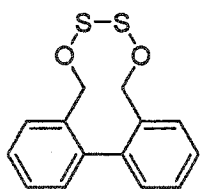

A solution of 2,2'-biphenyldimethanol **213** (214 mg, 1 mmol, 1 equiv) and NEt_3 (280 μL, 2 mmol, 2 equiv) in 10 mL of CH_2Cl_2 was allowed to stir under nitrogen at 0 °C. A solution of S_2Cl_2 (80 μL, 1.0 mmol, 1 equiv) in 10 mL of CH_2Cl_2 was added dropwise over *ca.* 10 min. The reaction mixture was allowed to stir for a further 5.5 h. The reaction mixture was quenched with 15 mL of H_2O. The organic phase was washed 3x 33 mL of H_2O. The organic phase was dried over $MgSO_4$. This mixture was vacuum filtered and the solvent was removed first under reduced pressure and then *in vacuo*. The crude mixture was flash chromatographed[21] in 10% CH_2Cl_2/hexanes as the eluant to

afford a fruity-smelling clear oil which solidified in the freezer. *Rf* (10% CH_2Cl_2/hexanes) 0.09. Yield: 25 %. ^1H NMR δ 7.51-7.40 (m, 5H), 7.36-7.31 (m, 2H), 7.21-7.12 (m, 2H), 5.15 (d, 0.4H, J = 12.30 Hz), 4.99 (d, 2H, J = 12.60 Hz), 4.59 (d, 2H, J = 12.60 Hz), 4.55 (d, 0.4H, J = 12.30 Hz); ^{13}C NMR δ 70.4, 76.5, 127.6, 127.8, 128.2, 128.9, 129.4, 129.6, 129.8, 131.4, 134.7, 135.8, 139.4, 140.7; 5:1 of two diastereomers as detected by ^{13}C NMR, ^1H NMR. MS (EI) *m/z* 276 ($M^{+\bullet}$), 228 ($M^{+\bullet}$ – SO) 196 ($M^{+\bullet}$ – S_2O); 179 ($M^{+\bullet}$ –S_2O_2H), 165 ($M^{+\bullet}$ – $S_2O_2CH_3$); HRMS. Calcd for $C_8H_8S_2O_2$: 276.0279. Found: 276.027(1).

6.5 References

(1) Frisch, M. J.; Trucks, G. W.; Sclegel, H. B.; Gill, P. M. W.; Johnson, B. G.; Robb, M. A.; Cheeseman, J. R.; Keith, T.; Petersson, G. A.; Montgomery, J. A.; Raghavachari, K.; Al-Laham, M. A.; Zakrzewski, V. G.; Ortiz, J. V.; Foresman, J. B.; Cioslowski, J.; Stefanov, B. B.; Nanayakkara, A.; Challacombe, M.; Peng, C. Y.; Ayala, P. Y.; Chen, W.; Wong, M. W.; Andres, J. L.; Replogle, E. S.; Gomperts, R.; Martin, R. L.; Fox, D. J.; Binkley, J. S.; Defrees, D. J.; Baker, J.; Stewart, J. P.; Head-Gordon, M.; Gonzalez, C.; Pople, J. A. *Gaussian 94*; Gaussian Inc.: Pittsburgh, PA, **1995**; Vol. revision D.4.

(2) Becke, A. D. *Int. J. Quantum Chem.* **1994**, *S28*, 625.

(3) Becke, A. D. *J. Chem. Phys.* **1993**, *98*, 5648.

(4) Lee, C.; Yang, W.; Parr, R. G. *Phys. Rev. B* **1988**, *37*, 785.

(5) Miehlich, B.; Savin, A.; Stoll, H.; Preuss, H. *Chem. Phys. Lett.* **1989**, *157*, 200.

(6) Ditchfield, R.; Hehre , W. J.; Pople, J. A. *J. Chem. Phys.* **1971**, *54*, 724.

(7) Hehre, W. J.; Ditchfield, R.; Pople, J. A. *J. Chem. Phys.* **1972**, *56*, 2257.

(8) Hariharan, P. C.; Pople, J. A. *Mol. Phys.* **1974**, *27*, 209.

(9) Gordon, M. S. *Chem. Phys. Lett.* **1980**, *76*, 163.

(10) Hariharan, P. C.; Pople, J. A. *Theo. Chim. Acta.* **1973**, *28*, 213.

(11) Mohamadi, F.; Richards, N. G. J.; Guida, W. C.; Liskamp, R.; Lipton, M.; Caufield, C.; Chang, G.; Hendrickson, T.; Still, W. C. *J. Comput. Chem.* **1990**, *4*, 440.

We have modified the MM3* force field to include new atom types and parameters to better handle the OSSO and OS(S)O functionalities.

(12) Møller, C.; Plesset, M. S. *Phys. Rev.* **1934**, *46*, 618.

(13) Head-Gordon, M.; Pople, J. A.; Frisch, M. J. *Chem. Phys. Lett.* **1988**, *153*, 503.

(14) Krishnan, R.; Binkley, J. S.; Seeger, R.; Pople, J. A. *J. Chem. Phys.* **1980**, *72*, 650.

(15) McLean, A. D.; Chandler, G. S. *J. Chem. Phys.* **1980**, *72*, 5639.

(16) An initial theoretical survey of the relative ground state energies of MeOSSOMe **6** and its constitutional isomer MeOS(S)OMe **6b** is available. See: Snyder, J. P.; Nevins, N.; Tardif, S. L.; Harpp, D. N. *J. Am. Chem. Soc.* **1997**, *119*, 12685. Though there is no experimental evidence to suggest the existence of branched isomer **6b**, it was nevertheless found to be 1.9 kcal/mol more stable than unbranched **6** at B3LYP/6-311G* + ZPVE with an MP2/6-311G(3d) unimolecular interconversion barrier between **6** and **6b** of 37.5 and from **6b** to **6** of 32.3 kcal/mol .

(17) Bickelhaupt, F. M.; Solà, M.; Schleyer, P. v. R. *J. Comput. Chem.* **1995**, *16*, 465.

(18) Steudel, R.; Miaskiewicz, K. *J. Chem. Soc. Dalton Trans.* **1991**, 2395.

(19) Jursic, B. S. *J. Comput. Chem.* **1996**, *17*, 835.

(20) Lösking, O.; Willner, H.; Baumgärtel, H.; Jochims, H. W.; Rühl, E. *Z. Anorg. Allg. Chem.* **1985**, *530*, 169.

(21) Still, W. C.; Kahn, M.; Mitra, A. *J. Org. Chem.* **1978**, *43*, 2923.

Chapter 7

Introduction: Polysulfides

7.1 Purpose for the Development of an Efficient Synthesis for Tri- and Tetrasulfides

One of the most heavily investigated and promising new modulators of gene expression is the phosphorothioate class of oligodeoxyribonucleotides.[1,2] These nuclease-resistant[3] antisense analogs are effective in inhibiting gene expression; the inhibitory mechanism is presumed to occur *via* the formation of a mRNA-antisense DNA duplex, which either impairs ribosomes from reading mRNA (inhibiting translation),[4] or promotes RNase H-mediated RNA cleavage of the bound mRNA strand.

Theoretically, any disease with a genetic cause could be targeted by the appropriate antisense analog.[5] Structurally, the phosphorothioates differ from natural DNA by the replacement of oxygen for sulfur at one of the two non-bridging positions at each interlinking phosphate group of the DNA backbone.

Antisense drugs have already been approved such as in formivirsen[6] (Vitravene), or in clinical trials in both Europe and the United States for the treatment of CMV retinitis in AIDS patients.[7] The development of economical and safe methods for the synthesis of these analogues has become a major focus of research; it is crucial that the sulfurization step be highly efficient for maximum nuclease-resistance.

There are two approaches for the synthesis of phosphorothioate oligonucleotides: the *H*-phosphonate approach or the phosphoramidite method. While the *H*-phosphonate method relies on a single post-chain assembly sulfurization step of all internucleotide

phosphate linkages (using S_8 dissolved in CS_2/pyridine), the phosphoramidite approach requires stepwise sulfurization after each coupling reaction. More efficient sulfurization occurs in the latter method and thus this is the preferred approach amongst researchers.

During the past few years, a variety of sulfurizing reagents have been investigated.[5,8-22] Of these, 3H-1,2-benzodithiol-3-one 1,1-dioxide (Beaucage reagent) **215** has been used frequently in large scale (>150 mmol) synthesis of phosphorothioate drugs. Apart from its high cost (>$100/g), and non-optimal solubility properties, this reagent suffers from inconsistent sulfurization efficiency due to the formation of a cyclic by-product **216** (3*H*-2,1-benzoxathiolan-3-one-1-oxide), that acts as a potent oxidizing reagent leading to the formation of undesirable phosphodiester linkages.

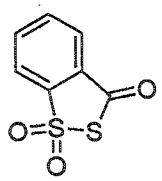

215

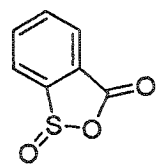

216

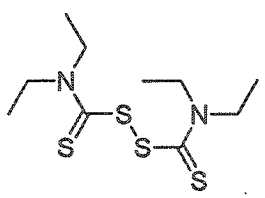

217

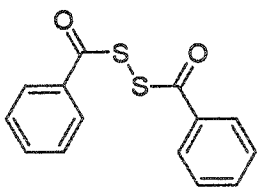

218

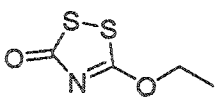

219

Phosphodiester formation is also possible *via* the presence of a contaminant in the peracid of the precursor to Beaucage reagent. Other sulfurizing reagents, such as tetraethylthiuram disulfide (TETD) **217**, phenylacyl disulfide (PADS) **218** and 3-ethoxy-

1,2,4-dithiazoline-5-one (EDITH) **219** suffer either from inefficient sulfurization rates or are expensive.

To facilitate the development of this research, there is a need for an inexpensive and efficient sulfurizing reagent that does not possess oxidative properties and is easy and economical to prepare. We seek to develop a general method for the synthesis of aromatic polysulfides as we believe that such structurally simple molecules might serve as potent sulfur-transfer reagents in the formation of phosphorothioates. In order to test our hypothesis, we have investigated the room temperature reactions of these polysulfides with a model phosphine to demonstrate their efficacy prior to use on oligonucleotides.

This chapter aims to provide a context for the reader of the general importance[23,24] of higher order polysulfides (RS_nR; $n > 2$) in important natural products, the current synthetic methods for their formation and some bonding and stereochemical features. The following two chapters chronicle our synthetic methodology and our resulting kinetics studies concerning the desulfurization of polysulfides by phosphines.

7.2 Survey of Some Interesting Natural Polysulfides

7.2.1 Acyclic Polysulfides

Many symmetric as well as asymmetric acyclic oligosulfides (RS_nR, $n = 3, 4$) occur naturally (Table **67**). They are prevalent in foods such as onions[25] and garlic,[26-30]

mushrooms,[31,32] aged beers,[33] and the unpleasant smelling durian fruit (bread fruit) that is found in Indochina.[34] It has recently been shown[35] that the polysulfides reported in earlier studies of garlic oil were formed as a result of the heating during the steam distillation process of naturally occurring allicin and diallyldisulfide; the concentration of these polysulfides decreases as the number of sulfur atoms increases.[36] These diallylpolysulfides most probably originated from thermally induced S-S and C-S homolytic bond cleavage and subsequent radical recombination.[37-39] Garlic research has been extensive given that diallyl polysulfides have been shown to demonstrate antimicrobial activity; allylmethyltrisulfide can also be detected during a methanol extraction. In the specific cases of *Heliobacter pylori*,[40] *Staphyolococcus aureus*, methicillin-resistant *S. aureus*, three *Candida* spp. and three *Aspergillus* spp.,[41] the bactereostatic properties increases with the number of sulfur atoms in the chain. In addition, unsaturated polysulfides inhibit the growth of certain tumours.[26,42]

Table 67. Some naturally occurring acyclic polysulfides (R_1-S_n-R_2)

R_1	R_2	*n*	source	ref
Me	Me	3, 4	shiitake mushroom	32
Me	Me	3	oil made from *Ferula asafoetide*	43
Me	Me	3	geotrichum candidum	44
Me	2-Bu	3	oil made from *Ferula asafoetide*	43
Me, Et, Pr	Me, Et, Pr	3	durian fruit	34
HOC_2H_4	HOC_2H_4	3	bacillus stearotheromophilus 222	45,46
Pr	Pr	3, 4	azadirachta indica	34
2-Bu	2-Bu	3, 4	oil made from *Ferula asafetida* (Afghanistan)	43
Bn	C_2H_4-OH	3	roots of *Petiveria alliaceae*	47
Allyl	Allyl	3-6	garlic oil	26,36,42
Allyl	Allyl	2-4	adenocalymma alliacaea	48,49
Alanyl	Alanyl	3, 4	wool hydrolysate 225a, 225b	50
3-Oxoundecyl	3-Oxoundecyl	3, 4	*Dictyopteris plagiogramma* (Hawaiian alga)	51
Me	Complex structure	3	*Micromonospora echinospora* (calicheamicin) 227	52
Me	Complex structure	3, 4	*Actrinomadura verrucosospora* (esperamicins)	53-55

Dimethyl trisulfide has been detected in disrupted cabbage tissue and its formation has been attributed to the reaction of H_2S with methyl methanethiosulfinate **220** and/or methyl methanethiosulfonate **221**, Scheme **52**.[56] The origin of compounds **220** and **221** is attributed to the cleavage of *S*-methyl-L-cysteine sulfoxide by C-S lyase (which first forms the sulfenic acid, which then couples to itself to form **220** with loss of H_2O; **221** forms during a second oxidative reaction).[56] Heating of *S*-propyl-L-cysteine and its sulfoxide in the presence of water participate in the formation of important volatile trisulfides in *Allium* vegetables.[57] Dimethyl trisulfide has also been detected as a minor flavouring component in most varieties of baked potato (Golden Wonder being the exception).[58] General reviews on polysulfide compounds in food are available.[59]

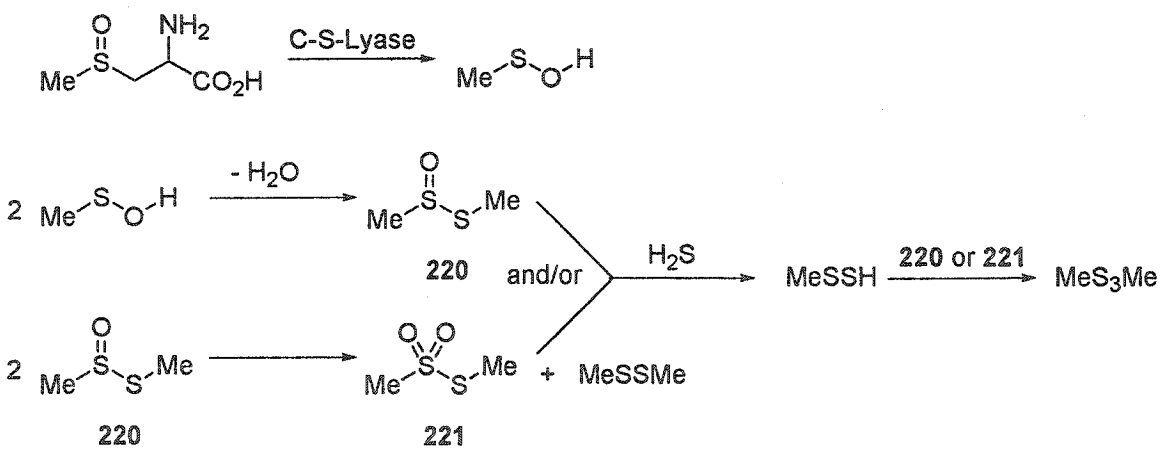

Scheme 52. Formation of MeS_3Me from damaged cabbage cell tissue.

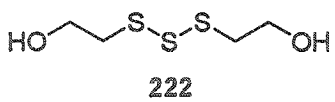

222

Acyclic polysulfides can be found in many organisms such as brown algae[60] as well as other organisms.[61] For instance, dimethyl trisulfide (MeSSSMe) has been isolated from the mandibular (defense) glands of the ponerine ant, *Paltothyreus tarsatus*[62] whereas

dimethyl tetrasulfide (MeSSSSMe) has been detected in the volatiles of swine manure.[61] Long-chain polsulfides have been isolated from a Hawaiian alga (Table 67).[51] Many polysulfides such as relatively unfunctionalized bis(2-hydroxyethyl) trisulfide **222**,[45,46] isolated from *Bacillus stearothermophilus* UK563, have cytotoxic effects: cytotoxicity against P815 mastocytoma cells, promoted increased NO formation, TNF and IL-1 production, and PGE_2 release in the peritoneal macrophages. In addition, the decomposition of Leinamycin **223** produces acyclic aliphatic polysulfides, which have been shown to induce DNA damage.[63]

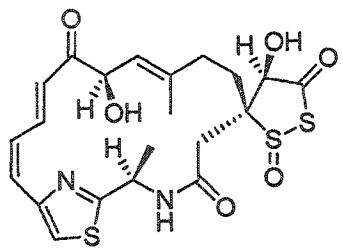

Leinamycin

223

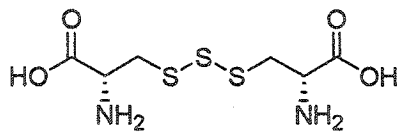

224

Trisulfides can also be generated *in vivo*; cystine, when heated in an acidic medium, converts to its trisulfide analog (Bactin or thiocystine), **224**, which has bacteriostatic action on Lactobacillus plantarum.[64,65] Thiocystine (cystine trisulfide) linkages are found in a derivative of the human growth hormone in which as much as 10% of the recombinant hormone produced in *Escherichia coli* exists as the trisulfide linkage (between Cys^{182} and Cys^{189} in this 191 protein).[66,67] Thiocystine has also been isolated from genetically engineered *Escherichia coli* bacteria[68] and has been observed in

recombinant DNA-derived methionyl human growth hormone as the bridge between residues 53 and 165.[69] Much research has also been done on analogs of the hormone oxytocin.[70] The mixed trisulfide between cysteine and glutathione has also been detected.[71]

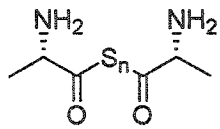

n = 3 **225a**
n = 4 **225b**

Although dialanyl polysulfides (**225a**, **225b**) have been detected in acidic wool hydrolysates, it is unclear whether related thiocystine is also part of the intrinsic wool structure or is itself derived from cystine during hydrolysis.[50,72] In general, thiocystine and other highly sulfurated compounds are formed in the anaerobic cysteine sulfur metabolism with the notable participation of enzymes such as cystathionase and rhodanese (thiosulfate: cyanide sulfurtransferase).[73] These compounds participate in cell regulation processes and contain antioxidant properties and themselves act as *in situ* sulfurizing agents for tRNA. They have also been shown to influence carcinogenesis and imunosuppression. A general review of the formation, regulation and activity of highly sulfurated compounds in the body is available.[74]

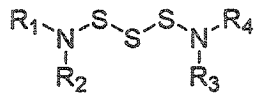

226

Diamino trisulfides **226** are used as pesticides as well as accelerators and crosslinking agents in rubber polymerization.[75] Many of these compounds have significant biological properties[76] and reviews of their presence and structure in marine organisms[77,78] have been published.

Of particular note are the Esperamicins[53-55] and Calicheamicin γ_1^I, **227**,[52,79] potent antineoplastic antibiotics[80] with modest selectivity for cancer cells.[81] The trisulfide linkage in these natural products, upon activation *via* nucleophilic attack (from a cellular thiol such as glutathione), acts as a trigger for a Bergman[82] cyclization (Scheme **53**) of an ene-diyne unit to ultimately give a 1,4-diyl intermediate. The resulting rehybridization of the bridgehead carbon (from sp^2 to sp^3), after the Michael addition by the now liberated thiolate, induces a conformational change that results in a decrease in the interatomic distance between the two termini of the ene-diyne subunit (from 3.35 Å to 3.16 Å). The energetically favourable Bergman cyclization then readily proceeds to afford the 1,4-diyl which can ultimately induce single strand cleavage and interstrand alkylation *via* the abstraction of two hydrogens from DNA.[79] The total synthesis of **227** has also been published.[76,83,84]

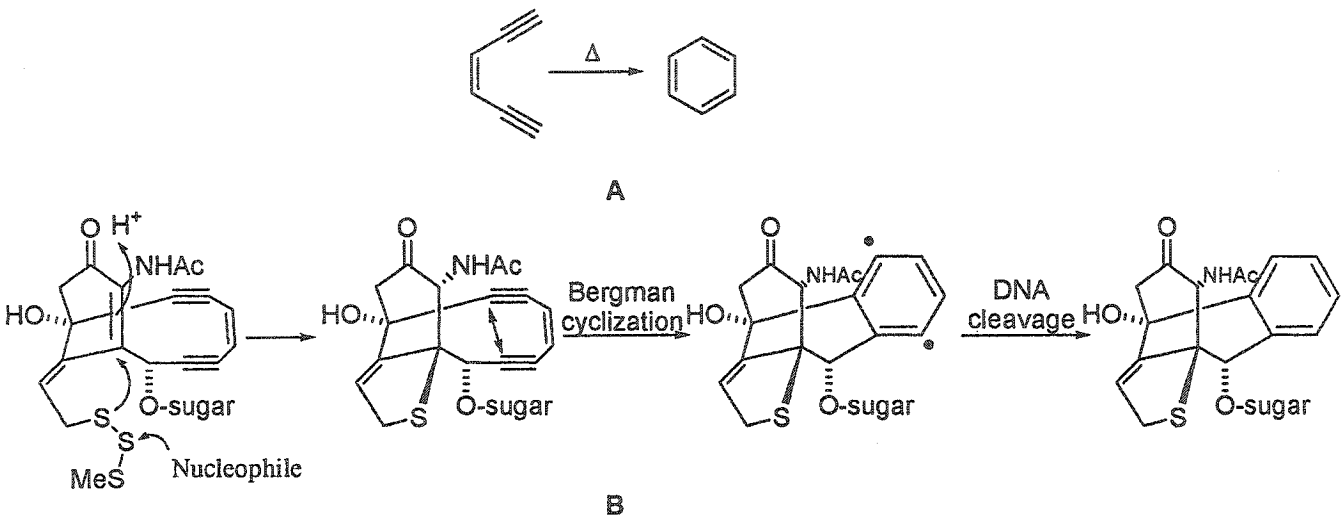

Scheme 53. A) Bergman cyclization. B) Bergman Cyclization in Calicheamicin γ_1^I **227**.

Adapted from Ref [79].

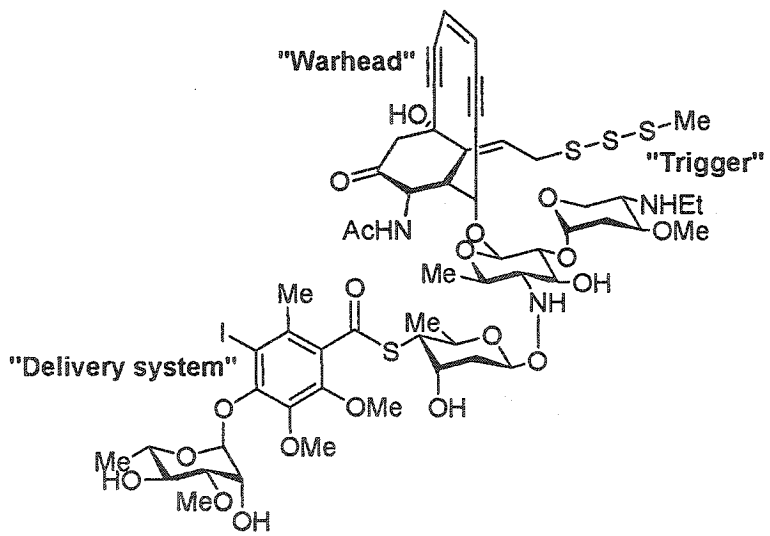

Calicheamicin γ_1^I

227

7.2.2 Cyclic Polysulfides

Cyclic polysulfides are also important compounds in foods. Lenthionine **228** is one of the major flavouring components isolated from the shiitake mushroom, *Lentinus edodes*

and was the first cyclic polysulfide isolated from an organism. Hydration of dried shiitake mushrooms followed by pentane extraction and subsequent analysis afforded mainly MeS_3Me, however when the hydration was carried out under basic conditions (pH 9) several cyclic polysulfides were indentified (**229** and **230**)[85,86] as important constituents Scheme **54**; acyclic polysulfides (Table **67**) were also detected.[31,32] It is widely accepted in the literature that highly sulfurated compounds such as **229** or **230** may be formed during isolation. Lenthionine and related cyclic methylene disulfides (ring sizes of 6-12) have also been isolated from *Chondria californica*, a red alga and from the seed of the mimosacea *Parkia speciosa*.[87,88]

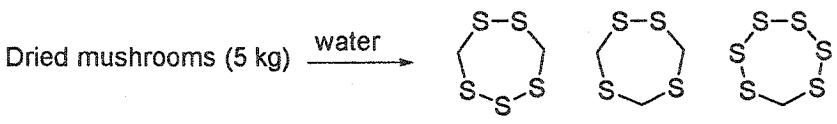

228 (560 mg) **229** (300 mg) **230** (7 mg)

Scheme **54**. Major naturally occurring cyclic polysulfides extracted from shiitake mushrooms at pH 9.

Many derivatives of 1,2,3-trithiane possess cytotoxic activity.[89] Compound **231** was isolated from the green alga[90,91] *Chara globulares* whereas related acid **232** was isolated from asparagus.[49] Functionalized cyclic trisulfide **233** has been isolated separately from the New Zealand ascidian[92] *Aplidium* sp. D as a yellow gum and from the related ascidian[93] *Hypsistozoa fasmeriana*. It shows remarkable antimicrobial, antileukemic and cytotoxic properties in *in vitro* testing.[92]

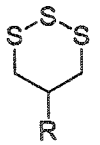

R = SMe **231**
R = COOH **232**

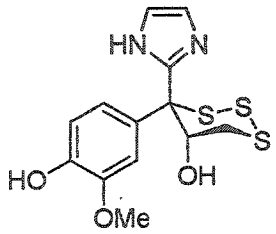

233

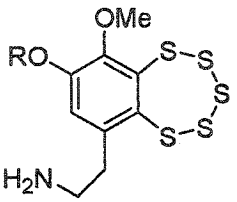

R = H **234**
R = Me **235**

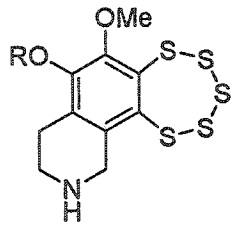

236

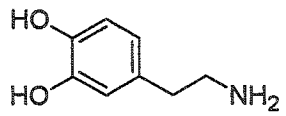

237

Benzopentathiepins are known to be biologically active. Related lissoclinotoxin A[94] **234** and B[95] **236** have both been isolated from the tunicate *Lissoclinum perforatum*. These two compounds exhibit potent antimicrobial, antifungal, and modest cytotoxic activities.[94,95] Varacin **235**,[96-98] a related benzopentathiepin has also been obtained from a tunicate and is also biologically active but unlike the lissoclinotoxins, does not possess any antimicrobial activity. The total synthesis of Varacin from vanillin has been reported.[99,100] These three compounds are all structurally related and possess a similar biosynthetic pathway to that of dopamine **237**.[96,99,100]

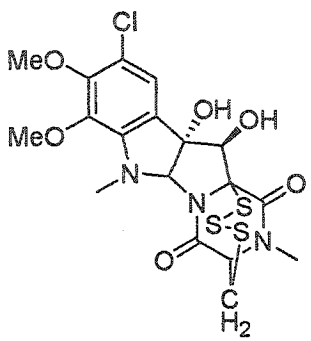

Sporidesmin C

238

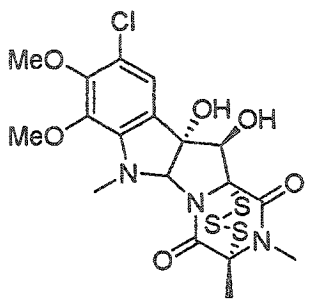

Sporidesmin E

239

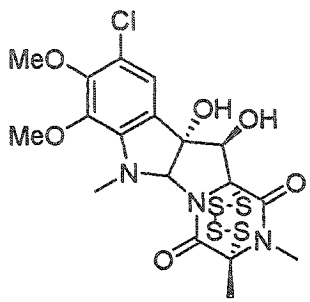

Sporidesmin G

240

Sporidesmin E[101,102] **239**, the trisulfide analog of Sporidesmin and related Sporidesmin C[103] **238** have been isolated from an extraction of *Pithomyces chartarum*,[101,102] a fungus which is found in New Zealand and which is responsible for liver damage and facial eczema in sheep. The same organism also produced the tetrasulfide analog, Sporidesmin G **240**.[104,105] The Sporidesmin series of compounds, all of which contain a core piperazinedione ring, all possess biological activity but are less well studied than the simpler cases reviewed above; Sporidesmin E is a particularly cytotoxic mould.[106,107]

Other compounds containing the piperazinedione core include the tri- **241a** and tetrasulfide **241b** homologues of acetylaranotin, an antiviral metabolite produced by *Aspergillus terrus* and *Arachniotus aureus*.[108,109] These compounds have been shown to have comparable antiviral activity to the parent. Thiodehydrogliotoxin **242** has been prepared from dehydrogliotoxin by reacting it with H_2S_2.[104] The chemistry and chiroptical properties of this compound have been extensively studied.[106,107,110,111] Sirodesmin C[112] **243** has been identified as a metabolite of the fungus *Sirodesmium diversum*. Structurally related hyaldendrin[113] **244** and Verticillin C[114] **245** and their respective tetrasulfide homologs have been isolated.[113,115,116]

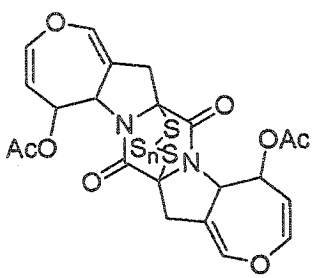

Trisulfide of acetylaranotin

n = 1 **241a**
n = 2 **241b**

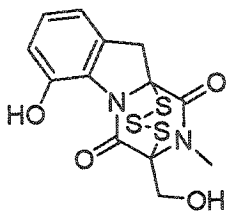

thiodehydrogliotoxin

242

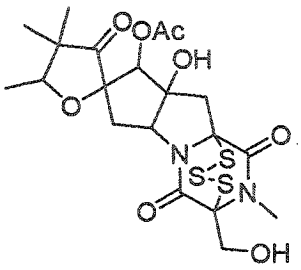

Sirodesmin C

243

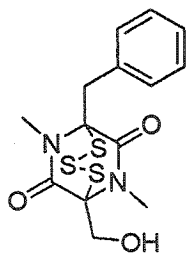

hyalodendrin

244

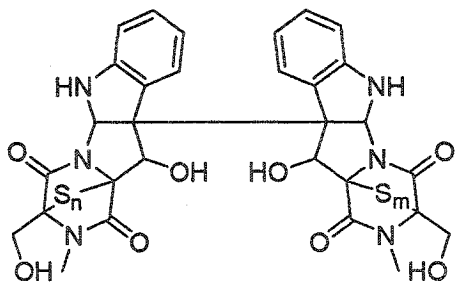

n = 2 and m = 3
or n = 3 and m = 2

Verticillin C

245

7.3 Synthesis of Polysulfides

The following sections represent a literature overview of the syntheis of polysulfides. Emphasis is placed on the preparation of symmetric acyclic tri- and tetrasulfides as it is these compounds that are highlighted in subsequent chapters. For context, the synthesis of acyclic unsymmetric tri- and tetrasulfides and higher order polysulfides (both cyclic and acyclic) are also covered.

7.3.1 The Synthesis of Acyclic Symmetric Tri- and Tetrasulfides

The preparation of symmetric, acyclic trisulfides is well documented.[23] The methods include the use of sulfur dichloride[117,118] with thiols in the absence of base (some authors have found it difficult to obtain consistently good yields[119]), the coupling of alkyl halides with sodium trisulfide in the presence[120] and absence[121] of phase transfer catalysts, mixtures of thiols[122,123] or disulfides with sulfur,[124] the reaction of a metal sulfide with alkanesulfenyl chlorides[125] and thiosulfonates,[119] the reduction of thiosulfonates and disulfonyl sulfides with phosphines[126] as well as sulfur insertion reactions into thiosulfinates, thiosulfonates,[127] sulfides and disulfides.[128,129] In a rare case, the reaction of trithiocarbonate (CS_3^{2-}) with aryl sulfenyl chlorides afforded the trisulfide in high yield (Scheme 55).[130]

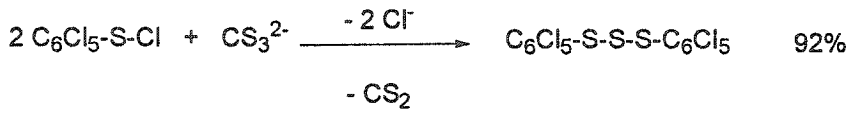

Scheme 55.

Preparation of the analogous tetrasulfides is not as well researched. To our knowledge, there exists no comprehensive study of the formation of this class. Oxidation of hydrodisulfides[131] in the presence of iodine, coupling of thiols with dialkoxy disulfides (ROSSOR),[132,133] sulfur insertion reactions[129] and electrophilic aromatic substitution with sulfur monochloride[134-136] have all been reported as preparative methods.

Compounds bearing the N-S_n-N linkage (**15**, **246-250**)[137,138] can be used as one and two sulfur transfer reagents in the formation of symmetric tri- and tetrasulfides *via* the

coupling of thiols.[139,140] Mild conditions and easy work-up due to the ease of collecting the insoluble amine (solvent: benzene) make this a highly attractive method and has been used in the synthesis of peptide trisulfides.[141]

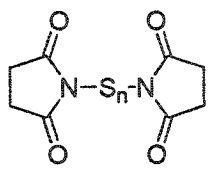

246

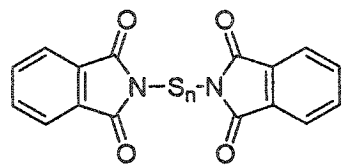

247

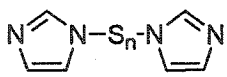

248

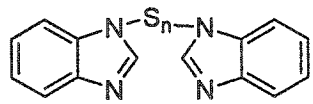

15

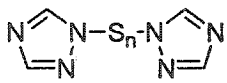

249

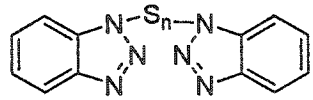

250

$n = 1, 2$

7.3.2 Synthesis of Acyclic Unsymmetric Tri- and Tetrasulfides

The synthesis of unsymmetric trisulfides is more difficult. Among the known procedures are the coupling of chlorodisulfides with thiols[142,143] or similarly with *N*-arylamidthiosulfites.[144] Other methods require the use of unwieldy and often unstable hydrodisulfides (RSSH)[145] or the deoxygenation of highly functionalized dialkanesulfonic thioanhydrides (RSO_2SSO_2R').[126] Unsymmetric trisulfides have been accessed through a mild sequential procedure developed by Barany[146] in modest to excellent yields (25-100%) wherein the key intermediate is an alkoxycarbonyldithiasulfenyl chloride (Scheme **56**). Petroleum additives displaying lubricating propertives have been synthesized *via* this protocol.[147] The use of stable alkyl

or aryl phthalimido disulfides as sulfur transfer reagents[148] has been used as a key step in the preparation of calicheamicin γ_1^I, **227**.[76] Another method involves the sequential coupling of two thiols using sulfur dichloride.[149]

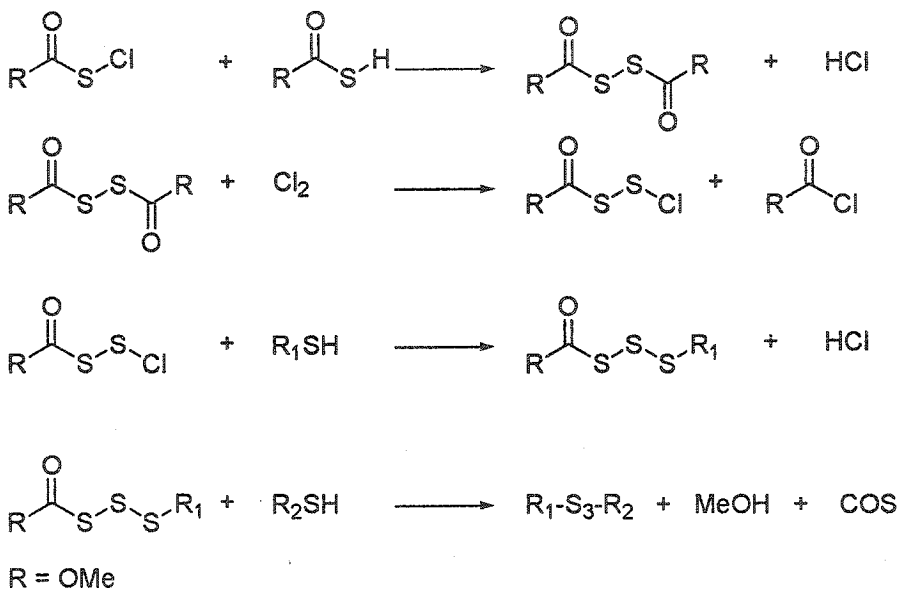

Scheme **56**. Sequential formation of unsymmetric trisulfides

The condensation of *N*-sulfenyl chloride (R_2N-SCl), which may be isolated from the reaction of a 1:1 ratio of SCl_2 to amine, with a thiol affords the unsymmetric R_2NSSR disulfide derivative. This intermediate may then be coupled to a second thiol, displacing the amine to prepare unsymmetric polysulfides.[148] To our knowledge, no generalized method exists for the formation of unsymmetric tetrasulfides in high yield although two such tetrasulfides were formed[149] using sulfur monochloride as the coupling reagent.

7.3.3 Synthesis of Higher Order Polysulfides

There are fewer methods to access consistently higher order polysulfides ($n > 4$). Recent methods include the use of titanocene polysulfide complexes,[150,151] *e.g.* Cp_2TiS_5,[152-155] $Cp_4Ti_2S_4$,[156] $Cp_2Ti_2S_6$,[157] (Cp = η^5-C_5H_5) and $Cp^*_2Ti_2S_3$[158] (Cp^* = η^5-$CH_3C_5H_4$). Although these conditions for the formation of polysulfides are mild, they suffer from the need to pre-synthesize chloropolysulfanes, a synthesis which is intolerant of protic functional groups; direct sulfur insertion into trityl chloride is also possible.[159] Titanocene polysulfides have been most notably used in the formation of sulfur allotropes S_7[160] and S_{14}.[159] Sequential coupling of thiols with alkoxy disulfides (to form the corresponding tetrasulfide) then with Cp_2TiS_5 has also been reported to form undecasulfides.[161] Other organometallic reagents such as ZDMC[162] or (TMEDA)ZnS_6[163] have also been used as sulfur transfer reagents both in the formation of organic[158,164] and inorganic[165] polychalcogens.

Access to higher order polysulfides is possible under thermal conditions through the use of elemental sulfur S_8, (usually in the presence of olefins[166]) which acts as an electrophilic source of sulfur in the presence of a catalyst such as NH_3,[167] DABCO[168] or Na_2S.[169-171] Sometimes with unusual unsaturation (Scheme 57)[172,173] or through the use of diazomethane,[174] the catalyst is not even needed; however these methods are not general. For example, squalene reacts with sulfur to form in part a bimolecular product with the formula $C_{60}H_{100}S_6$.[175] The synthesis of pentathiepins in low to moderate yield

from the thermolysis of 1,2,3-benzothiadiazoles in the presence of S_8 has also been reported.[168]

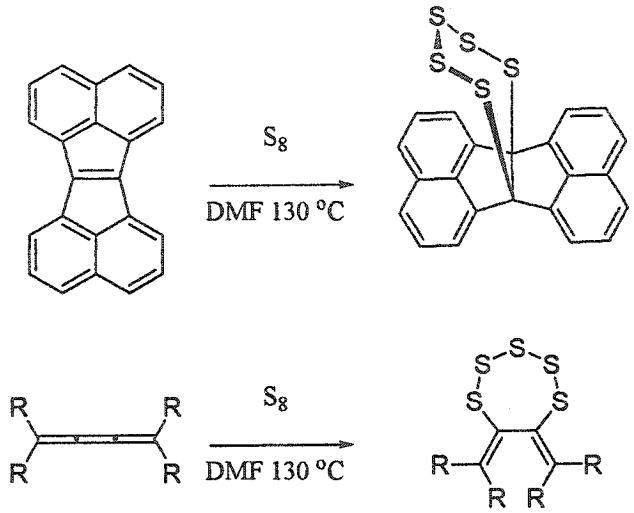

Scheme 57. Sulfur addition onto unsaturated systems in the absence of a catalyst

Although not synthetically useful, heptasulfide **251** was generated from what is believed to be *in situ* generation of S^{2-} from CS_2 and NaOEt/EtOH and subsequent concatenation and condensation with amine **252** and chloroacetone (Scheme 58).

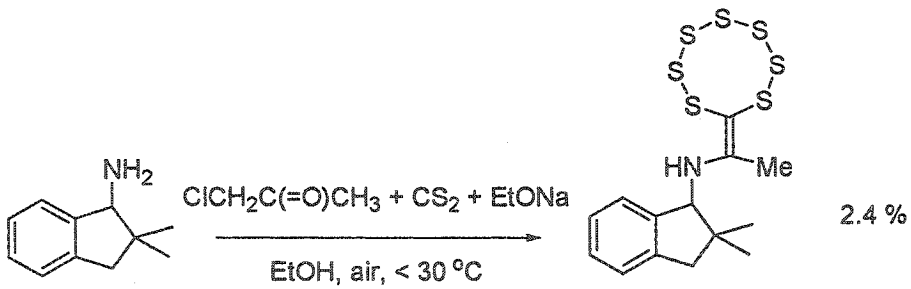

252 **251**

Scheme 58. *In situ* generation of S^{2-} in the formation of heptasulfide **251**

Highly reactive higher order dichloropolysulfanes such as S_3Cl_2 may also be prepared and then coupled with thiols in good yield.[176] Preformation of thermally labile hydrodisulfides such as Ph_3CSSH and subsequent reaction with SCl_2 afforded the

corresponding pentasulfide in modest yield.[177] Three-sulfur insertion into disulfides using $Ph_3CSSSCl$ provides access to symmetric pentasulfides in good to excellent yield.[128]

7.4 Connectivity of R-S_n-R (R = alkyl or H)

To date,[178] no organic polysulfide has been detected in the solid or liquid phase that contains a branched, thiosulfoxide arrangement (R_2S=S **94b**). The concept of hypervalent sulfur species was first introduced by Foss[179] although reports of the existence of thiosulfoxides are found in the literature dating from the early twentieth century, most specifically dealing with the distillation of Levinstein H (mustard gas).[180] The controversy surrounding the existence of thiosulfoxides both as reactive intermediates and as stable entities has not abated.

Recently[181] it has been shown *via* tandem mass spectrometry that in the gas phase, thiosulfoxides are stable entities both as radical cations as well as neutral species (R_2S=S, R = H, CH_3, C_2H_5). Steudel provided evidence by IR (bands at *ca.* 670 cm^{-1}) more than 30 years ago that branched-sulfur arrangements (-S-S(=S)-S-) could exist in sulfur homocycles at temperatures below -150 °C.[182,183] Calculations at the MP2/6-31G* level of theory now demonstrate that although the unbranched disulfide connectivity is more stable, that of the thiosulfoxide represents a local minimum.[184] Another study showed that although HSSH is the global minimum by *ca.* 38 kcal/mol in the isomerization of HSSH **69a** $\Leftrightarrow$ H_2S=S **69b**, H_2S=S **69b** was also nevertheless found to exist as a true local

minimum on the potential energy surface.[185] Schleyer,[186] in a comprehensive theoretical study, showed that the energy stabilization for XSSX **94a** (X = H **69a**, CH_3 **71a**) with respect to the branched isomer is large (averaging 33 kcal/mol and 19 kcal/mol respectively for **69a** and **71a**) and proportional to the S-S bond length. Bonding of hypervalent and non-hypervalent species of this type are similar and do not involve any special S-3*d* orbitals according to natural population analysis. The hypervalent-like structure of **94b** is better characterized as a polarized σ-bond (the terminal sulfur being negatively charged) with its strength depending on the electrostatic interactions and the origin of the X group.[187]

Steudel and co-workers showed *via ab initio* calculations that thiosulfoxides ($R_2S{=}S$, R = H, CH_3) should be both kinetically and thermally stable at low temperatures. However, they determined that the unimolecular isomerization barrier to the more stable disulfides (MeSSMe is calculated to be *ca.* 20 kcal/mol more stable than $Me_2S{=}S$ whereas HSSH

94a **94b** **253**

69a is calculated to be *ca.* 34 kcal/mol more stable than $H_2S{=}S$ **69b**) would be energetically unfavourable (*ca.* 81 kcal/mol and 52 kcal/mol respectively for Me and H for a X_2S_2 system) and that at low temperature they should exist as discrete entities.[184] These studies corroborate previous theoretical[187,188] and experimental[188-193] studies in this area. A corollary to this is that at lower temperatures (< 100 °C), thiosulfoxides cannot be invoked as intermediates in interconversion reactions involving polysulfides.

It should be noted that in a recent work, Steudel[194] probed the formation of sulfuranes **253** as possible hypervalent intermediates in the interconversion of sulfur allotropes and of chainlike polysulfides at moderate temperatures and found these species to be too energetically disfavoured; the formation of thiosulfoxides as intermediates at similar temperatures had previously been investigated and also found to be energetically disfavoured.[195] It was therefore concluded that such reactions proceed through a radical dissociation mechanism at higher temperatures and are initiated at more moderate temperatures by either trace nucleophile impurities in solution or by polar groups present on the reaction vessel which themselves may serve as catalysts.

Prior to the mass spectrometry study by Gerbaux[181] and co-workers, the existence of thiosulfoxides had only been inferred. Baechler and co-workers in two studies relating to sulfur-transfer proposed that thiosulfoxides are intermediates in the eventual deoxygenation of sulfoxides with thiophosphoryl bromide[196] $PSBr_3$ or phosphorus pentasulfide[197-199] P_4S_{10} (Scheme **59a** – probably proceeding in a similar manner to the oxaphosphetane formed during the Wittig reaction) as well as in the sulfurization then isomerization of allylic sulfoxides (*via* a [2,3]-sigmatropic shift) to the corresponding disulfide using B_2S_3 (Scheme **59b**);[200-202] thiosulfoxide intermediates have also been posited in the formation of sulfides from the reaction of sulfilimines (R_2S=N-X; X = H, Tos) or sulfur ylids with P_4S_{10}.[203-205] Phosphorus pentasulfide, P_4S_{10}, in particular has been synthetically useful. Illustrative examples include its use, in the presence of pyridine, to deoxygenate penicillin **254** and cephalosporin **255** sulfoxides[206] as well as allenyl sulfoxides.[207]

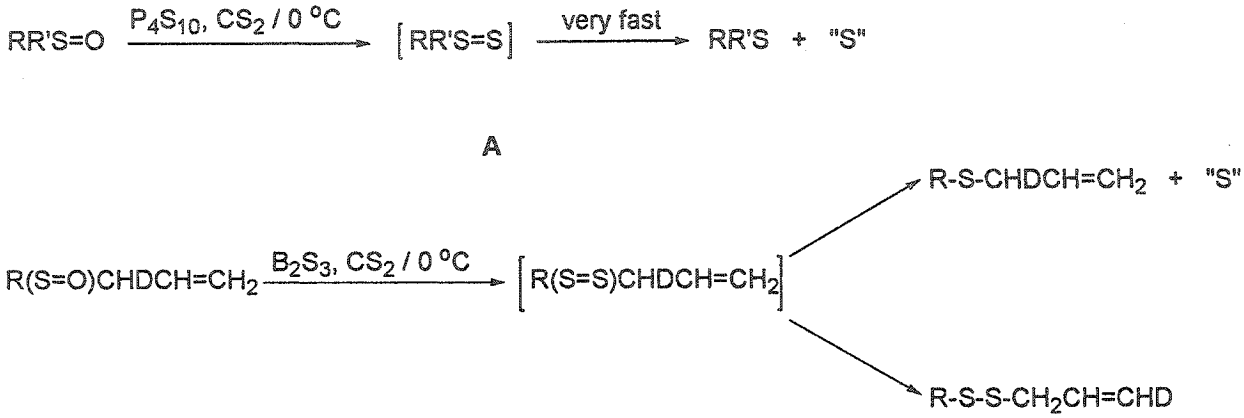

Scheme 59. Generation of thiosulfoxides as intermediates

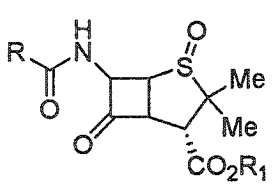

penicillin sulfoxide

254

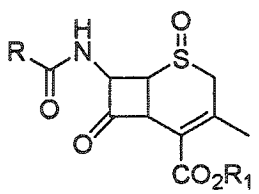

cephalosporin sulfoxide

255

The existence of an undetectably small equilibrium between allylic disulfides and their thiosulfoxide isomers was proposed by Mislow as far back as 1971 in order to account for the formation of allyl disulfides from the reaction of allyl sulfides with sulfur (Scheme **60a**)[208] or the sigmatropic rearrangement of allyl disulfides (Scheme **60b**).[209] Desulfurization of allyl disulfides with Ph_3P below 100 °C was also proposed to proceed *via* a thiosulfoxide transition state;[210] saturated disulfides did not desulfurize under these conditions.[211] Others have also implied the formation of thiosulfoxides although they too were not able to detect their existence.[199,212] Steudel[184] has calculated that even though MeSSAllyl is more stable than MeAllylS=S by *ca.* 20 kcal/mol, its isomerization only requires *ca.* 26 kcal/mol, much less than that calculated for saturated disulfides (*vide supra*).

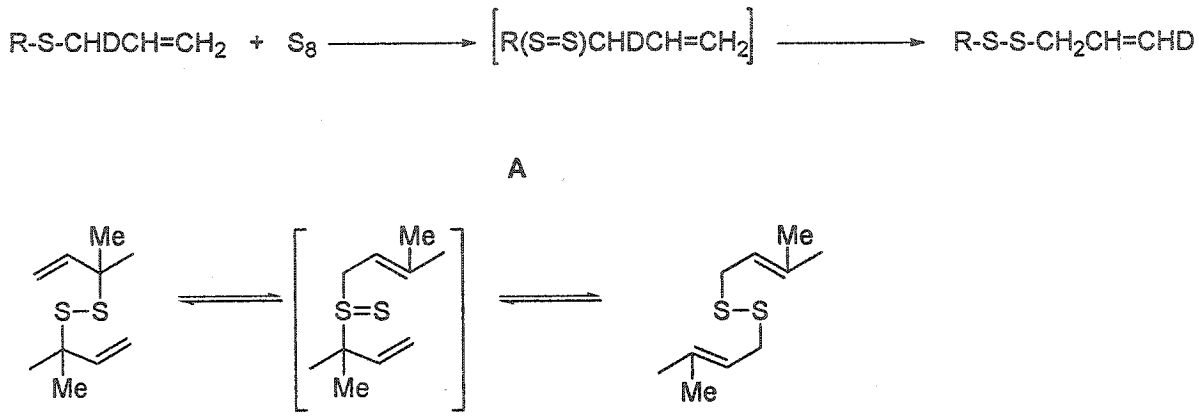

Scheme **60**. Thiosulfoxides as intermediates in isomerization reactions

Thiosulfoxides have been proposed as intermediates in photolytic[213] (Scheme **61a**) and thermolytic[214,215] (Scheme **61b**) desulfurization reactions.

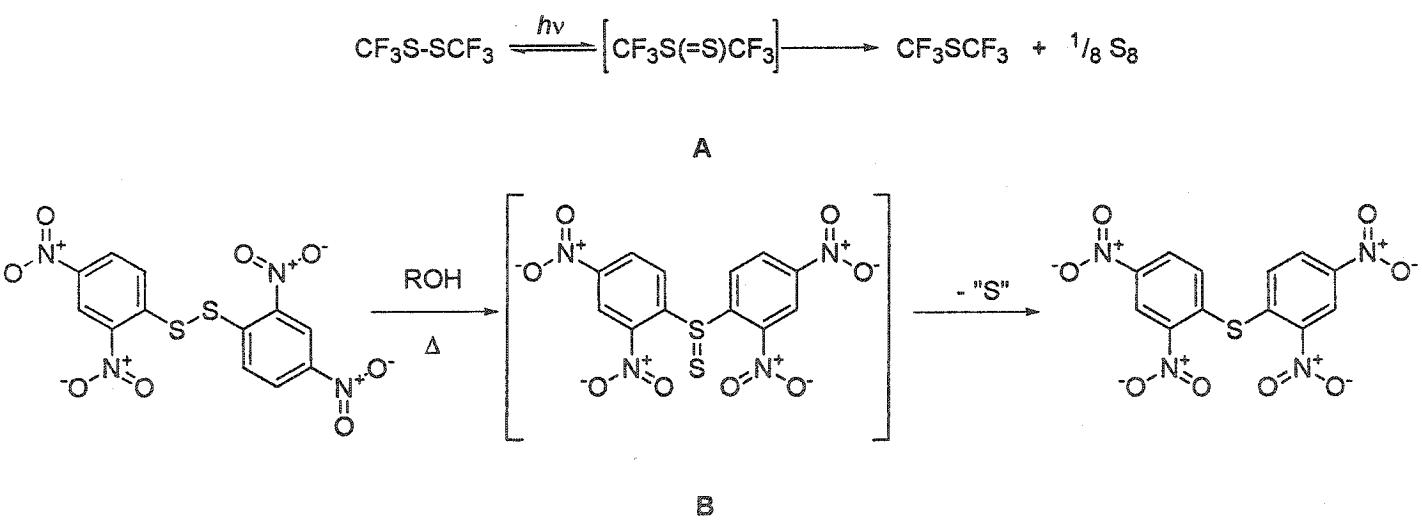

Scheme **61**. Thiosulfoxides as intermediates in thermal and photochemical reactions

Thiosulfoxides have also been postulated as intermediates in the efficient and efficacious reduction of sulfoxides with TFAA-H_2S system (>90%, 5 min)[216] or hexamethyldisilathiane[217] $[(Me)_3Si]_2S$ to the corresponding sulfide; in the latter case, the

increased strength of the Si-O (*ca.* 106 kcal/mol) bond over that of the Si-S (*ca.* 70 kcal/mol) bond provides the driving force for the reaction.

An explanation of the work to date suggests that the heat of formation of thiosulfoxides and branched sulfur species in the interconversion of sulfur homocycles[218] lie as little as *ca.* 10 kcal/mol above the unbranched disulfides.[215,219]

Little work has been done on the isomerization of higher order polysulfides to their respective branch-bonded isomers. Barnard has proposed a branch-bonded trisulfide as an intermediate in the thermal racemization of bis-(1,3-dimethylbut-2-enyl) trisulfide.[220] Safe and Taylor were proponents of an equilibrium between branched and unbranched trisulfides as an explanation of the conversion of disulfides to trisulfides by reaction with H_2S_2 **69**.[104] Recently the ground state energy difference between H_2S_6 and $(HSS)_2S{=}S$ has been calculated at a high level of theory (G3X-(MP2)) to be only *ca.* 13 kcal/mol at 0 K.[221] However, to date no evidence exists for branched isomers of polysulfides ($n > 2$).

Branch-bonded $X_2S{=}S$ structures have been detected and are considered stable entities when X is electronegative the physical properties of these compounds (where X = F, O, Cl, Br) are covered extensively in Chapter 2.

7.5 Structure and Conformational Analysis of Polysulfides

The conformational analysis of polysulfides has been reviewed.[222,223] To date, the crystal structures of more than 30 acyclic polysulfides have been resolved by X-Ray analysis.[224] In rare cases, electron diffraction has been used to elucidate the structures of R-S_n-R. In addition, the structures of sulfonium cations **256a**[225] and **256b**[226] have been determined.

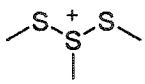

256a

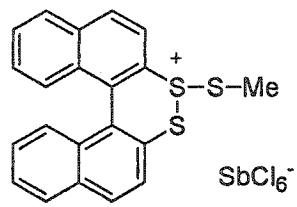

256b

As stated above, all crystal structures of polysulfides (up to nine sulfurs), indicate unbranched chains. Typical values for the geometry of polysulfides are r(S-S) = 2.05 ± 0.04 Å, θ(S-S-S) = 107 ± 3° and τ(S-S-S-S) = 85 ± 20°. Each S-S centered dihedral angle may exist in one of two forms as in Scheme **62**; in the case of disulfides this results in enantiomers.

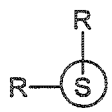

counterclockwise rotation
M or (-)

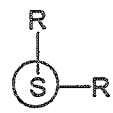

clockwise rotation
P or (+)

Scheme **62**. Two possible dihedral angles which may be adopted about the S-S bond and the nomenclature that characterizes these dihedral angles.

Thus a polysulfide may be characterized in terms of an overall helicity if all the dihedral angles are P (a right-handed helix) or M (a left-handed helix). It is also possible to have less ordered polysulfide chains although these are not as common. It is the minimization of the repulsion of non-bonding p electrons on adjacent sulfurs which is responsible for the observed *ca.* 90° dihedral angles; the $\sigma_{S\text{-}S}$ and $\sigma_{S\text{-}C}$ bonds are thus almost entirely p in character.

Recall that the rotational barrier[227] for MeS-SMe **71** was initially calculated to be 6.8 kcal/mol.[228] Allinger[229] determined that such a barrier was due to rotation through a *trans* transition state. The *cis* barrier was calculated to be *ca.* 3.5 kcal/mol greater than that of the *trans* barrier. IR[230] and Raman[231] measurements put this barrier at 7.3-9.5 kcal/mol. The *trans* barrier for HS-SH **69** was calculated to be 5.0 ± 0.2 kcal/mol.[232] The torsional barriers for higher order polysulfides have not been accurately determined but calculations for related H_2S_n (n = 2-4) systems suggests that such barriers decrease with sulfurs directly attached to the S-S moiety of interest (HSS-SSH barrier[233] found to be 6.2 kcal/mol). Calculations for HSSSH and MeSSSMe show rotational barriers of 7.1 and 7.4 kcal/mol respectively.[234] Such low barriers necessitate that rotamers are averaged on the NMR time scale and cannot therefore be distinguished from one another by this means.

Table 68. Geometric parameters of symmetrically substituted polysulfides R-S_n-R. Adapted from Ref 24.

R	method[a]	*n*	r(S-S) Å	θ(S-S-S) deg	τ(S-S)[b] deg	ref
Me	ED	3	2.046	107	80	235
2-nitrophenyl[c]	X-Ray	3	2.050, 2.054	106.4	81.7, 87. 8	236
2-nitrophenyl[d]	X-Ray	3	2.060	110.6	79.6	237
$(Me_3Si)_3C$	X-Ray	3	2.057, 2.066	112.5	93.2, 104.6	238
F_3C	ED	3	2.040	105.3	89	239
F_3C	X-Ray	3	2.041	106.7	88.5	240
Cl_3C	X-Ray	3	2.034	106.0	93, 95	241
n-$C_{18}H_{37}$	X-Ray	3	2.023, 2.030	106.3	72.8, 67.3	242
2-benzothiazoyl	X-Ray	4	2.027 (2x), 2.073	106.4	78.5	133
4-chlorophenyl	X-Ray	4	2.067, 2.036, 2.023	107.4, 108.4	75.5	133
CN	X-Ray	4	2.017, 2.068 (2x)	106.3, 106.7	84.8	243
F_3C	ED	4	2.034, 2.054	106.8	84, 98	239
n-$C_{18}H_{37}$	X-Ray	4	2.018, 2.060	105.3	63.5, 75.9	242
Ph_3C	X-Ray	5	2.04, 2.02, 2.05, 2.01	109, 106, 111	76-97	156
Ph_3C	X-Ray	6	2.024-2.070	104.8-108.5	88.7-101.4	156
CN	X-Ray	6	2.034-2.074	105.0-106.0	81.2-94.5	244
Cl_3C	X-Ray	7	2.018-2.059	103.6-107.1	79.7-91.1	155
CN	X-Ray	9	2.041-2.078	104.3-106.8	80.2-94.8	245

a) ED, electron diffraction (gas-phase). b) In the case of chiral molecules, the torsional angles of the corresponding enantiomers are all oppositely signed. c) Triclinic allotrope. d) Orthorhombic allotrope.

The geometric features of a representative set of polysulfides are shown in Table 68. Many of these compounds are chiral in the solid state (with helical chirality with point group symmetry of either C_n or D_n with n = 1, 2). It should also be noted that the parameters cited have widely varying errors and in the case of resolved X-ray structures, are influenced by intermolecular interactions. Although chiral molecules usually crystallize within the unit cell to afford equal populations of each enantiomer, there exist some cases in which enantiopure crystals have been obtained. For instance $S_9(CN)_2$ crystallizes from CS_2/*n*-hexane (enantiopure) despite the 2^{10} different conformations it can adopt (for rotation about S-S bonds).[245]

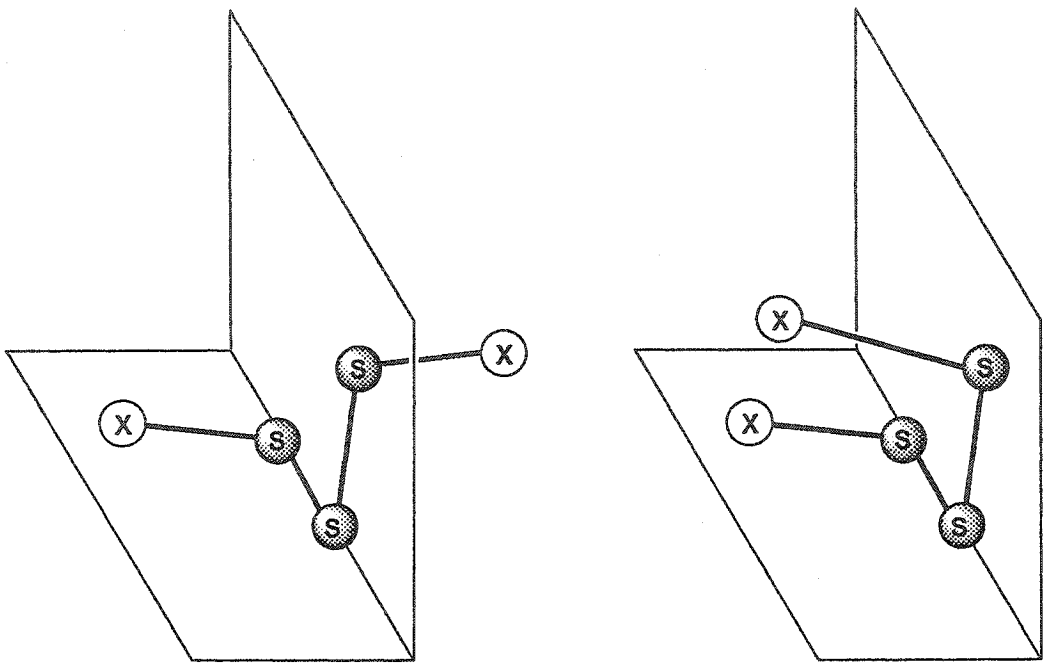

trans *cis*

A **B**

Figure **34**. Conformations of trisulfides

Most trisulfides adopt a *trans* conformation (Figure **34A**) with a local C_2 symmetry for the central trisulfide core and an organized helicity (M,M or P,P). Dicyanotrisulfide is an exception to this rule; it prefers to adopt the *cis* conformation (Figure **34B**) in the solid state.[246] It is believed that there exists a neighbouring group stabilization between the nitrile nitrogens and that of the central sulfur affording a M,P conformation (or P,M for its enantiomer). Similar stabilization is observed in bis(2-nitrophenyl) trisulfide which, in its triclinic form, contains weak interactions between the oxygens from the nitro groups and those of the neighbouring terminal sulfurs;[236] the orthorhombic crystals do not contain these interactions.[237] The conformational preference for a helicity within the S-S-S core is even kept with bulky R groups (R = $(Me_3Si)_3C$).[238] The electron diffraction for MeSSSMe was recently interpreted to be mostly that of the *trans* conformation (Figure

34A).[247] Molecular mechanics[234] and *ab initio*[247] work accurately describe the geometric parameters for MeSSSMe and both predict that the *trans* conformer is the most stable but interestingly Snyder[234] showed (albeit by a more primitive calculational method) that it was only so by *ca.* 1 kcal/mol; the difference being attributed to SH and SC dipole effects. Although the r(S-S) are similar for MeSSSMe to that of $Cl_3CSSSCCl_3$ and $F_3CSSSCF_3$ the latter two have decreased θ(S-S-S) and increased τ(S-S) angles. This may be due to the increased steric bulk of afforded by the trihalomethyl groups.

The four tetrasulfide crystal structures in Table **68** all exist in a *trans-trans* conformation all of which contain local helicity (Figure **35**). Local helicity is also observed in the only resolved crystal structure of a pentasulfide. However, this is not the case for the hexasulfides. These adopt a more compact, less ordered conformation. The crystal structure of $(Cl_3C)_2S_7$ is helical; in contrast, the conformation of $(CN)_2S_9$ is almost cyclic.

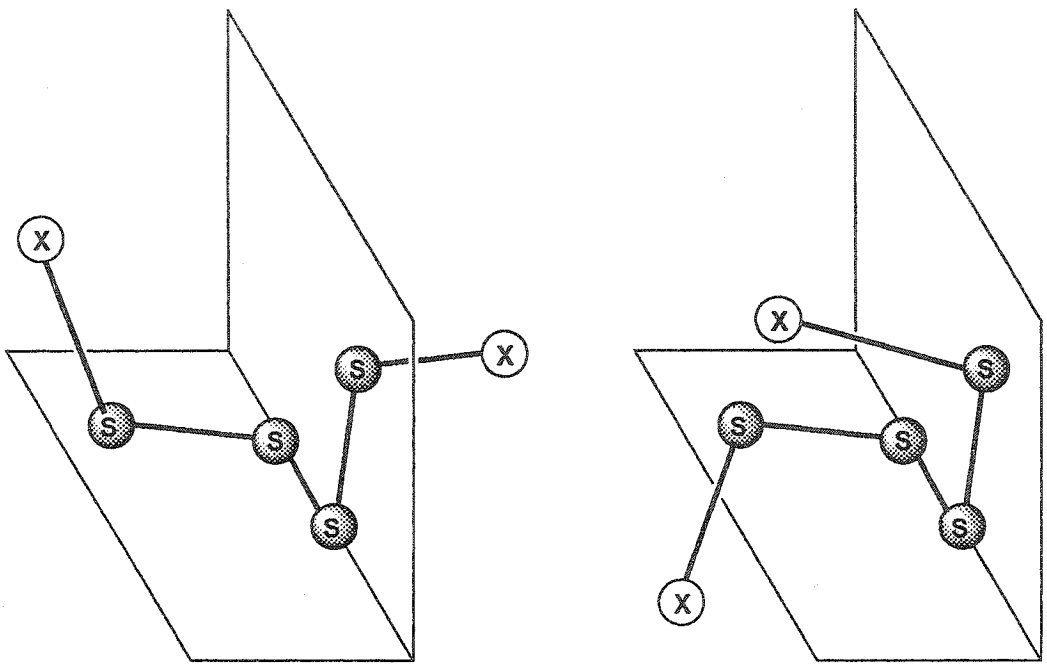

trans-trans *cis-cis*

A B

Figure 35. Conformations of tetrasulfides

7.6 Concluding Remarks

The preceding cogent review on polysulfides provides a firm basis for understanding the importance these classes of molecules play in Nature. It also provides a synopsis of the published synthetic methodology for polysulfides. This puts into a context our interest in optimizing the yields of tri- and tetrasulfides as well exploring their usefulness as sulfur transfer reagents and therapeutics.

7.7 References

(1) Zamecnik, P. C. *Prospects for Antisense Nucleic Acid Therapy for Cancer and AIDS*; Wiley Liss: New York, **1991**.

(2) Mirabelli, C. K.; Crooke, S. T. *Antisense Research and Applications*; CRC: Ann Arbor, **1993**.

(3) Eckstein, F. *Annu. Rev. Biochem.* **1985**, *54*, 367.

(4) Liebhaber, S. A.; Cash, F. E.; Shakin, S. H. *J. Biol. Chem.* **1984**, *259*, 15597.

(5) Cheruvallath, Z., S.; Carty, R. L.; Moore, M. N.; Capaldi, D. C.; Krotz, A. H.; Wheeler, P. D.; Turney, B. J.; Craig, S. R.; Gaus, H. J.; Scozzari, A. N.; Cole, D. L.; Ravikumar, V. T. *Organic Process Research & Development* **2000**, *4*, 199.

(6) Crooke, S. T. *Antisense and Nucleic Acid Drug Development* **1998**, *8*, vii.

(7) De Smet, M. D.; Meenken, C.; Van Den Horn, G. J. *Ocular Immunology and Inflammation* **1999**, *7*, 189.

(8) Xu, Q.; Musier-Forsyth, K.; Hammer, R. P.; Barany, G. *Nucleic Acids Research* **1996**, *24*, 1602.

(9) Xu, Q.; Barany, G.; Hammer, R. P.; Musier-Forsyth, K. *Nucleic Acids Research* **1996**, *24*, 3543.

(10) Ma, M. Y.-X.; Dignam, J. C.; Fong, G. W.; Li, L.; Gray, S. H.; Jacob-Samuel, B.; George, S. T. *Nucleic Acids Research* **1997**, *25*, 3590.

(11) Tang, J.-Y.; Han, Y.; Tang, J. X.; Zhang, Z. *Organic Process Research & Development* **2000**, *4*, 194.

(12) Brill, W. K.-D.; Tang, J.-Y.; Ma, Y.-X.; Caruthers, M. H. *J. Am. Chem. Soc.* **1989**, *111*, 2321.

(13) Iyer, R. P.; Phillips, L. R.; Egan, W.; Regan, J. B.; Beaucage, S. L. *J. Org. Chem.* **1990**, *55*, 4693.

(14) Iyer, R. P.; Egan, W.; Regan, J. B.; Beaucage, S. L. *J. Am. Chem. Soc.* **1990**, *112*, 1253.

(15) Vu, H.; Hirschbein, B. L. *Tetrahedron Lett.* **1991**, *32*, 3005.

(16) Stec, W. J.; Uznanski, B.; Wilk, A.; Hirschbein, B. L.; Fearon, K. L.; Bergot, B. J. *Tetrahedron Lett.* **1993**, *34*, 5317.

(17) Liu, X.; Reese, C. B. *J. Chem. Soc. Perkin. Trans. 1* **1995**, *13*, 1685.

(18) Stec, W. J.; Grajkowski, A.; Kobylanska, A.; Karwowski, B.; Koziolkiewicz, M.; Misiura, K.; Okruszek, A.; Wilk, A.; Guba, P.; Boczkowska, M. *J. Am. Chem. Soc.* **1995**, *117*, 12019.

(19) Almer, H.; Stawinski, J.; Stromberg, R. *Nucleic Acids Research* **1996**, *24*, 3811.

(20) Wyrzykiewicz, T. K.; Ravikumar, V. T. *Bioorganic & Medicinal Chemistry Letters* **1994**, *4*, 1519.

(21) Zhang, Z.; Nichols, A.; Tang, J. X.; Alsbeti, M.; Tang, J.-Y. *Nucleosides & Nucleotides* **1997**, *16*, 1585.

(22) Eleuteri, A.; Cheruvallath, Z., S.; Capaldi, D. C.; Cole, D. L.; Ravikumar, V. T. *Nucleosides & Nucleotides* **1999**, *18*, 1893.

(23) Steudel, R.; Kustos, M. In *Encyclopedia of Inorganic Chemistry*; King, R. B., Ed.; John Wiley & Sons: Athens, GA, 1994; Vol. 7, p 4009.

(24) Steudel, R. *Chem. Rev.* **2002**, *102*, 3905.

(25) Järvenpää, E. P.; Zhang, Z.; Huopalahti, R.; King, J. W. *Z. Lebensm Unters Forsch A* **1998**, *207*, 39.

(26) Block, E. *Angew. Chem. Int. Ed. Engl.* **1992**, *31*, 1135.

(27) Wijaya, C. H.; Nishimura, H.; Tanaka, T.; Mizutani, J. *J. Food Sci.* **1991**, *56*, 72.

(28) Hu, Q.; Yang, Q.; Yamato, O.; Yamasaki, M.; Maede, Y.; Yoshihara, T. *J. Agric. Food Chem.* **2002**, *50*, 1059.

(29) Wu, C. C.; Sheen, L. Y.; Chen, H.-W.; Tsai, S.-J.; Lii, C.-K. *Food and Chemical Toxicology* **2001**, *39*, 563.

(30) Pino, J.; Rosado, A.; Gonzalez, A. *Acta Alimentaria* **1991**, *20*, 163.

(31) Chen, C. C.; Chen, S. D.; Chen, J. J.; Wu, C. M. *J. Agric. Food Chem.* **1984**, *32*, 999.

(32) Chen, C. C.; Ho, C. T. *J. Agric. Food Chem.* **1986**, *34*, 830.

(33) Gijs, L.; Perpète, P.; Timmermans, A.; Collin, S. *J. Agric. Food Chem.* **2000**, *48*, 6196.

(34) Näf, R.; Velluz, A. *Flavour Fragr. J.* **1996**, *11*, 295.

(35) Block, E.; Iyer, R.; Grisoni, S.; Saha, C.; Belman, S.; Lossing, F. P. *J. Am. Chem. Soc.* **1988**, *110*, 7813.

(36) Lawson, L. D.; Wang, Z.-Y.; Hughes, B. G. *Planta Med.* **1991**, *57*, 363.

(37) Muller, E.; Hyne, J. B. *J. Am. Chem. Soc.* **1969**, *91*, 1907.

(38) Kende, I.; Pickering, T. L.; Tobolsky, A. V. *J. Am. Chem. Soc.* **1965**, *87*, 5582.

(39) Pickering, T. L.; Saunders, K. J.; Tobolsky, A. V. *J. Am. Chem. Soc.* **1967**, *89*, 2364.

(40) O'Gara, E. A.; Hill, D. J.; Maslin, D. J. *Appl Envirom. Microbiol.* **2000**, *66*, 2269.

(41) Tsao, S.-M.; Yin, M.-C. *J. Med. Microbiol.* **2001**, *50*, 646.

(42) Block, E. *Angew. Chem. Int. Ed. Engl.* **1992**, *104*, 1158.

(43) Rajanikanth, B.; Ravindranath, B.; Shankaranarayana, M. L. *Phytochemistry* **1984**, *23*, 899.

(44) Berger, C.; Khan, J. A.; Molimard, P.; Martin, N.; Spinnler, H. E. *Appl Envirom. Microbiol.* **1999**, *65*, 5510.

(45) Kohama, Y.; Iida, K.; Semba, T.; Inada, A.; Tanaka, K.; Nakanishi, T. *Chem. Pharm. Bull.* **1992**, *40*, 2210.

(46) Kohama, Y.; Iida, K.; Itoh, S.; Tsujikawa, K.; Mimura, T. *Biol. Pharm. Bull.* **1996**, *19*, 876.

(47) Von Szczepanaski, C.; Zgorzelak, P.; Hoyer, G. A. *Arzneim. Forschg.* **1972**, *22*, 1975.

(48) Apparo, M.; Kjaer, A.; Madsen, J. O.; Venkata Rao, E. *Phytochemistry* **1978**, *17*, 1660.

(49) Kasai, T.; Sakamura, S. *Agric. Biol. Chem.* **1982**, *46*, 821.

(50) Fletcher, J. C.; Robson, A. *Biochem. J.* **1963**, *87*, 553.

(51) Moore, R. E. *Chem. Commun.* **1971**, 1168.

(52) Lee, M. D.; Dunne, T. S.; Siegal, M. M.; Chang, C. C.; Morton, G. O.; Borders, D. B. *J. Am. Chem. Soc.* **1987**, *109*, 3464.

(53) Golik, J.; Clardy, J.; Dubay, G.; Groenewold, G.; Kawaguchi, H.; Masataka, K.; Krishnan, B.; Ohkuna, H.; Saitoh, K.-i.; Doyle, T. W. *J. Am. Chem. Soc.* **1987**, *109*, 3461.

(54) Golik, J.; Clardy, J.; Dubay, G.; Groenewold, G.; Kawaguchi, H.; Masataka, K.; Krishnan, B.; Ohkuna, H.; Saitoh, K.-i.; Doyle, T. W. *J. Am. Chem. Soc.* **1987**, *109*, 3462.

(55) Beutler, J. A.; Clark, P. A.; Alvarado, B. *Journal of Natural Products* **1994**, *57*, 629.

(56) Chin, H.-W. C.; Lindsay, R. C. *J. Agric. Food Chem.* **1994**, *42*, 1529.

(57) Kubec, R.; Drhová, V.; Velíšek, J. *J. Agric. Food Chem.* **1999**, *47*, 1132.

(58) Duckham, S. C.; Dodson, A. T.; Bakker, J.; Ames, J. M. *Nahrung/Food* **2001**, *45*, 317.

(59) *Sulfur Compounds in Foods*; Mussinan, C. J.; Keelan, M. E., Eds.; American Chemical Society: Washington D.C., 1994.

(60) Banerji, A.; Amonkar, S. V. B. *IN 75-B0344 19751127* India, **1975**

(61) Yasuhara, A.; Fuwa, K. *Bull. Chem. Soc. Japan* **1977**, *50*, 3029.

(62) Beroza, M. *Chemicals Controlling Insect Behavior*; Academic Press: New York, **1970**; p.117.

(63) Gates, K. S. *Chem. Res. Toxicol.* **2000**, *13*, 953.

(64) Jónsson, S.; Raa, J. *J. Food Sci.* **1980**, *45*, 1641.

(65) Ogasawara, Y.; Isoda, S.; Tanabe, S. *Toxicology Letters* **1998**, *99*, 191.

(66) Jespersen, A. M.; Christensen, T.; Klausen, N. K.; Nielsen, P. F.; Sørensen, H. H. *Eur. J. Biochem.* **1994**, *219*, 365.

(67) Andersson, C.; Edlund, P. O.; Gellesfors, P.; Hansson, Y.; Holmberg, E.; Hult, C.; Johansson, S.; Kordel, J.; Lundin, R.; Mended-Hartvig, I.; Noren, B.; Wehler, T.; Widmalm, G.; Ohman, J. *Int. J. Pept. Protein Res.* **1996**, *47*, 311.

(68) Jespersen, A. M.; Christensen, T.; Klausen, N. K.; Nielsen, P. F.; Sorensen, H. H. *Eur. J. Biochem.* **1994**, *219*, 365.

(69) Canova-Davis, E.; Baldonado, I. P.; Chloupek, R. C.; Ling, V. T.; Gehant, R.; Olson, K.; Gillece-Castro, B. L. *Anal. Chem.* **1996**, *68*, 4044.

(70) Chen, L.; Zoulíková, I.; Slaninová, J.; Barany, G. *J. Med. Chem* **1997**, *40*, 864.

(71) Sandy, J. D.; Davies, R. C.; Neuberger, A. *Biochem. J.* **1975**, *150*, 245.

(72) Bartle, K. D.; Fletcher, J. C.; Jones, D. W.; L'Amie, R. *Biochim. Biophys. Acta* **1968**, *160*, 106.

(73) Szczepkowski, T. W.; Wood, J. L. *Biochim. Biophys. Acta* **1967**, *139*, 469.

(74) Iciek, M.; Wlodek, L. *Polish J. Pharmacol.* **2001**, *53*, 215.

(75) Katritzky, A. R.; Zhao, X.; Hitchings, G. J. *Tetrahedron Lett.* **1990**, 473.

(76) Nicolaou, K. C.; Hummel, C. W.; Nakada, M.; Shibayama, K.; Pitsinos, E. N.; Saimoto, H.; Mizuno, Y.; Baldenius, K.-U.; Smith, A. L. *J. Am. Chem. Soc.* **1993**, *115*, 7625.

(77) Christopherson, C.; Anthoni, U. *Sulfur Reports* **1986**, *4*, 365.

(78) Faulkner, D. J. *Nat. Prod. Rep.* **2002**, *19*, 1.

(79) Nicolaou, K. C.; Dai, W.-M. *Angew. Chem. Int. Ed. Engl.* **1991**, *30*, 1387.

(80) König, B.; Pitsch, W.; Klein, M.; Vasold, R.; Prall, M.; Schreinder, P. R. *J. Org. Chem.* **2001**, *66*, 1742.

(81) Coalter, N. L.; Conclino, T. E.; Streib, N. E.; Hughes, C. G.; Rheinhold, A.; Zaleski, J. M. *J. Am. Chem. Soc.* **2000**, *122*, 3112.

(82) Bergman, R. *Acc. Chem. Res.* **1973**, *6*, 25.

(83) Groneberg, R. D.; Miyazaki, T.; Stylianides, N. A.; Schulze, T. J.; Stahl, W.; Schreiner, E. P.; Suzuki, T.; Iwabuchi, Y.; Smith, A. L.; Nicolaou, K. C. *J. Am. Chem. Soc.* **1993**, *115*, 7593.

(84) Smith, A. L.; Pitsinos, E. N.; Hwang, C. K.; Mizuno, Y.; Saimoto, H.; Scarlato, G. R.; Suzuki, T.; Nicolaou, K. C. *J. Am. Chem. Soc.* **1993**, *115*, 7612.

(85) Morita, K.; Kobayashi, S. *Tetrahedron Lett.* **1966**, 573.

(86) Morita, K.; Kobayashi, S. *Chem. Pharm. Bull.* **1967**, *15*, 988.

(87) Wratten, S. J.; Faulkner, D. J. *J. Org. Chem.* **1976**, *41*, 2465.

(88) Gmelin, R.; Susilo, R.; Fenwick, G. R. *Phytochemistry* **1981**, *20*, 2521.

(89) Kim, Y. H. In *Organic Sulfur Chemistry. Biochemical Aspects*; Oae, S., Okuyama, T., Eds.; CRC Press: Tokyo, 1992, p 137.

(90) Anthoni, U.; Christophersen, C.; Madsen, J. O.; Wium-Andersen, S.; Jacobsen, V. *Phytochemistry* **1980**, *19*, 1228.

(91) Anthoni, U.; Christophersen, C.; Jacobsen, V.; Svendsen, A. *Tetrahedron* **1982**, *38*, 2425.

(92) Copp, B. R.; Blunt, J. W.; Munro, M. H. G. *Tetrahedron Lett.* **1989**, *30*, 3703.

(93) Pearce, A. N.; Babcock, R. C.; Battershill, C. N.; Lambert, G.; Copp, B. R. *J. Org. Chem.* **2001**, *66*, 8257.

(94) Litaudon, M.; Guyot, M. *Tetrahedron Lett.* **1991**, *32*, 821.

(95) Litaudon, M.; Trigalo, F.; Martin, M.-T.; Frappier, F.; Guyot, M. *Tetrahedron* **1994**, *50*, 5323.

(96) Davidson, B. S.; Molinski, T. F.; Barrows, L. R.; Ireland, C. M. *J. Am. Chem. Soc.* **1991**, *113*, 4709.

(97) Greer, A. *J. Am. Chem. Soc.* **2001**, *123*, 10379.

(98) Brzostowska, E. M.; Greer, A. *J. Am. Chem. Soc.* **2003**, *125*, 396.

(99) Ford, P. W.; Davidson, B. S. *J. Org. Chem.* **1993**, *58*, 4522.

(100) Behar, V.; Danishefsky, S. J. *J. Am. Chem. Soc.* **1993**, *115*, 7017.

(101) Brewer, D.; Rahman, R.; Safe, S.; Taylor, A. *Chem. Commun.* **1968**, 1571.

(102) Rahman, R.; Safe, S.; Taylor, A. *J. Chem. Soc. C.* **1969**, 1665.

(103) Hodges, R.; Shannon, J. S. *Austral. J. Chem.* **1966**, *19*, 1059.

(104) Safe, S.; Taylor, A. *J. Chem. Soc. C.* **1970**, 432.

(105) Francis, E.; Rahman, R.; Safe, S.; Taylor, A. *J. Chem. Soc. Perkin. Trans. 1* **1972**, 470.

(106) Safe, S.; Taylor, A. *Chem. Commun.* **1969**, 1466.

(107) Safe, S.; Taylor, A. *J. Chem. Soc. C.* **1971**, 1189.

(108) Murdock, K. C.; Angier, R. B. *Chem. Commun.* **1970**, 55.

(109) Coffen, D. L.; Katonak, D. A.; Nelson, N. R.; Sencilio, F. D. *J. Org. Chem.* **1977**, *42*, 948.

(110) Herschield, J. D. M.; Tijhuis, M. W.; Noordik, J. H.; Ottenheijm, H. C. J. *J. Am. Chem. Soc.* **1979**, *101*, 1159.

(111) Sato, T.; Hino, T. *Tetrahedron* **1976**, *32*, 507.

(112) Curtis, P. J.; Greatbanks, D.; Hesp, B.; Cameron, A. F.; Freer, A. A. *J. Chem. Soc. Perkin. Trans. 1* **1977**, 180.

(113) Strunz, G. M.; Kakushima, M.; Stillwell, M. A. *Can. J. Chem.* **1974**, *53*, 295.

(114) Minato, H.; Matsumoto, M.; Katayama, T. *J. Chem. Soc. Perkin. Trans. 1* **1973**, 1819.

(115) Ahmed, F. R.; Przybylska, M. *Acta Cryst.* **1977**, *B33*, 168.

(116) Saito, T.; Koyoma, K.; Natori, S.; Iitaka, Y. *Tetrahedron Lett.* **1985**, *26*, 4731.

(117) Schoberl, A.; Wagner, A. *Methoden der Organishen Chemie*; 4th ed.; Houben-Weyl: Stuttgart, **1955**; Vol. 9; p.87.

(118) Clayton, J. O.; Etzler, D. H. *J. Chem. Soc.* **1974**, *69*, 974.

(119) Buckman, J. D.; Field, L. *J. Org. Chem.* **1967**, *32*, 454.

(120) Roberts, D.; Born, M.; Mieloszynski, J. L.; Paquer, D. *Phosphorus, Sulfur and Silicon And The Related Elements* **1993**, *83*, 49.

(121) Reid, E. E. *Organic Chemistry of Bivalent Sulfur*; Chemical Publishing Company: New York, **1960**; Vol. 3; p.387.

(122) Vineyard, B. D. *J. Org. Chem.* **1966**, *31*, 601.

(123) Otten, S.; Frohlich, R.; Haufe, G. *Heterocycles* **1999**, *51*, 505.

(124) Westlake Jr., H. E.; Laquer, H. L.; Smyth, C. P. *J. Am. Chem. Soc.* **1949**, *72*, 436.

(125) Wilson, R. M.; Buchanan, D. N. In *Methodicum Chimicum*; Zimmer, H., Niedenzu, K., Eds.; Thieme: New York, 1976; Vol. 7 Chapter 33.

(126) Hayashi, S.; Furukawa, M.; Yamamoto, J.; Hamamura, K. *Chem. Pharm. Bull.* **1967**, *15*, 1310.

(127) Capozzi, G.; Capperucci, A.; Degl'Innocenti, A.; Del Duce, R.; Menichetti, S. *Tetrahedron Lett.* **1989**, *30*, 2991.

(128) Harpp, D. N.; Hou, Y.; Abu-Yousef, I. A. *Tetrahedron Lett.* **2000**, *41*, 7809.

(129) Harpp, D. N.; Rys, A. Z. *Tetrahedron Lett.* **2000**, *41*, 7169.

(130) Hansen, H. C.; Senning, A.; Hazell, R. G. *Tetrahedron* **1985**, *41*, 5145.

(131) Kawamura, S.; Nakabayashi, T.; Horii, T.; Hamada, M. *Annual Report of the Radiation Center of Osaka Prefecture* **1977**, *18*, 81.

(132) Steudel, R.; Schmidt, H. *Chem. Ber.* **1994**, *127*, 1219.

(133) Steudel, R.; Kruger, P.; Florian, I.; Kustos, M. *Z. Anorg. Allg. Chem.* **1995**, *621*, 1021.

(134) Ricci, J. S.; Bernal, I. *J. Chem. Soc. (B)* **1979**, 1928.

(135) Ariyan, Z. S.; Wiles, L. A. *J. Chem. Soc.* **1962**, 4709.

(136) Yamomoto, K.; Jikei, M.; Miyatake, K.; Katoh, J.; Nishide, H.; Tsuchida, E. *Macromolecules* **1994**, *27*, 4312.

(137) Harpp, D. N.; Back, T. G. *Tetrahedron Lett.* **1972**, *15*, 1481.

(138) Harpp, D. N.; Steliou, K.; Chan, T. H. *J. Am. Chem. Soc.* **1978**, *100*, 1222.

(139) Sullivan, A. B.; Boustany, K. *Int. J. Sulfur Chem., A* **1971**, *1*, 207.

(140) Harpp, D. N.; Ash, D. K.; Back, T. G.; Gleason, J. G.; Orwig, B. A.; VanHorn, W. E.; Snyder, J. P. *Tetrahedron Lett.* **1970**, *11*, 3551.

(141) Lundin, R. H. L.; Norén, B. E.; Edlund, P. O. *Tetrahedron Lett.* **1994**, *35*, 6339.

(142) Böhme, H.; Van Ham, G. *Justus Liebigs Ann. Chem.* **1958**, *617*, 62.

(143) Von Szczepanaski, C.; Heindl, J.; Schroeder, E.; Kessler, H. J.; Redmann, U. Germany Patent, **1972**

(144) Nakabayashi, T.; Tsurugi, J. *J. Org. Chem.* **1961**, *26*, 2482.

(145) Kresze, G.; Patzscheke, J. *Chem. Ber.* **1960**, *93*, 380.

(146) Mott, A. W.; Barany, G. *Synthesis* **1984**, 657.

(147) Aberkane, O.; Mieloszynski, J. L.; Roberts, D.; Born, M.; Paquer, D. *Phosphorus, Sulfur and Silicon And The Related Elements* **1993**, *79*, 245.

(148) Harpp, D. N.; Ash, D. K. *Int. J. Sulfur Chem., A* **1971**, *1*, 211.

(149) Harpp, D. N.; Derbesy, G. *Tetrahedron Lett.* **1994**, *35*, 5381.

(150) Steudel, R.; Kustos, M.; Pridöhl, M.; Westphal, U. *Phosphorus, Sulfur and Silicon And The Related Elements* **1994**, *93-94*, 61.

(151) Steudel, R.; Münchow, V.; Pickardt, J. *Z. Anorg. Allg. Chem.* **1996**, *622*, 1594.

(152) Steudel, R.; Kustos, M. *Phosphorus, Sulfur and Silicon And The Related Elements* **1991**, *62*, 127.

(153) Steudel, R.; Förster, S.; Albertsen, J. *Chem. Ber.* **1991**, *124*, 2357.

(154) Steudel, R.; Kustos, M. *J. Org. Chem.* **1995**, *60*, 8056.

(155) Steudel, R.; Pridöhl, M.; Buschmann, J.; Luger, P. *Chem. Ber.* **1995**, *128*, 725.

(156) Steudel, R.; Kustos, M.; Pickardt, J.; Albertsen, J. *Z. Naturforsch. Part B: Chem Sci.* **1993**, *48*, 928.

(157) Albertsen, J., Technical University of Berlin, **1993**.

(158) Steudel, R.; Hassenberg, K.; Münchow, V.; Schumann, O.; Pickardt, J. *Eur. J. Inorg. Chem.* **2000**, 921.

(159) Steudel, R.; Schumann, O.; Buschmann, J.; Luger, P. *Angew. Chem. Int. Ed. Engl.* **1998**, *37*, 2377.

(160) Roesky, H. W.; Zamankhan, H.; Bats, J. W.; Fuess, H. *Angew. Chem. Int. Ed. Engl.* **1980**, *19*, 125.

(161) Steudel, R.; Schmidt, H. *Chem. Ber.* **1994**, *127*, 1219.

(162) Ossenkamp, G. C.; Kemmitt, T.; Johnston, J. H. *Journal of Colloid and Interface Science* **2002**, *249*, 464.

(163) Verma, A. K.; Rauchfuss, T. B.; Wilson, S. R. *Inorg. Chem.* **1995**, *34*, 3072.

(164) Steudel, R.; Hassenberg, K.; Pickardt, J. *Eur. J. Org. Chem.* **2001**.

(165) Verma, A. K.; Rauchfuss, T. B. *Inorg. Chem.* **1995**, *34*, 6199.

(166) Bloomfield, G. F. *J. Chem. Soc.* **1947**, *60*, 1547.

(167) Sato, R.; Satoh, S.-i.; Saito, M. *Chemistry Letters* **1990**, 139.

(168) Chenard, B. L.; Miller, T. J. *J. Org. Chem.* **1984**, *49*, 1221.

(169) Shields, T. C.; Kurtz, A. N. *J. Am. Chem. Soc.* **1969**, *91*, 5415.

(170) Bartlett, P. D.; Ghosh, T. *J. Org. Chem.* **1987**, *52*, 4937.

(171) Emsley, J.; Griffiths, D. W.; Jayne, G. J. J. *J. Chem. Soc. Perkin. Trans. 1* **1979**, 228.

(172) Sugihara, Y.; Takeda, H.; Nakayama, J. *Eur. J. Org. Chem.* **1999**, 597.

(173) Ando, W.; Tokitoh, N.; Kabe, Y. *Phosphorus, Sulfur and Silicon And The Related Elements* **1991**, *58*, 179.

(174) Takeda, N.; Tokitoh, N.; Imakubo, T.; Goto, M.; Okazaki, R. *Bull. Chem. Soc. Japan* **1995**, *68*, 2757.

(175) Bloomfield, G. F. *J. Chem. Soc.* **1947**, *60*, 1546.

(176) Féher, F.; Langer, M. *Tetrahedron Lett.* **1971**, *12*, 2125.

(177) Nakabayashi, T.; Tsurugi, J.; Yabuta, T. *J. Org. Chem.* **1964**, *29*, 1236.

(178) For a review on compounds containing the S=S bond see: Turnbull, K.; Kutney, G. W. *Chem. Rev.* **1982**, *82*, 333

(179) Foss, O. *Acta Chem. Scand.* **1950**, *4*, 404.

(180) Green, A. C. *J. Soc. Chem. Ind. London* **1919**, *38*, 459R.

(181) Gerbaux, P.; Salpin, J.-Y.; Bouchouxb, G.; Flammang, R. *Int J Mass Spectrom* **2000**, *195/196*, 239–249.

(182) Steudel, R. *Z. Anorg. Allg. Chem.* **1968**, 180.

(183) Steudel, R. *Z. Naturforsch. B* **1972**, *27B*, 469.

(184) Steudel, R.; Drozdova, Y.; Miaskiewicz, K.; Hertwig, R. H.; Koch, W. *J. Am. Chem. Soc.* **1997**, *119*, 1900.

(185) Marsden, C. J.; Smith, B. J. *J. Phys. Chem.* **1988**, *92*, 347.

(186) Schleyer, P. v. R.; Bickelhaupt, F. M.; Solà, M. *J. Comput. Chem.* **1995**, *16*, 465.

(187) Solà, M.; Mestres, J.; Carbó, R.; Duran, M. *J. Am. Chem. Soc.* **1994**, *116*, 5909.

(188) Bock, H.; Solouki, B. *Inorg. Chem.* **1977**, *16*, 665.

(189) Stevenson, D. P.; Beach, J. Y. *J. Am. Chem. Soc.* **1938**, *60*, 2872.

(190) Winnewisser, G.; Winnewisser, M.; Gordy, W. *J. Chem. Phys.* **1968**, *49*, 3465.

(191) Van Wart, H. E.; Cardinaux, F.; Scheraga, H. A. *J. Phys. Chem.* **1976**, *80*, 625.

(192) Yokozeki, A.; Bauer, S. H. *J. Phys. Chem.* **1976**, *80*, 618.

(193) Kushner, L. M.; Gorin, G.; Smyth, C. P. *J. Am. Chem. Soc.* **1950**, *72*, 477.

(194) Steudel, R.; Steudel, Y.; Miaskiewicz, K. *Chem. Eur. J.* **2001**, *7*, 3281.

(195) Steudel, R.; Laitinen, R. S.; Pakkanen, T. A. *J. Am. Chem. Soc.* **1987**, *109*, 710.

(196) Still, I. W. J.; Reed, J. N.; Turnbull, K. *Tetrahedron Lett.* **1979**, *20*, 1481.

(197) Baechler, Raymond D.; Daley, S. K. *Tetrahedron Lett.* **1978**, *19*, 101.

(198) Still, I. W. J.; Hasan, S. K.; Turnbull, K. *Synthesis* **1977**, 468.

(199) Still, I. W. J.; Hasan, S. K.; Turnbull, K. *Can. J. Chem.* **1978**, *56*, 1423.

(200) Baechler, Raymond D.; Daley, S. K.; Daly, B.; McGlynn, K. *Tetrahedron Lett.* **1978**, *19*, 105.

(201) Bálint, J.; Rákosi, M.; Bognár, R. *Phosphorus and Sulfur* **1979**, *6*, 23.

(202) Baechler, Raymond D.; San Filippo, L. J.; Schroll, A. *Tetrahedron Lett.* **1981**, *22*, 5247.

(203) Oae, S.; Yagihara, T.; Okabe, T. *Tetrahedron* **1972**, *28*, 3203.

(204) Oae, S.; Nakanishi, A.; Tsujimoto, N. *Tetrahedron* **1972**, *28*, 2981.

(205) Still, I. W. J.; Turnbull, K. *Synthesis* **1978**, 540.

(206) Micetich, R. G. *Tetrahedron Lett.* **1976**, *17*, 971.

(207) Cookson, R. C.; Parsons, P. J. *J. Chem. Soc. Chem. Commun.* **1978**, 822.

(208) Baechler, R. D.; Hummel, J. P.; Mislow, K. *J. Am. Chem. Soc.* **1973**, *95*, 4442.

(209) Höfle, G.; Baldwin, J. E. *J. Am. Chem. Soc.* **1971**, *93*, 6307.

(210) Exclusion of other mechanistic possibilities in the thermal isomerization of allyl-S_n-allyl and derivatives thereof, wherein $n = 2, 3$, is covered in detail in: Tidd, B. K. *Int. J. Sulfur Chem., C* **1971**, *6*, 101. Here it has been demonstrated that allylically unsaturated di- and trisulfides readily undergo a thermal [1,5]-sigmatropic rearrangement which results in *cis*, *trans*-isomerization of substituted compounds.

(211) Challenger, F.; Greenwood, D. *J. Chem. Soc.* **1950**.

(212) Green, M.; Lown, E. M.; Strausz, O. P. *J. Am. Chem. Soc.* **1984**, *106*, 6938.

(213) Brandt, G. A. R.; Emeleus, H. J.; Haszeldine, R. N. *J. Chem. Soc.* **1952**, 2198.

(214) Stepanov, B. I.; Rodionov, V. Y.; Chibisova, T. A. *J. Org. Chem. USSR (Engl. Transl.)* **1974**, *10*, 78.

(215) Turnbull, K.; Kutney, G. W. *Chem. Rev.* **1982**, *82*, 333.

(216) Drabowicz, J.; Oae, S. *Chem. Lett.* **1977**, 767.

(217) Soysa, H. S. D.; Weber, William P. *Tetrahedron Lett.* **1978**, *19*, 235.

(218) Tebbe, F. N.; Wasserman, E.; Peet, W. G.; Vatvars, A.; Hayman, A. C. *J. Am. Chem. Soc.* **1982**, *104*, 49.

(219) Benson, S. W. *Chem. Rev.* **1978**, *78*, 23.

(220) Barnard, D.; Houseman, T. H.; Porter, M.; Tidd, B. K. *Chem. Commun.* **1969**, 371.

(221) Wong, M. W.; Steudel, Y.; Steudel, R. *Chem. Phys. Lett.* **2002**, *364*, 387.

(222) Field, L. In *Organic Chemistry of Sulfur*; Oae, S., Ed.; Plenum Press: New York, 1977, p 303.

(223) Foss, O. In *Organic Sulfur Compounds*; Kharasch, N., Ed.; Pergammon Press Inc.: New York, 1961; Vol. 1, p 75.

(224) The Cambridge Crystallographic Database.

(225) Steudel, R.; Laitinen, R. S.; Weiss, R. *J. Chem. Soc. Dalton Trans.* **1986**, 1095.

(226) Lucchini, V.; Modena, G.; Pasquato, L. *J. Chem. Soc. Chem. Commun.* **1994**, 1565.

(227) A more detailed investigation on the origins of the rotational barriers about S-S bonds is covered in Chapter 2.

(228) Hubbard, W. N.; Douslin, D. R.; McCullough, J. P.; Scott, D. W.; Todd, S. S.; Messerly, J. F.; Hossenlopp, I. A.; George, A.; Waddington, G. *J. Am. Chem. Soc.* **1958**, *80*, 3547.

(229) Allinger, N. L.; Hickey, M. J.; Kao, J. *J. Am. Chem. Soc.* **1976**, *98*, 2741.

(230) El-Sabban, M. Z.; Scott, D. W. *U.S. Bur. Mines, Bull.* **1970**, *654*.

(231) Scoot, D. W.; Finke, H. L.; Gross, M. E.; Guthrie, G. B.; Huffman, H. M. *J. Am. Chem. Soc.* **1950**, *72*, 2424.

(232) Dixon, D. A.; Zeroka, D.; Wendoloski, J. J.; Wasserman, Z. R. *J. Phys. Chem.* **1985**, *89*, 5334.

(233) Steudel, R.; Drozdova, Y.; Miaskiewicz, K. *Z. Naturforsch. B* **1995**, *50*, 889.

(234) Harpp, D. N.; Snyder, J. P. *Tetrahedron Lett.* **1978**, *19*, 197.

(235) Donohue, J.; Schoemaker, V. *J. Chem. Phys.* **1948**, *16*, 92.

(236) Howie, R. A.; Wardell, J. L. *Acta Crystallogr.* **1996**, *C52*, 1533.

(237) Cox, P. J.; Wardell, J. L. *Acta Crystallogr.* **1997**, *C53*, 122.

(238) Ostrowski, M.; Jeske, J.; Jones, P. G.; du Mont, W.-W. *Chem. Ber.* **1993**, *126*, 1355.

(239) Gaensslen, M.; Minkwitz, R.; Molzbeck, W.; Oberhammer, H. *Inorg. Chem.* **1992**, *31*, 4147.

(240) Meyer, C.; Mootz, D.; Bäck, B.; Minkwitz, R. *Z. Naturforsch. B* **1997**, *52*, 69.

(241) Berthold, H. J. *Z. Anorg. Allg. Chem.* **1963**, *325*, 237.

(242) Gilardi, R. D.; Flippen-Anderson, J. L. *Acta Crystallogr. Sect. C.* **1985**, *41*, 72.

(243) Steudel, R.; Bergmann, K.; Kustos, M. *Z. Anorg. Allg. Chem.* **1994**, *620*, 117.

(244) Steudel, R.; Bergemann, K.; Buschmann, J.; Luger, P. *Inorg. Chem.* **1996**, *35*, 2184.

(245) Steudel, R.; Bergemann, K.; Buschmann, J.; Luger, P. *Angew. Chem. Int. Ed. Engl.* **1993**, *32*, 1702.

(246) Bats, J. W. *Acta Crystallogr. Sect. B.* **1977**, *33*, 2264.

(247) Shen, Q.; Wells, C.; Hagen, K. *Inorg. Chem.* **1998**, *37*, 3895.

Chapter 8

Synthesis of Acyclic Aromatic Polysulfides (Ar-S_n-Ar; $n > 2$)

8.1 Synthesis of Aromatic Tri- and Tetrasulfides

As part of our research effort dedicated to the pursuit of rapid and effective sulfurizing agents of oligonucleotides, we decided to test symmetric tri- and tetrasulfides as possible substrates. We thus required pure samples of a variety of symmetric polysulfides.

We report a modification of two literature procedures[1,2] (Scheme **63**) to form aromatic trisulfides **257a-d**, wherein yields and purity are significantly improved. We also report for the first time the synthesis of a corresponding set of aromatic tetrasulfides **258a-d**.[§] All compounds were characterized by ^{1}H NMR, ^{13}C NMR, MS, and HRMS or elemental analysis; crystal structures of **257b** and **258b** were also obtained.[3]

To solutions of easily accessible aromatic thiols **259a-d** and equimolar pyridine in anhydrous diethyl ether were added a freshly distilled solution of either sulfur dichloride SCl_2 (for **257a-d**) or sulfur monochloride S_2Cl_2 (for **258a-d**) at -78 °C (Scheme **63**). After workup, the sample was usually analytically pure but could be recrystallized in the freezer from *n*-pentane. The procedure was readily scaled up to 10 g.

[§] This work has been published: Zysman-Colman, E.; Harpp, D. N. *J. Org. Chem.* **2003**, *68*, 2487.

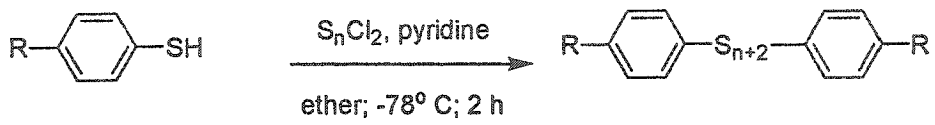

R = H	**259a**
R = CH_3	**259b**
R = Br	**259c**
R = NO_2	**259d**

R = H	n = 1 **257a**; n = 2 **258a**
R = CH_3	n = 1 **257b**; n = 2 **258b**
R = Br	n = 1 **257c**; n = 2 **258c**
R = NO_2	n = 1 **257d**; n = 2 **258d**

Scheme **63**.

The use of freshly distilled sulfur monochloride, ether as the solvent, with pyridine as a hydrochloride sink and possible activator, were all necessary components of the reaction in order to ensure the purity of the product and its high yield (Table **69**). Maintaining the temperature at -78 °C may also serve to increase purity as compared with previous syntheses.[4,5] We investigated this criterion by repeating the reaction for the production of **258b** at 0 °C and at room temperature, Table **70**. The yields remained high but decreased slightly with increasing temperature; the purity of the sample increased slightly with increasing temperature. It therefore seems that the coupling rate of the second equivalent of thiol to the intermediate (Scheme **64**) is faster than its potential decomposition.

Table 69. Data for Tri- and Tetrasulfides

Entry	Thiol	S_nCl_2[a]	Product	Yield[b] (%)	Mp (°C)	lit. Mp (°C)
1	**259a**	1	**257a**	61	62-63	*ca.* 5[6]
2		2	**258a**	71	41-42	34-35[7]
3	**259b**	1	**257b**	97	88-89	82-84[4]
4		2	**258b**	99	73-75	oil[8, d], 71-72[9]
5	**259c**	1	**257c**	97	72-75	68-71[5], 70-71[10]
6		2	**258c**	97	64-68	
7	**259d**	1	**257d**	90	140-145[c]	114-116[10]
8		2	**258d**	99	163-167	

a) n = 1 for sulfur dichloride, n = 2 for sulfur monochloride. b) Yields reported after one recrystallization. c) Sample turned dark yellow at 131-133 °C. d) The combustion analysis in the reference is not accurate and the claim of synthesis should be questioned.

Table 70. Temperature Study of Thiol Coupling with Sulfur Monochloride

Entry	Product	Temperature (°C)	Yield[b] (%)	Mp (°C)
1	**258b**	-78	99	73-75
2	**258b**	0	91	71-72
3	**258b**	RT[a]	86	74-75

a) RT = 25 ± 1 °C. b) Yields reported after one recrystallization.

The addition of pyridine as the amine base distinguishes this method from previous uses of sulfur dichloride or sulfur monochloride as coupling agents. While this is a simple alteration in the normal procedure, the greatly enhanced yields and purity clearly demonstrates the advantage. It is likely that the increased yield and higher purity is because the pyridinium salt is insoluble in the ether solvent. Upon addition of the yellow chlorosulfane to the thiol/pyridine solution, an immediate conversion to a white precipitate was observed. The precipitation of this pyridinium salt by-product apparently

drives the reaction to completion. It may also be that the activated intermediate is that of a sulfenyl pyridinium complex or a thiosulfenyl pyridinium complex (Scheme 64). Activated complexes of sulfur monochloride are not without precedent.[11]

The nitro analogues, **257d** and **258d** also precipitated from solution. In all cases, no higher order polysulfides were observed upon completion of the reaction. This proved to be important and beneficial as separation of polysulfides by chromatography is often problematic as a result of their very similar properties.

Compound **257a** had previously been reported to be an oil;[5,12,13] however, after being placed in the freezer in *n*-pentane for 24 h, pure crystals formed.

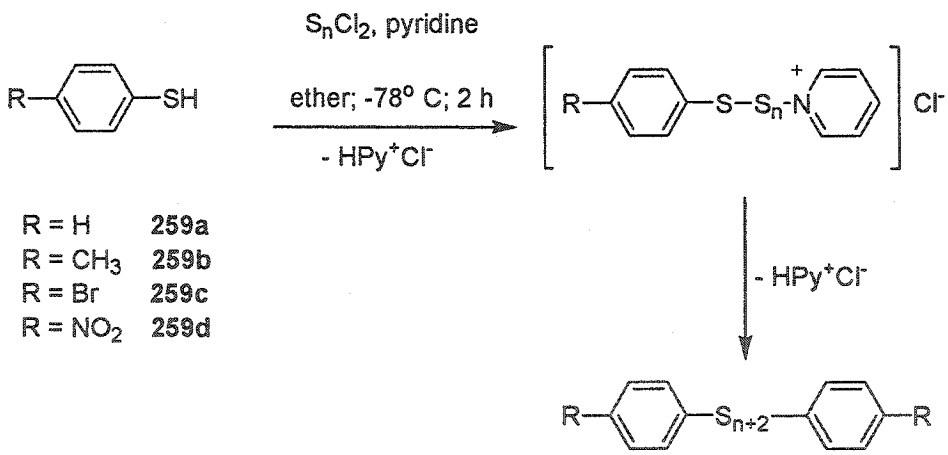

Scheme 64.

This optimized method provides a convenient preparation of acyclic aromatic tri- and tetrasulfides in high yield and purity from readily accessible materials under very mild conditions.

8.2 Physical Properties and Conformational Analysis of Aromatic Tri- and Tetrasulfides

Crystal structures of **257b** and **258b** were determined (Figure **36**). The geometry of these aromatic polysulfides for the most part is unexceptional[14-16] compared to that previously reported for others of this class (aromatic polysulfides), with an average S-S bond length of 2.045 Å for the two. The S-S-S bond angles are comparable with other aromatic trisulfides (*ca.* 107°).[14-16] Interestingly, whereas the conformation of **257b** contains left-handed helicity (P,P), that of **258b** is less ordered with a (M,P,P) conformation; the S-S dihedral angles are *ca.* 85°. This disorder is unusual in tetrasulfides.

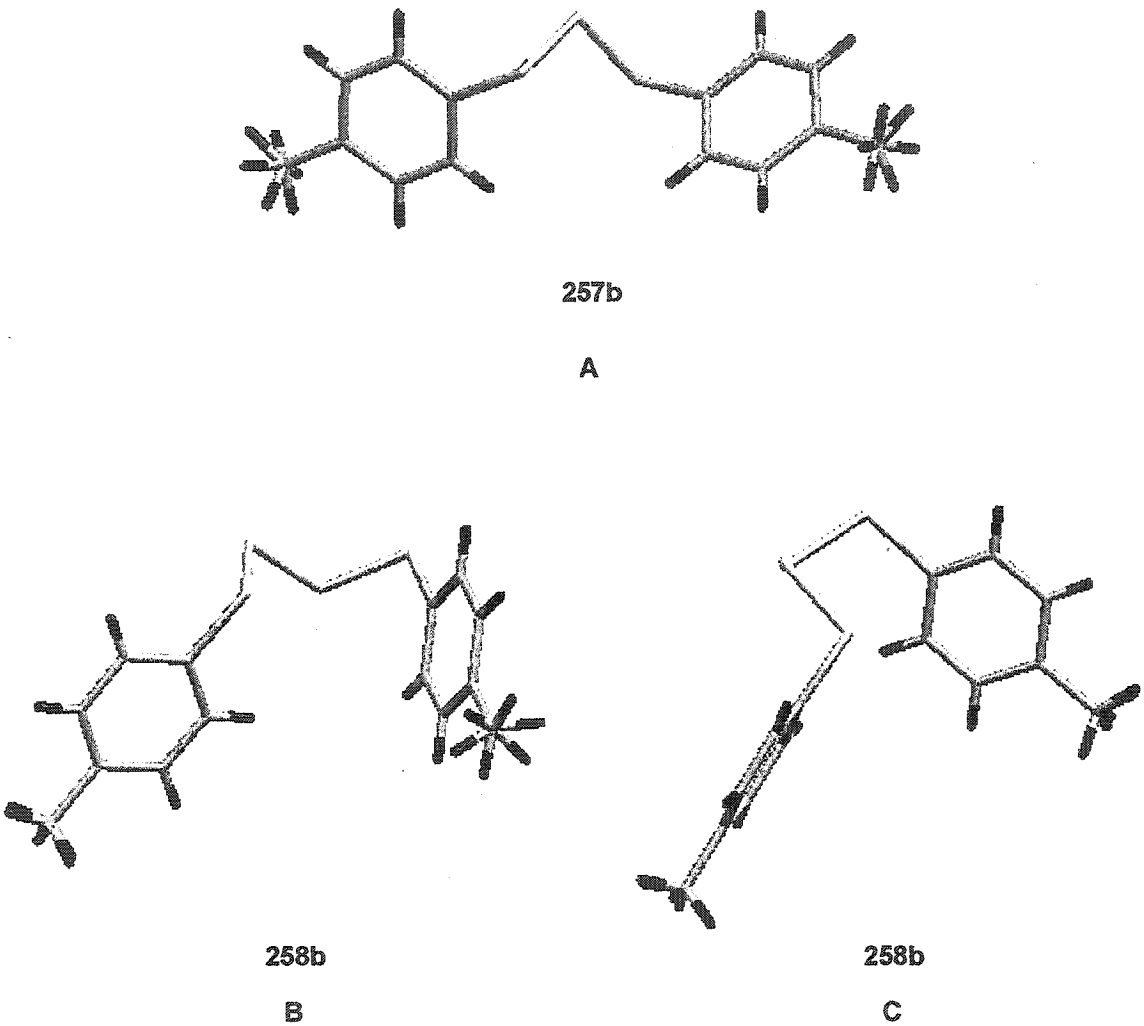

Figure 36. Stick representations of A) **257b**; B) **258b**; C) Newman projection of **258b**

Bis(4-methylbenzene)disulfide **260b** is a white solid whereas **257b** is light yellow and **258b** is dark yellow. We observed an initial correlation between the number of sulfur atoms in the polysulfide chain and the colour of the compound. The chromophore was being altered to absorb at longer wavelength with the inclusion of an increasing number of sulfur atoms. We thus undertook a UV study of **257b**, **258b** and **260b**, Figure 37. We hypothesized that there may exist a correlation between the number of sulfurs present in

the polysulfide chain and the observed λ_{max}. The λ_{max} values unfortunately were not diagnostic for the observed colour change. This may be due to the fact that we were at the edge of detection of the instrument with a larger signal-to-noise ratio in this region (*ca.* 250 nm); the observed yellow colours are due to our perception of the entire absorbance spectrum of each compound, a spectrum that would be expected to be detected at these short wavelengths.

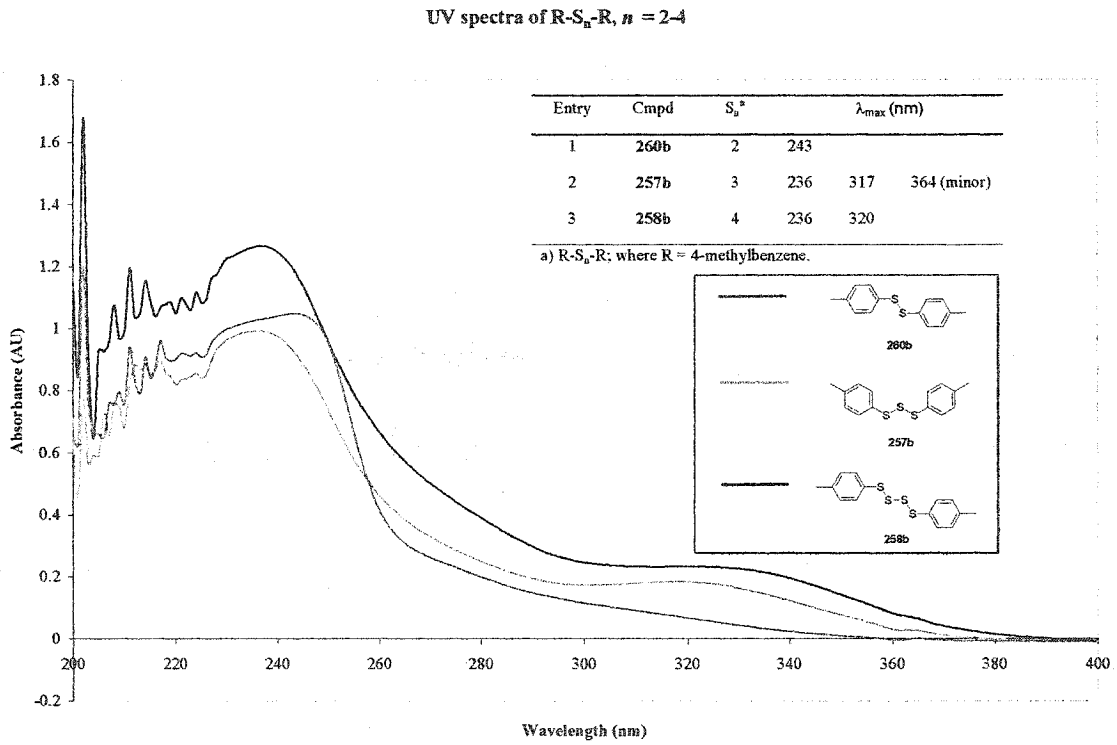

Figure 37. UV spectra of **257b**, **258b** and **260b** determined in $CDCl_3$

It has been shown that the downfield shifts of protons on carbons adjacent to polysulfides increase incrementally with increasing numbers of sulfur atoms.[17-20] Interestingly, the ^1H NMR chemical shift of the of the tolyl peak moved downfield as the number of sulfurs increased in the polysulfide chain from 1-6. This is graphically shown in Figure **38**. It is believed that we might be able to exploit the long-range influence of

the polysulfide moiety on the tolyl group by using this resolvable signal as a probe in kinetic reactions (*cf.* Chapter 9). To our knowledge this type of long-range communication of chemical shift information is rare. In this case it is most likely due to the rigidity of the tolyl group which, in essence, acts as if it were a methyl group as well as the ability of the benzene ring to act as a medium for communicating the number of sulfurs present in the polysulfide chain. This translation of ^{1}H NMR chemical information did not extend to ^{13}C NMR which remained virtually unchanged.

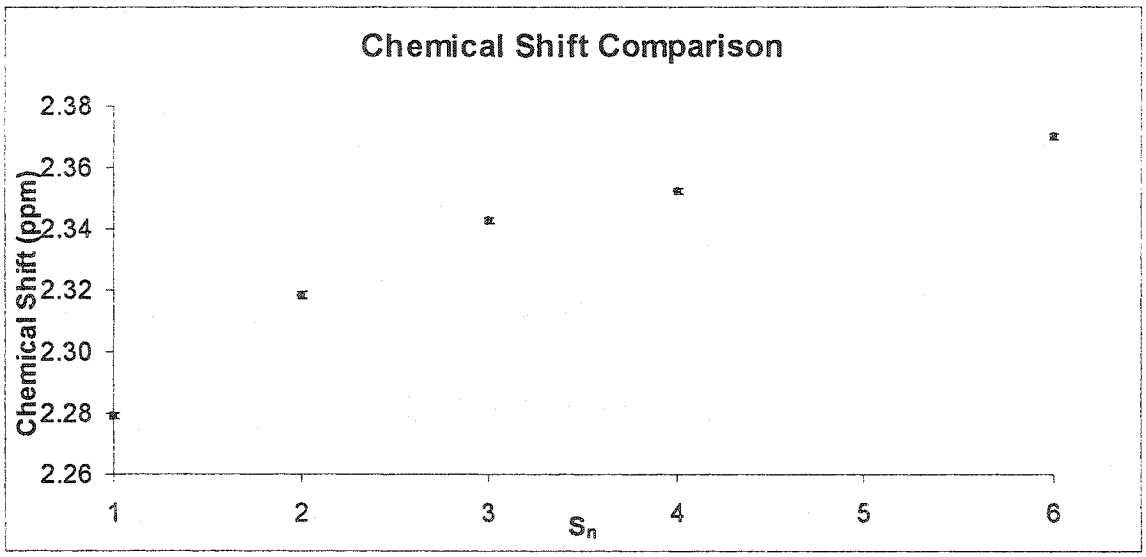

Figure **38**. Chemical shift of the 4-methylbenzene (tolyl) groups of **259b-262b**. Average error of 0.001 ppm estimated based on the standard deviation afforded from 10 independent ^{1}H NMRs of **257b**, **259b** and **260b**; the ^{1}H NMR of **258b** and **262b** were each determined twice with similar error.

Polysulfides can equilibrate thereby complicating product analysis.[21] This phenomenon can be accelerated in the presence of light and/or heat amongst other catalysts. Mass spectrometry may also be misleading as parent peaks in a mass spectrum can appear as a result of modest isomerization of the compound.[22] We were fortunate to

be able to detect the molecular ion in all cases. Moreover for **257a**, **257b**, **258a** and **258b**, we were able to detect successive loss of all labile sulfurs. For **257c**, **257d**, **258c** and **258d** this was only partially successful owing to the thermal lability of the Br and NO_2 groups.

All compounds in Table **69** were bench-stable for months; however, on exposure to light they would decompose in a matter of hours, forming different-order polysulfides of n = 2-6. No special precautions need be made with respect to air exposure if the compounds are weighed and used directly. Thermally, tetrasulfides were less stable than their trisulfide counterparts. It has been suggested that the increased conformational flexibility afforded by the extra sulfur atom increases the entropy and thus lowers the thermal stability.[23] The nitro group significantly increased the thermal stability of the compounds.

8.3 An Investigation into the Synthesis of Higher Order Polysulfides *via* Sulfur Insertion

We were also interested in developing a synthetic route for higher *p*-tolyl polysulfide homologues. This was particularly important as we required authentic samples with which we could compare the ^{1}H NMRs of the product distributions in our kinetics experiments (*vide infra*, Chapter 9). We thus undertook to try and synthesize bis(4-methylbenzene) pentasulfide **261b** and bis(4-methylbenzene) hexasulfide **262b**.

Previous work has demonstrated the facile insertion of 1-,[24] 2-,[25] and 3-sulfur[26] atoms into disulfides using tritylchloropolysulfanes (Tr-S_n-Cl, n = 1-3). We were particularly attracted to the reported facile use of the stable tritylthiosulfenyl chloride **263**.

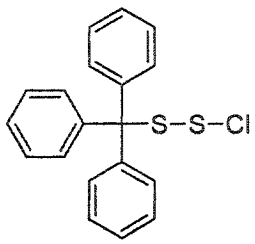

263

It was hoped that this insertion process might be extended to higher order polysulfides. The proposed mechanism of sulfur insertion is outlined in Scheme **65**. To a stirred solution of **258b** in a 1:1 mixture of CH_2Cl_2/AcOH was added equimolar **263** in CH_2Cl_2 and the mixture was allowed to stir for *ca.* 20 h at room temperature. This afforded **262b** in 91% yield. ^{1}H NMR analysis of the crude mixture indicated the presence of **262b** as well as a trityl alcohol by-product. The presence of **262b** was confirmed *via* HRMS; it is known that trityl functionalities are stable radical cations and its signal would not hinder identification of the then unknown polysulfide. As with **257b** and **258b**, the low resolution MS contained the molecular ion with peaks corresponding to the successive loss of each labile sulfur.

Attempts to synthesize **261b** in an analogous fashion from **257b** failed. The ^{1}H NMR analysis indicated the presence of mainly **258b** but also of unreacted **257b**. The presence of an unknown 4-methylbenzene group was inferred to be **261b** based on its relative chemical shift to that of other known authentic homologues. This is interesting as this

seems to mean that in this case **263** is acting mainly as a 1-sulfur transfer reagent whereas in the previous case it was acting as expected, as a 2-sulfur transfer reagent. It is unclear what accounts for this change in chemistry but sterics must be ruled out as Rys[25] had clearly shown that **260b** can insert 2 sulfurs to form **258b**.

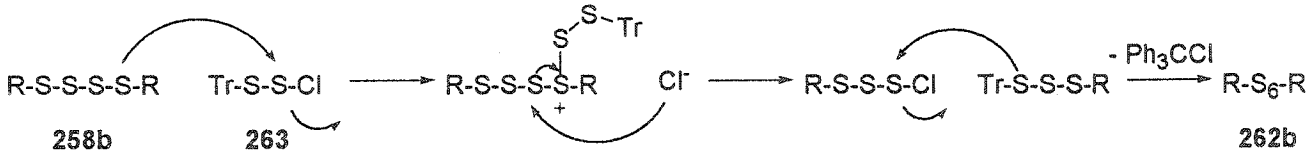

Scheme **65**. Formation of **262b** (R = 4-methylbenzene)

Originally Rys[25] had shown that the insertion reaction could be catalyzed through the addition of AcOH, which drastically reduced reaction times. This is most likely due to the stabilizing effects that the polar co-solvent imparts on the intermediates in Scheme **65**. Initial trials at comparable reaction times yielded poor conversion to desired **262b**. It was only by increasing the reaction time to 20 h that complete conversion could be attained. Nevertheless, the addition of AcOH proved crucial as without it, under similar reaction conditions, poor conversion to **262b** was observed.

We did not exploit or extend this methodology to other polysulfides or to see whether multiple 2-sulfur insertions might take place. One of our stated objectives here was to observe whether the tolyl groups for **259b-262b** were each distinctly resolvable. We have demonstrated this to be the case (*cf.* Figure **38**). However, our two step approach to the synthesis of symmetric penta- and hexasulfides may serve as an important synthetic alternative in the formation of these higher order homologues. Here there is no need to

pre-synthesize organochlorosulfanes or metallocene polysulfides; this is the standard method for the synthesis of higher order polysulfides (*vide supra* – Chapter **7.2.3**).

8.4 Synthetic Experimental Section

Synthesis of *p*-Aryl trisulfides: An example of the synthetic procedure is as follows.

A solution of thiol **259** (20 mmol, 1 equiv) and pyridine (20 mmol, 1 equiv) in 50 mL of Et_2O was allowed to stir under nitrogen at –78 °C. A solution of SCl_2 (10.0 mmol, 0.5 equiv) in 50 mL of Et_2O was added dropwise over 0.5 h. The reaction mixture was allowed to stir for a further 1.5 h. The reaction mixture was quenched with 25 mL of H_2O. The organic phase was washed 3x 25 mL of H_2O or until the aqueous phase became clear. The organic phase was dried over $MgSO_4$. This mixture was vacuum filtered, and the solvent was removed first under reduced pressure and then *in vacuo*.

Diphenyl trisulfide, 257a:

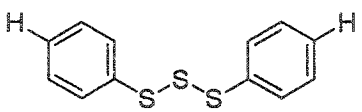

Yield: 61%; Recrystallization from *n*-pentane at -15 °C afforded light white needles; Mp 62-63 °C. (lit Mp[6] ~5 °C); ^{1}H NMR δ 7.14-7.34 (m, 6H), 7.47-7.59 (m, 4H); ^{13}C NMR δ 127.1, 127.5, 129.1, 137.0; MS (EI) *m/z* 250 ($M^{+\bullet}$), 218 ($M^{+\bullet}$ – S), 185 ($M^{+\bullet}$ – 2S) 154, 141 ($M^{+\bullet} - SC_6H_5$), 109 ($M^{+\bullet} - S_2C_6H_5$). HRMS for $C_{12}H_{10}S_3$: 249.9945. Found: 249.993(6).

Bis(4-methylbenzene) trisulfide, 257b:

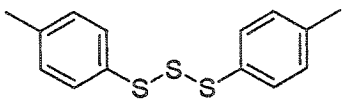

Yield: 97%; Recrystallization from *n*-pentane at -15 °C afforded light yellow needles; Mp 88-89 °C. (lit. Mp[4] 82-84 °C). ^{1}H NMR δ 2.35 (s, 6H), 7.40 (d, 4H, J_{AB} = 2.00 Hz), 7.42 (d, 4H, J_{AB} = 2.00 Hz); ^{13}C NMR δ 21.3, 129.7, 130.9, 132.8, 138.5; MS (EI) *m/z* 278 ($M^{+\bullet}$), 246 ($M^{+\bullet}$ – S), 214 ($M^{+\bullet}$ – 2S), 123 ($M^{+\bullet}$ – $S_2C_7H_7$), 91 ($M^{+\bullet}$ – $S_3C_7H_7$).

Bis(4-bromobenzene) trisulfide, 257c:

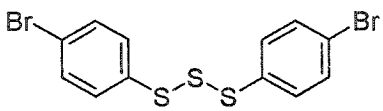

The product was a light, flaky solid. Yield: 97%; Mp 72-75 °C (lit Mp[10] 70-71 °C). ^{1}H NMR δ 7.32 (d, 4H, J_{AB} = 8.60 Hz), 7.41 (d, 4H, J_{AB} = 8.60 Hz); ^{13}C NMR δ 121.5, 129.4, 132.2, 135.7; MS (EI) *m/z* 408 ($M^{+\bullet}$), 376 ($M^{+\bullet}$ – S, 189 ($M^{+\bullet}$ – $S_2C_6H_4Br$), 108 ($M^{+\bullet}$ - $S_2C_6H_4Br_2$). Anal. Calcd for $C_{12}H_8S_3Br_2$: C, 34.85; H, 1.68; S, 23.24. Found: C, 35.30; H, 1.96; S, 23.56.

Bis(4-nitrobenzene) trisulfide, 257d:

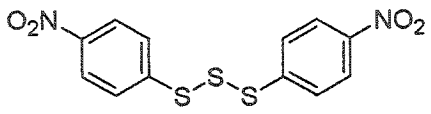

The above procedure was scaled up by a factor of 2. Upon quenching with 100 mL of H_2O, a grayish precipitate formed. This precipitate was vacuum filtered and further washed with 2x 100 mL of H_2O. The filtrate was further purified as above and the solute was dried. The products were combined to yield a tan-colored solid. Yield: 90%; Mp. 122-124 °C turning dark yellow then melting at 140-145 °C (lit. Mp[10] 114-116 °C). ^{1}H NMR δ 7.60 (d, 4H, J = 8.85 Hz), 8.17 (d, 4H, J = 8.85 Hz); ^{13}C NMR δ 124.4, 126.4, 144.0, 147.0; MS (CI) *m/z* 308 ($M^{+\bullet}$ – S). HRMS for $C_{12}H_8N_2O_4S_3$: 339.9646. Found: 339.965(7).

Synthesis of *p*-Aryl tetrasulfides. The following is a general example of the synthetic procedure. A solution of thiol **259** (40 mmol, 2 equiv) and pyridine (40 mmol, 2 equiv) in 100 mL of Et_2O was allowed to stir under nitrogen at –78 °C. A solution of S_2Cl_2 (20.0 mmol, 1 equiv) in 100 mL of Et_2O was added dropwise over 0.5 h. The reaction mixture was allowed to stir for a further 1.5 h. The reaction mixture was quenched with 100 mL of H_2O. The organic phase was washed 3x 50 mL of H_2O or until the aqueous phase became clear; the organic phase was dried over $MgSO_4$. This mixture was vacuum filtered, and the solvent was removed first under reduced pressure and then *in vacuo*.

Diphenyl tetrasulfide, 258a:

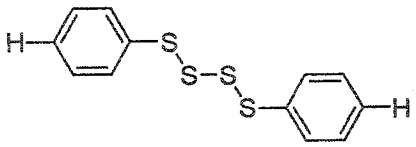

Yield: 71%; Recrystallization from *n*-pentane at -15 °C afforded light yellow needles; Mp 41-42 °C (lit. Mp[7] 34-35 °C). ^{1}H NMR δ 7.28-7.36 (m, 6H), 7.53-7.55 (m, 4H); ^{13}C NMR δ 128.3,129.1, 130.2, 136.2 ; MS (EI) *m/z* 282 ($M^{+\bullet}$), 250 ($M^{+\bullet}$ – S), 218 ($M^{+\bullet}$ – 2S), 185 ($M^{+\bullet}$ – 3S), 141 ($M^{+\bullet}$ – $S_2C_6H_5$, 109 ($M^{+\bullet}$ – $S_3C_6H_5$. HRMS for $C_{12}H_{10}S_4$: 281.9665, Found: 281.967(0).

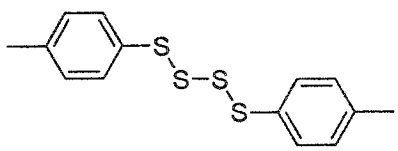

Bis(4-methylbenzene) tetrasulfide, 258b:

Yellow powder. Yield: 99%; Recrystallization from *n*-pentane at -15 °C afforded bright yellow needles; Mp 73-75 °C (lit. Mp. oil,[8] 71-72 °C[9]). ^{1}H NMR δ 2.35 (s, 6H), 7.12 (d, 4H J = 7.80 Hz), 7.44 (d, 4H, J = 7.80 Hz); ^{13}C NMR δ 21.4, 129.8, 130.9, 132.7, 138.7; MS (FAB) *m/z* 310 ($M^{+\bullet}$), 278 ($M^{+\bullet}$ – S, 246 ($M^{+\bullet}$ – 2S), 123 ($M^{+\bullet}$ – $S_3C_7H_7$); Anal. Calcd for $C_{14}H_{14}S_4$: C, 54.14; H, 4.45; S, 41.30. Found: C, 53.89; H, 4.10; S, 41.75.

Bis(4-bromobenzene) tetrasulfide, 258c:

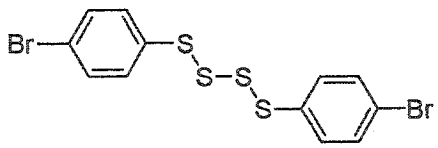

Light yellow, flaky solid. Yield: 97%; Mp 64-68 °C; ^{1}H NMR δ 7.35 (d, 4H J_{AB} = 8.40 Hz), 7.41 (d, 4H J_{AB} = 8.40 Hz); ^{13}C NMR δ 131.7, 132.3, 132.4, 132.4; MS (EI) *m/z* 440 ($M^{+\bullet}$), 408 ($M^{+\bullet}$ – S), 376 ($M^{+\bullet}$ – 2S), 189 ($M^{+\bullet}$ – $S_2C_6H_4Br$), 108 ($M^{+\bullet}$ – $S_2C_6H_4Br$). Anal. Calcd for $C_{12}H_8S_4Br_2$: C, 32.74; H, 1.83. Found: C, 32.77; H, 1.43.

Bis(4-nitrobenzene) tetrasulfide, 258d:

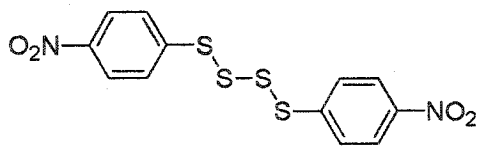

Upon quenching with 100 mL of H_2O, a grayish precipitate formed. This precipitate was vacuum filtered and further washed with 2x 100 mL of H_2O. The filtrate was further purified as above, and the solute was dried. The products were combined to yield a sandy coloured solid. Yield: 99%; Mp 163-167 °C; ^{1}H NMR δ 7.60 (d, 4H J = 8.20 Hz), 8.17 (d, 4H J = 8.20 Hz); ^{13}C NMR δ 124.4, 126.3, 144.0, 146.9; MS (CI) *m/z* 308 ($M^{+\bullet}$ – S). HRMS for $C_{12}H_8N_2O_4S_4$ + NH_4: 389.9711 Found: 389.971(6).

Attempt at the Synthesis of Bis(4-methylbenzene) pentasulfide, 261b. To a solution of bis(4-methylbenzene) trisulfide **257b** (60 mg, 0.19 mmol, 1 equiv.) in 2 mL CH_2Cl_2 and 2 mL glacial AcOH was slowly added a solution of tritylthiosulfenyl chloride[27] **263**

(65 mg, 0.19 mmol, 1 equiv) in 2 mL CH_2Cl_2 and allowed to stir at RT for 19 h. The solution was then evaporated to afford a light yellow solid which was determined by ^1H NMR to be a mixture of trityl alcohol, bis(4-methylbenzene) trisulfide **257b**, bis(4-methylbenzene) tetrasulfide **258b** and bis(4-methylbenzene) pentasulfide **261b**. The presence of bis(4-methylbenzene) trisulfide **257b** and bis(4-methylbenzene) tetrasulfide **258b** were confirmed by ^1H NMR comparison with authentic samples whereas the presence of **261b** was inferred based on the chemical shift of the CH_3 peak relative to other polysulfides.

Bis(4-methylbenzene) hexasulfide, 262b: To a solution of bis(4-methylbenzene) tetrasulfide **258b** (60 mg, 0.19 mmol, 1 equiv.) in 2 mL CH_2Cl_2 and 2 mL glacial AcOH was slowly added a solution of **263**[27] (65 mg, 0.19 mmol, 1 equiv) in 2 ml CH_2Cl_2 and allowed to stir at RT for 19 h. The solution was then evaporated to afford a light yellow solid which was determined by 1H NMR to be a 1:1 mixture of trityl alcohol:bis(4-methylbenzene) hexasulfide, **262b** (115.6 mg). This corresponds to a yield: 91%. ^1H NMR δ 2.37 (s, 6H), 7.15 (d, 4H J = 8.00 Hz), 7.48 (d, 4H J = 8.00 Hz); ^{13}C NMR δ 21.3, 127.6, 129.5, 132.7, 138.7; MS (EI) *m/z* 374 ($M^{+\bullet}$), 342 ($M^{+\bullet}$ – S), 310 ($M^{+\bullet}$ – 2S), 278 ($M^{+\bullet}$ – 3S), 246 ($M^{+\bullet}$ – 4S), 214 ($M^{+\bullet}$ – 5S), 183. HRMS for $C_{14}H_{14}S_6$: 373.9420, Found: 373.94(1)3.

8.5 References

(1) Schoberl, A.; Wagner, A. *Methoden der Organishen Chemie*; 4th ed.; Houben-Weyl: Stuttgart, **1955**; Vol. 9; p.87.

(2) Harpp, D. N.; Derbesy, G. *Tetrahedron Lett.* **1994**, *35*, 5381. The method in this article can be used to prepare the aliphatic analogues; however, the yields are not generally as high as in this modification.

(3) Harpp, D. N.; Zysman-Colman, E. *J. Org. Chem.* **2003**, *68*, 2487.

(4) Harpp, D. N.; Smith, R. A. *J. Org. Chem.* **1979**, *44*, 4140.

(5) Harpp, D. N.; Ash, D. K.; Smith, R. A. *J. Org. Chem.* **1980**, *45*, 5155.

(6) *Beilsteins Handbuchen Der Organischen Chemie*, **1965**; Vol. 6, E111; p.1047.

(7) Lechler, H.; Holzschneider, F. *Chem. Ber.* **1925**, *58*, 417.

(8) Saville, R. W. *J. Chem. Soc.* **1958**, 2880.

(9) Kawamura, S.; Horii, T.; Tsurugi, J. *J. Org. Chem.* **1971**, *36*, 3677.

(10) Feher, F.; Kurz, D. *Z. Naturforschg.* **1968**, *23 b*, 1030.

(11) Rees, C. W.; Rakitin, O. A.; Marcos, C. F.; Torroba, T. *J. Org. Chem.* **1999**, *64*, 4376.

(12) Harpp, D. N.; Granata, A. *Tetrahedron Lett.* **1976**, *35*, 3001.

(13) Capozzi, G.; Capperucci, A.; Degl'Innocenti, A.; Del Duce, R.; Menichetti, S. *Tetrahedron Lett.* **1989**, *30*, 2991.

(14) Steudel, R.; Kruger, P.; Florian, I.; Kustos, M. *Z. Anorg. Allg. Chem.* **1995**, *621*, 1021.

(15) Cox, P. J.; Wardell, J. L. *Acta Crystallogr.* **1997**, *C53*, 122.

(16) Howie, R. A.; Wardell, J. L. *Acta Crystallogr.* **1996**, *C52*, 1533.

(17) Clennan, E. L.; Stensaas, K. L. *J. Org. Chem.* **1996**, *61*, 7911.

(18) Steudel, R.; Kustos, M. *J. Org. Chem.* **1995**, *60*, 8056.

(19) Grant, D.; Van Wazer, J. R. *J. Am. Chem. Soc.* **1964**, *86*, 3012.

(20) Freeman, F.; Angeletakis, C. N.; Maricich, T. J. *Org. Magnetic Reson.* **1981**, *17*, 53.

(21) Tebbe, F. N.; Wasserman, E.; Peet, W. G.; Vatvars, A.; Hayman, A. C. *J. Am. Chem. Soc.* **1982**, *104*, 49.

(22) Litaudon, M.; Trigalo, F.; Martin, M.-T.; Frappier, F.; Guyot, M. *Tetrahedron* **1994**, *50*, 5323.

(23) Steudel, R. *Chem. Rev.* **2002**, *102*, 3905.

(24) Harpp, D. N.; Hou, Y.; Abu-Yousef, I. A.; Doung, Y. *Tetrahedron Lett.* **2001**, *42*, 8607.

(25) Harpp, D. N.; Rys, A. Z. *Tetrahedron Lett.* **2000**, *41*, 7169.

(26) Harpp, D. N.; Hou, Y.; Abu-Yousef, I. A. *Tetrahedron Lett.* **2000**, *41*, 7809.

(27) Compound **263** was generously donated by Dr. Andrzej Rys.

Chapter 9

Desulfurization of Aromatic Polysulfides with Triphenylphosphine

9.1 Introduction

As highlighted in Chapter 7, one of our goals was to determine whether structurally simple aromatic polysulfides could act as efficient sulfur transfer reagents in the synthesis of phosphorothioate oligonucleotide analogs.

Prior to biological testing, it was necessary to discover, by means of kinetics work on a model system, whether these polysulfides would indeed be efficacious. We chose triphenylphosphine (Ph_3P) as our model phosphine. Phosphines are generally weak bases but good nucleophiles. In addition, phosphorus can undergo valence expansion which makes them selective reducing agents.[1,2] Although phosphites are sulfurated in the synthesis of the nucleotides of interest, Arbuzov rearrangement would complicate the ^1H NMR product analysis.[3] Decomposition of simple aliphatic and aromatic trisulfides by phosphines has been studied previously, but only for the initial minutes of the reaction.[3-6] In addition, others[7,8] have carries out calculational studies to model the process. To our knowledge, no one had yet investigated the kinetics of desulfurization of tetrasulfides. Thus, this study should complement and expand the current understanding of the kinetics of desulfurization of polysulfides.[§]

[§] This work has been submitted: Zysman-Colman, E.; Farrell, P. G.; Harpp, D. N. *J. Sulfur Chem.*, **2003**.

9.2 Experimental Setup

9.2.1 Materials

Bis(4-methylbenzene) disulfide **260b**, 4-methylbenzenethiol, **259b**, Ph_3P and 1,3,5-tri-*t*-butylbenzene were all commercially available and were used without further purification. Bis(4-methylbenzene) trisulfide **257b** and bis(4-methylbenzene) tetrasulfide **258b** were synthesized according to the literature.[9] Deuterated chloroform ($CDCl_3$) was dried over molecular sieves.

9.2.2 Desulfurization of 257b or 258b

The following is a general example of the experimental procedure for the experiments detailed in Table 72 in Chapter **9.3.1**. A solution of 262 mg of Ph_3P (1 mmol, 1 equiv) and 278 mg of **257b** (1 mmol, 1 equiv) in 20 ml CH_2Cl_2 was allowed to stir at RT (see Table 72 for reaction times). The solvent was then removed under reduced pressure and the residue dried *in vacuo*. The resulting crude solid was chromatographed[10] (10% $CHCl_3$/hexanes slowly increasing to 80% $CHCl_3$/hexanes). For Entry 2 in Table 72 a yellow oil identified as a mixture of polysulfides **257b** and **258b**, R_f = 0.64 (50% $CHCl_3$/hexanes), and a white powder identified as triphenylphosphine sulfide $Ph_3P{=}S$, R_f = 0.47 (50% $CHCl_3$/hexanes) were the only recovered products. Yield of $Ph_3P{=}S$: 87%;[11] ^1H NMR δ 7.45 (m, 10H), 7.70 (m, 5H); ^{31}P NMR δ 44.48.

9.2.3 Instrumentation and Measurement Techniques in the Kinetics Studies

Kinetic studies were performed at 23.4 ± 0.8 °C on a 500 MHz machine. Stock solutions of **257b**, **258b** and **260b** in $CDCl_3$, each at 0.100 ± 0.002 M concentration, were kept in sealed volumetric glass flasks; these were shielded so as not to expose the solutions to the light. A stock solution of Ph_3P at 4.90 ± 0.08 M was used as the phosphine source. A stock solution of 1,3,5-tri-*t*-butylbenzene at 0.100 ± 0.002 M was used as the internal standard. These stock solutions were remade three times with variability amongst the concentration of the samples limited to 0.001 M. The total volume per sample was 600 μL which included 100 μL (0.01 mmol) of 1,3,5-tri-*tert*-butylbenzene as the internal standard (^{1}H NMR ($CDCl_3$) δ 1.34 (s, 27H), 7.26 (m, 3H)). To ensure pseudo-first-order kinetics with respect to Ph_3P, the ratio of Ph_3P to the substrate was either 16.3:1, 32.7:1 or 65.3:1, the substrate concentration being 0.025 M in all experiments. In order to ensure measurement accuracy, all volumes in each sample were measured using the same 500 μL syringe, which was itself washed only with solvent.

The delay time was set to 10 s.[12] The machine was shimmed with a dummy sample to afford peak resolution of less than 2 Hz. Data was acquired at 1 min intervals for the first 10 min followed by measurements at 20, 30 and 60 min. An infinity value for rate constant determination was estimated based on the extent of desulfurization that had occurred after 60 min.

Elucidating reactive intermediates spectroscopically can be difficult. Even starting materials such as polysulfides can equilibrate thereby complicating analysis.[13] For example, misleading parent peaks in a mass spectrum can appear as a result of modest isomerization of the compound.[14] Previous studies on the decomposition of polysulfides followed the reaction either through the measurement of the dielectric constant,[4] which was considered to be an indicator of product formation and where the assumption was that the reaction did not involve multiple steps, or by UV spectroscopy.[6,15] In this latter case, (where the nucleophile used was $(Et_2N)_3P$) due to the overlap of the aminophosphine peak (270-280 nm) with that of the starting material (*ca.* 255-260 nm which can extend beyond 325 nm), the UV_{max} of the trisulfide as the indicator could not be utilized.

We decided to use a model compound whereby it, as well as all the decomposition products could be dynamically monitored by ^1H NMR. We chose bis(4-methylbenzene) polysulfides as our model compounds as the methyl signals were entirely resolvable[16] and could be integrated using the 500 MHz NMR (*vide supra* Chapter 8).[17] The precision of the chemical shifts of the methyl signals from experiment to experiment was on average ± 0.002 ppm and is also an indication of the invariability of the concentration of the solutions used,[18] assuming that the chemical shift is in fact concentration dependent. This dependence does in fact exist and is shown in Figure 39 and Table 71.

Table 71. Chemical shifts of the 4-methylbenzene groups of **257b-260b** as a function of [Ph_3P]

[Ph_3P] (M)	Chemical Shifts (ppm)			
	258b	**257b**	**260b**	**259b**
0.00	2.352	2.343	2.318	-
0.42	2.339	2.331	2.306	2.285
0.83	2.323	2.317	2.290	2.272
1.67	2.296	2.289	2.261	2.243
m^a	-0.034	-0.032	-0.035	-0.033
b^a	2.353	2.343	2.319	2.299
$(R^2)^b$	0.998	0.999	0.999	1.000

a) Linear fit: $y = mx + b$ where m is the slope and b is the y-intercept. b) R^2 is the Pearson regression factor and is an indicator of the goodness of fit.

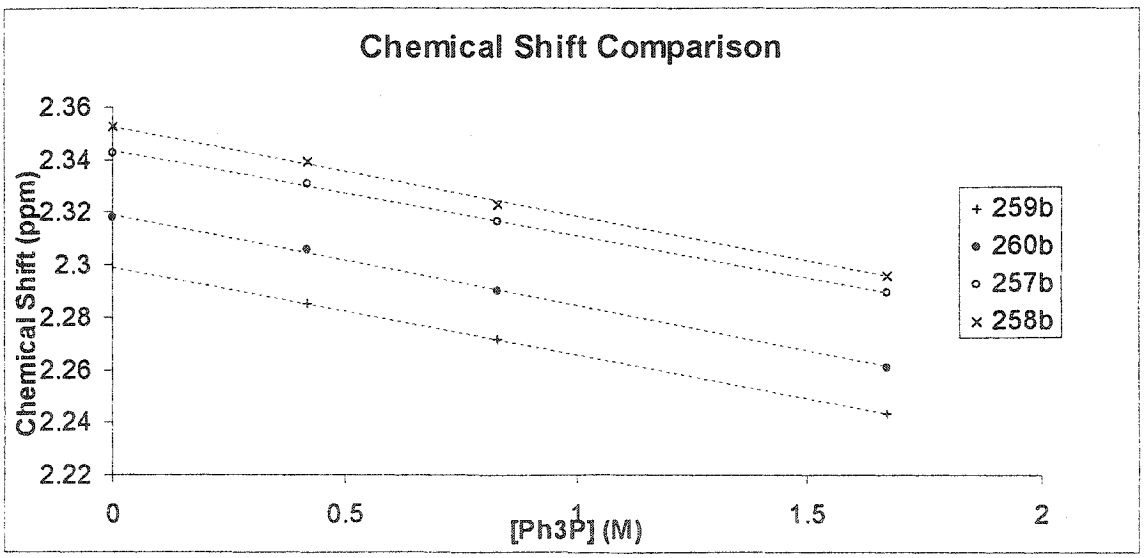

Figure 39. Dependence of the chemical shift of the methyl group on the concentration of Ph_3P.

9.2.4 Kinetics Methodology

Pseudo-first-order plots of $\ln(I_t - I_\infty)$ vs. time (where I_t, I_∞ are the ^{1}H NMR integrations of the methyl peaks at times t = t and t = t_∞ respectively) were determined for the decomposition of **260b** as well as the desulfurization of **257b** and **258b**. The initial t = 0 seconds point was taken as the time of the first NMR acquisition (usually *ca.* 4-5 minutes after the reagents were mixed). This delay was in part due to the need to shim the spectrometer to obtain good spectra. The values of the pseudo-first order rate constants, k_{obs}, were calculated using the method of least squares. Each experiment was repeated in triplicate and the average observed rate constant was reported. The reported error on k_{obs} was that of the standard error of the population. The rate constant k under pseudo-first order conditions is defined in equation (**21**) and the error on k is given in equation (**22**).[19] Although individual runs possessed good linear fits, reproducibility was poor. It is for this reason that the overall errors are large.

$$k = \frac{k_{obs}}{[Ph_3P]} \quad (21)$$

$$\sigma_k = \sqrt{\left(\frac{\sigma_{k_{obs}}}{[Ph_3P]}\right)^2 + \left(\frac{-k_{obs}}{[Ph_3P]^2}\right)^2 \sigma^2_{[Ph_3P]}} \quad (22)$$

9.3 Results and Discussion

9.3.1 Probing the reaction

Initially, we investigated the efficiency of desulfurization of **257b** and **258b** with Ph_3P in CH_2Cl_2 (Table 72). Room temperature desulfurization of **257b** reached 85% (isolation) in 10 min and did not significantly change, even after 4 h (Entry 1 *vs.* Entry 2), but under reflux (Entries 4 and 5), we were able to recover near quantitative amounts of $Ph_3P{=}S$. Increasing the number of sulfur atoms did not appreciably increase the yield of $Ph_3P{=}S$ (Entry 1 *vs.* Entry 3). We were interested in working at room temperature to parallel the standard sulfurization conditions used for oligonucleotides.

Table 72. Microscale desulfurization of **257b** and **258b** by equimolar Ph_3P in CH_2Cl_2

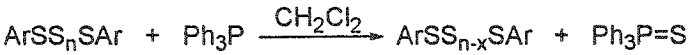

n = 1 **257b**
n = 2 **258b**

$x \leq n$

Entry	Cmpd.	Time (min)	Yield[a] (%)
1	**257b**	10	85
2	**257b**	240	87
3	**258b**	10	90
4[b]	**257b**	10	90
5[b]	**257b**	120	98

a) Yield of $Ph_3{=}S$ as isolated by silica gel chromatography.
b) Reaction was refluxed in CH_2Cl_2.

9.3.2 Kinetics of desulfurization

Having established that the desulfurization of **257b** and **258b** is facile and proceeds to near completion within minutes at room temperature in CH_2Cl_2, we then followed these reactions[3-6] *via* ^1H NMR. The rates of simple nucleophilic substitutions at a sulfenyl sulfur typically obey the following rate expression (eq. **23**).[20]

$$\text{Rate} = k[\text{R-S-X}][\text{Nu}^-] \quad \textbf{(23)}$$

The rate of attack on sulfur is dependent on a number of factors including solvent[6] and the steric bulk of the R group of the polysulfide.[21] In addition, thiolates are good leaving groups with pKa values of *ca.* 12 for R = alkyl[22] (*ca.* 6-7 for R = aryl - *vide infra*). This means that in rate studies on *alkyl* polysulfides, attack at carbon must also be considered. To ensure attack at sulfur, aromatic polysulfides, with R = 4-methylbenzene, were used in this study.

Given more than one type of sulfur, it is important to discuss where nucleophilic attack is likely to occur. In the context of nucleophilic displacement at sulfur, it has been shown[7,8,23,24] that the most thermodynamically stable leaving group (be it mercaptide or hydrodisulfide ion) will ultimately be displaced. The origin of the leaving group becomes most apparent if we compare the rates of exchange of methyl mercaptide (MeS^-) and the corresponding disulfide (MeSSMe)[25] with that of the disulfide and

$MeSS^{+}(Me)_2$.[26] Although the mercaptide ion is the better nucleophile, its exchange is 10^5 slower than the corresponding disulfide-thiosulfonium salt exchange.

The rate difference for this case must thus be entirely due to the stability of the leaving disulfide group versus that of the mercaptide ion. It is illustrative of the importance of the origin of the leaving group on the regioselectivity of attack by the nucleophile. Even though other systems also show this effect,[27] analyzing only the starting reagent and final product can lead to the wrong mechanistic conclusions. An example of the importance careful mechanistic studies entail is that of Hiskey and co-workers.[28] They found that in the cyanide ion cleavage of unsymmetrical disulfides, there is a reversible initial nucleophilic attack which occurs at the most positively polarized sulfur atom (kinetic step) followed by a slower step favoring the formation of the more stable cleavage product. Their results are shown in Scheme **66**.

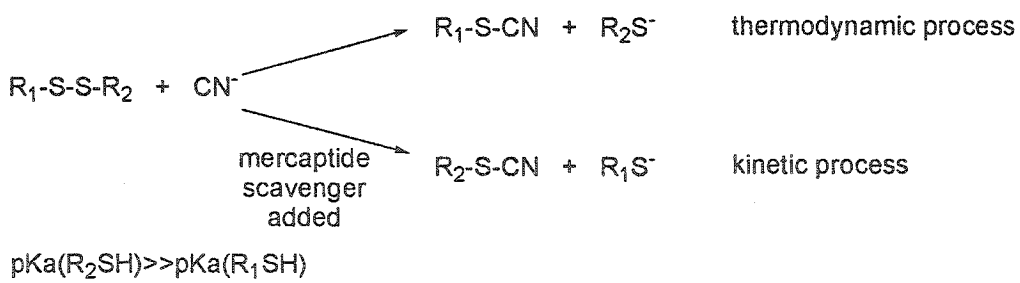

Scheme **66**.

Exploring our own system we note that the pKa of related PhSH was originally determined[29] to be 8.6 (9.3 for 4-methylbenzenethiol **259b**) but it has been more recently measured in the aqueous phase (either by acid-base titration or by changes in the UV-Vis spectrum as a function of pH) at *ca.* 6.6.[30,31] This latter value is in agreement with our calculational work[32] and so the early pKa value of **259b** should be viewed with

skepticism. The pKa for the corresponding phenyl hydrodisulfide has not been measured but has been calculated to be 5.9 in the gas phase.[32] The more acidic proton in this latter case is in agreement with studies of aliphatic analogs (*ca.* 5-6 for RSSH).[33] The aromatic hydrodisulfide ion ($ArSS^-$) may also be considered the better leaving group due to its increased resonance stabilization and inductive electron withdrawal from the adjacent sulfur atom[34] though the extent to which this occurs is a matter of some debate. In their examination of the effect of ring substitution on the chemical shift of the aromatic hydrodisulfide-SSH peak, Tsurugi and co-workers[35] concluded that the S-S bond does not transmit conjugation and permits only small inductive effects. Analogous trends are not seen in the chemical shifts of higher order polysulfanes, suggesting that the interpretation of electronic effects in compounds possessing -S-S- linkages is open to question.[36]

Block[37] has shown that the rate of S_N1 formation of $CH_3SCH_2^+$ is *ca.* 7000 times faster than that of $CH_3SSCH_2^+$. If the formation of positive phosphorus may be considered analogous to carbonium ion formation, then it is therefore reasonable to consider the corresponding thiophosphonium cation to be more stable that its dithiophosphonium analog. The extra sulfur atom effectively increases the activation energy in the formation of the intermediate. This assumption is in agreement with work reported by Saville, who hypothesized that attack by mercaptide ions occurs on a terminal sulfur of trisulfides.[34]

Recently, Steudel[38] and co-workers computed the relative acidities of a series of polysulfanes (HS_nH, n = 1, 4) in the gas phase. They determined that as the number of sulfur atoms increases, so does the acidity due to increased hyperconjugation across the

sulfur chain. These results are in agreement with the conclusion that RSS^- is a better leaving group than RS^- (R=alkyl or aryl).

It should be noted that we have been unable to obtain any spectroscopic evidence of pentacoordinated phosphorus intermediates (*cf.* Schemes **67** and **68**).[39] Examples of phosphoranes having two sulfurs bound to phosphorus are rare and have been shown to exist in equilibrium with their corresponding thiophosphonium salts;[40] mixed disulfide experiments have also strongly implicated the existence of a thiophosphonium salt intermediate.[41] As well, by analogy with sulfide insertion into polysulfides,[42] insertion of phosphorus into the chain should require considerably more energy than simple nucleophilic cleavage. We conducted ^{31}P NMR, ^{13}C NMR and ^{1}H NMR experiments over a wide range of chemical shift values and delay times but were unable to detect any thiophosphonium salt intermediate. Unlike Wittig-type phosphonium salts which are common and readily detectable,[43,44] there exist few reports of thiophosphonium species with Ph_3P and then only when they are complexed with a suitable counterion (such as SbF_6^-).[45]

Unlike the cleavage of disulfides,[46,47] there is a strong driving force in the desulfurization of higher order polysulfides towards formation of $Ph_3P{=}S$. Radiochemical studies on aromatic trisulfides[56,57] and the natural product Sporidesmin E[58,59] (*cf.* Chapter **7.2.2**) have demonstrated that the central sulfur is exclusively extruded by Ph_3P. However the central sulfur is the *only* sulfur available for removal because either the terminal sulfurs are adjacent to sp^2 hybridized aromatic carbons or to tertiary or

sterically hindered secondary carbons. Thus to extrapolate a general desulfurization mechanism for all trisulfide types based on these specific results may be misleading.

It has been determined that trisulfides react with phosphines much faster than the corresponding disulfides,[57,60] but only three kinetic studies of aromatic trisulfides have been reported in the literature;[4,5,15] all arriving at the same rate expression shown in equation (**24**).

Rate=k[phosphine][trisulfide] (**24**)

Earlier work[4,5] demonstrated that electron withdrawing groups on *para*-substitued aromatic trisulfides increase the rate of desulfurization. The presence of a solvent effect on the rates of desulfurization of trisulfides, as well as a negative ρ-value obtained in the Hammett correlation of the aryl substituents for the phosphine[15] and a corresponding positive ρ-value for the trisulfide,[4,5] is suggestive of a charged transition state. The effect of changing solvent is similar to that observed for aliphatic disulfides. A solvent effect was also observed in reactions of phosphites with unsymmetrical trisulfides containing a 4-methylbenzene group[3] (observed solvent effects are much larger for aliphatic trisulfides than aromatic trisulfides). In addition, phosphine-catalyzed trisulfide exchange experiments,[5,15] similar to those with disulfides (Scheme **67**), further establish both the existence of charged intermediates as well as the reversibility of their formation. These observations are all in agreement with the proposal that desulfurization proceeds *via* the

formation of thiophosphonium salt adducts, and evidence exists to support a phosphonium salt intermediate in nucleophilic phosphine reactions.[5,6]

Scheme 67. Reaction of bis(4-methylbenzene) disulfide **260b** with PPh_3

The desulfurization of trisulfide **257b** is shown in Figure 40, yielding excellent agreement with first order kinetics, Table 73 (R^2 >0.98).

Table 73. Rate constants for the desulfurization of **257b** and formation of **260b** in the reaction of 0.025 M **257b** with Ph_3P.

	Loss of **257b**[a]			Formation of **258b**[b]		
$[Ph_3P_{(initial)}]$[c] (M)	$k_{obs} \times 10^{-3}$ (s^{-1})[d]	$k \times 10^{-3}$ $(M^{-1} s^{-1})$	$t_{1/2}$ (*min*)	$k_{obs} \times 10^{-3}$ (s^{-1})[d]	$k \times 10^{-3}$ $(M^{-1} s^{-1})$	$t_{1/2}$ (*min*)
0.42	0.3 ± 0.1	0.7 ± 0.3	17.5	0.2 ± 0.1	0.6 ± 0.2	20.7
0.83	0.4 ± 0.1	0.5 ± 0.2	24.0	0.4 ± 0.2	0.5 ± 0.2	23.0
1.67	0.9 ± 0.2	0.5 ± 0.1	22.3	1.1 ± 0.6	0.7 ± 0.4	16.8

a) Partial order was determined to be 0.8. b) Partial order was determined to be 1.2. c) Error on concentration is estimated to be 0.08 M. d) 1st order rate constant.

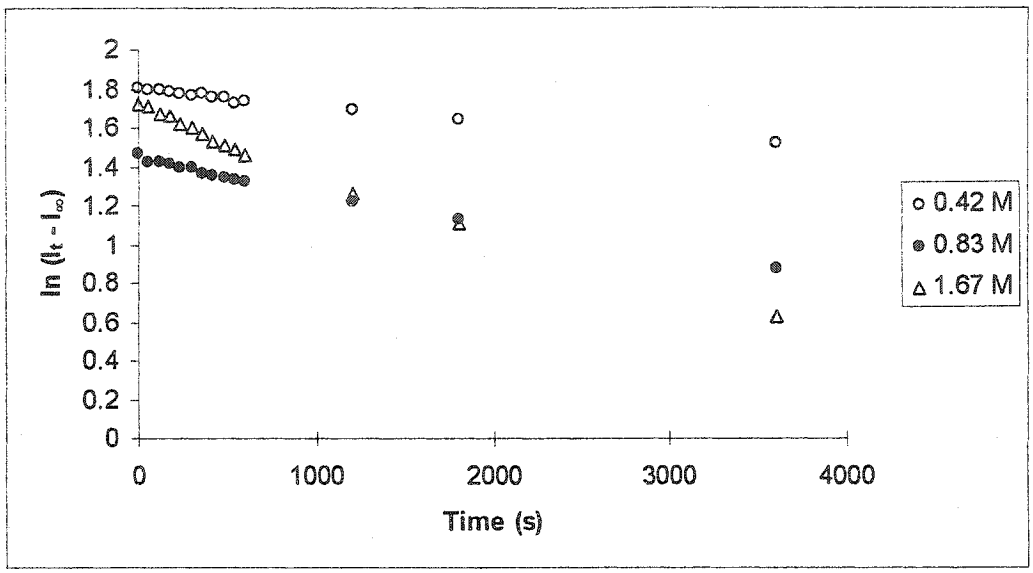

Figure **40**. 1st order rate plot of the desulfurization of 0.025 M **257b** at different concentrations of Ph_3P

The measured first order rate constant is reasonably close to the literature values (5.4 x 10^{-3} s^{-1} in benzene using $(Et_2N)_3P$ at 30 °C;[5] 1.25 x 10^{-3} s^{-1} in toluene using Ph_3P at 40 °C),[4] the differences being attributed to the different solvent systems and phosphine used as well as the slightly elevated temperatures of those studies.

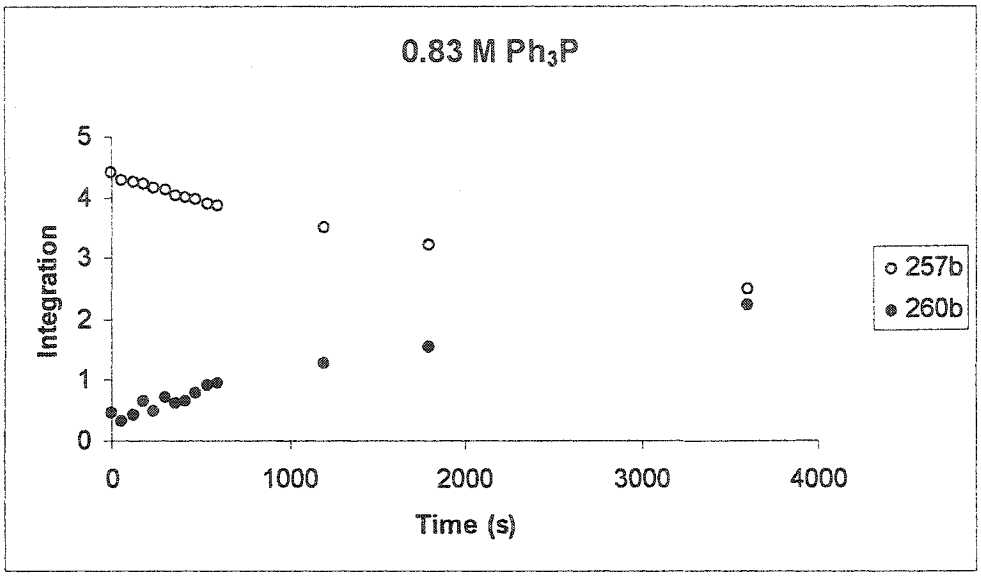

Figure 41. Representative time profile of reaction progression at 33:1 Ph_3P:**257b**

The rate constant for formation of the disulfide product **260b** was, within reasonable experimental error, equal to that of the decomposition of the trisulfide starting material **257b** (for a representative time profile see Figure 41). Furthermore, the behaviour in both the loss of **257b** as well as the resulting formation of **260b** remained first-order for the duration of the experiment (*ca.* 3 $t_{½}$). A small amount (*ca.* 10%) of 4-methylbenzenethiol **259b** was observed in the ^1H NMR spectra but does not affect the rate determining step of the reaction.[61]

Notwithstanding the absence of an observable intermediate, we may construct a possible reaction mechanism (Scheme **68**) in which the equilibrium positions of k_1 and k_2 are very likely in favour of the starting material (no higher order polysulfides were detected).

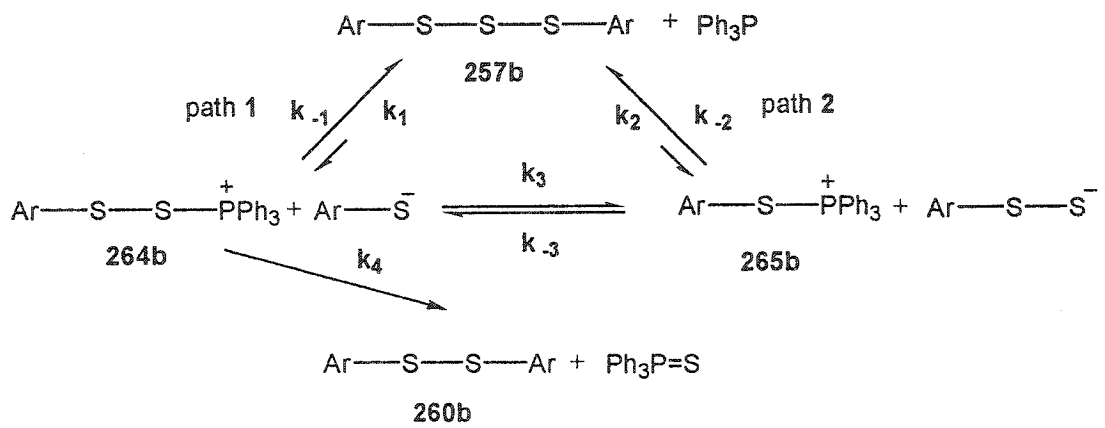

Scheme **68**. Mechanism for the desulfurization of aromatic trisulfides

Thiophosphonium ion **265b** is both the thermodynamically (pKa) and kinetically favored (polarization of sulfur atom) intermediate. Formation of this type of intermediate in the desulfurization of Calicheamicin γ_1^I **227** has been reported.[24] Calculations[7] have also suggested that nucleophilic attack on dimethyl trisulfide as well as methyl allyl trisulfide occurs at the terminal position (in the latter case, attack occurs terminal to the allyl group); this regeoselectivity was attributed both to a higher positive charge on the terminal sulfurs as well as less steric crowding.

However, in order to obtain **260b**, the reaction presumably proceeds *via* intermediate **264b**, assuming that the only sulfur that can be extruded is the central one *i.e.* nucleophilic attack on the 4-methylbenzene ring does not occur. This mechanistic

conclusion is also in keeping with the literature.[5,6] The final step, and the driving force of the reaction, would therefore involve the formation of $Ph_3P{=}S$ through attack of ArS^- at the terminal sulfenyl sulfur of **264b**. The fact that the rate of formation of **260b** is the same as that of the loss of **257b** (Table 73) argues that path 4 be the rate-determining step.

We thus arrive at the same mechanistic conclusions for aromatic trisulfides as those investigators who previously reported work on aliphatic trisulfides,[6] these latter cases based on a *second step attack on carbon* rather than sulfur in the formation of $Ph_3P{=}S$. It should be noted that we detected no higher-order polysulfides in the desulfurization of **257b** suggesting that the equilibrium of pathway 2 lies very largely to the side of **257b**. There is no evidence to support or refute the existence of a ligand exchange reaction governed by k_3.

Determining the mechanism of desulfurization of the corresponding tetrasulfide **258b** is somewhat more complicated. The rate of reaction of **258b** with Ph_3P is considerably greater than that of **257b**, resulting in a typical time profile of reaction as shown in Figure 42.

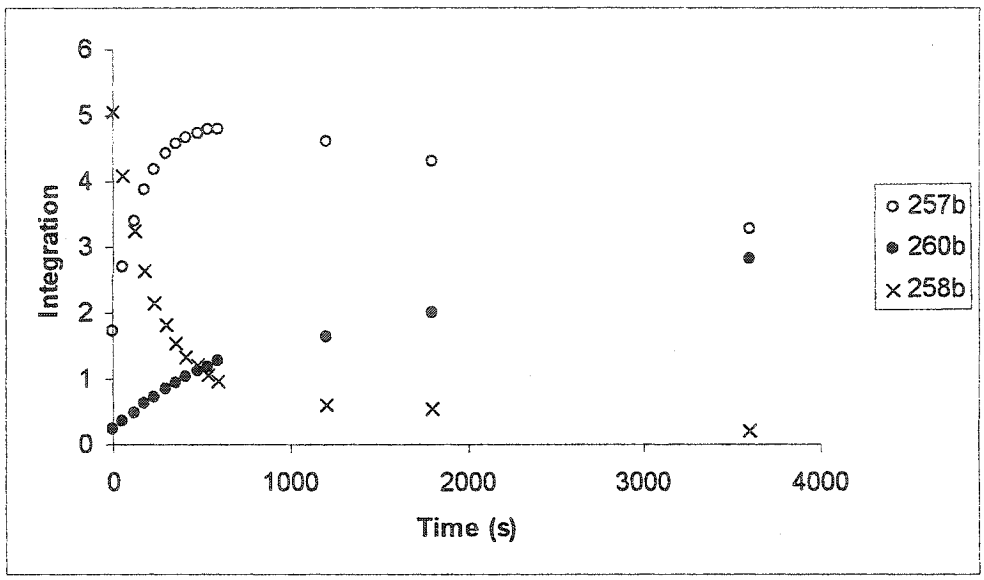

Figure 42. Time profile of the desulfurization of 0.025 M **258b** by 0.42 M Ph_3P.

To our knowledge, two studies on the desulfurization of aromatic tetrasulfides have been reported, but only with respect to polymers[63] or carried out in hydroxylic solvents.[62] We propose the following scheme for the initial desulfurization of **258b** (Scheme 69). It contains many parallel concepts to Schemes 67 and 68.

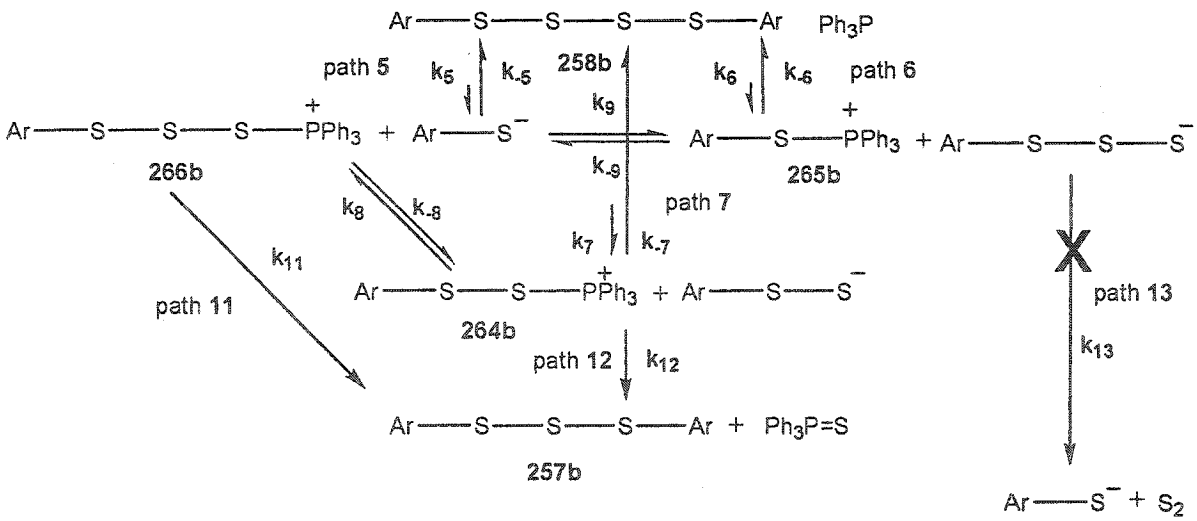

Scheme 69. Mechanism for the desulfurization of aromatic tetrasulfides

Intermediate **265b** through path **6** is likely to be a negligible contributor to the overall reaction due to the inherent room temperature instability of the trithiomercaptide ion,[36] even though in principle it is the best leaving group based on previous precedent (*vide supra*). If path **6** with the formation of $ArSSS^-$ were an important contributor then it would also be reasonably expected that this trisulfane anion could attack **258b** (which initially is in the largest concentration), thereby promoting the formation of higher order polysulfides; however, none were observed using carefully monitored control experiments. Thus path **13** would not be expected to be a contributor to the overall reaction scheme.

A modest amount of **260b** (*ca.* 17% of desulfurization products after 3 min regardless of Ph_3P concentration) that forms in the initial stages of the reaction and continues to form at rates comparable to those observed during the desulfurization of **257b** (*cf.* Table **73**). Given that tetrasulfides decompose much faster than their trisulfide counterparts (Figure **43**, Table **74**), the presence of **260b** in the initial stages of the reaction is a result of the subsequent desulfurization of formed trisulfide **257b**.[64]

However, since **257b** is the primary product that is formed at the fastest rate, paths **7** and **12** remain the primary routes for the desulfurization of **258b**.[66] A corollary to this is that either k_7 must be larger than k_5 or there is fast ligand exchange *via* k_8. It should be noted that in comparing the two pathways, path **7** affords the better leaving group and so should be favoured. As with the desulfurization of **257b**, we detected no higher-order polysulfides in the desulfurization of **258**.

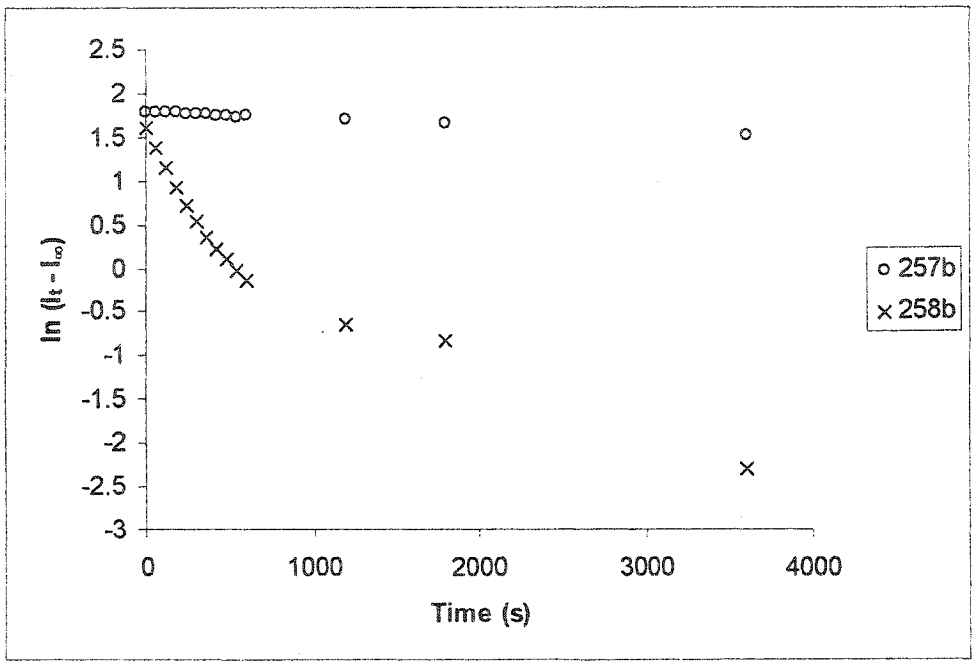

Figure **43**. Comparison of the desulfurization of **257b**, and **258b** at 0.42 M Ph_3P.

Table **74**. Comparison of the rates of desulfurization of **257b** and **258b**.

Entry	$[Ph_3P_{(initial)}]^a$ (M)	Cmpd	k_{obs} x 10^{-3} (s^{-1})	k x 10^{-3} (M^{-1} s^{-1})^b	k_{rel}^{c}	$t_{½}$ (min)
1	0.83	**257b**	0.4 ± 0.1	0.5 ± 0.2	1.0	24.0
2	0.83	**258b**	4.8 ± 1.4	5.8 ± 1.7	11.6	2.0

a) Error on concentration is estimated to be 0.08 M. b) 1st order rate constant. c) k_{rel} is the relative rate of decomposition with respect to **257b**.

It was difficult to ascertain rate constants for the loss of **258b** as almost all of the starting material was consumed within the first few observable minutes of the reaction. However, the initial cleavage rates of the desulfurization of tetrasulfide **258b** demonstrate a relative increase in the rate (compared with **257b**) by a factor of *ca.* 12 (Table **74**, k_{rel}). Thus by increasing the sulfur chain we increase the labilization of the sulfur atoms. We were able to determine the kinetics for the subsequent loss of trisulfide **257b** and the gain of product **260b** (Table **75**).

Table 75. Rate constants for the desulfurization of **257b** and **258b** and the formation of **260b** in the reaction of 0.025 M **258b** with Ph_3P.

	Loss of **258b**[a]			Loss of **258b**[b]			Formation of **257b**[c]		
$[Ph_3P_{(initial)}]$[d] (M)	k_{obs} x 10^{-3} (s^{-1})[e]	k x 10^{-3} (M^{-1} s^{-1})	$t_{1/2}$ (*min*)	k_{obs} x 10^{-3} (s^{-1})[e]	k x 10^{-3} (M^{-1} s^{-1})	$t_{1/2}$ (*min*)	k_{obs} x 10^{-3} (s^{-1})[e]	k x 10^{-3} (M^{-1} s^{-1})	$t_{1/2}$ (*min*)
0.42	4.8 ± 0.9	11.5 ± 2.6	1.0	0.2 ± 0.1	0.4 ± 0.1	28.8	0.5 ± 0.1	1.2 ± 0.3	9.9
0.83	4.8 ± 1.4	5.8 ± 1.7	2.0	0.8 ± 0.5	0.9 ± 0.6	12.5	0.6 ± 0.2	0.7 ± 0.3	15.9
1.67	3.2 ± 2.1	1.9 ± 1.3	6.1	1.1 ± 0.4	0.7 ± 0.3	17.0	1.2 ± 0.5	0.7 ± 0.3	16.3

a) The partial order was determined to be -0.3. b) Partial order was determined to be 1.4. c) Partial order was determined to be 0.6. d) Error on concentration is estimated to be 0.05 M. e) 1st order rate constant.

Within reasonable error, the rate constants for formation of **260b** are of the same order of magnitude as those for the loss of intermediate **257b** (Table 75), and approximate to those observed in the direct desulfurization of **257b** (Table 73). It should be noted that by utilizing ^{1}H NMR methods it is now possible to track intermediate and/or product formation as well as starting material loss, unlike previously reported kinetics studies on related systems.[4,5,15]

It is important to note that in both the desulfurization of **257b** and **258b**, the primary intermediate included the formation of the hydrodisulfide ion. The result of this is whereas desulfurization of **257b** proceeds *via initial* attack at the *terminal* sulfur, desulfurization of **258b** substantially proceeds with attack at one of the *central* sulfurs. This is also not without precedent[63] but still a matter of some debate.[8] Thus in the desulfurization of **257b** there exists a pre-equilibrium formation of **265b** as well as an $ArSS^{-}$ species prior to central sulfur extrusion. The existence of such pre-equilibriums is not without precedent as was demonstrated in the cyanide cleavage of disulfides.[28] However not inconsistent with this analysis are that in both the desulfurization of **257b** and **258b** the rate determining step is that of *central* sulfur extrusion. Scheme **69** can thus be simplified to Scheme **70**.

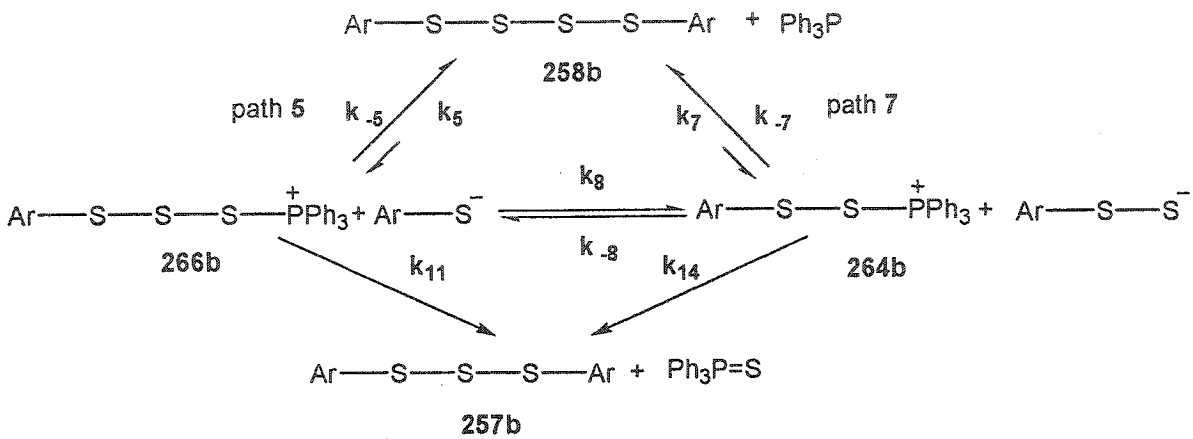

Scheme **69**. Mechanism for the desulfurization of aromatic tetrasulfides

The *ca.* twelve-fold increase in desulfurization rate in **258b** as compared with **257b** is due to both the presence of a better leaving group ($ArSS^-$ vs ArS^-) and a statistical doubling of the number of removable sulfurs in **258b**.

9.4 Concluding Remarks

Nucleophilic attack on polysulfides is an important reaction in organosulfur chemistry. To our knowledge, this work reports the first kinetic investigation of the desulfurization of tetrasulfides. This preliminary evaluation of **257b** and **258b** as phosphorothionation reagents indicates that when treated with an oligodeoxyribonucleotide substrate, they were not sufficiently reactive to classify as an effective sulfurizing reagent.[67] Recently, Gates has demonstrated the *in vivo* DNA cleavage properties of aliphatic polysulfides.[68,69] Our compounds may thus also possess DNA cleavage properties.

9.5 References

(1) Michaelis, A.; Kaehna, R. *Chem. Ber.* **1898**, *31*, 1048.

(2) Bhattacharya, A. K.; Thyagarajan, G. *Chem. Rev.* **1981**, *81*, 415.

(3) Harpp, D. N.; Smith, R. A. *J. Org. Chem.* **1979**, *44*, 4140.

(4) Féher, F.; Kurz, D. *Z. Naturforschg.* **1968**, *23B*, 1030.

(5) Harpp, D. N.; Ash, D. K.; Smith, R. A. *J. Org. Chem.* **1980**, *45*, 5155.

(6) Harpp, D. N.; Smith, R. A. *J. Am. Chem. Soc.* **1982**, *104*, 6045.

(7) Mulhearn, D. C.; Bachrach, S. M. *J. Am. Chem. Soc.* **1996**, *118*, 9415.

(8) Greer, A. *J. Am. Chem. Soc.* **2001**, *123*, 10379.

(9) Harpp, D. N.; Zysman-Colman, E. *J. Org. Chem.* **2003**, *68*, 2487.

(10) Still, W. C.; Kahn, M.; Mitra, A. *J. Org. Chem.* **1978**, *43*, 2923.

(11) In control experiments, it was possible to elute and then isolate 100% of $Ph_3P{=}S$ pre-loaded on a column.

(12) Control experiments were conducted with known ratios of **257b**, **258b** and **260** in order to reproduce these ratios through the integration of their respectively resolved methyl groups by ^{1}H NMR.

(13) Tebbe, F. N.; Wasserman, E.; Peet, W. G.; Vatvars, A.; Hayman, A. C. *J. Am. Chem. Soc.* **1982**, *104*, 49.

(14) Litaudon, M.; Trigalo, F.; Martin, M.-T.; Frappier, F.; Guyot, M. *Tetrahedron* **1994**, *50*, 5323.

(15) Hall, C. D.; Tweedy, B. R.; Kayhanian, R.; Lloyd, J. R. *J. Chem. Soc. Perkin. Trans. 2* **1992**, 775.

(16) van Wazer, J. R.; Grant, D. *J. Am. Chem. Soc.* **1964**, *86*, 1450.

(17) The methyl peaks in a solution containing 1% of **257b** with respect to **260b** were still resolvable.

(18) The chemical shifts of the methyl peaks of **257b-260b** were confirmed through independent control experiments.

(19) Through control experiments on the measurement of both the volume of solvent and the mass of Ph_3P, the error on [Ph_3P] was determined to be 0.08 M.

(20) Ciuffarin, E.; Fava, A. *Progress in Physical Organic Chemistry*; Interscience Division, John Wiley and Sons: New York, **1968**; Vol. 6; p.81.

(21) Kice, J. L. *Mechanisms of Reactions of Sulfur Compounds* **1968**, *3*, 91.

(22) Lowry, T. H.; Richardson, K. S. *Mechanism and Theory in Organic Chemistry*; Harper & Row: New York, **1987**.

(23) Parker, A. J.; Kharasch, N. *J. Am. Chem. Soc.* **1960**, *82*, 3071.

(24) Ellestad, G. A.; Hamann, P. R.; Zein, N.; Morton, G. O.; Siegal, M. M.; Pastel, M.; Borders, D. B.; McGahren, W. J. *Tetrahedron Lett.* **1989**, *30*, 3033.

(25) Fava, A.; Iliceto, A.; Camera, E. *J. Am. Chem. Soc.* **1957**, *79*, 833.

(26) Kice, J. L.; Favstritsky, N. A. *J. Am. Chem. Soc.* **1969**, *91*, 1751.

(27) Harpp, D. N.; Granata, A. *J. Org. Chem.* **1980**, *45*, 271.

(28) Harpp, D. N.; Hiskey, R. G. *J. Am. Chem. Soc.* **1964**, *86*, 2014.

(29) Dmuchovsky, B.; Zienty, F. B.; Vredenburgh, W. A. *J. Org. Chem.* **1966**, *31*, 865.

(30) Jencks, W. P.; Salvesen, K. *J. Am. Chem. Soc.* **1971**, *93*, 4433.

(31) DeCollo, T. V.; Lees, W. J. *J. Org. Chem.* **2001**, *66*, 4244.

(32) Snyder, J. P. *Private Communication* **2002**.

(33) Everett, S. A.; Folkes, L. K.; Wardman, P.; Asmus, K.-D. *Free Radical Res.* **1994**, *20*, 387.

(34) Evans, M. B.; Saville, B. *Proc. Chem. Soc. London* **1962**, 18.

(35) Kawamura, S.; Horii, T.; Tsurugi, J. *J. Org. Chem.* **1971**, *36*, 3677.

(36) Langer, H. J.; Hyne, J. B. *Can. J. Chem.* **1973**, *51*, 3403.

(37) Block, E. *J. Org. Chem.* **1974**, *39*, 734.

(38) Steudel, R.; Otto, A. H. *Eur. J. Inorg. Chem.* **1999**, 2057.

(39) Control ^{31}P NMR, ^{13}C NMR and ^{1}H NMR experiments were conducted over a 200 ppm, 170 ppm and 15 ppm range respectively for the detection of possible tetra- or pentacoordinated intermediates. None were detected on the NMR time scale. This does not preclude the existence of such species but merely indicates their low concentration.

(40) Burros, B. C.; De'Ath, N. J.; Denney, D. B.; Denney, D. Z.; Kipnis, I. J. *J. Am. Chem. Soc.* **1978**, *100*, 7300.

(41) Harpp, D. N.; Gleason, J. G.; Snyder, J. P. *J. Am. Chem. Soc.* **1968**, *90*, 4181.

(42) Steudel, R.; Steudel, Y.; Miaskiewicz, K. *Chem. Eur. J.* **2001**, *7*, 3281.

(43) Bangerter, F.; Karpf, M.; Meier, L. A.; Rys, P.; Skrabal, P. *J. Am. Chem. Soc.* **1998**, *120*, 10653.

(44) Puke, C.; Erker, G.; Wibbeling, B.; Fröhlich, R. *Eur. J. Org. Chem.* **1999**, *8*, 1831.

(45) Tebby, J. C.; Maier, L.; Diel, P. J. *Handbook of Phosphorus-31 Nuclear Magnetic Resonance Data*; CRC Press: Boston, **2000**.

(46) The partial order for the cleavage of disulfide **260b** was determined to be ~0.1 suggesting an independence on its concentration. The only products detected were small amounts of trisulfide **257b** and trace amounts of thiophenol **259b**.

(47) No SH proton was detected for **259b** but the identity of the CH_3 peak was confirmed by comparison with authentic **259b**. This indicates that the thiophosphonium salt is (in part) decomposing, picking up a deuteron from the solvent. In general, desulfurization of aromatic disulfides by triphenylphosphine in the absence of alcoholic solvent[48-53] is only possible at elevated temperatures.[54,55].

(48) Schönberg, A.; Barakat, M. Z. *J. Chem. Soc.* **1949**, 892.

(49) Humphrey, R. E.; Hawkins, J. M. *Anal. Chem.* **1964**, *36*, 1812.

(50) Davidson, R. S. *J. Chem. Soc.* **1967**, *21*, 2131.

(51) Overman, L. E.; Metzinger, D.; O'Connor, E. M.; Overman, J. D. *J. Am. Chem. Soc.* **1974**, *96*, 6081.

(52) Overman, L. E.; Petty, S. T. *J. Org. Chem.* **1975**, *40*, 2779.

(53) Overman, L. E.; O'Connor, E. M. *J. Am. Chem. Soc.* **1976**, *98*, 771.

(54) Harpp, D. N.; Kader, H. A.; Smith, R. A. *Sulfur Letters* **1982**, *1*, 59.

(55) Middleton, D. L.; Samsel, E. G.; Wiegand, G. H. *Phosphorus and Sulfur* **1979**, *7*, 339.

(56) Harpp, D. N.; Ash, D. K. *Chem. Commun.* **1970**, 811.

(57) Ash, D. K. Ph. D. thesis, McGill University, **1973**.

(58) Safe, S.; Taylor, A. *J. Chem. Soc. C.* **1971**, 1189.

(59) Safe, S.; Taylor, A. *Chem. Commun.* **1969**, 1466.

(60) Gleason, J. G. Ph.D. thesis, McGill University, **1970**.

(61) Besides the expected desulfurized product **260b**, only one other product was detected, which was identified as **259b**, (the SH-peak was not present). The absence of alcoholic hydroxyl[62] or water signals detected by ^{1}H NMR combined with the absence of an SH peak for **259b** suggests that a competing reaction may convert some of the

assumed thiophosphonium intermediate into **259b** and that the reduction source is deuterated.

(62) Démarcq, M. C. *J. Chem. Res.* **1993**, *M*, 3052.

(63) Ganesh, K.; Kishore, K. *Macromolecules* **1995**, *28*, 2483.

(64) In contrast, Hayashi[65] reported that it was easier and faster to desulfurize **260b** compared with **257b** with Ph_3P. This appears to be an erroneous conclusion since the desulfurization of aromatic disulfides is possible only at high temperatures.[54].

(65) Hayashi, S.; Furukawa, M.; Yamamoto, J.; Hamamura, K. *Chem. Pharm. Bull.* **1967**, *15*, 1310.

(66) It is also possible that intermediate **266b** could decompose directly to either to **260b** or to **257b** by reaction with Ar-S$^{\cdot}$. In the former case the most probable reaction here is attack at the terminal sulfur of **266b** with concomitant formation of $Ph_3P{=}S$ and "S" which would itself then concatenate to form S_8, whereas in the latter case attack would occur at the central sulfur with the formation of $Ph_3P{=}S$ as the sole by-product. This anion could also come from the 2-sulfur loss of unstable Ar-SSS$^{\cdot}$. Other reactions

such as that of Ar-S^- with tetrasulfide **258b** can not be ruled out as pathways in the generation of trisulfide **257b**.

(67) Although **258b** was optimal for kinetic investigation (*vide supra*), we are currently investigating the desulfurization of bis(*p*-nitrophenyl) tetrasulfide **258d** which, due to its electron withdrawing groups, would be projected to be a much faster sulfur transfer reagent than **258b**.

(68) Gates, K. S. *Chem. Res. Toxicol.* **2000**, *13*, 953.

(69) Gates, K. S.; Breydo, L. *Bioorganic & Medicinal Chemistry Letters* **2000**, *10*, 885.

Contributions to Original Knowledge

Theory from Alkoxy Disulfides:

1. A high-level computational survey was conducted in order to ascertain the least expensive method for accurately modeling alkoxy disulfides and thionosulfites (Chapter 3).
2. NBO analysis of gas phase calculations demonstrated that the high barrier to rotation about the S-S bond in alkoxy disulfides was due to two negative hyperconjugative interactions between each of the sulfur lone pairs with their adjacent S-O antibonding orbitals (Chapter 3).
3. Theoretical work was performed in order to ascertain the influencing factors on the relative ground state energies of isomeric alkoxy disulfides and thionosulfites. It was determined that the relative energy difference was proportional to the ring size. Predictions indicate that coupling of 1,4-diols with sulfur transfer reagents should afford *both* the alkoxy disulfide and the thionosulfite. This was experimentally verified (Chapter 6)

Experimental Results for Alkoxy Disulfides

4. The synthesis of acyclic alkoxy disulfides was optimized. A series of 11 alcohols were used in the substituent survey. Of the alkoxy disulfides formed, two had not been previously reported (*bis*(*p*-*t*-butylbenzyloxy)disulfide and *bis*(benzhydroloxy) disulfide) while the yields of five others were optimized (Chapter 4).
5. A substituent study of the rotational barrier about the OS-SO bond in acyclic alkoxy disulfides was carried out. Modification of the substituent did not

appreciably influence the torsional barrier. This represents the first such study for alkoxy disulfides where only the electronics of the substituent were altered (Chapter 4).

6. A solvent study of the S-S rotational barrier in acyclic alkoxy disulfides was conducted. Although calculations predicted a solvent effect, measurements of the rotational barrier in six solvents indicate that within experimental error, it was not affected. This represents the first such solvent study designed to elicit activation parameters for S-S rotation for this class of compounds (Chapter 4).
7. The thermolysis of acyclic alkoxy disulfides was investigated for the first time. Results indicate that alkoxy disulfides undergo initial S-O bond homolysis and their decomposition follow first order kinetics. Products were identified by ^{1}H NMR comparison with authentic samples. Activation parameters were calculated indicating that the thermal decomposition of alkoxy disulfides is *ca.* 8 kcal/mol more demanding than the S-S rotational barrier (Chapter 4).
8. Relevant to this study, three closely related and unusual molecules have been prepared. These are the first cyclic alkoxy disulfide **171**, its valence-bond isomer **172** representing the first medium-sized ring thionosulfite and a cyclic dimer of **171** that contains two OSSO moieties, **173**. X-ray crystal structures of all three of these molecules have been obtained (Chapter 5). In addition, a second new cyclic alkoxy disulfide, a 10-membered ring derived from 2,2'-biphenyldimethanol, has been fully characterized. Unique to this compound is the presence of two chiral axes indicating the presence of diasteomeric conformations that were detected by ^{1}H NMR and ^{13}C NMR (Chapter 6).

9. Conformational analysis on **171-173** as well as an analogous sulfite **174** (X-ray structure obtained) were carried out (Chapter **5**).

Experimental Results for Polysulfides

10. The synthesis of symmetric acyclic aromatic tri- and tetrasulfides were optimized (Chapter **8**).

11. The kinetics of desulfurization of bis(4-methylbenzene) trisulfide and bis(4-methylbenzene) tetrasulfide with triphenylphosphine was carried out by ^{1}H NMR. This work provides dynamic monitoring of all intermediates, products as well as starting material. Rate constants were determined and a consistent mechanism for the desulfurization of tetrasulfides was postulated (Chapter **9**).

APPENDICES

APPENDIX I. General Synthetic Experimental

All commercially available reagents were obtained from Aldrich Chemical Company. They were used without further purification unless otherwise stated below.

Methylene chloride (CH_2Cl_2), triethylamine (NEt_3) and hexamethyl disilazane ($C_6H_{19}NSi_2$ - HMDS) were distilled over calcium hydride. Tetrahydrofuran (THF) was distilled from the blue sodium-benzophenone ketyl. Diethyl ether (Et_2O) and Carbon tetrachloride (CCl_4) were dried over activated 4Å molecular sieves. Sulfur monochloride, S_2Cl_2, (135-137 °C) was distilled according to procedures adapted from Fieser and Fieser (100:4:1 S_2Cl_2:sulfur:charcoal).[1] Sulfur dichloride, SCl_2 (59-60 °C), was fractionally distilled over 0.1% phosphorus pentachloride, PCl_5. Both S_2Cl_2 and SCl_2 were used immediately after distillation.

Thin Layer Chromatography (TLC) was performed on 0.25 mm Merck silica plates with aluminum backing and visualized under UV light and/or by dipping in a solution of ammonium molybdate ($(NH_4)_6Mo_7O_{24}{\cdot}H_2O$) (10 g) and ceric ammonium sulfate ($(NH_4)_4Ce(SO_4)_4$) (4 g) in 10% v/v aqueous sulfuric acid (H_2SO_4) (400 ml) followed by heating. Sometimes commercially available phosphomolybdic acid solution (PMA) was used as alternative visualization solution. Flash column chromatography[2] was conducted using 230-400 mesh silica gel purchased from Silicycle.

^1H NMR spectra were recorded in $CDCl_3$ at 200 MHz on a Varian Mercury-200 spectrometer, at 300 MHz on a Varian Mercury-300 spectrometer, at 400 MHz on a Varian Mercury-400 spectrometer, or at 500 MHz a Varian Unity-500 spectrometer. ^{13}C

NMR were obtained on the latter three instruments at 75, 101, or 125 MHz, respectively. ^{31}P NMR were recorded at 81 MHz and were obtained on a Varian Mercury-200 spectrometer. Deuterated chloroform ($CDCl_3$), dried over 4Å molecular sieves, was used as the solvent of record and ^{1}H NMR and ^{13}C NMR. The chemical shifts, δ, of the spectra, measured in parts per million, (ppm), were referenced relative to tetramethylsilane (TMS) or to the solvent peak. ^{31}P NMR spectra were referenced to phosphoric acid, H_3PO_4. The following abbreviations have been used for multiplicity assignments: "s" for singlet, "d" for doublet, "t" for triplet, "q" for quartet, "m" for multiplet, "AB" for a spectrum containing a second-order AB splitting pattern. Some yields were determined by ^{1}H NMR by comparison with an internal standard. 1,3,5-Tri-*tert*-butyl benzene was used as the internal standard as it was inert to the reaction conditions.

Infrared spectra were recorded on an ABB Bomem MB100 FT-IR spectrometer. The FT-Raman spectra were recorded on a Bruker Model IFS-88 FT-IR spectrometer equipped with a Bruker FRA-106 Raman module containing a liquid nitrogen-cooled, 300 mW Nd^{3+}-YAG laser operating at 1064 nm at 4 cm^{-1} resolution. Data are reported in wavenumbers (cm^{-1}). Ultra-Visible (UV) spectra were recorded on a HP 8453 diode array UV/VIS spectrophotometer.

Low resolution electron impact (EI), chemical ionization (CI) or fast atom bombardment (FAB) mass spectra were recorded using a Kratos MS 25RFA instrument equipped with a 70 eV ionizing energy source. Mr. Nadim Saadé (McGill University) or

Dr. Gaston Boulay (Université de Sherbrooke) performed the analysis. The data are reported according to their charge to mass ratio (*m/z*) and their assignment. High resolution mass spectra (HRMS) were carried out at the Université de Sherbrooke, Sherbrooke, QC, Canada by Dr. Gaston Boulay.

The elemental analysis of **257c**, **258b** and **258c** were performed at Quantitative Technologies Inc., Whitehouse, NJ, USA.

The X-Ray crystal structures for **257b** and **258b** were solved by Dr. Anne-Marie Lebuis formerly of McGill University. The structures were solved using the SHELXS-96 program on an Enraf Nonius CAD-4 diffractometer at Univeristé de Montréal. The crystal structures of **171-174** were determined by Dr. Fracine Bélanger-Gariépy of Univeristé de Montréal. These structures were solved using the SHELXTL (1997) ver. 5.10 program on a Bruker AXS Smart 2K/Platform CCD diffractometer.

Melting points (Mp.) were recorded on a Gallenkamp K 8500 melting point apparatus using open end capillaries and are corrected. Differential scanning calorimetry (DSC) spectra were recorded on a TA Instruments DSC 2010 differential scanning calorimeter and are corrected.

All glassware was either oven-dried overnight (140 °C) then cooled in a desiccator containing Drierite or flame-dried and cooled under a nitrogen stream. All reactions were performed under a nitrogen atmosphere (N_2) unless otherwise stated.

APPENDIX II. X-Ray Structures

APPENDIX II.1

CRYSTAL AND MOLECULAR STRUCTURE OF

C8 H8 O2 S2 COMPOUND

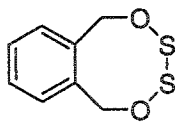

171

Structure solved and refined in the laboratory of X-ray diffraction
Université de Montréal by Francine Bélanger Gariépy.

Table II.1.1 Crystal data and structure refinement for C8 H8 O2 S2.

Empirical formula	C8 H8 O2 S2
Formula weight	200.26
Temperature	220(2)K
Wavelength	1.54178 Å
Crystal system	Monoclinic
Space group	P21/n
Unit cell dimensions	a = 4.82000(10) Å $\alpha = 90^\circ$ b = 15.6821(2) Å $\beta = 94.1410(10)^\circ$ c = 11.5593(2) Å $\gamma = 90^\circ$
Volume	871.46(3)Å^3
Z	4
Density (calculated)	1.526 Mg/m^3
Absorption coefficient	5.174 mm^{-1}
F(000)	416
Crystal size	0.49 x 0.05 x 0.05 mm
Theta range for data collection	4.76 to 72.74°
Index ranges	$-5 \leq h \leq 5$, $-19 \leq k \leq 19$, $-14 \leq \ell \leq 14$
Reflections collected	10561
Independent reflections	1712 [R_{int} = 0.030]
Absorption correction	Semi-empirical from equivalents
Max. and min. transmission	0.8400 and 0.5800
Refinement method	Full-matrix least-squares on F^2
Data / restraints / parameters	1712 / 0 / 109
Goodness-of-fit on F^2	1.024
Final R indices [I>2sigma(I)]	R_1 = 0.0382, wR_2 = 0.1037
R indices (all data)	R_1 = 0.0473, wR_2 = 0.1078
Largest diff. peak and hole	0.364 and -0.250 e/Å^3

Table II.1.2 Atomic coordinates (x 10^4) and equivalent isotropic displacement parameters ($Å^2$ x 10^3) for C8 H8 O2 S2.

U_{eq} is defined as one third of the trace of the orthogonalized Uij tensor.

	x	y	z	U_{eq}
S(1)	8935(1)	6777(1)	5197(1)	40(1)
O(2)	6188(3)	6147(1)	5202(1)	44(1)
C(3)	5363(5)	5850(2)	6320(2)	40(1)
C(4)	7722(5)	5519(2)	7119(2)	32(1)
C(5)	8633(5)	4695(2)	6966(2)	40(1)
C(6)	10800(5)	4351(2)	7666(2)	43(1)
C(7)	12040(6)	4835(2)	8548(2)	46(1)
C(8)	11163(5)	5656(2)	8722(2)	41(1)
C(9)	9004(5)	6017(1)	8014(2)	33(1)
C(10)	8259(6)	6937(2)	8220(2)	45(1)
O(11)	9835(4)	7509(1)	7523(2)	50(1)
S(12)	8384(2)	7747(1)	6223(1)	54(1)

Table II.1.3 Hydrogen coordinates (x 10^4) and isotropic displacement parameters ($Å^2$ x 10^3) for C8 H8 O2 S2.

	x	y	z	U_{eq}
H(3A)	3982	5395	6187	47
H(3B)	4466	6321	6706	47
H(5)	7760	4359	6373	48
H(6)	11416	3792	7539	51
H(7)	13495	4604	9036	55
H(8)	12033	5981	9328	49
H(10A)	6265	7020	8024	54
H(10B)	8645	7074	9043	54

Table II.1.4 Anisotropic parameters ($Å^2$ x 10^3) for C8 H8 O2 S2.

The anisotropic displacement factor exponent takes the form:

$$-2\pi^2 [h^2 a^{*2} U_{11} + ... + 2 h k a^* b^* U_{12}]$$

	U11	U22	U33	U23	U13	U12
S(1)	41(1)	43(1)	37(1)	3(1)	3(1)	-1(1)
O(2)	41(1)	54(1)	34(1)	0(1)	-6(1)	-9(1)
C(3)	32(1)	47(1)	40(1)	3(1)	-1(1)	-5(1)
C(4)	27(1)	37(1)	32(1)	2(1)	4(1)	-6(1)
C(5)	46(2)	35(1)	39(1)	-3(1)	4(1)	-9(1)
C(6)	49(2)	33(1)	47(2)	8(1)	7(1)	3(1)
C(7)	47(2)	50(2)	39(1)	14(1)	-3(1)	5(1)
C(8)	45(2)	48(1)	28(1)	-1(1)	-1(1)	-3(1)
C(9)	34(1)	37(1)	29(1)	0(1)	6(1)	-1(1)
C(10)	55(2)	45(2)	36(1)	-10(1)	5(1)	7(1)
O(11)	66(1)	35(1)	47(1)	-5(1)	-9(1)	-5(1)
S(12)	76(1)	32(1)	53(1)	3(1)	-7(1)	5(1)

Table II.1.5 Bond lengths [Å] and angles [°] for C8 H8 O2 S2

S(1)-O(2)	1.6521(18)	C(5)-C(4)-C(9)	119.2(2)
S(1)-S(12)	1.9588(10)	C(5)-C(4)-C(3)	118.5(2)
O(2)-C(3)	1.456(3)	C(9)-C(4)-C(3)	122.2(2)
C(3)-C(4)	1.504(3)	C(4)-C(5)-C(6)	121.6(2)
C(4)-C(5)	1.380(3)	C(7)-C(6)-C(5)	119.2(2)
C(4)-C(9)	1.404(3)	C(6)-C(7)-C(8)	120.3(2)
C(5)-C(6)	1.383(3)	C(7)-C(8)-C(9)	121.2(2)
C(6)-C(7)	1.374(4)	C(8)-C(9)-C(4)	118.4(2)
C(7)-C(8)	1.374(4)	C(8)-C(9)-C(10)	118.1(2)
C(8)-C(9)	1.397(3)	C(4)-C(9)-C(10)	123.5(2)
C(9)-C(10)	1.509(3)	O(11)-C(10)-C(9)	111.2(2)
C(10)-O(11)	1.456(3)	C(10)-O(11)-S(12)	116.01(16)
O(11)-S(12)	1.6539(19)	O(11)-S(12)-S(1)	107.94(7)
O(2)-S(1)-S(12)	108.57(8)		
C(3)-O(2)-S(1)	117.68(14)		
O(2)-C(3)-C(4)	114.39(19)		

Table II.1.6 Torsion angles [°] for C8 H8 O2 S2.

S(12)-S(1)-O(2)-C(3)	-53.90(18)
S(1)-O(2)-C(3)-C(4)	-46.6(3)
O(2)-C(3)-C(4)-C(5)	-81.3(3)
O(2)-C(3)-C(4)-C(9)	99.1(3)
C(9)-C(4)-C(5)-C(6)	-0.7(4)
C(3)-C(4)-C(5)-C(6)	179.7(2)
C(4)-C(5)-C(6)-C(7)	1.3(4)
C(5)-C(6)-C(7)-C(8)	-1.0(4)
C(6)-C(7)-C(8)-C(9)	0.1(4)
C(7)-C(8)-C(9)-C(4)	0.5(4)
C(7)-C(8)-C(9)-C(10)	-176.9(2)
C(5)-C(4)-C(9)-C(8)	-0.2(3)
C(3)-C(4)-C(9)-C(8)	179.4(2)
C(5)-C(4)-C(9)-C(10)	177.1(2)
C(3)-C(4)-C(9)-C(10)	-3.4(4)
C(8)-C(9)-C(10)-O(11)	90.5(3)
C(4)-C(9)-C(10)-O(11)	-86.7(3)
C(9)-C(10)-O(11)-S(12)	90.2(2)
C(10)-O(11)-S(12)-S(1)	-77.89(17)
O(2)-S(1)-S(12)-O(11)	93.20(11)

References

International Tables for Crystallography (1992). Vol. C. Tables 4.2.6.8 and 6.1.1.4, Dordrecht: Kluwer Academic Publishers.

SAINT (1999) Release 6.06; Integration Software for Single Crystal Data. Bruker AXS Inc., Madison, WI 53719-1173.

Sheldrick, G.M. (1996). SADABS, Bruker Area Detector Absorption Corrections. Bruker AXS Inc., Madison, WI 53719-1173.

Sheldrick, G.M. (1997). SHELXS97, Program for the Solution of Crystal Structures. Univ. of Gottingen, Germany.

Sheldrick, G.M. (1997). SHELXL97, Program for the Refinement of Crystal Structures. Univ. of Gottingen, Germany.

SHELXTL (1997) Release 5.10; The Complete Software Package for Single Crystal Structure Determination. Bruker AXS Inc., Madison, WI 53719-1173.

SMART (1999) Release 5.059; Bruker Molecular Analysis Research Tool. Bruker AXS Inc., Madison, WI 53719-1173.

Spek, A.L. (2000). PLATON, Molecular Geometry Program, 2000 version. University of Utrecht, Utrecht, Holland.

XPREP (1997) Release 5.10; X-ray data Preparation and Reciprocal space Exploration Program. Bruker AXS Inc., Madison, WI 53719-1173.

Supplementary Angles:

Distance HH

3.4464	H3A - H10A
4.6695	H3A - H10B
2.0217	H3B - H10A
3.4591	H3B - H10B
2.4384	H3A - H5
3.4964	H3B - H5
3.4716	H10A - H8
2.3735	H10B - H8
1.5816	H3A - H3B
1.5858	H10A - H10B

Least-squares planes (x,y,z in crystal coordinates) and deviations from them
(* indicates atom used to define plane)

- 3.3799 (0.0061) x - 5.1980 (0.0396) y + 7.8626 (0.0283) z = 0.1173 (0.0438)

*	-0.0016 (0.0011)	C3
*	0.0015 (0.0010)	C4
*	0.0019 (0.0013)	C5
*	-0.0018 (0.0012)	C6
	0.5975 (0.0031)	H3A
	0.3600 (0.0027)	H3B

Rms deviation of fitted atoms = 0.0017

- 3.3975 (0.0088) x - 4.8617 (0.0306) y + 7.9439 (0.0310) z = 0.3670 (0.0509)

Angle to previous plane (with approximate esd) = 1.31 (0.42)

*	-0.0156 (0.0012)	C10
*	0.0145 (0.0011)	C9
*	0.0188 (0.0014)	C8
*	-0.0177 (0.0014)	C7
	0.4656 (0.0025)	H10A
	0.4403 (0.0035)	H10B

Rms deviation of fitted atoms = 0.0167

APPENDIX II.2

CRYSTAL AND MOLECULAR STRUCTURE OF

C8 H8 O2 S2 COMPOUND

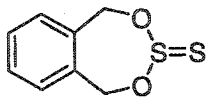

172

Structure solved and refined in the laboratory of X-ray diffraction
Emory University.

Table II.2.1 Crystal data and structure refinement for C8 H8 O2 S2.

Identification code	jsso3s	
Empirical formula	C8 H8 O2 S2	
Formula weight	200.26	
Temperature	100(2) K	
Wavelength	1.54178 Å	
Crystal system	Monoclinic	
Space group	P2(1)/c	
Unit cell dimensions	a = 7.8807(5) Å	α= 90°.
	b = 15.0240(8) Å	β= 93.278(4)°.
	c = 7.2198(4) Å	γ = 90°.
Volume	853.42(9) $Å^3$	
Z	4	
Density (calculated)	1.559 Mg/m^3	
Absorption coefficient	5.283 mm^{-1}	
F(000)	416	
Crystal size	0.32 x 0.22 x 0.19 mm^3	
Theta range for data collection	5.62 to 66.69°.	
Index ranges	-9<=h<=9, -17<=k<=15, -8<=l<=7	
Reflections collected	3792	
Independent reflections	1369 [R(int) = 0.0268]	
Completeness to theta = 66.69°	90.8 %	
Absorption correction	SADABS	
Max. and min. transmission	0.4334 and 0.2827	

Refinement method	Full-matrix least-squares on F^2
Data / restraints / parameters	1369 / 0 / 141
Goodness-of-fit on F^2	1.030
Final R indices [I>2sigma(I)]	R1 = 0.0390, wR2 = 0.1174
R indices (all data)	R1 = 0.0399, wR2 = 0.1187
Largest diff. peak and hole	0.419 and -0.638 e.$Å^{-3}$

Table II.2.2 Atomic coordinates (x 10^4) and equivalent isotropic displacement parameters ($Å^2$x 10^3) for JSSO3s. U(eq) is defined as one third of the trace of the orthogonalized U^{ij} tensor.

	x	y	z	U(eq)
C(1)	9012(3)	1606(2)	2712(3)	19(1)
C(2)	9697(3)	1366(1)	4633(3)	15(1)
C(3)	11368(3)	1566(2)	5182(3)	19(1)
C(4)	12040(3)	1360(2)	6953(3)	19(1)
C(5)	11009(3)	959(2)	8211(3)	19(1)
C(6)	9323(3)	760(2)	7677(3)	18(1)
C(7)	8663(3)	948(1)	5897(3)	14(1)
C(8)	6847(3)	697(2)	5359(3)	17(1)
O(1)	7630(2)	2252(1)	2787(2)	20(1)
O(2)	5771(2)	1474(1)	4968(2)	18(1)
S(1)	5700(1)	1909(1)	2908(1)	17(1)
S(2)	5260(1)	974(1)	1097(1)	22(1)

Table II.2.3 Bond lengths [Å] and angles [°] for JSSO3s.

C(1)-O(1)	1.462(3)
C(1)-C(2)	1.503(3)
C(2)-C(3)	1.387(3)
C(2)-C(7)	1.406(3)
C(3)-C(4)	1.391(3)
C(4)-C(5)	1.390(3)
C(5)-C(6)	1.394(3)
C(6)-C(7)	1.388(3)
C(7)-C(8)	1.509(3)
C(8)-O(2)	1.460(3)
O(1)-S(1)	1.6126(17)
O(2)-S(1)	1.6233(15)
S(1)-S(2)	1.9361(8)
O(1)-C(1)-C(2)	110.76(18)
C(3)-C(2)-C(7)	119.2(2)
C(3)-C(2)-C(1)	119.8(2)
C(7)-C(2)-C(1)	121.0(2)
C(2)-C(3)-C(4)	121.3(2)
C(5)-C(4)-C(3)	119.4(2)
C(4)-C(5)-C(6)	119.7(2)
C(7)-C(6)-C(5)	120.9(2)
C(6)-C(7)-C(2)	119.4(2)
C(6)-C(7)-C(8)	119.2(2)
C(2)-C(7)-C(8)	121.4(2)
O(2)-C(8)-C(7)	112.45(18)
C(1)-O(1)-S(1)	119.78(14)
C(8)-O(2)-S(1)	119.21(14)
O(1)-S(1)-O(2)	101.24(9)
O(1)-S(1)-S(2)	109.18(7)
O(2)-S(1)-S(2)	108.79(7)

Symmetry transformations used to generate equivalent atoms:

Table II.2.4 Anisotropic displacement parameters ($Å^2 x\ 10^3$) for JSSO3s. The anisotropic displacement factor exponent takes the form: $-2\pi^2[\ h^2\ a^{*2}U^{11} + ... + 2\ h\ k\ a^*\ b^*\ U^{12}\ ]$

	U^{11}	U^{22}	U^{33}	U^{23}	U^{13}	U^{12}
C(1)	18(1)	22(1)	18(1)	3(1)	8(1)	-1(1)
C(2)	17(1)	11(1)	17(1)	-1(1)	7(1)	3(1)
C(3)	19(1)	16(1)	23(1)	1(1)	7(1)	0(1)
C(4)	17(1)	16(1)	25(1)	-2(1)	1(1)	4(1)
C(5)	21(1)	16(1)	20(1)	-1(1)	2(1)	4(1)
C(6)	23(1)	15(1)	18(1)	1(1)	8(1)	0(1)
C(7)	16(1)	10(1)	18(1)	-1(1)	6(1)	1(1)
C(8)	18(1)	16(1)	18(1)	5(1)	4(1)	-2(1)
O(1)	19(1)	14(1)	25(1)	5(1)	2(1)	-2(1)
O(2)	17(1)	22(1)	18(1)	1(1)	6(1)	3(1)
S(1)	18(1)	15(1)	19(1)	1(1)	3(1)	1(1)
S(2)	25(1)	22(1)	19(1)	-2(1)	1(1)	-4(1)

Table II.2.5 Hydrogen coordinates (x 10^4) and isotropic displacement parameters ($Å^2$x 10^3) for JSSO3s.

	x	y	z	U(eq)
H(1)	8540(30)	1088(18)	1980(40)	19(7)
H(2)	9910(40)	1902(18)	2030(40)	20(7)
H(3)	12110(40)	1910(19)	4250(40)	27(8)
H(4)	13200(30)	1506(16)	7360(30)	13(6)
H(5)	11430(30)	836(17)	9460(40)	13(6)
H(6)	8570(40)	489(18)	8490(40)	24(7)
H(7)	6730(40)	330(19)	4210(40)	26(7)
H(8)	6400(40)	390(19)	6350(40)	32(8)

Table II.2.6 Torsion angles [°] for JSSO3s.

O(1)-C(1)-C(2)-C(3)	-116.8(2)
O(1)-C(1)-C(2)-C(7)	62.4(3)
C(7)-C(2)-C(3)-C(4)	0.2(3)
C(1)-C(2)-C(3)-C(4)	179.5(2)
C(2)-C(3)-C(4)-C(5)	-1.2(4)
C(3)-C(4)-C(5)-C(6)	0.8(3)
C(4)-C(5)-C(6)-C(7)	0.6(3)
C(5)-C(6)-C(7)-C(2)	-1.6(3)
C(5)-C(6)-C(7)-C(8)	178.3(2)
C(3)-C(2)-C(7)-C(6)	1.2(3)
C(1)-C(2)-C(7)-C(6)	-178.1(2)
C(3)-C(2)-C(7)-C(8)	-178.7(2)
C(1)-C(2)-C(7)-C(8)	2.0(3)
C(6)-C(7)-C(8)-O(2)	114.8(2)
C(2)-C(7)-C(8)-O(2)	-65.3(3)
C(2)-C(1)-O(1)-S(1)	-89.1(2)
C(7)-C(8)-O(2)-S(1)	85.1(2)
C(1)-O(1)-S(1)-O(2)	68.14(16)
C(1)-O(1)-S(1)-S(2)	-46.49(16)
C(8)-O(2)-S(1)-O(1)	-64.50(16)
C(8)-O(2)-S(1)-S(2)	50.43(16)

Crystal Structure Analysis

A suitable crystal of **JSSO3** was coated with Paratone N oil, suspended in a small fiber loop and placed in a cooled nitrogen gas stream at 100 K on a Bruker D8 SMART 1000 CCD sealed tube diffractometer with graphite monochromated CuK_α (1.54178 Å) radiation. Data were measured using a series of combinations of phi and omega scans with 10 second frame exposures and 0.3° frame widths. Data collection, indexing and initial cell refinements were all carried out using SMART[1] software. Frame integration and final cell refinements were done using SAINT[2] software. The final cell parameters were determined from least-squares refinement on 3545 reflections. The SADABS[3] program was used to carry out absorption corrections.

The structure was solved using Direct methods and difference Fourier techniques (SHELXTL, V5.10).[4] All the hydrogen atoms were located in a difference Fourier map and were included in the final cycles of least squares with isotropic U_{ij} 's; all non-hydrogen atoms were refined anisotropically. Scattering factors and anomalous dispersion corrections are taken from the *International Tables for X-ray Crystallography*[5]. Structure solution, refinement, graphics and generation of publication materials were performed by using SHELXTL, V5.10 software. Additional details of data collection and structure refinement are given in Table 1.

References

SMART Version 5.55, **2000**, Bruker AXS, Inc., Analytical X-ray Systems, 5465 East Cheryl Parkway, Madison WI 53711-5373.

SAINT Version 6.02, **1999**, Bruker AXS, Inc., Analytical X-ray Systems, 5465 East Cheryl Parkway, Madison WI 53711-5373.

SADABS, **1996**, George Sheldrick, University of Göttingen,

SHELXTL V5.10, **1997**, Bruker AXS, Inc., Analytical X-ray Systems, 5465 East Cheryl Parkway, Madison WI 53711-5373.

A. J. C. Wilson (ed), *International Tables for X-ray Crystallography, Volume C.* Kynoch, Academic Publishers, Dordrecht, **1992**, Tables 6.1.1.4 (pp. 500-502) and 4.2.6.8 (pp. 219-222).

APPENDIX II.3

CRYSTAL AND MOLECULAR STRUCTURE OF

C16 H16 O4 S4 COMPOUND

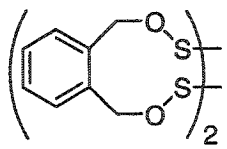

173

Structure solved and refined in the laboratory of X-ray diffraction
Université de Montréal by Francine Bélanger-Gariépy.

Table II.3.1 Crystal data and structure refinement for C16 H16 O4 S4.

Empirical formula	C16 H16 O4 S4
Formula weight	400.53
Temperature	220(2)K
Wavelength	1.54178 Å
Crystal system	Orthorhombic
Space group	Pba2
Unit cell dimensions	a = 13.5485(2) Å α = 90° b = 14.9235(2) Å β = 90° c = 4.37660(10) Å γ = 90°
Volume	884.91(3)Å^3
Z	2
Density (calculated)	1.503 Mg/m^3
Absorption coefficient	5.095 mm^{-1}
F(000)	416
Crystal size	0.27 x 0.15 x 0.11 mm
Theta range for data collection	4.41 to 72.76°
Index ranges	$-16 \leq h \leq 16$, $-17 \leq k \leq 18$, $-5 \leq \ell \leq 4$
Reflections collected	5381
Independent reflections	1485 [R_{int} = 0.031]
Absorption correction	Semi-empirical from equivalents
Max. and min. transmission	0.6900 and 0.3300
Refinement method	Full-matrix least-squares on F^2
Data / restraints / parameters	1485 / 1 / 109
Goodness-of-fit on F^2	1.039
Final R indices [I>2sigma(I)]	R_1 = 0.0382, wR_2 = 0.1013
R indices (all data)	R_1 = 0.0423, wR_2 = 0.1031
Absolute structure parameter	0.07(3)
Largest diff. peak and hole	0.300 and -0.285 e/Å^3

Table II.3.2 Atomic coordinates (x 10^4) and equivalent isotropic displacement parameters ($Å^2$ x 10^3) for C16 H16 O4 S4.

U_{eq} is defined as one third of the trace of the orthogonalized Uij tensor.

	x	y	z	U_{eq}
S(1)	7597(1)	9643(1)	7055(2)	41(1)
O(2)	6787(2)	8927(1)	8474(6)	40(1)
C(3)	6576(2)	8154(2)	6543(8)	36(1)
C(4)	5842(2)	7595(2)	8257(8)	35(1)
C(5)	6126(2)	6784(2)	9509(11)	44(1)
C(6)	5482(3)	6259(2)	11141(10)	51(1)
C(7)	4514(3)	6543(2)	11532(10)	48(1)
C(8)	4219(3)	7352(2)	10295(10)	42(1)
C(9)	4859(2)	7882(2)	8663(8)	36(1)
C(10)	4518(2)	8772(2)	7417(10)	42(1)
O(11)	3508(2)	8670(1)	6398(7)	47(1)
S(12)	3091(1)	9524(1)	4309(2)	45(1)

Table II.3.3 Hydrogen coordinates (x 10^4) and isotropic displacement parameters ($Å^2$ x 10^3) for C16 H16 O4 S4.

	x	y	z	U_{eq}
H(3A)	7180	7811	6155	43
H(3B)	6300	8347	4580	43
H(5)	6779	6586	9235	53
H(6)	5694	5713	11985	61
H(7)	4064	6188	12628	58
H(8)	3564	7544	10578	51
H(10A)	4557	9232	9009	51
H(10B)	4939	8955	5706	51

Table II.3.4 Anisotropic parameters ($Å^2$ x 10^3) for C16 H16 O4 S4.

The anisotropic displacement factor exponent takes the form:

$$-2\pi^2 [h^2 a^{*2} U_{11} + ... + 2 h k a^* b^* U_{12}]$$

	U11	U22	U33	U23	U13	U12
S(1)	30(1)	34(1)	57(1)	-5(1)	6(1)	1(1)
O(2)	43(1)	32(1)	44(2)	-6(1)	4(1)	-5(1)
C(3)	35(2)	31(2)	40(2)	-11(1)	2(2)	4(1)
C(4)	32(1)	30(2)	41(2)	-9(1)	-1(1)	0(1)
C(5)	37(2)	33(2)	62(2)	-7(2)	-7(2)	6(1)
C(6)	50(2)	30(2)	74(3)	8(2)	-11(2)	1(2)
C(7)	49(2)	37(2)	58(3)	5(2)	5(2)	-10(2)
C(8)	36(2)	34(2)	57(2)	-3(2)	4(2)	1(2)
C(9)	33(1)	30(2)	44(2)	-6(1)	-1(1)	2(1)
C(10)	34(2)	35(2)	58(3)	1(2)	-4(2)	1(1)
O(11)	35(1)	34(1)	71(2)	0(1)	-7(1)	0(1)
S(12)	44(1)	41(1)	48(1)	-2(1)	-11(1)	3(1)

Table II.3.5 Bond lengths [Å] and angles [°] for C16 H16 O4 S4

S(1)-O(2)	1.653(2)
S(1)-S(12)#1	1.9637(13)
O(2)-C(3)	1.458(3)
C(3)-C(4)	1.500(4)
C(4)-C(5)	1.383(4)
C(4)-C(9)	1.410(4)
C(5)-C(6)	1.374(5)
C(6)-C(7)	1.388(5)
C(7)-C(8)	1.382(5)
C(8)-C(9)	1.374(5)
C(9)-C(10)	1.509(4)
C(10)-O(11)	1.447(4)
O(11)-S(12)	1.667(2)
S(12)-S(1)#1	1.9637(13)
O(2)-S(1)-S(12)#1	108.91(9)
C(3)-O(2)-S(1)	115.07(19)
O(2)-C(3)-C(4)	106.3(2)
C(5)-C(4)-C(9)	118.6(3)
C(5)-C(4)-C(3)	120.0(3)
C(9)-C(4)-C(3)	121.3(3)
C(6)-C(5)-C(4)	121.8(3)
C(5)-C(6)-C(7)	119.4(3)
C(8)-C(7)-C(6)	119.4(4)
C(9)-C(8)-C(7)	121.6(3)
C(8)-C(9)-C(4)	119.2(3)
C(8)-C(9)-C(10)	120.1(3)
C(4)-C(9)-C(10)	120.7(3)
O(11)-C(10)-C(9)	108.0(2)
C(10)-O(11)-S(12)	114.19(19)
O(11)-S(12)-S(1)#1	108.00(11)

Symmetry transformations used to generate equivalent atoms:

#1 -x+1,-y+2,z

Table II.3.6 Torsion angles [°] for C16 H16 O4 S4.

S(12)#1-S(1)-O(2)-C(3)	84.4(2)
S(1)-O(2)-C(3)-C(4)	179.4(2)
O(2)-C(3)-C(4)-C(5)	-108.8(3)
O(2)-C(3)-C(4)-C(9)	70.4(4)
C(9)-C(4)-C(5)-C(6)	-0.4(6)
C(3)-C(4)-C(5)-C(6)	178.8(3)
C(4)-C(5)-C(6)-C(7)	0.5(6)
C(5)-C(6)-C(7)-C(8)	-0.6(6)
C(6)-C(7)-C(8)-C(9)	0.5(6)
C(7)-C(8)-C(9)-C(4)	-0.4(6)
C(7)-C(8)-C(9)-C(10)	-178.4(3)
C(5)-C(4)-C(9)-C(8)	0.3(5)
C(3)-C(4)-C(9)-C(8)	-178.9(3)
C(5)-C(4)-C(9)-C(10)	178.4(3)
C(3)-C(4)-C(9)-C(10)	-0.9(5)
C(8)-C(9)-C(10)-O(11)	-37.6(5)
C(4)-C(9)-C(10)-O(11)	144.4(3)
C(9)-C(10)-O(11)-S(12)	-168.0(2)
C(10)-O(11)-S(12)-S(1)#1	-94.4(2)
O(2)-S(1)-S(12)#1-O(11)#1	87.6(1)

Symmetry transformations used to generate equivalent atoms:

#1 -x+1,-y+2,z

References

Flack, H.D. (1983). Acta Cryst. A39, 876-881.

Flack, H.D. and Schwarzenbach, D. (1988). Acta Cryst. A44, 499-506.

International Tables for Crystallography (1992). Vol. C. Tables 4.2.6.8 and 6.1.1.4, Dordrecht: Kluwer Academic Publishers.

SAINT (1999) Release 6.06; Integration Software for Single Crystal Data. Bruker AXS Inc., Madison, WI 53719-1173.

Sheldrick, G.M. (1996). SADABS, Bruker Area Detector Absorption Corrections. Bruker AXS Inc., Madison, WI 53719-1173.

Sheldrick, G.M. (1997). SHELXS97, Program for the Solution of Crystal Structures. Univ. of Gottingen, Germany.

Sheldrick, G.M. (1997). SHELXL97, Program for the Refinement of Crystal Structures. Univ. of Gottingen, Germany.

SHELXTL (1997) Release 5.10; The Complete Software Package for Single Crystal Structure Determination. Bruker AXS Inc., Madison, WI 53719-1173.

SMART (1999) Release 5.059; Bruker Molecular Analysis Research Tool. Bruker AXS Inc., Madison, WI 53719-1173.

Spek, A.L. (2000). PLATON, Molecular Geometry Program, 2000 version. University of Utrecht, Utrecht, Holland.

XPREP (1997) Release 5.10; X-ray data Preparation and Reciprocal space Exploration Program. Bruker AXS Inc., Madison, WI 53719-1173.

APPENDIX II.4

CRYSTAL AND MOLECULAR STRUCTURE OF

C8 H8 O3 S COMPOUND

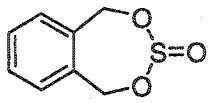

174

Structure solved and refined in the laboratory of X-ray diffraction
Université de Montréal by Francine Bélanger-Gariépy.

Table II.4.1 Crystal data and structure refinement for C8 H8 O3 S.

Empirical formula	C8 H8 O3 S
Formula weight	184.20
Temperature	220(2)K
Wavelength	1.54178 Å
Crystal system	Orthorhombic
Space group	Pbca
Unit cell dimensions	a = 11.2787(2) Å $\alpha = 90^\circ$ b = 8.8934(2) Å $\beta = 90^\circ$ c = 16.4636(3) Å $\gamma = 90^\circ$
Volume	1651.40(6)$Å^3$
Z	8
Density (calculated)	1.482 Mg/m^3
Absorption coefficient	3.200 mm^{-1}
F(000)	768
Crystal size	0.60 x 0.27 x 0.08 mm
Theta range for data collection	5.37 to 55.16°
Index ranges	$-11 \leq h \leq 11$, $-8 \leq k \leq 9$, $-17 \leq \ell \leq 16$
Reflections collected	10293
Independent reflections	1037 [R_{int} = 0.050]
Absorption correction	Semi-empirical from equivalents
Max. and min. transmission	0.8300 and 0.2400
Refinement method	Full-matrix least-squares on F^2
Data / restraints / parameters	1037 / 372 / 219
Goodness-of-fit on F^2	1.004
Final R indices [I>2sigma(I)]	R_1 = 0.0372, wR_2 = 0.0954
R indices (all data)	R_1 = 0.0434, wR_2 = 0.0997
Extinction coefficient	0.0026(4)
Largest diff. peak and hole	0.187 and -0.272 $e/Å^3$

Table II.4.2 Atomic coordinates (x 10^4) and equivalent isotropic displacement parameters ($Å^2$ x 10^3) for C8 H8 O3 S.

U_{eq} is defined as one third of the trace of the orthogonalized Uij tensor.

	Occ.	x	y	z	U_{eq}
O(11)	0.899(3)	3414(3)	-788(3)	2728(2)	82(1)
S(11)	0.899(3)	2738(1)	527(1)	2498(1)	63(1)
O(12)	0.899(3)	3669(2)	1820(2)	2281(1)	63(1)
C(13)	0.899(3)	4695(2)	1438(3)	1768(2)	57(1)
C(14)	0.899(3)	4394(4)	1617(5)	883(2)	48(1)
C(15)	0.899(3)	4974(5)	2683(7)	419(2)	64(1)
C(16)	0.899(3)	4719(4)	2854(5)	-395(3)	76(1)
C(17)	0.899(3)	3878(4)	1965(5)	-747(2)	75(1)
C(18)	0.899(3)	3283(4)	896(4)	-293(2)	61(1)
C(19)	0.899(3)	3537(4)	711(4)	519(2)	45(1)
C(110)	0.899(3)	2873(4)	-448(4)	1000(2)	56(1)
O(111)	0.899(3)	2147(2)	254(4)	1630(1)	60(1)
O(21)	0.101(3)	2683(18)	250(20)	3092(10)	123(7)
S(21)	0.101(3)	3116(9)	-588(11)	2400(6)	81(3)
O(22)	0.101(3)	4370(10)	108(15)	2127(9)	88(4)
C(23)	0.101(3)	4350(30)	1710(19)	1893(12)	58(5)
C(24)	0.101(3)	4360(40)	1840(50)	979(13)	49(4)
C(25)	0.101(3)	5140(40)	2830(60)	611(15)	48(5)
C(26)	0.101(3)	5080(30)	3090(50)	-213(16)	58(5)
C(27)	0.101(3)	4310(40)	2290(50)	-673(13)	57(6)
C(28)	0.101(3)	3490(40)	1330(50)	-320(13)	53(5)
C(29)	0.101(3)	3540(30)	1060(40)	508(12)	49(5)
C(210)	0.101(3)	2920(30)	-310(30)	831(11)	52(5)
O(211)	0.101(3)	2361(16)	-40(40)	1620(10)	58(5)

Table II.4.3 Hydrogen coordinates (x 10^4) and isotropic displacement parameters ($Å^2$ x 10^3) for C8 H8 O3 S.

	Occ.	x	y	z	U_{eq}
H(13A)	0.899(3)	4936	397	1873	69
H(13B)	0.899(3)	5363	2096	1905	69
H(15)	0.899(3)	5549	3301	662	77
H(16)	0.899(3)	5123	3578	-706	91
H(17)	0.899(3)	3700	2080	-1301	90
H(18)	0.899(3)	2703	291	-541	73
H(11A)	0.899(3)	2363	-1031	635	67
H(11B)	0.899(3)	3439	-1142	1253	67
H(23A)	0.101(3)	5040	2225	2122	70
H(23B)	0.101(3)	3633	2189	2109	70
H(25)	0.101(3)	5721	3321	926	57
H(26)	0.101(3)	5575	3821	-455	70
H(27)	0.101(3)	4322	2393	-1241	69
H(28)	0.101(3)	2914	853	-641	63
H(21A)	0.101(3)	2319	-632	441	63
H(21B)	0.101(3)	3502	-1125	886	63

Table II.4.4 Anisotropic parameters ($Å^2$ x 10^3) for C8 H8 O3 S.

The anisotropic displacement factor exponent takes the form:

$$-2\,\pi^2\,[\,h^2\,a^{*2}\,U_{11} + \ldots + 2\,h\,k\,a^*\,b^*\,U_{12}\,]$$

	U11	U22	U33	U23	U13	U12
O(11)	86(2)	80(2)	80(2)	25(1)	-6(1)	17(1)
S(11)	69(1)	66(1)	54(1)	11(1)	10(1)	10(1)
O(12)	75(1)	58(1)	56(1)	-9(1)	5(1)	6(1)
C(13)	49(2)	60(2)	63(2)	-8(1)	-4(1)	-3(1)
C(14)	44(1)	39(2)	62(2)	-3(1)	7(1)	3(1)
C(15)	61(2)	49(2)	81(3)	1(3)	16(2)	-2(1)
C(16)	89(4)	49(3)	89(3)	13(3)	43(3)	8(2)
C(17)	99(3)	67(3)	58(2)	6(2)	17(2)	24(2)
C(18)	74(2)	52(3)	56(2)	-4(1)	1(1)	9(2)
C(19)	49(2)	36(2)	50(2)	-3(1)	2(1)	7(1)
C(110)	55(2)	52(2)	61(2)	-8(1)	3(2)	-9(1)
O(111)	48(1)	66(2)	66(1)	8(1)	5(1)	5(1)
O(21)	137(16)	149(15)	82(14)	33(12)	25(12)	-47(13)
S(21)	100(7)	47(6)	94(7)	6(4)	4(5)	-16(5)
O(22)	98(9)	74(8)	92(8)	16(7)	-28(8)	5(7)
C(23)	59(9)	49(8)	67(9)	-8(8)	-23(8)	-4(8)
C(24)	46(8)	41(8)	60(7)	-18(7)	4(7)	-1(7)
C(25)	53(10)	37(9)	53(9)	-10(9)	2(8)	3(8)
C(26)	65(11)	45(10)	64(10)	-15(9)	8(9)	3(8)
C(27)	74(11)	46(10)	52(10)	13(9)	17(9)	-5(10)
C(28)	64(9)	43(9)	52(8)	-8(8)	1(8)	-8(8)
C(29)	53(8)	40(8)	53(8)	0(7)	14(8)	4(8)
C(210)	51(9)	51(9)	55(8)	-3(8)	-2(8)	15(8)
O(211)	53(8)	51(8)	71(8)	8(7)	4(7)	13(7)

Table II.4.5 Bond lengths [Å] and angles [°] for C8 H8 O3 S

O(11)-S(11)	1.447(3)	C(28)-C(29)-C(24)	119.2(1)
S(11)-O(111)	1.595(2)	C(28)-C(29)-C(210)	118.10(13)
S(11)-O(12)	1.5980(18)	C(24)-C(29)-C(210)	120.90(14)
O(12)-C(13)	1.472(3)	O(211)-C(210)-C(29)	112.50(14)
C(13)-C(14)	1.505(4)	C(210)-O(211)-S(21)	115.30(13)
C(14)-C(15)	1.382(3)		
C(14)-C(19)	1.394(3)		
C(15)-C(16)	1.379(5)		
C(16)-C(17)	1.364(5)		
C(17)-C(18)	1.382(5)		
C(18)-C(19)	1.377(3)		
C(19)-C(110)	1.501(3)		
C(110)-O(111)	1.462(3)		
O(21)-S(21)	1.445(9)		
S(21)-O(22)	1.608(9)		
S(21)-O(211)	1.616(9)		
O(22)-C(23)	1.476(10)		
C(23)-C(24)	1.509(9)		
C(24)-C(25)	1.383(9)		
C(24)-C(29)	1.396(9)		
C(25)-C(26)	1.38(1)		
C(26)-C(27)	1.361(10)		
C(27)-C(28)	1.383(10)		
C(28)-C(29)	1.384(9)		
C(29)-C(210)	1.50(1)		
C(210)-O(211)	1.465(9)		
O(11)-S(11)-O(111)	109.4(2)		
O(11)-S(11)-O(12)	107.11(15)		
O(111)-S(11)-O(12)	100.54(13)		
C(13)-O(12)-S(11)	118.64(15)		
O(12)-C(13)-C(14)	110.7(3)		
C(15)-C(14)-C(19)	119.1(3)		
C(15)-C(14)-C(13)	120.1(3)		
C(19)-C(14)-C(13)	120.8(2)		
C(16)-C(15)-C(14)	121.0(3)		
C(17)-C(16)-C(15)	119.5(3)		
C(16)-C(17)-C(18)	120.5(3)		
C(19)-C(18)-C(17)	120.4(3)		
C(18)-C(19)-C(14)	119.5(2)		
C(18)-C(19)-C(110)	119.4(2)		
C(14)-C(19)-C(110)	121.1(2)		
O(111)-C(110)-C(19)	111.1(2)		
C(110)-O(111)-S(11)	117.8(2)		
O(21)-S(21)-O(22)	108.6(9)		
O(21)-S(21)-O(211)	107.00(12)		
O(22)-S(21)-O(211)	97.2(9)		
C(23)-O(22)-S(21)	115.50(12)		
O(22)-C(23)-C(24)	109.50(15)		
C(25)-C(24)-C(29)	119.8(1)		
C(25)-C(24)-C(23)	119.50(12)		
C(29)-C(24)-C(23)	120.60(13)		
C(26)-C(25)-C(24)	120.50(12)		
C(27)-C(26)-C(25)	119.30(12)		
C(26)-C(27)-C(28)	121.20(12)		
C(27)-C(28)-C(29)	119.70(12)		

Table II.4.6 Torsion angles [°] for C8 H8 O3 S.

O(11)-S(11)-O(12)-C(13)	45.1(2)
O(111)-S(11)-O(12)-C(13)	-69.1(2)
S(11)-O(12)-C(13)-C(14)	88.3(2)
O(12)-C(13)-C(14)-C(15)	115.9(5)
O(12)-C(13)-C(14)-C(19)	-64.4(5)
C(19)-C(14)-C(15)-C(16)	-0.4(9)
C(13)-C(14)-C(15)-C(16)	179.3(5)
C(14)-C(15)-C(16)-C(17)	0.5(9)
C(15)-C(16)-C(17)-C(18)	-0.2(7)
C(16)-C(17)-C(18)-C(19)	-0.2(6)
C(17)-C(18)-C(19)-C(14)	0.3(6)
C(17)-C(18)-C(19)-C(110)	179.5(4)
C(15)-C(14)-C(19)-C(18)	0.0(7)
C(13)-C(14)-C(19)-C(18)	-179.7(4)
C(15)-C(14)-C(19)-C(110)	-179.2(5)
C(13)-C(14)-C(19)-C(110)	1.1(6)
C(18)-C(19)-C(110)-O(111)	-115.1(4)
C(14)-C(19)-C(110)-O(111)	64.1(5)
C(19)-C(110)-O(111)-S(11)	-89.5(3)
O(11)-S(11)-O(111)-C(110)	-43.0(3)
O(12)-S(11)-O(111)-C(110)	69.4(3)
O(21)-S(21)-O(22)-C(23)	-59.50(18)
O(211)-S(21)-O(22)-C(23)	51.30(19)
S(21)-O(22)-C(23)-C(24)	-101.90(19)
O(22)-C(23)-C(24)-C(25)	-132(5)
O(22)-C(23)-C(24)-C(29)	53(5)
C(29)-C(24)-C(25)-C(26)	2(9)
C(23)-C(24)-C(25)-C(26)	-173(5)
C(24)-C(25)-C(26)-C(27)	-5(9)
C(25)-C(26)-C(27)-C(28)	7(9)
C(26)-C(27)-C(28)-C(29)	-6(8)
C(27)-C(28)-C(29)-C(24)	3(7)
C(27)-C(28)-C(29)-C(210)	-161(5)
C(25)-C(24)-C(29)-C(28)	-2(7)
C(23)-C(24)-C(29)-C(28)	173(4)
C(25)-C(24)-C(29)-C(210)	163(5)
C(23)-C(24)-C(29)-C(210)	-23(6)
C(28)-C(29)-C(210)-O(211)	-143(4)
C(24)-C(29)-C(210)-O(211)	53(5)
C(29)-C(210)-O(211)-S(21)	-98(2)
O(21)-S(21)-O(211)-C(210)	158.30(19)
O(22)-S(21)-O(211)-C(210)	46(2)

References

International Tables for Crystallography (1992). Vol. C. Tables 4.2.6.8 and 6.1.1.4, Dordrecht: Kluwer Academic Publishers.

SAINT (1999) Release 6.06; Integration Software for Single Crystal Data. Bruker AXS Inc., Madison, WI 53719-1173.

Sheldrick, G.M. (1996). SADABS, Bruker Area Detector Absorption Corrections. Bruker AXS Inc., Madison, WI 53719-1173.

Sheldrick, G.M. (1997). SHELXS97, Program for the Solution of Crystal Structures. Univ. of Gottingen, Germany.

Sheldrick, G.M. (1997). SHELXL97, Program for the Refinement of Crystal Structures. Univ. of Gottingen, Germany.

SHELXTL (1997) Release 5.10; The Complete Software Package for Single Crystal Structure Determination. Bruker AXS Inc., Madison, WI 53719-1173.

SMART (1999) Release 5.059; Bruker Molecular Analysis Research Tool. Bruker AXS Inc., Madison, WI 53719-1173.

Spek, A.L. (2000). PLATON, Molecular Geometry Program, 2000 version. University of Utrecht, Utrecht, Holland.

XPREP (1997) Release 5.10; X-ray data Preparation and Reciprocal space Exploration Program. Bruker AXS Inc., Madison, WI 53719-1173.

APPENDIX II.5

CRYSTAL AND MOLECULAR STRUCTURE OF

C14 H14 S3 COMPOUND

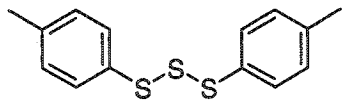

257b

Structure solved by X-Ray crystallography laboratory, chemistry department, McGill University by Dr Anne-Marie Lebuis.

Table II.4.1 Crystal data and structure refinement for C14 H14 S3.

Empirical formula	C14 H14 S3	
Formula weight, Mr	278.43	
Cell setting	Orthorhombic	
Space group	P2(1)2(1)2	
Unit cell dimensions (A, deg)	a = 7.5363(4)	α = 90
	b = 16.1028(8)	β = 90
	c = 5.8308(3)	γ = 90
Volume of unit cell, V	707.60(6)$Å^3$	
Formula units per cell, Z	2	
Formula units per assymetric unit, Z'	1/2	
Density calculated from formula and cell, Dx (Mg/m^3)	1.307	
F(000)	292	
Radiation type	CuK\a	
Wavelength, lambda (A)	1.54178	
No. of reflections for cell measurement	1002	
Theta range (deg)	5.9 to 71.3	
Linear absorption coefficient, mu (mm^-1)	4.573	
Measurement temperature (K)	293(2)	
Crystal shape	plate	
Colour	colourless	
Size (mm)	0.494 x 0.160 x 0.011	
Data collection		
Diffractometer type	Bruker AXS Smart 2K/Platform	
Data-collection method	phi scans	
Absorption correction type	Multi scan	
Max and min transmission values	0.97 and 0.30	

No. of reflections measured	8496
No. of independent reflections	1347
Completeness of data to Theta max	0.970
No. of observed reflections	1022
Criterion for observed reflections	>2sigma(I)
Rint	0.1120
Theta range for data collection	5.49 to 72.58 deg.
Ranges of h,k,l	$-9 \leq h \leq 9$, $-19 \leq k \leq 19$, $-6 \leq \ell \leq 6$
No. of standard reflections	64
Intensity decay (%)	none
Refinement	
Refinement method	Full-matrix on F^2
Final R indices, I>2sigma(I)	R1 = 0.0458, wR2 = 0.1168
R indices, all data	R1 = 0.0625, wR2 = 0.1168
Goodness-of-fit on F^2, S	0.957

R1 = sum (absabs Foabs -abs Fcabsabs)/sum (abs Foabs),
wR2 = [sum [w(Fo^2^-Fc^2^)^2^]/sum [w(Fo^2^)^2^]]^1*2^ and
GoF = [sum [w(Fo^2^-Fc^2^)^2^]/(No. of reflns - No. of params.)]^1*2^

Data / restraints / parameters	1347 / 0 / 78
Method of refining and locating H atoms	riding
Weighting scheme	based on measured s.u.'s
Function minimized	sum w(Fo^2^-Fc^2^)

calc w=1/[\s^2^(Fo^2^)+(0.0665P)^2^]

Maximum shift/sigma	0.000
Largest diff. peak and hole	0.365 and -0.216 e.A^*3
Absolute structure parameter	0.09(4)

Table II.5.2 Atomic coordinates and equivalent isotropic displacement parameters (A^2^ x 10 ^2^) for C14 H14 S3.

U~eq~ = (1/3)sum~i~sum~j~U~ij~a^*^~i~a^*^~j~a~i~.a~j~.

	x	y	z	U(eq)
S(1)	0.29321(14)	0.46585(6)	0.1188(2)	7.05(4)
S(2)	0.5000	0.5000	-0.0870(2)	6.28(4)
C(1)	0.3391(4)	0.3606(2)	0.1899(6)	5.12(9)
C(2)	0.4207(4)	0.3416(2)	0.3972(6)	5.82(9)
C(3)	0.4489(5)	0.2598(3)	0.4575(6)	5.75(9)
C(4)	0.3950(4)	0.1952(2)	0.3175(6)	4.98(8)
C(5)	0.3150(4)	0.2158(2)	0.1110(6)	5.07(8)
C(6)	0.2864(4)	0.2972(2)	0.0482(5)	5.07(8)
C(7)	0.4246(5)	0.1070(2)	0.3880(9)	7.25(11)

Table II.5.3 Bond lengths (A) and angles (deg) for C14 H14 S3.

S(1)-C(1)	1.779(4)	S(1)-S(2)	2.0422(14)
S(2)-S(1)#1	2.0422(14)	C(1)-C(6)	1.373(4)
C(1)-C(2)	1.390(5)	C(2)-C(3)	1.380(5)
C(2)-H(2)	0.9300	C(3)-C(4)	1.383(5)
C(3)-H(3)	0.9300	C(4)-C(5)	1.387(5)
C(4)-C(7)	1.495(5)	C(5)-C(6)	1.377(4)
C(5)-H(5)	0.9300	C(6)-H(6)	0.9300
C(7)-H(7A)	0.9600	C(7)-H(7B)	0.9600
C(7)-H(7C)	0.9600	C(7)-H(7D)	0.9600
C(7)-H(7E)	0.9600	C(7)-H(7F)	0.9600

C(1)-S(1)-S(2)	104.18(11)	S(1)#1-S(2)-S(1)	108.04(9)
C(6)-C(1)-C(2)	119.2(3)	C(6)-C(1)-S(1)	120.8(3)
C(2)-C(1)-S(1)	119.9(3)	C(3)-C(2)-C(1)	120.0(3)
C(3)-C(2)-H(2)	120.0	C(1)-C(2)-H(2)	120.0
C(2)-C(3)-C(4)	121.5(3)	C(2)-C(3)-H(3)	119.3
C(4)-C(3)-H(3)	119.3	C(3)-C(4)-C(5)	117.4(3)
C(3)-C(4)-C(7)	120.5(3)	C(5)-C(4)-C(7)	122.1(3)
C(6)-C(5)-C(4)	121.8(3)	C(6)-C(5)-H(5)	119.1
C(4)-C(5)-H(5)	119.1	C(1)-C(6)-C(5)	120.2(3)
C(1)-C(6)-H(6)	119.9	C(5)-C(6)-H(6)	119.9
C(4)-C(7)-H(7A)	109.5	C(4)-C(7)-H(7B)	109.5
H(7A)-C(7)-H(7B)	109.5	C(4)-C(7)-H(7C)	109.5
H(7A)-C(7)-H(7C)	109.5	H(7B)-C(7)-H(7C)	109.5
C(4)-C(7)-H(7D)	109.5	H(7A)-C(7)-H(7D)	141.1
H(7B)-C(7)-H(7D)	56.3	H(7C)-C(7)-H(7D)	56.3
C(4)-C(7)-H(7E)	109.5	H(7A)-C(7)-H(7E)	56.3
H(7B)-C(7)-H(7E)	141.1	H(7C)-C(7)-H(7E)	56.3
HH(7D)-C(7)-H(7E)	109.5	C(4)-C(7)-H(7F)	109.5
H(7A)-C(7)-H(7F)	56.3	H(7B)-C(7)-H(7F)	56.3
H(7C)-C(7)-H(7F)	141.1	H(7D)-C(7)-H(7F)	109.5
H(7E)-C(7)-H(7F)	109.5		

Symmetry transformations used to generate equivalent atoms:
#1 -x+1,-y+1,z

Table II.5.4 Torsion angles (deg) for C14 H14 S3.

C(1)-S(1)-S(2)-S(1)#1	-83.47(13)
S(2)-S(1)-C(1)-C(6)	-86.0(3)
S(2)-S(1)-C(1)-C(2)	97.6(3)
C(6)-C(1)-C(2)-C(3)	0.5(5)
S(1)-C(1)-C(2)-C(3)	177.0(3)
C(1)-C(2)-C(3)-C(4)	-1.1(5)
C(2)-C(3)-C(4)-C(5)	1.5(5)
C(2)-C(3)-C(4)-C(7)	-179.1(3)
C(3)-C(4)-C(5)-C(6)	-1.4(5)
C(7)-C(4)-C(5)-C(6)	179.3(3)
C(2)-C(1)-C(6)-C(5)	-0.3(5)
S(1)-C(1)-C(6)-C(5)	-176.8(3)
C(4)-C(5)-C(6)-C(1)	0.8(5)
C(1)-S(1)-S(2)-S(1)#1	-83.47(13)

Symmetry transformations used to generate equivalent atoms:
#1 -x+1,-y+1,z

Table II.5.5 Hydrogen coordinates and isotropic displacement parameters (A^2^ x 10 ^2^) for C14 H14 S3.

	x	y	z	U~iso~
H(2)	0.4562	0.3840	0.4953	7.0
H(3)	0.5055	0.2478	0.5954	6.9
H(5)	0.2798	0.1736	0.0122	6.1
H(6)	0.2313	0.3091	-0.0906	6.1
H(7A)	0.3794	0.0706	0.2716	10.9
H(7B)	0.3642	0.0965	0.5300	10.9
H(7C)	0.5494	0.0974	0.4077	10.9
H(7D)	0.4826	0.1057	0.5346	10.9
H(7E)	0.4978	0.0798	0.2762	10.9
H(7F)	0.3126	0.0789	0.3985	10.9

Table II.5.6 Anisotropic parameters (A^2 x 10^2) for C14 H14 S3.

The anisotropic displacement factor exponent takes the form:

-2 pi^2 [h^2 a*^2 U11 + ... + 2 h k a* b* U12]

	U11	U22	U33	U23	U13	U12
S(1)	6.58(6)	5.31(5)	9.24(8)	-0.04(5)	0.67(6)	0.77(5)
S(2)	8.84(10)	4.97(7)	5.03(7)	0.0	0.0	-0.40(6)
C(1)	4.64(19)	5.4(2)	5.3(2)	-0.89(16)	0.74(15)	-0.39(15)
C(2)	6.1(2)	6.6(2)	4.7(2)	-1.8(2)	-0.15(17)	-0.92(18)
C(3)	5.8(2)	7.2(3)	4.3(2)	0.19(17)	-0.58(15)	-0.16(19)
C(4)	4.09(17)	5.8(2)	5.0(2)	0.41(17)	0.44(15)	-0.35(16)
C(5)	5.40(18)	5.4(2)	4.38(19)	-1.04(16)	-0.22(18)	-0.68(16)
C(6)	4.85(17)	6.3(2)	4.1(2)	-0.24(15)	-0.43(15)	-0.06(18)
C(7)	7.1(2)	6.8(3)	7.8(3)	1.3(2)	0.1(2)	-0.70(19)

Table II.5.7 Distances to the weighted least-squares planes for C14 H14 S3.

(x,y,z in crystal coordinates, * indicates atom used to define plane)

6.7259 (0.0048) x + 0.2811 (0.0226) y - 2.6283 (0.0074) z = 1.8837 (0.0072)

*	-0.0006 (0.0021)	C1
*	-0.0023 (0.0024)	C2
*	0.0061 (0.0024)	C3
*	-0.0069 (0.0022)	C4
*	0.0042 (0.0022)	C5
*	-0.0004 (0.0022)	C6
	-0.0173 (0.0061)	C7

Rms deviation of fitted atoms = 0.0043

Discussion data collection, structure determination and refinement procedure

X-ray crystallographic data for I were collected from a single crystal sample, which was mounted on a glass fiber. Data were collected using a Bruker Platform diffractometer, equipped with a Bruker SMART 2K Charged-Coupled Device (CCD) Area Detector using the program SMART and normal focus sealed tube source graphite monochromated Cu-KALPHA radiation. The crystal-to-detector distance was 4.908 cm, and the data collection was carried out in 512 x 512 pixel mode, utilizing 4 x 4 pixel binning. The initial unit cell parameters were determined by a least-squares fit of the angular setting of strong reflections, collected by a 9.0 degree scan in 30 frames over four different parts of the reciprocal space (120 frames total). One complete sphere of data was collected, to better than 0.8\%A resolution. Upon completion of the data collection, the first 101 frames were recollected in order to improve the decay correction analysis.

Data reduction processing was carried out by the use of the program SAINT (Bruker, 1999), which applied Lorentz and polarization corrections to three-dimensionally integrated diffraction spots.
The program SADABS (Sheldrick, 1996) was utilized for the scaling of diffraction data, the application of a decay correction, and an empirical absorption correction based on redundant reflections. The space group was confirmed by XPREP routine in SHELXTL program (Sheldrick, 1997).
The structure was solved by direct method using SHELXS97 (Sheldrick,1997) and difmap synthesis using SHELXL96 (Sheldrick, 1996). All non-hydrogen atoms are anisotropic, hydrogen atoms are isotropic. Hydrogen atoms are constrained to the parent site using a riding model; SHELXL96 defaults, C-H 0.93 to 0.97\%A. The hydrogen atoms on the methyl groups are disordered over 2 orientations related by an 180 degree rotation, with each at half occupancy. The isotropic factors, Uiso, were adjusted to a value 50% higher then U(eq) of the parent site (methyl) and 20% higher (others).

A final verification of possible voids was performed using the VOID routine of the PLATON program (Spek, 1995).

The molecule sits on a two-fold axis, the asymmetric unit is 1/2 molecule. The second half is identical

References

Flack, H.D. (1983). Acta Cryst. A39, 876-881.

Flack, H.D. and Schwarzenbach, D. (1988). Acta Cryst. A44, 499-506.

International Tables for Crystallography (1992). Vol. C. Tables 4.2.6.8 and 6.1.1.4, Dordrecht: Kluwer Academic Publishers.

SAINT (1999) Release 6.06; Integration Software for Single Crystal Data. Bruker AXS Inc., Madison, WI 53719-1173.

Sheldrick, G.M. (1996). SADABS, Bruker Area Detector Absorption Corrections. Bruker AXS Inc., Madison, WI 53719-1173.

SHELXTL (1997) Release 5.10; The Complete Software Package for Single Crystal Structure Determination. Bruker AXS Inc., Madison, WI 53719-1173.

SMART (1999) Release 5.059; Bruker Molecular Analysis Research Tool. Bruker AXS Inc., Madison, WI 53719-1173.

Spek, A.L. (1995. PLATON, Molecular Geometry Program, July 1995 version. University of Utrecht, Utrecht, Holland. (version 190499 at McGill)

XPREP (1997) Release 5.10; X-ray data Preparation and Reciprocal space Exploration Program. Bruker AXS Inc., Madison, WI 53719-1173.

APPENDIX II.6

CRYSTAL AND MOLECULAR STRUCTURE OF

C14 H14 S4 COMPOUND

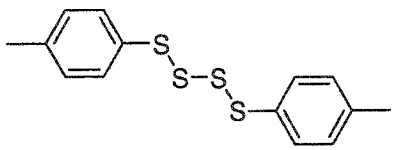

258b

Structure solved by X-Ray crystallography laboratory, chemistry department, McGill University by Dr Anne-Marie Lebuis.

Table II.6.1 Crystal data and structure refinement for C14 H14 S4.

Empirical formula	C14 H14 S4
Formula weight, Mr	310.49
Cell setting	Monoclinic
Space group	P2(1)/c
Unit cell dimensions (A, deg)	a = 14.1087(4) α = 90 b = 6.1715(2) β = 101.223(2) c = 17.5195(5) γ = 90
Volume of unit cell, V	1496.28(8)$Å^3$
Formula units per cell, Z	4
Formula units per asymmetric unit, Z'	1
Density calculated from formula and cell, Dx (Mg/m^3)	1.378
F(000)	648
Radiation type	CuK\a
Wavelength, lambda (A)	1.54178
No. of reflections for cell measurement	1018
Theta range (deg)	5.1 to 71.9
Linear absorption coefficient, mu (mm^-1)	5.653
Measurement temperature (K)	223(2)
Crystal shape	stick
Colour	colourless
Size (mm)	0.555 x 0.076 x 0.023
Data collection	
Diffractometer type	Bruker AXS SMART 2K/Platform
Data-collection method	phi scans
Absorption correction type	Semi-empirical from equivalents
Max and min transmission values	0.91 and 0.43

No. of reflections measured	17709
No. of independent reflections	2900
Completeness of data to Theta max	0.979
No. of observed reflections	2197
Criterion for observed reflections	>2sigma(I)
Rint	0.0946
Theta range for data collection	3.19 to 72.58 deg.
Ranges of h,k,l	$-17 \leq h \leq 16$, $-7 \leq k \leq 7$, $-21 \leq \ell \leq 21$
No. of standard reflections	123
Intensity decay (%)	none

Refinement

Refinement method	Full-matrix on F^2
Final R indices, I>2sigma(I)	R1 = 0.0497, wR2 = 0.1299
R indices, all data	R1 = 0.0610, wR2 = 0.1299
Goodness-of-fit on F^2, S	0.959

R1 = sum (absabs Foabs -abs Fcabsabs)/sum (abs Foabs),
wR2 = [sum [w(Fo^2^-Fc^2^)^2^]/sum [w(Fo^2^)^2^]]^1*2^ and
GoF = [sum [w(Fo^2^-Fc^2^)^2^]/(No. of reflns - No. of params.)]^1*2^

Data / restraints / parameters	2900 / 0 / 163
Method of refining and locating H atoms	mixed
Weighting scheme	based on measured s.u.'s
Function minimized	sum w(Fo^2^-Fc^2^)

calc w=1/[\s^2^(Fo^2^)+(0.0810P)^2^]

Maximum shift/sigma	0.001
Largest diff. peak and hole	0.363 and -0.339 e.A^*3

Table II.6.2 Atomic coordinates and equivalent isotropic displacement parameters (A^2^ x 10 ^2^) for C14 H14 S4.

U~eq~ = (1/3)sum~i~sum~j~U~ij~a^*^~i~a^*^~j~a~i~.a~j~.

	x	y	z	U(eq)
S(1)	0.53464(5)	1.24776(12)	0.43508(4)	5.06(2)
S(2)	0.62789(5)	1.21229(12)	0.53903(4)	4.96(2)
S(3)	0.73676(5)	1.43373(12)	0.54033(4)	5.51(2)
S(4)	0.83373(6)	1.29797(14)	0.48103(5)	5.68(2)
C(1)	0.58463(18)	1.0760(4)	0.37096(15)	4.22(6)
C(2)	0.58668(19)	1.1520(5)	0.29771(16)	4.64(6)
C(3)	0.62299(19)	1.0211(5)	0.24529(16)	4.81(7)
C(4)	0.65882(19)	0.8166(5)	0.26630(15)	4.45(6)
C(5)	0.6557(2)	0.7430(4)	0.34092(17)	4.77(7)
C(6)	0.6183(2)	0.8686(5)	0.39220(16)	4.89(7)
C(7)	0.6995(2)	0.6768(6)	0.21001(18)	6.25(8)
C(8)	0.91196(19)	1.1447(5)	0.55316(16)	4.51(6)
C(9)	1.0036(2)	1.2195(5)	0.58247(18)	5.45(7)
C(10)	1.0659(2)	1.0953(6)	0.63585(19)	5.96(8)
C(11)	1.0388(2)	0.8976(5)	0.66121(17)	5.38(7)
C(12)	0.9462(2)	0.8248(5)	0.6304(2)	6.10(8)
C(13)	0.8833(2)	0.9465(5)	0.57691(19)	5.70(8)
C(14)	1.1067(3)	0.7636(6)	0.7192(2)	7.48(10)

Table II.6.3 Bond lengths (A) and angles (deg) for C14 H14 S4.

S(1)-C(1)	1.786(3)	S(1)-S(2)	2.0402(10)
S(2)-S(3)	2.0528(11)	S(3)-S(4)	2.0510(11)
S(4)-C(8)	1.780(3)	C(1)-C(2)	1.372(4)
C(1)-C(6)	1.391(4)	C(2)-C(3)	1.393(4)
C(2)-H(2)	0.9300	C(3)-C(4)	1.382(4)
C(3)-H(3)	0.9300	C(4)-C(5)	1.393(4)
C(4)-C(7)	1.506(4)	C(5)-C(6)	1.368(4)
C(5)-H(5)	0.9300	C(6)-H(6)	0.9300
C(7)-H(7A)	0.9600	C(7)-H(7B)	0.9600
C(7)-H(7C)	0.9600	C(7)-H(7D)	0.9600
C(7)-H(7E)	0.9600	C(7)-H(7F)	0.9600
C(8)-C(9)	1.375(4)	C(8)-C(13)	1.378(4)
C(9)-C(10)	1.384(4)	C(9)-H(9)	0.9300
C(10)-C(11)	1.378(4)	C(10)-H(10)	0.9300
C(11)-C(12)	1.387(4)	C(11)-C(14)	1.503(4)
C(12)-C(13)	1.381(4)	C(12)-H(12)	0.9300
C(13)-H(13)	0.9300	C(14)-H(14A)	0.9600
C(14)-H(14B)	0.9600	C(14)-H(14C)	0.9600
C(14)-H(14D)	0.9600	C(14)-H(14E)	0.9600
C(14)-H(14F)	0.9600		

C(1)-S(1)-S(2)	103.46(9)	S(1)-S(2)-S(3)	106.84(4)
S(4)-S(3)-S(2)	107.09(4)	C(8)-S(4)-S(3)	103.90(10)
C(2)-C(1)-C(6)	119.8(3)	C(2)-C(1)-S(1)	117.9(2)
C(6)-C(1)-S(1)	122.3(2)	C(1)-C(2)-C(3)	119.7(3)
C(1)-C(2)-H(2)	120.1	C(3)-C(2)-H(2)	120.1
C(4)-C(3)-C(2)	121.1(3)	C(4)-C(3)-H(3)	119.5
C(2)-C(3)-H(3)	119.5	C(3)-C(4)-C(5)	118.1(3)
C(3)-C(4)-C(7)	121.0(3)	C(5)-C(4)-C(7)	120.9(3)
C(6)-C(5)-C(4)	121.2(3)	C(6)-C(5)-H(5)	119.4
C(4)-C(5)-H(5)	119.4	C(5)-C(6)-C(1)	120.1(3)
C(5)-C(6)-H(6)	120.0	C(1)-C(6)-H(6)	120.0
C(4)-C(7)-H(7A)	109.5	C(4)-C(7)-H(7B)	109.5
H(7A)-C(7)-H(7B)	109.5	C(4)-C(7)-H(7C)	109.5
H(7A)-C(7)-H(7C)	109.5	H(7B)-C(7)-H(7C)	109.5
C(4)-C(7)-H(7D)	109.5	H(7A)-C(7)-H(7D)	141.1
H(7B)-C(7)-H(7D)	56.3	H(7C)-C(7)-H(7D)	56.3
C(4)-C(7)-H(7E)	109.5	H(7A)-C(7)-H(7E)	56.3
H(7B)-C(7)-H(7E)	141.1	H(7C)-C(7)-H(7E)	56.3
H(7D)-C(7)-H(7E)	109.5	C(4)-C(7)-H(7F)	109.5
HH(7A)-C(7)-H(7F)	56.3	H(7B)-C(7)-H(7F)	56.3
H(7C)-C(7)-H(7F)	141.1	H(7D)-C(7)-H(7F)	109.5
H(7E)-C(7)-H(7F)	109.5	C(9)-C(8)-C(13)	119.7(3)
C(9)-C(8)-S(4)	119.7(2)	C(13)-C(8)-S(4)	120.6(2)
C(8)-C(9)-C(10)	119.6(3)	C(8)-C(9)-H(9)	120.2
C(10)-C(9)-H(9)	120.2	C(11)-C(10)-C(9)	121.9(3)
C(11)-C(10)-H(10)	119.0	C(9)-C(10)-H(10)	119.0
C(10)-C(11)-C(12)	117.4(3)	C(10)-C(11)-C(14)	121.7(3)
C(12)-C(11)-C(14)	120.9(3)	C(13)-C(12)-C(11)	121.4(3)
C(13)-C(12)-H(12)	119.3	C(11)-C(12)-H(12)	119.3
C(8)-C(13)-C(12)	120.0(3)	C(8)-C(13)-H(13)	120.0
C(12)-C(13)-H(13)	120.0	C(11)-C(14)-H(14A)	109.5
C(11)-C(14)-H(14B)	109.5	H(14A)-C(14)-H(14B)	109.5
C(11)-C(14)-H(14C)	109.5	H(14A)-C(14)-H(14C)	109.5

H(14B)-C(14)-H(14C)	109.5	C(11)-C(14)-H(14D)	109.5
H(14A)-C(14)-H(14D)	141.1	H(14B)-C(14)-H(14D)	56.3
H(14C)-C(14)-H(14D)	56.3	C(11)-C(14)-H(14E)	109.5
H(14A)-C(14)-H(14E)	56.3	H(14B)-C(14)-H(14E)	141.1
H(14C)-C(14)-H(14E)	56.3	H(14D)-C(14)-H(14E)	109.5
C(11)-C(14)-H(14F)	109.5	H(14A)-C(14)-H(14F)	56.3
H(14B)-C(14)-H(14F)	56.3	H(14C)-C(14)-H(14F)	141.1
H(14D)-C(14)-H(14F)	109.5	H(14E)-C(14)-H(14F)	109.5

Table II.6.4 Torsion angles (deg) for C14 H14 S4.

C(1)-S(1)-S(2)-S(3)	86.82(10)
S(1)-S(2)-S(3)-S(4)	-82.74(5)
S(2)-S(3)-S(4)-C(8)	-86.46(11)
S(2)-S(1)-C(1)-C(2)	-137.7(2)
S(2)-S(1)-C(1)-C(6)	44.3(2)
C(6)-C(1)-C(2)-C(3)	-0.4(4)
S(1)-C(1)-C(2)-C(3)	-178.5(2)
C(1)-C(2)-C(3)-C(4)	-1.2(4)
C(2)-C(3)-C(4)-C(5)	1.4(4)
C(2)-C(3)-C(4)-C(7)	-179.0(3)
C(3)-C(4)-C(5)-C(6)	0.0(4)
C(7)-C(4)-C(5)-C(6)	-179.6(3)
C(4)-C(5)-C(6)-C(1)	-1.6(4)
C(2)-C(1)-C(6)-C(5)	1.8(4)
S(1)-C(1)-C(6)-C(5)	179.8(2)
S(3)-S(4)-C(8)-C(9)	-105.6(2)
S(3)-S(4)-C(8)-C(13)	77.8(3)
C(13)-C(8)-C(9)-C(10)	-0.3(5)
S(4)-C(8)-C(9)-C(10)	-177.0(2)
C(8)-C(9)-C(10)-C(11)	-0.3(5)
C(9)-C(10)-C(11)-C(12)	0.8(5)
C(9)-C(10)-C(11)-C(14)	-180.0(3)
C(10)-C(11)-C(12)-C(13)	-0.7(5)
C(14)-C(11)-C(12)-C(13)	-179.9(3)
C(9)-C(8)-C(13)-C(12)	0.5(5)
S(4)-C(8)-C(13)-C(12)	177.1(2)
C(11)-C(12)-C(13)-C(8)	0.0(5)

Table II.6.5 Hydrogen coordinates and isotropic displacement parameters (A^2^ x 10 ^2^) for C14 H14 S4.

	x	y	z	U~iso~
H(2)	0.5639	1.2902	0.2831	5.6
H(3)	0.6231	1.0721	0.1954	5.8
H(5)	0.6795	0.6059	0.3562	5.7
H(6)	0.6153	0.8151	0.4413	5.9
H(7A)	0.7208	0.5413	0.2344	9.4
H(7B)	0.7533	0.7494	0.1950	9.4
H(7C)	0.6505	0.6504	0.1647	9.4
H(7D)	0.6956	0.7528	0.1617	9.4
H(7E)	0.6631	0.5447	0.2010	9.4
H(7F)	0.7659	0.6437	0.2314	9.4
H(9)	1.0236	1.3527	0.5665	6.5
H(10)	1.1278	1.1467	0.6552	7.2
H(12)	0.9261	0.6912	0.6460	7.3
H(13)	0.8215	0.8947	0.5569	6.8
H(14A)	1.0751	0.6322	0.7296	11.2
H(14B)	1.1255	0.8440	0.7667	11.2
H(14C)	1.1631	0.7289	0.6985	11.2
H(14D)	1.1674	0.8379	0.7336	11.2
H(14E)	1.1169	0.6261	0.6965	11.2
H(14F)	1.0793	0.7411	0.7647	11.2

Table II.6.6 Anisotropic parameters (A^2 x 10^2) for C14 H14 S4.

The anisotropic displacement factor exponent takes the form:

$$-2\pi^2 [h^2 a^{*2} U11 + ... + 2 h k a^* b^* U12]$$

	U11	U22	U33	U23	U13	U12
S(1)	4.15(4)	5.93(5)	5.09(4)	-0.29(3)	0.85(3)	0.78(3)
S(2)	5.03(4)	6.02(5)	4.08(4)	0.14(3)	1.47(3)	0.14(3)
S(3)	5.41(4)	4.59(4)	6.28(5)	-0.70(3)	0.51(3)	0.05(3)
S(4)	4.82(4)	7.02(5)	5.36(5)	1.30(3)	1.37(3)	-0.02(3)
C(1)	3.58(13)	4.45(15)	4.57(15)	-0.02(11)	0.64(11)	-0.22(11)
C(2)	4.33(14)	4.79(16)	4.66(15)	0.62(12)	0.52(12)	0.14(12)
C(3)	4.76(15)	5.44(17)	4.19(15)	0.84(12)	0.80(12)	-0.47(13)
C(4)	3.67(14)	5.24(16)	4.37(15)	-0.26(11)	0.62(11)	-0.44(12)
C(5)	5.19(16)	4.06(15)	4.97(16)	0.21(12)	0.75(13)	0.18(12)
C(6)	5.72(17)	4.99(17)	4.02(15)	0.77(12)	1.07(12)	0.14(13)
C(7)	6.4(2)	7.3(2)	5.19(18)	-0.90(15)	1.29(15)	0.71(17)
C(8)	4.07(14)	4.95(16)	4.76(15)	0.26(12)	1.48(11)	0.10(12)
C(9)	4.78(16)	5.43(18)	6.25(19)	0.43(13)	1.35(14)	-0.86(14)
C(10)	3.98(15)	6.8(2)	7.0(2)	-0.14(16)	0.81(14)	-0.98(14)
C(11)	4.70(16)	6.29(19)	5.41(17)	0.35(14)	1.58(13)	0.75(14)
C(12)	5.85(19)	5.01(18)	7.7(2)	0.95(15)	2.03(16)	-0.26(15)
C(13)	4.37(15)	5.31(19)	7.4(2)	0.29(14)	1.03(14)	-1.02(13)
C(14)	6.6(2)	8.7(3)	7.0(2)	1.81(18)	0.93(18)	0.97(18)

Table II.6.7 Least-squares planes (x,y,z in crystal coordinates) and deviations from them for C14 H14 S4.

(* indicates atom used to define plane)

PLANE 1

- 6.9424 (0.0164) x + 2.7714 (0.0072) y + 14.4940 (0.0122) z = 4.8552 (0.0217)

*	0.0035	(0.0021)	C8
*	-0.0006	(0.0022)	C9
*	-0.0034	(0.0023)	C10
*	0.0046	(0.0022)	C11
*	-0.0018	(0.0023)	C12
*	-0.0023	(0.0022)	C13
	0.0022	(0.0057)	C14
	-0.0740	(0.0042)	S4

Rms deviation of fitted atoms = 0.0030

PLANE 2

12.1626 (0.0077) x + 2.3467 (0.0063) y + 2.8183 (0.0195) z = 10.6743 (0.0034)

Angle to previous plane (with approximate esd) = 89.80 (0.09)

*	0.0068	(0.0018)	C1
*	0.0035	(0.0019)	C2
*	-0.0097	(0.0019)	C3
*	0.0055	(0.0019)	C4
*	0.0050	(0.0020)	C5
*	-0.0110	(0.0020)	C6
	0.0140	(0.0047)	C7
	-0.0174	(0.0036)	S1

Rms deviation of fitted atoms = 0.0074

Discussion data collection, structure determination and refinement procedure

X-ray crystallographic data for I were collected from a single crystal sample, which was mounted on a glass fiber. Data were collected using a Bruker Platform diffractometer, equipped with a Bruker SMART 2K Charged-Coupled Device (CCD) Area Detector using the program SMART and normal focus sealed tube source graphite monochromated Cu-K(radiation. The crystal-to-detector distance was 4.908 cm, and the data collection was carried out in 512 x 512 pixel mode, utilizing 4 x 4 pixel binning. The initial unit cell parameters were determined by a least-squares fit of the angular setting of strong reflections, collected by a 9.0 degree scan in 30 frames over four different parts of the reciprocal space (120 frames total). One complete sphere of data was collected, to better than 0.8Å resolution. Upon compleetion of the data collection, the first 101 frames were recollected in order to improve the decay correction analysis.

Data reduction processing was carried out by the use of the program SAINT (Bruker, 1999), which applied Lorentz and polarization corrections to three-dimensionally integrated diffraction spots.
The program SADABS (Sheldrick, 1996) was utilized for the scaling of diffraction data, the application of a decay correction, and an empirical absorption correction based on redundant reflections. The space group was confirmed by XPREP routine in SHELXTL program (Sheldrick, 1997). The structure was solved by direct method using SHELXS97 (Sheldrick, 1997) and difmap synthesis using SHELXL96 (Sheldrick, 1996). All non-hydrogen atoms are anisotropic, hydrogen atoms are isotropic. Hydrogen atoms are constrained to the parent site using a riding model; SHELXL96 defaults, C-H 0.93 to 0.97Å. The hydrogens on the methyl groups are disordered over 2 orientations related by an 180(rotation, with each at half occupancy. The isotropic factors, Uiso, were adjusted to a value 50% higher then U(eq) of the parent site (methyl) and 20% higher (others).
A final verification of possible voids was performed using the VOID routine of the PLATON program (Spek, 1995).

References

Flack, H.D. (1983). Acta Cryst. A39, 876-881.

Flack, H.D. and Schwarzenbach, D. (1988). Acta Cryst. A44, 499-506.

International Tables for Crystallography (1992). Vol. C. Tables 4.2.6.8 and 6.1.1.4, Dordrecht: Kluwer Academic Publishers.

SAINT (1999) Release 6.06; Integration Software for Single Crystal Data. Bruker AXS Inc., Madison, WI 53719-1173.

Sheldrick, G.M. (1996). SADABS, Bruker Area Detector Absorption Corrections. Bruker AXS Inc., Madison, WI 53719-1173.

SHELXTL (1997) Release 5.10; The Complete Software Package for Single Crystal Structure Determination. Bruker AXS Inc., Madison, WI 53719-1173.

SMART (1999) Release 5.059; Bruker Molecular Analysis Research Tool. Bruker AXS Inc., Madison, WI 53719-1173.

Spek, A.L. (1995b). PLUTON Molecular Graphics Program, July 1995 version. University of Utrecht, Utrecht, Holland.

Spek, A.L. (1995. PLATON, Molecular Geometry Program, July 1995 version. University of Utrecht, Utrecht, Holland. (version 190499 at McGill)

XPREP (1997) Release 5.10; X-ray data Preparation and Reciprocal space Exploration Program. Bruker AXS Inc., Madison, WI 53719-1173.

APPENDIX III. DSC Spectra

Sample: indium control - 3.5 mg
Size: 3.5000 mg
Method: Eli
Comment: indium - 3.5 mg

DSC

File: E:\Eli\indium.003
Operator: Eli
Run Date: 6-May-03 15:18

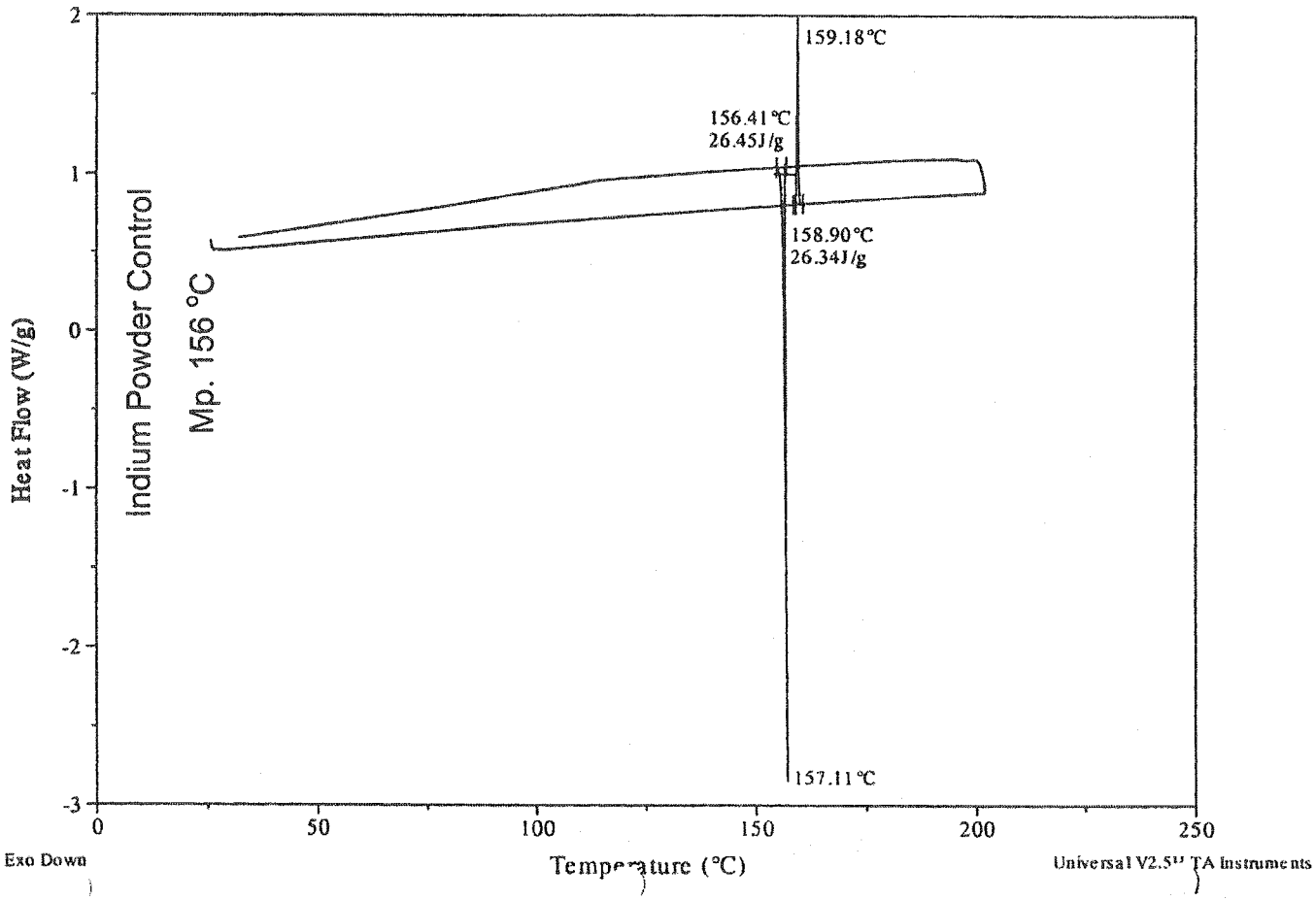

Sample: benzoic acid control
Size: 1.0000 mg
Method: Eli
Comment: benzoic acid control - triple point - 122

DSC

File: E:\Eli\control.002
Operator: Eli
Run Date: 2-May-03 09:52

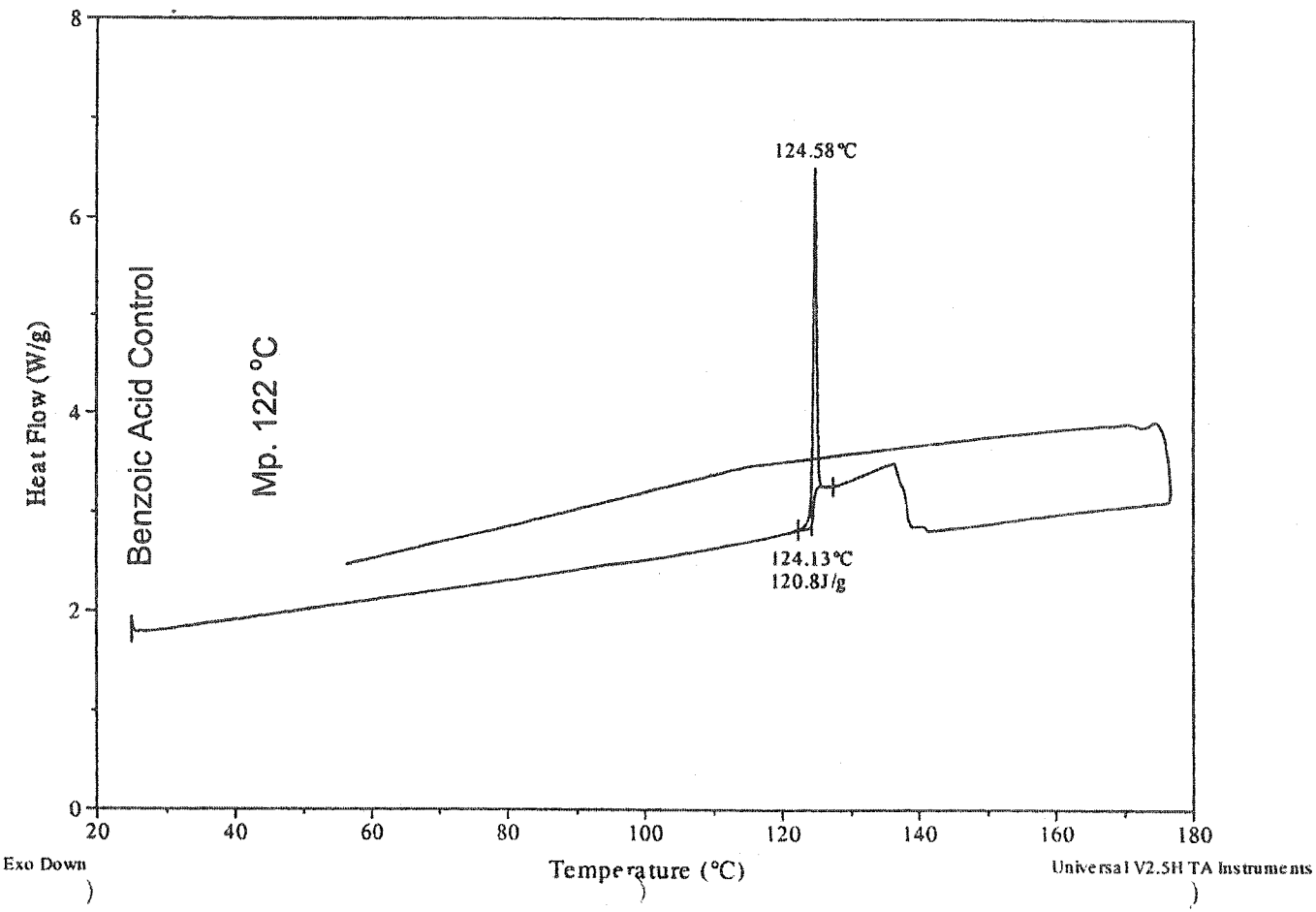

Sample: monomer of Eli System
Size: 4.8000 mg
Method: Eli

DSC

File: EZC_06_51_frac_6_8_trial...
Operator: Eli
Run Date: 11-Apr-03 12:04

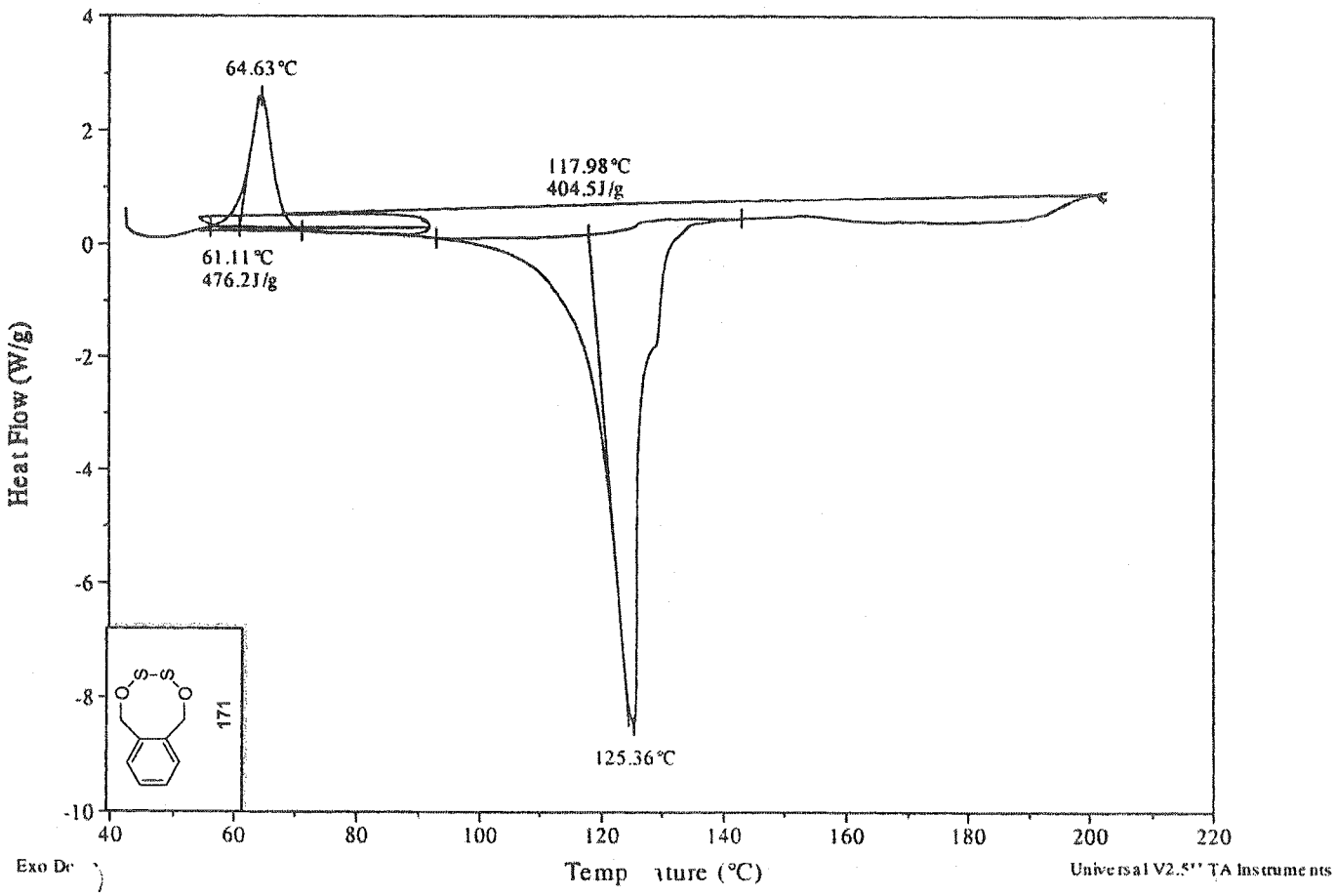

Sample: Eli's Sample 0.5mg
Size: 0.5000 mg
Method: Eli1
Comment: thiono

DSC

File: E:\Eli\042403.001
Operator: Eli
Run Date: 24-Apr-03 20:16

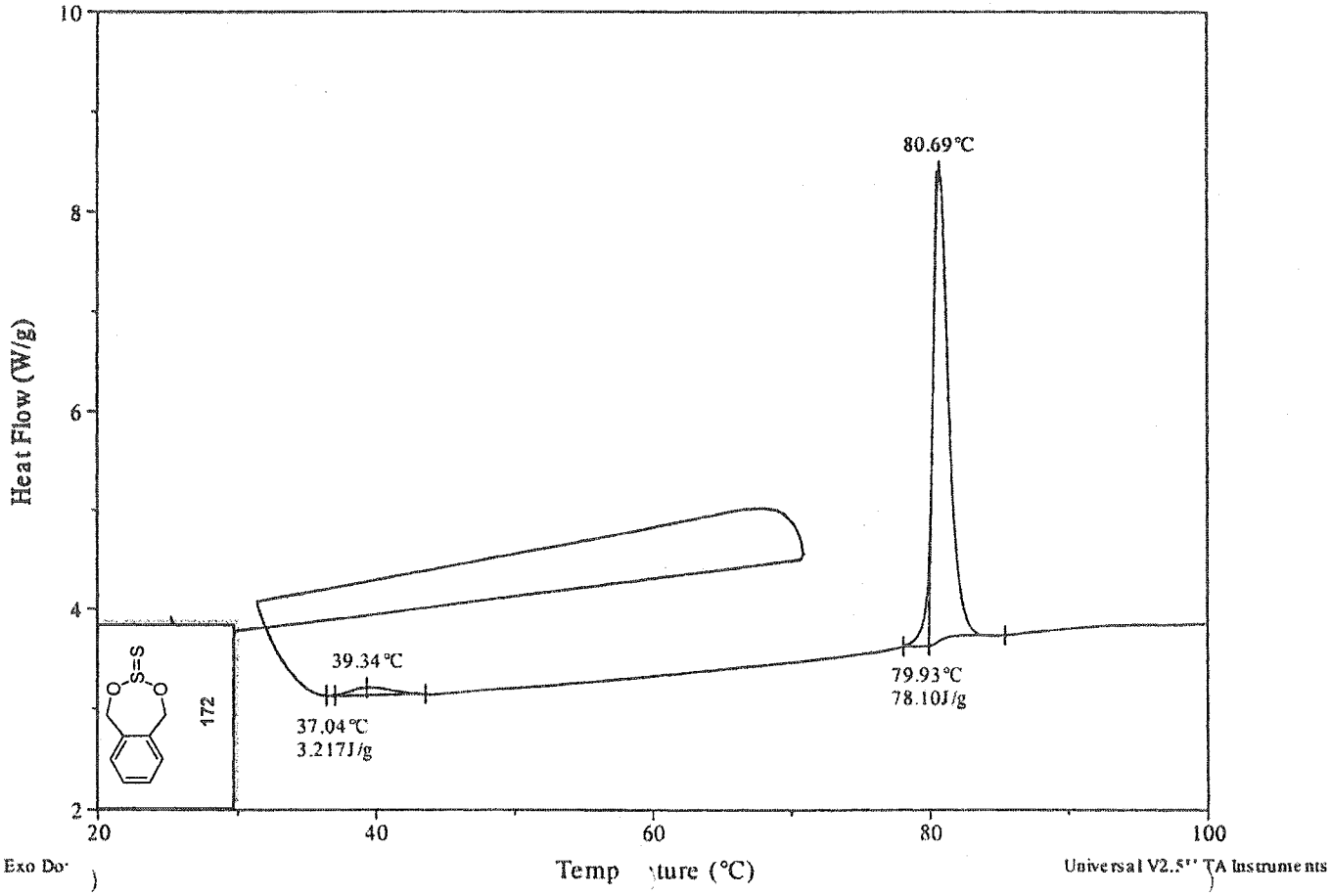

Sample: dimer from EZC-07-15-frac-12-20
Size: 0.2000 mg
Method: Eli
Comment: dimer from EZC-07-15-frac-12-20

DSC

File: E:\Eli\dimer.001
Operator: Eli
Run Date: 1-May-03 11:42

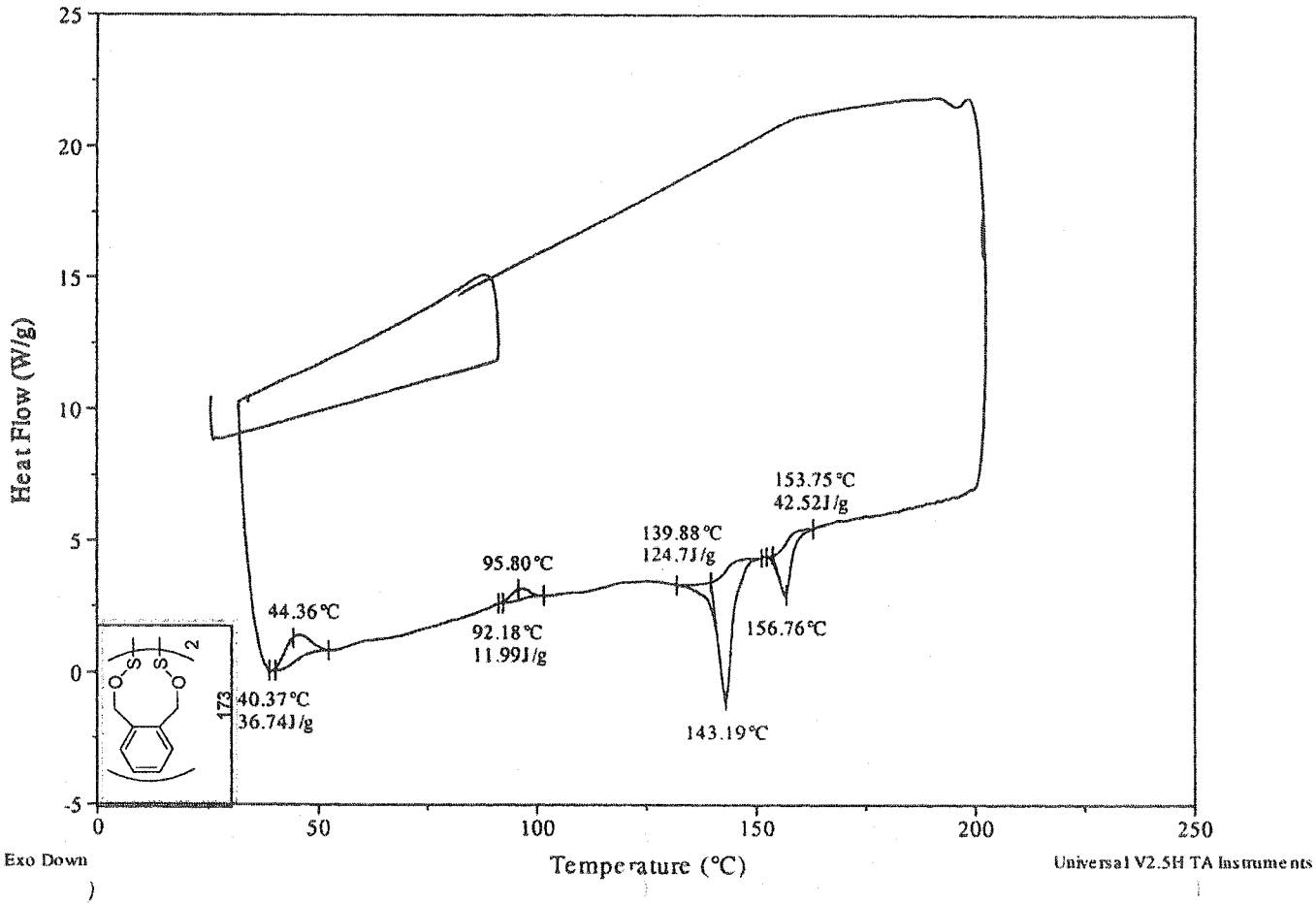

APPENDIX IV. IR Spectra

File # 1 : MONOMER3 Mode = 2 (Mid-IR) 4/25/03 9:39 AM

Sample Desription = monomer by kbr

Scans = 8 Res = 2 cm-1 11 scans/min Apod = Cosine

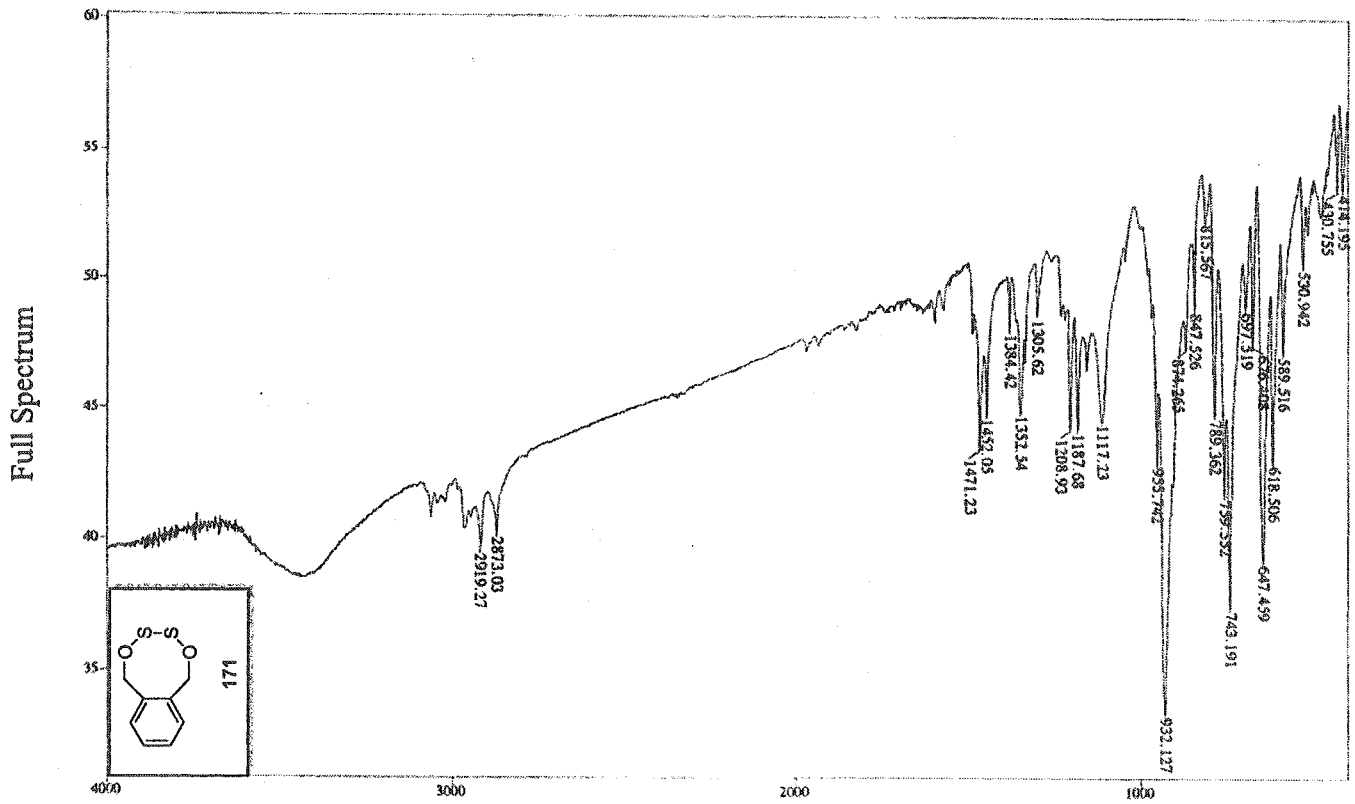

File # 1 : MONOMER3 Mode = 2 (Mid-IR) 4/25/03 9:59 AM

Sample Description = monomer by kbr

Scans = 8 Res = 2 cm-1 11 scans/min Apod = Cosine

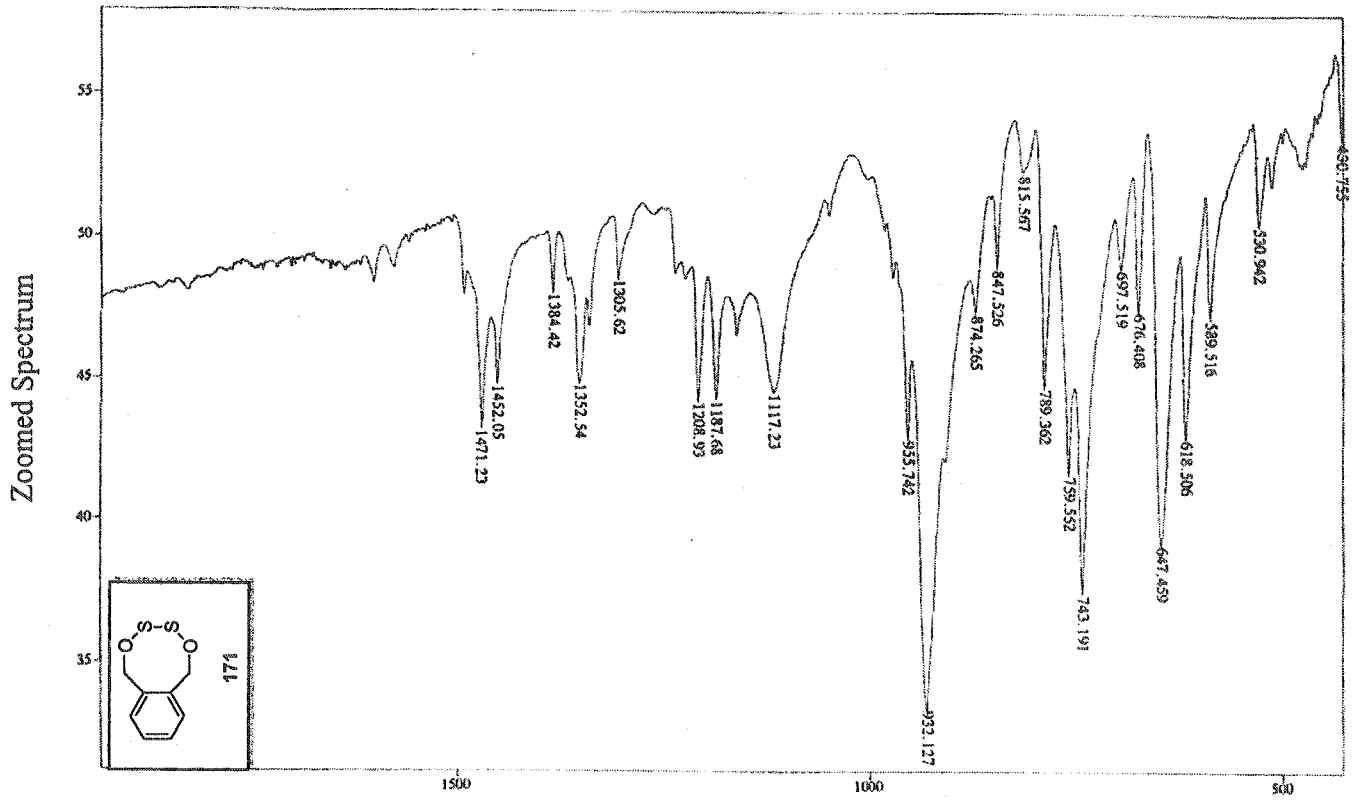

Transmittance / W... ...umber (cm-1)

Full Spectrum
File # 1 : THIONO3
Mode = 2 (Mid-IR)
4/25/03 10:29 AM
Sample Description = thiono by kbr
Scans = 8
Res = 2 cm-1 11 scans/min
Apod = Cosine
Transmittance / %
Number (cm-1)
4000
3000
2000
1000
45
50
55
60
65
172
3745.4
1496.24
1441.79
1454.9
1384.46
1242.34
1218.68
1186.03
1118.27
947.4
931.791
892.676
852.673
774.398
738.546
696.527
685.208
668.784
632.422
595.256
539.631
485.599

File # 1 : THIONO3
Mode = 2 (Mid-IR)
4/25/03 10:29 AM
Sample Description = thiono by khr
Scans = 8
Res = 2 cm-1 11 scans/min
Apod = Cosine
Zoomed Spectrum
Transmittance : Wavenumber (cm-1)
172
1496.24
1454.9
1441.79
1384.46
1242.34
1218.68
1186.03
1118.27
947.4
892.676
852.673
774.398
738.346
696.527
685.208
668.784
632.422
595.256
539.631
455.793

File # 1 : OVERLAY | Mode = 2 (Mid-IR) | 4/25/03 9:59 AM

Sample Desription = monomer by kbr

Scans = 8 | Res = 2 cm-1 11 scans/min | Apod = Cosine

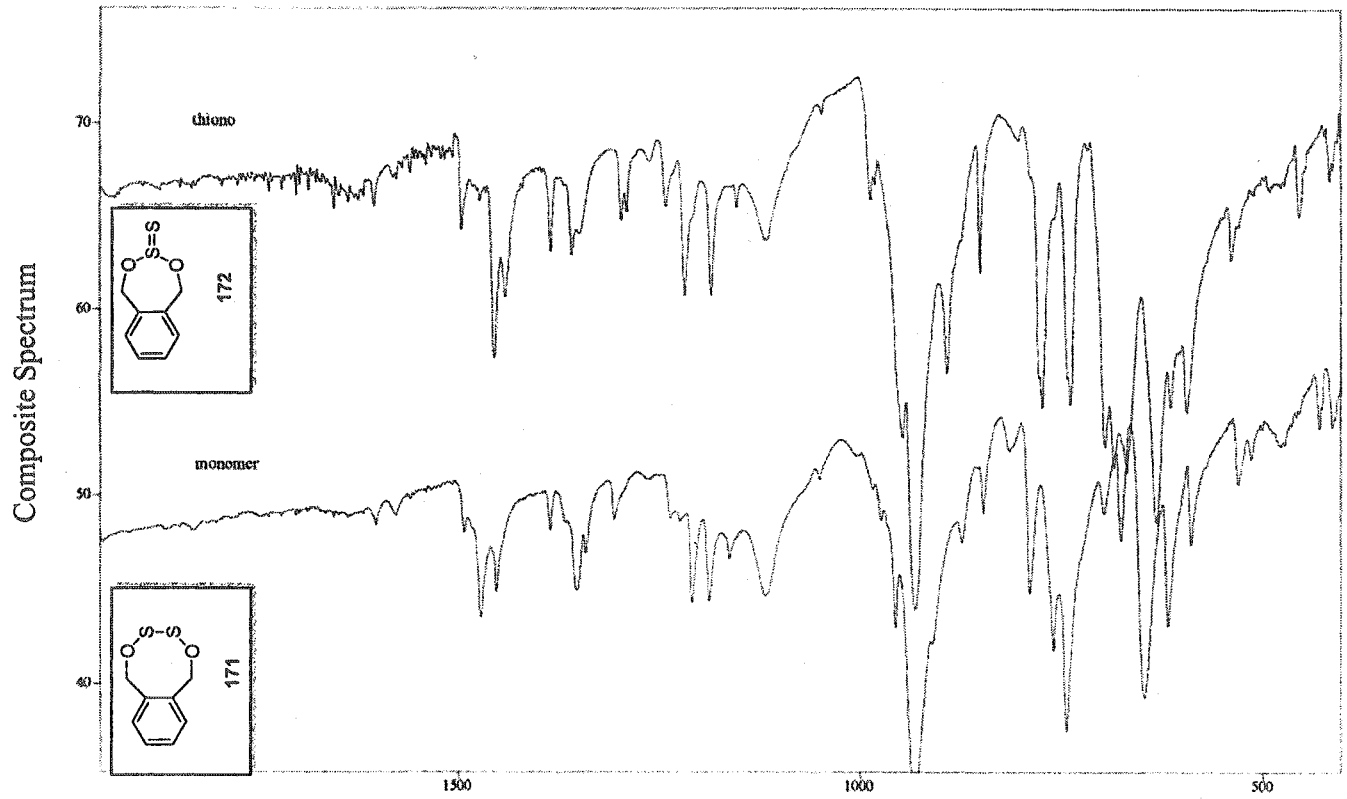

Transmittance / W. Number (cm-1)

File # 1 : 053003 Mode = 2 (Mid-IR) 5/1/03 11:33 AM

Sample Desription = dimer - KBr - from EZC-07-15-frac-12-20

Scans = 8 Res = 2 cm-1 11 scans/min Apod = Cosine

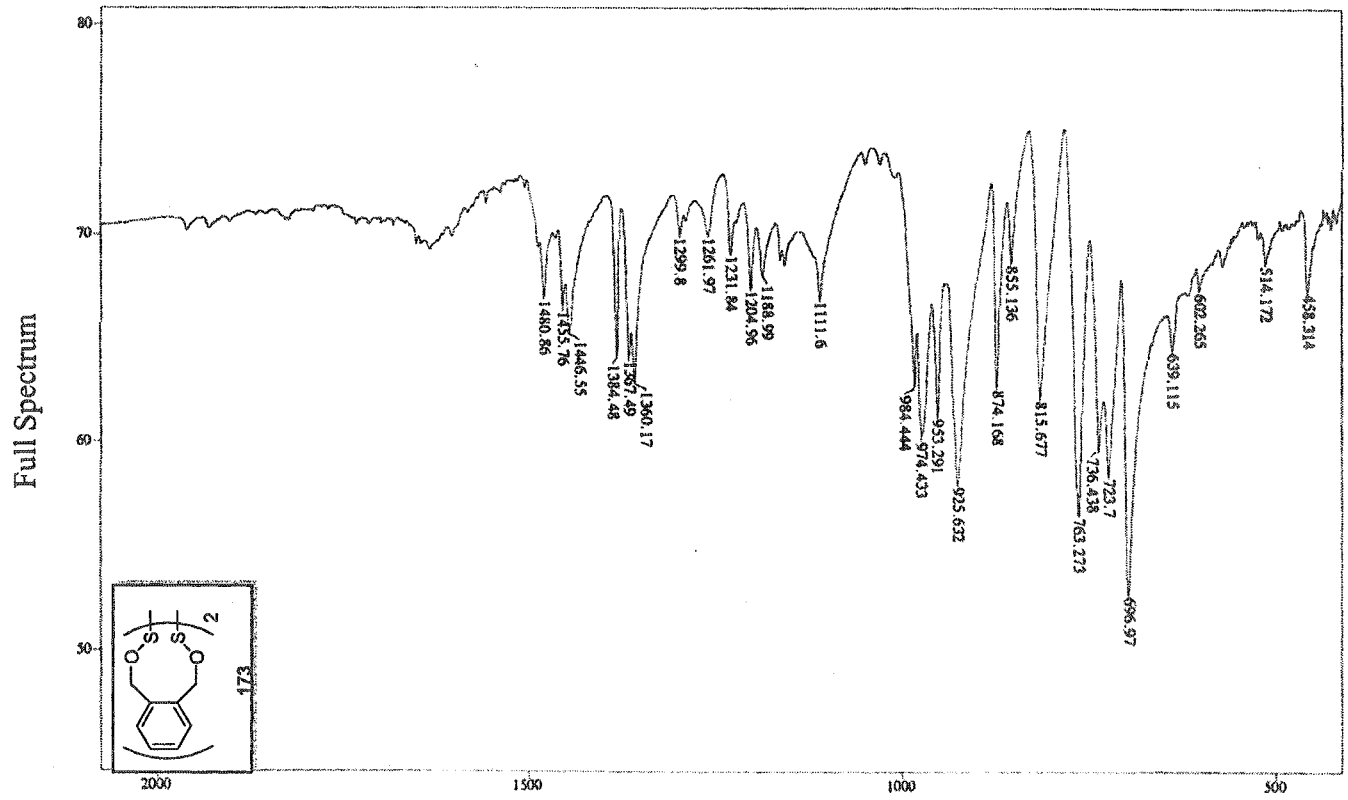

Transmittance / W- Number (cm-1)

APPENDIX V. Raman Spectra

C:\OPUS_NT\DATA\DEPT\ELI\MONOMER.0 5/15/03 02:30:58 PM

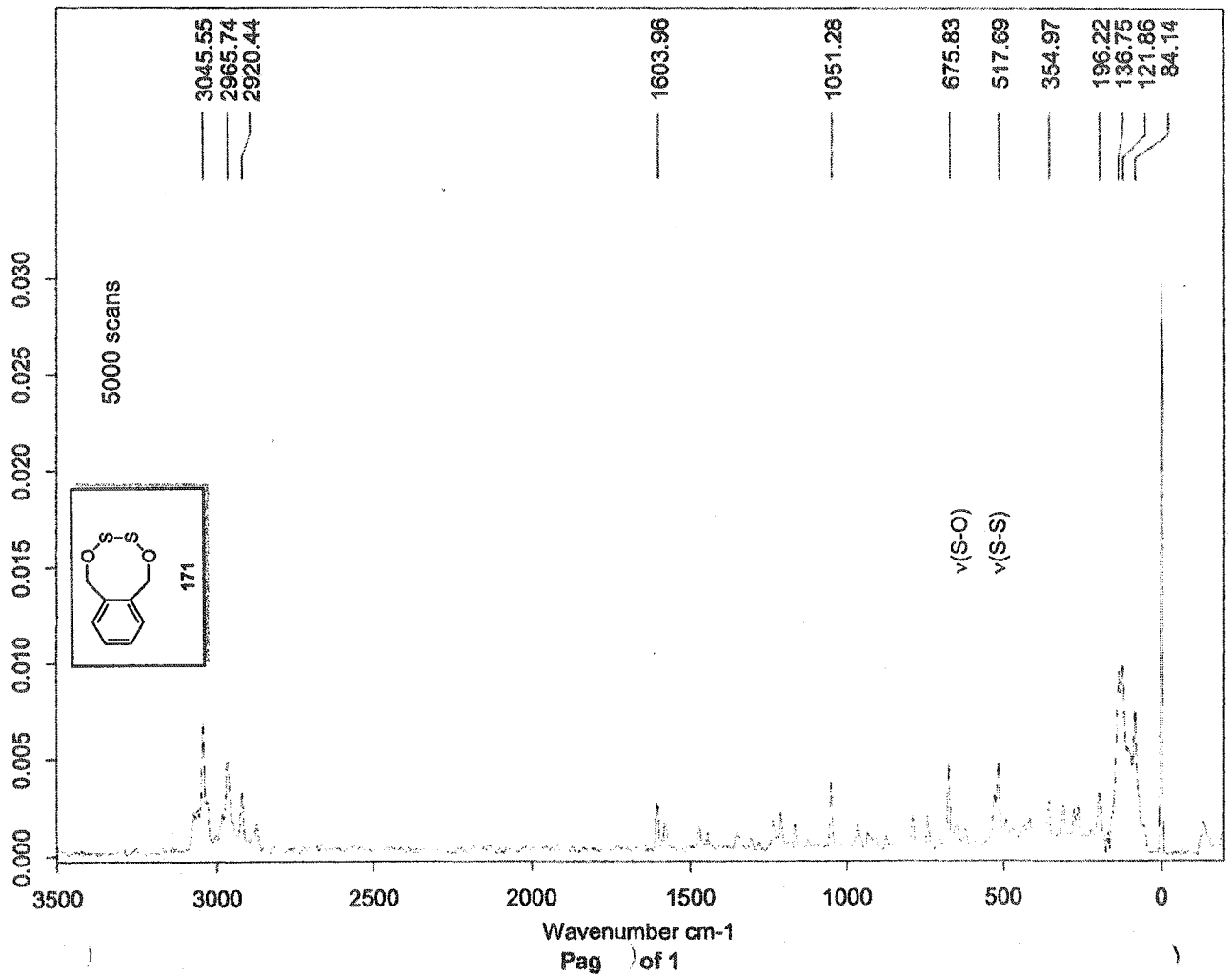

C:\OPUS_NT\DATA\DEPTEL\THIONO.0
0.000
0.005
0.010
0.015
0.020
0.025
0.030
3500
3000
2500
2000
1500
1000
500
0
Wavenumber cm-1
Page)of 1
1000 scans
172
3046.55
2983.10
1606.09
1219.97
1160.25
1048.00
744.63
632.76
540.02
337.35
304.28
178.93
134.59
86.89
57.61
ν(S-O)
ν(S=S)
5/15/03 01:33:32 PM